Proceedings of the 15th International Workshop on Laser Ranging

Extending the Range

Volume 2

October 15-20, 2006
Canberra, Australia

TABLE OF CONTENTS

Karel Hamal Obituary
I Prochazka *1*

Preface
J Luck *3*

Foreword
R Thompson *4*

Welcome Note
W Gurtner *5*

Workshop Summary
M Pearlman *7*

Science Products Session

Summary
S Klosko *9*

Enhanced Modelling of the Non-Gravitational Forces Acting on LAGEOS
J Andres, R Noomen *12*

Calibrating GNSS Orbts with SLR Tracking Data
C Urschl, G Beutler, W Gurtner, U Hugentobler, S Schaer *23*

GIOVE-A and GPS-35/36 Orbit Determination and Analysis of Dynamical Properties Based on SLR-only Tracking Data
S Melachroinos, F Perosanz, F Deleflie, R Biancalel, O Laurain, P Exertier *27*

Orbit Determination and Analysis for Giove-A using SLR Tracking Data
R Govind *39*

Orbit Determination for GIOVE-A using SLR Tracking Data
C Urschl, G Beutler, W Gurtner, U Hugentobler, M Ploner *40*

Satellite Laser Ranging in the National (Australian) Collaborative Research Infrastructure Proposal for Geospatial R&D
K Lambeck *47*

Time-Variable Gravity from SLR and DORIS Tracking
F Lemoine, S Klosko, C Cox, T Johnson *48*

Global Glacial Isostatic Adjustment: Target Fields for Space Geodesy
W Peltier *55*

Recent Results from SLR Experiments in Fundamental Physics: Frame Dragging Observed with Satellite Laser Ranging.
E Pavlis, I Ciufolini, R Konig *69*

A "Web Service" to Compare Geodetic Time Series
F Deleflie *79*

Least-Square Mean Effect: Application to the Analysis of SLR Time Series
D Coulot, P Berio, A Pollet *80*

Some Aspects Concerning the SLR Part of ITRF2005
H Mueller, D Angermann *91*

Determination of the Temporal Variations of the Earth's Centre of Mass from Multi-Year Satellite Laser Ranging Data
R Govind *98*

Contribution of Satellite and Lunar Laser Ranging to Earth Orientation Monitoring
D Gambis, R Biancale *99*

Station Positioning and the ITRF
Z Altamimi *100*

Station Coordinates, Earth Rotation Parameters and Low Degree Harmonics from SLR within GGOS-D
R Koenig, H Mueller *106*

An Original Approach to Compute Satellite Laser Ranging Biases
D Coulot, P Berio, O Laurain, D Feraudy, P Exertier *110*

Analysis of 13 Years (1993-2005) of Satellite Laser Ranging Data on the Two LAGEOS Satellites for Terrestrial Reference Frames and Earth Orientation Parameters
D Coulot, P Berio, O Laurain, D Feraudy, P Exertier, F Deleflie 120

Network Performance and Results Session

Summary
C Luceri, M Torrence 131

The SLR Network from a QC Perspective
R Noomen 132

The ILRS Standard Products: a Quality Assessment
G Bianco, V Luceri, C Sciarretta 141

Systematic Range Bias 2005-06
T Otsubo, N Obara 148

A Reassessment of Laser Ranging Accuracy at SGF Herstmonceux, UK
P Gibbs, G Appleby, C Potter 154

The Global SLR Network and the Origin and Scale of the TRF in the GGOS Era
E Pavlis 159

FTLRS Ajaccio Campaigns: Operations and Positioning Analysis over 2002/2005
F Pierron, B Gourine, P Exertier, P Berio, P Bonnefond, D Coulot et al 167

SLR-based Evaluation and Validation Studies of Candidate ITRF2005 Products
E Pavlis, M Kuzmicz-Cieslak, D Pavlis 173

An Optimised Global SLR Network for Terrestrial Reference Frame Definition
R Govind 180

Performance of Southern Hemisphere Stations
J Luck 181

The Evolution of SLR/LLR in Response to Mission Needs
P Shelus 188

Assessment of SLR Network Performance
M Torrence, P Dunn 189

Performance of WPLTN Stations
J Luck 191

Archiving and Infrastructure Support at the ILRS Data Centers
C Noll, M Torrence, W Seemueller 198

Minico Calibration of System Delay Calibration at Mount Stromlo SLR
J Luck 202

A Summary of Observations of Giove A, taken from Mt Stromlo SLR Station
C Moore 203

Lasers and Detectors Session

Summary
J Degnan, I Prochaska 210

Photon Counting Module for Laser Time Transfer Space Mission
K Hamal, I Prochazka, L Kral, Y Fumin 211

Picosecond Lasers with Raman Frequency and Pulsewidth Conversion for Range Finding
N Andreev, E Grishin, O Kulagin, A Sergeev, M Valley 217

Advanced Solid State Laser System for Space Tracking
Y Gao, Y Wang, B Greene, C Smith, A Chan, A Gray, J Vear, M Blundell 222

Altimetry Session

Summary
F Lemoine 223

Second-Generation, Scanning, 3D Imaging Lidars Based on Photon-Counting
J Degnan, D Wells, R Machan, E Leventhal, D Lawrence, Y Zheng, S Mitchell, C Field, W Hasselbrack 224

The BELA - The First European Planetary Laser Altimeter: Conceptional Design and Technical Status
H Michaelis, T Spohn, J Oberst, N Thomas, K Seiferlin, U Christensen, M Hilchenbach, U Schreiber 229

Timing System for the Laser Altimeter for Planetary Exploration Technology Demonstrator
P Jirousek, I Prochazka, K Hamal, M Fedyszynova, U Schreiber, H Michaelis, Y Fumin, H Peicheng 236

A Compact Low Power Altimetry Laser for Lunar Applications
T Varghese, R Burnham 242

Lasercomm at Sea - Trident Warrior 06
R Burris

Kilohertz Session

Summary
G Kirchner, G Appleby 243

Portable Pico Event Timer and SLR Control (P-PET-C) System
K Hamal, I Prochazka, Y Fumin 244

Some Early Results of Kilohertz Laser Ranging at Herstmonceux
P Gibbs, C Potter, R Sherwood, M Wilkinson, D Benham, V Smith, G Appleby 250

Performance of Liquid Crystal Optical Gate for Suppressing Laser Backscatter in Monostatic Kilohertz SLR Systems
J Degnan, D Caplan 259

SLR2000: The Path toward Completion
J McGarry, T Zagwodzki 265

Determination of AJISAI Spin Parameters using Graz kHz SLR Data
G Kirchner, W Hausleitner, E Cristea 270

New Methods to Determine Gravity Probe-B Spin Parameters using Graz kHz SLR Data
G Kirchner, D Kucharski, E Cristea 276

LAGEOS-1 Spin Determination, using Comparisons between Graz kHz SLR Data and Simulations
D Kucharski, G Kirchner 285

Measuring Atmospheric Seeing with KHz SLR
G Kirchner, D Kucharski, F Koidl, J Weingrill 293

Timing Systems Session

Summary
Y Fumin 299

A032-ET Experimental Test on Changchun SLR
C Fan, X Dong, Y Zhao, X Han 300

Event Timing System for Riga SLR Station
Y Artyukh, V Bespal'ko, K Lapushka, A Rybakov 306

Instrumentation for Creating KHz SLR Timing Systems
Y Artyukh, E Boole, V Vedin 311

OCA Event Timer
E Samain, J-M Torre, D Albanese, Ph Guillemot, F Para, J Paris, I Petitbon, P Vrancken, J Weick 316

The Model A032-ET of Riga Event Timers
V Bespal'ko, E Boole, V Vedin 321

Upgrading of Integration of Time to Digit Converter on a Single FPGA
Y Zhang, P Huang, R Zhu 327

High-Speed Enhancement to HTSI Event Timer Systems
D McClure, C Steggerda, S Wetzel 331

Low-Noise Frequency Synthesis for High Accuracy Picosecond Satellite Laser Ranging Timing Systems
J Kolbl, P Sperber, G Kirchner, F Koidl 338

Multiple Wavelength and Refraction Session

Summary
E Pavlis 340

Analysis of Multi-Wavelength SLR Tracking Data Using Precise Orbits
H Mueller 341

Improvement of Current Refraction Modeling in Satellite Laser Ranging (SLR) by Ray Tracing through Meterological Data
G Hulley, E Pavlis 345

Two-Color Calibration of the Zimmerwald SLR System
W Gurtner, E Pop, J Utzinger 351

Multi Color Satellite Laser Ranging
K Hamal, I Prochazka, J Blazej, Y Fumin, H Jingfu, Z Zhongping, H Kunimori, B Greene, G Kirchner, F Koidl, S Riepfel, W Gurtner 356

Telescopes, Stations and Upgrades Session

Summary
C Smith 358

Grasse Laser Stations in Evolutions to Future and Technological Developments
F Pierron, E Samain, J-M Torre, M Pierron, M Furia et al 359

New Russian Systems for SLR, Angular Measurements and Photometry
V Burmistrov, N Parkhomenko, V Shargorodsky, V Vasiliev 365

TLRS-3 Return to Operations
H Donovan, D McCollums, D Patterson, J Horvath, M Heinick, S Wetzel, D Carter 370

Korean Plan for SLR System Development
H-C Lim, J-U Park, S-K Jeong, B-S Kim 375

Study on Servo-Control System of Astronomical Telescopes
Z Li, X Zheng, Y Xiong 378

Russian Laser Tracking Network
V Burmistrov, A Fedotov, N Parkhomenko, V Pasinkov, V Shargorodsky, V Vasiliev 381

TLRS-4 Deployment to Maui, Hawaii
S Wetzell, H Donovan, M Blount, D McCollums, C Foreman, M Heinick 384

New SLR Station Running in San Juan of Argentina
T Wang, F Qu, Y Han, W Liu, E Actis, R Podesta 390

System Improvement and GIOVE-A Observation of Changchun SLR
Y Zhao, C Fan, X Han, D Yang, N Chen, F Xue, L Geng, C Liu, J Shi, Z Zhang, B Shao, H Zhang, X Dong 399

Advanced Concepts and Time Transfer Session

Summary
H Kunimori 405

Progress on Laser Time Transfer Project
Y Fumin, H Peicheng, C Wanzhen, Z Zhongping, W Yuanming, C Juping, G Fang, Z Guangnan, L Ying, I Prochazka, K Hamal 406

T2L2 - Time Transfer by Laser Link
E Samain, Ph Guillemot, D Albanese, Ph Berio, F Deleflie, P Exertier, F Para, J Paris, I Petitbon, J-M Torre, P Vrancken, J Weick 414

New Application of KHz Laser Ranging: Time Transfer via Ajisai
T Otsubo, H Kunimori, T Gotoh 420

A Satellite Tracking Demonstration on Ground Using 100mm Aperture Optical Antenna for Space Laser Communication
H Kunimori, M Okawa, H Watanabe,Y Yasuda 425

The NASA Satellite Laser Ranging Network: Current Status and Future Plans
D Carter 430

Possibility of Laser Ranging Support for the Next-Generation Space VLBI Mission, ASTRO-G
T Otsubo, T Kubo-oka, H Saito, H Hirabayashi, T Kato, M Yoshikawa, Y Murata, Y Asaki, S Nakamura 434

Electron Multiplying CCD Camera Performance Tests
D Lewova, M Nemec, I Prochazka, K Hamal, G Kirchner, F Koidl, D Kucharski, Y Fumin 438

LIDAR Experiments at the Space Geodesy Facility, Herstmonceux, UK
G Appleby, C Potter, P Gibbs, R Jones 441

Possibility of the Near Earth Objects Distance Measurement with Laser Ranging Device
M Abele, L Osipova 444

Transponder Session

Summary
U Schreiber 450

Laser Ranging at Interplanetary Distances
G Neumann, J Cavanaugh, B Coyle, J McGarry, D Smith, X Sun, M Torrence, T Zagwodski, M Zuber 451

Simulating Interplanetary Transponder and Laser Communications Experiments via Dual Station Ranging to SLR Satellites
J Degnan 457

Laser Ranging at Planetary Distances from SLR2000
J McGarry, T Zagwodzki, P Dabney, P Dunn, J Cheek 463

Laser Ranging to the Lunar Reconnaissance Orbiter (LRO)
D Smith, M Zuber, M Torrence, J McGarry, M Pearlman 468

Un-cooperative Targets Session

Summary
C Smith 472

The Experimental Laser Ranging System for Space Debris at Shanghai
Y Fumin, C Wanzhen, Z Zhongping, C Juping, W Yuanming, K Hamal, I Prochazka 473

Simultaneous Optical and Laser Space Objects Tracking
M Nemec, I Prochazka, K Hamal, G Kirchner, F Koidl, W Voller 479

Software and Automation Session

Summary
W Gurtner, J McGarry 485

A Comparison of Performance Statistics for Manual and Automated Operations at Mt. Stromlo
C Moore 486

EOS Software Systems for Satellite Laser Ranging and General Astronomical Observatory Applications
M Pearson 490

Electro-Control System of San Juan SLR Station
P Wang, T Guo, X Li, Y Han, W Liu, T Wang, F Qu, Y Tan, T Zou 495

Integrated Upgrades of Control System for TROS
L Xin, G Tangyong, A Tong, W Peiyuan, T Yechun, X Jiening, Z Yunyao D Ruilin 498

CCD and SLR Dual-use of the Zimmerwald Tracking System
W Gurtner, M Ploner 500

Automated Transmitter Beam Size and Divergence Control in the SLR2000 System
J Degnan, G Jodor, H Bourges 507

Obtaining the High-resolution Epoch with the FPGA Technology
Q Li, F Qu, Z Wei 513

New FTLRS Software Tools for Tuning Observations Schedule and Remote Control
M Pierron et al 516

Recursive Filter Algorithm for Noise Reduction in SLR
M Heiner, U Schreiber, N Brandl 520

The Impact and Resolution of "Collision Bands" on Tracking Targets at Various Ranges
C Moore 526

Web Application for the Engineering Data Files Processing
K Salminsh 532

Consolidated Laser Prediction and Data Formats: Supporting New Technology
R Ricklefs 535

Lunar Laser Ranging Session

Summary
T Murphy 539

APOLLO Springs to Life: One-millimeter Lunar Laser Ranging
T Murphy, E Adelberger, J Battat, C Hoyle, E Michelsen, C Stubbs, H Swanson 540

Targets and Return Signal Strength Session

Summary
T Murphy 546

Retroreflector Studies
D Arnold 547

The INFN-LNF Space Climatic Facility for LARES and ETRUSCO
D Arnold, G Bellettini, A Cantone, I Ciufolini, D Currie, S Dell'Agnello, G Delle-Monache, M Franceschi, M Garattini, N Intaglietta, A Lucantoni, T Napolitano, A Paolozzi, E Pavlis, R Tauraso, R Vittori 550

Absolute Calibration of LLR Signal: Reflector Health Status
T Murphy, E Adelberger, J Battat, C Hoyle, E Michelsen, C Stubbs, H Swanson 556

Experimental Return Strengths from Optus-B and GPS
J Luck, C Moore 562

Spherical Glass Target Microsatellite
V Shargorodsky, V Vasiliev, M Belov, I Gashkin, N Parkhomenko 566

Overflow Session

Summary
M Pearlman 571

Current Status of "Simeiz-1873" Station
A Dmytrotsa, O Minin, D Neyachenko 572

Overview and Performance of the Ukrainian SLR station "Lviv-1831"
K Martynyuk-Lototsky, J Blahodyr, A Bilinskiy, O Lohvynenko 575

Results of the TLRS-4/Moblas-7 Intercomparison Test
J Horvath, M Blount, C Clarke, H Donovan, C Foreman, M Heinick, A Mann, D Patterson, D McCollums, T Oldham, S Wetzel, D Carter 576

The Accuracy Verification for GPS Receiver of ALOS by SLR
N Kudo, S Nakamura, R Nakamura 582

Fulfillment of SLR Daylight Tracking of Changchun Station
Y Zhao, X Han, C Fan, T Dai 587

GLONASS Status Update and MCC Activity in GLONASS Program
V Glotov, S Revnivykh, V Mitrikas 593

PARTICIPANTS

Attendees 597

Group Photo 19 October 2006 600

TIMING SYSTEMS SESSION SUMMARY

Chair: Yang Fumin

More Event Timers are available, for 2 KHz and even higher repetition rates:

- A032-ET from Latvia, precision 10 ps, 10 KHz
- P-PET-C from Prague, Czech Republic, precision 2.5 ps, 2 KHz
- T2L2 ET from OCA, France, precision 2 ps, ~2 KHz
- ET from HTSI, USA, precision 2 ps, ~50 KHz

With much improved linearity and thermal drift.

Question: Are the prices for these ETs available?

Y. Zhang from Shanghai showed in a poster that only one FPGA chip can work as a timer for future space applications or other compact systems.

A032-ET Experimental Test on Changchun SLR

FAN Cunbo[1], DONG Xue[1,2], ZHAO You[1], HAN Xinwei[1]

1. National Astronomical Observatories/Changchun Observatory, CAS
2. Graduate University of Chinese Academy of Sciences (CAS), Beijing

Abstract

This paper introduces the experimental test of A032 Event Timer on Changchun SLR. First, the pulse delay generator DG535 is used to generate two path signals to simulate the start and stop signal, and the A032-ET to measure the intervals. Then, it also gives out the system hardware connection diagram, analyzes signal time sequence and shows the software flow chart. Finally it shows the results of ranging the ground target and the satellites.

Key Words: Event Timer, A032-ET, Satellite Laser Ranging (SLR), Simulation

Introduction

Satellite Laser Ranging (SLR) is the most accurate satellite tracking technique available with single shot positional accuracy under a centimeter and normal point corrected data able to claim precision of just a few millimeters. The SLR tracking method requires a pulsed laser source and a telescope which is used to collect the reflected laser light on its return. The laser provides a detectable link between a fixed station and a distant satellite moving in the space. The telescope and associated equipment determine a very precise location and velocity for both the satellite and station from the data provided by the laser beam. Time interval from station to the satellite and back can be calculated by counters, which is transferred into the range we want.

The SLR data are used to improve the orbital predictions for the tracked satellites which, in turn, make the satellites easier to track. In other words, the more data we get the better precision of orbit prediction we can calculate. Increasing the firing frequency is a convenient way to increase data, and there are many stations around the world trying to do KHz SLR system. SLR, in essence, is a method of satellite tracking. The key equipment for increasing the firing frequency are the counter and laser source. But now the KHz laser source is available in the world. And here we put the emphasis on the counter. There are two kinds of counters: the Time Interval counter and the Event Timer counter. The interval counter measures the time the laser flight from the station to satellite and back. HP5370 and SR620 are the most popular used interval timers in the global SLR society. The Event Timer records the epochs of signals received by both channel A (start) and B (stop) and puts them into buffer. Then the epochs are matched by range gate prediction. Event Timer calculates intervals with epochs, and in theory, with no rate limits but reading and processing data.

While using Event Timer, sending range gate is the most important technical difficulty, and the match of start and stop signals is also very important. Many stations in the world are adopting Event Timer as counter to advance their systems. PET4 has been used in Wettzell station, which is assembled by Dassualt model; P-PET 2000 begun to work in San Fernando in 2004, and Graz station have already completed KHz system; the KHz system in Herstmonceux is on developing stage, and almost finished. A032-ET developed by Latvia University using EET method also fits for KHz system in theory.

Status In Changchun

There are two interval counters in Changchun station: HP5370B is used routinely and SR620 as a standby. The observation in Changchun is excellent these years and the system is steady. The single shot precision is less than 2cm, and the passes observed every year are more than 4,000. However, the laser fire frequency is not very high: 8Hz for low orbit satellites and 5 Hz or 4Hz for high orbit satellites. We plan to use the Event Timer to increase firing frequency to 10Hz and even higher so as to increase the quantity of data. After analyzing all Event Timers, the A032-ET was chosen for Changchun experiment, and the purpose is to increase the firing frequency for all satellites to 10Hz, and even higher. As an Event Timer, A032-ET is superior to interval counter; some specifications are shown in Table 1.

Table 1: *A032-ET specifications*

Single shot RMS		<10 ps
Dead time		60 ns
Nor-linearity error		< 1 ps
Offset temperature stability		<0.1 ps
FIFO depth		1,200
Measurement rate	Option 1	Up to 10KHz continually
	Option 2	Up to 500Hz cycle repetition rate

Figure 1. *Hardware of A032-ET*

There are two currently available options of the A032-ET, which use the same specialized hardware (Figure 1 shows the hardware of A032-ET) but differ by the software. These options provide alternatively two basic kinds of measurement: The option A032.1 provides continuous (gapless) measurement of events at high (up to 10 KHZ) mean measurement rate. It is well suitable to measure the overlapped time intervals between Start and Stop events that come at the separate inputs (either A or B) of the Event Timer in any order. Specifically this is the case of advanced SLR at KHz repetition rate. The option A032.2 provides cyclical measurement of events that come at the separate inputs of the ET-device in the strict order. Specifically this is the case of conventional SLR where the measured Start-Stop time intervals do not exceed the repetition period of Start events. Considering our purpose, we choose A032.1 option to do the experiment, and the range gate has to be redesigned to fit for the new counter.

Experiment test and real observation on Changchun SLR

Before experiment we redesign the range gate control circuit, and the scheme is represented in Figure 2.

Range gate control circuit is assembled by three circuits, which are designed by the same module. The three circuits generate gate signal circularly and then are imported into an OR gate. Finally, the RG_out is transmitted as the range gate we want.

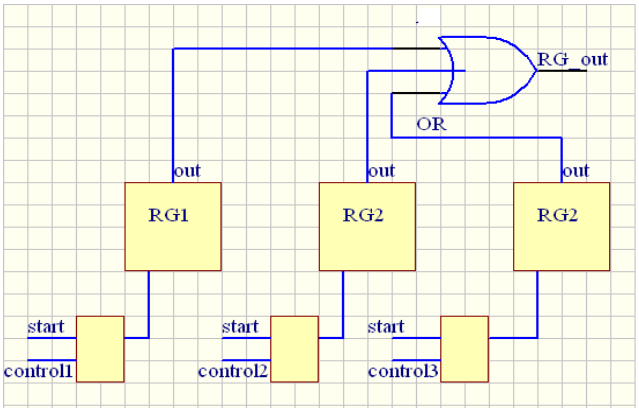

Figure 2. *Range gate control circuit*

Simulation

In this simulation, we use pulse generator DG535 as a signal source. It generates two NIM signals, and the interval was measured by A032-ET. The rate is set to 10Hz for the purpose is increasing the frequency to 10Hz. The interval sent by DG535 is static and the trigger is interior. The hardware connection scheme is shown in Figure 3, and the software flow chart is showed in Figure 4. All through the test, A032-ET worked normally, it measured the interval with the precision of ps under the condition of 10Hz

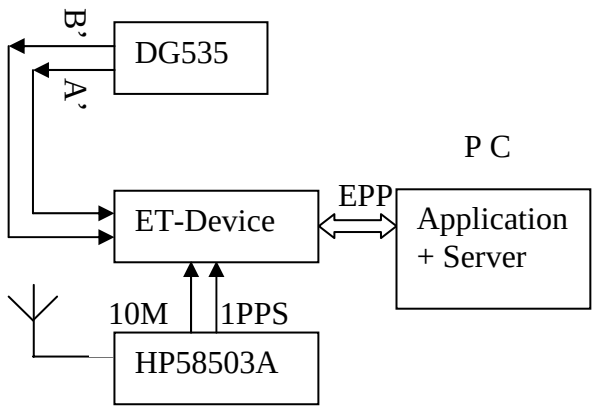

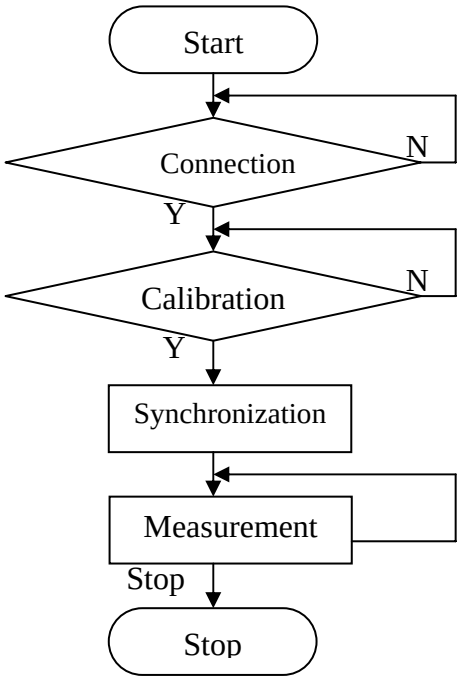

Figure 3. *Simulation scheme*

Figure 4. *Software flow chart*

Range gate measurement

Range gate is measured with A032-ET to find out the matching of start and stop signals. In this experiment, the start pulse is generated by DG535, which is triggered by laser firing, and output of the range gate is used as the stop pulse. Range gate measurement is to simulate observation condition and make some improvement for the software. The main function written in VC++ language is compiled as Dynamic Link Library. The data received by A032-ET is transferred into control software written in VB for

calculating the time interval. The data transferred into VB with the form of an array included time-tags that the events happened in channel A, B. The time-tags are matched well with range gate prediction.

Real Observations

The firing frequency is increased to 10Hz for all satellites and A032-ET is used as a new timer to calculate the time interval instead. The hardware connection scheme is presented in Figure 5. The main pulse is imported into channel A as start signal and the return pulse as stop signal. A032-ET could distinguish only NIM pulses; the 10MHz and 1pps signals are given by GPS HP58503A. Figure 6 shows the time sequence of Changchun SLR system. In the scheme, T1 and T4 is laser fire time, T2 is the epoch time of the main pulse, and T3 is the epoch time of the return pulse.

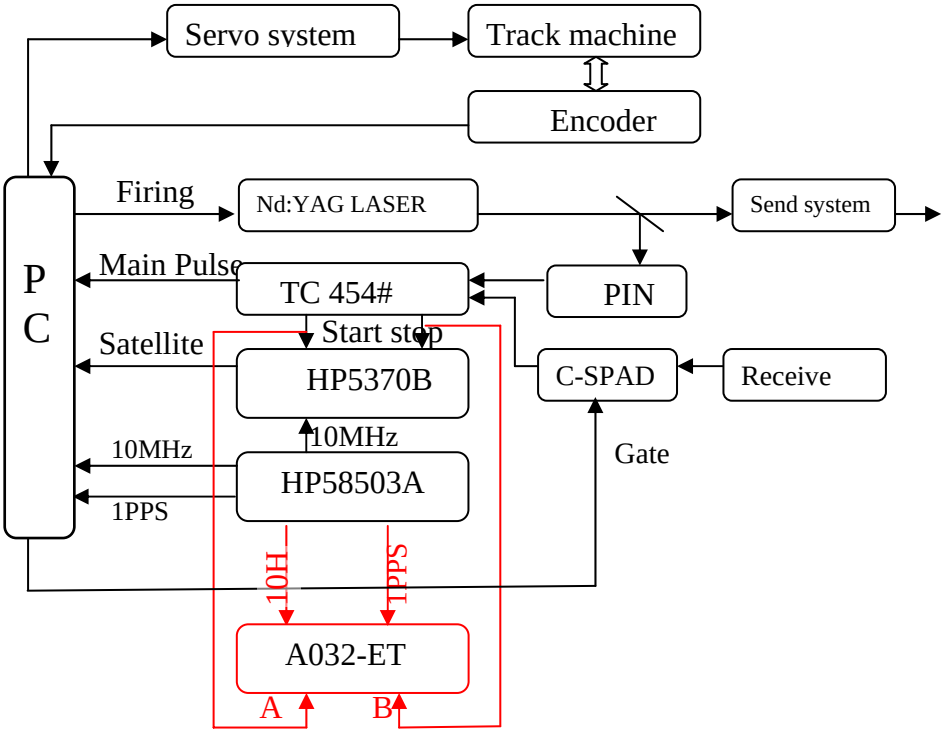

Figure 5. *Hardware connection*

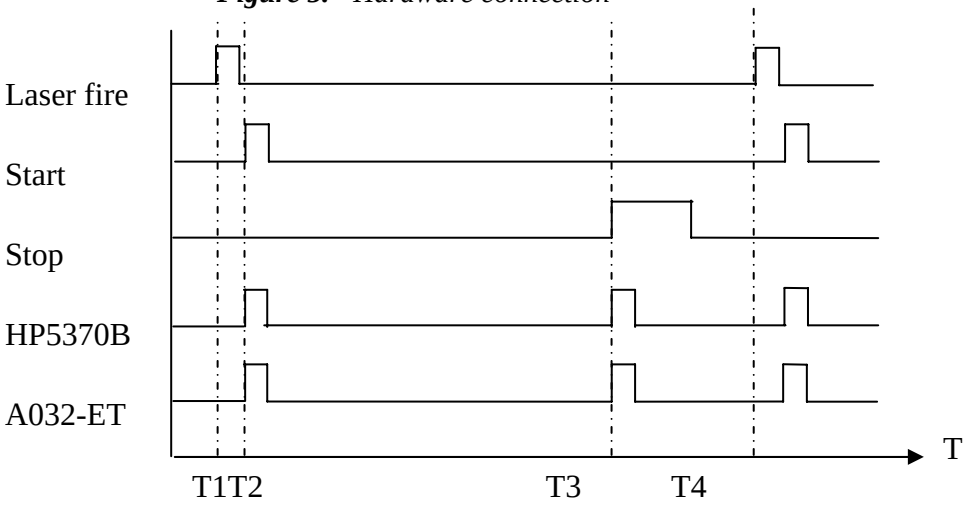

Figure 6. *Time sequence of Changchun SLR system*

Figure 7 shows the Etalon-2 measurement interface. The firing rate is 10Hz. From this picture, the return signal line can be clearly seen. From the satellite observation, we can see that the system works very well with A032-ET under the condition of 10Hz firing frequency. The return signal rate of high orbit satellites is increased.

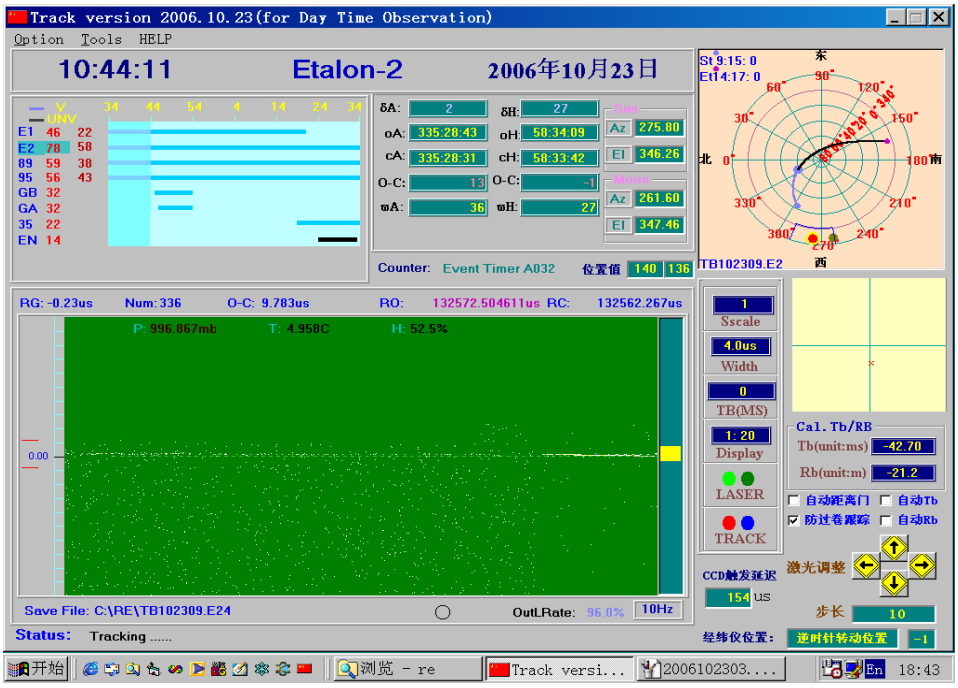

Figure 7. *Etalon-2 measurement interface*

Conclusion

From analysis report such as Toshi's report, we can see A032-ET works well as Event Timer. The precision is 1cm more or less. It could be used in SLR system normally. Because the laser pulse is about 200ps in Changchun station, the precision of the whole system does not increase obviously after the event timer is used. Since Oct.23 of 2006, A032-ET has been used in the satellite laser ranging routinely for the all satellites tracked with the firing frequency of 10Hz in Changchun station. Table 2 shows the data quantity from 2006-10-23 to 2006-12-31. There are too many passes. Now, it works very well and the experiment is very successful. Next, we plan to increase to KHz observation if the laser source is available.

Table 2: *Data of Changchun SLR Station (2006-10-23 to 2006-12-31)*

Site Information		Data Volume			
Column 1	2	3	4	5	6
Location	Station Number	LEO pass Tot	LAGEOS pass Tot	High pass Tot	Total passes
Changchun	7237	1095	153	209	1457

Acknowledgement

The authors would like to thank SHI Jianyong and ZHANG Haitao who partially participate in the work. And also express their appreciation to Prof. Yu. Artyukh and his colleague Eugene Buls of University of Latvia for their technical supports.

The authors gratefully acknowledge the support of K.C.Wong Education Foundation, Hong Kong.

References

[1] Yu. Artyukh: "Selective Time Interval Counter for SLR Applications", Proc. of 11th International Workshop on Laser Ranging, Deggendort, Germany, 1998.

[2] Yang, F.M.: "Current status and future plans for the Chinese Satellite Laser Ranging Network", Surv. Geophys. 22 (6): 465-471 2001.

[3] P. Gibbs: "Comparisons of a single SR620 timer against a variety of timers from the Eurolas network", Proceedings of 13th International Workshop on Laser Ranging, Washington D.C. 2002.

[4] P. Gibbs: "Inter-comparison of Various Timing Devices Against a Single SR Timer", Proceedings of 13th International Laser Ranging Workshop, Washington D.C., USA. 2002.

[5] Yu. Artyukh, V. Bespal: "A New Line of Timing Systems for Satellite Laser Ranging", Proceeding of the 8th Biennial Electronics Conference, Tallinnl, Estonia, 2002, pp. 239-240.

[6] Yu. Artyukh, V. Bespal: "A010 Family of Time Interval Counter Adapted to SLR Application", Proceedings of the 13th International Laser Ranging Workshop, Washington D.C. 2002.

[7] Liu Chengzhi, Zhao You, Fan Cunbo, etc.: "The Performance of Changchun Satellite Laser Ranging Station", Proceeding of 14th International Laser Ranging Workshop, San Fernando, Spain, 2004, pp. 175-177.

[8] Yu. Artyukh, V. Bespal: "A Version of the A032-ET Event Timer for KHz SLR", Proceedings of KHz SLR Meeting, Graz, Austria, 2004.

[9] C. Selke, F. Koidl, G. Kirchner: "Tests of the Stability and Linearity of the A032ET Event Timer at Graz Station", Proceeding of 14th International Laser Ranging Workshop, San Fernando, Spain, 2004, pp. 337-341.

[10] G. Kirchner, 2004, SLR Graz: The RGG (Range Gate Generator), Proceedings of KHz SLR Meeting, Graz, Austria.

[11] G. Appleby, P. Gibbs: "SGF Herstmonseux: Current Status and Future Upgrades", Proceeding of 14th International Laser Ranging Workshop, San Fernando, Spain, 2004, pp. 213-216.

[12] K. Hamal, I. Prochazka: "Portable Pico Event Timer 2 KHz", Proceeding of 14th International Laser Ranging Workshop, San Fernando, Spain, 2004, pp. 333-335.

[13] G. Kirchner, F. Koidl: "Graz KHz SLR System: Design, Experiences and Results", Proceeding of 14th International Laser Ranging Workshop, San Fernando, Spain, 2004, pp. 501-505.

[14] G. Kirchner: "Riga A032-ET in Graz", ILRS 2005 Workshop, Eastbourne, England, 2005.

Event Timing System for Riga SLR Station

Yu. Artyukh[1], V. Bespal'ko[1], K. Lapushka[2], A. Rybakov[1]

1. Institute of Electronics and Computer Science, Riga, Latvia.
2. Astronomical Institute of University of Latvia, Riga, Latvia.

Contact: artyukh@edi.lv, riglas@lanet.lv

Abstract

The new Riga Event Timing System (RTS) is designed and built in 2006 for SLR station Riga-1884 to improve its measurement equipment in precision, functionality and reliability of operation. The RTS is a multimode instrument for satellite ranging at 10 Hz repetition rate with parallel measurement of PMT-pulse amplitudes for the range bias correction. The RTS can support millimetre accuracy of SLR although the overall system accuracy is limited by the other equipment of Riga SLR station. As compared to the previous version of Riga timing system, the RTS offers considerably better performance and functionality and provides a good basis for further improving the Riga SLR station as a whole.

Introduction

The Riga Event Timing System (RTS) is designed and built in 2006 for Riga SLR station to upgrade its measurement equipment. The RTS maintains the basic functional possibilities of the previous Riga timing system but is advanced in many essential respects. Specifically, the RTS is based on employment of the latest Riga Event Timer A032-ET [1]. As compared to the previously used instrument, the A032-ET provides much better single-shot resolution (8 ps RMS instead of the previous 25 ps) and much smaller “dead time” (60 ns instead of the previous 400 ns).

A new hardware design is made to integrate the most of specialized hardware means within a single stand-alone device. There are new functional possibilities of digital signal processing and system control that have to increase the SLR efficiency. Some optional functional capabilities are added for experimental investigations with the aim to improve the performance of Riga station as a whole.

A special feature of the RTS is that it provides pre-processing of STOP pulses coming from either traditional single or special doubled receiver based on Photo Multiplier Tubes (PMT). The doubled receiver generates the pulses overlapping only when the true STOP pulse is being received [2]. It makes possible to reduce the noise influence when the satellite ranging is performed by day. Like the previous Riga timing system, the RTS performs PMT pulse amplitude measurement to correct the range bias [3].

Principles of operation

The RTS supports the following operational modes:

- SLR system calibration in the range from 9 to 375 m with parallel measurement of STOP-pulse amplitudes;
- Satellite ranging to 25,500 km at 10 Hz repetition rate with parallel measurement of STOP-pulse amplitudes;
- Integrated mode when the SLR system calibration and satellite ranging are performed simultaneously (for optional use);
- Measurement of pulse noises.

Structurally the RTS combines the RTS hardware and a PC with the RTS software (Fig.1).

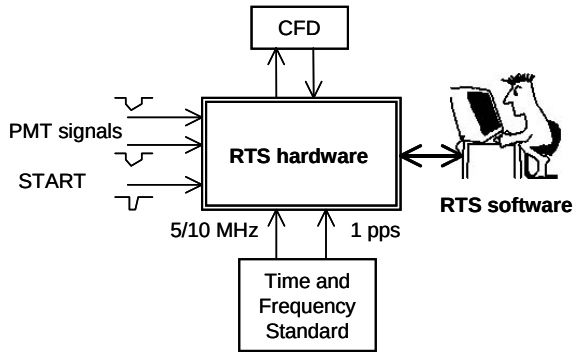

Figure 1. *RTS architecture*

Additionally the RTS includes two commonly used external devices: Time and Frequency Standard and Constant Fraction Discriminator (CFD).

The RTS hardware

The RTS hardware contains three functional units: Signal Processing block, Event Timer Block and Master Clock; each implemented as a separate board. These boards and their power supply are housed in 19'' 2U rack module (Fig.2).

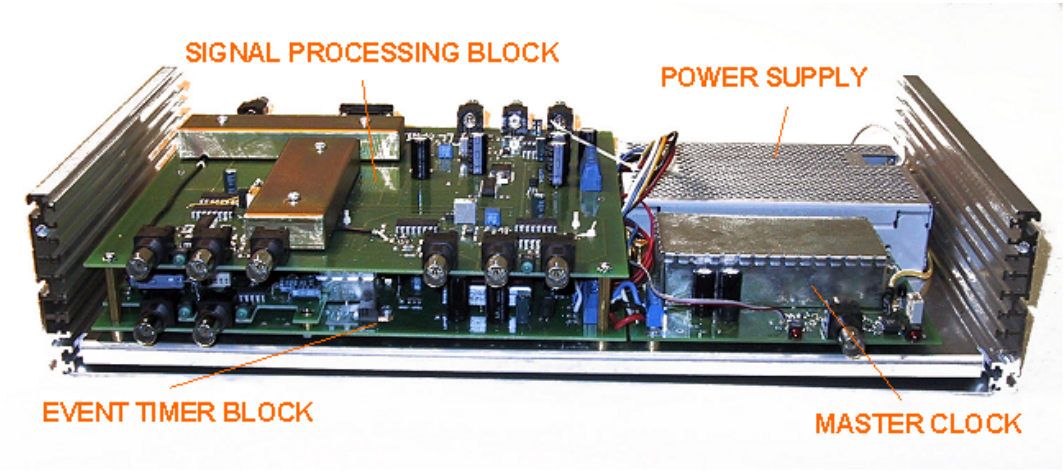

Figure 2. *RTS hardware assembly*

The Signal Processing Block receives the PMT pulses (3 to 7 ns width range; -0.1 to -3.0 V amplitude range) and, in interaction with the CFD, produces normalised NIM pulses for the Event Timer Block. The Event Timer Block measures time instants of these pulses and START pulses coming. Then the measurement results come to PC for further data processing, displaying and memorizing. The Master Clock represents a voltage-controlled crystal oscillator disciplined by an external high-stable 5 or 10 MHz reference frequency using PLL circuit. It generates a low-jittered 100 MHz clock signal required for precise event measurement and synchronization of Signal Processing Block operation as a whole.

Signal Processing Block

The Signal Processing Block performs a few basic operations with PMT pulses before their measurement by the Event Timer Block (Fig.3).

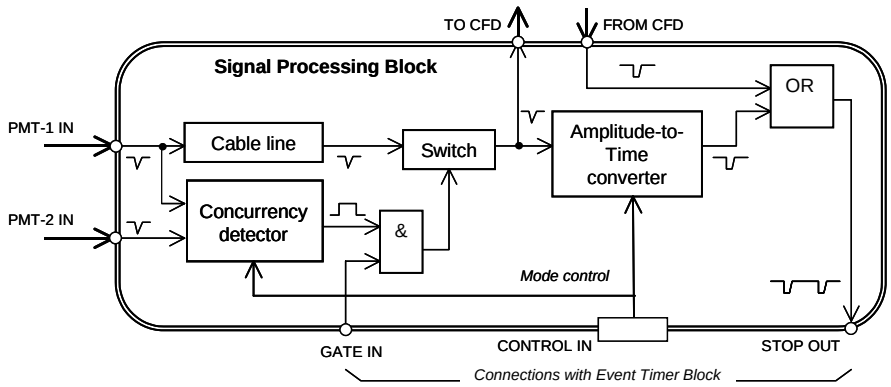

Figure 3. *Functional diagram of the Signal Processing Block*

At first it selects PMT pulses which probably conform only to the returned laser pulses. To do that either single ("PMT-1 IN") input or two ("PMT-1 IN" and "PMT-2 IN") inputs for PMT pulses can be used. In the last case it is supposed that the PMT pulses overlap only when the true return is being received. In the case of concurrency of these pulses one of them ("PMT-1") is selected using the wideband switch. Such selection acts together with the online programmable gating provided by the Event Timer Block.

The selected pulses from the switch output come to the CFD. The CFD generates normalized NIM pulse in response to each input PMT pulse. This NIM pulse comes to the input "FROM CFD" of the Signal Processing Block. However the CFD cannot fully avoid the time-uncertainty of PMT pulse coming. For this reason the amplitude of each PMT pulses is additionally measured as the amplitude values are related to the range bias. To do that, the Amplitude-to-Time converter generates the NIM pulse in response to the same PMT pulse with some delay proportional to the PMT pulse amplitude. In this way every selected PMT pulse is being converted into two NIM pulses where the first one represents directly the returned signal and time interval from the first pulse to the second one reflects its amplitude (Fig.4). Resolution of such amplitude measurement is about 9 bits.

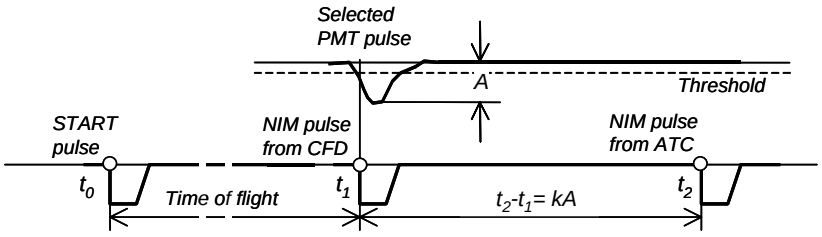

Figure 4. *Time diagram illustrating PMT pulse amplitude conversion*

Then the Event Timer Block measures time instants of these pulses and START pulse coming at each ranging cycle so as to give out complete data for further satellite ranging. As shown in [3], the mentioned technique of PMT signal amplitude measurement makes it possible to effectively correct the range bias caused by the PMT features.

Event Timer Block

The Event Timer Block precisely measures the instants at which input events occur. Every event is associated with certain fixed point on the leading edge of input NIM pulses. Used method of event timing is untraditional in many respects. Specifically, it

supports not only high precision but high speed as well. Using 100 MHz internal clocks this method provides each single measurement with 7-8 ps RMS resolution during 60 ns only.

The event measurement is performed in two stages. At first, the Event Timer Block transforms every input event into single 80-bit timing data block (subsequently referred to as TD-block) and sequentially accumulates them in a FIFO memory. Each TD-block contains the counting data (39 bits; 10 ns resolution) and interpolating data (40 bits), as well as one-bit mark specifying the kind of measured event (either Start or Stop). The interpolating data are presented initially in an intermediate redundant form.

At the next stage the PC takes out TD-blocks from the FIFO memory and processes them to obtain the corresponding epoch time-tags in a unified form. Further these time-tags are additionally processed to display the ranging results in real time. To achieve the best precision, processing of TD-blocks takes into account the actual physical characteristics of time interpolation under actual operating conditions; these characteristics are defined through so called scaling (hardware calibration) before the measurement.

The Event Timer Block is flexibly controllable and allows writing TD-blocks in the FIFO memory and reading them by the PC in different order. Specifically, the RTS provides cyclical measurement of events. In the beginning of each cycle the RTS measures a single Start-event, and only then - a number of Stop-events. According to the modes of RTS operation, the Event Timer Block measures up to 3 events in the System calibration and Satellite ranging modes, up to 5 events in the “Integrated mode” and up to 10000 events when pulse noise is measured. In all cases the Event Timer Block at first accumulates TD-blocks in the FIFO memory during some defined waiting period, starting from Start-event registration. During this time the PC processes TD-blocks that have been read out from the Event Timer Block in the previous cycle. Then the PC stops the event registration, reads the currently accumulated TD-blocks and allows starting the next similar cycle. The waiting period is strictly adapted to the repetition rate (10 Hz) of RTS operation. Optionally the RTS can provide the repetition rate up to 30 Hz.

In addition to the event measurement the Event Timer Block generates NIM pulses, which come to the input “GATE IN” of the Signal Processing Block to provide online programmable PMT pulse gating.

The RTS software

The RTS software performs real-time procedures which depend on the selected operating mode, current user control, etc. There are also various auxiliary procedures to prepare the system to operation (clock synchronization, calibration of measurement hardware, system checking, etc). For example, in the conventional Satellite ranging mode the RTS software performs in real time the following procedures:

- periodically checks the RTS hardware to detect the START pulse coming;
- when the START pulse is detected, triggers the internal time-out and begins processing of the previously taken data;
- when the time-out is finished, stops the measurement, reads the data from the RTS hardware, writes to it a new data concerning the STOP pulse gating and makes next cycle available.

Correspondingly the data processing performed during the time-out includes:

- conversion of TD-blocks to the unified form of epoch time-tags;

- calculation of the gate delay and residual, time interval reflected the STOP pulse amplitude and new data concerning the STOP pulse gating in the next cycle;
- displaying (Fig.5) and memorizing the measurement results.

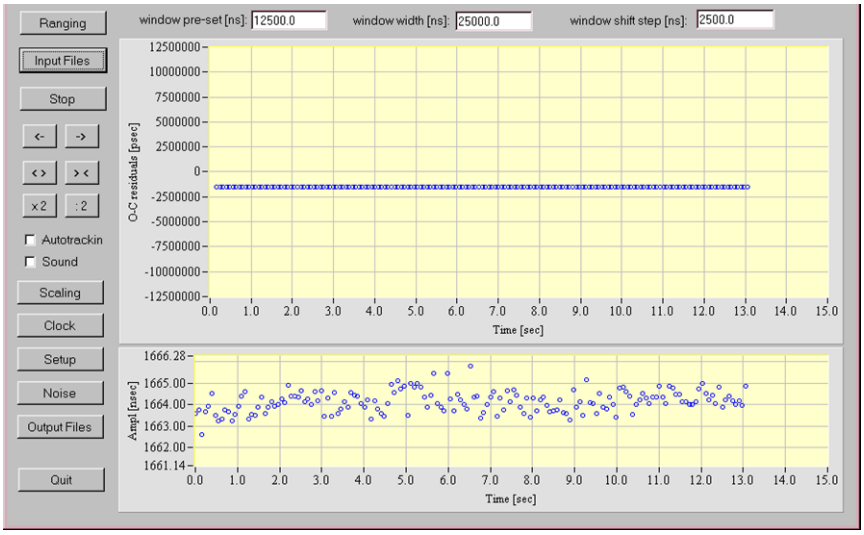

Figure 5. *Example of displaying the measurement results. Upper plot shows residuals; bottom plot indicates amplitudes of PMT pulses*

The RTS software offers optionally an autotracking of satellite in range after its initial acquisition. When the autotracking is on, possible trend of the residuals is actually excluded due to the automatic gate delay correction. Algorithm of the autotracking is based on median selection of current residuals to exclude their possible abnormal values, and continuous generation of a special piecewise-linear function for gate delay correction. Every piece of this function is being determined using regression analysis of the current fraction of residuals. In this case the gate delay correction is performed at 1 Hz rate approx., allowing considerable errors in initial predetermination of the function “RANGE vs. START TIME”.

The RTS software is written in *C* language for LabWindows/CVI ver.6.0 and works under Windows XP.

Conclusion

As compared to the previous version of Riga timing system, the RTS offers considerably better performance in terms of accuracy, functionality, and reliability in operation. This provides a good basis for further advancing the Riga SLR Station as a whole. In 2006 the RTS was involved in trial operation; the first series of successful SLR results has been obtained.

Reference

[1] V. Bespalko, E. Boole, V. Vedin. The Model A032-ET of Riga Event Timers. Proceedings of the 15th International Workshop on Laser Ranging, Canberra Australia, October 16-20, 2006.

[2] ILRS 2003-2004 Annual Report, p. B-38.

[3] Yu. Artyukh, V. Bespalko, K. Lapushka, A. Rybakov. PMT signals caused range-bias correction at the SLR Station Riga-1884. Proceedings of the 12th International Workshop on Laser Ranging. Matera, Italy, November 13-17, 2000.

Instrumentation for Creating KHz SLR Timing Systems

Yu. Artyukh, E. Boole, V. Vedin

1. Institute of Electronics and Computer Science, Riga, LATVIA.

Contact: artyukh@edi.lv

Abstract

The instrumentation provides basic tools for creating SLR timing systems operating at repetition rate up to a few KHz. There is a test setup to simulate the process of ranging to various satellites and to evaluate capabilities of this instrumentation for the KHz system design. The simulation of the CHAMP laser ranging at 2 KHz repetition rate is considered as an example. Test results show that the proposed instrumentation offers sufficient performance to be used in the KHz SLR systems.

Timing system architecture

As known, increasing the SLR repetition rate up to KHz provides a variety of essential benefits. Currently there are a few SLR stations which already use this technique or will have it in the near future. However KHz SLR usually need essential upgrading of SLR equipment, including the timing system for satellite range measurement. In view of that we propose an instrumental basis to create various KHz SLR timing systems adapted to the specific user requirements.

There is the well-known custom timing system for KHz SLR at Graz SLR station [1]. In general terms, architecture of timing systems based on the proposed instrumentation and principles of their operation are similar. But there are distinctions in some essential details. Specifically, in our case the specialized hardware is offered as two compatible stand-alone devices (Event Timer A032-ET and Range Gate Generator). PC interacts with these devices and coordinates their operation via standard parallel ports working in the EPP (Enhanced Parallel Port) mode (Fig.1).

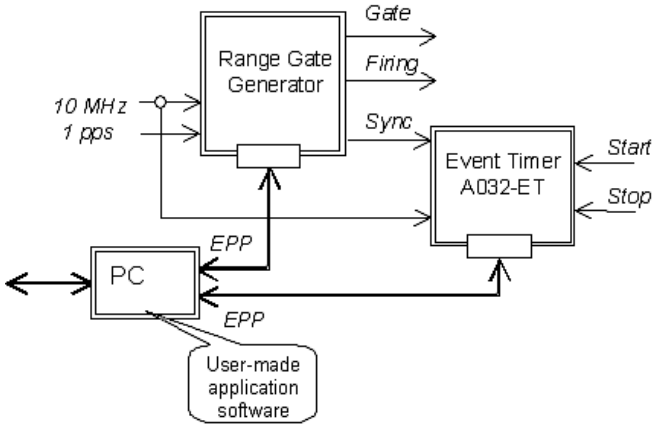

Figure 1. *Timing system architecture*

As for the application software, it should be custom-made according to the specific application requirements with the reference to the sample program (source code written in *C*). This program defines device-specific software functions which can be directly built in the user software to support the interactions with hardware. In this way the instrumentation can be used as a basis for various timing system designs.

System hardware

Event Timer

The basic system hardware component is Riga Event Timer A032-ET. It offers two independent inputs for *Start* and *Stop* measurement with RMS resolution about 7-8 ps. Distinctive feature of this device is exceptionally small "dead time" (60 ns) due to the advanced interpolating technique of event timing. This allows sequential measurement of *Start* and *Stop* using simple single-channel hardware structure (Fig.2). Note that such solution simplifies the timer's implementation and makes it relatively inexpensive.

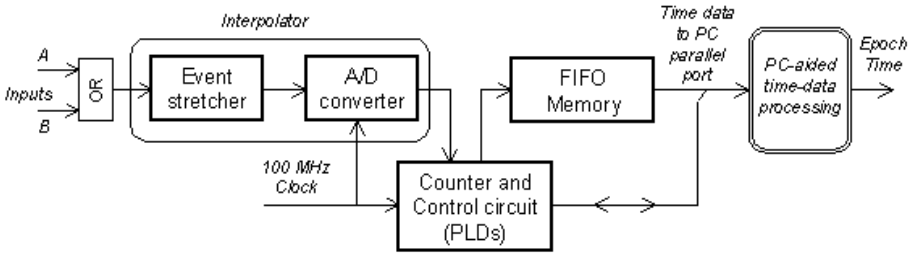

Figure 2. *Schematic block diagram of the Event Timer*

Although small "dead time" allows the burst rate of event timing up to 17 MHz (for up to 12K sequential events), the average rate is limited down to 10-15 KHz by the available speed of data transfer to PC. However it seems that this rate is quite enough for KHz SLR. In more details the A032-ET features are described in [2].

Range Gate Generator

The Range Gate Generator (RGG) is based on the well-known scheme of Digit-to-Event conversion (Fig.3). Continuous counting of 100 MHz clock pulses forms the 25-bit time-scale with 335 ms periodicity. Such periodicity directly conforms to the maximum value of range gate delay.

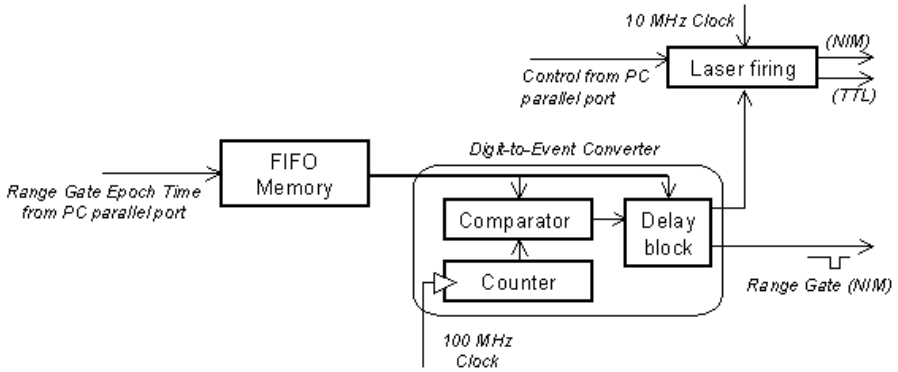

Figure 3. *Schematic block diagram of the Range Gate Generator*

Dual-ported FIFO memory receives the time data (Range Gate Epoch Time) from PC. In this case the data writing to this memory and data reading from it are independent asynchronous processes. Digital comparator compares the data from the FIFO memory with the current state of time-scale, providing the range gate generation with 10 ns resolution. Additional 7-bit controlled delay block (based on MC100EP196 delay chip) increases resolution up to 80 ps. However there is noticeable differential non-linearity for this chip, resulting in a noise-like error of range gate generation (80 ps RMS approx.). Most of the RGG digital functions are implemented on CPLD basis.

An important feature of the RGG is a specific firing generation. As known, the range measurement can be corrupted when a transmitted laser pulse is close to the received one. To avoid such problems each firing is generated so that it never can occur within some protected zone around any gate being generated (Fig.4).

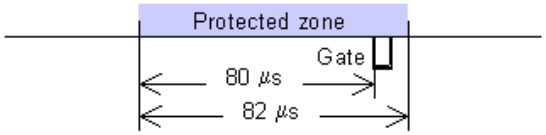

Figure 4. *Zone protected from firing*

To provide such condition, initially specified period of firings may sometimes be automatically (without any pre-calculations) incremented by quarter of its value. The nominal value of firing period can be set in the range from 100 μs to 167 ms with 0.64 μs resolution. In other words, the timing system is able to operate in a wide range of repetition rate, starting from 6 Hz.

Generally the RGG has been designed not only for KHz SLR applications. For this reason it also provides some additional features that are beyond of the direct KHz SLR needs. Specifically, it offers FIFO memory depth up to 16,000 data blocks defining the epoch times, cyclical offline operation, has two selectable outputs for two-channel event generation, etc. These features may be useful for other applications such as tests of timing devices.

General performance limitation

In the process of *Stop* gating each *Start* brings about corresponding control data at the RGG interface with some delay called “response time”. The response time is a system parameter that defines both the SLR maximum repetition rate and allowable minimum of satellite range.

There are three main components of the response time: time of data reading from the Event Timer, time of data processing and time of data writing to RGG. Usually it is desirable to dedicate the maximum time for real-time data processing. Correspondingly the total time of data reading (10 Bytes) and data writing (5 Bytes) via PC parallel ports (see Fig.1) has to be reduced as far as possible. Although formally the EPP should provide the data transfer rate up to 1-2 MB/s, actually it considerably depends on the PC operating system and its configuration. Specifically, our experiments with different MS-Windows operating systems showed that the total time of data reading/writing on average varies from 25 μs (for Windows-98) to 150 μs (for Windows XP). Furthermore, this time is not stable, resulting in significant variation of the response time from cycle to cycle. Unfortunately it was not possible to check other operating systems that could be better suited for real-time operation.

Experimental evaluation of system potentialities

To evaluate the potential of the proposed instrumentation a test setup has been used. This test setup has a structure which is similar to that shown in Fig.1. In this case each firing simulates *Start* and each generated gate simulates *Stop* for the Event Timer. Correspondingly a test program simulates application software. The test program performs the simplest real-time data processing related mainly to the Range Gate Epoch Time calculation and memorizing of the measurement results (no time-consuming operations such as real-time data displaying). Evaluation of the

measurement results is performed offline. The test program works under Windows XP. In this case the average response time was about 250 μs and its maximum value - about 1 ms. Most of the response time was consumed for the data reading/writing. These timing conditions correspond to the possibility of satellite ranging from 1 ms at repetition rate up to 4 KHz.

Other experiments were related to simulations of LEO satellites laser ranging as this represents a worst case for the timing system operation in possible real applications (the higher orbit, the less problems with the response time limitations). Specifically, the simulation of the CHAMP laser ranging at 2 KHz repetition rate was performed (Fig.5). There are 550,000 sequential readings obtained continuously during 275 seconds of the CHAMP pass simulation. The satellite range is from 2.45 ms up to 7.48 ms.

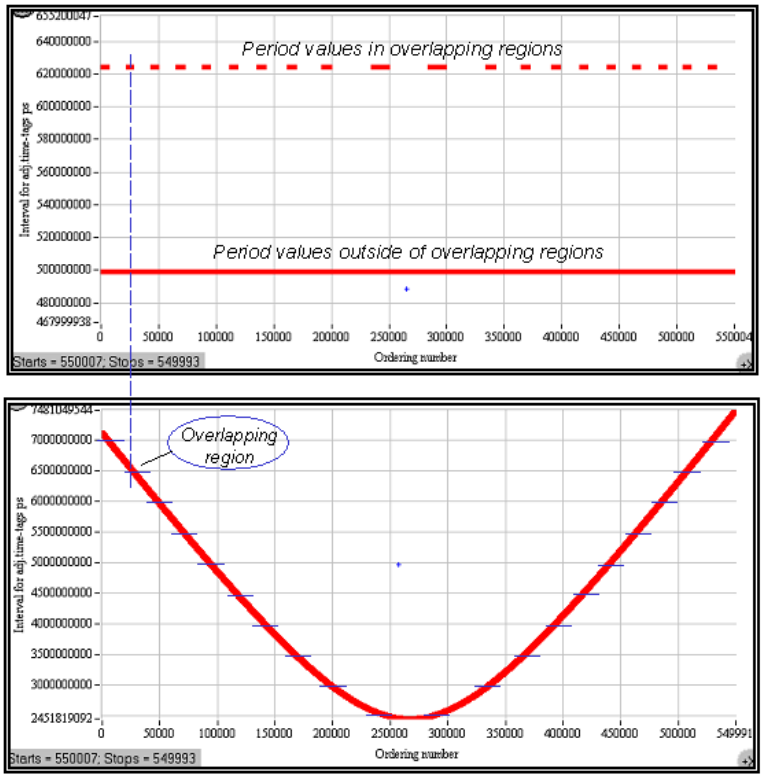

Figure 5. *Period of laser firing (upper graph) and measured range (in bottom) vs. cycle number for CHAMP laser ranging simulation*

As can be seen from the simulation result, there are a number of regions where the transmitting and receiving of laser pulses may overlap. Although the nominal value of repetition period was 499.2 μs, the actual average period was increased up to 502.157 μs (by 0.59%) due to incrementing of some firing periods (~2.4% of total number) by 0.125 ms to avoid these overlaps. Under these conditions any distortions or gaps in the measurement process were not detected. However, it should be taken into account that actually the real-time data processing can be much more complicated than that for the test setup. For this reason it is preferable to use the real-time operating systems to ensure the necessary time for data processing.

Additionally the residuals have been calculated to evaluate the system instrumental errors. When the Range Gate Epoch Times are defined for RGG with the maximum resolution (80 ps), there is a maximum non-linearity in the range gate generation (the

RGG interpolation delay varies in the full 10 ns range). Correspondingly in this case the calculated residuals reflect mainly the non-linearity errors of range gate generation (Fig.6). As can be seen, the peak-to-peak error is about 440 ps.

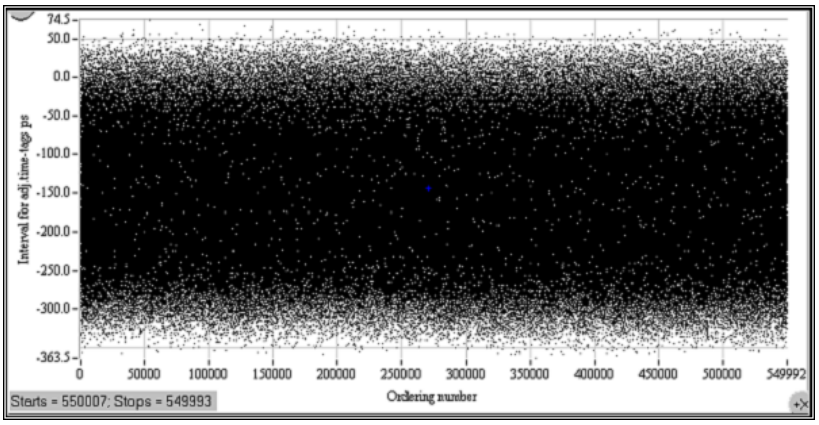

Figure 6. *Residuals vs. cycle number for CHAMP laser ranging simulation*

When the Range Gate Epoch Times are defined with 10 ns resolution, there is no noticeable non-linearity in range gate generation (since the RGG interpolation delay does not vary). Correspondingly in this case the residuals reflect both the errors of event timing and jitter of range gate generation. In our experiment the RMS of residual variation was about 8.9 ps. Since the actual RMS resolution of Event Timer is about 7.5 ps (this is specified by a separate test), it can be concluded that the RMS jitter of range gate generation is about 4.8 ps. Such jitter is negligible as compared to the actual RGG non-linearity.

Conclusion

We presume that KHz SLR is of vital interest for many SLR stations. Taking that into account, the proposed instrumentation offers sufficient performance for such applications and can be useful for creating new timing systems that provide SLR at repetition rate up to a few KHz. In this case the problems of timing system design can be reduced down to the development of user-specific application software.

Special thanks to Dr. Kirchner for his assistance and promotion of our latest designs. His well-known achievements concerning the KHz SLR at Graz station in many respects stimulated our activity in this area.

References

[1] [1] G. Kirchner. Present Status of the Graz kHz SLR System. Proceedings of the kHz SLR Meeting, Graz, Austria, October 27-29, 2004.

[2] [2] V. Bespal'ko, E. Boole, V. Vedin. The Model A032-ET of Riga Event Timers. Proceedings of the 15th International Workshop on Laser Ranging, Canberra, Australia, October 16-20, 2006.

OCA Event Timer

E. Samain[1], Jean Marie Torre[1], D. Albanese[1], Ph. Guillemot[2],
F. Para[1], J. Paris[1], I. Petitbon[2], P. Vrancken[1], J. Weick[1]

1. Observatoire. de la Côte d'Azur, Caussols, France.

2 CNES, Toulouse, France.

Contact: etienne.samain@obs-azur.fr

Abstract

In the framework of T2L2[1,2,3] project, OCA and CNES designed an ultra stable event timer[4]. It includes on a unique card, a vernier, a logic counter, a 100 MHz frequency synthesis and a module for communications and internal calibrations. It has a precision better than 2 ps, linearity below 1 ps and a thermal drift in the range of 0.5 ps per degree. The dead time between two consecutive events is 3 µs.

For the T2L2 ground operations both the start time and the return time of laser pulses are required and not only the differences between the events. In order to run properly the T2L2 project, it will be necessary to upgrade some of the laser stations in that way. A T2L2 questionnaire was sent to the ILRS community to identify precisely the needs of each station.

For these reasons it has been decided to develop from the studies of the space design an event timer dedicated for ground operations. It could have the same characteristics than the flight model even if it seems possible to increase the frequency of the vernier to reach a sub picosecond precision and to decrease the dead time below 1 µs.

Introduction

An event timer is a system able to get the time position of an event in the time scale of a clock. It can be consider as a counter driven by the clock which is the time reference. When an event occurs, the value of the counter is extracted and this value represents the arrival time of the event. The time origin of such an event timer has to be measured with a reference signal like a PPS. A time interval is computed from the difference between two arrival times. The most important characteristics of an event timer are: the precision, the linearity, the time stability and the dead time.

Ideally, the linearity error has to be good enough so that the precision of the timer do not rely on the position of the event in the time scale produced by the clock. A precision of few picoseconds requires then a linearity error in the range of one picosecond. The time stability $\sigma_x(\tau)$ permits to evaluate the performances of the instrument when the events are acquired during τ. In the framework of the laser ranging activities, this is an important characteristic to construct the normal point. In the frame of the time transfer this important to evaluate the noise introduce by the timer as compared to the noise introduce by the clocks. The start time and the arrival time can be measured from the same event timer if the dead time between two consecutive measurements is small enough. A dead time in the range of 3 µs permits to range ground targets at 500 m. This is a minimum requirement to be able to calibrate a laser station with an external ground target.

A first breadboard of the T2L2 space instrumentation was built at OCA in 2002. Since then, T2L2 project was accepted by CNES on the satellite Jason2. We started the development of the space instrumentation in mid 2005. Three models were built: a prototype, an engineering model and the flight model. The flight model is now ready

to be integrated on the satellite.

Description of the T2L2 event timer

The event timer is made with 4 distinct modules on a unique card (figure 1):

- A vernier having a time resolution of 0.1 ps
- Frequency synthesis @ 100 MHz controlled from an external 10 MHz clock signal coming from the DORIS system.
- Calibration module to improve the long term time stability
- Digital module for communication through a RS422 serial bus

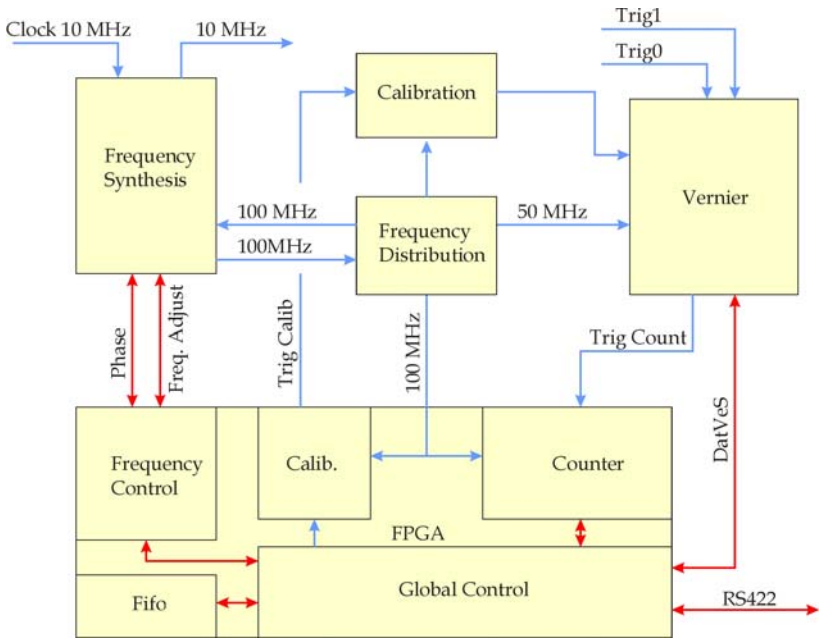

Figure 1 : *Synoptic of the event timer.*

The most important module is the vernier which give the arrival time of the event with a resolution of 0.1 ps. It is driven by the digital frequency synthesis module designed to translate the 10 MHz clock signal to 50 and 100 MHz. The global performances of the timer rely on these two modules. The calibration module permits to improve the long-term stability of the timer. It generates calibrated events that are timed by the event timer. The frequency synthesis is built from an ultra low noise quartz oscillator @ 100 MHz (ArElectronic) controlled with a Phase Lock Loop based on a digital phase measurement. Figure 2 gives the time stability specification of both the DORIS Oscillator and the ArElectronic oscillator. The PLL is tuned to get a frequency cut at 100 Hz with a damping factor of 3. The digital module is divided in 2 parts. The first one is a digital counter driven by the frequency synthesis signal. It gives the arrival time of the event with a time resolution equal to the period of this signal: 10 ns. The second one is the global control of the timer. It controls all the modules and the serial bus.

The complete T2L2 space instrument includes four more cards, two for the detection, one for the computer and memory and one for the power supply. It also includes an optical module made with an avalanche photodiode provided by PESO [5]. All these modules are gathered in a compact aluminium box (figure 3), which is placed inside the satellite payload. The instrument is completed with a detection module located

outside the satellite and very close to the Laser Ranging Array provided by ITE inc.

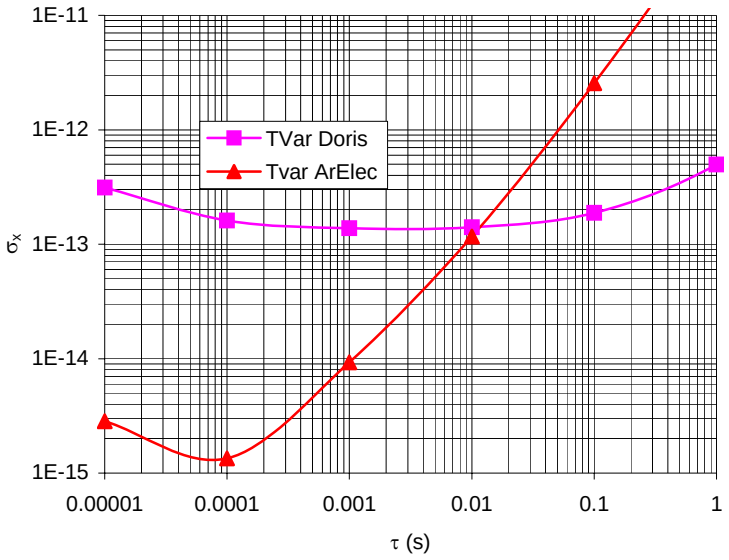

Figure 2 : *Time stability of both the local oscillator and the external oscillator*

The global characteristics of the event timer are:

Input frequency	10 MHz sinus 0 dBm
Event input	2 inputs, ECL level
Local oscillator	100 MHz; noise floor : -165 dBc
Logical frequency	100 MHz
Dynamic	5.7 years
Vernier period	20 ns
Vernier resolution	0.1 ps
Vernier precision	< 2 ps rms
Vernier linearity	< 1 ps rms
Vernier Time Stability	< 30 fs over 1000 s
Vernier Thermal sensitivity	< 1 ps/°C
Vernier Magnetic field sensitivity	< 1ps /100 µT
Calibration Precision	0.9 ps rms
Freq synthesis stability	$\sigma_x = 0.2 \times 10^{-12}\ \tau^{-1/2}$ s @ τ0 = 40 ms
Communication	RS422 @ 1 Mbits
Continuous rate	7000 Hz
Dead time	3 µs
Memory	2 frames
Size	220 x 180 mm²
Power consumption	15 W

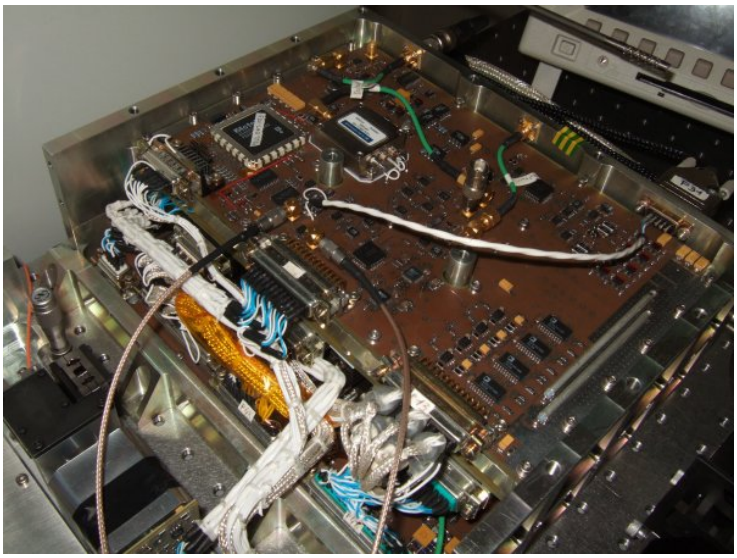

Figure 3 : *T2L2 Electronic instrumentation. The electronic card (in the center of the photography) is the event timer. A part of the Geiger photo detector can be seen on the left side.*

T2L2 ground instrumentation

For the T2L2 ground operations, both the start time and the return time of laser pulses are required and not only the differences between the events. In order for the T2L2 project to run properly, it will be necessary to upgrade laser stations in that way. A T2L2 questionnaire has been sent to the ILRS community to identify precisely the needs of each station. The questionnaire will help us to define the specifications and the design of the event timer: communication, size, number of entry, input frequency, etc.The event timer designed for T2L2 is not dedicated for T2L2: it will also be perfectly well suited for laser ranging. The timer could have the same characteristics than the flight model even if it seems possible to increase the frequency of the vernier to reach a sub picosecond precision and to decrease the dead time below 1 µs.

Conclusions

With an expected improvement of one order of magnitude as compared to existing time transfer techniques, T2L2 will allow the calibration of various existing radiofrequency time and frequency transfer systems like GPS or TWSTFT, and comparisons of cold atomic clocks at a level never reached before. Both the characterizations of the engineering model and the first measurement of the flight model allow us to be confident about the whole performances of the project. The T2L2 space model could also be used in the future in the framework of some interplanetary projects like TIPO [6] (One way laser ranging in the solar system) and Astrod [7] (Astrodynamical Space Test of relativity using optical devices) or LATOR.

Figure 4 : *laser ranging network : Event timer status in September 2006. In yellow laser station requiring an upgrade ; in green, compatible laser station (from the questionnaire)*

For a ground application, the performances of the event timer are at least one order of magnitude better than the performances of the other sensitive elements in the chain: laser – photo-detection. The short dead time between two consecutive measurements (that could be below 1 µs for the ground design) could permit to envision a laser station with only one timer and one photo detection system that will allow a direct accurate laser ranging measurement without any external calibration.

References

[1] P. Fridelance, E. Samain and C. Veillet, "*T2L2 - Time transfer by Laser link: a new optical time transfer generation*", Experimental Astronomy Vol.7 Num.3 Sept.97

[2] Samain, E., J. Weick, P. Vrancken, F. Para, D. Albanese, J. Paris, J.-M. Torre, C. Zhao, Ph. Guillemot and I. Petitbon, "Time Transfer by Laser Link: The T2L2 Experiment on Jason 2 and further Experiments", Int. Journal of Modern Phys. D, World Sci. Publ. Company, (2007), (in press)

[3] Guillemot, Ph., K. Gasc, I. Petitbon, E. Samain, P. Vrancken, J. Weick, D. Albanese, F. Para, J.-M. Torre, "Time Transfer by Laser Link: The T2L2 experiment on Jason 2", Proceedings of the IEEE International Frequency Control Symposium, p. 771-778, (2006)

[4] E. Samain, "*An Ultra Stable Event Timer*", Proceedings of the 13th International Workshop on laser ranging instrumentation, 2002.

[5] I. Procazka , K. Hamal, "*Recent achievements in solid state detector technology for laser ranging*", 2 , 469, Proceedings of the 9th International Workshop on laser ranging instrumentation, 1994

[6] E. Samain, One way laser ranging in the solar system, the TIPO Project (Télémétrie InterPlanétaire Optique), EGS, 2002.

[7] Wei-Tou Ni, Proceedings of the first International ASTROD symposium on laser astrodynamics, space test of relativity and gravitational – Wave astronomy, International journal of modern physics, 2002.

The Model A032-ET of Riga Event Timers

V. Bespal'ko, E. Boole, V. Vedin

1. Institute of Electronics and Computer Science, Riga, LATVIA.

Contact: artyukh@edi.lv

Abstract

The Event Timer A032-ET is an advanced version of the earlier model A031-ET of Riga event timers. As compared to this model, the A032-ET offers better single-shot resolution (<10 ps RMS) and is adapted to KHz SLR, supporting continuous measurement at the mean rate up to 10 KHz. At the same time it satisfies basic demands of conventional (low-rate) SLR. In this paper the principles of operation and basic features of the A032-ET are considered. Typical test results concerning the evaluation of single-shot resolution, linearity and offset drift are presented.

Introduction

Riga Event Timer A032-ET was designed in 2005 as an advanced version of the previous model A031-ET [1] with the main aim to adapt it to KHz SLR and improve its operating characteristics. As a result the following additional features of the A032-ET have been achieved:

- Continuous measurement at mean rate up to 10 KHz;
- Client-Server interaction supporting full remote control from the Client;
- Increased single-shot resolution (better than 10 ps RMS);
- Decreased "dead time" (not more than 60 ns);
- Built-in online programmable Stop pulse gating.

At the same time the A032-ET satisfies basic demands of conventional SLR at repetition rate up to tens of Hz and remains affordable at price. A032-ET is already known for some part of users. In particular, during one year after its designing about 10 instruments were delivered to different SLR stations. In this paper the principles of operation and basic features of the A032-ET are considered in more detail.

A032-ET main features

The A032-ET is a computer-based instrument that precisely measures epoch times when events (input pulse comings) occur. There are two alternative modes of the A032-ET operation that are tailored to the high-rate SLR and conventional low-rate SLR respectively:

- **"True Timer"** provides continuous (gapless) measurement of events at high (up to 10 KHz) mean measurement rate, allowing bursts up to 16 MHz. This mode suits well to measure Start and Stop events that come at the separate inputs (either *A* or *B*) of the A032-ET in any order.
- **"Multi-Stop Counter"** provides cyclical measurement of events that come at the separate inputs of the A032-ET in the strict order: in every cycle at first the A032-ET measures a single Start event coming at the input *A*, and then – a user-defined number of Stop events (up to 12,000) coming at the input *B*. The Stop events can be measured with online programmable gate delay.

Such measurements are performed with 7-9 ps RMS resolution in practically unlimited range. Extreme low measurement non-linearity (<1 ps) is supported.

A032-ET architecture

Like the most of virtual instruments, the A032-ET performs its measurement functions partly by hardware means and partly by software means. The measurement software provides interfacing with a user program via TCP/IP based network according to the well-known "Client/Server" scheme. The application program using TCP/IP service utilities can control the A032-ET and receive measurement data from it for further specific-application processing.

In terms of the Client/Server architecture the A032-ET can be considered as a combination of a specialised timing device (ET-device), and a specialised Server (ET-server) dedicated both to managing the ET-device and primary processing the timing data obtained from it (Fig.1).

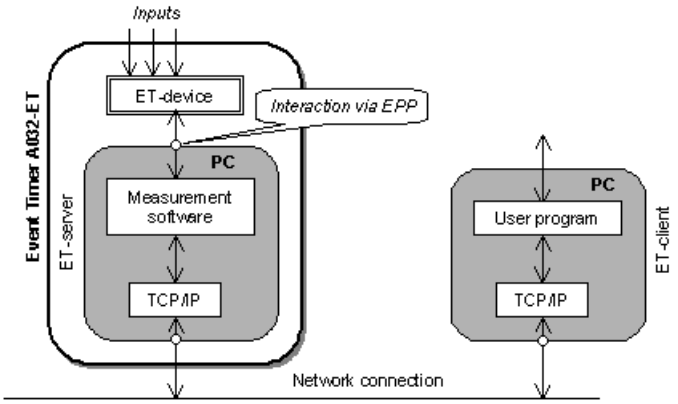

Figure 1. *Network architecture of the Event Timer*

In this case the ET-client is a PC on which user runs his application, using the specific ET-server resources via network. In many cases a single PC under MS-Windows can serve as both the ET-server and the ET-client although a separate PC for the ET-server is preferable to achieve the highest operating speed.

Principles of operation

The A032-ET performs the measurement of input events in two stages. At first, the ET-device transforms every input event into single 80-bit timing data block (TD-block) and sequentially accumulates such blocks in a buffer FIFO memory. Each TD-block contains the clock counter data (39 bits) and interpolating data (40 bits) about the time of event incoming, as well as one-bit mark specifying the input (either *A* or *B*) providing the measured event. The interpolating data are presented initially in an intermediate redundant form and need further an additional processing by the ET-server.

The used unconventional method of event timing supports both high precision and high speed. Specifically, using the 100 MHz internal clocks the method provides each single measurement with <10 ps RMS resolution during 60 ns only. This gives the maximum available rate of event timing about 16 MHz. At this rate the applied FIFO memory is able to accumulate up to 12,000 TD-blocks. An additional attractive feature of this event timing method is that it leads to the relative simplicity of hardware implementation (Fig.2). At the next stage the ET-server reads TD-blocks from the FIFO memory and processes them to obtain the corresponding time-tags in a unified form. Further these time-tags are sent to the ET-client via network.

The ET-device is flexibly controllable and applies two different procedures of TD-

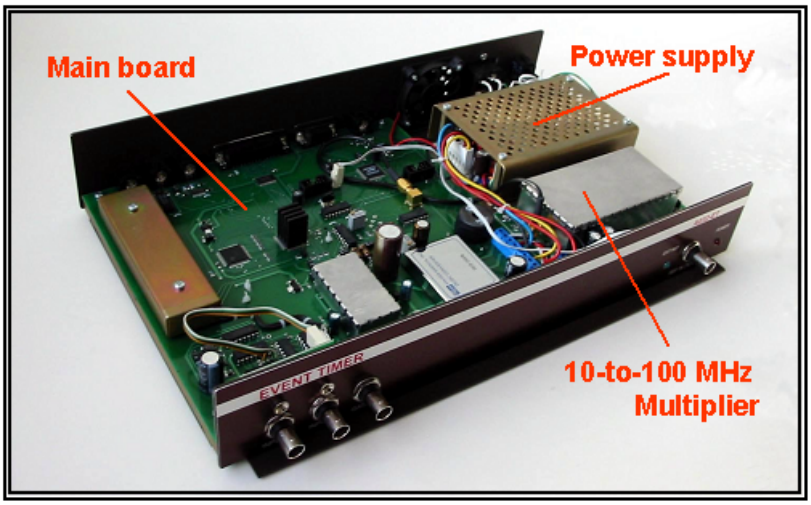

Figure 2. *Hardware design*

block accumulation in the FIFO memory and TD-block reading by the ET-server for two operation modes respectively

In the **"True Timer"** mode the ET-device provides continuous event measurement during practically unlimited time. To do that, the ET-device continuously accumulates TD-blocks in FIFO memory in order of measured event incoming. Concurrently with this process, the ET-server continuously monitors the current state of the FIFO memory with some user-defined period to detect the state when the amount of TD-blocks exceeds the user-selectable value (204, 102, 50, or 25 TD-blocks). The rest of the FIFO memory capacity is used to damp possible bursts of input event intensity. When the specified FIFO state is detected, the ET-server takes out the defined amount of TD-blocks from the ET-device, processes them and sends the corresponding time-tags to the ET-client. Such procedure is being cyclically repeated. In this way continuous event registration goes together with cyclical timing data processing and sending the time-tags to the ET-client via network. The mean rate of such continuous measurement is limited mainly by the available speed of TD-block reading and processing by the PC of the ET-server. Typically (although it may depend on the actual performance of the PC) the total time of single TD-block reading and processing on average is about 0.1 ms, resulting in the maximum mean measurement rate about 10 KHz.

In the **"Multi-Stop Counter"** mode the ET-device provides cyclical measurement of events. In the beginning of each cycle the A032-ET measures a single Start-event coming at the Input *A* of the ET-device, and only then - a number of Stop-events (up to 12,000) coming at the Input *B*. In this case the ET-device accumulates TD-blocks in the FIFO memory during some user-defined waiting period, starting from Start-event registration. During this time the ET-server processes TD-blocks, which are read from the ET-device in previous cycle, and sends the corresponding time-tags to the ET-client. Then the ET-server stops the event registration, reads the accumulated TD-blocks (but not more than the user-defined amount) and starts the next similar cycle. The waiting period can be defined in a wide range with a 1 ms step.

During the waiting period the ET-server can receive a command from the ET-client to restart the measurement with modified gate delay. In this way online cycle-to-cycle controllable gating is possible. However it should be taken into account that the real network may produce some unexpected delays for data exchange, resulting in

episodic loss of synchronism in such interactive operation at a high (more than tens of Hz) repetition rate of measurement cycles.

Precision characteristics

Although, in fact, the A032-ET measures the separate events, its precision is specified for time interval between two measured events. In this case the total measurement error ΔT_j for time interval T_j represented by difference of any two time-tags can be expressed as follows:

$$\Delta T_j = B(t) + E(T_j) + \xi_j,$$

where:

$B(t)$ – time-varying offset in measurement;

$E(T_j)$ – non-linearity error that depends on the value of measured time interval;

ξ_j – unbiased random error.

Specific values of these components of measurement error are evaluated for each instrument. Let's consider some typical examples of such evaluations.

Single shot RMS resolution

The A032-ET provides the best RMS resolution (standard deviation of the error ξ_j) directly after ET-device calibration. Then the resolution may slightly degrade under time-varying temperature conditions (Fig.3).

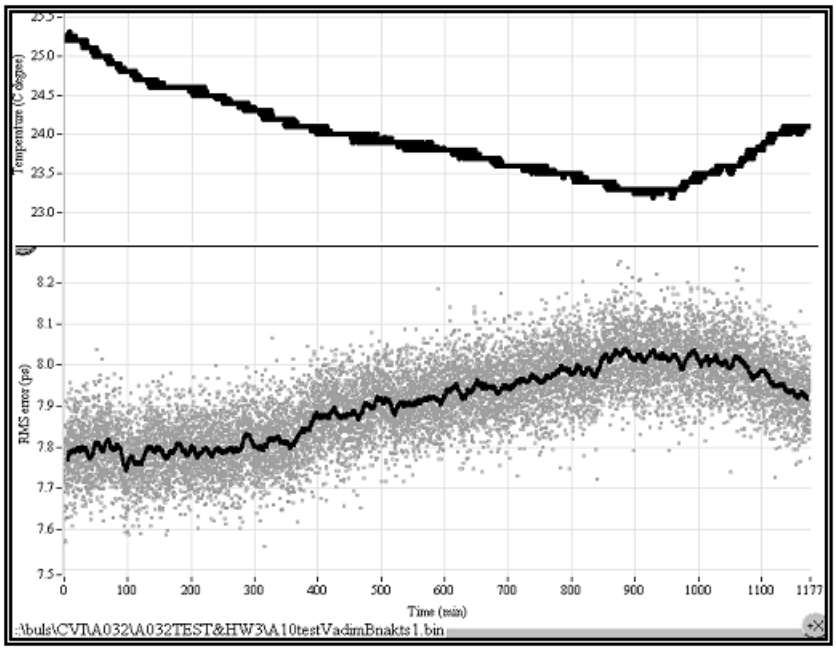

Figure 3. *Ambient-temperature and RMS resolution vs. time*

As can be seen, initially the RMS resolution is about 7.8 ps. During the next 15 hours the ambient-temperature is gradually changed for 2°C, resulting in decreasing of the RMS resolution down to 8 ps (about 0.1 ps/°C).

Linearity

There is some damping transient in electrical circuits responsible for event measurement. If such transient is not completed by the beginning of the following measurement it will be performed with some error. This error depends on the time interval between previous event and event currently measured, causing non-linearity in event measurement.

The A032-ET corrects such non-linearity but cannot exclude it completely, leaving slight, noise-like residual non-linearity in the range up to 2000 ns. This non-linearity appears as errors, which are particular and constant for every 1 ns step of time interval incrementing (Fig.4). In the range exceeding 2000 ns the non-linearity is negligible.

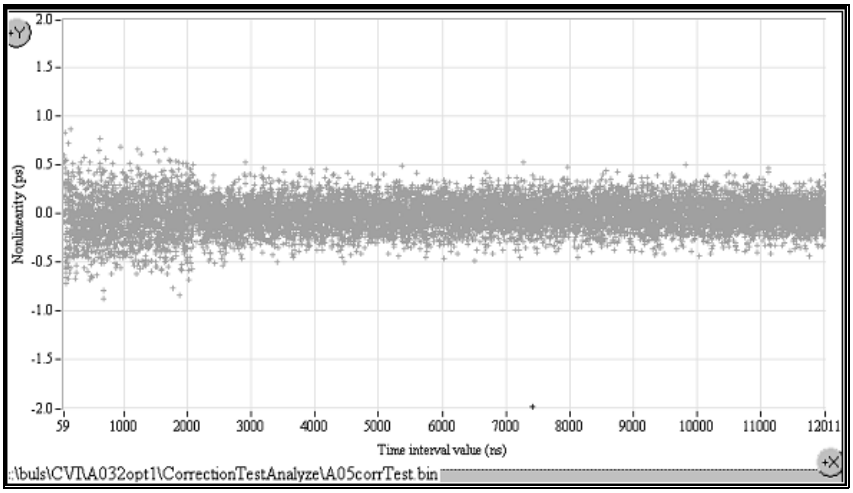

Figure 4. *Typical result of non-linearity error testing*

As can be seen, the maximum non-linearity does not exceed ±1 ps. However such estimate is overstated by reason of the additive evaluation errors (these errors are directly present in the range from 2000 ns). Actually the non-linearity is much smaller.

Offset drift

All events coming at either input of the ET-device are measured sequentially in the same manner and by the same means. Owing to this there is no any noticeable offset in time intervals between measured events when these events come at the same input. However when the events come at the different inputs it results in some offset. The offset is caused by a difference between internal propagation delays of input signals before their coming to the common measurement unit. These delays slightly vary with the ambient-temperature change, thus causing certain offset drift and corresponding long-term instability in time interval measurements.

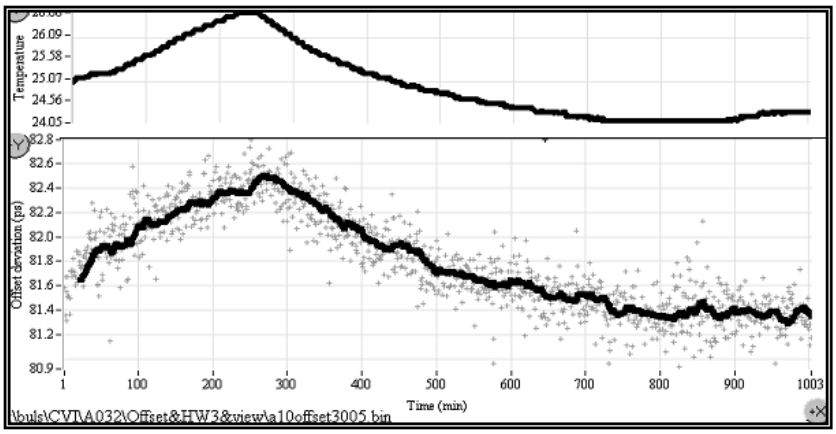

Figure 5. *Ambient-temperature and offset vs. time*

As can be seen from the example shown in Fig.5, the offset variation is directly related to the temperature variation, indicating in this case the offset temperature stability about 0.48 ps/°C. Generally this parameter value depends on the specific operating conditions.

A032-ET summary specification

Generalizing the test results that have been obtained at least for 15 units of the A032-ET, the following summary specification can be stated:

Inputs (BNC): INPUT A	NIM pulse (falling edge; >5 ns width)
INPUT B	NIM pulse (falling edge; >5 ns width)
SYNC IN	TTL pulse (rising edge, 1 pps)
TRIG IN	TTL pulse (rising edge)
REF IN	10 MHz (>0.5 V p-p)
Single-shot RMS resolution	<10 ps
Dead time	60 ns
Non-linearity error	<1 ps (<3-5 ps for time intervals less than 100 ns)
Offset temperature stability	<0.5 ps/^{0}C after warm-up
Warm-up time	2 hours
FIFO depth	12,000 time-tags
Measurement rate (True Timer)	up to 10 KHz continuously
Stop pulse gating (Multi-Stop Counter)	online programmable via network (10 ns LSD, 60 ns to 167 ms range)
Control	fully remote control from a user program via the network
Application interface	over TCP/IP
Hardware interface	via PC parallel port supporting EPP mode
Server software	MS-Windows based
Accessory software	DEMO application software
Hardware dimension, weight	375x60x233 mm (desktop); 3.0 kg
Power supply	100-240 VAC

It should be pointed that the A032-ET is a custom instrument manufactured in a limited quantity and only on request. For this reason such instruments may differ from one to another in some details. Additionally it should be taken into account that the measurement rate may depend on the actual performance of the user's PC and network.

Additional notices

The A032-ET is currently available in the following configuration:

- ET-device;
- Server software A032.1 that provides **"True Timer"** mode;
- Server software A032.2 that provides **"Multi-Stop Counter"** mode;
- DEMO Client software (including source codes in *C*) that illustrates the manner in which the user can create own specific application.

Optionally the Sample program (source code in *C*) is available. This program defines the device-specific software functions to communicate with the A032-ET hardware via PC Parallel Port. These functions can be directly built in the user software when the user desires to create fully integrated timing system.

References

[1] http://ilrs.gsfc.nasa.gov/docs/timing/Event-Timer-A031-ET.pdf

Upgrading of Integration of Time to Digit Converter on a Single FPGA

Young Zhang[1,2], Peicheng Huang[1] and Renjie Zhu[1,2]

1. Shanghai Astronomy Observatory, Chinese Academy of Sciences, 80 Nan Dan Road, Shanghai, China 200030
2. Graduate School of the Chinese Academy of Sciences, 19A Yu Quan Road, Beijing, China 100039

Contact: zhang.young@gmail.com , pchuang@shao.ac.cn and zhurj@shao.ac.cn

Abstract

A Time to Digit Converter (TDC), which can achieve resolution 50-60 picoseconds, is integrated on a single FPGA. Implementing a TDC on an FPGA provides not only higher precision and shorter dead time compared to traditional methods, but also higher scale of integration. As the system can be integrated into single chip, it is especially suitable for portable and satellite-borne system. Besides, the resolution is expected to be improved to less than 30 picoseconds. Principle of operation, architecture of the prototype, the construction of this TDC and the nonlinearity are presented in this paper.

Introduction

Traditional high-precision time interval measurement techniques include time stretching method, time-to-amplitude method and Vernier method, tapped delay line method and differential delay line method [1]. There are two examples of TDC integration on a single FPGA: Jozef Kalisz *et al* adopted differential delay line method on QuickLogic's pASIC2 FPGA, which achieved 100 ps LSB [2]. Zielinski and Chaberski, using tapped delay line method, implemented a module on Xilinx's XCV300 with 100 ps resolution [3]. In this paper, a TDC is implemented on a XC4VSX35 FPGA with 50-60 picoseconds resolution. Table 1 lists main parameters of this module as below.

***Table 1**: Design Summary*

Standard uncertainty	50--60 picoseconds
Resolution/LSB	50--60 picoseconds (expected to reduce to 20-30)
Measurement Range	0-99999 seconds
Input Reference Clock	10MHz Rb Atom Clock
Calibration Mode	Real time Calibration

General Design

Interpolating Principle

Interpolating methods are widely used because of its advantages in both long measurement range and high resolution. With interpolating methods, a time interval T generally consists of three parts. A major part, nT_p, is measured in real time by reference clock. The remaining two short intervals ΔT_1 and ΔT_2 are defined at the beginning and at

the end of time interval *T*, which are measured by insulators. In this design, they are measured by two tapped delay lines. Fig. 1 gives the math relation between them.

Reference clock

The input 10MHz reference clock from Rb atom clock is quite stable but not high enough for interpolating. With built-in DCM on FPGA, it is synthesized into 200MHz. As shown in Fig.1, the time interval nT_p is counted by the reference clock 200MHz. The measurement jitter of 200MHz reference clock is about 60 picoseconds.

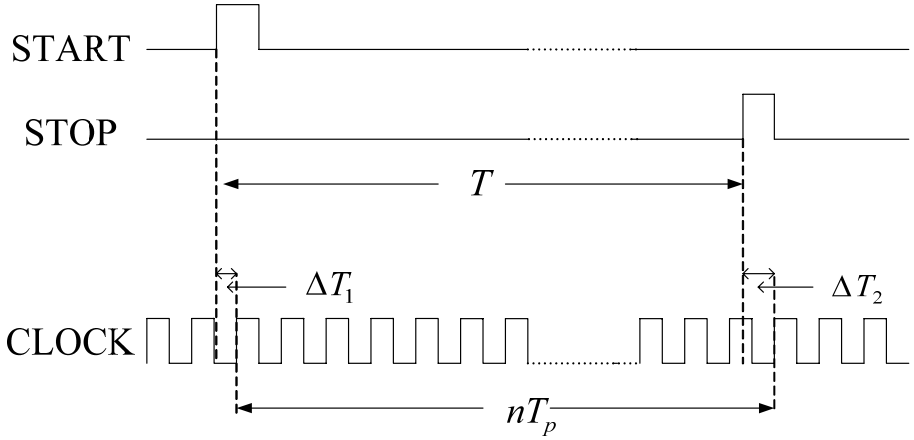

$$T = nT_p + \Delta T_1 - \Delta T_2$$

Figure 1. *Interpolating Principle*

Tapped Delay line

The tapped delay line is made of slices - the basic unit of the Virtex FPGA. As shown in Fig.2, a delay unit and a D flip-flop, is in the dashed line. The dashed part of delay logic can be implemented in a single slice, as shown in Fig. 3. These slices cascade to form a slice chain, i.e., a tapped delay line. Two delay lines of this kind, measure the short time interval ΔT_1 and ΔT_2 respectively.

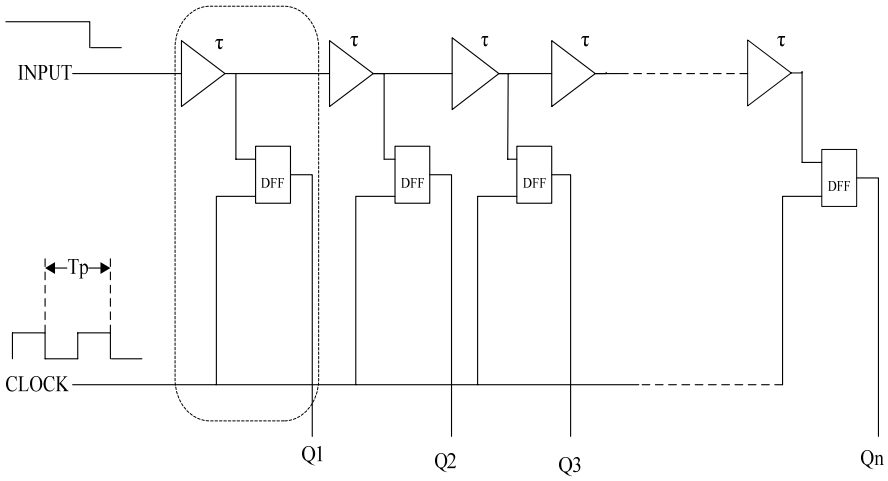

Figure 2. *Tapped delay line made of slices.*

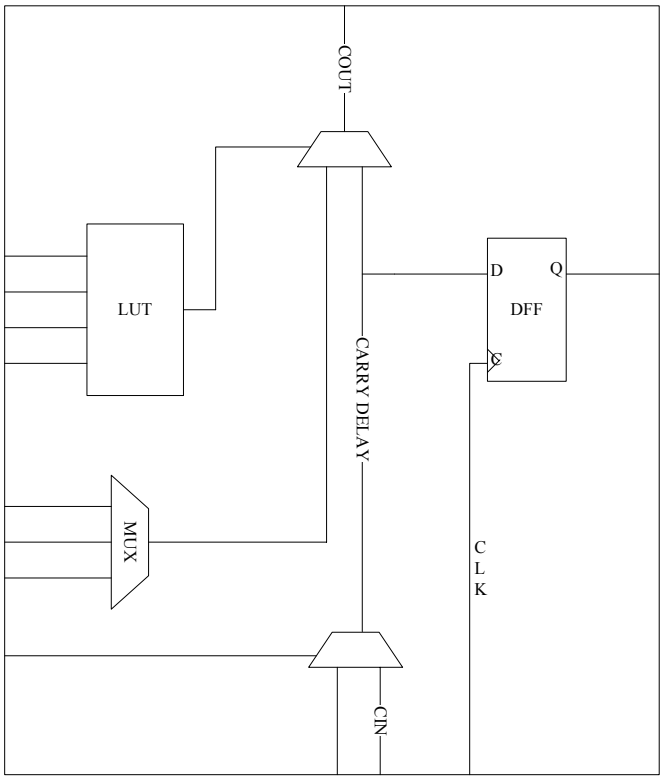

Figure 3. *Simplified slice configuration as delay unit.*

The delay unit of slice utilizes the fastest path, fast carry logic, to obtain the highest resolution. It's assumed that all delay units are of the same delay time τ. The measurement average delay τ, which determines the resolution or least significant bit of this module, is about 50-60 ps. However, this assumption does not fit the facts perfectly. The nonlinearity of the tapped delay line is measured and analyzed in the next part.

Measurement data

In this part, the measurement data of this module is compared with those of SRS's SR620. To demonstrate the resolution of this high-precision TDC, y axis of Fig 4 is marked with TDC measurement, while the x axis is marked with SR620 measurement.

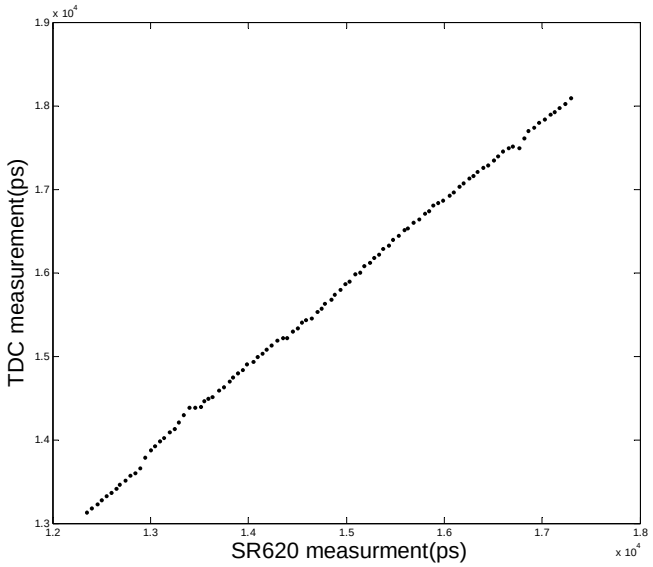

Figure 4*. Comparison of TDC measurement with SR620 measurement*

The difference between two groups of measurement, which is equal to the differential nonlinearity, is given in Fig. 5. In Fig.5, the maximum difference is about 300 picoseconds. The difference measurement can be repeated in other time cycle, which means it can be corrected with prior knowledge of it. This will be part of further research. Besides, with a little internal modification, the resolution is expected to reduce to less than 30 picoseconds, which means 50% improvement in resolution. This will be part of our future work.

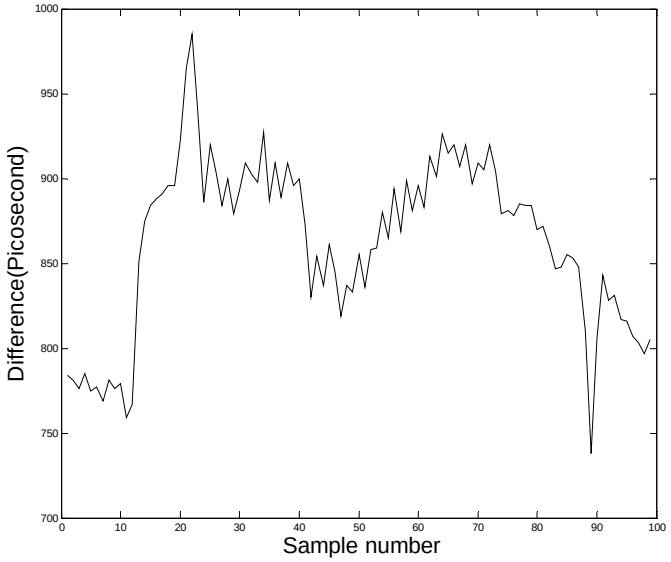

Figure 5. Difference between TDC and SR620

Fig.6 is a snapshot of our measurement experiment.

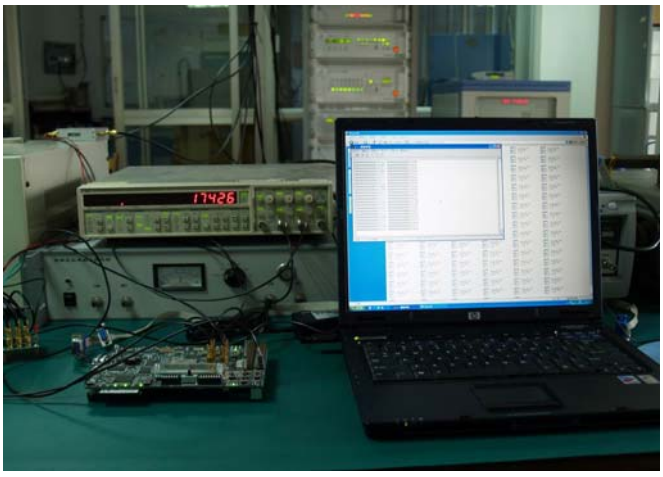

Figure 6. Measurement experiment

References

[1] Józef Kalisz, 2004. Review of methods for time interval measurements with picosecond resolution Institute of Physics Publishing Metrologia, vol 41 pp17-32.

[2] Szplet R, Kalisz J and Szymanowski R., 2000. Interpolating time counter with 100 ps resolution on a single FPGA device IEEE Trans. Instrum. Meas. vol 49, pp.879-883.

[3] Zielinski M, Chaberski D., and Grzelak S., 2003. Time-interval measuring module with short dead-time Metrol. Meas. Syst. 10.

High-Speed Enhancement to HTSI Event Timer System

D. McClure, C. Steggerda, S. Wetzel

1. Honeywell Technology Solutions Inc., 7515 Mission Drive, Lanham, MD USA 20706

Contact: scott.wetzel@honeywell.com

Abstract

HTSI has developed a high-performance Event Timer Controller to pair with the HTSI Event Timer that allows acquisition of UTC tagged event epochs with <2ps jitter and 0.5ps resolution from up to 12 input event channels at continuous asynchronous event acquisition rates of over 50kHz. The increase in sustainable data rate allows easy integration of multiple or arrays of detectors and generation of a single real-time stream of UTC epoch'd event data with associated channel ID flags.

This paper describes the upgrades to the HTSI event timer system that enable the high-speed capability. The content will include a data comparison of ILRS stations utilizing the HTSI event timer as well as a discussion of current usage applications and potentials for future use.

High-Speed Enhancement to HTSI Event Timer System

The HTSI Event Timer was designed and built in the 1990s by Charles Steggerda based on his years of experience designing timing devices. Initial laboratory and MOBLAS-7 test results were reported in July 1998 at the 19th International Laser and Radar Conference in Annapolis, MD in a paper titled *Instrumentation Development and Calibration for the Matera Laser Ranging Observatory*. Today's paper follows up after 8 years of use and describes an important new capability that can be utilized by the current and next generation of high rate laser ranging stations. Figure 1 shows the HTSI Event Timer.

Figure 1: *HTSI Event Timer*

HTSI Event Timer Description

The HTSI Event Timer (ET) generates precise epoch time-tags ideal for Satellite Laser Ranging, Lunar Laser Ranging, and other precision timing applications. The ET facilitates measurement of delays between one or more pulses without a range/delay

dependant effect on timing error and supports applications with multiple shots in the air required by high laser fire rates or extended time of flight to targets (i.e. geosynchronous, lunar, or beyond). The basic design and capability hasn't changed since that reported in July 1998 at the 19th International Laser and Radar Conference. The ET couples a precise synchronous counter with from 1 to 4 analog verniers and a computer synchronized to UTC. In the single vernier configuration, the ET provides better than 2 ps of resolution and less than 4 ps of Root-Mean-Square (RMS) jitter. In the four vernier configuration, the ET provides measurement redundancy and increases the effective resolution to <500 fs with an RMS jitter of < 2 ps.

Clock Speed (Internal)	500 MHz, Locks to external 10MHz
Input Channels	12 SMA inputs; NIM type; 50 Ohm termination; negative pulses (unused channels do not require termination)
Resolution	Better than 2ps (1 vernier), 500 femtoseconds (4 vernier)
Dead-Time	100 Nanoseconds
RMS Jitter	<5ps for 1 vernier; <2ps for 4 vernier
FIFO Depth	512
Interface	32 bit DIO, Optional computer allows additional interfaces
Software	UNIX (HP-UX, Linux), MS Windows, etc.
Power	Auto ranging (100-240V; 50-60Hz)

Figure 2: *Summary of Specifications*

Twelve external inputs are provided and events sampled on each channel are tagged with an identification flag in hardware. When coupled with a computer that receives coarse time via time code or GPS, a full event epoch can be generated. Events can be sampled by the hardware at a rate of 10MHz, but are input into a high-speed FIFO buffer that can only store 512 events. Thus the specification of maximum sustainable event sample rate is dependant on the DIO and processing speed of the specific event timer controller.

HTSI Event Timer Past Performance

The initial HTSI event timer development was started in 1995 to support the Matera Laser Ranging Observatory (MLRO). Initial testing of the ET prototype was performed at NASA Goddard Space Flight Center's MOBLAS-7 reference station. Comparison results between the prototype ET and MOBLAS-7 indicated addition of the Event Timer produced an immediate 30-40% improvement in MOBLAS 7 data quality over the existing HP-5370 counter data decreasing LAGEOS range data RMS from 9mm to 5mm.

Later in 1998, the final 4-vernier MLRO and 1 vernier SLR2000 event timers were built. In 2002, a dual vernier model was built for the Global High Accuracy Trajectory Station (GUTS) to be located in Tanegashima, Japan. The MLRO and GUTS event timers supported both stations in achieving best case performance of 2mm ground calibration and 5mm LAGEOS RMS. Both stations utilized the multiple inputs to support fire, dual color PMTs (MLRO), amplified channels for Lunar (MLRO) and Geosynchronous ranging (GUTS), system calibration inputs, on-time pulses, etc. And in 2006, an Event Timer is being built for the US Naval Research Laboratories (NRL)

- **MOBLAS 7** – (Prototype Event Timer; 1998; 3ps RMS)
  - 5 Hz fire, 2 events per frame
  - Use of the HTSI Event Timer produced an immediate 30-40% improvement in MOBLAS 7 data quality over the HP-5370 TIU (Lageos-1 data improved from 9 mm RMS to 5 mm RMS).
- **SLR2000 Prototype** – (Delivered in 1998; 4ps RMS)
  - 2 kHz fire, multiple events per frame, quad PMT
- **MLRO** – (Used in Greenbelt, MD in 1998 and Matera, Italy since 2000; 2ps RMS)
  - 10 Hz fire, 8 events per frame
  - Multiple laser & PMT detection path signals sampled by one event timer.
  - Supported station in achieving 2 mm calibration and 5 mm LAGEOS RMS.
  - Supported station in acquiring two-color and lunar data.
- **GUTS** – (Used in MD in 2002 and Tanegashima, Japan since 2004; 4ps RMS)
  - 10 Hz fire, 4 events per frame
  - Supported station in achieving 2 mm calibration and 5 mm LAGEOS RMS.
  - Supported station in acquiring data from geosynchronous targets.
- **NRL** – Being developed as a stand alone ET for delivery in 2006/2007
- **GUTS Spare** – Being developed for delivery in 2007

Figure 3: *HTSI Event Timer Past Performance*

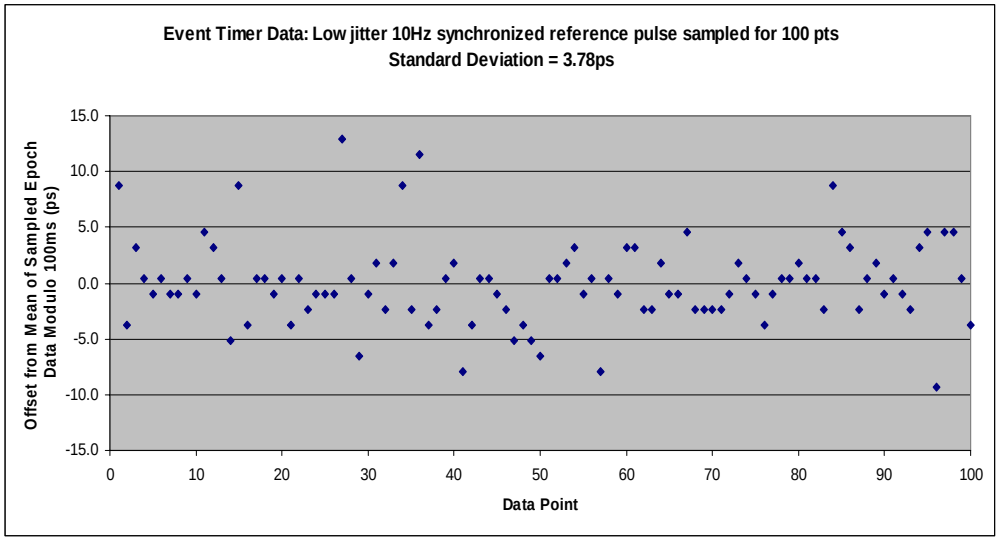

Figure 4: *Event Timer Accuracy*

HTSI Event Timer Data

Figure 4 demonstrates typical Event Timer Accuracy / RMS when configured with a single vernier. To generate this graph, a precise 10Hz electrical reference pulse was sampled 100 times by the event timer. The epoch data was then normalized to the mean repetition frequency. The graph shows raw, unfiltered offset data that demonstrates a 3.78ps RMS jitter. If you look closely, you can see data banding demonstrating that the single vernier bit resolution is <2ps.

Figure 5 demonstrates the potential single shot RMS of stations that utilize the HTSI event timer showing the MLRO and GUTS stations as having the lowest reported LAGEOS single shot RMS in the ILRS network. Note that the event timer, while crucial, is coupled with excellent optics and low-noise optical detection to produce these results.

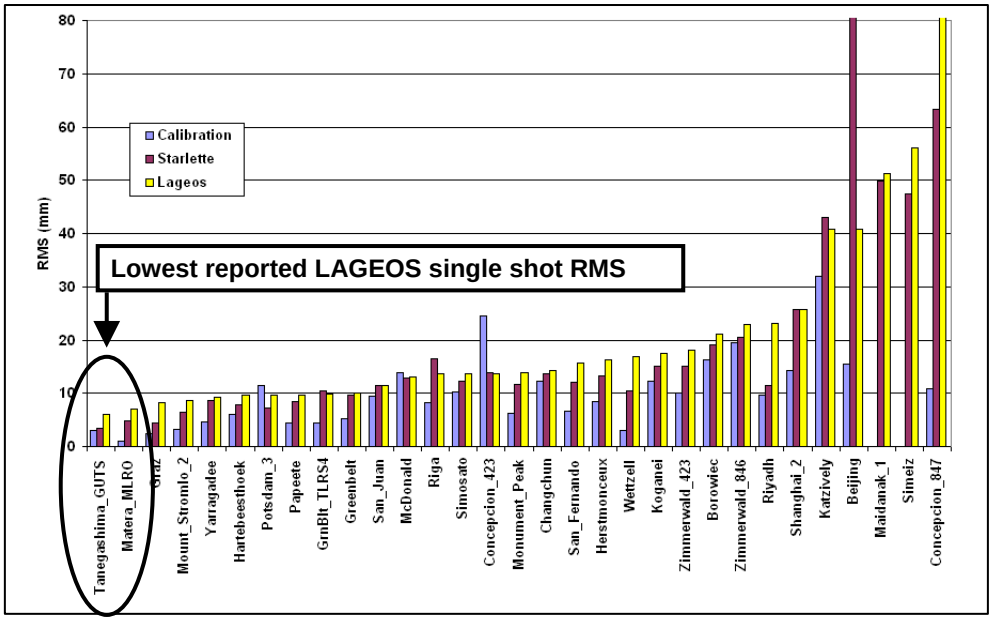

Figure 5: *ILRS Station Single Shot RMS Data for 2Q 2006*

HTSI Event Timer Controller High Speed Enhancement

The HTSI ET has always supported Mega-event per second sample rates, but has been limited by the speed of its control computer in emptying the 512 event deep hardware FIFO. The GUTS and MLRO ET controllers used non-DMA DIO to communicate with the ET at a maximum event rate of approximately 200 events per second (while also performing tracking and controlling other equipment). Counter and verniers were manually addressed by the controller. For SLR2000, HTSI converted the ET to use a high-speed DIO card. In addition, the counter and vernier became auto-addressed allowing for DMA transfer operations. The ultimate data rate was still limited from sharing control computers with other tasks, 10Mbps Ethernet speeds and generation of individual event interrupts.

The advances in computer processing speeds and network bandwidth since 1998 have allowed the design of a high-performance controller to utilize the hardware to its full potential. This high-performance controller enables the HTSI event timer to immediately gain a factor of 10 in sustainable rate (from multi-KHz samples per sec to at least 50ksamples/sec) and promises to allow for further growth in the future as the world transitions to dual core processors and 10GB Ethernet. In addition, the enhanced controller removes the complex issue of DIO interface, driver, and data handling replacing them with a simplistic network accessible design. The enhanced Event Timer controller provides a real-time stream of epoch'd ET data across a dedicated LAN to a station tracking computer. DIO transfer rate is maximized by allowing the ET FIFOs to buffer data. Data is immediately calibrated, combined with UTC coarse time, sent to Ethernet, and received on the tracking computer. A prototype of the enhanced controller has been built in Greenbelt, MD, and is still in the process of software development and testing.

Figure 6 shows the block diagram of the Event Timer Controller that has been built in our integration lab. Notice that all components exist to produce high accuracy time epochs referenced to UTC.

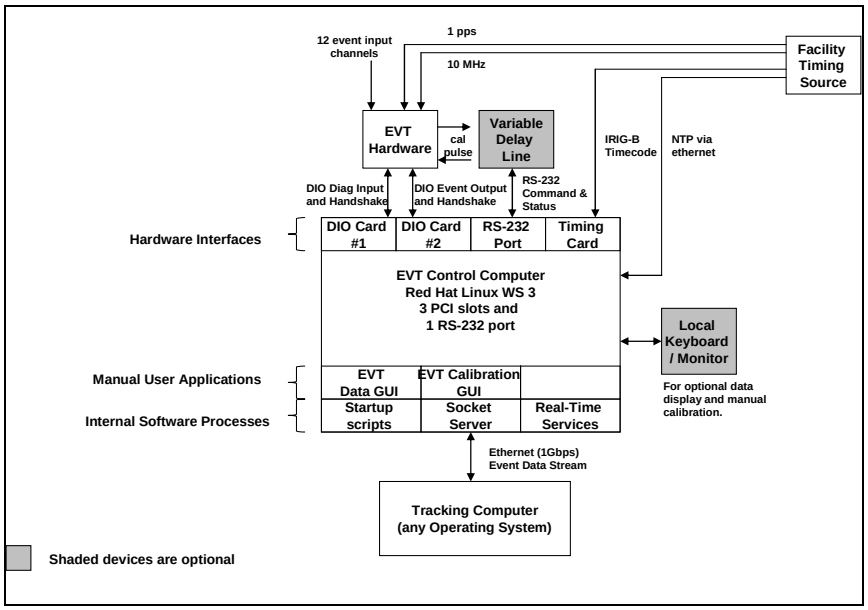

Figure 6: *Enhanced Event Timer Controller: Block Diagram*

Figure 7 shows the internal software architecture and data flows within the Enhanced Event Timer Controller. The Event Timer Software architecture is based on modular C++ UNIX processes inherited from the MLRO and GUTS software heritage. Event Data moves from right to left in this figure. Event Timer and Time Code Generator data is merged to produce a real-time stream of event epoch data. Vernier non-linearity's are then removed via calibration in real-time. The event data is then distributed to client tracking computers via a network socket server.

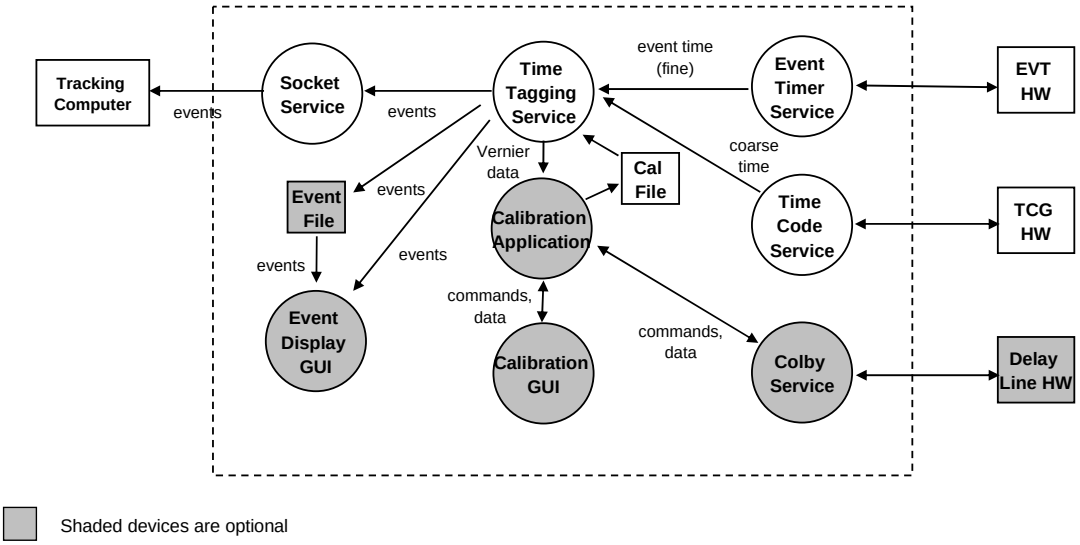

Figure 7: *Enhanced Event Timer Controller Software Architecture*

Optional software modules allow for local calibration of the event timer or independent use of the ET controller by storing event data in a file. Optional modules include a delay line interface, a calibration process and GUI, and an event display GUI.

HTSI Enhanced Event Timer Controller: Initial Results

DIO Performance

Figure 8 shows initial results of high speed testing with the Enhanced Event Timer Controller. Initial DIO laboratory performance tests were able to read reference pulse event times from the ET FIFO buffer at a sustained rate of 5Msamples/sec or **1.25 Million events per second** with a 3 vernier + 1 counter ET. DIO card specifications indicate that the maximum continuous handshaking I/O rate for the DIO-6533 is 17.3 Msamples/sec potentially enabling the reading of. **4.3Million events per second** with a 3 vernier + 1 counter event timer.

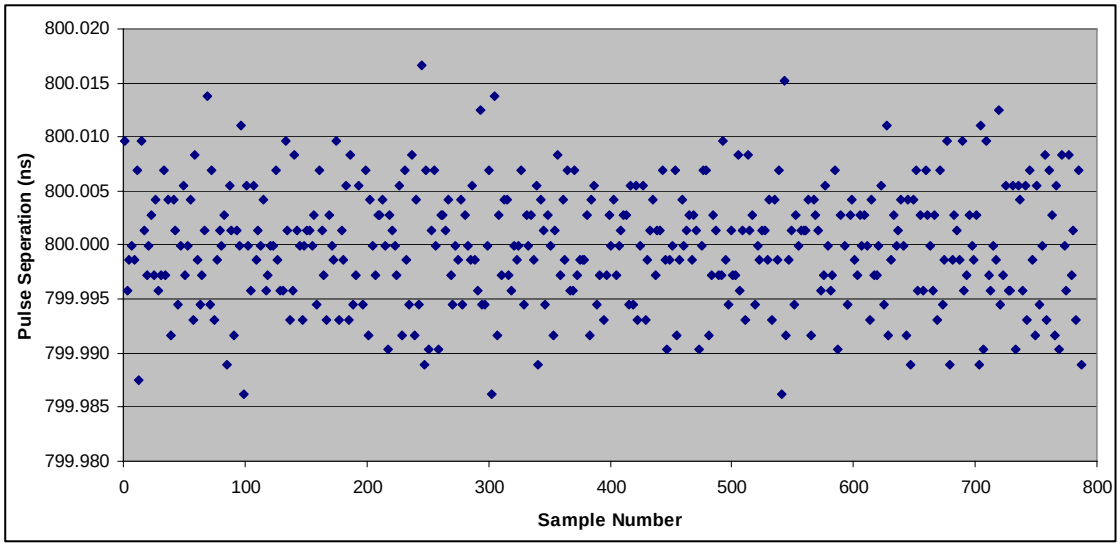

Figure 8: *Initial Enhanced Event Timer Controller High Speed DIO Test Data*

LAN Performance

Preliminary tests demonstrate that it is possible to sustain network transfer rates of **61,035 events per second** on our current 100Mbps testing LAN (no network traffic analysis tool was available to determine actual network bandwidth usage). Further increase in speed is theoretically possible after tuning of packet sizes and enhancing our laboratory with a 1Gbps network switch. These results match initial computations to first order predicting that 50,000 events per second requires a minimum of 25Mbps dedicated network bandwidth on an isolated LAN (assuming 1,024 bit packets holding (8) 112 bit events or 896 bits of user data each and a factor of four compensation for traffic).

HTSI Event Timer: Future Applications

The newly developed HTSI High-Speed Event Timer Controller when combined with the HTSI Event Timer produces a system that can enable many future applications in addition to those currently being supported. Currently the HTSI Event Timer has been used to support:

- 10Hz single and dual laser fire and return with station calibration events (single and multi-wavelength)
- 10Hz geosynchronous and lunar laser ranging (multiple shots in the air)
- 2kHz tracking with 3 high-rate event inputs (6KEvents/sec)

The Enhanced HTSI Event Timer System meets the needs of the SLR data community to acquire data at higher and higher repetition rates with more detectors and enables the design of the next decade of forward reaching experiments. A few of the additional potential applications that can be extrapolated includes:

- 2kHz operations with multiple fire and detection events (i.e. for multiple wavelengths / dual PMTs)
- 2kHz operations with additional station delay diagnostic event inputs
- Use of arrays of detectors at 2kHz (3x3; 3x4; 4x4 would require external event coupling)
- Recording of high rate event epoch data approaching 1 Million events per second
- Laser fire and return pairs several orders of magnitudes faster than 2kHz
- Time transfer experiments (ground and on-orbit)
- Station construction with reduced event timer integration time
- Station construction with reduced real-time tracking controller complexity and cost (ethernet vs. DIO)

References:

[1] *Instrumentation Development and Calibration for the Matera Laser Ranging Observatory*, July 1998, 19th International Laser and Radar Conference in Annapolis, MD, C. Steggerda, M. Selden, C. B. Clarke, R. Stringfellow, J. M. Heinick, D. McClure, Dr. G. Bianco

[2] Time of Flight Devices Manufacturer Specifications Comparison Table, ILRS Web Site, http://ilrs.gsfc.nasa.gov/engineering_technology/timing/tof_devices/manufacture_spec/index.html

[3] SLR Global Performance Report Card 2Q 2006, ILRS Web Site, http://ilrs.gsfc.nasa.gov/stations/site_info/global_report_cards/perf_2006q2_wLLR.html

Low-Noise Frequency Synthesis for High Accuracy Picosecond Satellite Laser Ranging Timing Systems

Josef Kölbl[1], Peter Sperber[1], Georg Kirchner[2], Franz Koidl[2]

1. Deggendorf University of Applied Sciences
2. Austrian Academy of Sciences, Observatory Lustbühel

Abstract

The developed Frequency Multiplier from 10 MHz to 200 MHz is fully compatible to the Thales Multiplier and can be directly interfaced to the Thales Event Timing Modules by "plug and play". The new Multiplier designed at Deggendorf University of Applied Sciences shows high sub-harmonic attenuation in the frequency domain of greater than 110 dB.

Whereas, in the time domain the 200 fs rms cycle-to-cycle jitter specification is observed when measuring the output signal with a high-bandwidth sampling oscilloscope. Measurements in the time domain and frequency domain of the new multipliers show better specifications to existing frequency synthesizers.

The 10 MHz to 80 MHz Frequency Multiplier is in continuous operation at Mount Stromlo SLR Station and in various Keystone SLR Stations in Japan. Modules are available through our partner company MPF Optics Ltd.

Introduction

Tests carried out at SLR station Lustbühel, Graz:
Graz E.T. / Dassault Modules:
Comparison between Dassault Clock and Deggendorf-Clock

- DeggendorfClock is mechanically / electrical connections identical to Dassault Clock;
- Measurements in Graz were made using both clock modules alternatively;
- Measurement description:
    - Standard Laser Firing pulse (TTL), Power Splitter 50 Ohm;
    - 1 Pulse direct into E.T. Start;
    - Splitted pulse delayed with cable, into E.T.Stop;
    - Standard Calibration Program used, Single Time Intervals stored;
    - Results checked with Program DRAW, 2.2 Sigma Iteration;
- For ease of tests: Clock module 200 MHz outputs (both clocks) connected via standard RG58 Cables / SMA connectors into Start / Stop Modules (instead of Dassault Semi-Rigid Cables). All Tests performed in this configuration.
- At each change of Setup: E.T. switched off; new sync / new offsets after each switch on.

Results (in ps) / No Sigma iteration

Cal_1: 9215.94 ± 3.87 [ps]	Dassault Clock	Semi-Rigid Cables (Graz Original Setup)
Cal_2: 9216.04 ± 3.34 [ps]	Dassault Clock	RG 58 cable
Cal_3: 9217.14 ± 3.58 [ps]	Deggendorf clock	RG 58 cable
Cal_4: 9214.83 ± 3.34 [ps]	Dassault Clock	RG 58 cable
Cal_5: 9216.45 ± 3.32 [ps]	Deggendorf clock	RG 58 cable

Results (in ps) / 2.2 Sigma iteration:

Cal_1: 9215.94 ± 2.84 [ps]	Dassault Clock	Semi-Rigid Cables (Graz Original Setup)
Cal_2: 9216.12 ± 2.79 [ps]	Dassault Clock	RG 58 cable
Cal_3: 9217.00 ± 2.82 [ps]	Deggendorf clock	RG 58 cable
Cal_4: 9214.73 ± 3.07 [ps]	Dassault Clock	RG 58 cable
Cal_5: 9216.45 ± 2.57 [ps]	Deggendorf clock	RG 58 cable

Remarks

- Variation in absolute values (1-2 ps): Due to new offsets between start/stop modules after switch ON.
- Several other calibration runs were made, with different cable length etc.; all giving similar results.
- The Deggendorf clock module seems to have at least the same specs than the Dassault; no difference visible.

Editor's Note

The technical data specification for the frequency multiplier unit can be found on the accompanying CD.

MULTIPLE WAVELENGTH AND REFRACTION SESSION SUMMARY

Chair: Erricos Pavlis

Gurtner presented recent changes at Zimmerwald. The system used internal, near realtime calibration until June 2006. The change was necessitated after routine operations with a second wavelength (infrared) revealed differences between the calibrated ranges of the two colors that could not be explained as errors in the applied refraction models. It turned out that the internal calibration values of the infrared chain showed variations that had not much to do with system calibration. The source of these variations could not be identified. In June 2006 the station switched to external calibration and the differential biases were by and large eliminated. One of the concluding remarks was the need of a 100-fold improvement in the dual wavelength data if they are to be used for refraction modeling.

Müller reported that Lageos-1/2 multi-wavelength normal point data from Zimmerwald and Concepcion were reduced with DGFI's s/w, to estimate station coordinates and color dependent biases. The statistics and the history of bias differences for the Marini-Murray and Mendes-Pavlis refraction models were shown. Full-rate tracking data were also analysed to determine if they lead to results different from the use of onsite normal points. The switch from internal to external calibration at Zimmerwald resulted in a significant improvement of the relative biases, mainly for the infrared side. The tests indicated the superior performance of the new refraction model of Mendes-Pavlis.

Pavlis (for Hulley) presented the validation of the new, sub-millimeter accuracy, zenith delay model of Mendes and Pavlis, [2004] and the sub-centimeter accuracy mapping function of Mendes et al., [2002], using global data from the Atmospheric Infrared Sounder (AIRS), the European Center for Medium Weather Forecasting (ECMWF) and the National Center for Environmental Prediction (NCEP). The models however are still far from the required sub-millimeter accuracy goal for future SLR analysis standards and the requirements place on SLR by the Global Geodetic Surveying System (GGOS) [Pearlman et al., 2005]. They thus developed a new technique, using 3D ray tracing that includes the effects of horizontal refractivity gradients. Global statistics for two years indicated delays can reach even 5 cm at an elevation angle of 10° at certain times of the year and at some locations. Application of the method to a two-year set of global SLR data resulted in variance reduction of the residuals by up to 45%, and 3 mm in RMS.

Hamal reported on a joint activity with Chinese groups using multiple wavelength SLR. He described a novel use of a Single Photon Avalanche Detector (SPAD) for sub-centimeter ranging precision in infrared and sub-millimeter precision ranging in the visible region. This optimum configuration was implemented at the Shanghai station. Ranging was done successfully to satellites distances of 30000 km with one-centimeter precision. The results of direct measurements of atmosphere dispersion were compared to existing refraction models.

Sierk gave a lengthy, entertaining and very animated report of the upgrading activities at Wettzell and Conception in an impromptu, unscheduled entry in the session. The brief, 2-slide presentation turned out to be several dozens of slides rolling recollection of every gory detail, of the elaborate steps in upgrading the two systems. At the behest of the anxiously awaiting next presenter, the late Karel Hamal, the chairman had to almost resort to force to put an end to the captivating performance.

Analysis of Multi-Wavelength SLR Tracking Data Using Precise Orbits

H. Mueller

1. Deutsches Geodaetisches Forschungsinstitut, Muenchen.

Contact: mueller@dgfi.badw.de / Fax: +49 89 23031 1240

Abstract

Using precise Lageos-1/2 orbit generated by the DOGS (DGFI Orbit and Geodetic Parameter estimation Software) Package (http://ilrsac.dgfi.badw.de/dogs), multi-wavelength tracking data from Zimmerwald and Concepcion were analysed. We solved for station coordinates and color dependent biases. Some statistics and the history of bias differences for various tropspheric refraction models are shown. Additionally the available full-rate tracking data were analysed to see if there are differences to the biases obtained from the onsite normal points. The results show that the switch from internal to external calibration at Zimmerwald give a significant improvment of the relative biases, mainly from the infrared part. Finally we tried to rate the refraction models from the resulting bias differences.

Introduction

After an email request from Werner Gurtner to investigate if the new calibration scheme for Zimmerwald, Switzerland, since June 21 2006, has improved the quality of the two frequency data, we decided to reprocess all Zimmerwald data for 2005 and 2006 with the new DOGS programme, version 4.07, (Angermann et al. 2004) and strategy.

For the period 2005/06 we solved weekly Lageos-1/2 arcs using the same models as in the weekly position and EOP series. The parameters solved in this weekly arcs are:

- internal arc parameters
- earth orientation parameters
- station coordinates
- weekly biases for selected stations
- for Zimmerwald additionally a colour dependent bias per pass

Analysis

In a first step we looked into the range residual for the two colours, not solving for biases to see if the discrepancy between red and blue range residuals decrease after the calibration change. It is evident, that the range residuals reduced after the change in the Zimmerwald calibration from internal to external. In figure 1 the residuals prior and after the event are plotted. As next test we compared the relative biases between red and blue to see whether we could see an improvement of the data quality, too. In figure 2 the relative biases red-blue are summarized.

Using these results we tried to look for systematic characteristics in the relative biases. Unfortunately we did not see any correlation between bias and elevation resp. atmospheric data. The relative bias between is small after the change in calibration, see figure 3, but the precision is still not good enough to make full use of information contained in the two colors.

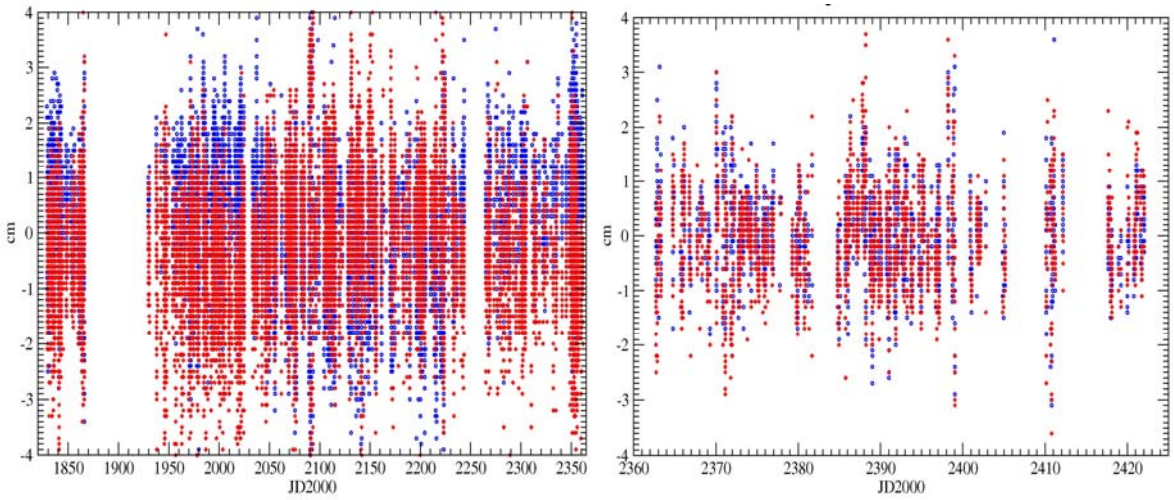

Figure 1. *Lageos-1 range residuals (red and blue Laser) for Zimmerwald*

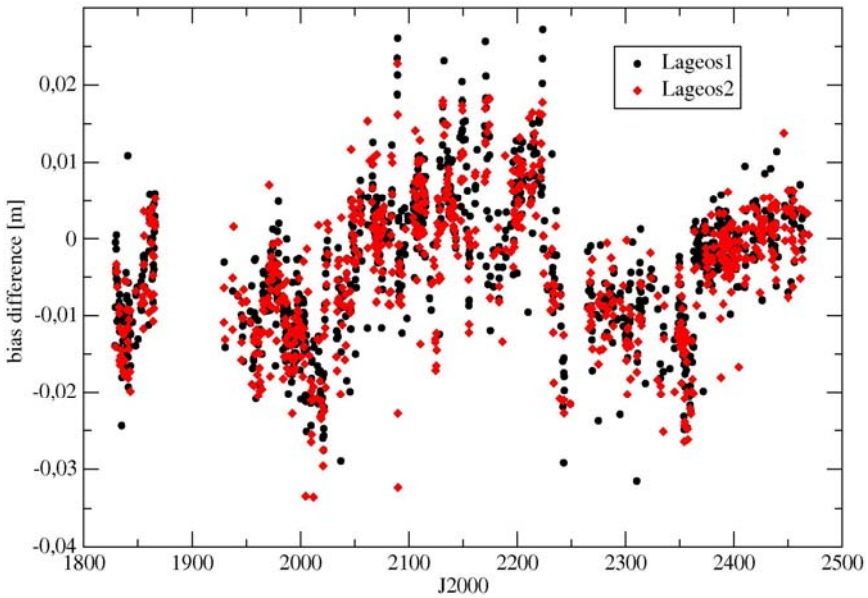

Figure 2. *Relative bias between red and blue Laser (cal. change at 2362.5 JD2000)*

A test to use the full rate tracking data provided for some of the Zimmerwald passes, did also fail because the epochs of the returned pulses are not identical and an interpolation to simultaneous results did not reach the required accuracy.

There is another station, Concepcion in Chile, operated by the TIGO system, which has the capability of two frequency ranging. We also tried to analyse these tracking data, but there is also no evidence of any systematic in the relative residuals. Mainly due to the fact the most of the time TIGO only delivers red wavelength tracking data, see figure 4, for all two-frequency passes available in 2005/06. The only result is that the biases are bigger than the Zimmerwald biases which could indicate that the calibration of the TIGO system is not stable enough because the tropospheric conditions in Chile are not so different to Europe. But there could also be other reasons for that higher noise in the relative biases.

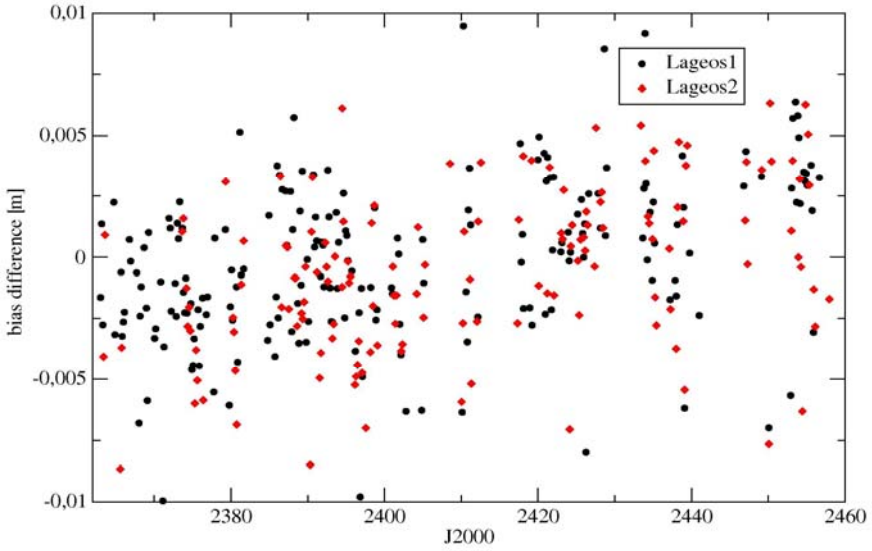

Figure 3. *Relative bias after calibration change for Lageos-1/2*

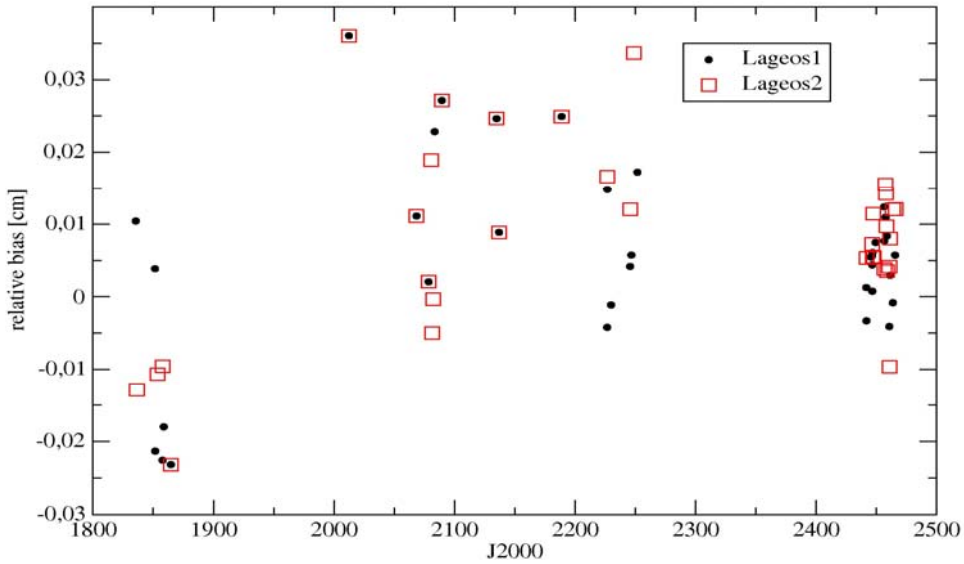

Figure 4. *Relative biases for Concepcion in Chile (TIGO system)*

Analysis of Troposphere Models.

To get at least some results from our computations we tried to see if there is a difference in the relative biases for the presently used Model Marini-Murray and the new Mendes-Pavlis model. There is no direct improvement if we look into the relative biases only, see figure 5. But if we look into the orbital fit, a clear indication that the new Mendes-Pavlis model gives an improvement is the mean weekly r.m.s. fit for the Zimmerwald SLR station which decrease significantly. In figure 6 we see the weekly r.m.s for Lageos-2 for Zimmerwald with solved station coordinates and relative range biases.

Conclusion

The new calibration at Zimmerwald, Switzerland, improved the quality of the two frequency SLR tracking data but there is still not enough precision in the relative biases to make full use of the data. The other two wavelength tracking system TIGO

at Concepcion in Chile has higher relative biases which could be the cause of calibration problems, like the Zimmerwald system.

The new Mendes-Pavlis tropospheric delay model gives, at least for the two frequency systems, an improvement compared to the old Marini-Murray model.

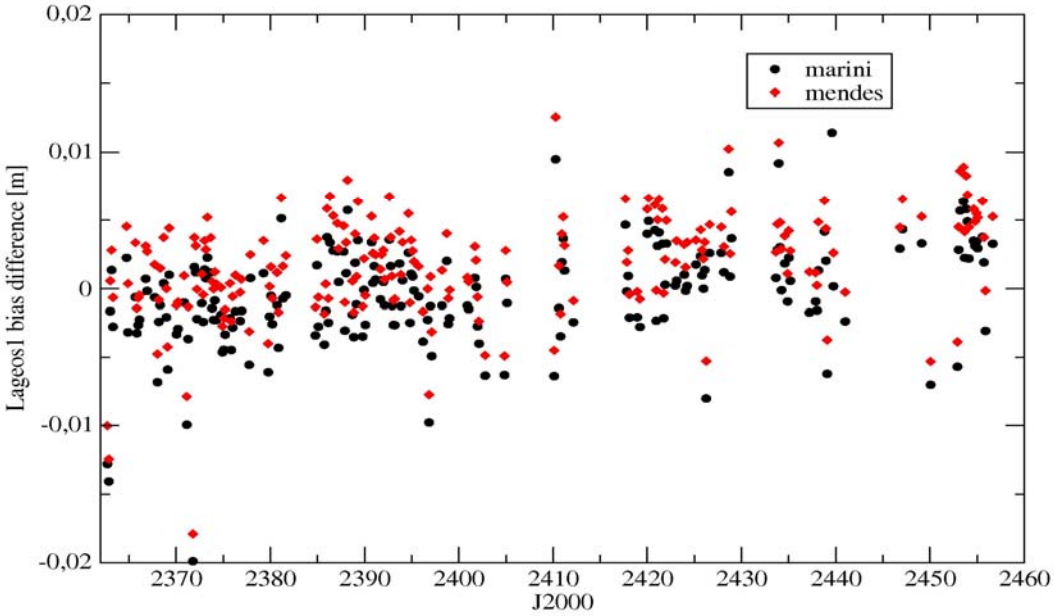

Figure 5. *Relative biases for Lageos-1 using Marini and Mendes refraction model*

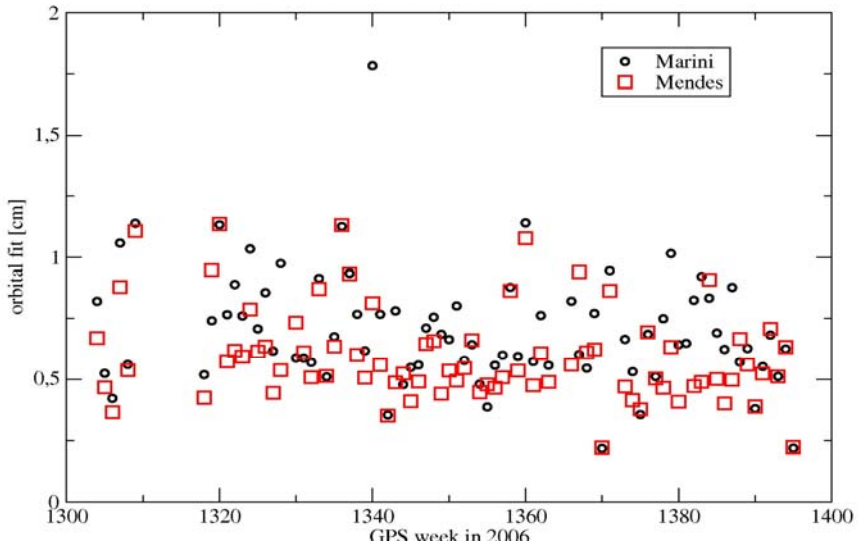

Figure 6. *Mean weekly residuals of Lageos-2 arcs for Zimmerwald*

References

[1] Angermann D, Drewes H, Krügel M, Meisel B, Gerstl M, Kelm R, Müller H, Seemüller W, Tesmer V (2004) ITRS Combination Center at DGFI: A terrestrial reference frame realization 2003, Deutsche Geodätische Kommission, Reihe B, Heft Nr. 313.

[2] Marini, J.W. and C.W. Murray, Corrections of laser range tracking data for atmospheric refraction at elevations above 10 degrees, NASA-TM-X-70555, Goddard Space Flight Center, Greenbelt, MD, 1973.

[3] Mendes, V.B., E.C. Pavlis, High-accuracy zenith delay prediction at optical wavelengths, Geophysical research letters, Vol. 31, 2004.

Improvement of Current Refraction Modeling in Satellite Laser Ranging (SLR) by Ray Tracing through Meteorological Data

G. Hulley and E. C. Pavlis

1. Joint Center for Earth Systems Technology (JCET), UMBC, Baltimore, MD, USA.

Contact: ghulley1@umbc.edu , epavlis@umbc.edu / Fax: +1 410 455 5868

Abstract

The accuracy of current modern space-based geodetic systems such as Satellite Laser Ranging (SLR), Very Long Baseline Interferometry (VLBI), the Global Positioning System (GPS), and satellite altimetry all suffer from limitations in the modeling of atmospheric refraction corrections. The current modeling of atmospheric refraction in the analysis of SLR data comprises the determination of the atmospheric delay in the zenith direction and subsequent projection to a given elevation angle, using a mapping function (MF). Recently a new zenith delay (ZD) model of sub-millimeter accuracy [Mendes and Pavlis, 2004] and a new MF of sub-centimeter accuracy [Mendes et al., 2002] were developed, applicable to the wavelengths used in modern SLR instrumentation.

We have already assessed and validated the new ZD model and MF's using 2-d ray tracing and globally distributed data from the Atmospheric Infrared Sounder (AIRS), the European Center for Medium Weather Forecasting (ECMWF) and the National Center for Environmental Prediction (NCEP). However, the models still remain far from the required sub-millimeter accuracy goal for future SLR analysis standards as set forth by the International Laser Ranging Service (ILRS) based on the requirements place on SLR by the Global Geodetic Surveying System (GGOS) [Pearlman et al., 2005].

To further improve atmospheric delay modeling, we need to look at the application of ray tracing and horizontal refractivity gradients on SLR data collected at the core SLR sites around the globe. We have found horizontal gradient delays of up to 5 cm at an elevation angle of 10° at certain times of year and SLR site locations. The effects of applying ray tracing results, including horizontal gradients to a set of global SLR geodetic data resulted in reduction of the observation residuals by up to 45% in variance, and 3 mm in RMS. This is a highly significant contribution for the SLR technique's effort to reach an accuracy at the 1-mm level this decade.

Introduction

All current models of atmospheric delay for SLR observations assume a spherically symmetric atmosphere, ignoring horizontal gradients in the refractive index of the atmosphere. In order to improve models of atmospheric delay, horizontal gradients in the atmospheric refractive index need to be understood and modeled on a global scale. Currently, ignoring horizontal gradients is the largest source of error in atmospheric delay models for SLR at low elevation angles. We have demonstrated that the contribution of horizontal gradients to the total atmospheric delay is primarily at the few-centimeter level at 10° elevation, and can be as large as 5 cm at certain locations (where SLR stations operate) and times of year. Although centimeter delay corrections seem small, horizontal gradients need to be taken into account because they can lead to significant errors in estimated vertical and to a lesser extent, horizontal station coordinates, which in turn affect the accuracy of the scale and origin of the International Terrestrial Reference Frame (ITRF) [*Altamimi et al.*, 2002].

Presently, we are attempting to develop the infrastructure and enabling science that will allow us to develop future ITRF's with an origin accurate to 1 mm at its epoch of definition and a stability of 0.1 mm/year or better, a tenfold improvement over our current capabilities that are no better than 0.4 parts per billion (~3 mm) in origin stability. Part of this effort requires the improvement of our atmospheric delay corrections to the SLR data with an accuracy of 1 mm or better. In the past, VLBI groups used NCEP fields to calculate refractivity gradients in order to make comparisons with results obtained from their VLBI geodetic data. However, we are entering a new era where global snapshots are available from satellite-borne instruments on a daily basis and at much higher spatial resolution than weather models. We will primarily be using atmospheric profiles from the AIRS instrument on NASA's AQUA Earth Observing System (EOS) platform in order to compute the atmospheric delay by ray tracing and including horizontal refractivity gradient contributions. We also use global data sets from ECMWF and NCEP to supplement, compare, and validate the AIRS results.

Methodology

The optical path length between the tracking station and satellite is defined as the integral of the group refractive index along the path of the ray. We define the atmospheric delay as the difference between the optical path length and the geometric path length:

$$d_{atm} = \int_{ray} n ds - \int_{vac} ds \tag{1}$$

where n is the group refractive index, and $ds = dr/sin\theta$ is a differential element of length along the path of the ray. The subscripts ray and vac in the integral indicate the actual ray path and vacuum path of the signal. If we express the group refractive index in terms of the group refractivity, N

$$n = 1 + 10^{-6} N \tag{2}$$

then the atmospheric delay can be expressed as:

$$d_{atm} = 10^{-6} \int_{ray} N ds + \left[\int_{ray} ds - \int_{vac} ds \right] \tag{3}$$

where the first term represents the excess path delay or velocity error, and the bracketed term is the delay due to the bending of the ray, called the geometric delay (d_{geo}).

By expanding the refractivity, N, in a Taylor's series expansion around the laser site [*Gardner*, 1977], the total atmospheric delay including gradients, can be written as:

$$d_{atm} = 10^{-6} \int_{r_s}^{r_a} \frac{N(r)}{sin\theta} dr + d_{geo} + \left[\int_{r_s}^{r_a} \frac{N_{ns}(r)\rho}{sin\theta} dr \right] cos\alpha + \left[\int_{r_s}^{r_a} \frac{N_{ew}(r)\rho}{sin\theta} dr \right] sin\alpha \tag{4}$$

where θ is the elevation angle at altitude calculated using Snell's law, $\rho = r\phi$ represents horizontal arc distance from the station, r_s is the geocentric radius of the station, and r_a is the geocentric radius at the top of the atmosphere. The third and fourth terms are the contribution to the total delay from horizontal gradients, where N_{ns} and N_{ew} are the North-South (NS) and East-West (EW) components of the horizontal refractivity gradient. The $cos\alpha$ and $sin\alpha$ terms project the NS and EW gradient components onto the azimuth of the observation.

Ray Tracing

The most accurate and comprehensive way of calculating the atmospheric delay is by using a technique known as ray tracing. The computation process is based on geometric optics theory applied over a series of thin spherical shells, concentric with the earth, within which a constant refractivity is assumed. Using Snell's law to calculate elevation changes and horizontal refractivity gradients to calculate azimuth changes along the ray's path, one can trace the ray accurately through the atmosphere in two or three dimensions and calculate the total delay by integrating the incremental delay at each atmospheric layer until the top of the atmosphere using equation (4).

Atmospheric delay modeling has been neglected for decades, with the official model for SLR being that of Marini and Murray [1973], developed in the early 70's. Only in recent years, has an improved ZD model [*Mendes and Pavlis*, 2004] and MF [*Mendes et al.*, 2002] been developed, applicable to the wavelengths used in present day SLR. The new ZD model and MF, called the Mendes-Pavlis (M-P) model, was adopted for the reanalysis of all SLR data from 1976 till present, and in the production of the weekly operational products, beginning January 1, 2007. However, these are still models and the assumption of uniform, spherically symmetric refractive index layers made in their development is unreasonable as it makes the delay only dependent on elevation and not on azimuth. We now have the capability to use atmospheric fields from AIRS that are available at near-real time, twice-daily (day and night), and on a global scale. This enables us to compute the total delay, including gradients, by ray tracing at any elevation and azimuth using real-time atmospheric conditions at any chosen SLR site on the globe. Although ray tracing can be computationally expensive and involves many steps, the results are more physically meaningful than those calculated from delay models, and with the computing facilities available today, the benefits far outweigh the costs. Furthermore, the process can be highly automated at a single, "clearinghouse" type location, with the results disseminated to the users via Internet services and the World Wide Web.

Horizontal Refractivity Gradients

Until now, the contribution from horizontal refractivity gradients to the total atmospheric delay has essentially been ignored in the analysis of SLR data. Previous studies of horizontal gradients (see, for example, *Gardner et al.*, 1978; *MacMillan*, 1995; *Chen and Herring*, 1997) were all based on developing models to account for the gradient delay. We have found these models to be unreasonable in estimating the delay for several reasons: The mapping function used by *Chen and Herring* [1997] ignores higher order terms in the expansion of the continued fraction used in calculating the mapping function, and the development is based on the fact that the gradients have the same direction at all levels in the atmosphere. The model developed by *MacMillan* [1995] includes an extra term, $cot(e)$, that accounts for larger gradient changes at low elevation angles, but the delay becomes infinite at small elevation angles as a result. The *Gardner* [1978] gradient model is dependent on surface gradient values of temperature and pressure, thereby ignoring gradient values at higher altitudes that could introduce significant errors in the magnitude and sign of the gradient delay.

We calculate the gradients in a more direct and accurate way by ray tracing using the third and fourth terms in equation (6) combined with atmospheric profiles from AIRS, ECMWF, and NCEP. Our initial results show that the largest gradient variations occur as a result of seasonal and diurnal changes. Stations situated in mountainous regions,

such as McDonald, TX and Monument Peak, CA had larger horizontal pressure gradients, while stations in close proximity to large bodies of water such as Yarragadee, Australia, had larger horizontal temperature gradients. No significant non-hydrostatic (wet) gradients were found, with maximum wet delays only reaching a few tenths of a millimeter during the summer at Greenbelt, MD. Maximum NS gradient delays of up to 5 cm were found at Yarragadee and Herstmonceux, UK, at an elevation angle of 10°, while standard deviations ranged from 6-12 mm depending on location and time of year. The EW gradients were smaller in magnitude and variability than the NS gradients.

Results

We now look at the impact of using ray tracing with AIRS, ECMWF and NCEP data on the analysis of a set of real SLR data for the geodetic satellite LAGEOS 1 during 2004 and 2005 and for 10 of the globally distributed core SLR stations. We analyze our results by looking at the RMS and variance percent difference between the 'corrected' SLR residuals with the atmospheric delay estimated by ray tracing and including horizontal gradients, and the 'original' residuals, that use the M-P model for calculating the atmospheric delay. The total number of observations used in the statistics for all stations is 47664. Positive values of RMS and variance indicate improvement in the results.

The results when including the gradients in Figure 1 (i.e. delay = model + gradients) show that the residual variances when using AIRS data are reduced by up to 10-15% in variance when only gradient corrections are applied. ECMWF and NCEP results also show improvement with residual reductions ranging from 5-10%. AIRS ray tracing results had a greater improvement in RMS and variance when compared to

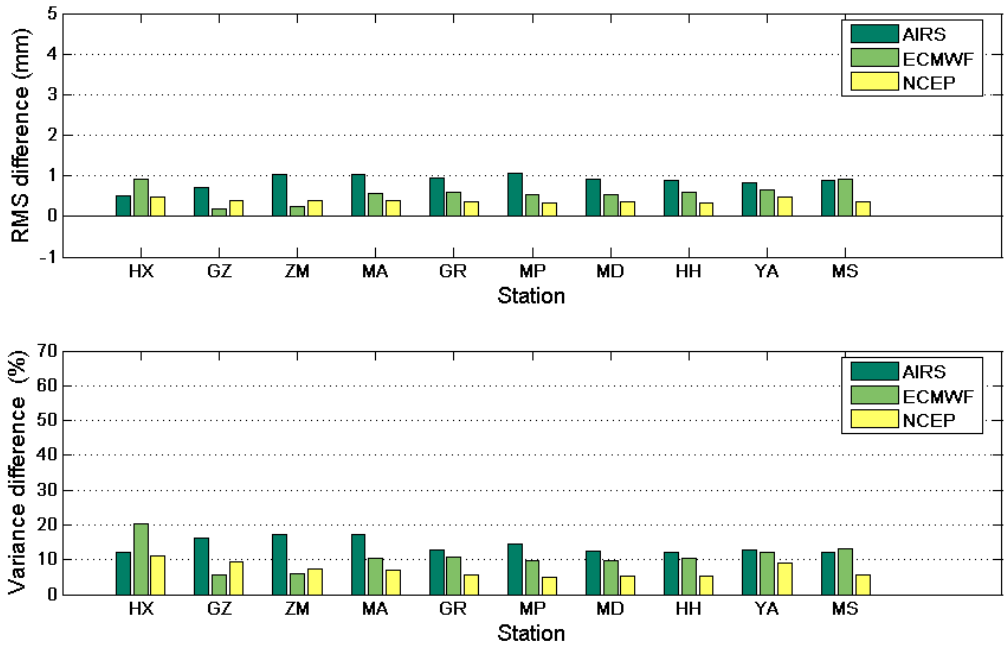

***Figure 1**. RMS (top) and variance (bottom) differences between the original residuals (model) and the gradient-corrected residuals (model + gradients) for stations: HX (Herstmonceux, UK), GZ (Graz, Austria), ZM (Zimmerwald, Switzerland), MA (Matera, Italy), GR (Greenbelt, MD), MP (Monument Peak, CA), MD (McDonald, TX), HH (Hartebeesthoek, South Africa), YA (Yarragadee, Australia), and MS (Mt. Stromlo, Australia).*

NCEP and ECMWF results for all stations. This can probably be attributed to the higher resolution of the AIRS data, providing the ability to calculate the gradients on a much finer scale.

When the total correction is applied (i.e. delay = ray tracing + gradients) with no dependence on the model, the NCEP results actually show larger improvements than AIRS and ECMWF (Figure 2). However, it is interesting to note that there are instances where we see negative RMS differences for NCEP at Herstmonceux, Graz and Greenbelt, even though the corresponding variances show improvement. This is most likely due to either a large positive or negative bias in the mean of the corrected residuals. There is an overall greater improvement in the results when the total correction is applied, and this can be seen as an increase in variance percent difference from Figure 1 to Figure 2. However, at Yarragadee and Mt Stromlo, AIRS total correction actually does slightly worse than the gradient correction. AIRS variances decrease from 12.8% for the gradient correction, to 12.4% for the total correction at Yarragadee and from 12.3% to 9.8% at Mt Stromlo. High AIRS variabilities in boundary layer pressure and temperatures on the interface between land and ocean at these stations could be a factor in this case.

Summary and future plans

Our current and near-term plans are to improve and generalize our 3-d ray tracing process and to include as many sources as presently available. In a second step, we plan to establish an automated daily service for all SLR-tracked targets with high-accuracy requirements (i.e. those used for the ITRF, sea-level monitoring, etc.), and provide the community with value-added data sets including these improved atmospheric delay corrections.

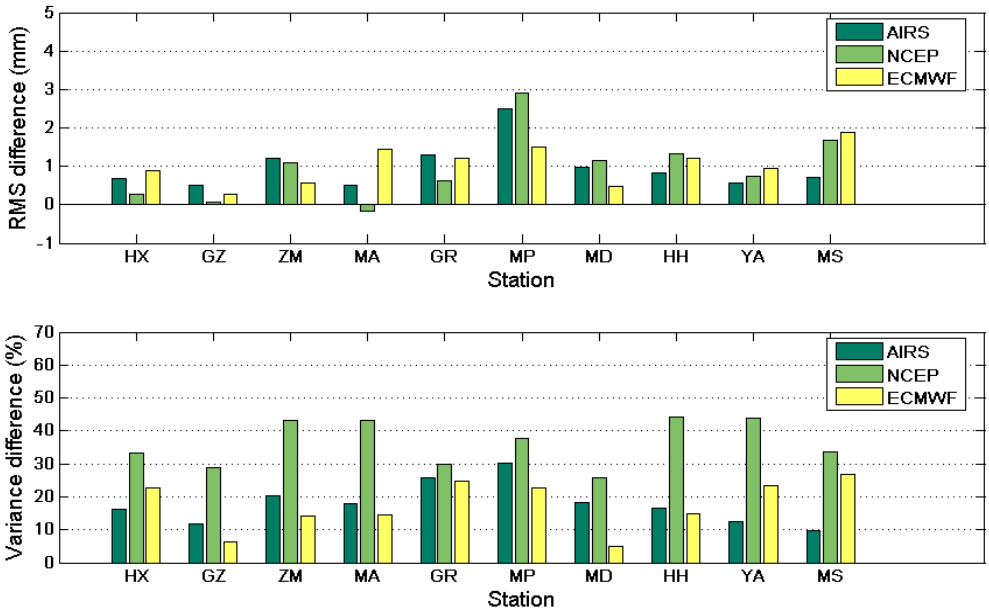

Figure 2. *Differences between the original residuals (model) and the total-corrected residuals (ray-tracing + gradients).*

References

[1] Altamimi, Z., P. Sillard, and Claude Boucher (2002), ITRF2000: A new release of the International Terrestrial Frame for earth science applications, *J. Geophys. Res.*, *107*, NO. B10, 2214, doi:10.1029/2001JB000561

[2] Chen, G.E. and T.A. Herring (1997), Effects of atmospheric azimuthal asymmetry on the analysis of space geodetic data, *J. Geophys. Res.*, *102*, pp. 20,489-20,502.

[3] Gardner, C.S. (1977), Correction of laser tracking data for the effects of horizontal refractivity gradients, *Appl. Opt.*, *16*, *No. 9*, pp. 2427-2432

[4] Gardner, C.S., J.R. Rowlett, and B.E. Hendrickson (1978), Ray tracing evaluation of a technique for correcting the refraction errors in satellite tracking data, *Appl. Opt.*, *17*, *No. 19*, pp. 3143-3145

[5] MacMillan, D.S. (1995), Atmospheric gradients from very long baseline interferometry observations, *Geophys. Res. Lett.*, *22*, pp. 1041-1044.

[6] Marini, J.W., and C.W. Murray (1973), Correction of laser range tracking data for atmospheric refraction at elevations above 10 degrees, *NASA Rep. X-591-73-351*, Goddard Space Flight Cent., Greenbelt, MD

[7] Mendes, V.B., G. Prates, E.C. Pavlis, D.E. Pavlis, and R.B. Langley (2002), Improved Mapping Functions for Atmospheric Refraction Correction in SLR, *Geophys. Res. Lett.*, *29*(10), 1414, doi:10.1029/2001GL014394.

[8] Mendes, V.B., and E. C. Pavlis (2004), High-Accuracy Zenith Delay Prediction at Optical Wavelengths, *Geophys. Res. Lett.*, *31*, L14602, doi:10.1029/2004GL020308.

[9] Pearlman M., and Coauthors (2005), Global geodetic observing system - Considerations for the Geodetic network infrastructure, 2005 IAG/IAPSO/IABO Joint Assembly, Cairns, Australia, August 22-26

Two-Color Calibration of The Zimmerwald SLR System

W. Gurtner, E. Pop, J. Utzinger

1. Astronomical Institute, University of Bern.

Contact: gurtner@aiub.unibe.ch

Abstract

The current and the preceding Zimmerwald SLR systems have used internal, near-realtime calibration with apparently good success. The addition of the second wavelength (infrared) to our system revealed, after some time of routine operation, differences between the calibrated ranges of the two colors that could not be explained with errors in the applied refraction models. It turned out that the internal calibration values of the infrared chain showed variations that had not much to do with system calibration. The source of these variations could not be identified. In June 2006 we switched to external calibration by necessity.

Introduction

The 1-meter Zimmerwald satellite laser ranging system, installed in 1997, has been designed for two-color ranging right from the beginning. In order to have two wavelengths with suitable sensors and reasonable reception signal power at our disposal we chose a Titanium-Sapphire laser with the primary wavelength at 846 nm (near infrared) and the second harmonic at 423 nm (blue).

As receivers we are currently using a compensated SPAD at 423 nm and a Hamamatsu H7422P-50 photomultiplier at 846 nm. The time walk of the latter is compensated using an empirical correction table in function of the measured return pulse energy.

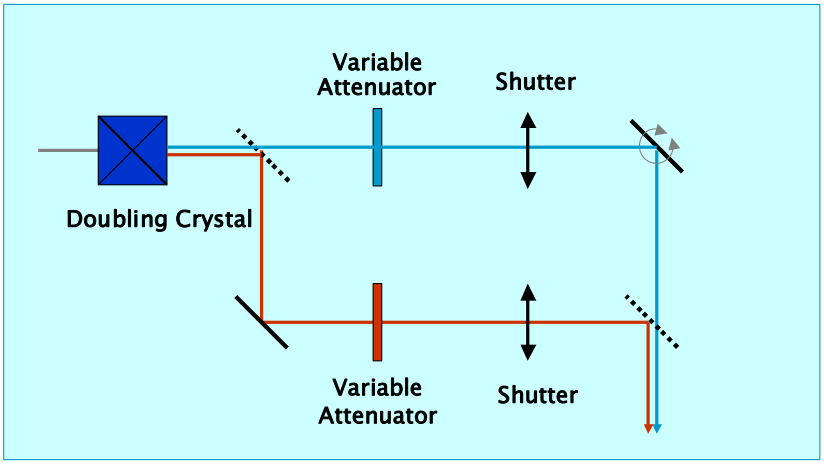

Figure 1: *Transmit path: Individual attenuation*

Single-shot precision is of the order of 60 ps in blue and 150 ps in infrared.
The optical paths to and from the telescope have been optimized for transmission for the two wavelengths. The two beams can be individually attenuated, both in the transmit as well as in the receiving path.

At the International Laser Ranging Workshop 2002 in Washington we reported (Gurtner, 2002) first results of dual-wavelength operation. We concluded;

- *The average difference between infrared and blue residuals per pulse is between 0 and 0.05 ns after a Marini-Murray refraction correction using onsite surface met values.*
- *Apart from the above mentioned tendency we could not yet detect any systematic behavior of the differences so far.*
- *The differential Marini-Murray refraction corrections between 423 and 846 nm seem to be better than < 10 mm.*
- *However, there could still be range biases between the two reception channels of the same order of magnitude.*

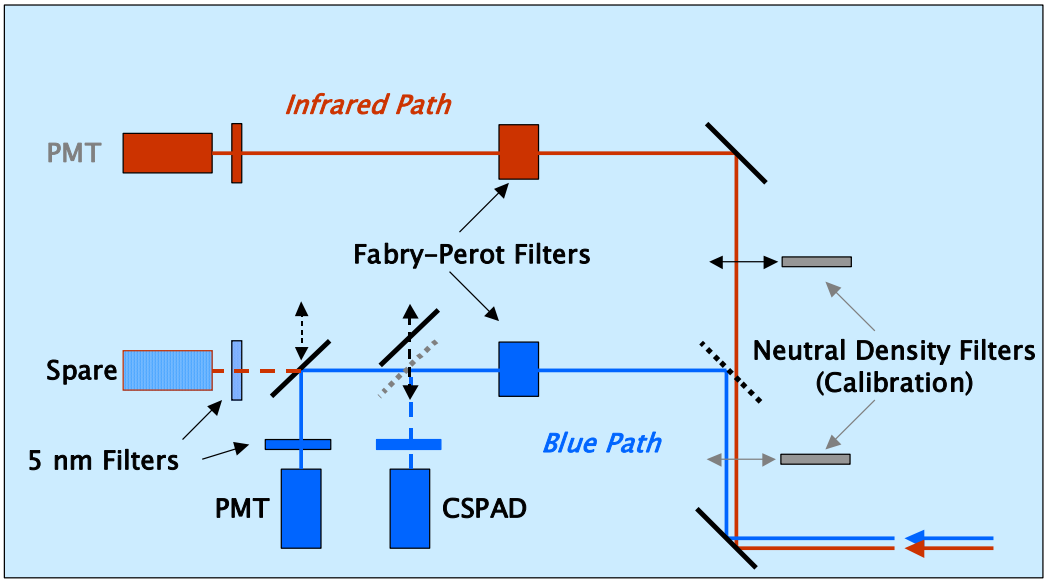

Figure 2: *Receiving path: Separation of the two colors*

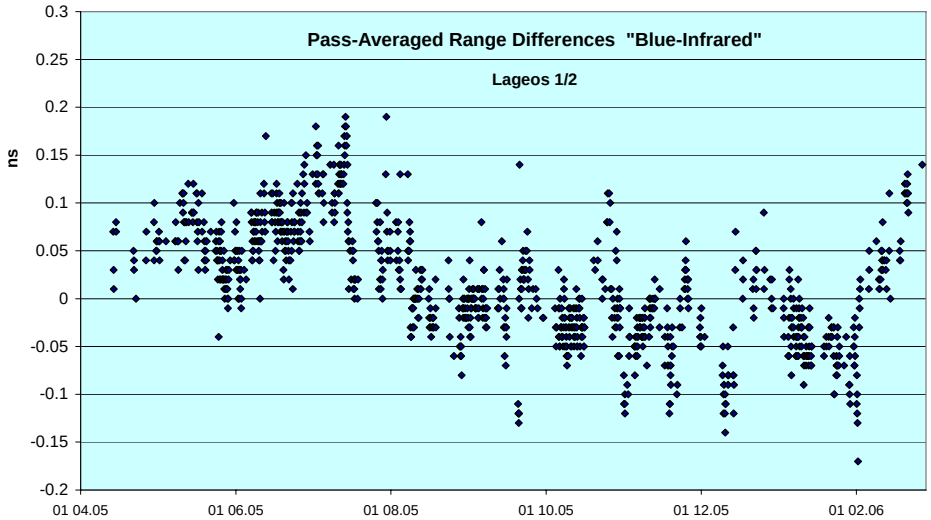

Figure 3: *On-site-determined differences blue-infrared*

Slowly Varying Systematic Differences

In the meantime, however, the refraction-corrected pass-average differences between the two colors showed slowly varying systematic effects that have nothing to do with remaining errors in the applied refraction corrections. These variations could be seen

in on-site generated differences (Figure 3) as well as in the pass-averaged residuals of global analyses performed by ILRS analysis centers (Figure 4). These variations were as large as plus and minus 2 cm!

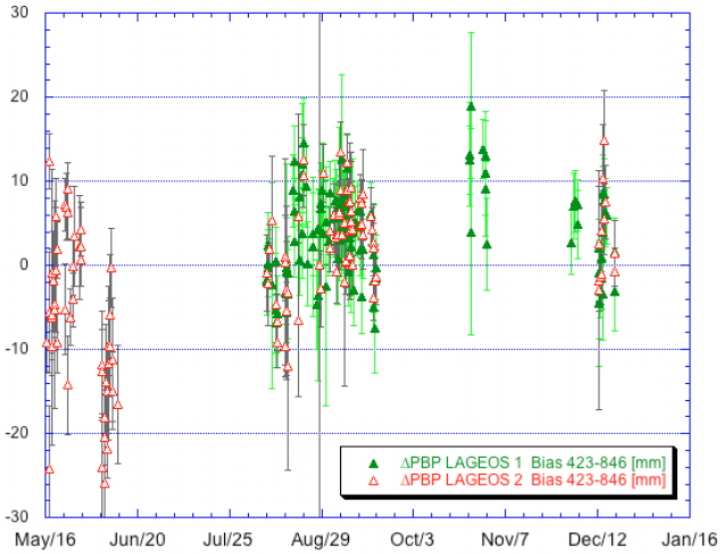

Figure 4: *Pass-averaged biases between blue and infrared (JCET analysis center, 2004)*

A closer investigation showed that these inter-color bias variations highly correlated with the calibration values used to correct the infrared ranges to the satellites (Fig. 5).

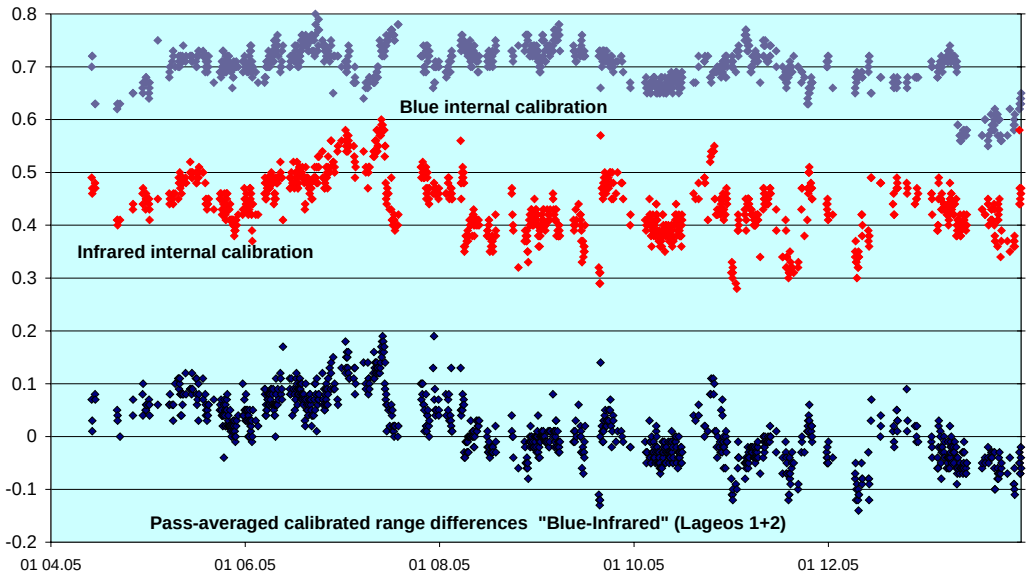

Figure 5 : *Time series of internal calibration values and inter-color biases*

It can be clearly seen that the time series of the infrared calibration values (middle series, covering about 10 months from April 2005 to February 2006) shows the same features as the pass-averaged calibrated range differences between blue and infrared.

The standard calibration procedure used so-called internal calibrations: During the satellite passes, interleaved with the ranging to the satellites, flight time measurements of a weak calibration beam extracted from the main laser pulse and sent through an internal path of known length are performed to keep track of small changes in the

system behavior (e.g. temperature changes) leading to errors in the measured satellite ranges.

The differences between the calibrated ranges (corrected for tropospheric refraction) to the satellites in the two colors should then only contain biases from residual errors in the tropospheric corrections and the applied calibration values, and various random errors from the measurement procedures. The fact that we see slowly varying inter-color biases correlated with the infrared calibration lets us assume that there is a problem with the respective calibration procedure.

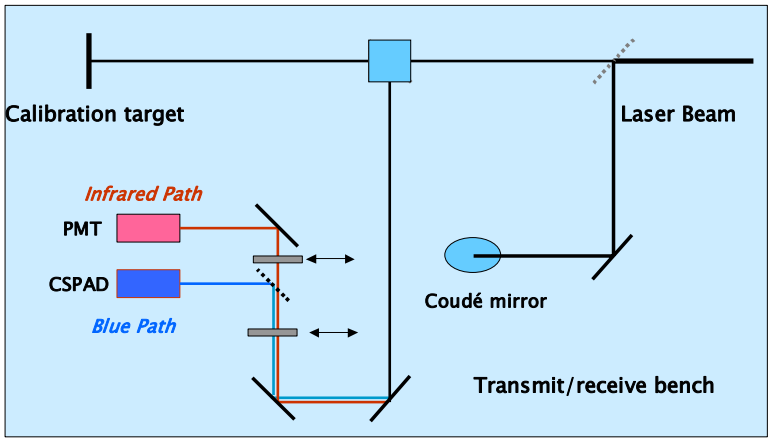

Figure 6: *Internal Calibration*

Occasionally we also perform calibration observations to an external target at about 600 m distance. Figure 7 shows time series of separate internal and external calibration sessions for infrared over the same 10 months and again the pass-averaged differences of calibrated blue-infrared satellite ranges. It is obvious that the external calibrations do not show the same variations.

A possible reason for the problem with the internal calibration (in infrared) could be the behavior of the respective Stanford counter at the very short time of flight (a few tens of nanoseconds). However, a comparison between the two counters used in the two receiver chains (blue and infrared) and the newly purchased A032ET event timers

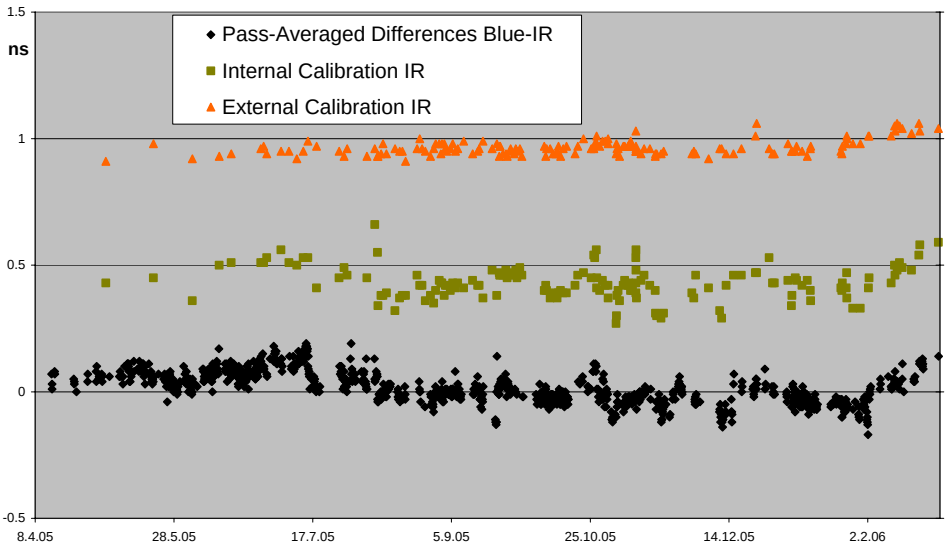

Figure 7: *Internal/external calibration, inter-color biases*

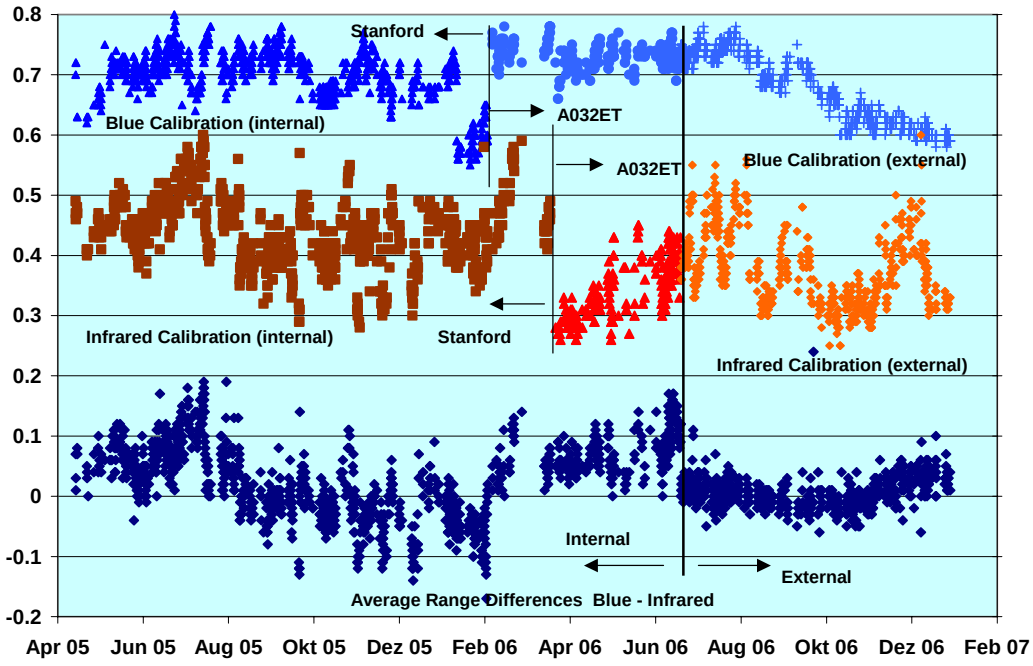

Figure 8: *Calibrations, inter-range biases*

did not reveal anything suspicious. The later replacement of the Stanford counters by the event timers in spring 2006 did not solve the problem either.

Consequently we decided to replace the internal calibration procedure by calibrations to the external target. We modified the observation procedures accordingly: The scheduler inserts now approximately every half hour a short calibration session into the satellite passes.

Figure 8 shows now the behavior of the inter-color biases before and after the modification of the calibration procedures on June 21, 2006. The variations (bottom time series in the Figure) became significantly smaller. There still seems to be a small signature in the time series. We will have to closely monitor these differences and hopefully be able to later correlate these variations with some system parameters.

References

[1] Gurtner, W., E. Pop, J. Utzinger, “Zimmerwald Dual-Wavelength Observations: First Experiences”, 13th International Workshop on Laser Ranging, Washington D.C, October 7-11, 2002

Multi Color Satellite Laser Ranging At Czech Technical University

Karel Hamal[1], Ivan Prochazka[1], Josef Blazej[1],Yang Fumin[2], Hu Jingfu[2], Zhang Zhongping[2], Hiroo Kunimori[3], Ben Greene[4], Georg Kirchner[5], Franz Koidl[5], Stephan Riepfel[6], Werner Gurtner[7]

1. Czech Technical University in Prague, Brehova 7, 115 19 Prague 1, Czech Republic
2. Shanghai Observatory, People Republic of China,
3. CRL, Japan,
4. EOS, Australia,
5. Graz Observatory, Austria
6. Wettzell Observatory, Germany
7. Zimmerwald Observatory, Switzerland

Abstract

We are reporting on our activity on Satellite Laser Ranging (SLR) using multiple wavelengths. The reasons for simultaneous multi-frequency laser ranging of artificial Earth satellites are discussed. Atmospheric dispersion study and the eye-safe wavelength region are both considered. To detect the returned signal, the Single Photon Avalanche Detector (SPAD) is operated in so-called Geiger mode. The silicon, germanium, and gallium arsenide phosphide based SPAD are used depending on wavelength to cover nearly the entire optical region having the single photon response, temporal resolution better than 120ps FWHM, and quantum efficiency of about 15%. The active area size and the compact design of the detector packages permitted their application in satellite laser ranging yielding sub-centimeter ranging precision in infrared and sub-millimeter precision ranging in the visible region. The active area of the detector used is from 100 to 200 µm. Detectors for the visible region are cooled thermo-electrically and detectors for infrared, based on germanium, are cooled cryogenically with a custom design liquid nitrogen Dewar. The design and diagnostics of a hydrogen Raman-shifted picosecond Nd:YAG laser operated at 10 Hz repetition rate are presented. Both the far-field beam structure and temporal picosecond pulse profile are monitored for different laser configurations. The optimum laser configuration has been implemented to the SLR station in Shanghai for two color ranging. To operate the SLR station in Graz in visible range, three color ranging is accomplished by Nd:YAG SHG 532 nm, the first Stokes Raman at 682 nm and the first anti Stokes at 432 nm using Hydrogen. To operate the eye safe SLR in Tokyo at the 1540 nm wavelength, the laser was operating at 1064 nm to pump the first Stokes at 1540 nm using methane. To operate the SLR in Bern and Wettzell (move to Chile) Titanium-Sapphire based laser has been operating at 852 nm and SHG 426 nm. The color set has been established at the Shanghai observatory since 2004. The ranging has been successfully accomplished for retro-reflector equipped satellites up to a distance 30000 km with one centimeter precision. The results of direct measurements of atmosphere dispersion are presented and compared existing atmosphere models.

Introduction

We have the experience in field of SLR since the seventies of last century. To range satellites or Moon one has to consider several “contributors” to the overall accuracy of the SLR measurement chain: the station itself, satellite retroreflector array, and the atmosphere as well. Current SLR technology aims toward millimeter accuracy. From the point of view of the SLR station, rms of the laser pulse duration, Start and Stop detectors rms and the Event Timer jitter are involved. Related to the atmospheric dispersion, the existing models are not yet explaining the contribution at millimeter

accuracy level. The SLR at different wavelengths might help to understand the atmospheric mapping function down to millimeter and consequently sub-millimeter level. In fact, multi-color SLR is a unique method for overall optical path dispersion model direct verification.

Experiment arrangement

Assuming the atmospheric dispersion, to find the right laser for multiple wavelength millimeter SLR, one can consider the Nd:YAG / SHG / THG, Nd:YAG / SHG / Raman First Stokes / First antiStokes in hydrogen, Nd:YAG / SHG / Raman First Stokes in methane and the Titanium Sapphire Fundamental / SHG, all of them at different repetition rates. The basic of Raman conversion is described by eq. 1.

$$\frac{1}{\lambda_{shifted}} = \frac{1}{\lambda_{pump}} + k \cdot \nu_R \text{, where } k \in \left(-\infty, -1\right\rangle \cup \left\langle 1, \infty\right) \quad (1)$$

Where λ is symbol for the wavelength and ν is material constant describing Raman shift for the selected gas. For hydrogen it is 4155 cm^{-1}, for methane 2914 cm^{-1}, and for deuterium 2987 cm^{-1}.

The selection of the laser transmitter concept is influenced by the required reliability in the routine field operation. Considering that the 6 picoseconds round trip time corresponds to one millimeter range, therefore to reach the millimeter goal, the acceptable laser pulse width within the range of 10 to 50 picoseconds is desirable. The experiment energy budget requires the energy in one pulse in order of several tens of millijoules. The selection of the right wavelength pair is determined by the atmospheric dispersion mentioned above, by atmosphere transparency, and by the availability of high effective frequency shifters. In principle it is difficult to use to independent lasers due to the required picosecond synchronization.

The available detectors have to be considered. Our laboratory has long term experience in the field of picosecond temporal resolution solid state detectors[1]. For the visible range we did examine mainly silicon based SPADs, for the eyesafe SLR Germanium based SPADs. The silicon one can be operated at thermoelectrically cooling temperature. The germanium based cooled detector is suitable for eyesafe wavelengths; however it has to be cooled by liquid nitrogen. Using the Quantel YG580 Laser 30 mJ / 1.06 μm, 35 ps, different Raman tubes filled by Hydrogen at different pressure, different focusing lens, we were getting 8 mJ / 0.68 μm, 1 mJ / 0.45 μm. Considering the eyesafe SLR using Raman shift in methane from fundamental we were getting 3 mJ / 1.54 μm.

Conclusion

We are presenting a review of our activities on multiple color SLR and recent results from Shanghai SLR observatory[2]. The selection of the right wavelength pair is discussed and together with our experience with available and effective frequency shifters selection and tuning. The multiple color laser transmitter based on Nd:YAG picosecond laser generating the second harmonic frequency and the Raman Stokes and anti Stokes frequencies is dedicated for the new Shanghai SLR station, the part of Western Pacific Laser Ranging Network.

References

[1] Procházka, I., Hamal, K., Sopko, B.: ”Recent Achievements in Single Photon Detectors and Their Applications”, Journal of Modern Optics. 2004, vol. 51, no. 9-10, pp. 1298-1313. ISSN 0950-0340.

[2] Hu, Jingfu, Yang, Fumin, Zhang, Zhongping, Hamal, K., Prochazka, I., Blazej, J.: ”A Raman laser system for multi-wavelength satellite laser ranging”, Science in China Series G: Physics and Astronomy. 2004, vol. 47, no. 6, pp. 737-743. ISSN 1672-1799

TELESCOPES, STATIONS AND UPGRADES SESSION SUMMARY

Chair: Craig Smith

The session on telescopes, systems and upgrades demonstrated that the field of satellite laser ranging (SLR) is healthy and growing. Speakers during the session described a wide range of new and refurbished SLR instruments all over the globe.

Probably the most ambitious project described came from the Russian Federation where 6 new SLR systems have recently been completed and there are plans to build up to a further 15 stations by 2010, all in support the upgraded Glonass Global Navigation System (GNS).

Not to be outdone, we heard from NASA and US Contractors about a revitalized SLR program that has returned a number of stations to operations (TLRS3 and 4) as well as maintenance and development of the MOBLAS network. SLR 2000 development has also been continued.

Not to be outdone by Russia or the US, China too has entered a new era of significant SLR development as contributions to the Galileo GNS has spurred on rapid SLR activity in this country too. Excellent presentations were provided about a new SLR station built in San Juan, Argentina, as well as significant upgrades to existing stations at Yunnan, Changchun and Shanghai SLR Observatories.

SLR work however, is a global enterprise and from France we heard that after 30 years of operations the old SLR station (7835) at Grasse has been decommissioned. This station has been replaced by new and more capable systems FLTRS and MEO, whilst the old telescope will find new life as an SLR telescope in Matjiesfontein, South Africa. Plans were also presented for new SLR network in South Korea.

We look forward to hearing about the progress of all these ambitious projects and exciting developments at the next ILRS workshop.

Grasse laser stations in evolutions to future and technological developments

F. Pierron[1], E. Samain[1], JM Torre[1], M. Pierron[1], M. Furia[1] and the Grasse laser staff

1. Observatoire de la Côte d'Azur, GEMINI/UMR 6203-CNRS, Av N. Copernic, 06130 Grasse, France.

Abstract

A very important project in term of buildings and technology for telescopes, mount and dome has been started at the Grasse Observatory since September 2005.

A new laboratory has been built in place of historical SLR fixed station (7835) to receive mobile SLR system (FTLRS) for upgrade, development and operations between field missions.

The current LLR station (7845), renamed MeO (for Metrology and Optics), is being completely rebuilt to track and range in the future from "Low Earth orbiting satellites" to the Moon and even further to support new missions in the solar system. The project status will be reported in this presentation with both technological issues and new potentialities for such installations at Grasse.

Introduction and short report 1980-2005 period

The Grasse LLR system with a large and accurate 1.5 meter telescope got first moon returns in 1982.

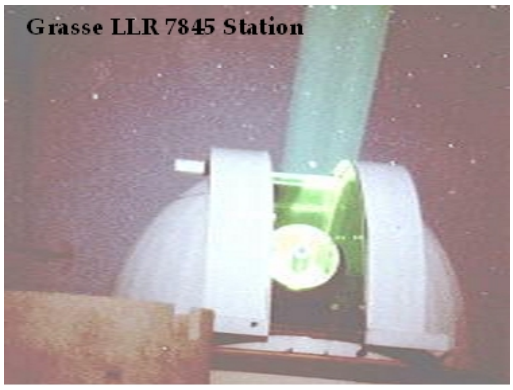

In this configuration (0.2 Hertz ruby laser with 3 nanoseconds pulses), 1166 normal points have been acquired in 5 years with an RMS of about 20 centimeters.

In 1987 a major upgrade was achieved on this system with a new Yag laser (10 hertz-300 ps pulses) and timing system (Dassault event timer).

During this very operational period, about 8500 npts (65% of the global network) were acquired with an rms of 3 cm and a stability at some millimeters level.

The station stopped in summer 2005 for new developments described below in this paper.

This very efficient SLR system installed at Grasse observatory in 1975 at 30 meter from the LLR system tracked in thirty years about 35000 satellites passes.

The quality and quantity of data over the years of this core station is very impressive and scientific community can thanks a lot observers, engineers and scientists involved in this process very consuming in term of manpower.

The station stopped definitively his activity in summer 2005 to involve laser staff in new evolution for SLR/LLR activity.

Historical SLR station definitively stopped, waiting South Africa collaboration

In September 2005, telescope and mount were dismantled and temporarily installed in the old trailer waiting new future abroad.

In fact for some years, South African colleagues are promoting an LLR/SLR development for this country in collaboration with global scientific community.

OCA/CNES/GRGS proposed to participate to this venture in putting this one meter telescope at South African geodesists disposal. Of course the mount and mechanical devices of this system will have to be refurbished (encoders, drive motors, coude mirrors etc.) and a budget is already planned by this partner for renewing this telescope/mount at HartRAO.

In the context of this interesting project in South Hemisphere a new site has been found in a very favorable place for SLR/LLR activity in term of meteorological conditions. We can see here on the next photo, this future site for Space Geodesy Observatory near Matjiesfontein at about 250 km north of Cape Town and 70 km south of GFZ Geodynamics Observatory and South African Astronomical Observatory.

After some administrative agreements in progress, OCA 1 meter telescope/mount should be shipped to South Africa before summer 2007.

Future site for Space Geodesy Observatory in South Africa

1 meter Telescope/mount in trailer at OCA in 2006

New laboratory for FTLRS developments and operations built in place of old telescope :

Just in the place of old one meter telescope, we built a new laboratory perfectly suited to host mobile system between fields campaigns.

The configuration of the setup has very original features.

The group laser /mount /telescope is installed on a platform elevator with two possible positions:

-One down in the laboratory to achieve technological developments tuning and maintenance in good conditions (left picture).

-The other one 1.40m higher (right picture) with the roof open and the telescope able to view the sky and to achieve operations on satellites in normal conditions with operator control facilities inside the building.

The reference point of the station in high position has been designed to be very stable and repetitive at better that one millimeter level. In this observation place, the station is no more supported by but lie on a metallic square embedded in the roof concrete, such a way the platform can be down in this phase**.**

For the campaigns setup the group laser/mount/ telescope is took off from the special support fixed on the elevator in the laboratory and installed in the tripod which can be easily packed for shipping and deployed on site to the concrete pad.

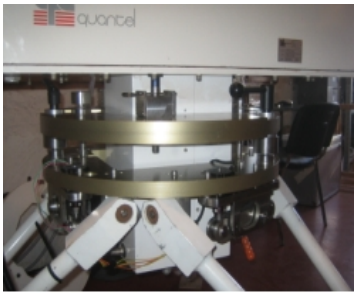

New devices (electric jacks software controlled) to easily adjust leveling in automatic mode have been developed. This new facility is very important to assist local observers with remote control capability during outside campaign.

Ftlrs in campaign configuration – Ajaccio 2005

LLR Station renamed to MEO and completely rebuilt

In summer 2005 we stopped temporarily the old LLR station in order to modernize and to imply it in more goals (science programs and technology).

This important project in term of funding and manpower implied for design and buildings had been prepared for three years with detailed technical studies and looking in the future for emerging new projects on next 20 years.

The main idea is to have flexibility in different configurations :

- **A new generation of Laser Ranging station**
  – From 400 km to the Moon
  – One Way Interplanetary mission
  – Highly Automatic
- **Research & Development facility**
  – New optical links
  – Time transfer experiments
  – One Way Interplanetary missions
  - Detection, Event Timer

A. Telescope/mount

In the future, the mount will be able to have a speed compatible with SLR on lower satellites and this is a very strong constraint on such an heavy system.

We decided to install in this new design powerful and precise direct torque motors on the axes in such a way to have speed multiplied by an important factor .

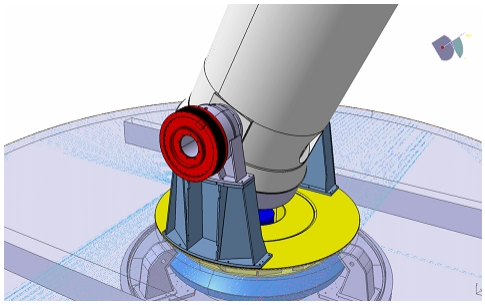

Nevertheless, the pointing accuracy remains an important challenge especially to range moon and future spacecrafts in solar systems.

The quality of the encoders installed on the axes and the mechanical stability of the whole setup are been carefully designed and should lead to an absolute pointing accuracy below 1 arc second.

B. Dome

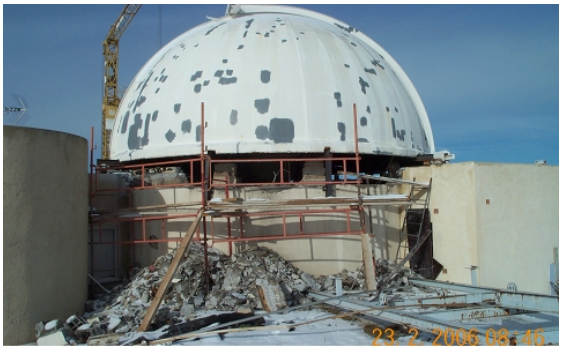

Similar constraints are applied on the dome and in order to remain compatible with mount speediness a lot of modifications are today achieved.

This dome is twenty five years old today and at this occasion the Observatory workshops undertook heavy maintenance works on metallic structures to hope reliable operations in future.

C. Laser and focal laboratories

To track both moon and HEO satellites, two lasers systems in different rooms were operated the past years (Quantel with 300ps and BMI with 20 ps).

A very important work and new design have been achieved to combine both lasers on a single bench with three capabilities

- 800 mJ in 10ns at 10 Hz
- 250 mJ in 300ps at 10 Hz
-250 mJ in 14 x 20ps at 10 Hz

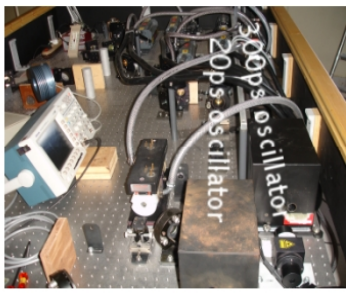

The last configuration with 14 pulses of 20 ps is a very original design to range the moon very accurately comparable with current SLR systems and achieving a return rate similar to previous configuration (single pulse of 300 ps).

In future, at least **3 focal laboratories** will be installed under the telescope to have different R&D experiments and routine operations accessible with a fast and easy mirror switch on the coude.

Conclusion

- **SLR fixed station (7835) stopped in june 2005**
  - 30 years of fruitful operations
  - Telescope and mount moved in the trailer waiting eventual collaboration abroad

- **New laboratory build in this place for FTLRS**
  - Two position capability with elevator system and opening roof
    - Technology developments
    - Operation on satellites to Lageos.

- **Old LLR Station renamed to MEO and completely refurbished.**
  - Earth satellite capability 800 to 36000 km Moon reflectors.
  - R&D studies and new experiments (Time transfer, transponder…).

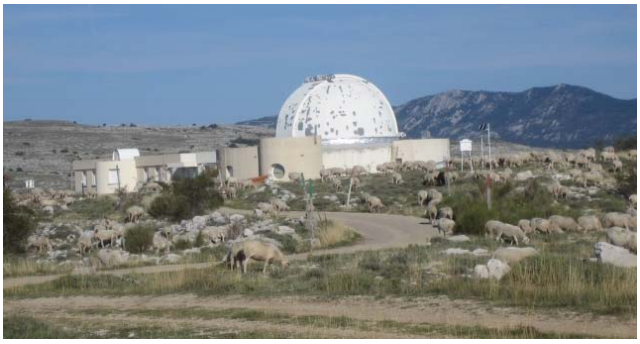

- **New SLR facilities in 12/18 months**
  - Two observing systems (0,13 and 1,50 m telescopes) occasionally collocated.
  - Fields campaign for FTLRS (maximum 6 months/year).

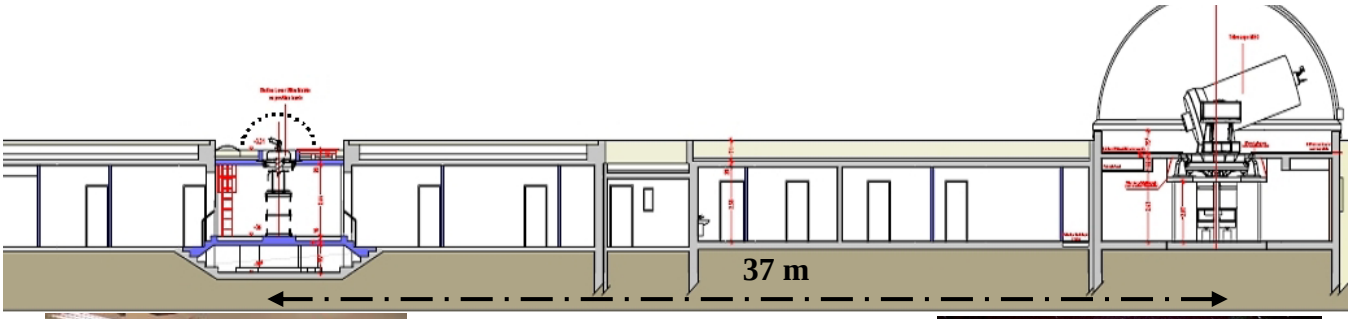

New Russian Systems for SLR, Angular Measurements, and Photometry

V.B. Burmistrov, N.N. Parkhomenko, V.D. Shargorodsky, V.P. Vasiliev

1. Institute for Precision Instrument Engineering, Moscow, Russia.

Contact: www.niipp-moskva.ru

Abstract

A brief description is presented of two novel-type stations providing satellite laser ranging, angular measurements, and photometry (in reflected sunlight), recently developed in the Institute for Precision Instruments Engineering (IPIE). Putting the stations in operation will expand the Russian Laser Tracking Network to six stations.

Compact station

The compact station with two 25-cm diameter optical systems (the first one used for transmission/reception of laser ranging signals, and the second one for angular measurements and photometry) has the following design features:

- The weight of any single unit of the system (in package) does not exceed 50kg, with system total weight less than 300kg. Thus, no special lifting mechanisms are needed for installation.
- An autonomous cover for the optical unit and mount allows installation on a small pier, without erection of a special fixed tower.
- Low power consumption (≤2.5 kW) allows supply from single-phase mains or from a portable power generator.
- Low cost in serial production (about 750K USD) and simple technology provides manufacturing by existing industrial firms.

Compact Laser/Optical Station Parameters

SLR of spacecraft with retroreflectors

- Spacecraft orbit height range: 400 to 40000 km
- Daytime and nighttime measurements for spacecraft with orbit heights 400 to 6000 km
- NP RMS errors 0.5 to 2 cm (averaging interval 60 s)
- Residual (systematic error) 0.5 to 2 cm
- Elevation range 20 to 85 deg.

Angular measurements

- Visual star magnitude: ≤ 12^m
- RMS error for spacecraft angular velocity up to 40 arcsec: ≤ 2’’

Photometry

- Visual star magnitude: ≤ 10^m
- Brightness determination error: ≤ 0.2^m

The option for mounting on a fixed position has a weight of 170 kg (optics + mount). No lifting mechanisms are needed for installation. The station has been tested near the 6-

meter telescope of Russian Academy of Sciences (in Northern Caucasus) during 2005. Currently, serial manufacturing is organized of the compact station for the Russian Laser Tracking Network. It is planned to produce 15 stations more until 2010.

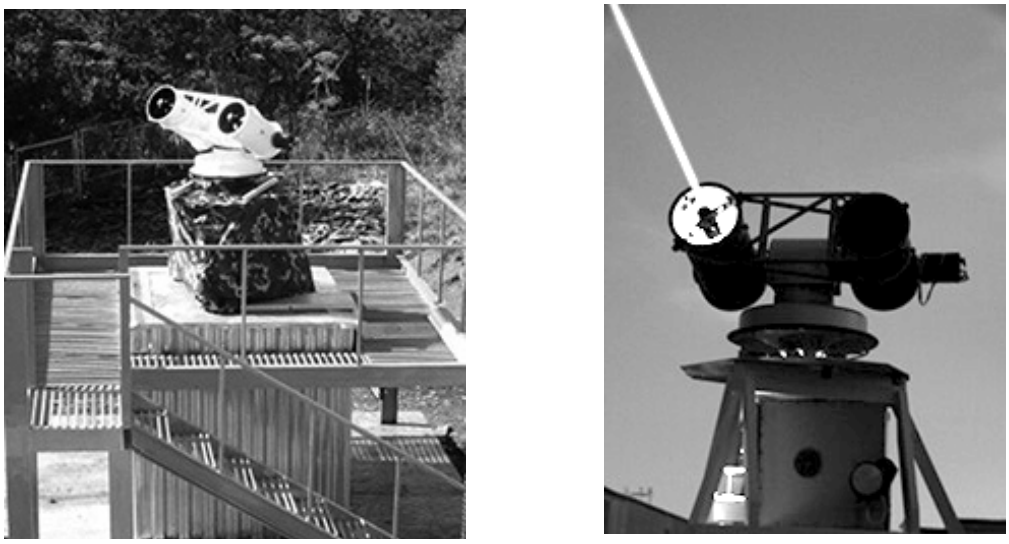

Figure 1: *Compact SLR station in operation*

Mobile Station

The mobile station is placed into 3 containers installed on wheels for transportation. The weight of optics and mount units is 12 tons. Except this unit, the system comprises an equipment container with operator's workplace, as well as a "house" for operator's rest. The mobile station acceptance tests have been completed on the Russian cosmodrome "Baikonur" in Kazachstan.

Pointing/tracking system and mount of the compact station

Mount parameters

- Mount type: Az-El, with two flanges for equipment mounting
- Digitally controlled torque motor drive
- Equipment weight on each mount flange:≤ 20 kg
- The mount is provided with an autonomous cover
- Angular rotation range:
  - Elevation: 5 to 95 deg
  - Azimuth: -278 to +278 deg
- Maximum angular speed 30deg/s;
- maximum angular acceleration 30deg/s^2

Mobile laser/optical station parameters

SLR of spacecraft with retroreflectors

- Spacecraft orbit height range: 400 to 40000 km

- Daytime and nighttime measurements for spacecraft with orbit heights 400 to 6000 km
- NP RMS errors 0.5 to 2 cm (averaging interval 10 s)
- Residual (systematic error) 0.5 to 2 cm
- Elevation range 20 to 85 deg

Angular measurements

- Visual star magnitude:≤ 14^{m}
- RMS error for spacecraft angular velocity up to 40 arcsec:≤2”

Photometry

- Visual star magnitude:≤ 12^{m}
- Brightness determination error: ≤ 0.2^{m}

The mobile station with a 60 cm diameter receive telescope and two separate optical systems for laser beam collimation and TV camera, has the following basic parameters.

Station of both types have similar laser ranging system with the following parameters:

Operation wavelength..... 0.532 μm
Pulse repetition rate..... 300 Hz
Laser pulse duration ..... 250 ps
Laser pulse energy..... 2.5 mJ
Output beam divergence ..... 5 arcsec
Receive telescope diameter
– compact station ..... 25 cm
– mobile station ..... 60 cm
Timing accuracy (measurement position on time scale) ..... 200 ns

Figure 2*: Operation site with installed equipment (containers and telescope)*

***Figure 3**: Mobile station preparation for operation*

***Figure 4:** Mobile station during transportation*

***Figure 5**: Mobile station in operation*

***Figure 6**: Mobile station operator workspace*

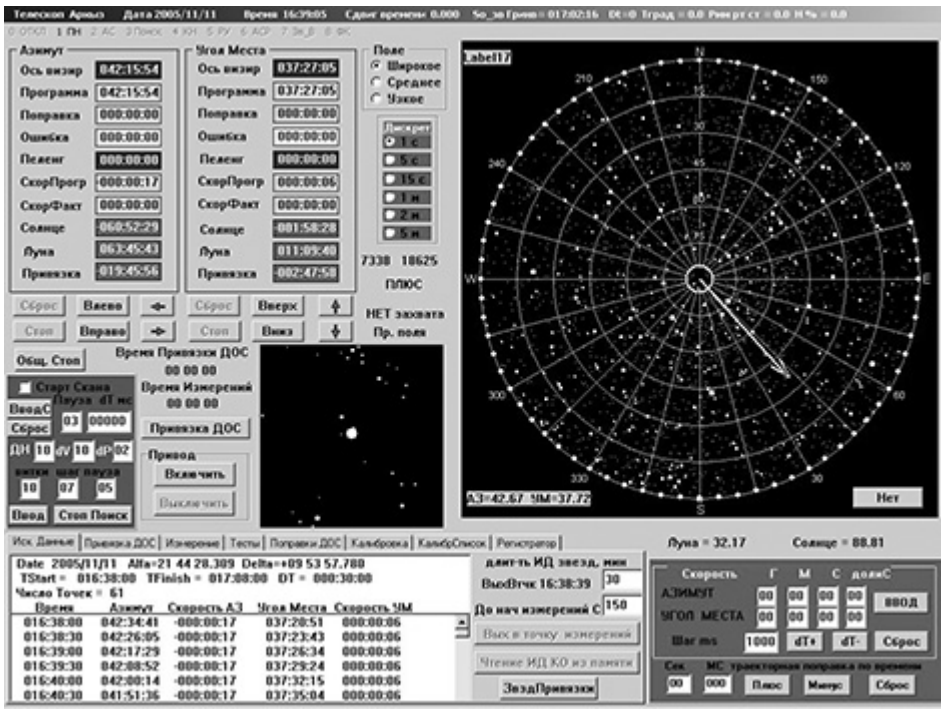

***Figure 7:** Versatile pointing/tracking control virtual panel*

Right: image of star catalog.

Center: image of calculated catalog star positions in the TV camera field of view (around the telescope pointing direction).

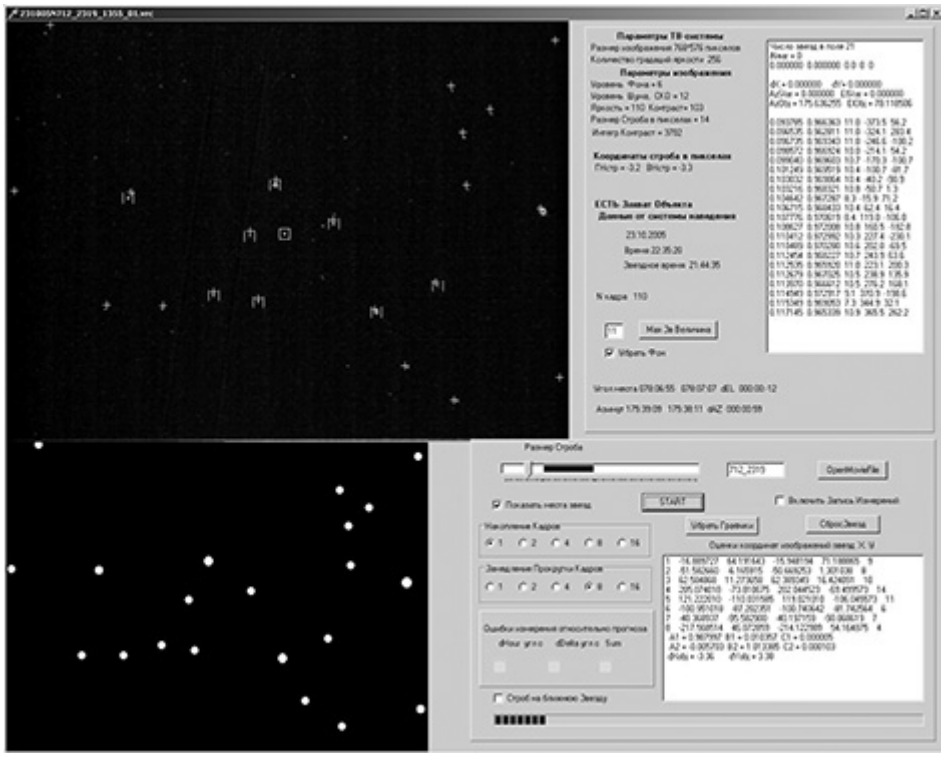

Upper left: TV frame with GLONASS-712 spacecraft in the center.

Lower left: star catalog fragment. + marks: position of catalog stars in the TV frame.

II marks: star tracking gates (stars selected for spacecraft angular position measurements).

Figure 8: *Versatile angular measurement (astrometric) virtual control panel*

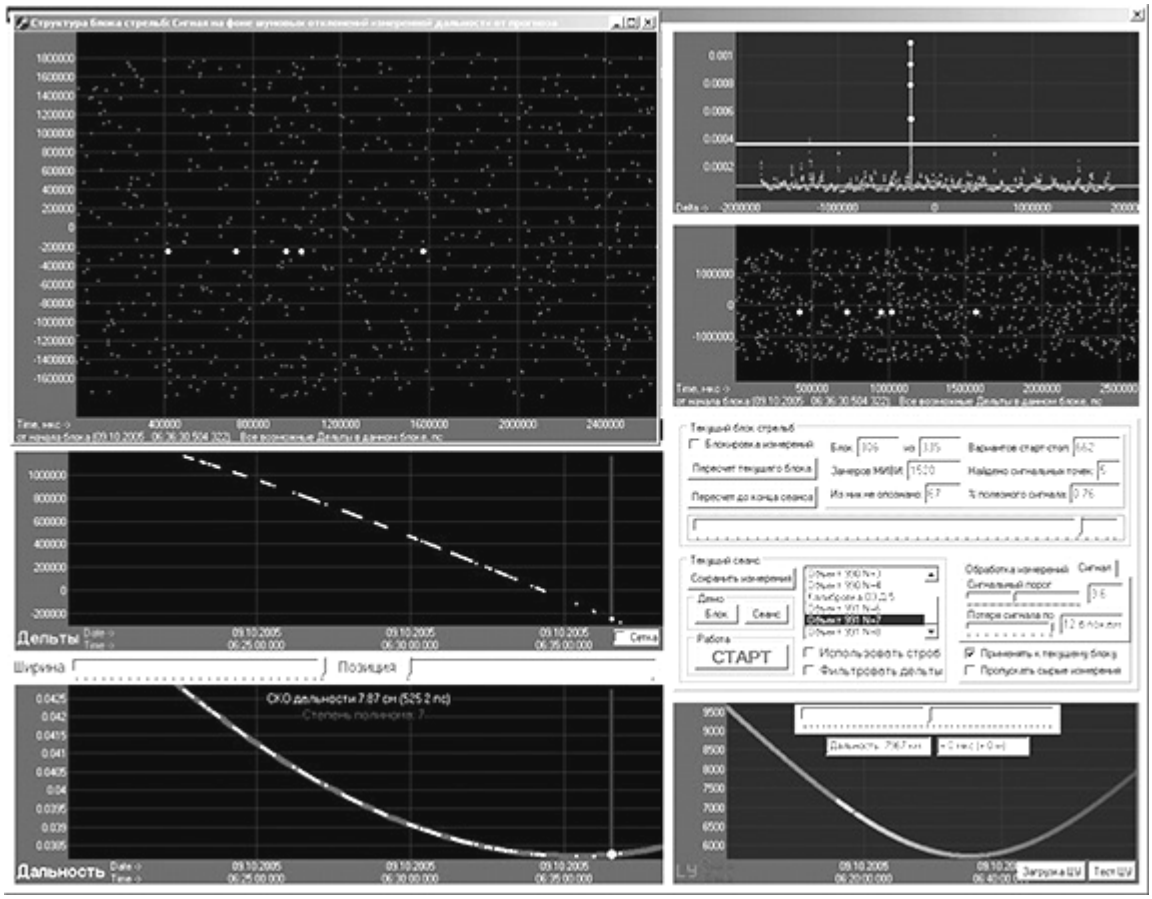

Figure 9: *Laser ranging control virtual panel (daytime observation of LAGEOS)*

TLRS-3 Return To Operations

Howard Donovan[1], Dennis McCollums[1], Don Patterson[1], Julie Horvath[1], Michael Heinick[1], Scott Wetzel[1], David Carter[2]

1. Honeywell Technology Solutions Inc. 7515 Mission Dr., Lanham, MD, USA 20771.

2. NASA Goddard Space Flight Center, Code 453, Greenbelt, MD, USA 20771.

Contact: Howard.Donovan@Honeywell.com

Abstract

The Transportable Laser Ranging Station 3 (TLRS-3) tracked from the Arequipa, Peru site for almost twelve years when the station was decommissioned in January of 2004. Replacing the SAO-2 in 1992 in a partnership between NASA and the Universidad Naciaonal De San Agustin, the TLRS-3 had travelled between Cerro Tololo, Chile and Arequipa, Peru after beginning its first operations in 1988 visiting the Mojave site in Goldstone, California. This paper will discuss the repairs, upgrades, and modifications accomplished at the TLRS-3 as well as the results of the first data collected.

History of TLRS-3 in Arequipa, Peru

The TLRS-3 replaced the SAO-2 system as the primary tracking station in Arequipa, Peru on August 7, 1992 with the tracking of an ERS-1 pass. In an agreement between NASA and the Universidad Naciaonal De San Agustin (UNSA), UNSA provided the operational crew while HTSI provided engineering support. TLRS-3 operated very well for almost twelve years until NASA budget reductions necessitated the closing of TLRS-3. On January 27, 2004 TLRS-3 tracked its last pass, a Starlette. In the fall of 2005, NASA tasked HTSI to return TLRS-3 to operational status. The UNSA crew returned to the station on December 12, 2005 to begin the task of reinitializing the system. HTSI working, with NASA and UNSA, began restoring the TLRS-3 to full operations, returning to the station in January 2006. The task of returning TLRS-3 to operations was done concurrently with the TLRS-4 Return to Operations effort.

TLRS-3 Return to Operations Strategy

With the TLRS-4 Return to Operations effort preceding the TLRS-3 effort by a few months, the TLRS-3 effort was able to take advantage of the multiple enhancements, upgrades and repair strategies used to quickly bring TLRS-4 back to operational status. Unlike the TLRS-4 though, the TLRS-3 had been without power and had not seen any type of maintenance for two years. Scheduled for TLRS-3 would be a full system inspection, implementation of the software and hardware improvements made to TLRS-4, a full system characterization using the System Operational Verification Test (SOVT) process, and a full validation of system performance prior to release of data to the ILRS.

Significant Engineering Issues

The TLRS-3 was off line for over 2 years with no HVAC control, no humidity control, and no air filtration. The system had not been exercised in any way. As a result the integrity of the station computers, system electronics, telescope optics, laser system, and

gimbal were of concern. With the lack of humidity control, corrosion issues were of concern as well, especially with the wire wrap boards, ICs and IC sockets, connectors, switches, etc. and the metal surfaces within the system, especially the laser. Because of the uncontrolled atmosphere within the trailers, temperature cycling presented a connection issue with wire wrap boards, connectors, etc. also. Maintenance of the site and main power system had not been performed either.

Planned and Implemented Upgrades

Upgrades planned for the TLRS-3 had already been implemented and proven to the TLRS-4. The Upper Deck received several enhancements to reduce maintenance and improve lifetime of the optics, improve the accuracy of the star calibration and reduce the time required to accomplish the calibration, and to improve throughput of the daylight filter. The optical system of the entire Upper Deck was enclosed to assist in keeping the optics clean, improve daylight tracking, and provide additional operator safety. A camera system was installed to increase the accuracy of the star calibrations. The optics layout was also redesigned so that optics did not have to be removed to perform the star calibration and so that the laser and star image could be easily co-aligned. The 10 angstrom daylight filter was replaced with a unit that has a 68% throughput and is quite temperature stable. The telescope was returned to NASA SLR Engineering in the USA and was completely disassembled, inspected, cleaned, and realigned. Throughput increased from ~ 50% to 87%. The T/R Switch was upgraded to an improved stepper motor design which was much more temperature stable than the old design. The Photek MCP Upgrade was installed replacing the failing ITT MCP. The upgrade included a newly calibrated CFD as well. The Controller Computer received improved Sattrk and Monitor programs. With these improvements came the Window/Window Upgrade, Mode Change Bias Reset, enhanced “Record All frames” function, 5pps and 4pps Thread Matching and Automated Switching, Sun Avoidance, Horizon Mask, the new Go/No Go software, and the high voltage power supply scaling upgrade. The new TLRS-4 microprocessor based Trackball was installed as well. Maintenance to site power was performed which included refurbishing the site power transformer.

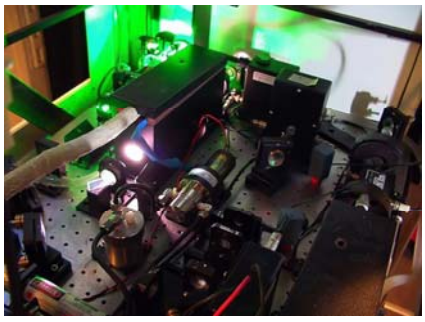

Current Status

The TLRS-3 is producing high quality data. Over 90 pass segments have been acquired with a data quality of <10mm RMS on Lageos and Starlette and <20 mm RMS on Ajisai. CHAMP and Grace B have been tracked. Average ground calibration is excellent at the 5.4 mm level.

Future Plans

Though significant progress has been made in bringing the TLRS-3 back to operational

status, there are still some unfinished tasks. Optimization of gimbal tracking performance, completion of the 4pps upgrade, completion of the Controller and Processor software upgrades and testing, calibration of system test equipment, restocking of system spares, completion of a site safety inspection and the performance of the site survey.

Test Data

Graphical examples of the Lageos satellite data and a listing of all the passes acquired by TLRS-3 during the upgrade are provided below. Included in the pass listing are calibration RMS, satellite RMS, system delay shift, calibration observation count, and satellite observation count.

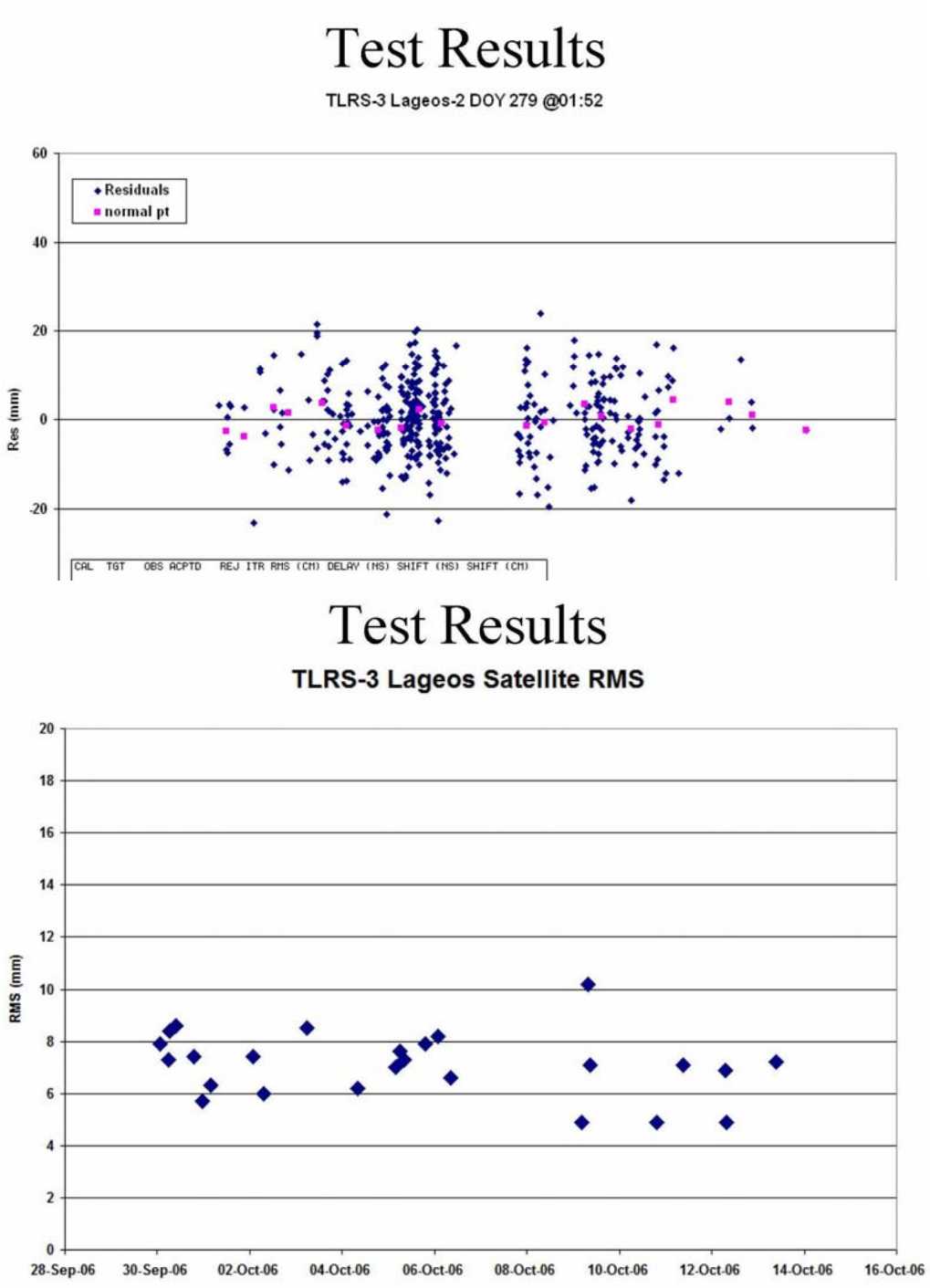

Test Results

PASS DATE	OCC NUM	SATID	TARGET	TARGET DISTANCE	# CAL OBS	# CAL REJ	CAL RMS (mm)	APPLIED DELAY	SHIFT (mm)	# SAT OBS	# SAT REJ	SAT RMS (mm)	MEAN TEMP ©	MEAN PRESS (mbars)	HUMIDITY (%)	NUM NP DATA BINS	NUM NP
29-Sep-06 00:53	03	1500	BC	105981	1948	14	4.5	3637.2	-1.07	93	15	22.2	13.32	761.2	51	30	18
30-Sep-06 01:21	03	5986	BC	105981	2188	9	5.9	3643.9	6.16	92	0	7.9	12.31	760.5	46	4	4
30-Sep-06 01:43	03	4378	BC	105981	2188	9	5.9	3643.9	6.16	19	6	4.2	11.73	760.6	45	28	6
30-Sep-06 02:03	03	1500	BC	105981	2188	9	5.9	3643.9	6.16	341	23	17.3	11.57	760.7	45	20	19
30-Sep-06 05:51	03	5986	BC	105981	2046	5	6.4	3643.5	-1.46	10	0	7.3	10.27	759.7	43	2	2
30-Sep-06 06:11	03	1155	BC	105981	2046	5	6.4	3643.5	-1.46	224	1	8.4	10.29	759.5	42	13	13
30-Sep-06 06:56	03	317	BC	105981	2034	4	6.4	3644.6	0.65	343	23	14.2	9.88	759.5	41	27	19
30-Sep-06 08:05	03	1134	BC	105981	2065	10	5.9	3646.7	1.72	100	7	8.4	8.91	759.6	45	5	5
30-Sep-06 08:52	03	643	BC	105981	2014	1	5.8	3646.2	-0.95	67	3	10	9.51	759.7	42	4	4
30-Sep-06 09:52	03	5986	BC	105981	2043	1	6.4	3646.4	1.37	159	1	8.6	9.15	760	39	14	10
30-Sep-06 18:58	03	1155	BC	105981	2249	10	5	3646.2	-0.35	132	1	7.4	23.14	760.5	15	6	6
30-Sep-06 23:04	03	1134	BC	105981	2022	3	5	3644.5	2.06	372	63	8.9	16.08	761.7	28	19	13
30-Sep-06 23:31	03	5986	BC	105981	2022	3	5	3644.5	2.06	38	1	5.7	14.37	762.1	32	10	8
01-Oct-06 01:11	03	1500	BC	105981	2233	16	4.7	3640	2.66	1063	231	21.7	11.35	762.5	39	17	17
01-Oct-06 02:37	03	6179	BC	105981	2015	32	4.4	3641.1	2.11	43	0	19.9	10.51	762.6	36	5	5
01-Oct-06 03:05	03	6178	BC	105981	2015	32	4.4	3641.1	2.11	127	14	22.4	10.7	762.6	32	6	6
01-Oct-06 03:13	03	5557	BC	105981	2015	32	4.4	3641.1	2.11	109	12	6.1	10.55	762.5	31	7	7
01-Oct-06 03:33	03	5986	BC	105981	2015	32	4.4	3641.1	2.11	109	3	6.3	8.9	762.3	36	13	11
02-Oct-06 00:34	03	4378	BC	105981	2131	39	4.6	3638.1	-0.65	192	3	7.3	12.12	761.9	35	27	23
02-Oct-06 01:13	03	8004	BC	105981	2157	60	4.7	3637.3	-1.4	402	22	14.6	11.46	762.2	35	45	34
02-Oct-06 01:31	03	5986	BC	105981	2157	60	4.7	3637.3	-1.4	405	4	7.4	10.85	762.2	36	21	18
02-Oct-06 02:36	03	6178	BC	105981	2455	66	4.8	3636.3	1.11	59	8	8	10.9	762.2	32	11	10
02-Oct-06 05:14	03	8501	BC	105981	2059	43	5.3	3639.4	-1.09	44	1	6.8	8.48	761.1	37	7	6
02-Oct-06 05:28	03	317	BC	105981	2059	43	5.3	3639.4	-1.09	192	15	14.3	8.69	760.8	35	26	12
02-Oct-06 06:53	03	8501	BC	105981	2083	28	5.3	3638.1	-0.4	8	0	10.1	8.2	760.2	34	2	2
02-Oct-06 06:55	03	1134	BC	105981	2083	28	5.3	3638.1	-0.4	168	10	10.7	8.18	760.2	34	10	10
02-Oct-06 07:05	03	1155	BC	105981	2083	28	5.3	3638.1	-0.4	38	0	6	8.29	760.1	36	3	3
02-Oct-06 07:19	03	317	BC	105981	2083	28	5.3	3638.1	-0.4	371	40	9.3	7.7	760.1	34	34	21
02-Oct-06 07:59	03	643	BC	105981	2025	19	5.4	3638.4	0.16	13	0	5.7	7.41	760.1	36	3	3
02-Oct-06 08:48	03	1134	BC	105981	2035	7	5.5	3640.3	0.91	30	3	7.9	7.8	759.9	34	4	4
02-Oct-06 12:57	03	1500	BA	105981	1018	8	6.3	3645.6	0	460	65	16.3	18.1	761.4	18	12	12
03-Oct-06 01:32	03	1500	BB	105981	1007	32	4.8	3636.8	0	182	5	14.8	10.52	761.4	41	4	4
03-Oct-06 02:48	03	5557	BC	105981	2031	139	5.3	3638.3	-0.94	99	6	7.6	10.69	761.7	40	10	8
03-Oct-06 04:45	03	317	BC	105981	1837	27	5.2	3639.4	-1.4	157	6	9.9	9.58	760.6	40	21	18
03-Oct-06 05:32	03	1155	BC	105981	2034	37	5	3638.3	1.67	243	3	8.5	9.13	760.3	41	12	12
03-Oct-06 06:19	03	8501	BC	105981	2039	41	5	3639.6	-0.1	129	15	16.9	9.6	759.8	36	4	4
03-Oct-06 06:40	03	317	BC	105981	2039	41	5	3639.6	-0.1	119	2	8.5	8.85	759.5	36	11	11
03-Oct-06 07:16	03	1134	BC	105981	2017	34	5.3	3640.5	2.09	17	0	6.9	9.2	759.3	32	1	1
04-Oct-06 05:48	03	8501	BC	105981	2031	6	5.1	3644.3	1.81	165	7	7.2	9.8	759.4	33	9	9
04-Oct-06 07:38	03	1134	BC	105981	2040	8	5.1	3643.3	-0.55	272	8	7.9	8.42	758.6	32	7	7
04-Oct-06 07:49	03	317	BC	105981	2040	8	5.1	3643.3	-0.55	26	0	7.1	8.99	758.5	30	7	7
04-Oct-06 07:53	03	1155	BC	105981	2040	8	5.1	3643.3	-0.55	12	0	6.2	8.61	758.6	34	6	5
05-Oct-06 02:11	03	6179	BC	105981	1237	15	5	3643.2	-1.85	249	55	7.9	10.57	760	41	22	20
05-Oct-06 02:29	03	5557	BC	105981	1237	15	5	3643.2	-1.85	23	1	9.7	10.5	760.1	40	2	2
05-Oct-06 02:40	03	6178	BC	105981	1237	15	5	3643.2	-1.85	346	23	8.9	10.61	760.2	39	20	19
05-Oct-06 02:47	03	8002	BC	105981	1237	15	5	3643.2	-1.85	109	6	10.8	10.47	760.2	39	16	11
05-Oct-06 03:54	03	5986	BC	105981	2277	59	5.5	3642.8	1.2	119	1	7	9.88	759.6	39	17	17
05-Oct-06 05:10	03	317	BC	105981	2046	10	5.5	3643.1	1.29	59	3	10.3	9.7	758.9	34	18	8
05-Oct-06 06:12	03	1155	BC	105981	2146	8	5.5	3647.4	0.67	109	0	7.6	9.37	758.3	22	12	4
05-Oct-06 07:04	03	317	BC	105981	2146	8	5.5	3647.4	0.67	306	20	11.1	8.84	758.1	21	19	19
05-Oct-06 07:54	03	1134	BC	105981	2143	8	5.5	3647.9	1.36	405	51	11.1	9.59	757.8	18	11	11
05-Oct-06 08:20	03	643	BC	105981	2143	8	5.5	3647.9	1.36	130	11	6.7	9.38	757.7	17	6	6
05-Oct-06 08:28	03	5986	BC	105981	2143	8	5.5	3647.9	1.36	54	0	7.3	9.31	757.6	17	8	6
05-Oct-06 18:05	03	8501	BC	105981	2060	10	6.7	3655.7	-7.68	47	2	5.9	23.44	758	16	6	6
05-Oct-06 19:22	03	1155	BC	105981	1687	20	5.5	3654.1	1.19	15	1	7.9	23.11	757.5	17	3	2
05-Oct-06 22:41	03	1500	BC	105981	2064	11	5.6	3654.2	1.87	700	91	21.9	18.21	758.7	22	19	19
06-Oct-06 01:53	03	5986	BC	105981	2590	23	5.3	3646	5.19	417	0	8.2	12.35	760.9	33	24	20
06-Oct-06 03:03	03	5557	BC	105981	2174	5	5.4	3649.3	-1.43	33	3	6.1	10.5	761	35	3	3
06-Oct-06 03:19	03	6179	BC	105981	2174	5	5.4	3649.3	-1.43	127	9	7	11.17	761.1	33	9	9
06-Oct-06 06:16	03	317	BC	105981	2063	5	5.6	3650.2	-0.2	450	19	13.1	10.39	759.9	34	27	25
06-Oct-06 06:28	03	1134	BC	105981	2063	5	5.6	3650.2	-0.2	202	41	9.4	10.33	759.9	33	5	5
06-Oct-06 08:14	03	1155	BC	105981	2021	6	5.6	3652.2	0.49	110	0	6.6	10.14	759.2	30	22	15
08-Oct-06 21:59	03	1500	BC	105981	2026	54	4.7	3655.6	0.51	1417	260	17.7	19.89	760.3	24	25	24
08-Oct-06 23:21	03	4378	BC	105981	2192	106	5.2	3653.8	2.72	116	11	7.5	15.79	761	33	20	14
09-Oct-06 04:10	03	317	BC	105981	1527	175	5.7	3649.4	-1.07	11	0	6.5	11.4	761.6	34	2	2
09-Oct-06 04:30	03	1155	BC	105981	1527	175	5.7	3649.4	-1.07	44	5	4.9	11.34	761.4	32	8	7
09-Oct-06 05:37	03	1134	BC	105981	1540	151	5.5	3647.1	-0.87	134	25	6.9	11.5	760.8	29	5	5
09-Oct-06 07:46	03	1155	BC	105981	2063	181	5.4	3647.1	1.83	39	1	10.2	10.03	760	29	6	4
09-Oct-06 08:15	03	643	BC	105981	2063	181	5.4	3647.1	1.83	33	5	6.5	9.1	759.9	25	2	2
09-Oct-06 08:56	03	5986	BC	105981	2044	259	5.4	3647.1	-2.6	272	23	7.1	9.24	760	23	20	14
10-Oct-06 19:01	03	1134	BC	105981	1234	3	6	3660.7	5.77	241	19	7.1	22.35	761.9	20	20	12
10-Oct-06 19:35	03	1155	BC	105981	1234	3	6	3660.7	5.77	60	1	4.9	22.97	761.8	20	5	5
11-Oct-06 09:10	03	5986	BA	105981	1020	1	5.3	3658.7	0	56	0	7.1	12.22	760.9	17	17	6
12-Oct-06 04:42	03	1134	BC	105981	2048	6	5.1	3660	0.29	156	6	5.9	11.84	762.6	29	14	5
12-Oct-06 06:39	03	8501	BC	105981	2023	5	5	3660.5	-0.34	10	0	8.4	11.4	761.5	31	2	2
12-Oct-06 07:11	03	1155	BC	105981	2124	5	4.8	3661.4	-0.14	108	0	6.9	11.57	761.2	30	6	6
12-Oct-06 07:34	03	1155	BC	105981	2124	5	4.8	3661.4	-0.14	32	0	4.9	11.96	761.2	29	6	6
12-Oct-06 08:31	03	643	BC	105981	2092	9	4.5	3659.8	-0.08	96	12	9.5	11.16	761.1	30	4	4
12-Oct-06 10:03	03	1500	BC	105981	2051	8	5	3658.9	-0.77	1083	111	17	11.35	761.6	30	17	17
12-Oct-06 10:56	03	4378	BC	105981	2019	6	5.6	3662.9	2.36	24	0	6	11.6	762	30	6	6
12-Oct-06 17:52	03	1134	BC	105981	1926	17	5	3666.7	-0.02	133	7	7	24.29	761.1	16	14	10
13-Oct-06 08:09	03	643	BB	105981	1041	47	7.3	3654	0	48	3	16.5	9.6	761.1	36	4	2
13-Oct-06 09:39	03	5986	BC	105981	2085	46	6.3	3656.2	-0.8	377	2	7.2	9.03	761.4	36	14	13

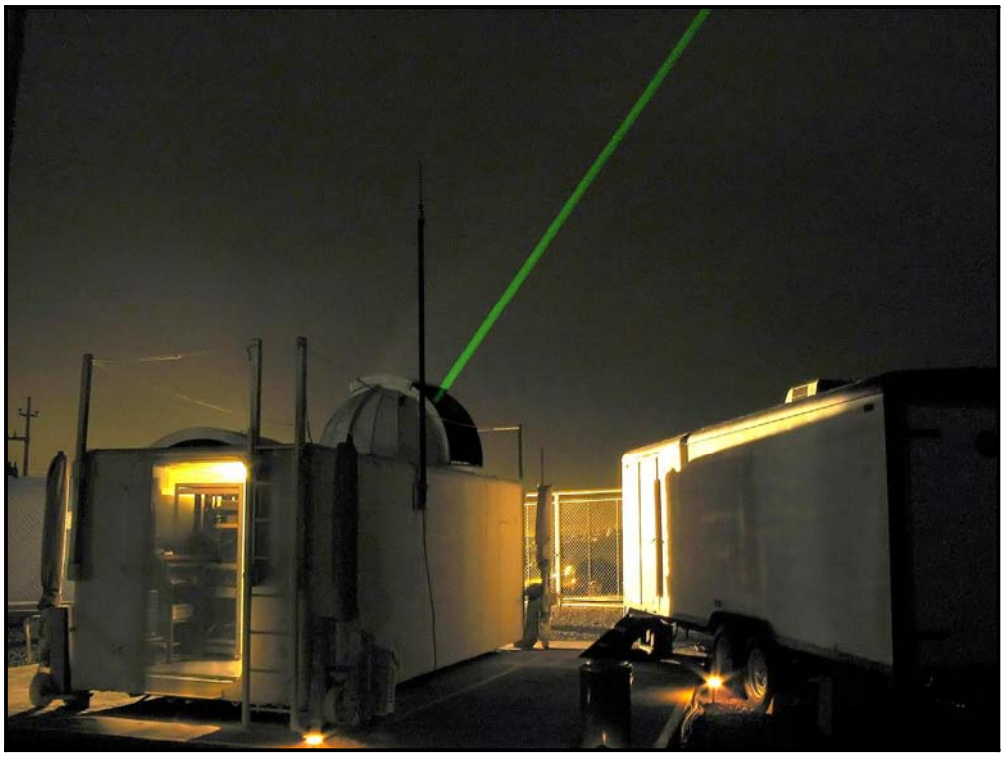

Korean Plan for SLR System Development

Hyung-Chul Lim[1, 2], Jong-Uk Park[1], Sang-Ki Jeong[2], Byung-Su Kim[2]

1. Korea Astronomy and Space Science Institute, Daejeon, Korea
2. Korea Institute of Science and Technology Evaluation and Planning, Seoul, Korea

Contact: hclim@kasi.re.kr

Abstract

There are about 70 GNSS stations in Korea for GNSS applications including space geodesy, and 3 VLBI stations will be constructed by 2007 for astronomical and geodetic research. In addition, two Korean satellites with a laser retro-reflector array, STSAT-2 and KOMPSAT-5, will be launched in 2008 and 2010, respectively. Thus, SLR system is considered to be necessary in Korea for constructed for satellite laser tracking and space geodesy research. KASI has a plan to develop a fixed SLR station and a mobile SLR station in the near future. In this study, future Korean plans of SLR system development will be presented.

Introduction

More than 70 GNSS (Global Navigation Satellite System) stations have been operated by several institutes, including KASI (Korea Astronomy and Space Science Institute), for accomplishing missions of navigation, space geodesy, and so on. From 1995, KASI has been playing an important role in IGS (International GNSS Service) and IERS (International Earth Rotation and Reference Systems Service) as global GNSS station, and operating an IGS global data center from 1996. Except GPS applications, KASI has a wide variety of research areas like optical, radio, theoretical and observational astronomy research, and is expanding its area through astronomical research in space. So, KASI has been constructing 3 VLBI (Very Long Baseline Interferometry) stations with receivers working in the frequencies 2/8, 22 and 43GHz bands which will be completed by 2007 for radio astronomy research including space geodesy. Fundamental stations for geodesy operate three geodetic space techniques at one location: VLBI, GNSS and SLR (Satellite Laser Ranging), which can give a powerful tool for space geodesy such as global reference frame. KASI has a plan of operating a fundamental station in Jeju island in which a GNSS station is already operated and a VLBI station will be completed in 2007. So, KASI wants to develop a SLR system for constructing a fundamental station, and it has tried to raise funds for SLR system development from Korean government.

After KITSAT-1 was launched in 1992, which was the first Korean satellite, Korea launched 6 LEO (Low Earth Orbit) satellites made by Korean technology. They are not all equipped with LRA (Laser Retro-reflector Array) because precise orbit determination is not required in their missions. However, two Korean satellites with LRA will be launched in 2008 and 2010, respectively: Science Technology SATellite-2 (STSAT-2) with a Lyman-alpha imaging solar telescope and Korea Multi-Purpose SATellie-5 (KOMPSAT-5) with a Synthetic Aperture Radar (SAR). STSAT-2 LRA was developed through international collaboration between SaTReC(Satellite Technology Research Center), Korea and Shanghai Astronomical Observatory, China. But KOMPSAT-5 will have the same LRA as Champ, Grace and TerraSAR-X satellites, whose LRA will be made by GFZ (GeoForschungsZentrum Potsdam), Germany.

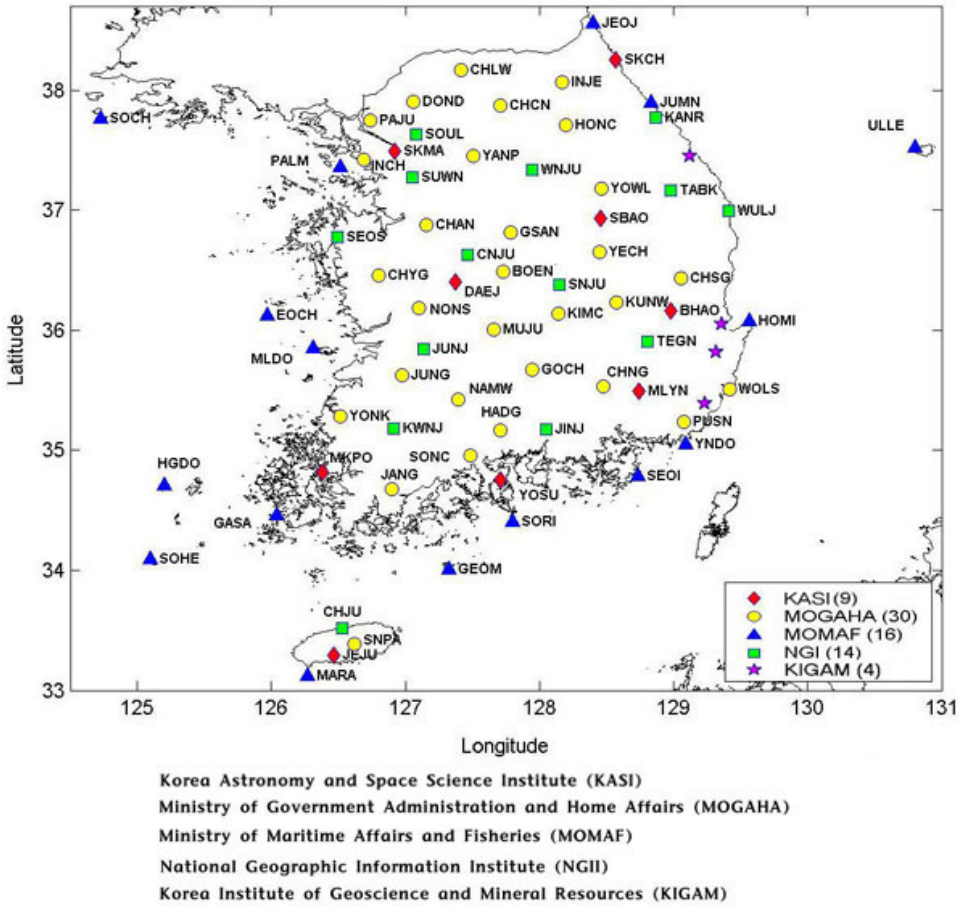

Korea Astronomy and Space Science Institute (KASI)
Ministry of Government Administration and Home Affairs (MOGAHA)
Ministry of Maritime Affairs and Fisheries (MOMAF)
National Geographic Information Institute (NGII)
Korea Institute of Geoscience and Mineral Resources (KIGAM)

***Figure 1**. Korean GNSS Network*

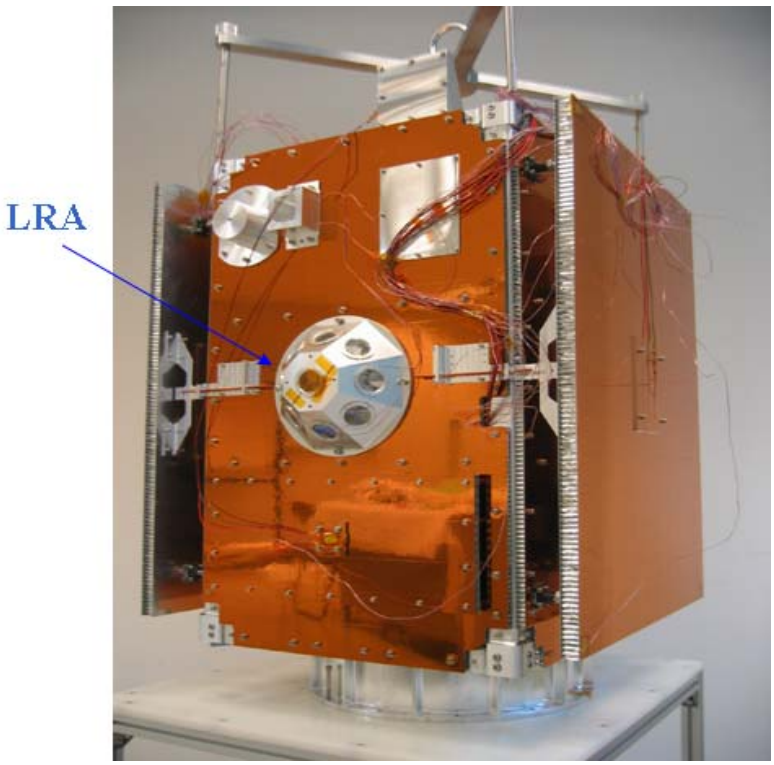

***Figure 2**. STSAT-2(first Korean satellite with LRA)*

Future Plan for SLR system development

KASI conducted the preliminary study for SLR system development from December 2004 to November 2005 with KAERI (Korea Atomic Energy Research Institute), KIMM (Korea Institute of Machinery and Materials) and SaTReC (Satellite Technology Research Center). In the preliminary study, KASI carried out a feasibility study on SLR system development and made the conceptual design of Tx/Rx telescope and Control & Operating System. The conceptual design of the laser generator was done by KAERI, the tracking mount by KIMM, and the Tx/Rx electric system by SaTReC. KASI has tried to obtain the financial support of the Korean government for SLR system development (KSLR project) since this preliminary study, and wants to start the KSLR project in 2008 with KAERI, KIMM and SaTReC. In this project, one fixed system with a 1m Rx telescope and one mobile system with 40cm Rx telescope will be developed for 5 years. The detailed requirements of a fixed system are shown in Table 1. The mobile system will be integrated by introducing the core subsystems from abroad, and the fixed system will be developed through the international and domestic collaboration. So, it will take about 3 years to develop a mobile system but 5 years (subsystem development: 3.5yr, system integration: 0.5yr, test operation: 1yr) to develop a fixed system. After a fixed SLR system is constructed, KASI will join to ILRS (International Laser Ranging Service) for the contribution of the international SLR society.

As mentioned in the previous section, STSAT-2 will be launched in 2008 when Korea will not be capable of tracking it. So a mobile system (TROS, Transportable Ranging Observation System) will be introduced in China this June for laser tracking of STSAT-2 but the detailed schedule is not fixed

Table 1. *Requirements of the future Korean SLR system*

Items	Requirements
Tracking Coverage	• Possible to track satellites in the altitude of 25,000km • STSAT-2, KOMPSAT-5, GPS, Galileo Satellites and so on.
Ranging Accuracy	• Lageos : 10mm(SS), 1-2mm(NP) • GPS and Galileo : 20mm(SS), 3-5mm(NP) • Ground Target : 3mm(SS), 1mm(NP)
Automatic Operation	• Remote control from the remote site via internet or dedicated line. • Aircraft detection using radar and automatic observation according to the schedule.
Etc	• Daylight tracking. • Optical tracking of the space launch vehicle (if possible).

Summary

Two Korean satellites with LRA, STSAT-2 and KOMPSAT-5 will be launched in 2007 and 2009, respectively. Therefore, SLR system is steadily required to be established in Korea not only for satellite tracking, but also for space geodesy research by using GNSS and VLBI. In response to this demand, KASI have prepared for development of SLR system for several years, and expect to launch the project for the development of SLR system from 2008. KASI has a plan to develop one mobile and one fixed SLR systems for 5 years. After a fixed SLR system is constructed, KASI will join ILRS and participate in the international tracking campaign.

References

[1] Lee, J. H., Kim, S. B., Kim, K. H., Lee, S. H., Im, Y. J., Fumin, Y., Wanzhen, C., “Korea’s First Satellite for Satellite Laser Ranging”, Acta Astronautica, 2004.

Study on Servo-Control System of Astronomical Telescopes

Li Zhu-lian, Zheng Xiang-ming, Xiong Yao-heng

1. National Astronomical Observatories/Yunnan Observatory, Chinese Academy of Sciences, Kunming 650011,China

Abstract

Based on recent and modern control theories, this paper describes an analysis of the control system compensation function and its application to astronomical telescope servo control requirements. It discusses corresponding compensation networks for modern astronomical telescopes.

Keywords: *Servo System, Compensation Network, SLR/LLR telescope*

Introduction

Most of modern telescopes servo-control systems are computer closed loop control systems which are based on classical control theories and are composed of one or more feedback control loop. Typical feedback control system is shown in Fig.1. In theory, control system designed according to this block diagram might meet the requirements. However, in a concrete project, control system simply designed like this way is not simultaneously satisfied with all the requirements until it is compensated properly.

C(s) represents controlled output, its value is sent back through feedback controller

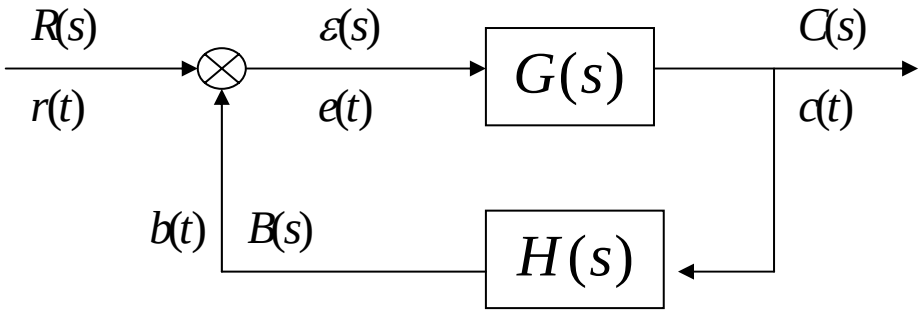

Fig.1 *Typical Feedback Control Loop*

whose transfer function is H(s). Its output B(s) is compared with expected output R(s), i.e. input of whole control system, the error which R(s) substracts B(s) is sent into controller G(s), which adjusts the error to near zero.

Compensation of Control System

In order to carry out expected capability, modifying and adjusting the control system structure is named compensation. In another words, compensation is used to adjust structure for compensating defect of system. PD (Proportion Differential) Compensation Network and PI (Proportion Integral) are often used in modern control system design. Corresponding control loop block diagram is shown as Fig.2. Gc(s) is the transfer function of the compensation network. [1]

PD Compensation Network Function

When compensation network transfer function $G_c(s)$ is:

$$G_c(s) \approx \frac{k}{p} s$$

it is a PD type compensation Network.[2] Fig.3 is its corresponding bode graph, which is magnitude versus phase plot. It could be clearly seen that magnitude gain increases with frequency and phase is greater than zero. This means that PD compensation can offer additional phase for primary system without compensation network.

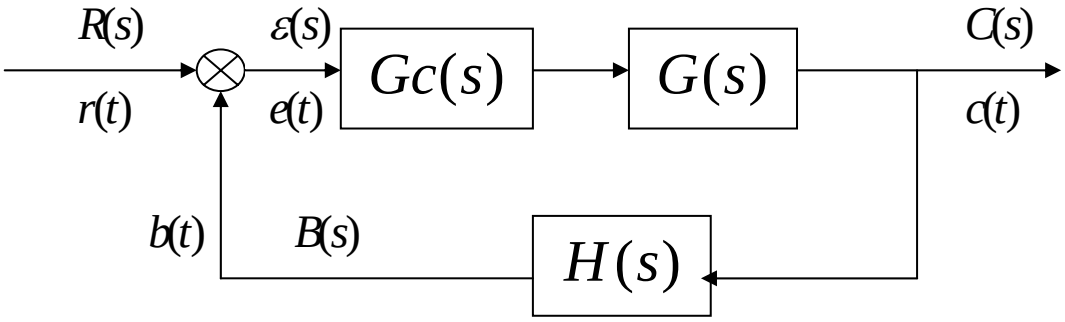

Fig.2 *Feedback Control Loop with Compensation*

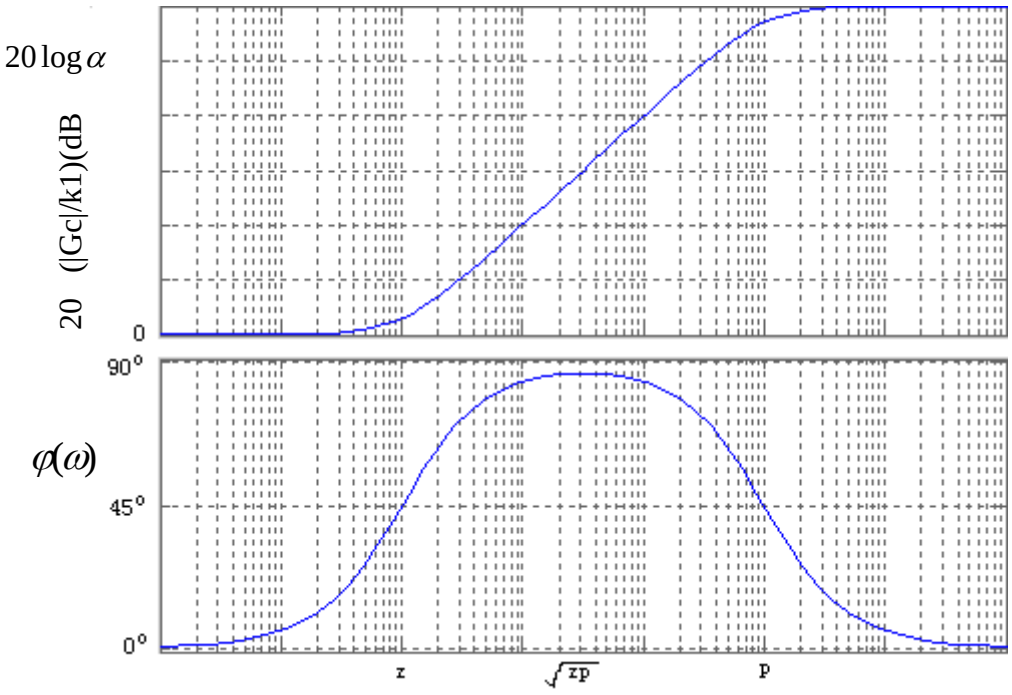

Fig.3 *The Bode Graph of PD Compensation*

Therefore, to make system response more quickly and strengthen system stability is the function of PD compensation.

PI Compensation Network Function

When compensation network transfer function $G_c(s)$ is :

$$G_c(s) \approx \frac{k}{ps}$$

it is a PI type compensation Network.[2] Fig.4 is its corresponding bode graph, which is magnitude versus phase plot. It is obvious that magnitude gain descends with frequency and phase is negative. This shows that PI compensation can offer delay phase for

primary system without compensation network. So, the function of PI compensation is to improve system accuracy of stability. To sum up, PD compensation may be used to improve instantaneous response and PI can be used to meliorate stable response.

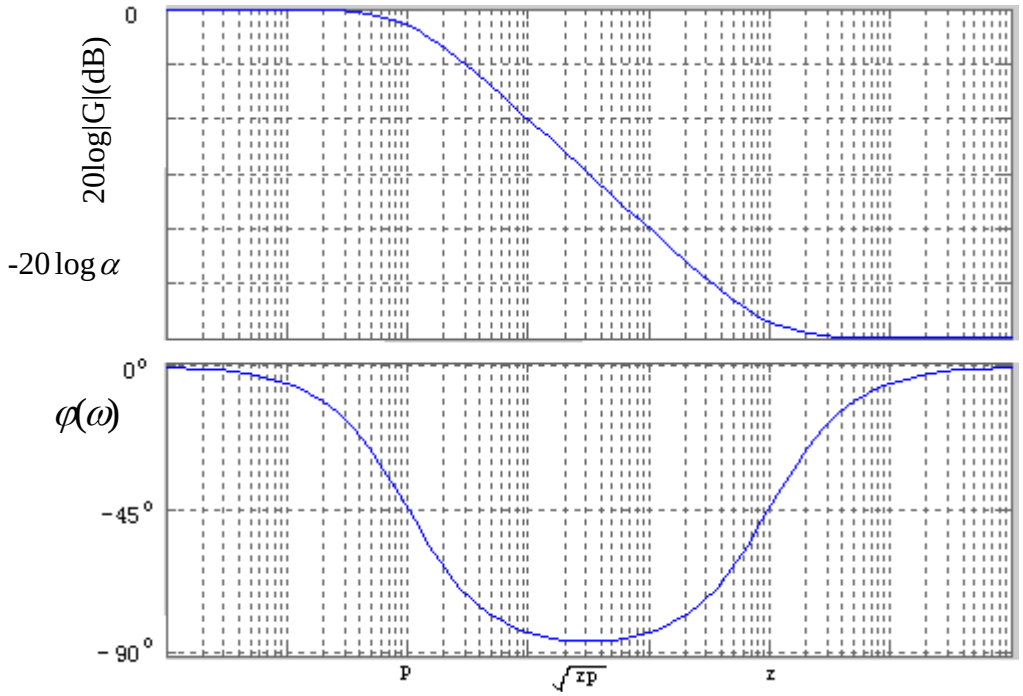

Fig.4 *The Bode Graph of PI Compensation*

Compensation Network Design for Telescope Servo System

According to characters of the compensation network which were analysed above, we could design a proper servo control system for any astronomical telescope.

If a telescope is required to track quick motion celestial bodies, such as satellites near the Earth, we would design the control system compensation network as PD compensation, or PI compensation would be better to observe slow motion celestial bodies for a telescope.

Of course, when a telescope is not require to track quick motion celestial bodies but slow motion bodies, to combine advantages of PI and PD could gain the expected performance or we could directly design the control system compensation network as PID compensation.

Discussion

Though PID compensation network could attain better capability, its disadvantage is that needs more devices and increases design cost. Therefore, if a telescope need track both quick and slow bodies, in order to save resource, we'd better select PD compensation network, then through software methods to compensate the accuracy of stability.

References

[1] Richard C., Dorf, Robert H and Bishop. Modern Control System (eighth edition). Translation by Xie Hong-wei, Zou Feng-xing and Zhang Ming. Beijing Higher Education Press.

[2] Dai Bei-qian, Qian Zhi-yuan. Linear Electronic Circuit. HeFei:University of Science and Technology of China Press.

Russian Laser Tracking Network

V.B. Burmistrov, A.A. Fedotov, N.N. Parkhomenko,
V. Pasinkov, V.D. Shargorodsky, V.P. Vasiliev

1. Institute for Precision Instrument Engineering, Moscow, Russia.

Contact: www.niipp-moskva.ru

Abstract

Basic parameter are presented of six laser tracking stations now installed in Russia. Besides SLR, the stations also provide angular measurement and photometry. Some applications of obtained data are also specified.

Introduction

The Russian SLR stations comprise three optical channels: ranging channel, angular measurement channel, and photometric channel, providing the following accuracy of measurements:

- Ranging: 5 - 10 mm (RMS of NP)
- Angular measurements (in reflected sunlight): 1 arcsec

Photometry (in reflected sunlight): ≈0.2 star magnitude.

Ranging data applications

The high precision of laser ranging allows use of SLR as a single source of calibration data for GLONASS ephemeris determination, providing solution of following problems:

- Estimation of accuracy, and calibration of radio-frequency means for GLONASS orbit measurements.
- Providing SLR stations with geodetic-class RF navigation receivers connected to hydrogen maser frequency standards allows monitoring of on-board clocks and use of the data for operational control of GLONASS time and ephemeris data.
- SLR station coordinates are used as geodetic base for the GLONASS reference frame.
- SLR data are used to provide declared values of ephemeris precision, as well as to provide computation and forwarding of accuracy factor in the navigation frame of GLONASS – M spacecraft.

Angular measurement data applications

Angular measurement data obtained on SLR stations are used for implementation of single-point scheme of flight control for commercial geostationary spacecraft with periodical measurements of orbit inclination to provide retaining of the geostationary spacecraft standpoint within ±0.1 deg. in longitude and ±0.1 deg. in latitude.

Photometric data applications

- The presence of a high-sensitivity TV channel provides registration of flight phases (motors turn-on, booster separation, etc.) during launching of spacecraft on high elliptical and geostationary orbits.

- The photometric channel supports determination of spacecraft motion relative to its center-of-mass, as well as of its attitude stability.

Taking into account the unfavorable astro-climatic conditions on most of the country territory, efforts are made to expand the Russian laser tracking network. Currently, five SLR stations are in operation. In 5 years, the number of stations will increase to 15…20, as declared in the new Global Navigation System Federal program.

Russian laser tracking network

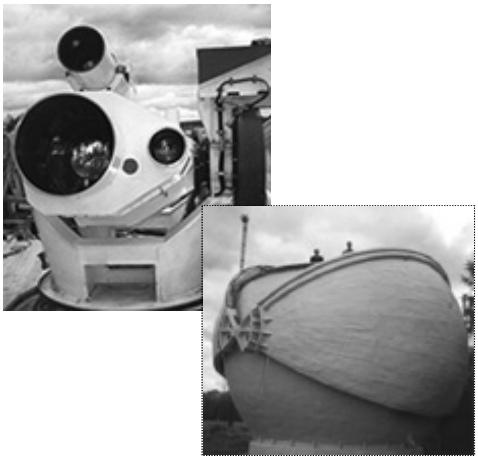

Figure 1: *SLR Station in Shelkovo (near Moscow)*

Figure 2:*Altay Optical and Laser Tracking Center*

Figure 3:*Komsomolsk SLR station*

Figure 4: *Compact SLR station installed in Arkhys (North Cuacasus)*

Figure 5: *Maidanak Optical and Laser stations (Uzbekistan) (currently, an inter-state agreement is under preparation concerning the mutual control and operation of this station).*

Figure 6: *Mobile SLR station installed in Baikonur*

Figure 7: *Russian laser tracking network*

TLRS-4 Deployment to Maui, Hawaii

Scott Wetzel[1], Howard Donovan[1], Maceo Blount[1], Dennis McCollums[1], Craig Foreman[1], Michael Heinick[1,] Daniel O'Gara[2], David Carter[3]

1. Honeywell Technology Solutions Inc., 7515 Mission Drive, Lanham, MD USA 20706
2. University of Hawaii, Institute for Astronomy, Maui, HI, USA 96790
3. NASA Goddard Space Flight Center, Code 453, Greenbelt, MD, USA 20771

Abstract

With the completion of the TLRS-4 Operational Readiness Review in the fall of 2005, Honeywell Technology Solutions Inc (HTSI) working with the University of Hawaii Institute for Astronomy (IfA), deployed the NASA TLRS-4 system to the 10,000 foot summit of the Haleakala volcano on September 7th, 2006. TLRS-4 is returning a critical data point to the ILRS Global solution following the closure of the HOLLAS SLR station in 2004. This paper describes the planning, deployment, current status and future at the Haleakala Observatory.

Background

The NASA Transportable Laser Ranging System (TLRS) number 4, TLRS-4, was returned to operations during spring and summer of 2005, following approximately 10 years of inactivity as an operational station in the NASA SLR Network. A highly successful inter-comparison test with Moblas 7 validated that TLRS-4 was ready for deployment. Following the Operational Readiness Review on September 15, 2005, TLRS-4 was readied for deployment to the 10,000 ft summit of the Haleakala volcano on Maui, Hawaii. The system was to be operated by the University of Hawaii (UH), Institute for Astronomy (IfA) under contract to NASA, returning a critical data point in the Pacific Ocean. As the Hollas system had been decommissioned in 2004 following budget reductions at NASA, the site was converted to the new PanStarrs Observatory. To return SLR to the Haleakala Observatory, the TLRS-4 system was provided and would be moved to a pad within approximately 100 meters of the Hollas station. The figure below shows the location of the former Hollas system and the location of where TLRS-4 system would be deployed.

Haleakala Observatory Site Preparations

As the Hollas site was no longer available for SLR, a suitable location for TLRS-4 was required. One was found near the Mees Solar Observatory, however there was inadequate infrastructure to support SLR operations. Improved infrastructure to be considered included: pad, power, grounding voice and data communications, calibrations piers, site safety and site and system survey. Even though the IfA had no

formal contract in place with NASA, they provided excellent coordination for all efforts of site preparations that would be required to locate TLRS-4 at the observatory.

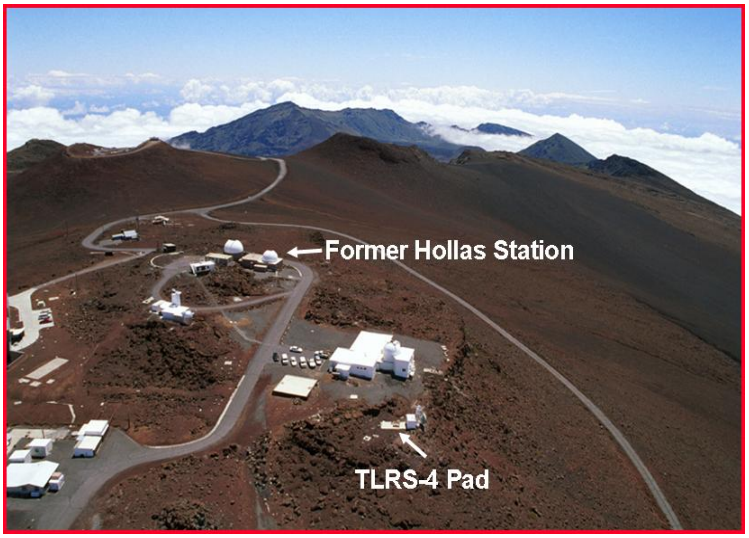

During this period when no contract existed with the IfA, the system remained in a semi-operational mode at the Goddard Geophysical and Astronomical Observatory (GGAO) in Greenbelt, Maryland at NASA SLR Headquarters.

Also, during this time, a dome safety retrofit project occurred in Maryland to provide a remotely operated and weather hardened dome and shutter to meet with the sometimes harsh wind and rain conditions at the summit of the Haleakala volcano. Additionally, an upgrade to provide for 4 Hz tracking for high orbital satellites occurred and the TLRS systems were not originally designed to high satellite tracking.

In April 2006, in anticipation of the IfA, NASA contract being finalized and due to the time required to transport the system from Maryland to Hawaii, it was determined to ship the system to Maui. The system arrived in Maui in late May 2006. As the contract had not been finalized, the shipment consisting of the Ranging Van, the Support Trailer and the radar platform and tracking dome, were placed at the Waiakoa, IfA office property located at 3,000 feet for holding until the system could be sent to the summit. A key milestone to be completed once the contract was in place was a site occupancy permit and permit to perform infrastructure modifications at the observatory.

When the contract was approved in late spring a occupation and building permit was applied for by the IfA. The permit was received in mid-August 2006 and site preparations were begun.

The Haleakala volcano is rich in native Hawaiian history, culture and religion. A cultural observer was required to approve and oversee all work performed on the site

where any disturbance may occur to native soils. Special requirements and permissions for excavation, removal and replacement of ground were followed and it was required that any person working on the project to be provided with a training and a cultural introduction to the religious and historical significance and understanding of working in Hawaii.

Following this training and receipt of the permitting, both HTSI and IfA worked aggressively to ready the site for occupation of the TLRS-4 system. Major components of site infrastructure included the calibration piers and site power. The previous figures show the unoccupied pad and the construction of the calibration piers. Temporary site power was provided from the Mees Observatory.

On September 6, 2006, the TLRS-4 was readied for transport from the IfA offices in Waiakoa to the summit. The newly fabricated dome and radar platform were installed at the Waiakoa office prior to loading the tracking van on the flatbed for the trip to the summit.

The Operations Van and the Support Trailer were delivered and installed on a rainy September 7th and placed on the pad shown above. Since that time, connection to the temporary site power, setup of the two vans and the reenergizing of the system began with the IfA and HTSI team.

An interesting point of working at the Haleakala Observatory is that the crew is required to drive from either sea level or near sea level to the 10,000 foot summit daily. Working conditions with such a daily change in altitude affect how the workers exert effort both mentally and physically. As one never completely adapts to the high altitude, greater concentration in routine physical and mental tasks, are required.

Transition of the TLRS-4 from the HTSI team to the IfA was seamless due to the extensive background in SLR that was retained by the University of Hawaii with key people such as Dan O'Gara and Jake Kamibayashi, the close similarities between the TLRS-4 software architecture and the Hollas system. More significantly, the new TLRS-4 Station Manager, Craig Foreman, spent months in Maryland in the restart effort of the TLRS-4 system and was responsible for many of the modifications of the system to operate in the Haleakala summit environment. Craig's success was ensured by working with the HTSI team especially Maceo Blount who lead the installation team to Maui for the installation and training of the other IfA personal.

Current Status

At the time of this report, the TLRS-4 station setup is completed. During the startup of the system, there was a laser failure that was being troubleshot. Also, during this time, optical alignments were being completed and the other components and subsystems were being verified. Site power to the system was being used on a temporary basis from the Mees Observatory while a permanent source was being developed.

Remaining efforts and future plans for TLRS-4 include completing the System Operational Verification Tests (SOVT), ground calibration testing, satellite tracking and validation of data acquired. Also required actions include completing the site survey analysis and report generation, updating of the Site Log, and completion of the training aspect of TLRS-4 to the IfA crew.

Power switchover to a more permanent solution will require further effort, approval by the cultural observer and contracting with local contractors and the local power company. During this period, the ground field will be enhanced to reduce ground currents on station. Locating an SLR station located at the top of a dormant volcano produce unique grounding opportunities that must be resolved in unique ways.

Conclusion

In conclusion, acknowledgements of the many extra efforts and the dedicated team that worked to reach a successful conclusion to the project that restores an important piece of the global puzzle for the reference frame and for SLR go to NASA with the leadership provided by David Carter. Also to the HTSI Team led by Howard Donovan and his the team of professionals including Don Patterson, Dennis McCollums, Tony Mann, Michael Heinick, Julie Horvath, Bart Clarke, Oscar Brogdon, Maceo Blount, and Craig Foreman. And finally, the team from the University of Hawaii, Institute for Astronomy and the extra efforts provided by Dan O'Gara, Mike Maberry, Jeff Kuhn, Jake Kamibayashi and Les Hieda.

New SLR Station Running in San Juan of Argentina

T. Wang[1], F. Qu[1], Y. Han[2], W. Liu[2], E. L. Actis[3], R. Podesta[3]

1. Chinese Academy of Surveying and Mapping (CASM)
2. National Astronomical Observatories, Chinese Academy of Sciences (NAOC)
3. Observatorio Astronomico Felix Aguilar (FELIX)

Contact: wangtq@casm.ac.cn /Fax:0086-10-68218654

Abstract

The new SLR station in San Juan of Argentina is the result of a kind of cooperation of science and technology between China and Argentina and it was running by the twenty second of February of 2006. The whole SLR system in the station was designed and developed by Chinese Academy of Surveying and Mapping (CASM) and National Astronomical Observatories (NAO) of Chinese Academy of Sciences in the years of 2000 to 2003. The investor for the SLR system is the Ministry of Science and Technology of China. The new station building including the dome in the field of Observatorio Astronomico Felix Aguilar(FELIX), Astronomical Observatories of San Juan National University of Argentina, was designed and constructed by San Juan National University of Argentina. The approximate site position of the station is 31°30´31".050S, 68°37´23".377W and the height is 727.22m. The new SLR facility in San Juan station features a good accurate and prolific SLR system according to the data reports of ILRS data analysis centers. The current status, the future update and some questions for the SLR system in San Juan station are also mentioned in this paper

Background

The new SLR system in San Juan of Argentina is based on the Science and Technology cooperation between National Astronomical Observatories (NAO), Chinese Academy of Sciences and San Juan National University of Argentina. The supporter and investor for the project are the Ministries of Science and Technology of the two countries. In fact, for more than 10 years the Felix Aguilar Astronomical Observatory of San Juan National University of Argentina (OAFA) and National Astronomical Observatories (NAO), Chinese Academy of Sciences have developed friendly cooperation on astronomical research and observation. Under the efforts of the both Observatories the cooperation on cataloguing the Southern Parts of the Earth and astronomy geodynamics using the photoelectric astrolabe MARK II (PA II) has been successful and got lot of interesting results.

At November of 2000, National Astronomical Observatories (NAO), Chinese Academy of Sciences and Felix Aguilar Astronomical Observatory of San Juan National University of Argentina (OAFA) subscribed a cooperation agreement on satellite laser ranging (SLR) to extend the relationship between the two observatories for astronomical observation and research. It is very beneficial to set up a new fixed SLR station in Argentina of South America, which located in the southern parts of the Earth, as the distribution of the SLR stations in the world will be improved better.

According to the agreements of the cooperation the Chinese Academy of Surveying and Mapping (CASM) is responsible for design, developing, installing and debugging of whole SLR system and technical training to the persons from National Astronomical Observatories (NAO) of Chinese Academy of Science and Felix Aguilar Astronomical Observatory of San Juan National University of Argentina (OAFA).The National

Astronomical Observatories (NAO) of Chinese Academy of Science is in charge of packaging of whole SLR system and to ship it to Argentina. And San Juan National University of Argentina with its Felix Aguilar Astronomical Observatory takes charge for whole constructions and decorations of the SLR room including the mobile roof of the building.

The whole SLR system was designed and developed by Chinese Academy of Surveying and Mapping (CASM) and National Astronomical Observatories (NAO) of Chinese Academy of Science in the years of 2000 to 2003 and checked and accepted by China Ministries of Science and Technology at 12th of January, 2004. The main body of the new station building in Felix Aguilar Astronomical Observatory of San Juan National University of Argentina (OAFA) was completed in August of 2005 by San Juan National University of Argentina.

So there are three layers for the scientific and technical cooperation between China and Argentina. The first and top layer, the government layer, is between the two Scientific and Technical Ministries of the two countries and this is on the layer of policy. The second layer is between National Astronomical Observatories (NAO) of Chinese Academy of Sciences and San Juan National University of Argentina and this is on the layer of administration. The third layer is between Chinese Academy of Surveying and Mapping (CASM) and National Astronomical Observatories (NAO) of Chinese Academy of Science and this is on the layer of putting in practice.

Figure 1: *San Juan SLR Station*

Figure 2: *SLR Telescope*

Site Installation

The San Juan SLR station is located in the site of Felix Aguilar Astronomical Observatory in San Juan. San Juan city is 1300km Northwest from Buenos Aires the Capital of Argentina and it is the capital city of San Juan province. San Juan is No.12 of biggest city in Argentina with its population of 20,000 citizens in downtown area. The weather in San Juan region can go up to 50º in summer with very dry character of desert Climate and it is not cold in winter time with the lowest temperature of 5º. There are plenty of fruits and melons in harvest seasons especially the grape. So San Juan is very famous for its good quality and high productivity of the wine.

Felix Aguilar Astronomical Observatory has two observation stations, the Felix Aguilar station and Leonato station. The Felix Aguilar station is about 10 km from the city center of San Juan and the office building of the Observatory is there as well as the

SLR station. The Leonato station near Andes Mountains is 200 km from San Juan city and some astronomical instruments from Germany, America and Spain in use for science and technology cooperation.

So the San Juan SLR station not far from the city San Juan and with 300 good days for SLR observations is a excellent site for astronomical observations. The geographic positions of the site are 31°30´31".050S, 68°37´23".377W and 727.22m. There is an another astronomical device in use for nearly 10 years long the photoelectric astrolabe MARK II (PA II) also cooperated with National Astronomical Observatories of China. The groundwork for the SLR telescope is not good with its screen and sand underground and no base stones within 100 meters in deep.

Installation Time Table

The whole set of the SLR device reached San Juan of Argentina on 6th of Aug., 2005. Then we were waiting for the inspecting from Argentina customs for a month and opened the cargo container on 24th of Sep. From this date to about 20th of Nov., 2005 we were waiting for the decoration of the SLR buildings and for modifying the base pillar of the telescope and the bottom of the laser. On 28th of Nov., 2005 the installing started and the installing ended on 23rd of Feb., 2006 with the first Lageos pass of data returns received last night of the date before. That means we got the first SLR pass of satellites data in San Juan Station on the night of twenty second of Feb., 2006 and sent the data to ILRS and running the station on 23rd of Feb., 2006.

Installation Difficulties

The first difficulty is insufficient for the space of installing. For safety of the transportation from China to Argentina we packaged the whole SLR systems separately to the minimum units. And we needed the base pillar of the telescope and the whole second floor under the dome that must be strong enough and stable enough to the work to do the main mirror and second mirror installing and debugging. But the base pillar still needed to repair and the second floor under the dome was made of thin wood board

***Figure 3**: Installing and debugging*

so the mirrors installing and debugging have to be in a big storage. It was not easy to do such a kind of working in a storage so it takes our nearly a month.

The second thing is the Base pillar of the telescope not fit with the telescope in height and orientation. So we have to change the height of concrete base pillar and some holes in positions and sizes. And that is very hard to do. Base for laser platform is too high and we spend lot of energy to cut the base by electric drilling machine.

Figure 4: *Base of laser platform and Base pillar of the telescope modifying*

Decoration for whole laser building not finished. So we have to do the installing and debugging for the SLR system and the decorating for the SLR building at same time. The mobile roof of the telescope we call it “dome” moves unreasonable. That repeatedly made problems with us and not safe as well.

Installation Personnel

Professor T. Wang from Chinese Academy of Surveying and Mapping (CASM) is responsible for whole installing and debugging and in charge of optics and telescope star calibrations. Professor T. Guo from Institute of Seismology, China Earthquake Administrations is responsible for electronics design and installing. Senior engineer W. Liu from National Astronomical Observatories of China is responsible for electronics and laser installing, debugging and daily maintain. Senior engineer D. Huang also from National Astronomical Observatories of China is responsible for installing and daily observations. Engineer Q. Xiang from Chinese Academy of Surveying and Mapping (CASM) is responsible for installing and daily observations. Senior engineer A. Gonzalez from Felix Aguilar Astronomical Observatory of San Juan National University of Argentina (OAFA) is responsible for electronics installing and The daily observation and maintains. Senior engineer R. Podesta from Felix Aguilar Astronomical Observatory of San Juan National University of Argentina (OAFA) is responsible for daily observations and maintains. Senior engineer E. L. Actis from Felix Aguilar Astronomical Observatory of San Juan National University of Argentina (OAFA) is responsible for daily observations and maintains. Senior engineer E. Alonso from Felix Aguilar Astronomical Observatory of San Juan National University of Argentina (OAFA) is responsible for daily observations and maintains. Senior engineer

Figure 5*: The San Juan SLR Station Team*

A. M. Pacheco from Felix Aguilar Astronomical Observatory of San Juan National University of Argentina (OAFA) is responsible for daily observations and maintains.

Daily Observations and Maintenance

To Argentina side: Monday through Wednesday 4 persons are shift on duty for observations but every day a Chinese people must be present at beginning.
To China side: Thursday to Sunday 3 persons are shift on duty and every day the free person in china side is in charge of cleaning, cooking and shopping for their living. So the work is heavy for every one.

Hope:

We hope getting 6000 passes of satellite data from all SLR satellites a year including 1200 passes from satellites Lageos-1 and Lageos-2 each year. And we hope the all data we get will have good quality.

Figure 6: *Daily Observations and review*

Problems and Questions:

The San Juan SLR station can get 6000 passes of satellite data from all laser satellites per year and they are all night productivities. That means the SLR system in San Juan station has no daytime ability now. This question refers to the laser system itself and we need a stable laser to finish the daytime ability to the SLR system.

In San Juan station the Laser is not only unstable and the spare parts damaged badly. Maybe in the laser system there are some designs unreasonable and we need to adjust the laser system every 3 or 4 days. We have only 3 sets of spare mirrors for the laser and short time after they are all damaged. So recently we have to change the positions of the damaged mirrors maintaining the laser beam output with very unstable some times. This is the second problem in San Juan station.

Some times different persons produce different quality for the data due to laser instability. Not every person can be in control of the laser adjusting so different data quality was produced in the people's shift of on duty from time to time. Dome moves difficulty and not safety are the problems and questions also. At beginning the data have big range bias due to the damaged chip in timing circuit board and now it is ok by change the chip. Running is more difficult compare to in China due to the delay of time for the spare parts transportation from China to Argentina.

Future Plan

The National Astronomical Observatories (NAO) of Chinese Academy of Sciences and Felix Aguilar Astronomical Observatory of San Juan National University of Argentina (OAFA) and Chinese Academy of Surveying and Mapping (CASM) will continue cooperate to the updating of SLR system in San Juan in the near future. The upgrading in first step is to change the SLR system to a new generation system that means we will have KHz and daytime ranging ability of course the semiconductor pumped laser as well.

But it is not soon due to the three layers cooperation and time is needed for finance support from the government and also the performance and the development of the new system need lot of time to do lot of things from China to Argentina.

The Instrumentation

The System Profiles:

The telescope was mostly rebuilt in a storage in San Juan station. It consisted of a Cassegrain receiving telescope of 60 cm aperture and a separated Galilei Telescope which collimated the laser beam with a factor of about 4.

The control computer is a common PC, even a notebook can be also, under windows operating system. All programs like satellite predictions, tracking the targets, ranging the data, data preprocessing and send the data to ILRS etc. are running on the same machine. The control computer is connected to the control interface box by parallel line and the servo system accessed to the control interface box by serial communications.

- Laser system is a Nd:YAG passive mod-locked dye laser with 30ps pulse width and single pulse energy of 30mj in green light.
- The detector is Compensated Single Photon Avalanche Diode (C-SPAD) from Czech Technical University.
- Stanford Counter SR-620

- TV system is Image Intensifier plus CCD and it collect the star and laser beam image by the main receiving telescope.
- Timing and frequency is by HP58503A GPS time and frequency receiver.
- Calibration short distance target, out-install, inside the dome.

The frame diagram of profiles for the whole system is shown as following diagram.

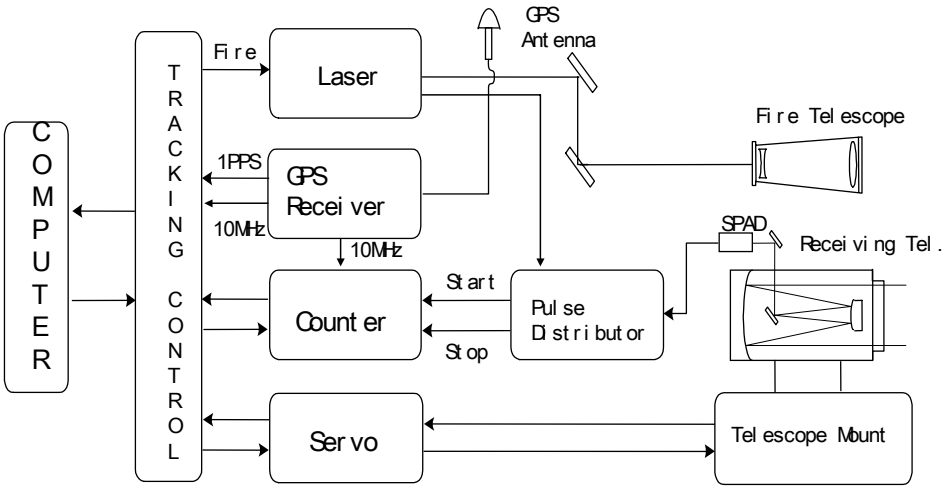

Figure 7: The frame diagram of profiles for the system

***Figure 8**: Control Room for SLR*

***Figure 9:** The Laser System*

***Figure 10**: The short distance Ground Target*

***Figure 11**: Monitoring Screen*

Optical System:

The optical receiving system has a microcrystalline glass main mirror (weight 80kg) with the diameter of 630mm and a microcrystalline glass secondary mirror with the diameter of 200mm. Also there are a spectroscope, an adjustable set of pinhole, an autocollimator and a broadband filter of 10nm in the optical receiving system. The optical receiving system is able to receive both visible light for ICCD and green laser for ranging detector without any additional adjustment due to the spectroscope.

For the transmitting path the laser beam can be guided to the Coude path via 2 reflecting mirrors and a beam expander of 2 times from the laser platform. The Coude path has 6 reflecting mirrors and from the Coude path the laser beam is guided to 16 cm diameter transmitting telescope and to the satellites.

The optical receiving and transmitting path can be shown as following drawing:

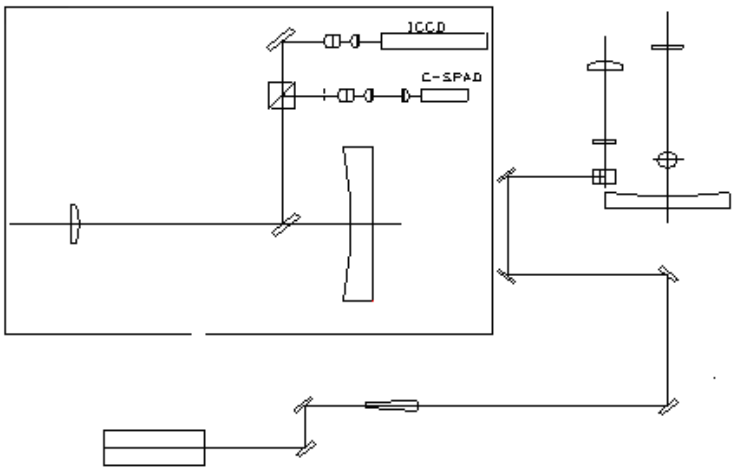

Figure 12: *Optical TR path.*

Laser System:

The computer controlled passive mode-locked laser (Nd: YAG) firing rate up to 10Hz has the pulse width of 30ps and pulse energy of 30mj for wavelength 532nm laser. It is produced by Shanghai Optics and Electronics Institute. The principle diagram of the laser is shown as following diagram:

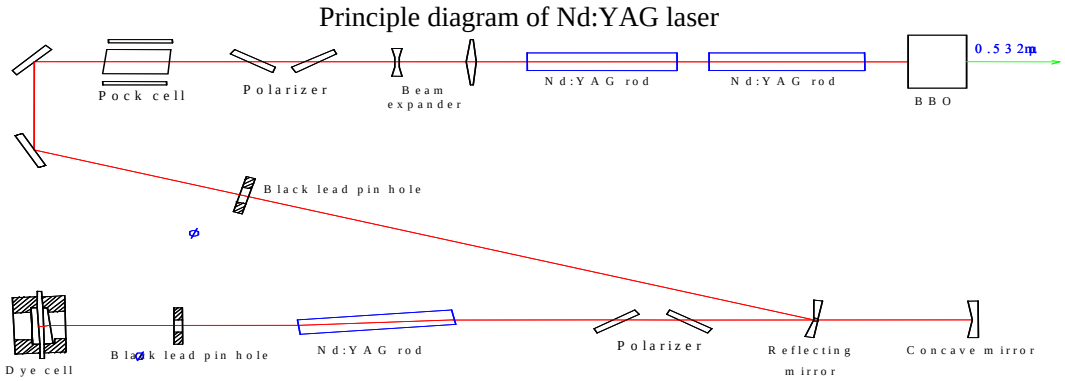

Figure 13: *Laser System.*

Tracking Control and Servo:

A common PC computer is used for telescope control, range gate setting, laser firing and data acquisition etc. All software including satellite predictions and data pretreatment is running in windows operation system and all things can be done just by the computer mouse.

Summaries

The New SLR station in San Juan of Argentina has being running since 23rd of Feb. 2006 and up to 30th of Sep. 2006 nearly 4000 passes of SLR data were sent to the analysis centers of ILRS including 799 Lageos passes and 509 high satellite passes in about 7 months (220 days) from the 2006 3rd quarter report of SLR Global Performance Report Card. That means the San Juan station has the possibility to get 6450 passes for all SLR satellites including 1325 Lageos passes and 844 high satellite passes.

Especially for the Galileo satellite GIOVE-A the San Juan station got 36 passes and it is the number 2 in the quantity line of GIOVE-A satellite by stations only following the station 7090 Yarragadee in Australia which got 45 passes.

The data quality is also very good with the calibration, satellite and Lageos precisions (RMS) of 12.4, 11.0 and 13.3 mm also from from the 2006 3rd quarter report of SLR Global Performance Report Card.

The fact above can prove the cooperation of science and technology between China and Argentina in the field of Satellite Laser Ranging is excellent successful. The SLR system in San Juan station developed by the scientists of China and Argentina has fine capability and stability although the laser is not stable and needs lot of work to maintain. The weather in San Juan station is very good we can say and be reassurance about it.

There are lots of acknowledgments to Professor Guo Tangyong from Institute of Seismology of China Earthquake Administrations and the people from Shanghai SLR station and other stations in China Laser Tracking Network for their efforts in the project.

System Improvement and GIOVE-A Observation of Changchun SLR

ZHAO You[1], FAN Cunbo[1], HAN Xinwei[1], YANG Dingjiang[2], CHEN Nianjiang[2], XUE Feng[2], GENG Lin[2], LIU Chengzhi[1], SHI Jianyong[1], ZHANG Ziang[1], SHAO Baodong[1], ZHANG Haitong[1], DONG Xue[1,3]

1. National Astronomical Observatories/Changchun Observatory, CAS
2. North China Research Institute of Electro-Optics, CGI, Beijing
3. Graduate University of Chinese Academy of Sciences, Beijing

Abstract

This paper introduces the system improvement for tracking GIOVE-A in Changchun station. During the more than two months improvement, the new servo and encoder systems were installed. And primary mirror, second mirror and some other mirrors have been cleaned and recoated. The laser system was adjusted in order to improve the laser efficiency and output. The paper gives out the improvement results, and the GIOVE-A satellite observation results.

Key Words: *system improvement, GIOVE-A observation, SLR*

Introduction of project background

Galileo system consists of 27 satellites distributed in three uniformly separated planes. In 2006, two GSTB-V2 satellites were planned in orbit. The nominal lifetime is 2 years. Four IOV Galileo satellites were planed to be launched towards the end of 2007. Full Deployment Phase and Long Term Operation will be followed the IOV. Galileo In-Orbit Validation Element (GIOVE) satellites: GIOVE-A and GIOVE-B. The objectives of the deployment of these two satellites are to:

- secure use of the frequencies allocated by the International Telecommunication Union (ITU) for the Galileo system
- verify the most critical technologies of the operational Galileo system, such as the on-board atomic clocks and the navigation signal generators
- characterize the novel features of the Galileo signal design, including the verification of user receivers and their resistance to interference and multipath, and
- characterize the radiation environment of the medium-Earth orbit (MEO) planned for the Galileo constellation.

GIOVE-A and -B were built in parallel to provide in-orbit redundancy and to secure the mission objectives. They provide complementary capabilities. GIOVE-A was launched on December 28, 2005, into an MEO with an altitude of 23,260 kilometers. Carrying a payload of rubidium clocks, signal-generation units, and a phase-array antenna of individual L-band elements, GIOVE-A started broadcasting on January 28, 2006, securing the frequencies allocated by the ITU for Galileo. Performance of the on-board atomic clocks, antenna infrastructure, and signal properties is evaluated through precise orbit determination, supported by Satellite Laser Ranging (SLR), an independent high-precision range measurement technique for orbit determination based on a global network of stations that measure the round-trip flight-time of ultra short laser pulses to satellites equipped with laser retro reflector arrays (LRAs). SLR provides instantaneous range measurements of millimeter-level precision which can be compiled to provide accurate orbits and to measure the on-board clock error.

Fig.1. *Changchun SLR telescope*

Due to the urgent need, it is necessary to select an existing SLR station to provide laser ranging service for GSTB-V2 satellites. Given the importance of SLR data for the characterization of the GIOVE clocks, the People's Republic of China contributed to the Galileo program the refurbishing of a Chinese SLR station to provide GIOVE laser-ranging observations. The Changchun station in northeast China was selected among the Chinese stations contributing to the ILRS because it had demonstrated strong MEO satellite tracking; collocation with an existing International GPS Service station; and good weather conditions. There are 5 fixed SLR stations in China nowadays. Among the stations, Changchun station possesses the best performance. Its data quantity is the most in China. It has the ability to range to the distance more than 20,000km with the accuracy less than 2cm. So Changchun SLR Station is selected to service for Galileo in the early stage. Followings are photos of Changchun station and SLR telescope:

Fig.2. *Bird view of Changchun station*

Changchun Observatory (ChO) of National Astronomical Observatory, Chinese Academy of Sciences, is a member of global SLR and GPS networks. It started Satellite Laser Ranging (SLR) since the early of 80th last century. The third generation of SLR in ChO was established during 1985. The system has the ability of tracking satellites with the distance of more than 20000km. Single-shot RMS is less than 2cm. From years ago, ChO SLR has been the best one in Chinese network, and got the No.10 rank in the

global SLR network. It is also an important and high performance station in the International Laser Ranging Service (ILRS). According to the report of ILRS, ChO SLR has the ability of tracking the high orbit satellites, such as Glonass, Etalon and GPS which have orbit height more than 20000km. Based on the Galileo satellite orbit height and the effective area of Laser Retro-Reflectors Array (LRA), the strength of return signal from Galileo satellites will be similar to that from GPS or Glonass satellites. So ChO SLR has the ability of tracking Galileo satellites.

Contents of SLR improvements

Though ChO SLR has the ability of tracking the high orbit satellites such as Glonass, Etalon, GPS and Galileo satellites, it can only get less return signal from above satellites. This is caused by the following causes:

- The coated film of the primary mirror and second mirror are damaged seriously, and now they have low reflectivity.
- The tracking system has lower precision. The mount of the telescope shakes so hard that less data can be obtained from high orbit satellite.
- The energy of output laser pulse is a little low.

Following is the Changchun SLR system structure. The dark color parts are the parts which are to be refurnished for GIOVE-A observation.

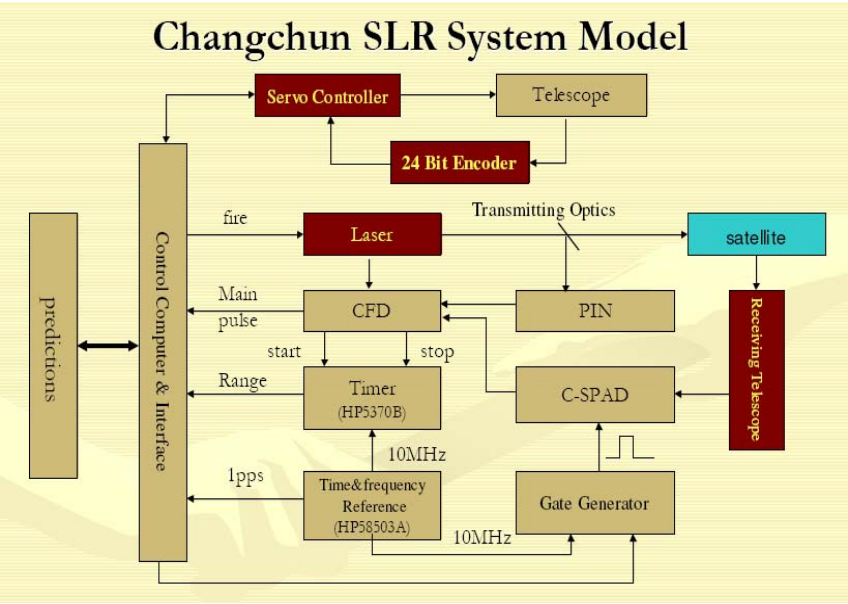

Fig.3. *Changchun SLR System*

If these parts were not improved, it would be very difficult for us to get more data from Galileo satellites and to support a long-term tracking of the satellites routinely. In order to track the Galileo satellites and get more SLR data with high precision, the following things will be done in short-term:

- Telescope. Primary mirror and second mirror of the receiving telescope must be recoated, tested, adjusted and calibrated. This will result in higher transparency of the receiving optics.
- Encoder. A new type photoelectric encoder will be installed in the tracking mount to replace the old one. This will improve the resolution of the angular sensor of the

tracking mount. This can be done in the same period with the telescope modification.

- Servo System. A new type of servo driver will be used to improve the telescope tracking performance. This will heighten the tracking precision.
- Laser System. The old laser components will be replaced in order to heighten the laser output energy up to 70-100mj and improve output stability. This will greatly increase the number of photons reflected back from the satellites.

After the system improvement, the tracking system can have less than 2" tracking precision for high orbit satellites, the output laser energy will be stronger. And these will benefit to improve the return rate and the tracking capability for high orbit satellite of ChO SLR. Finally, the system can execute the Galileo mission and get more data routinely.

Table 1. *System Specifications*

Label	*Unit name*	*Spec. name*	*Spec*	*Listed in Addendum*	*To be Tested*	*Reason*
M1	Mirrors	Reflectivity of Primary Mirror	≧98% (532nm)	Yes (p17)	Yes	
M2	Mirrors	Reflectivity of Secondary Mirror	≧99% (532nm)	Yes (p17)	Yes	
M3	Mirrors	Reflectivity of 45° Mirror	≧99% (532nm)	Yes (p17)	Yes	
E1	Encoder	Temperature Characteristics	Independent	Yes (p18)	No	Determined by principle (digital electro-optic encoder)
E2	Encoder	Current	Tens of mA	Yes (p18)	No	It's a middle spec and can be reflected by accuracy
E3	Encoder	Resolution	0.078″	No	Yes	It's critical spec of a encoder
E4	Encoder	Accuracy	σ≤1"	No	Yes	It's critical spec of a encoder
E5	Encoder	Sampling rate	500Hz	No	Yes	It's critical spec of a encoder
S1	Servo	Elevation Max Speed	8°/s	Yes (p18)	Yes	
S2	Servo	Elevation Max Acceleration	12°/s^2	Yes (p18)	Yes	
S3	Servo	Elevation Min Speed	<5″/s	Yes (p18)	Yes	
S4	Servo	Azimuth Max Speed	10°/s	Yes (p18)	Yes	
S5	Servo	Azimuth Max Acceleration	15°/s^2	Yes (p18)	Yes	
S6	Servo	Azimuth Min Speed	<5"/s	Yes (p18)	Yes	
L1	Laser	Pulse Energy	80mJ	Yes (p18)	Yes	

Performance after improvement

Table 1 lists the specifications to be tested after system refurbishment and the results. All are met the specified value. After recoated, the reflectivity and transparency of the mirrors for 532nm are as follows: primary mirror: 97.29%; second mirror: 99.049%; dichroic mirror: 99.55%; 45°reflector: 99.83%. After system modification, tracking speed and stability of the system greatly improved and output laser energy increased from 30mj to 100mj. Ranging ability increased obviously and points and passes from high satellites increased.

Following are the photos to show the recoated primary mirror, new operation console, laser output on screen, and the encoder system.

The recoated primary mirror

New operation console

Laser output on monitor

New encoder system

Up to Dec.12 of 2006, there are 28 passes of GIOVE-A and 12 passes of GPS-35, -36 to be tracked. Refurbishing work had been finished and acceptance tests were underway. The observations performed by Changchun at the time of the campaign were included in the data set as the data revealed itself to be of high value for the analysis carried out. The geographical location of Changchun (see Figures 4) was of primary importance in providing better laser-ranging coverage of GIOVE-A.

Fig.4. *World map showing geographical distribution of the first GIOVE-A ranging campaign*

Acknowledgement

The authors would like to thank Prof. WANG Jianli, Prof. XU Zhijun (Changchun Institute of Optics, Fine Mechanics and Physics, CAS); Prof. YANG Fuming, Prof. CHEN Wanzhen (Shanghai Astronomical Observatory, CAS); Prof. WANG Tanqiang (Chinese Academy of Surveying and Mapping) who partially participate in the work and their kind help.

The authors gratefully acknowledge the support of K.C.Wong Education Foundation, Hong Kong.

References

[1] Acceptance Test Plan for Phase I of Galileo Project in Changchun Station.

[2] Satellite Laser Ranging For Galileo Project in Changchun Station.

[3] Zhao You: “Upgrade of Changchun SLR System”, Proceedings of 11th International Workshop on Laser Ranging, Sep. 1998 Deggendorf, Germany, pp. 188-196.

[4] Yang Fumin, Xiao Zhikun, Chen Wanzhen, et al, “Design and Observations of the Satellite Laser Ranging System for Daylight Tracking at Shanghai Observatory”, Science in China Series A, Vol 42, No. 2, pp 198-206, 1999.

[5] You ZHAO, Cunbo FAN, Chengzhi LIU, Xinwei HAN, Jianyong SHI, Xinhua ZHANG, Haitao ZHANG: “System Stability Improvement of Changchun SLR”, Proceedings of 13th International Workshop on Laser Ranging, Oct. 2002, USA.

[6] ILRS publications SLR Station Performance Report Card 2005, on the Internet.

[7] You Zhao, Cunbo Fan, Xinwei Han, Chengzhi Liu, Xinhua Zhang, Jianyong Shi: “Progress for daylight tracking in Changchun SLR system”, Proceedings of 14th International Workshop on Laser Ranging, June of 2004, Spain, pp 179-182.

[8] Marco Falcone, Daniel Navarro-Reyes, Jörg Hahn, Michiel Otten, Ricardo Piriz, Mike Pearlman: “Satellite Laser-Ranging Campaigns”, GPS World, Nov 1, 2006.

ADVANCED CONCEPTS AND TIME TRANSFER SESSION SUMMARY

Chair: Hiroo Kunimori

New applications using all or part of SLR instrumentation were the subjects of papers presented in this session. SLR was born and has grown up in the fields of geodesy, geodynamics, and orbital mechanics, and since then has interacted with many other fields to open up new applications and users. In addition to the obvious value of SLR as a contributor to fundamental physics, geodesy and the reference frame, each organization has its own interests to use SLR for different applications. Here we have 5 oral papers and 3 poster papers including Time Transfer, Communications, Radio Astronomy, Lidar and NEO Tracking.

Time Transfer

"Progress on Laser Time Transfer Project" by Y. Fumin et al described the China LTT mission on a satellite, hopefully to be approved in the next three months. It uses dual SPAD, TDC module and Laser Retroreflector Array. The engineering model and testing are in progress. The experiment is now planned only within the China network.

"T2L2 Status Update" by E. Samain, F. Deleflie et al gave news of the Time Transfer by Laser Link project, a LASSO follow-on mission at last approved for the JASON-2 mission for 2008 launch, 30 years after the concept was made. Tests using the space segment engineering model and the ground prototype are ongoing, and an international network is being modelled.

"New Application of KHz Laser Ranging: Time Transfer by Ajisai" by T. Otsubo et al presented a simulation study for AJISAI TT revised 14 years after the concept was introduced in equation form, including a search algorithm and link budget in the KHz SLR era.

Communications

"Satellite Tracking Demonstration on Ground Using 100mm Aperture Optical Antenna for Space Laser Communication" by H. Kunimori et al described how SLR using optical communications equipment were present in a course of development of a next-generation Laser Comm terminal, and present-generation LEO-GND Laser Comm was described.

Also, in another session, a free space Laser Comm experiment over ocean over 10 miles was presented.

Radio Astronomy

"Possibility of Laser Ranging Support for the Next-Generation Space VLBI Mission ASTRO-G" by T. Otsubo et al discussed the role of SLR in POD at altitudes higher than GPS, and the engineering problems.

LIDAR

"LIDAR Experiments at the Space Geodesy Facility, Herstmonceux, UK" by G. Appleby et al.

NEO Tracking and Monitoring

"Electron Multiplying CCD Camera Performance Tests" by D. Lewova et al.

"Possibility of Near Earth Objects Distance Measurement with Laser Ranging Device" by M. Abele and L. Osipova.

Progress on Laser Time Transfer Project

Yang Fumin[1], Huang Peicheng[1], Chen Wanzhen[1], Zhang Zhongping[1], Wang Yuanming[1], Chen Juping[1], Guo Fang[1],Zou Guangnan[2], Liao Ying[2], Ivan Prochazka[3], Karel Hamal[3]

1. Shanghai Observatory, Chinese Academy of Science, Shanghai, China
2. China Academy of Space Technology, Beijing, China
3. Czech Technical University in Prague, Czech Republic

Abstract

The purposes of the Laser Time Transfer (LTT) experiment are to synchronize the atomic clocks in space to ones on the ground, and to verify the relativity theory. The LTT payload in space includes a dual-SPAD detector, a timer based on TDC device, control unit and a LRA. The expected uncertainty of measurement of clock differences for single shot is about 200ps, and the uncertainty of measurement for the relative frequency differences for two rubidium clocks is about 5×10^{-14}/ 1000 seconds. The LTT flight module is ready and is waiting for the flight mission in 2007-2008.

Introduction

Based on the successful time transfer by laser pulses between ground stations in 2003[1], the Laser Time Transfer (LTT) project between satellite and ground stations was initiated in 2004. The goals of the LTT are as follows: 1) Evaluation of performance of space clocks which are rubidium's now, and will be hydrogen clocks in the future. 2) Verification of the relativity

Shanghai Astronomical Observatory, in cooperation with the China Academy of Space Technology in Beijing, has been in charge of the LTT project. The Philosophy of the project is to make a payload as simple as possible on a satellite in a short time to verify the capability of the time transfer by laser pulses between space and ground clocks. So, a simple 40um SPAD detector with 100ps timing resolution[2] and the TDC devices with lower resolution(125ps)[3] have been chosen for the space module. The LTT project has kept going smoothly since 2004. The flight module has been built and has passed the space environmental testings.

Principle of LTT

Fig.1. shows the principle of LTT. ΔT –time difference of second pulses between space and ground clocks. T_G – time interval between the transmitting laser pulse and second pulse of the ground clock. T_S – time interval between the received laser pulse and second pulse of the space clock. τ – flight time of laser pulse between ground station and satellite. So we have:

$$\Delta T = \frac{\tau}{2} - T_G - T_S$$

where the relativity effect, system delays, atmospheric correction and so on are not included.

Fig.2. shows the block diagram of LTT. There are three main parts onboard: detector, timer and retro-reflectors.

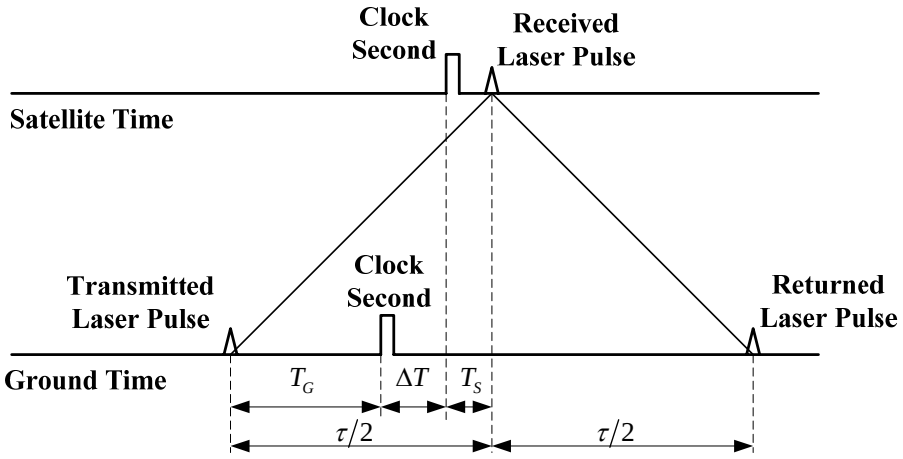

Fig.1. *Principle of Laser Time Transfer*

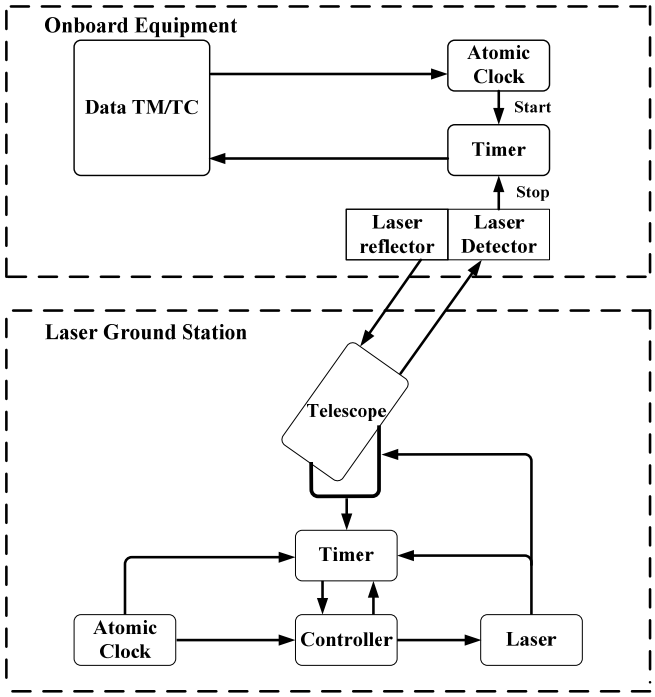

Fig.2. *Diagram of LTT*

Specifications of space module

Laser Reflector Array (LRA)

The LTT module will be installed on the satellite with an orbital altitude of about 20000km. The LRA made by Shanghai Astronomical Observatory has a planar panel with 42 retros. The single retro has an aperture of 33mm without coating on back surfaces. The LRA has the reflective area of 360cm2, and total mass of 2.5kg.

LTT module

Fig.3. is the block diagram of the LTT module. The detector is 40um SPAD made by the Czech Technical University.

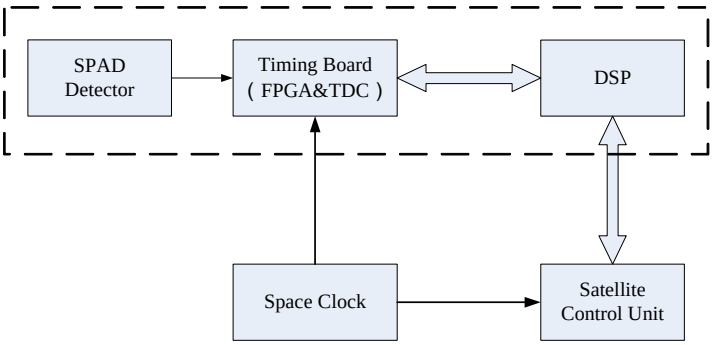

Fig.3. *Block Diagram of LTT Module*

The Specification of the detector is as follows:

- Configuration dual photon counting detector based on Silicon K14 SPAD
- active area circular 25 um diameter
- timing resolution < 100 psec
- operating temp. -30ºC~ +60ºC, no cooling, no stabilisation
- power consumption < 400 mW
- optical damage th. full Solar flux 100 nm BW > 8 hr
- lifetime in space > 5 years

Fig.4. shows the LTT detector. There are two SPAD detectors in the box, one is for spare part and can be switched by telecontrol command from ground. There aren't any lenses in front of the SPAD chips, so the receiving area on board is 40um SPAD chip only. The field of view of the detector is about 30º. There is a 10nm bandwidth filter in front of the SPAD chips.

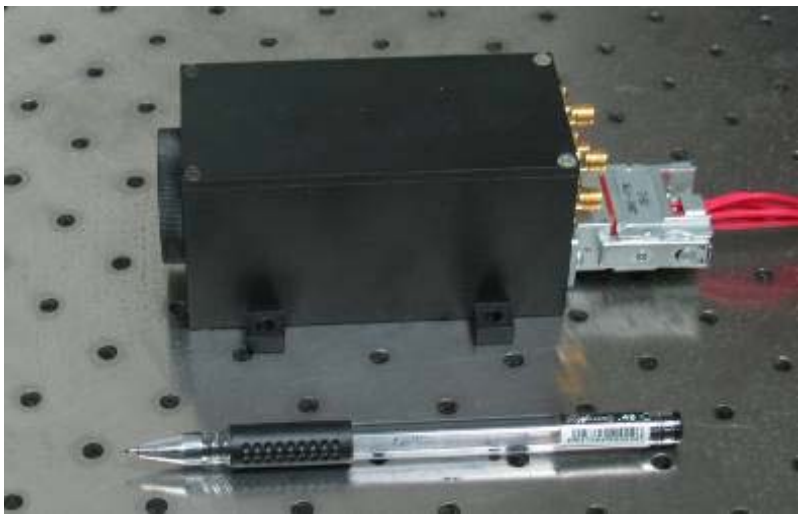

Fig.4. LTT Detector

The received photons onboard NP can be estimated by:

$$N_P = \frac{4 \cdot E \cdot S \cdot A_P \cdot K_t \cdot K_r \cdot T \cdot \alpha}{\pi \cdot R^2 \cdot \theta_t^2}$$

where

E: Laser pulse energy, 50mJ (532nm)

S: Number of photons per joule (532nm), 2.7×10^{18}

A_P: 40μm SPAD without any lenses, diameter of active area, 0.025mm
Kt: Eff. of transmitting optics, 0.60
Kr: Eff. of receiving optics, 0.60
T: Atmospheric transmission (one way), 0.55
R: Range of satellite, for MEO orbit at elevation 30°, 22600Km
θt: Divergency of laser beam from telescope, 10 arcsec
α: Attenuation factor, 0.5

We have, Np=7.0 (Photons)

It can be detected by the 40 μm SPAD detector.

The principle of the LTT timer is shown in Fig.5. The main device is TDC (Time Digit Converter) made by ACAM company in Germany. The TDC-GP1 with resolution of 125ps which had passed the radiation testing in Germany was adopted. Fig.6. shows the LTT timer.

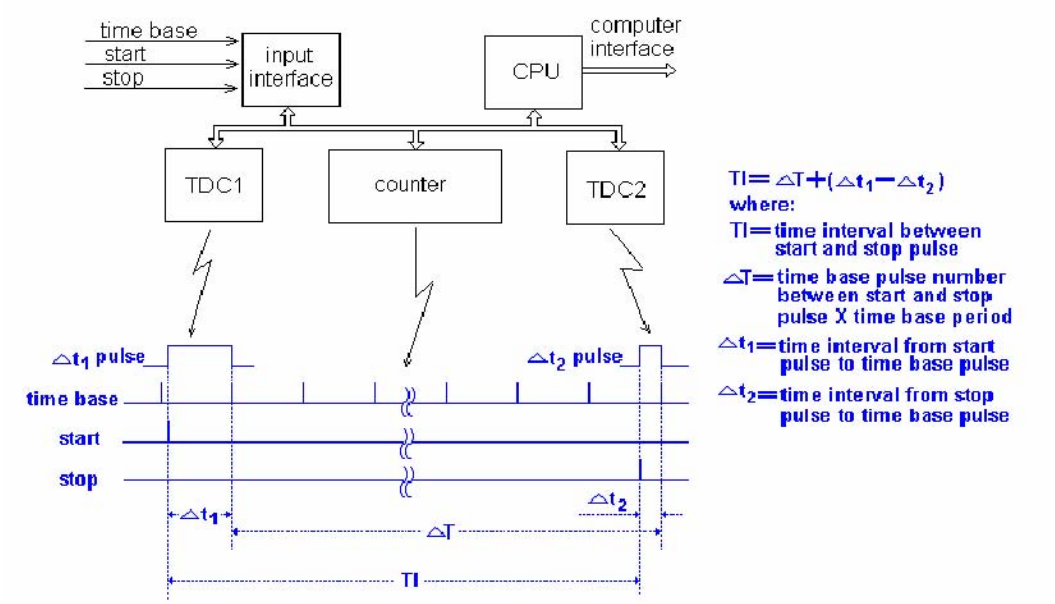

Fig.5. *Principle of the LTT Timer*

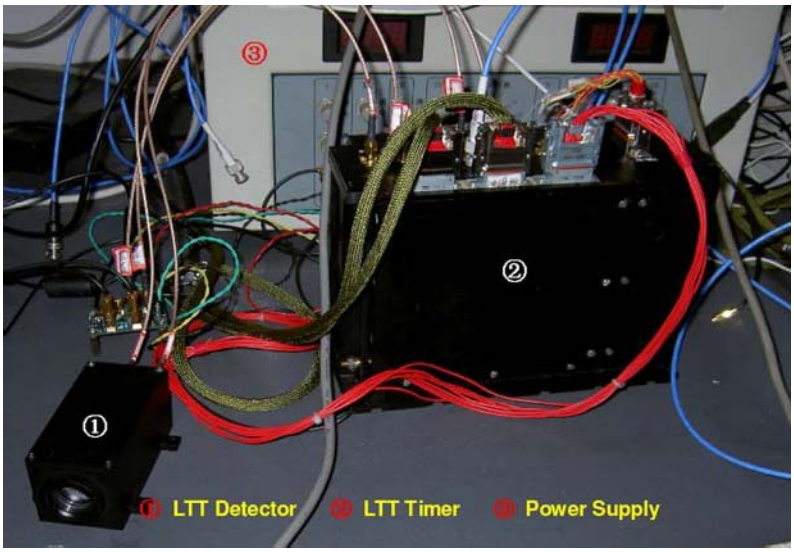

Fig.6. *LTT Timer and Detector*

The specification of the LTT timer is as follows:

- Resolution of timing 10ps
- Precision of timing 100ps
- Mass (dual-timer) 4.3Kg
- Power consumption 17W
- Size 240×100×167mm

Laser firing control for ground stations

For simplification of the module, a 40um SPAD detector without gating circuit and cooling was adopted. In order to keep from the noises produced by the albedo of the ground and the atmosphere, and the detector itself, the ground station will be asked to control strictly the laser firing epoch according to the flight time from ground station to the detector onboard, and let the laser signals arrive at the detector just after the second pulses of the clock onboard, which will start the timer onboard, by 200 ns or so. The laser pulses will stop the timer. So, it is equal to have a gate onboard.

To meet the timing requirement, the laser on the ground station should be actively switched, and the passive switch (or active-passive) can not be used. The accuracy of the prediction of the satellite's range will be about 10m, it equals to 67ns. The uncertainty of laser firing pulses can be controlled within 10ns. The prediction of the difference between the space clock's second and the ground clock's one will be better than 20ns. So we can actually control the received laser pulses with relative to the second pulses of the space clock. Therefore, it means that the time intervals among the laser firings at the station are not constant, and will vary with the distances between the ground station and the satellite.

Ground testing for timing accuracy of LTT module

Fig.7. is the block diagram for the ground testing on the timing accuracy of the LTT module. The specifications of the equipment for the testing are as follows:

- MicroChip Laser
  - Output performance
    - Output power 3μJ
    - Pulse width 650ps
  - Repetition rate 1-100Hz
  - Dimensions (L×W×H) 150×36.4×31mm
  - Weight: 250g
- Rubidium Standard 2 sets, Datum 8000
- Counter (SR620) 2 sets, Stanford Research

Fig.8. and Fig.9. show the instruments for the testing. Table 1 shows the measurement results of the ground testing.

As shown in Table 1, the accuracy of the time difference measurement is 196ps (rms). In Fig.10, line 1 is the result of clock differences by LTT, and line 2 is by the timer SR620 directly. The slope rates of the two lines are: -2.3279×10^{-10} and -2.3285×10^{-10} respectively, and they are coincident very well.

Fig.11. shows several LTT results with 2 sets of Rb clock. The uncertainty for measuring relative frequency difference is about 4×10^{-13} in 200 second and about 5×10^{-14} in 1000 seconds.

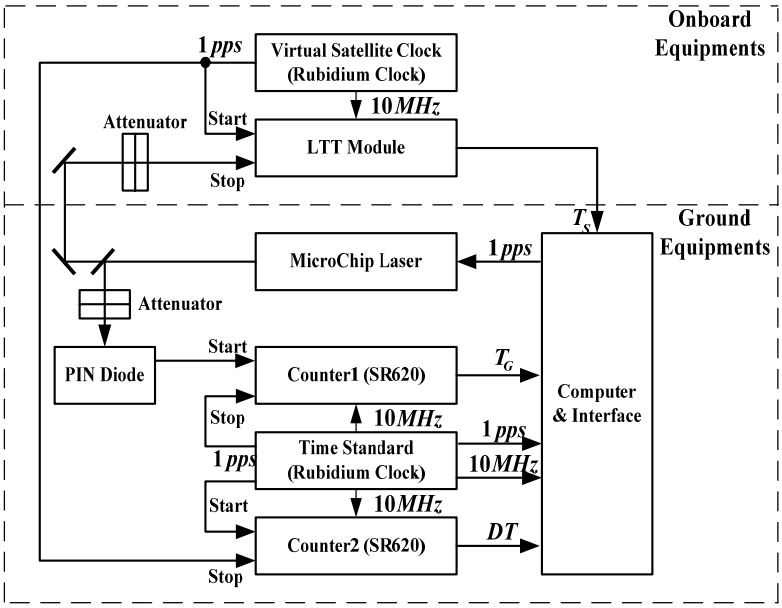

Fig.7. *Diagram of the Testing*

Fig.8. *Ground Testing Instruments*

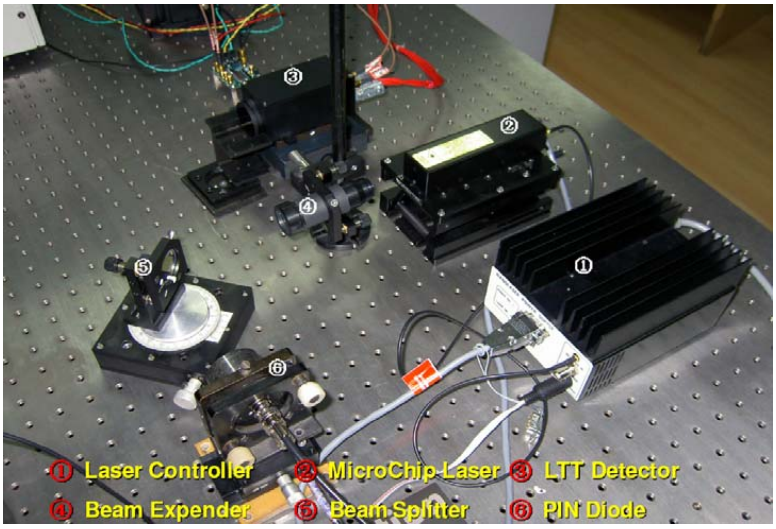

Fig.9. *MicroChip Laser and transmitting Optics*

Table1. *Result of the Ground Testing*

Epoch(s)	(1) Clock Difference by Laser(ns)	(2) Clock Difference by Counter (ns)	(1) (2) (ns)	RMS(ps)	Number of Measurement
3508.7	250300.4	250264.7	35.754	178.4	104
3953.8	250196.3	250160.5	35.783	190.6	139
4246.1	250128.3	250092.6	35.742	165.3	136
4588.9	250048.6	250012.8	35.748	266.7	148
5022.8	249946.8	249911.1	35.751	212.9	84
5498.9	249836.3	249800.5	35.792	73.1	56
5736.5	249781.4	249745.7	35.731	231.2	96
5923.8	249737.7	249702.0	35.687	224.1	103
6187.9	249676.3	249640.7	35.619	199.8	90
6374.8	249633.0	249597.5	35.488	221.6	96
Mean			35.709±0.092	196.4	

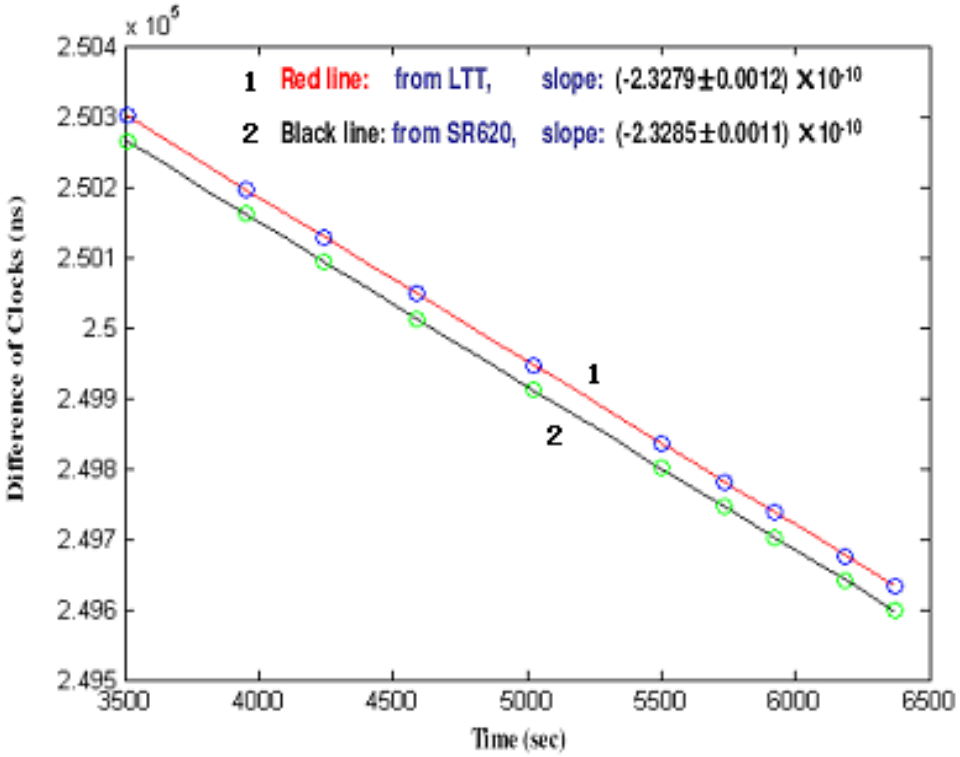

Fig.10. *Results of LTT with two Rb Clocks*

Space Environment Testing

The LTT module has passed the following testing: vibrations, shock, acceleration, thermal circulation, -40--65ºC, thermal vacuum, -40--65ºC, EMC and long term testing in high temperature.

Conclusions

The flight module for Laser Time Transfer experiment has been completed and is waiting for the mission 2007-2008. With the built-in spare parts together, the characteristics of the flight module are as follows:

- Mass 4.6Kg
- Power consumption 17W
- Dimensions:

  - 240×100×167mm (dual-timer, interfaces and power supply)
  - 105×70×50mm (dual-detector)
- Uncertainty of measurement for the relative frequency differences by laser link for two rubidium standards:
  - 4.0×10^{-13} in 200 seconds
  - 5×10^{-14} in 1000 seconds

References

[1] Yang Fumin, Zhang Zhongping, Chen Wanzhen, Li Xin, Chen Juping, Wang Bin, Time Transfer by Laser Pulses between Ground Stations, 14th International Workshop on Laser Ranging, San Fernando, Spain, 7-11 June, 2004

[2] Ivan Prochazka, Karel Hamal, Lukas Kral, Yang Fumin, Photon Counting Module for Laser Time Transfer Space Mission, 15th International Workshop on Laser Ranging, Canberra, Australia, 15-20 October, 2006

[3] TDC-GP1 User Guide, http://www.acam.de/Documents/English/DB_GP1_e.pd

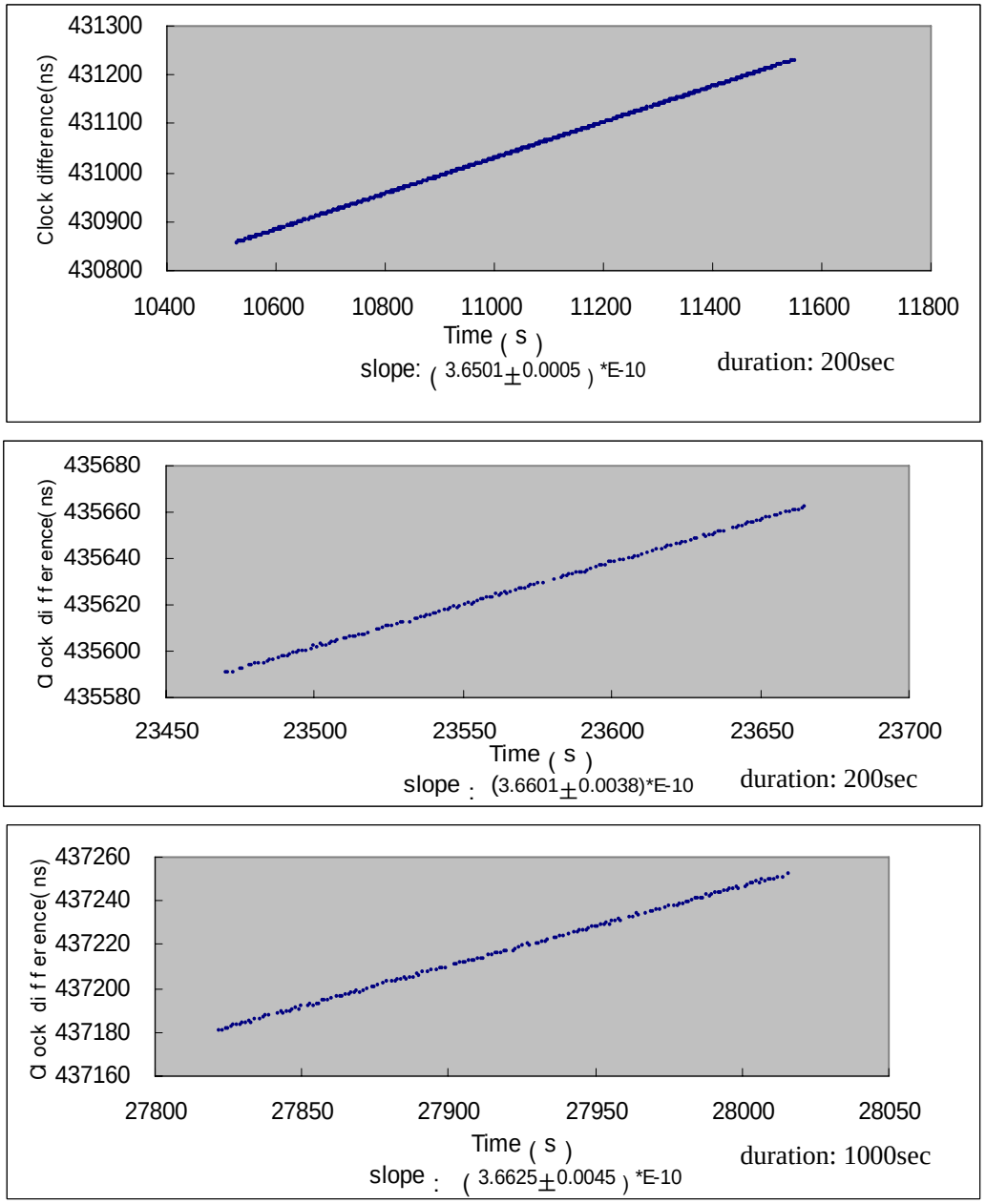

Fig.11. *LTT Results with 2 sets of Rb Clock*

T2L2 – Time Transfer by Laser Link

E. Samain[1], Ph. Guillemot[2], D. Albanese[1], Ph. Berio[1], F. Deleflie[1], P. Exertier[1], F. Para[1], F. Pierron[1], J. Paris[1], I. Petitbon[2], J.-M. Torre[1], P. Vrancken[1], J. Weick[1]

1. OCA - Observatoire de la Côte d'Azur, 06460 Caussols, France.

2. CNES - Centre National d'Etudes Spatiales, 34100 Toulouse, France.

Contact: Etienne.Samain@obs-azur.fr

Abstract

The new generation of optical time transfer T2L2 [1,2] (Time Transfer by Laser Link) has recently been accepted as a passenger of the Jason 2 satellite. The main objective of T2L2 on Jason2 is to compare remote clocks on earth. The project will also permit to follow-up from the ground, the on board clock of the DORIS[1] System. The performances expected are enhanced by one or two order of magnitudes as compared to existing microwave time transfer techniques, like GPS and TWSTFT[2]. After a description of the space instrumentation principle, we will present the metrological performances and give the current status of the project. Jason 2 will be launched in 2008 for a nominal mission duration of 3 years (5 expected) .

Introduction

The Time Transfer by Laser Link experiment (T2L2), initiated by OCA (Observatoire de la Côte d'Azur) and accepted by CNES (Centre National d'Etudes Spatiales), France, will be launched in mid-2008 on the altimetric satellite Jason 2. The experiment principle is issued from the classical laser telemetry techniques, with a specific instrumentation implemented onboard the satellite capable to tag the arrival time of laser pulses.

T2L2 history

T2L2 is the follow-on mission to LASSO (LAser Synchronization from Stationary Orbit) which was proposed in 1972 and launched in 1988 onboard the geostationary orbit satellite Meteosat P2. A first optical time transfer had successfully been achieved in 1992 between OCA, France and MacDonald, Texas [3]. This experiment measured a stability of 10^{-13} over 1000s and validated the feasibility of the concept. In 1996, a T2L2 instrument was proposed in the framework of the French PERSEUS mission to the Russian space station MIR, but the project was finally stopped at the end of the phase A. In the meantime it was accepted by ESA in the ACES (Atomic Clock Ensemble in Space) program scheduled on the International Space Station (ISS). T2L2 was one of the three scientific proposals of ACES, but had to be de-scoped in 2001 for some technical reasons concerning the whole ACES mission. Feasibility studies have been led by CNES and OCA for other flight opportunities (Myriade Micro-satellite, Galileo Test Bed), and finally a new opportunity appeared at the end of 2004, when NASA decided to abandon the WSOA instrument, an American contribution to the Jason-2 mission. A preliminary analysis confirmed the high interest to put a T2L2 instrument onto this altimetry-dedicated space vehicle and CNES decided to select the T2L2 instrument as a passenger on the Jason 2 mission.

[1] DORIS : Radio electric positioning system
[2] TWSTFT: Two-Way Satellite Time and Frequency Transfer

Principle and purpose of the experiment

T2L2 is an optical experiment that is able to establish a temporal link between remote clocks. The principle is based on the propagation of light pulses between laser stations and a satellite equipped with a specific instrumentation. The T2L2 payload is made with a photodetection device, a time-tagging unit, a clock (the DORIS ultra-stable oscillator (USO)) and a Laser Ranging Array (LRA). The ground station emits asynchronous laser pulses towards the satellite. LRA return a fraction of the received photons back to the station, while another fraction is detected and timed in the temporal reference frame of the onboard clock as (t_{board}). Each station records the start (t_{start}) and return (t_{return}) time each light pulse.

For a given light pulse emitted from station A, the synchronization χ_{AS} between the ground clock A and the satellite clock S is then derived from these data:

$$\chi_{AS} = \frac{t_{start} + t_{return}}{2} - t_{board} + \tau_{relativity} + \tau_{atmosphere} + \tau_{geometry} \quad (1)$$

$\tau_{relativity}$ is coming from relativistic effects, $\tau_{atmosphere}$ is the atmospheric delay and $\tau_{geometry}$ takes account of the geometrical offset between the reflection and detection equivalent points, depending on the relative position of the station and the satellite.

The same experiment can be lead from another station B and χ_{BS} can then be measured. The time transfer between A and B is then deduced from the difference between χ_{AS} and χ_{BS}. In a common view configuration, i.e. the two laser ranging stations are firing simultaneously towards the satellite, the noise of the onboard oscillator has to be considered over a very short time (time interval between consecutive pulses), so that it can be considered as negligible in the global error budget.

In a non-common view mode, the satellite local oscillator carries the temporal information over the distance separating laser stations. In the case of Jason 2 (driven by a quartz oscillator), we will have a significant degradation of the performances as soon as the time interval between passes is a few seconds (the maximum distance that allow this common view mode is roughly 7000 km). But in some cases, it will possible to keep a good time transfer performances even if the distance is greater than 7000 km by the use of intermediary laser stations located between station A and B. These stations will permit to build a virtual DORIS time scale from the clocks of each station.

Participation to the T2L2 experiment

The T2L2 ground segment is a laser station equipped with instrumentation to measure accurately both the start and return time of laser pulses. The laser station has to shoot with a 532 nm pulsed Nd:YAG laser having a pulse width between 10 to 200ps FWHM. The station can work between 10 Hz to a few Khz. Concerning the link budget, the conception of the space segment has been studied to detect low energy signals: the detection level onboard is comparable to the level in the ground. As a rule, if the ground station detects the impulse back, the same impulse should have been detected onboard as well.

Among the 40 laser stations in the world, 25 regularly range Jason 1 and will probably track Jason 2. Many laser stations have indicated their interest in participating to the T2L2 experiment (Figure 1).

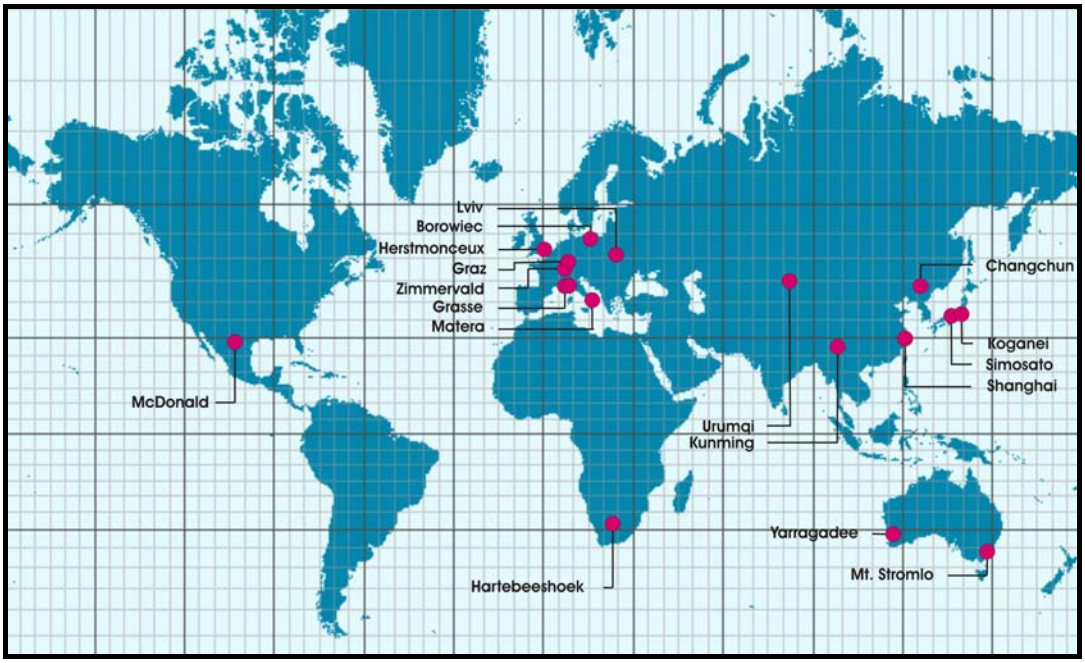

Figure 1: *T2L2 participation (October 2006)*

T2L2 on Jason 2

Jason 2 is a French-American follow-on mission to Jason 1 and Topex/Poseidon. Conducted by CNES and NASA, its goal is to study the internal structure and dynamics of ocean currents mainly by radar altimetry.

Jason 2 is build around a Proteus platform equipped with a dual-frequency radar altimeter Poseidon-3 and a microwave radiometer. For the needs of precise determination of the satellite orbit, three independent positioning systems are embarked: a Doris transponder, a GPS receiver and a LRA (Laser Ranging Array) target. The T2L2 instrument and two radiation studying payloads (Carmen-2, France and LPT, Japan) are supplementing the satellite instrumentation with some complementary objectives.

The satellite will be placed by a Delta launcher on the Jason 1's orbit at an altitude of 1,336 km and an inclination of 66°. This orbit allows common views at continental scale (about 7000 km baseline between stations). The time interval between two passes varies from 2 to 14 hours with an average duration of about 1000 s. The T2L2 specific instrumentation has a mass of 10 kg and a power consumption of 45 W. It includes (Figure 2):

- Two photo detection units located outside the main Jason 2 payload on the LRA boom (figure 3 right). Both are composed of avalanche photo detectors. The first one is working in a Geiger mode for precise chronometry[4,5] The other is in linear gain mode in order to trigger the whole detection chain and to measure the received optical energy and the reflected solar flux (earth albedo). To minimise the false detection rate, the detection threshold may be adjusted either by remote control or automatically as a function of the solar flux measurement.
- The electronic unit, located inside the Jason 2 payload module is composed of two main items (figure 3 right). The detection unit ensures the conversion of the laser pulse into an electronic signal and the event timer [6].

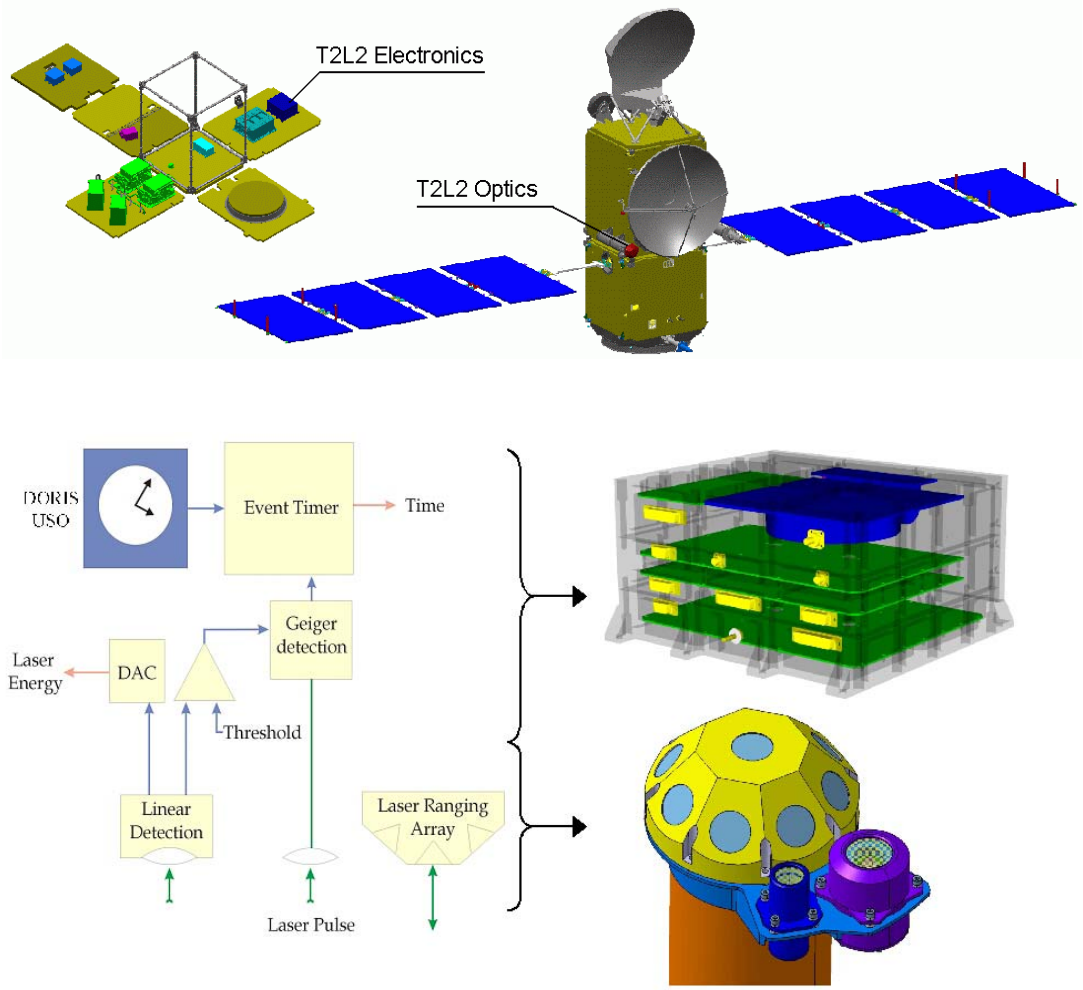

***Figure 2**: The integration of the T2L2 device inside the Jason-2 spacecraft*

Mission's objectives

The objectives of the T2L2 experiment on Jason 2 are threefold:

- Validation of optical time transfer, including the validation of the experiment, its time stability and accuracy. T2L2 will be a first step and a demonstration for future experiment based on one way laser ranging techniques in an interplanetary range: TIPO[3]. It should also allow the de-correlation of the effects coming from the target signature. In that way, it will permit to improve the precision of the telemetry.
- Scientific applications concerning time and frequency metrology allowing the calibration of radiofrequency time transfer (GPS and Two-Way), fundamental physics with the measurement of light speed anisotropy and alpha fine structure constant, Earth observation and very long baseline interferometry (VLBI).
- Characterization of the onboard Doris oscillator's drift, especially above the South Atlantic Anomaly (SAA) where the environment is highly irradiative. The two radiation instruments onboard will give the possibility to find a correlation between the expected and measured drift and propose adequate corrections.

Performance budget

T2L2 has ground-ground time transfer accuracy better than 100 ps. This will allow inter calibration between different time transfer methods by extracting the error

[3] TIPO: *Télémétrie InterPlanétaire Optique* / Optical InterPlanetary Telemetry

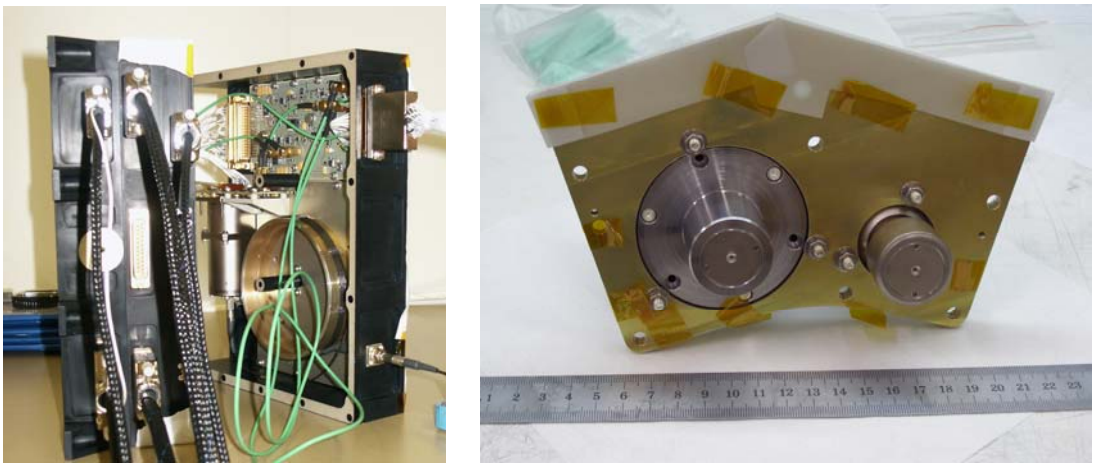

Figure 3: *Left : electronic of the flight model. The cylinder on the right side, support an multi mode optical fiber that generate a delay between the 2 photo detection. Right: the photo detection module (linear photo detector on the left side)*

caused by the transfer techniques themselves. T2L2 is particularly interesting to calibrate the regular time transfer used for the construction of international time scales (TAI) in particular the "Two-Way" (TWSTFT) that is about to become the quality reference for these scales. T2L2 will also permit to validate and to qualify the time transfers of Two-Way phase or GPS phase.

In term of stability, the comparison of T2L2 with the existing microwave links is shown on Figure 4. In a common view configuration (red bottom curve), the stability is better than 1 ps over an integration of 1,000 s. In non-common view, when conditions will not permit to build a virtual DORIS time scale, T2L2 will still offer an interesting alternative for radiofrequency calibration campaigns.

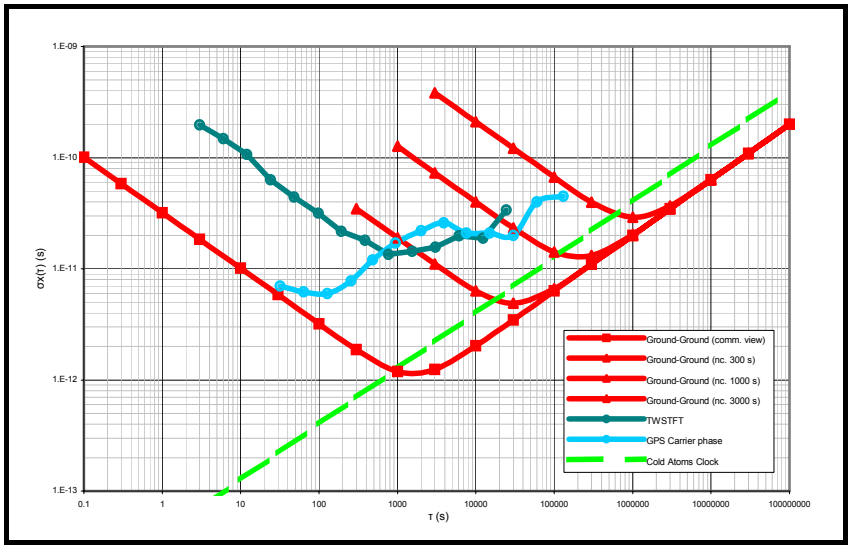

Figure 4: *T2L2 stability in common and non-common view configuration in* $\sqrt{\text{TVAR}}$

Current Status

The decision to put the T2L2 instrument in the Jason-2 satellite was taken on July 2005. The phase B started in September 2005 and entered in phase C/D in January 2006. Only one proto-flight model was built for the optics, while the electronics was developed in three steps: prototype boards, engineering model (EM) and flight model (FM). Metrological tests on EM have been done in July 2006. The flight model is now

fully integrated and the qualification processes is running now. The delivery of the instrument for the integration on the Jason 2 satellite is expected in April 2007.

A test bed has been developed at OCA to evaluate the metrological performances of the T2L2 space instrument and to perform some calibrations of both electronics and optics. This test bed will precisely reproduce the experimental conditions that will meet in orbit. The optical subsystem of the test bed was designed to simulate laser stations by illuminating the optics with faint laser pulses and also background illumination. The T2L2 photo detection module is mounted on 2 axes gimbals able to emulate the attitudes of the satellite in the range of ±60°. A high performance timing system is used as a timing reference. The experimental setup also includes a DORIS space clock engineering model in order to simulate the conditions on the satellite Jason 2, and alternatively a Cesium standard for time accuracy measurements. The tests that were so far conducted on the engineering model show the compliance with the metrology specifications for both the photo detection and the event timer.

Conclusion

With an improvement of one order of magnitude as compared to microwave time transfer techniques, T2L2 will give the possibility to compare cold atoms clocks at a level never reached before. It will allow the calibration of the existing radiofrequency links like GPS and TWSTFT with an improvement of at least one order of magnitude. T2L2 will also allow the precise characterization of the DORIS USO onboard Jason 2. The validation of the time and frequency transfer in space by T2L2 will represent an important step for further missions using this kind of technology, especially in a one-way mode in the solar system [7,8]. Jason 2 will be launched mid-2008 for a nominal duration of 3 years.

References

[1] Fridelance, P., E. Samain and C. Veillet, “Time Tranfer by Laser Link: a new optical time transfer generation”, Experimental Astronomy 7, 191, (1997)

[2] Samain, E., J. Weick, P. Vrancken, F. Para, D. Albanese, J. Paris, J.-M. Torre, C. Zhao, Ph. Guillemot and I. Petitbon, “Time Transfer by Laser Link: The T2L2 Experiment on Jason 2 and further Experiments”, Int. Journal of Modern Phys. D, World Sci. Publ. Company, (2007), (in press)

[3] P. Fridelance, C. Veillet, “*Operation and data analysis in the LASSO experiment*”, Metrologia, 32, 27-33, 1995

[4] I. Procazka , K. Hamal, “*Recent achievements in solid state detector technology for laser ranging*”, 2 , 469, Proceedings of the 9th International Workshop on laser ranging instrumentation, 1994

[5] E. Samain , “*Timing of optical pulses by photodiode in Geiger mode*”, Applied Optics, 37, No 3, pp 502-506, 1998.

[6] Samain, E. et al, OCA Event Timer , this proceedings 2006.

[7] E. Samain, One way laser ranging in the solar system, the TIPO Project (Télémétrie InterPlanétaire Optique), EGS, 2002.

[8] Wei-Tou Ni, Proceedings of the first International ASTROD symposium on laser astrodynamics, space test of relativity and gravitational – Wave astronomy, International journal of modern physics, 2002.

New Application for Khz Laser Ranging: Time Transfer Via Ajisai

Toshimichi Otsubo[1], Hiroo Kunimori[2] and Tadahiro Gotoh[2]

1. Kashima Space Research Center, National Institute of Information and Communications Technology, 893-1 Hirai, Kashima 314-8501 Japan
2. Koganei Headquarters, National Institute of Information and Communications Technology, 4-2-1 Nukui-kita, Koganei 184-8795 Japan

Contact: otsubo@nict.go.jp / FAX : +81-299-84-7160

Introduction

It was 14 years ago when the use of laser ranging technique was proposed for time transfer application for the first time (Kunimori, et al., 1992). The concept is to exchange laser pulses between two laser ranging stations via the curved mirrors carried on the AJISAI satellite (Sasaki and Hashimoto, 1987) shown in Fig. 1. The AJISAI satellite, launched in August 1996, carries 314 mirror panels as well as 1436 retroreflectors. Laser ranging stations usually detect retroreflected signals from the retroreflectors. However, the optical reflection by the mirrors were expected to be useful as if they were a two-way 'zero-delay' optical transponder, although they were originally designed to be used for photographical observations. It should be also emphasised that the optical components on the AJISAI satellite has almost no limit of lifetime, and therefore it can be used for many decades with no risk factors for long-term variation of transponder delay, etc.

This concept has not been realised yet. In this paper, the difficulties we have encountered for the realisation of this concept are briefly reviewed. Then, some new possible approaches, especially the use of the kHz laser ranging technology, are proposed. A possible scenario is lastly given based on the assumption of multiple kHz laser ranging station in Europe region (Kirchner and Koidl, 2004; Gibbs, et al., 2006).

Time Transfer via AJISAI: Concept and Difficulties

As seen in Fig. 1, the surface of the AJISAI satellite is mostly covered by the mirrors whose curvature is 8.5 to 9 metres. The size of each mirror panel is approximately 400 cm2 (~ 20 cm by 20 cm) at maximum. The laser retroreflectors (12 retroreflectors in one holder) are placed in the gap of the mirror panels.

This satellite flashes three or six times per its rotation period when it is illuminated by the sun. This is because three mirror panels located in the same row point toward the same latitudal angle. The placement of mirror panels was arranged so that the flashed mirror panels can be identified by the time intervals between flashes.

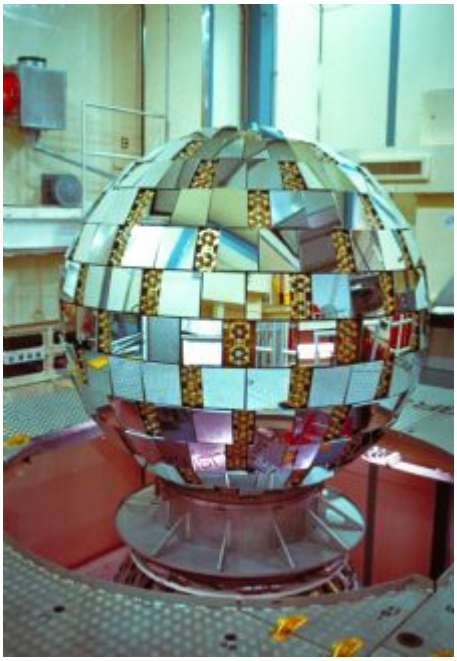

Figure. 1. *Japanese geodetic satellite AJISAI (photo: courtesy of JAXA).*

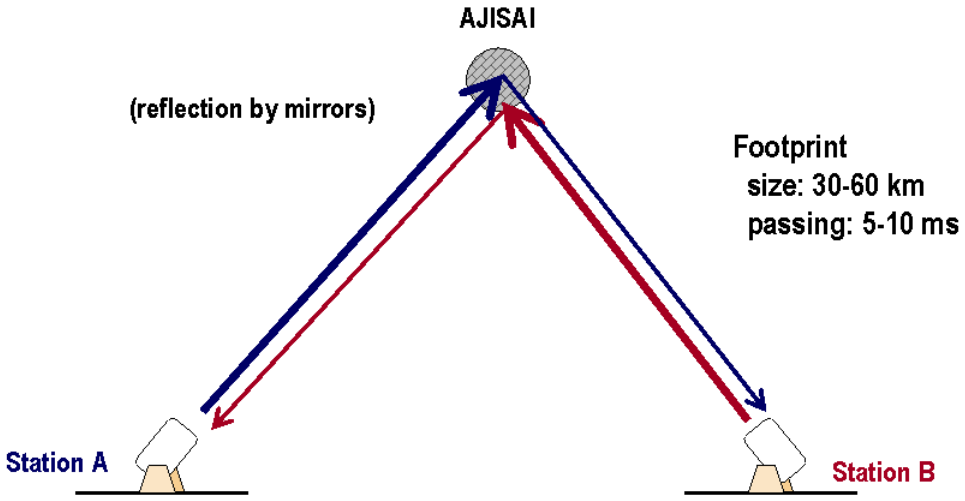

Figure 2. *AJISAI time transfer experiment: basic concept.*

A schematic view of the time transfer experiment via AJISAI proposed by Kunimori et al. (1992) is shown in Fig. 2. Like the radio-based two-way time transfer, the signal transmitted from one station goes to the other and vice versa. The curved mirrors make the reflection beam much wider to about 30 to 60 km size. Such a large footprint passes the receiving station just in 5 or 10 milliseconds.

The time diagram of signal passage between station A and B is illustrated in Fig. 3 where the 'ordinary' ranging of the station A and the signal transfer from the station A to the station B are shown. The signal transfer from the station B to the station A is simply given just by swapping the subscripts A and B. The case [1] is the prediction where the distance (in a time unit) R_{A1}* is the predicted one-way distance from the station A to the satellite and the time duration D_{A1}* is the predicted one-way internal system delay. The laser pulse is intended to hit the satellite at epoch t_0 of an imaginary 'true' clock. Assuming the clock of the station A is fast by ΔT_A compared to the 'true' clock, the station-transmission and the satellite-hit events come earlier by ΔT_A (case [2]). In reality, the laser does not exactly fire at the commanded epoch, and the delay is hereby set to L_A (case [3]). Now the start event $t_T(A)$ is given as:

$$t_T(A) = t_0 - \Delta T_A - R_{A1}^{*} - D_{A1}^{*} + L_A \quad (\text{'true' clock})$$
$$= t_0 - R_{A1}^{*} - D_{A1}^{*} + L_A \quad (\text{station A's clock})$$

Then, neglecting the centre-of-mass correction of the satellite, the reflected signal by retroreflectors comes back to the station A at:

$$t_R(A \to A) = t_0 - \Delta T_A + R_{A2} + (R_{A1} - R_{A1}^{*}) + D_{A2} + (D_{A1} - D_{A1}^{*}) + L_A \quad (\text{'true' clock})$$
$$= t_0 + R_{A2} + (R_{A1} - R_{A1}^{*}) + D_{A2} + (D_{A1} - D_{A1}^{*}) + L_A \quad (\text{station A's clock})$$

where R_{A1} and R_{A2} are the true outgoing and incoming one-way distance and D_{A1} and D_{A2} are the true outgoing and incoming one-way internal system delay.

What we usually use for the laser ranging is the difference (time interval) of the above two:

$$t_R(A \to A) - t_T(A) = R_{A1} + R_{A2} + D_{A1} + D_{A2}$$

from which we subtract the internal system delay D_{A1} +D_{A2} to obtain the two-way distance R_{A1} +R_{A2}. The clock offset ΔT_A and the laser firing delay L_A does not appear here, and therefore they are hardly observable from the ordinary laser ranging measurement.

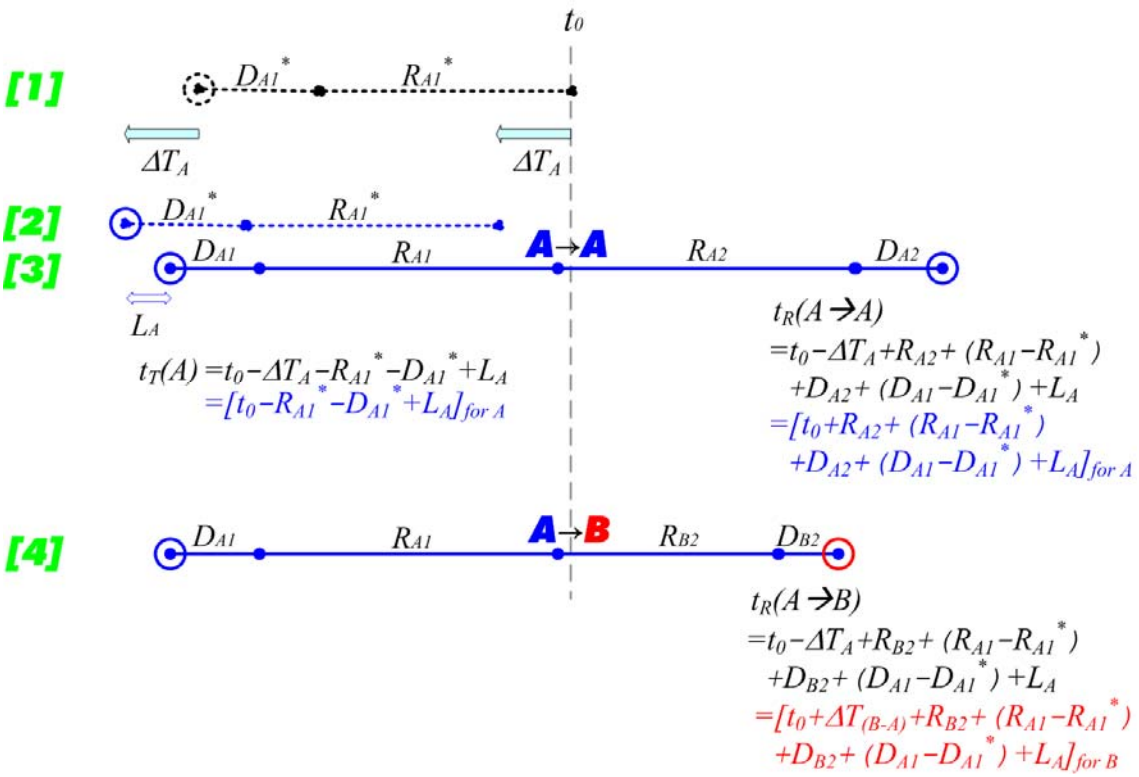

Figure 3. *Time diagram of ordinary laser ranging (A→A) and time transfer (A→B).*

Coming back to Fig. 3, the case [4] shows the signal transfer from the station A to the station B. The stop event at the station B comes at:

$$t_R(A \to B) = t_0 - \Delta T_A + R_{B2} + (R_{A1} - R_{A1}^*) + D_{B2} + (D_{A1} - D_{A1}^*) + L_A \quad \text{('true' clock)}$$
$$= t_0 + \Delta T_{B-A} + R_{B2} + (R_{A1} - R_{A1}^*) + D_{B2} + (D_{A1} - D_{A1}^*) + L_A$$
(station B's clock)

where the subscript B corresponds to variables for the station B. The opposite direction from the station B to the station A is given by an equation of swapping A and B in the above formulae. Using them, the two-way time transfer to obtain the difference of the clock offset, $\Delta T_{B\text{-}A} = \Delta T_B - \Delta T_A$ is given as the difference of two range observations $\rho_{A\text{->}B}$ and $\rho_{B\text{->}A}$, as below:

$$\rho_{A\to B} - \rho_{B\to A}$$
$$= t_R(A \to B) - t_T(A) - t_R(B \to A) + t_T(B)$$
$$\vdots$$
$$= 2\Delta T_{B-A} + [(R_{B2} - R_{B1}) - (R_{A2} - R_{A1})] + D_{B2} - D_{B1} - D_{A2} + D_{A1}$$

Now the double-difference $[(R_{B2} - R_{B1}) - (R_{A2} - R_{A1})]$ can be precisely calculated from the orbital motion of the satellite. On the other hand, the double-difference of the incoming/outgoing one-way internal system delay should be given to obtain the absolute value of $\Delta T_{B\text{-}A}$. That is, either (1) incoming minus outgoing (D_{A1} - D_{A2}) and (D_{B1} – D_{B2}) should be given, or (2) inter-station difference of one-way internal system delay (D_{B1} - D_{A1}) and (D_{B2} – D_{A2}) should be given. These values cannot be easily measured from the ordinary laser ranging systems. Note that, in spite of the difficulties in deriving the absolute accurate $\Delta T_{B\text{-}A}$, the variation of clock offsets would be relatively easily observed, leaving the constant offset of the '*D*' values and assuming them to be constant.

Beside this issue, the experiment itself has seemed unrealistic due to the following problems:

(a) The footprint passage time duration is just 5 to 10 ms. Compared to the laser firing interval of 100 to 200 ms (5 to 10 Hz lasers), it is much shorter. The footprint passage happens usually only three times per the rotation period of AJISAI, currently ~ 2s. Hence, the probability of hitting the laser at the right time was just 2.5 to 10 %. The chance was very limited.

(b) The mirror-reflection signal should reach the other station. If one wants to use a single range gate (common to laser ranging observation), the signals from the station A and the station B should hit the satellite almost at the same time. The multiple stop events should also be recorded, which is not possible by the ordinary time interval counters.

(c) The expected number of photons was just 1 to a few photons for the mirror-reflection signals, assuming a 100mJ/pulse laser. Very high sensitivity (or very strong laser) was required.

Expected breakthrough using kHz laser ranging technology

The problems (a) and (b) in the previous section are likely to be solved by the newly emerging kHz laser ranging networks. Firstly, as for the problem (a), the kHz laser (2 kHz in this case) fires 10 to 20 times per the footprint passage duration. The observation opportunity will not be missed. The kHz laser ranging systems almost automatically requires an event timer, instead of a time interval counter, due to the longer satellite ranges compared to the laser firing interval. The problem (b) will also be solved.

Especially in the European laser ranging network, multiple stations are moving toward the kHz laser ranging, following a very successful achievement at Graz, Austria. This region might be useful to exchange time signals via AJISAI between ~1000 km distant stations.

On the other hand, the link budget issue (the problem (c) in the previous section) gets more serious with kHz lasers. For instance the laser energy transmitted from the Graz system is 400 μJ/pulse, which is only 0.4 % of a traditional 100 mJ/pulse laser. The expected number of photons becomes a few hundredths of photons/pulse, and 1/10 to 1 photons/footprint passage. This would probably be the key issue for the realization of this experiment. We need to increase the laser energy and/or enhance the optical efficiency.

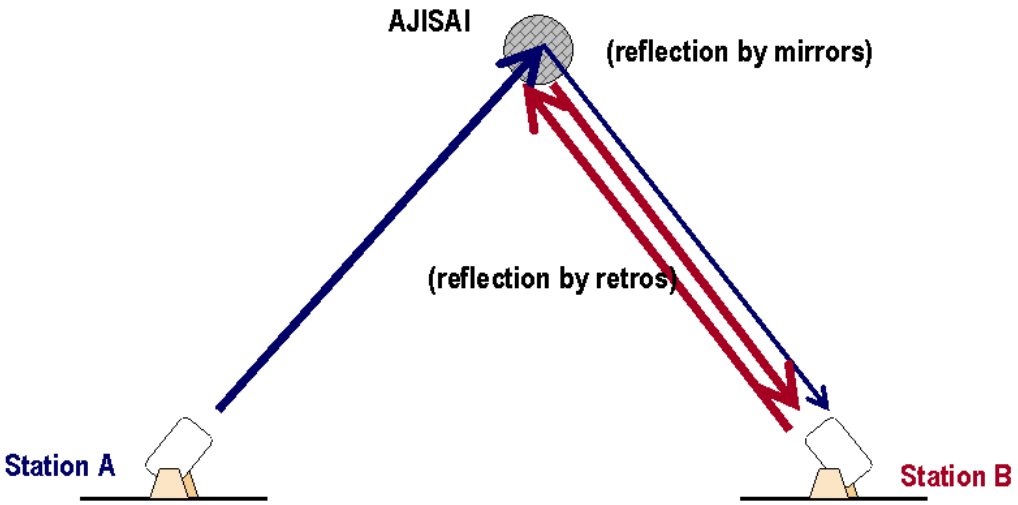

Figure 4. *AJISAI time transfer experiment: new concept.*

New experiment algorithms

As the single (A→B or B→A) signal transfer itself seems an uneasy task due to the weak link, we cannot expect the two-way (A→B and B→A) signal transfer at least at the initial stage. We re-examined the time diagram (Fig. 3) and conceived a novel way to achieve the time comparison experiment, as follows.

Let us assume the situation illustrated in Fig. 4, that is, one gets the single (A→B) signal transfer and the laser ranging (B→B). Subtracting the former range observation $\rho_{A->B}$ by the latter range observation $\rho_{B->B}$:

$$\begin{aligned}
&\rho_{A\to B} - \rho_{B\to B} \\
&= t_R(A \to B) - t_T(A) - t_R(B \to B) + t_T(B) \\
&\quad \vdots \\
&= \Delta T_{B-A} + [R_{A1} - R_{B1}] + [D_{A1} - D_{B1}]
\end{aligned}$$

where the clock offset difference $\Delta T_{B\text{-}A}$ appears. The second term, one-way range difference $[R_{A1} - R_{B1}]$, can be given at a few cm precision from an orbit determination procedure. The centre-of-mass corrections for R_{A1} and R_{B1} are different in this case due to the different reflection point: a mirror and retroreflectors, which should be taken into account for sub-nanosecond time comparison. The third term, difference of one-way outgoing system delay $[D_{A1} - D_{B1}]$, is still a problem to be solved, like the case of the two-way signal transfer. It is, nevertheless, now a difference of outgoing system delay, not the double difference of outgoing and incoming system delay.

Likewise, for example, by subtracting $\rho_{A->B}$ by $\rho_{A->A}$, the outgoing path will be cancelled and the incoming differences should be considered.

In this way, the clock offset information can be obtained by the single signal transfer and the ordinary laser ranging observation. This will ease the difficulties, especially on the weak link budget.

Conclusions

The time transfer via AJISAI is a long-lasting technology potentially with a very high precision/accuracy of 100 ps or even better. This will be one of new fields for a newly emerging kHz laser ranging 'network', especially in Europe. We have also derived a new algorithm which requires only single signal transfer, which will ease the weak link problem.

References

[1] Kunimori, H., F. Takahashi, T. Itabe, A. Yamamoto, "Laser ranging application to time transfer using geodetic satellite and to other Japanese space programs," Proc. 8th International Workshop on Laser Ranging Instrumentation, 1-34—1-42, 1992.

[2] Sasaki, M. and H. Hashimoto, "Launch and observation program of the experimental geodetic satellite of Japan," IEEE Trans. Geoscience and Remote Sensing, GE-25, 5, 526-533, 1987.

[3] Kirchner, G. and F. Koidl, "Graz KHz SLR System: Design, Experiences and Results," Proc. 14th International Workshop on Laser Ranging, 501-505, 2004.

[4] Gibbs, P., C. Potter, R. Sherwood, M. Wilkinson, D. Benham, V. Smith, "Some Early Results of Kilohertz Laser Ranging at Herstmonceux," in these proceedings, 2006.

A Satellite Tracking Demonstration on Ground Using a 100mm Aperture Optical Antenna for Space Laser Communication

H. Kunimori[1], M.Okawa[1], H.Watanabe[1], Y. Yasuda[2]

1. National Institute of Information and Communications Technology
2. Emeritus Waseda University, Japan
Contact: kuni@nict.go.jp , 4-2-1 Nukui-kita, Koganei 184-8795 Japan

Abstract

The Next Generation LEO System (NeLS) optical terminal was designed for 1.5um wavelength and 2Gbps data rate communication between 500 km – 3000 km inter-satellite link. In the course of ground validation test, using Coarse Pointing Mechanism and Optical Antenna, we demonstrated open tracking capability by ranging to a satellite AJISAI.

Introduction

The Next Generation LEO System Research Center (NeLS) in National Institute of Information and Communications Technology (NICT), of Japan, formed in 1997 for the key technology development of space communication network in future [1,2]. Fig. 1 and Fig. 2 show a concept and development schedule for optical communication part, respectively. Since 2002, it has focusing on the development of optical inter-satellite link technology for the future communication demanding a high data transmission for global multimedia service, as well as requirement of earth observation/ science data communication to ground.

Figure 1: *Concept of NeLS: Next Generation LEO System*

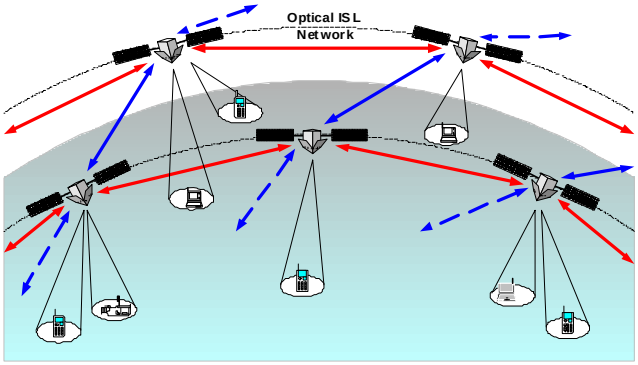

Optical terminal and key components

Fig. 3 shows block diagram of optical terminal. The optical terminal consists of four units, namely 1) Coarse Pointing Mechanism (CPM) located outside the spacecraft on mission panel, 2) Optical Antenna (OANT) as one of fixed part of optics located on mission panel 3) AT&P unit located outside the spacecraft, and 4) Communication Unit which interface both transmit & receive by optical fibers, located inside the spacecraft.

Figure 2: *NeLS Optcal Engineering Model Development Schedule*

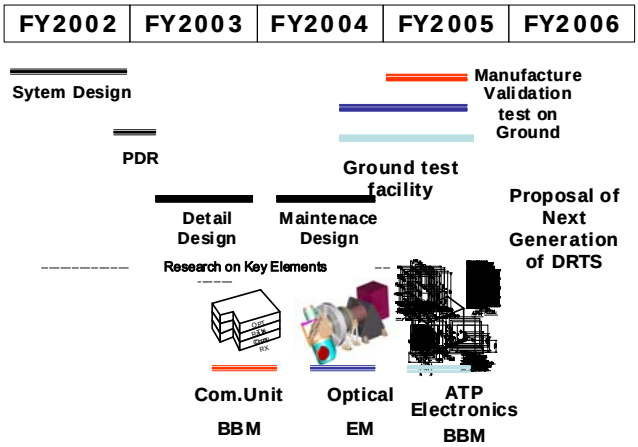

Figure 3: *NeLS Optical Terminal*

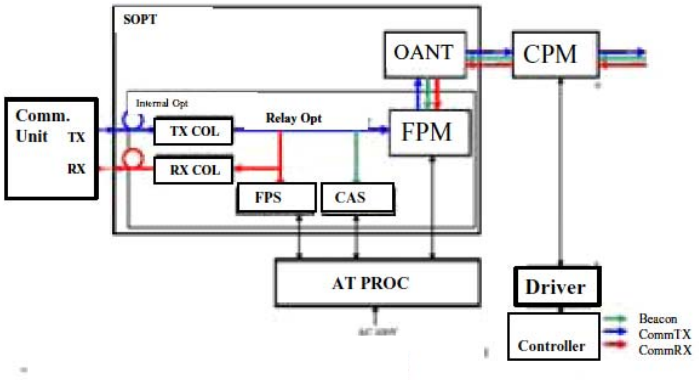

Figure 4: *A 10cm class Coarse Pointing Mechanizm (CPM)*

Item	Specification
Range of drive axis	Az:+/-275deg EL:+/-110deg
Maximum drive speed	3.0deg(slew) 1.0deg(track
Effective aperture size	85mm
Resolution of encorders	2/10000deg
Weight	16kg

CPM utilizes two-flat mirror type 2-axis gimbals (shown in Fig.4 picture and specification) so-called elbow-type has been adopted to cover all direction in space, where optical antenna fixed to satellite body.

In addition to OANT, as a fixed part of optics, a wide range Fine Pointing Mechanism (FPM), a Coarse Acquisition Sensor (CAS), a Fine Pointing Sensor (FPS), a Transmitting Collimator (TX COL), and a Receiving Collimator (RX COL) are integrated onto an optical bench with relay optics. AT&P UNIT includes terminal control processor circuit and power supply.

The Optical Antenna shown in Fig.5 has type of Cassegrain, where secondary mirror is supported by tripod and main reflector diameter of 125mm diameter, made by material of SiC with gold coating. Total effective focal length is 2600mm and magnification is about 20.

Other key components of internal optics include a fine pointing mirror made by voice coil actuators and GAP sensors, and transmitting and receiving fiber couplers has been tested as space qualification devices(Fig.6).

Figure5: *Subsystem - OPTICAL ANTENNA*

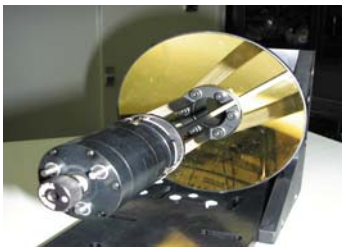

Figure 6: *Key components of internal optics*

Fine Pointing Mirror (FPM)

Transmitting Fiber Coupler (left)
Receiving Fiber Coupler& QD (right)

Utilities for ground test

To perform functional test and validation of optical terminal, we have developed one of utilities an optical tracking simulators utilized in a room spacing several meters between optical terminal and target

Figure 7: *Optical Tracking Simulator for ground experiment*

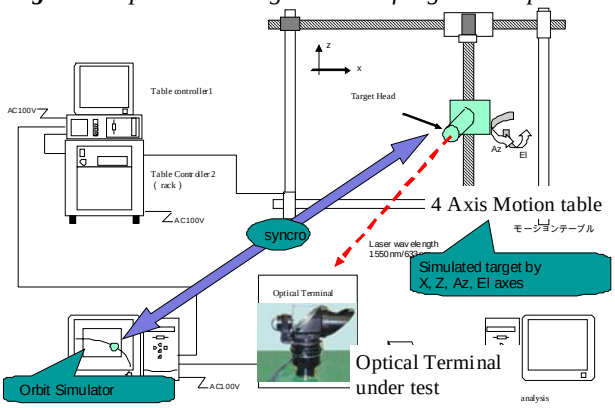

antenna. The target has on 4 axes (X-Z, Tip/Tilt) movement platform and has optical INPUT/OUTPUT capability. Fig.7 shows a schematic configuration of optical tracking simulator. The movement is programmed based on orbit simulation. Although the optical characteristics of terminal is different from that of far field, a basic function of acquisition and tracking during communication has been tested and 2.5Gbps communication BER data acquired and application of HDTV was demonstrated.

Another utility for optical terminal on ground outside, air-conditioned enclosed dome with a 30cm diameter optical window has been developed (Fig.8). The dome has axis of azimuth and rotor on azimuth structure made of stainless steel. The dome is on a box with 2 x 1 x 1 meters dimension, in which there is optical table set as vibration isolated manner, carrying optics and mechanics. Under table there are room and also carrying drivers of dome and electronics and power supply for optical terminal.

Fig.9 shows a schematic view of arrangement in a dome box called MML (Micro Mobile Laser) utility box. It also has optics for satellite laser ranging set that sharing beam through CPM by 45 degrees flat mirror.

Satellite Pointing capability test

Figure 8: *Utility development for Ground outside experiment*

The CPM was set up on optical bench so that mechanical & optical axis is aligned to gravity field (i.e. leveling) and other principal axis of equipments (laser and receivers). Two axis intersection angle offset orthogonality was measured as 80 ± 5 arcseconds. And star calibration of axis resulted in several arcseconds rms after rigorous alignment work done. Fig.10 shows a follow-on error when CPM tracking a Starlette satellite simulation pass which maximum elevation of 85 degrees. Two passes consecutively run shown. Since keyhole effect exists at zenith on Alt/Az axis gimbals, the performance of Az axis about maximum elevation was degraded to 10 arcseconds, however most of errors except key hole was within one arcsecond. Elevation axis has the same characteristics, but mean following error was larger (2 arcseconds rms) than that of Azimuth. Using standard SLR equipment with a nano second pulse width and 20mJ/pulse Nd:YAG lasers set up on table. We have performed laser ranging to a satellite AJISAI. Return proves the tracking system as open loop (means no use of beacon from satellite) working. Fig.11

Figure 9: *Configuration of Optical comm. and SLR equipments*

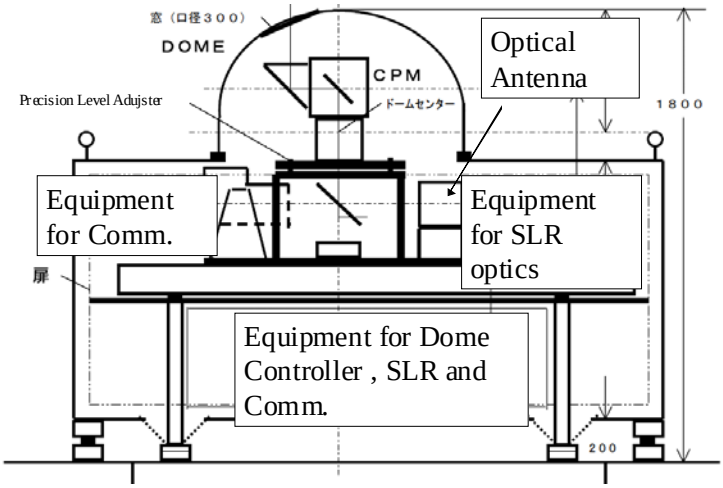

shows range residual vs observation time and there is a series of dots among dark noise and background noises that is from satellite returns. Fig.11 shows range residual vs observation time and there is a series of dots among dark noise and background noises that is from satellite returns.

We have had such four passes acquiring satellite returns during two weeks campaign. During campaign ranging to fix target to a 20meters to 4km distance was used as calibration of range as well as beam divergence and direction. The location of 4km distance is used as fixed distance communication experiment being done almost paralleled.

Figure 10: *LEO Tracking follow-on error evaluation of CPM by Starlette 85 deg elevation pass*

Black dot: Following Error Axis range+- 15arcsec
Red dot error RMS(2sec avarage) Axis range 0-10arcsec

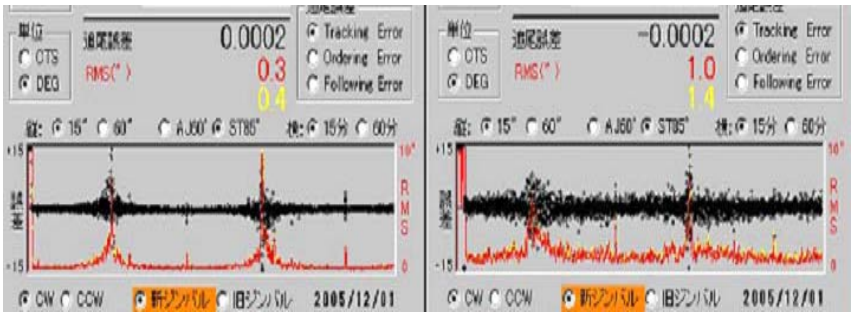

AZ axis:
<1arcsec rms except around zenith about 10arcsec rms

EL axis:
< 2arcsec rms except around zenith about 6 arcsec rms

Summary

The Next Generation Inter-satellite Laser Communication Terminal Optical Part Engineering Model has been developed. By using newly developed utility for ground

test validation, such as 4 axis motion table, mobile dome, optical terminal for 1.5um wavelength and 2.4Gbps data rate was evaluated in near-field (5m-5km) including ATP performance with atmospheric existence. Using Coarse Pointing Mechanism (CPM) and 10 cm class Optical antenna and, and associated 532nm pulse laser connection pass, we have demonstrated open-loop satellite tracking capability by ranging to AJISAI. Next Step is now using evaluation of those, we are proposing the next generation of DRTS (Data Relay Technology Satellite) in early 2010's

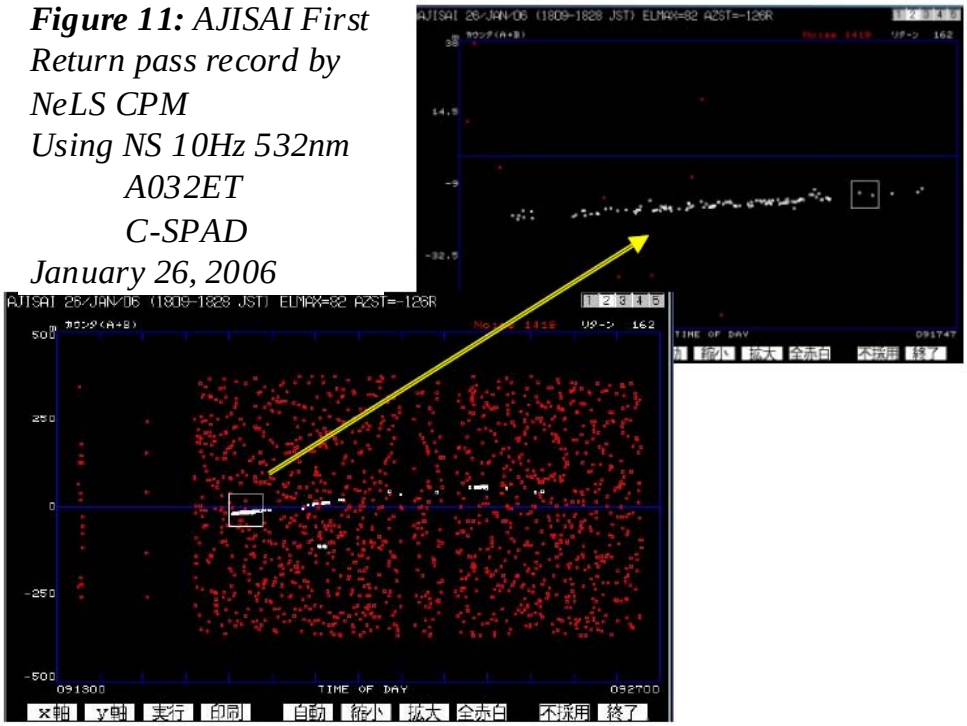

Figure 11: *AJISAI First Return pass record by NeLS CPM Using NS 10Hz 532nm A032ET C-SPAD January 26, 2006*

Acknowledgement

Authors would like to special thanks to who support the NeLS ground-satellite test experiment, namely N.Endo (INDECO), T.Yamaguchi (DENOH), Y.Suzaki (UNIVERSE), A.Hasegawa (SHOTOKU) and J.Guilfoyle (MTP).

References

[1] E. Morikawa, et.al, "R&D of A Next Generation LEO System for Global Multimedia Mobile Satellite Communications", 53th International Astronautical Congress, IAC-02-M.4.02, Huston US, 10-19 Oct. 2002.

[2] Y. Koyama, et.al., " Optical terminal for NeLS in-orbit demonstration", Proc.SPIE .Vo.5338, pp29-36., Jan.2005.

The NASA Satellite Laser Ranging Network: Current Status and Future Plans

David L. Carter[1]

1. NASA Goddard Space Flight Center, Code 453, Greenbelt, Maryland, USA 20771

Abstract

Over the past few years, the NASA Satellite Laser Ranging (SLR) Program has experience a resurgence of energy. In preparation for the completion and deployment of the SLR 2000 Replacement Systems, the NASA heritage SLR network continues to provide quality SLR data products to the International Laser Ranging Service (ILRS). Recently, NASA made the decision to return two critical stations in Maui, Hawaii and Arequipa, Peru back to operational status. NASA has been working hard to bring these two stations back on-line with the replacement of the HOLLAS station with the TLRS-4 system and the re-start of the TLRS-3 system. Other highlights have occurred throughout the NASA SLR network. The current status and the future plans of the NASA SLR Network will be discussed in this paper.

Background

The NASA SLR network consists of eight stations. NASA built five trailer-based Mobile Laser Ranging Stations (MOBLAS) and two highly compact Transportable Laser Ranging Systems (TLRS). The University of Hawaii and the University of Texas have operated two high performing Observatory SLR systems at their respective Universities. The University of Texas system has Lunar Laser Ranging (LLR) capability. NASA also has partnerships with foreign Government agencies and Universities for the operations and maintenance of MOBLAS systems. Under these partnerships, NASA continues to provide the SLR system, training, engineering support, and spare parts to maintain operations. The host country provides the site, local infrastructure, and the operating crew.

In February 2004, a forty percent decrease in the NASA SLR budget caused major reductions to the NASA SLR Network. The reductions included reduced network infrastructure, operational coverage at the stations, sustaining engineering staff, and data operational support. The MOBLAS-7 (Greenbelt, Maryland), McDonald Laser Ranging System (MLRS) (Fort Davis, Texas), and HOLLAS (Maui, Hawaii) stations were reduced to one shift operations. The NASA operator was removed from MOBLAS-8 site in Tahiti. In addition, the TLRS-3 site in Arequipa, Peru closed in February 2004, and the HOLLAS site in Maui, Hawaii closed in June 2004.

Resurgence of NASA SLR Network

In October 2004, the NASA SLR program experienced a resurgence of energy. Additional funding was provided by NASA Headquarters to re-open the TLRS-3 system in Arequipa, Peru. The TLRS-4 system, which was in caretaker status at Goddard Space Flight Center, was returned to operational status and shipped to Maui to replace the HOLLAS station. Another operational shift was added to the MLRS in Fort Davis, Texas. Additional highlights occurred throughout the NASA SLR network which are listed below.

MOBLAS-4 (Monument Peak, California):

NASA continued its collaboration with HTSI for the operations and maintenance of the MOBLAS-4 system. The site installed new Geoscience equipment. A Doppler Orbitography and Radiopositioning Integrated by Satellite (DORIS) instrument and a seismic instrument were installed at the SLR site. The DORIS instrument is from the Institut Geographique National (IGN) in France and the seismic instrument is from SCRIPPS Institution of Oceanography in San Diego, California. The site also installed a newly High Performance forWireless Research and Education Network (HPWREN) high speed internet access. The station is continuing three shift operations, five days per week, twenty-four hours per day.

MOBLAS-5 (Yarragadee, Australia):

NASA continued its collaboration with Geoscience Australia (GA) for operations and maintenance of the MOBLAS-5 system. The MOBLAS-5 crew continues to be one of the top data producing station in the ILRS. The station is continuing three shift operations, seven days per week, twenty-four hours per day.

MOBLAS-6 (Hartebeesthoek, South Africa)

NASA continued its collaboration with the South African National Research Foundation and the Hartebeesthoek Radio Astronomical Observatory (HRAO) for operations and maintenance of the MOBLAS-6 system. The system was originally

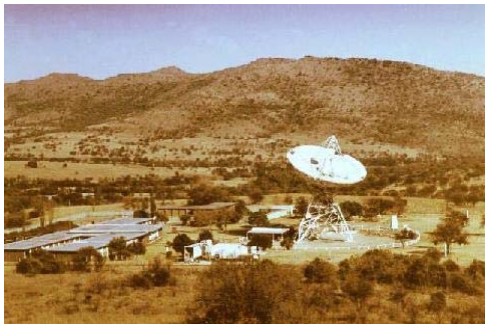

installed in HRAO in June 2000. The MOBLAS-6 operations began in August 2000. The site dedication ceremony occurred in November 2000. The HRAO site is collocated with Very Long Baseline Interferometry (VLBI), Global Positioning System (GPS), and DORIS. The station is continuing three shift operations, five days per week, twenty-four hours per day.

MOBLAS-7 (Greenbelt, Maryland)

NASA continued its collaboration with HTSI for the operations and maintenance of the MOBLAS-7 system. MOBLAS-7 continues to perform outstandingly despite the reduction in operational shifts. The system is used by NASA to test all upgrades and modifications to the NASA network prior to being installed in the field sites. The station is continuing one shift operations, five days per week.

MOBLAS-8 (Tahiti, French Polynesia)

NASA continued its collaboration with Centre National d'Etudes Spatiales (CNES) and the University of French Polynesia (UFP) for the operations and maintenance of the MOBLAS-8 system in Tahiti, French Polynesia. The Tahiti Geodetic Observatory recently named Dr. Jean Pierre Barriot as its new Director. The station was affected by the removal of a NASA operator and trainer due to budget reduction in 2004. The staff has done an excellent job operating and maintaining the station despite poor weather conditions at times. The MOBLAS-8 system was originally shipped to Tahiti in August 1997. The site dedication ceremony occurred in May 1998. The system is collocated with a GPS and DORIS system. The station will be providing two shift operations, five days per week.

TLRS-3 (Arequipa, Peru)

NASA re-newed its collaboration with the Universidad Nacional de San Agustin (UNSA) for the operations and maintenance of the TLRS-3 system in October 2005. The TLRS-3 crew working with Honeywell Technical Solutions Incorporated (HTSI) engineers began restoring the site to full operations. The restoration of the site included repairs to the laser, controller computer, HP5370, gimbal, dome controller, and telescope. The system's first light was September 23, 2006. As of the October 16, 2006, 90 pass segments had been acquired with a data quality of < 10 mm RMS on Lageos. The average ground calibration was at the 5.4 mm level. The station is providing two shift operations, day and night, five days per week.

TLRS-4 (Maui, Hawaii)

NASA renewed its collaboration with the University of Hawaii, Institute for Astronomy (IfA). After the HOLLAS system was decommissioned in June 2004, the site was converted to the new PanStarrs Observatory. NASA decided to bring the TLRS-4 system to operational status and ship it to the Haleakala Observatory in Maui, Hawaii. The TLRS-4 system had a highly successful inter-comparison test with MOBLAS-7. The system passed an Operational Readiness Review in September 2005. After 10 years on non-operations, TLRS-4 was shipped to Maui in April 2006. HTSI working with the University of Hawaii IfA personnel, prepared the site and installed the system on new pad on top of Mount Haleakala. The system's first light was in October 2006. The station will be providing two shift operations, day and night, seven days per week.

MLRS (Fort Davis, Texas)

NASA continued its collaboration with the University of Texas and the Center for Space Research (CSR) for operations and maintenance of the MLRS system in Fort Davis, Texas. MLRS provided SLR and LLR tracking data. CSR continued its data analysis support for the ILRS network. The station will be providing operations seven days per week, twelve hours per day.

Conclusion

The future of the NASA SLR Program is exciting. The resurgence of energy can be seen by the recent accomplishments of the various stations. NASA is increasing its infrastructure as well as plans are in place to increase stations operational shifts. The TLRS-3 system in Arequipa and the TLRS-4 system in Maui will be fully operational in December 2006. Dedication ceremonies for re-opening both sites are being organized for January/February 2007 timeframe. In addition, significant progress continues on the SLR2000 prototype development. We would like acknowledge the extraordinary efforts and dedication of the team supporting the NASA SLR network which includes NASA personnel, contractors, universities, and our foreign partners.

Possibility of Laser Ranging Support For The Next-Generation Space VLBI Mission, Astro-G

Toshimichi Otsubo[1], Toshihiro Kubo-oka[1], Hirobumi Saito[2], Hisashi Hirabayashi[2], Takaji Kato[2], Makoto Yoshikawa[2], Yasuhiro Murata[2], Yoshiharu Asaki[2], and Shinichi Nakamura[3]

1. Kashima Space Research Center, National Institute of Information and Communications Technology, 893-1 Hirai, Kashima 314-8501 Japan
2. Institute of Space and Astronautical Science, Japan Aerospace Exploration Agency, 3-1-1 Yoshinodai, Sagamihara, 229-8510 Japan
3. Consolidated Space Tracking and Data Acquisition Department, Japan Aerospace Exploration Agency, 2-1-1 Sengen, Tsukuba, 305-8505 Japan

Contact: otsubo@nict.go.jp / Fax: +81-299-84-7160

Introduction

Space VLBI (Very Long Baseline Interferometry) missions enable us to extend the baseline length beyond the diameter of the Earth and, as a result, to obtain more precise images of astronomical radio sources. Following the first successful space VLBI mission, HALCA (Hirabayashi, et al., 1998), which launched in 1997 and finished in 2005, JAXA (Japan Aerospace Exploration Agency) approved the next-generation space VLBI satellite called ASTRO-G (Hirabayashi, 2005) in 2006. It is scheduled to be launched in 2012. This new satellite, with a 9.6-metre mesh antenna, will receive high frequency radio signals up to 43 GHz and enhance the resolution of images by approximately 10 times than the former mission. It is expected to provide high-resolution imaging of active galactic nuclei, motion in galactic star forming regions, observations of extragalactic water masers, and so on.

The space VLBI satellite observes stellar objects in collaboration with ground VLBI network. One of the observation modes is called phase compensation observation. That is, the VLBI antenna switches the pointing direction by 2 or 3 degrees every minute to see a target object and a reference object. This makes it possible to compensate the atmospheric delay for ground VLBI stations. In this observation mode, very precise orbits up to a few cm precision are required throughout the trajectory.

Its orbit is highly elliptic. With an eccentricity of 0.62, its altitude varies from 1000 km (perigee) to 25000 km (apogee). The orbital period is about 7.5 hours and the inclination is set to 31 degrees. In contrast to spherical geodetic satellites, the area-mass ratio is large and its shape is very complicated. Therefore, it will experience large and complicated perturbation forces mainly due to solar radiation pressure. Although the cm-order orbit determination for near-circular orbits is nowadays fairly common, that for such an elliptic orbit is a highly challenging problem. We

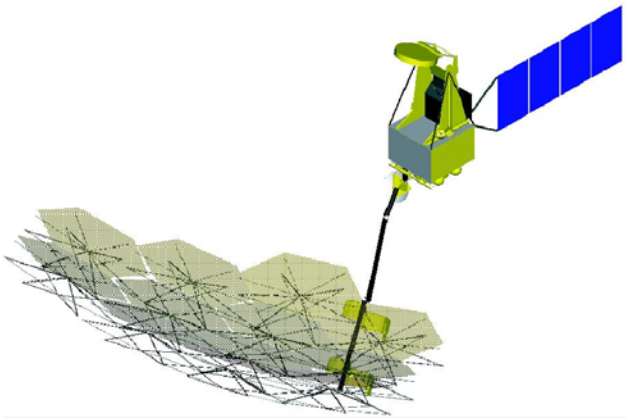

Figure 1. *ASTRO-G satellite.*

are currently investigating possible instruments for high-precision orbit determination. This paper deals a quick-look, first-step simulation of GPS and SLR data.

Possible instruments for precise orbit determination

In the following discussions, we assume these virtual orbital elements of ASTRO-G:

Epoch: 0h UT, 26 Apr 2004
Semimajor axis: 19378 km
Eccentricity: 0.6193
Inclination: 31 deg
Longitude of ascending node: 0 deg
Argument of perigee: 0 deg
True anomaly: 0 deg

After several experiments since 1990's, an onboard GPS receiver is found to be useful for precise orbit determination of low earth orbit (LEO) satellites, and the number of LEO satellites carrying this instrument is rapidly increasing.

We currently consider GPS receiver(s) as the primary instrument for precise orbit measurement. The apogee of ASTRO-G is 25000 km of altitude which is higher than the GPS satellites (20000 km). The beam divergence of GPS microwave signal is almost the size of the earth, so it gets out of the main lobe of the GPS signal (~ 20 degrees for L1 frequency) as its altitude gets high (~ typically a few thousand km).

The number of 'visible' GPS satellites on track was plotted in Fig. 2 using the true GPS constellation on the day. The bottom graph is the geocentric distance of the ASTRO-G satellite. This graph covers 15 hours, almost 2 revolution periods. The 'visibility' is defined so that the ASTRO-G satellite is within the 20-degree beam divergence and it is out of the Earth's shadow. First, assuming a single GPS receiver that always points away from the geocentre, the 'visible' number of GPS satellites is the dotted (blue) line in the top graph. Only when it is close to the perigee, one hour per the 7.5 hours period, it can see more than four satellites. Then, we simulated multiple receivers which provide no limit in terms of direction. The result is plotted as the solid (red) line in the top graph. With the contribution from GPS satellites that locate opposite side of the earth, the 'visible' number increases. Even away from the perigee, a few GPS satellites can be visible, but the number is far less than four in most cases.

In order to overcome this situation, we need to look into the possibility of the use of sidelobe GPS signal. Also, other GNSS satellites like GLONASS and GALILEO are also possible to improve the situation. Nevertheless, we stick to the above condition (solid red line) for the rest of this paper.

In these circumstances, laser ranging seems to play an important role for precise orbits. We have not looked into the specifications, but the reflector array size should be similar to that of GPS or GLONASS satellites. Other possibilities, such as an accelerometer or VLBI delay measurements, are also being considered, but not included in this paper.

Quick-look POD simulations

We simulated the following data set for the 15 hours in Fig. 2:

- GPS: every 30 seconds, pseudorange and carrier phase, L1 and L2 frequency
  (assumed observation error = 10 cm for carrier phase, and 3 m for pseudorange)
- SLR: normal points every 120 seconds
  (assumed observation error = 6 cm)

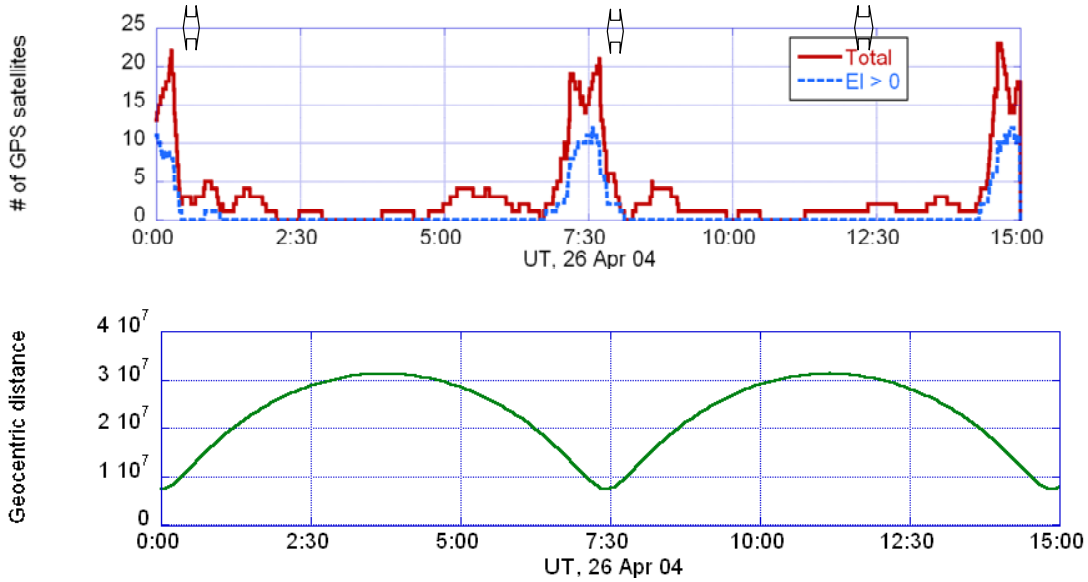

Figure 2. *Number of visible GPS satellites (top) and geocentric distance (bottom) of ASTRO-G simulated orbit. The three two-headed arrows are the duration of assumed SLR observations.*

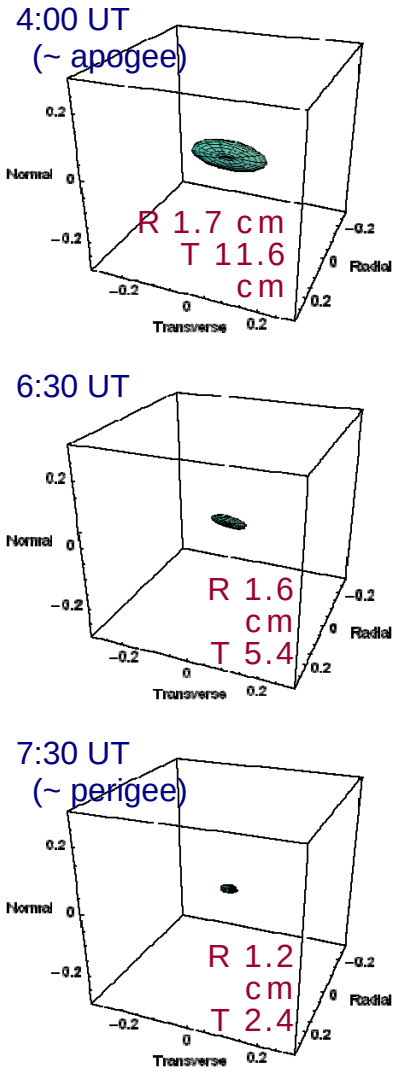

Figure 3. *Error ellipsoids for the GPS-only case.*

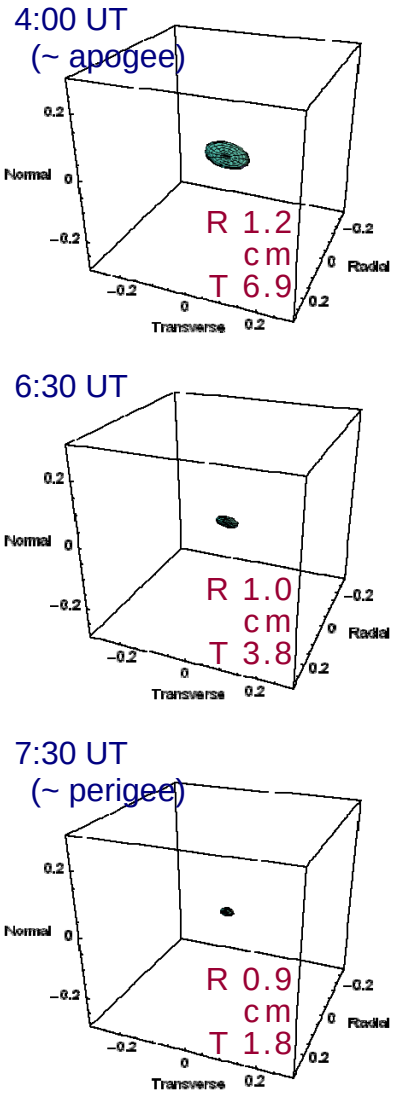

Figure 4. *Error ellipsoids for the GPS+SLR case.*

The orbital parameters, six elements, constant along-track acceleration and once-per-rev along-track acceleration, are estimated at 4:00 (close to the apogee), 6:30 and 7:30 (close to the perigee), instead of the starting time (0:00) of the arc. The clock offsets at each epoch and the ambiguities of ion-free GPS carrier phase are also solved for. We look into the covariance matrix of the orbit positional solution to obtain the estimation error. The covariance matrices given in the XYZ inertial coordinate system are then converted to the RTN satellite-fixed system, that is, in Radial, Transverse and Normal direction.

We firstly simulated the GPS data only. The ellipsoidal bodies in Fig. 3 show the size of three-dimensional errors for the three epochs. The error in the transverse component (= along-track component at the apogee and the perigee) is dominant in all cases. As expected, the ellipsoid gets larger around the apogee where GPS signal is merely detected.

Then we added the SLR data, the three 30-minute passes shown in Fig. 2, to the GPS data. The ellipsoids are shown in Fig. 4. It is obviously seen that the errors in the transverse and radial components are significantly reduced by the addition of the small amount of SLR data. Although we cannot expect dense tracking from the SLR network, this result suggests the SLR data will significantly contribute to the improvement of the orbit of ASTRO-G.

Discussions for future studies

The precise orbit monitoring instrument for the ASTRO-G satellite is being investigated. SLR observations will significantly improve the orbit compared to the GPS-only case. With further analyses we need to consider the details on the instruments such as the number and arrangement of GPS antennas and SLR retroreflectors.

The International Laser Ranging Service (ILRS) had a small experience of highly elliptic orbit satellite in the LRE (Laser Ranging Equipment) test mission launched to a geostationary transfer orbit in 2001 (Otsubo, et al., 2002). If the satellite actually carries retroreflectors for SLR, we would like to ask the ILRS stations to adapt their tracking system to highly elliptic orbits.

Due to the complicated shape of the satellite and the large area-per-mass ratio, this satellite is to experience largely complicated perturbation forces from solar radiation pressure that is about 100 times of LAGEOS. Therefore, along with the orbit measurement instruments discussed in this paper, the establishment of a precise force model is also essential for the precise orbit determination of this satellite.

References

[1] Hirabayashi, H., H. Hirosawa, H. Kobayashi, Y. Murata, P. G. Edwards, E. B. Fomalont, K. Fujisawa, T. Ichikawa, T. Kii, T. Lovell, G. A. Moellenbrock, R. Okayasu, M. Inoue, N. Kawaguchi, S. Kameno, K. M. Shibata, Y. Asaki, T. Bushimata, S. Enome, S. Horiuchi, T. Miyaji, T. Umemoto, V. Migenes, K. Wajima, J. Nakajima, M. Morimoto, J. Ellis, D. L. Meier, D. W. Murphy, R. A. Preston, J. G. Smith, S. J. Tingay, D. L. Traub, R. D. Wietfeldt, J. M. Benson, M. J. Claussen, C. Flatters, J. D. Romney, J. S. Ulvestad, L. R. D'Addario, G. I. Langston, A. H. Minter, B. R. Carlson, P. E. Dewdney, D. L. Jauncey, J. E. Reynolds, A. R. Taylor, P. M. McCulloch, W. H. Cannon, L. I. Gurvits, A. J. Mioduszewski, R. T. Schilizzi, R. S. Booth, “Overview and Initial Results of the Very Long Baseline Interferometry Space Observatory Programme,” Science, 281, 1825, 1998.

[2] Hirabayashi, H., “Next Generation Space VLBI,” EAS Publications Series, 15, 465-478, 2005.

[3] T. Otsubo, H. Kunimori, K. Yoshihara, H. Hashimoto, “Laser Reflector Arrangement on H2A-LRE Satellite for Monitoring the Spin Rate and the Optical Degradation,” Applied Optics, 41, 27, 5672-5677, 2002.

Electron Multiplying CCD Camera Performance Tests

D. Lewová[1], M. Němec[1], I. Procházka[1], K. Hamal[1],G. Kirchner[2], F. Koidl[2], D. Kucharski[3], Yang Fumin[4]

1. Czech Technical University in Prague, Brehova 7, 115 19 Prague 1, Czech Republic,

2. Graz Observatory, Austrian Academy of Sciences, Austria

3. Space Research Centre, Polish Academy of Sciences, Poland

4. Shanghai Observatory, Chinese Academy of Science, China

Contact: lew.dana@gmail.com , nemecm1@troja.fjfi.cvut.cz

Abstract

For satellite laser ranging, TV guiding is widely used to point the laser beam on the satellite. The ISIT (Intensified Silicon-Intensifier Target) camera has been applied in last years for its high sensitivity, which enabled to track all satellites of interest. However, there is a strict limitation to use it for daylight observation. The new type of CCD camera Electron Multiplying CCD (EMCCD) provides high sensitivity for short integration time required for fast real time tracking while maintaining the high ruggedness for daylight tracking. An additional internal gain reaches a factor up to 200 in comparison with regular CCD. During our tests in Graz and Shanghai, we did demonstrate the ability for satellite laser ranging during the daylight and during the night time exploiting the higher sensitivity, as well. The test results and a comparison with ISIT technology will be presented.

EMCCD Camera Performance Tests

- EMCCD provides high sensitivity for short integration time required for fast real time tracking
- In comparison with ISIT, EMCCD offers adjustability of exposure time and EM gain and beside the Analog video output it has very fast native Digital output allowing better image enhancement post-processing
- During our tests in Graz and Shanghai we did demonstrate the ability for SLR during daylight and night operations

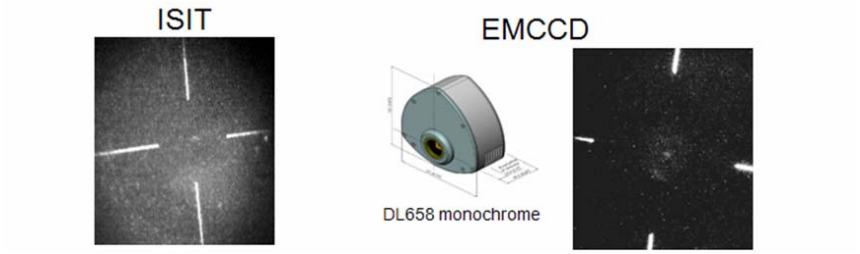

EMCCD Camera Performance Tests

EMCCD Images of GPS, Etalon 2, Glonass and Lageos 2 illuminated by Sun only

Digital output – no enhancement
(Images are captured with the same EMCCD settings and inverted)

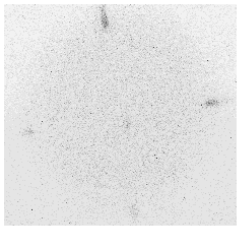

Gps BIIA-24, 0.2s, Gain 250
2006-08-25T20:07:39 UTC
Sun only, Altitude ~ 20,100 km

10x10pixels	Object	Backgr.
Standard Deviation	350,37	243,86
Mean	939,13	818,49
Maximum	2603	2263
Total Counts	375652	327396

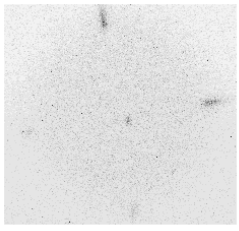

Etalon2, 0.2s, Gain 250
2006-08-25T20:39:42 UTC
Sun only, Altitude ~ 19,100 km

10x10pixels	Object	Backgr.
Standard Deviation	471,25	274,1
Mean	1024,35	820,27
Maximum	4129	2119
Total Counts	375652	328106

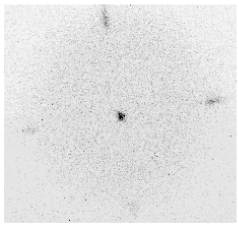

G87- Glonass, 0.2s, Gain 250
2006-08-25T22:53:02 UTC
Sun only, Altitude ~ 19,100 km

10x10pixels	Object	Backgr.
Standard Deviation	1508,39	310,89
Mean	1870,07	869,8
Maximum	10835	2235
Total Counts	748028	347920

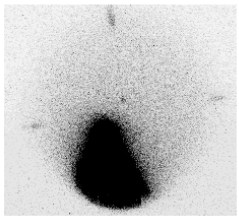

Lageos2, 0.2s, Gain 250
2006-08-25T19:27:57 UTC
Sun only (Laser outside the object)
Altitude ~ 5625 km

10x10pixels	Object	Backgr.
St. Deviation	629,62	503,65
Mean	1713,28	1495,48
Maximum	4375	3389
Total Counts	685310	598194

EMCCD Camera Performance Tests

Analog video output enhancement

On-line video filter - Contrast enhancement
GPS 36

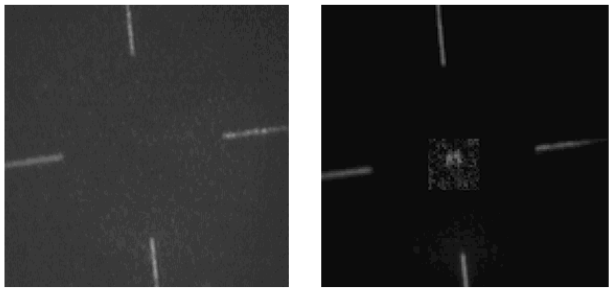

before after

On-line video filter - Pseudocolor mapping

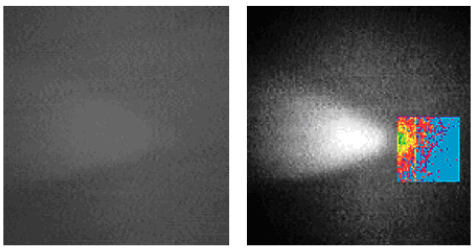

before after

For more details see the following Poster.

Electron Multiplying CCD Camera Performance Tests

D. Lewova, M. Němec, I. Procházka, K. Hamal (1)
G. Kirchner, F.Koidl (2)
Yang Fumin(3), D. Kucharski (4)

(1) Czech Technical University in Prague, Czech Republic, (2) Satellite Laser Station Graz, Austrian Academy of Sciences, Austria
(3) Chinese Academy of Sciences, Shanghai, China, (4) Space Research Centre, Polish Academy of Sciences,Poland

For satellite laser ranging, TV guiding is widely used to point the laser beam on the satellite. The ISIT (Intensified Silicon-Intensifier Target) camera has been applied in last years for its high sensitivity, which enabled to track all satellites of interest. However, there is a strict limitation to use it for daylight observation. The new type of CCD camera Electron Multiplying CCD (EMCCD) provides high sensitivity for short integration time required for fast real time tracking while maintaining the high ruggedness for daylight tracking. An additional internal gain reaches a factor up to 200 in comparison with regular CCD. During our tests in Graz and Shanghai we did demonstrate the ability for satellite laser ranging during the daylight and during the night time while exploiting the higher sensitivity , as well. The test results and a comparison with ISIT technology will be presented.

Andor Luca DL658 (monochrome)

Technology	Electron Multiplying CCD ("gain off" operable)
Active Pixels (horiz x vert)	658 x 496
Pixel Size (horiz x vert; µm)	10 x 10
Image Area (mm)	6.58 x 4.96
Sensor	TIL
Peak Q.E.	52%
Minimum Oper. Temp (°C)	-20
Active Area Pixel Well Depth(e⁻ typical)	25,000
Conventional Register Pixel Well Depth (e⁻ typical)	100,000
Pixel Readout Rate	12.5
Read Noise (e-)	25
Min Operating Temp (°C)	-20
Digitization	14-bit
Max. Frame rate	30 full frames/sec
PC Interface	USB 2.0 only
Price	$8850 / €7500
Software	Solis (Not Recommended) $1500 / €1400

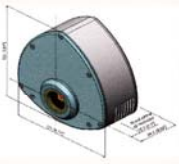

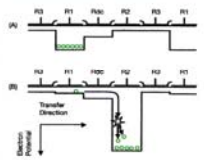

Gain register operation

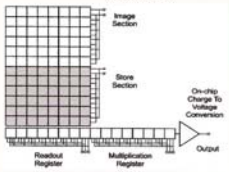

EMCCD structure

EMCCD Camera Tests

Shanghai Observatory

Graz Observatory

Test conditions:

optics	Canon lens TV-16, 1;1.4, f=50 mm, C-mount
optics settings	f/D = 22, additional ND filters 12 x each, 3 pieces
signal source	red LED, 7m distance, dark room
software	ANDOR Solis for imaging, ver. 4.3.0.0
PC notebook	UMAX Vision Book 632LX, Celeron D, 2.5GHz, 512 MB,USB2.0

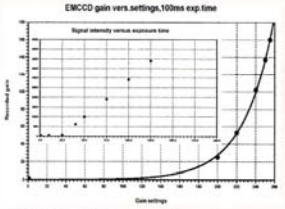

EMCCD and ISIT, Graz, 2006

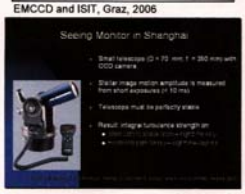

ISIT vs. EMCCD Comparison

Satellite object max/background level : 1,3

ISIT
only night observation
high FPS (30)

Satellite object max/background level : 3

EMCCD
Negs.:
night + day observing
up to 30 FPS
only 5 FPS
(for the same results)
EM ageing / anti-ageing
Pros.:
lower sensitivity
lower noise (EM gain on)
adjustability of exposure time and EM gain

EMCCD Gain experiment :

- green LED
- additional 2 ND filters inserted into optical path
- exposure time set to 100 ms
- the "EMDAC setting" set to values in the range of 1 to 255

Exposure time linearity:

- the gain setting =1 (no EM additional gain)
- one ND filter inserted into optical path
- the image intensity evaluated as a function of image exposure time (linear dependence expected)
- the gain increases with exposure time starting at 1 ms exposures
- the gain increase is linear only for exposure times >= 25 ms !

Gps BIIA-24, 0.2s, Gain 250
2006-08-25T20:07:39 UTC
Sun only, Altitude ~ 20,100 km

10x10pixels	Object	Backgr.
Standard Deviation	350,37	243,86
Mean	939,13	818,49
Maximum	2603	2263
Total Counts	375652	327396

Etalon2 0.2s, Gain 250
2006-08-25T20:39:42 UTC
Sun only, Altitude ~ 19,100 km

10x10pixels	Object	Backgr.
Standard Deviation	471,25	274,1
Mean	1024,35	820,27
Maximum	4129	2119
Total Counts	409740	328106

G87- Glonass, 0.2s, Gain 250
2006-08-25T22:53:02 UTC
Sun only, Altitude ~ 19,100 km

10x10pixels	Object	Backgr.
Standard Deviation	1508,39	310,89
Mean	1870,07	869,8
Maximum	10835	2235
Total Counts	748028	347920

Lageos2, 0.2s, Gain 250
2006-08-25T19:27:57 UTC
Sun only (Laser outside),
Altitude ~ 5625 km

10x10pixels	Object	Backgr.
St. Deviation	629,62	503,65
Mean	1713,28	1495,48
Maximum	4375	3389
Total Counts	685310	598194

Data Mining - HW

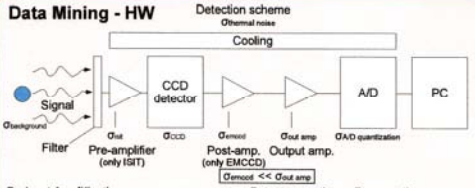

Pre/post Amplification
- decreasing readout noises levels (Low-noise internal amplification of signal before high-noise external output amplification)
- Increasing influence of S/N

Detectors settings - Exposure time
- Internal binning
- Post/pre amplifications

Filtration - interested wave-lengths pass only
- background influence(level) elimination

Cooling - Decreasing thermal noises

GPS BIIA-24 on-line filter
2006-08-25T22:09:39 UTC
Averaging - 25 frames
Selected area – contrast enhanced

Adjusted Contrast and brightness in the selected area

PC – Software methods

Methods for S/N increasing :
SW binning – 3D (integration in time + 2D in space)
SW Exposure - summation of frames
Averaging (mean; time)
Flatfield – Intensity levels calibration
Background Reduction
- Bcg. Frame subtraction(frame without object)
- AVG Filter
- Median Filter

} Artificial Background estimation and subtraction

Original image | Estimated background by median filter | Estimated Background Image subtraction

Visualization

Methods for better visibility of objects in real time :

Levels selection - Image histogram
Adjusting of contrast and brightness
Gama correction
Color inverting
Pseudo-color mapping

Pseudo color mapping

40W, 2J laser Moon shooting

Shanghai observatory

Replacing dichroic mirror

During tests in Graz and Shanghai we did demonstrate the ability for satellite laser ranging during the daylight and during the night time while exploiting the higher sensitivity

15th International Workshop on Laser Ranging, Canberra, Australia,15-20 October, 2006

LIDAR Experiments At The Space Geodesy Facility, Herstmonceux, Uk

Graham Appleby[1], Christopher Potter[1], Philip Gibbs[1] and Roderic Jones[2]

1. NERC Space Geodesy Facility, Herstmonceux, Hailsham, UK

2. Department of Chemistry, University of Cambridge, Lensfield Road, Cambridge, UK

Introduction

We are developing a LIDAR capability, ultimately to run concurrently with satellite laser ranging measurements, at Herstmonceux, UK. Our interest is in monitoring atmospheric pollution, boundary layer heights and cirrus properties over the site. For preliminary testing we have developed a modified version of the laser ranging software and used the existing laser ranging hardware to detect backscatter at a range of heights of from one to 14 km vertically above the site. During experimental runs the C-SPAD detector is gated in few-hundred metre increments from close to the telescope to beyond the tropopause, and time-tagged single-photon backscatter events are detected. Over the experimental period of a few minutes a vertical profile of atmospheric response is mapped and various layers detected. In this paper we discuss some analysis of these preliminary results and state plans for future enhancements.

Backscatter experiments

With the telescope set towards the zenith, we gate the C-SPAD for usually 30-seconds at each height above the site, from 1000 to 14,000m and collect backscatter events. The initial height of 1000m is imposed on this experiment by the separation between the transmit-receive telescopes, whose fields-of-view begin to intersect about 800m from the mount.

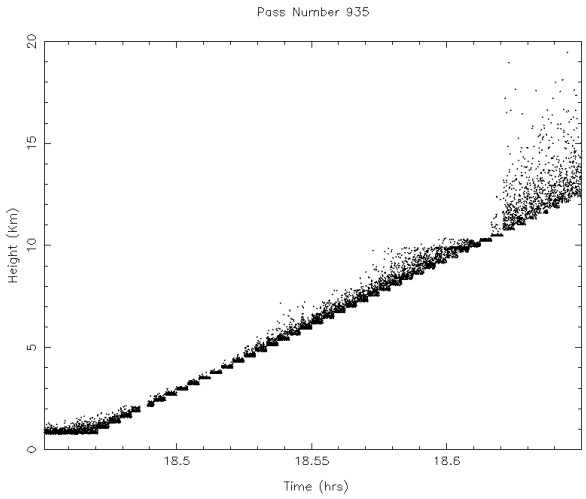

Figure 1. *Raw observations of backscatter events vertically above Herstmonceux*

The plot in Figure 1 shows the 'stepladder' that results when the raw event-height results are plotted against time. During the setup process at the first height, neutral density filters (ND) were entered manually into the receiver optical path to ensure that the range gate was approximately uniformly filled with events. Thereafter, ND values were not changed.

Preliminary analysis

We carry out a preliminary analysis of the backscatter measurements by taking the raw observations and computing for each noise point its distance above the station, on the assumption that for night-time observations all data shown in Figure 1 result from laser backscatter in the atmosphere. On this assumption and, at this stage, ignoring the decrease of laser energy with height, we therefore are able to measure return energy as a function of height and thus probe atmospheric particulate density.

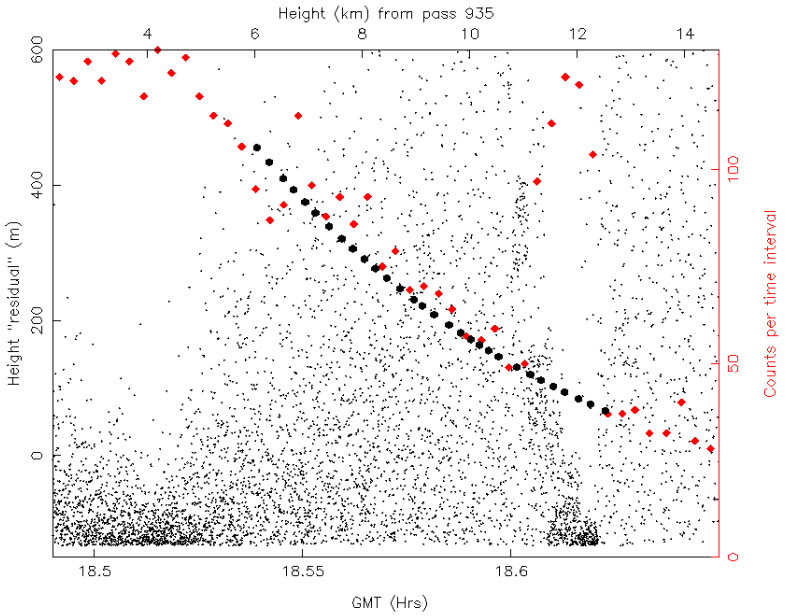

Figure 2. *Backscatter events plotted as a function of time and height in the atmosphere*

Figure 2 shows the results of this simple analysis applied to the observational session of Figure 1. If the degree of backscatter from the atmosphere was independent of height, the plot would show a uniform density of points. However, this is clearly not the case, and from the plot we suggest that a haze layer can be seen at about 4-5Km above the site, followed by a further layer at 12 km, probably identified with the tropopause. The red dots, plotted against the right-hand vertical axis, give the total number of events detected in each 3-minute interval throughout the experiment. We have fitted to those red points, strictly between the two haze layers (6 to 11km), the exponential decay curve shown by the black dots, and determine from it an atmospheric scale height of approximately 6km. Note that this fitted curve is extended in the plot beyond the region of the fit, through the high level layer, where it links with the observational totals for 13km and above. More work will be required to refine this analysis, in particular to estimate the decrease of laser energy with height.

Monitoring cloud and contrail optical density

In a related study, we are interested in the possibility of monitoring contrail and cirrus optical depth during standard laser ranging. The airspace over Herstmonceux is a busy flight path to Gatwick as well as a gateway into the UK for transatlantic routes, and a recent study into contrails over this part of the country (Stuber *et al*, *NATURE*, June 2006) has highlighted the importance of contrails as contributions to warming effects. However, little is known about the characteristics of contrails, and estimates of their optical depth vary greatly.

During laser ranging, the tracking software automatically maintains the average return level at single photons by inserting varying degrees of ND filters in the detector optical path. Compared with a model of the link budget for the ranging process, the degree of ND actually required to achieve single photon returns is a measure of departure of atmospheric transparency from that in the model. In particular, if the pass transits a contrail, the required change (reduction) in ND necessary to maintain single photon returns is a direct measurement of the additional optical depth of the atmosphere due to the trail.

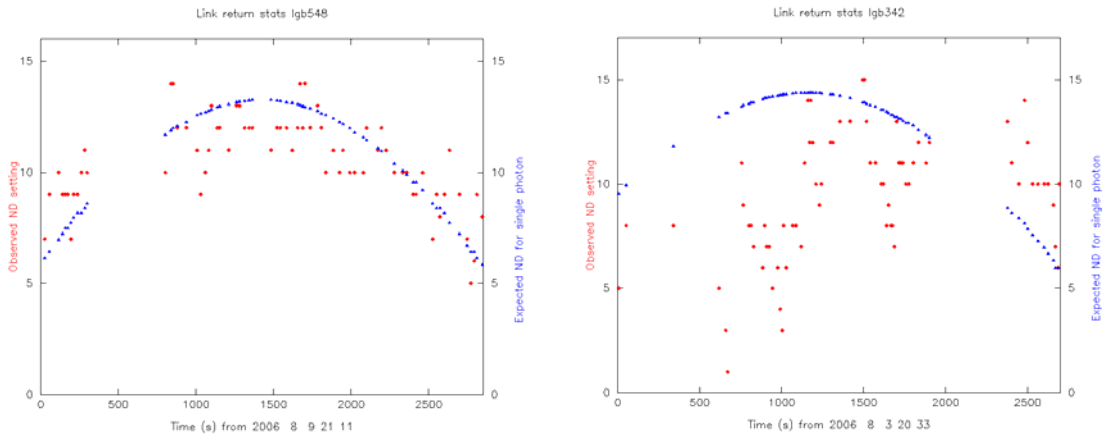

***Figure 3**. Comparison of theoretical (blue) and measured (red) ND required for single-photon laser return from LAGEOS-2.*

The plots in Figure 3 above show two tracking instances of modelled (blue points in smooth curves) and actual ND (red, scattered points) inserted by the operating system; the left plot is in a clear sky and the right plot shows three passages of the satellite behind contrails. The clear sky data follows the predicted ND values fairly well, the small changes being due to pointing variations from optimal. During the contrail passages, ND is systematically removed and replaced, giving a profile of contrail optical density.

Conclusion.

Both the observational experiments reported in this paper are at preliminary stages. Much more work is required to improve and automate the observational methods, quantify systematic effects and analyse the results. We also plan to design and integrate on the telescope a LIDAR system that is independent of, but which will run simultaneously with, standard laser ranging operations.

Possibility of the Near Earth Objects Distance Measurement with Laser Ranging Device

M.Ābele, L.Osipova

Institute of Astronomy, University of Latvia, Raiņa bulv. 19, Rīga LV-1586, Latvia

Abstract

The orbit perihelion of a some of minor planets is nearer from the Sun than the Earth's orbit. Observations are possible only in a small part of the orbit. Orbital elements of them cannot be determined accurately because we have only angular coordinates. The use of a laser ranging device for distance measurements will greatly improve the precision of determining orbital elements.

Keywords: *minor planets, laser ranging*

Introduction

We know a number of minor planets whose orbital perihelion is nearer from the Sun than the Earth's orbit.[1] Accurate forecasting of their motion is not possible, because they can be observed only in the vicinity of aphelion when their lighted sides are turned toward the Earth, and the Sun is located on the opposite side. Observations are possible only for a small part of the orbit because the planets are small in size and it is not possible to observe them from the Earth even with powerful telescopes. In order to determine orbits more accurately, we assess the possibility to measure the distance to these orbits with a laser ranging device. [2, 3, 4]

Possible measurements of minor planets with laser ranging device

A possible scheme of the experiment is shown in Fig. 1. The laser device LAS, which is situated on the Earth, radiates impulses of light in the direction of the minor planet MP. The distance is L and the diameter of the laser beam is d_{la}:

$$d_{la} = 2 \cdot L \cdot \mathrm{tg}\, r_d \tag{1}$$

where r_d is the diffraction, the angle radius $r_d = 1.2197\ \lambda/d_t$ that depends on the radiation optics' diameter d_t and the wavelength λ [5].

As the energy l_i diffraction image is irregular, the energy radiated in the direction of the minor planet E_{ep} can be calculated using formula

$$E_{ep} = E_{las} \cdot c_{at} \cdot c_{op} \frac{\int_0^{d/2} l_i(r) \cdot r \cdot dr}{\int_0^{r_d} l_i(r) \cdot r \cdot dr} \tag{2}$$

where E_{las} – laser emanated energy;

c_{at} – light transmissivity of the atmosphere;

c_{op} – light transmissivity of the optical system;

d – diameter of the minor planet.

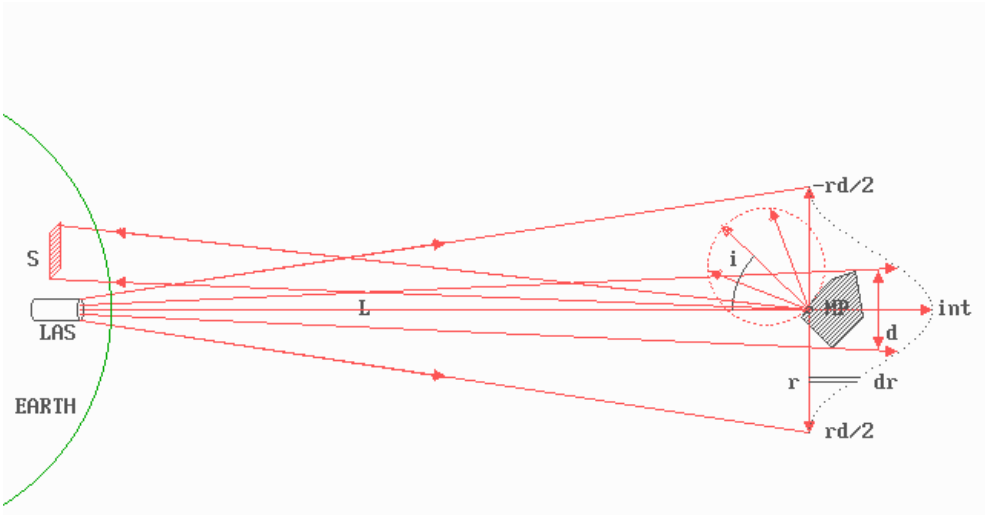

Fig. 1. Measurments of minor planets with laser ranging device

The surface of the minor planet is matted and its each element reflects the light in accordance with the Lambert Law. Area S on the Earth receives radiated energy E_e:

$$E_e = E_p \cdot c_{at} \cdot a \cdot \cos i \cdot \frac{S}{\pi L} \qquad (3)$$

where i – mean surface normal angle turned in the direction of the Earth;

a – reflection coefficient (albedo).

As E_e is very weak, the reflected energy can be described with the number of photons per unit of area $n_f = E_e/E_{fot}$, where E_{fot} – photon energy:

$$E_{fot} = h \cdot \nu \qquad (4)$$

where h – Planck's constant ($h = 6.622 \cdot 10^{-34}$ J·s);

ν – frequency of light wavelength.

The calculation results are showed in Table 1:

Laser energ. = 10 J

Laser wave length = 0.694 mkm

Laser beem diverġence = 0.5819907" (2 r difr)

Atmospher transmitance = 0.8

Telescope transmitance = 0.9

Planets albedo = 10 % (black)

	Planets diameter, m				
	50	100	200	400	800
Range, km	Reflected photons on 1 km^2				
50000	1.953181E+7	6.593346E+7	1.413264E+8	1.583503E+8	1.631335E+8
100000	1275306	4882952	1.648337E+7	3.53316E+7	3.598758E+7
200000	80588	318826	1220738	4120841	8832901
400000	5052	20147	79706	305184	1030210
800000	316	1263	5036	19926	76296
1600000	19	79	315	1259	4981
3200000	1	4	19	78	314
6400000	0	0	1	4	19
1.28E+7	0	0	0	0	1
2.56E+7	0	0	0	0	0

Table 1*. Reflected photons from minor planet.*

The minor planet is irradiated by the Sun. Energy received by the minor planet per second is:

$$E_{sp} = W_s \cdot \pi \cdot \frac{d^2}{4} , \tag{5}$$

where W_s – constant of the Sun (near the Earth W_s = 1360 W/m^2).

Of late, CCD devices with very high sensitivity in red waveband 0.694 μm wavelength laser have been used. In this waveband, the Sun's radiation is less intense than in the visible range. If wavelength is dλ, energy in the zone is

$$\varepsilon_\lambda = \frac{2\pi hc^2 \cdot d\lambda}{\lambda^5 \cdot e^{\frac{hc}{\lambda kT}} - 1} . \tag{6}$$

Energy of the reflected light is

$$E_{st} = E_{sp} \cdot \frac{\varepsilon_\lambda}{\varepsilon} \cdot c_{at} \cdot a \cdot \cos i \cdot \frac{S_{tr}}{\pi L} , \tag{7}$$

where S_{tr} is the area of the reflected light:

$$S_{tr} = \pi \cdot \frac{D_{dt}^2}{4} . \tag{8}$$

And the frequency f_n is

$$f_n = \frac{E_{st} \cdot q}{E_{fot}} , \tag{9}$$

where q – receiver quantum efficiency.

The probability that at least one photon enters the telescope aperture is small. If a telescope with 1.6 m diameter is used, about 50 reflected pulses may be detected in one hour, the noise from the solar background is 249 pulses per second on the average. If a larger receiving telescope is used, a minor planet's trajectory can be spotted better, the measurements can be done at a larger distance and the reflected pulses received with a higher frequency (Fig. 2).

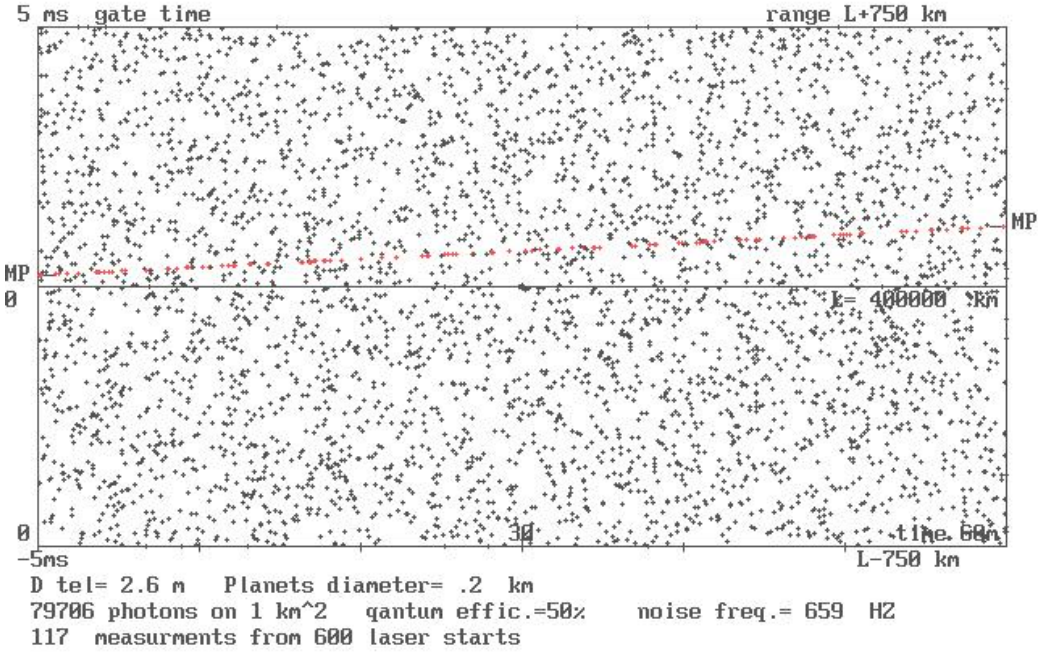

Fig.2. Reflected laser pulses and noise from minor planet

Experiment realization possibility

Described experiment is in planning stage. In order to ensure irradiation of the minor

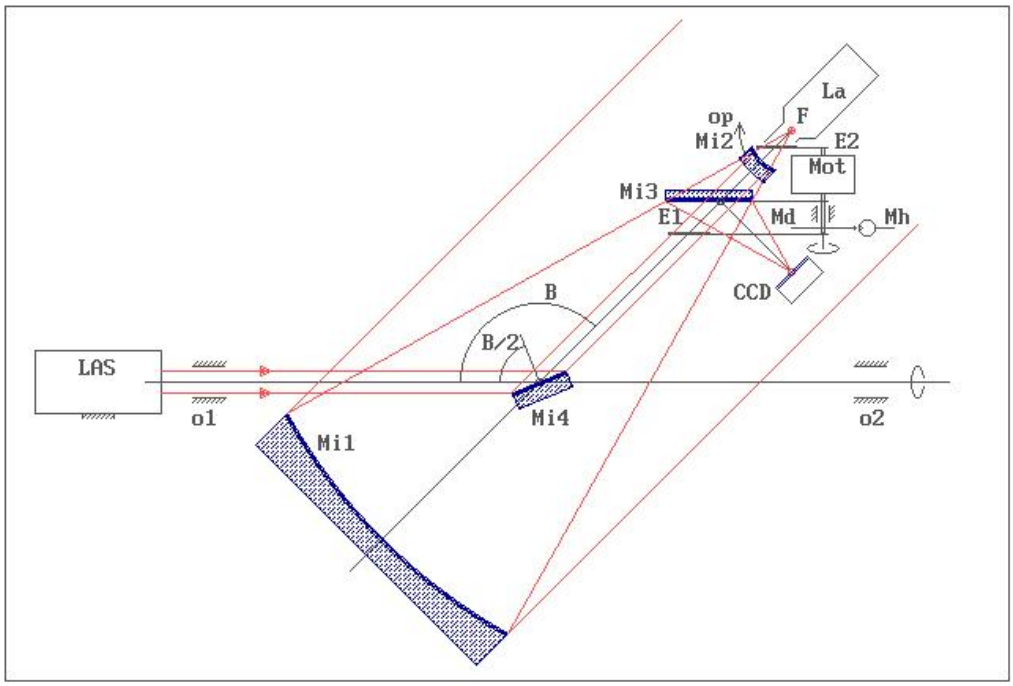

Fig.3. The laser arangement relative to the telescope

planet with a laser beam, a telescope for lighting up cosmic objects from the Earth is being devised at the Institute of Astronomy of the University of Latvia [Fig. 3, 4].

Its main optical element is the paraboloid mirror, 600 mm in diameter, that is put in a special mounting with a horizontal first axis of mounting. It allows for the laser beam to be directed to the irradiation object by a single additional mirror. [6] A laser device with the power level of 10 J can be manufactured in Lithuania by EKSPLA Company.

The receiver telescope of the reflected signal can be placed in a large distance from the transmitting source. Any astrophysical telescope with a mirror of over 1 meter in diameter could be used, and the 1.6 m telescope of the Moletai Observatory (Lithuania) could be a good option. In order to minimize the signals reflected from the Sun, for background impulses the exit of the telescope needs to be equipped with the narrow-band light filter.

Fig.4*. The telescope model.*

Taking into account that the transmitting and receiving devices are situated in a large distance each from the other, it is difficult to harmonize their frequency ranges. The frequencies of transmitted and reflected energy may also differ due to the Doppler Effect. Therefore, it is convenient to make use of a spectrograph with its exit equipped with a charge coupled device (CCD) camera. The scheme of the measurement device is showed in Figure 5.

The spectrum of the minor planet is projected on the outer column of the charge matrix CCD. At the time moment when the re-transmitted impulse from the planet can be expected, a frequency from the silica generator GEN, which moves the accumulated information along j axis, is supplied by the help of an electronic switch whose operation has been synchronized with the GPS time scale. When all matrix cells are filled consistently with the ordinary algorithm with the help of the synchronization scheme SINH through a digital amplitude modifying device, the matrix content is fed to the computer DAT. The available information covers ~ 1000

spectrum zones. One of them can capture the retransmitted impulses from the surface of the minor planet. Any needed zone can afterwards be found from within the absorption zones of the Sun. If a frequency that shifts information from one matrix column to another is 15 MHZ, the distance measurement discreet is 10 m. This allows realization of the showed algorithm of measure.

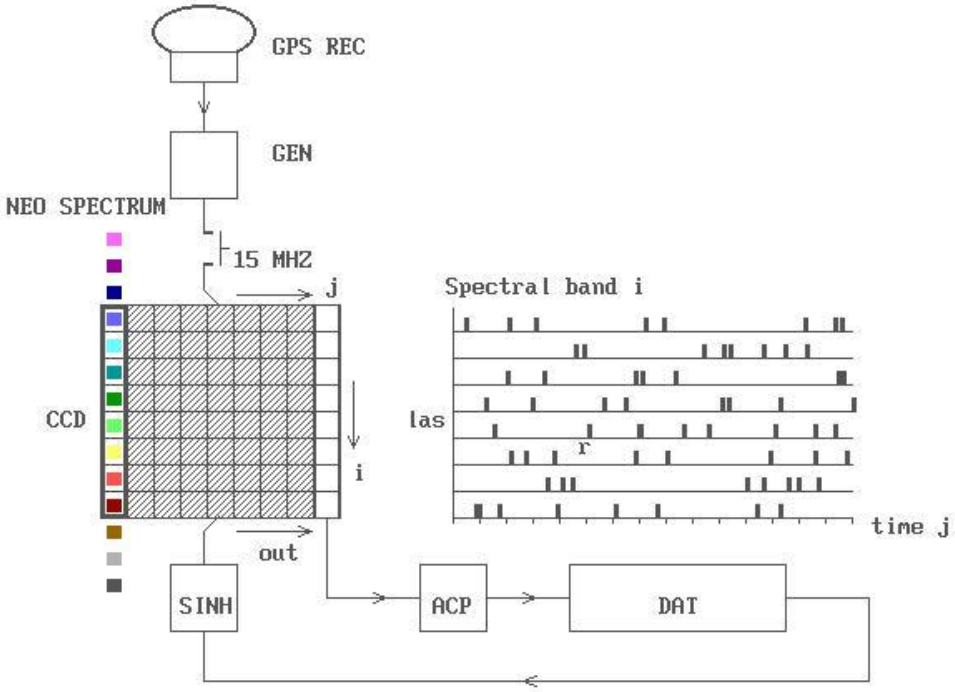

Fig. 5. Spectrograph for reflected pulses measurment

Conclusions

This project can be carried out in co-operation with other astronomers of the Baltic States. Its implementation would enable scientists to improve significantly the orbital elements of the minor planets that present danger to the Earth and to forecast their motion in the future.

References

[1] IAU Minor Planet Center. Unusual Minor Planets. 2002 Sept. 10. http://cfa-www. harvard. edu/iau/lists/Unusual. html

[2] Abele M., Osipova L. Determination of NEO orbits based on laser ranging measurements. Latvian Journal of Physics and Technical Sciences. 2004. 1. p. 31-36.

[3] Abele M., Balklavs-Grinhofs A., Osipova L. Possibility of minor planets distance measurement with laser ranging device. Latvian Journal of Physics and Tehnical Sciences. 2004. 2. p. 54-61,

[4] Degnan John J. Unified Approach to Photon-Couting Microlaser Rangers, Transponders, and Altimeters. Surveys in Geophysics Kluver Academic Publishers. 2002.

[5] Д.Д.Максутов. Астрономическая оптика. 1946. (rus.)

[6] Abele M., Vjaters J., Ubelis A., Osipova L. A telescope to spot space objects from the Earth surface. Latvian Journal of Physics and Tehnical Sciences. 2005. 3. p. 20-28.

TRANSPONDERS SESSION SUMMARY

Chair: Ulli Schreiber

Transponder applications are becoming a real option. Feasibility studies using the optical facility at Goddard and the MOLA on the Mars Explorer and MLA on the Messenger spacecraft have demonstrated successfully one-way and two-way optical ranging at interplanetary distances. These experiments became possible because of the lucky opportunity based on the availability of missions for the test of at least some mission aspects of transponders. A full transponder concept is in preparation for the Lunar Reconnaissance Orbiter (LRO) with the goal of improving the orbit determination for the altimeter application. This will be the first mission where ILRS support is required for a transponder application. Currently there are several simulation and evaluation efforts under way in order to improve the understanding of the potential of transponders, both in simulation and in a collocated ranging experiment.

Laser Ranging at Interplanetary Distances

G. A. Neumann[1], J. F. Cavanaugh[1], D. B. Coyle[1], J. McGarry[1], D. E. Smith[1], X. Sun[1], M. Torrence[1], T. W. Zagwodski[1], and M. T. Zuber[2]

1. NASA Godddard Space Flight Center

2. Massachusetts Institute of Technology

Contact: neumann@tharsis.gsfc.nasa.gov /Tel. 301 614 6026/Fax 301 614 6015.

Abstract

In May 2005, timed observations of short laser pulses of light between the Mercury Laser Altimeter (MLA) instrument aboard the MESSENGER spacecraft, and the Goddard Geophysical Astronomical Observatory (GGAO) measured the two-way range time-of-flight with sub-nanosecond precision. A one-way optical experiment was conducted a few months later from GGAO to the Mars Orbiter Laser Altimeter (MOLA) aboard the Mars Global Surveyor (MGS) spacecraft at a distance of 81 Gm (0.54 AU). These experiments demonstrated the possibility of interplanetary communication and precise ranging using modest power.

Introduction

Laser ranging in space began with ranging to retroreflectors on the Moon placed by the Apollo [Faller et al., 1969] and Luna missions. Pulses fired by a powerful, earth-based laser are reflected back to the transmitting site, where time-of-flight measurements are made using standardized clocks. Such measurements routinely achieve decimeter precision using very short pulses and single-photon detectors. Laser ranges require only small corrections for atmospheric transmission, and provide precise constraints on the dynamics of the Earth-Moon system. With retroreflectors, the number of photons available for timing decreases with the fourth power of the distance, making distances much beyond the Moon's orbit impractical. A transponder, on the other hand, receives pulses and sends pulses back in a coherent fashion so that the photon count decreases only by the square of distance in both directions, making ranging possible at far greater distances. The Mercury Laser Altimeter (MLA) ranging experiment in May, 2005 demonstrated the concept of asynchronous transponders [Degnan, 2002] in which two laser terminals independently fire pulses at each other, with timing recorded for analysis at a common location. The times of the paired observations are then used to solve for two-way range as well as a spacecraft clock offset. Multiple transponder observations can additionally constrain the spacecraft clock drift, the range rate and the range acceleration.

The MLA experiment used the 1.2-m telescope facility of the Goddard Geophysical Astronomical Observatory (GGAO) to fire at and detect pulses from MLA at a distance of 24 Gm, or 0.16 AU. It served to calibrate the instrument transmitter and detector far field characteristics and alignment, as well as confirm the distance inferred from radio tracking. The results of this experiment were communicated in brief [Smith et al., 2006]. In September 2005, one-way laser transmission was achieved to the Mars Orbiter Laser Altimeter (MOLA) instrument at Mars [Abshire et al., 2006] from GGAO using a more powerful laser firing at 49 Hz. MOLA no longer had its laser or timing capability but could record the rate of detector triggers using the spacecraft 8-Hz timing signal. An encoded sequence was transmitted using a 1-Hz shutter. The number of pulses received was strongly correlated with the modulation of the outgoing pulses. This experiment demonstrated the feasibility of laser

communication at 81 Gm, and confirmed the spacecraft clock offset of Mars Global Surveyor to a precision of ~4 ms.

We provide here further details regarding these experiments and prospects for future laser ranging and communication in deep space.

Ground Transmitter and Receiver

The HOMER life-test laser [Coyle and Stysley, 2005] employed in the MLA-Earth experiment produced 16 mJ per shot at 240 Hz. MLA received pulses at 8 Hz, the electronics allowing about 14 ms in each shot interval for returns. Thus it was anticipated that the laser would place three or more pulses inside the timing window. A 10X beam expander collimated the outgoing beam divergence to approximately 50 microradians (90% energy) after transmission through a portion of the 1.2-m telescope of the Goddard Geophysical Astronomical Observatory (GGAO). The energy per shot at the entrance to the 0.0417-m^2 MLA telescope would be 0.6 fJ, neglecting losses in transmission and atmospheric attenuation. The energy at the telescope measured from shots detected at low and high thresholds by the MLA was 0.083 ± 0.04 fJ. After the experiment, it was found that coatings on six folding mirrors in the GGAO optical path had been optimized for 532 nm operation and transmitted only 70% of 1064 nm light, reducing total transmission to about 12%. The effective transmitted energy of the ground system was reduced accordingly, amounting to about 2 mJ per shot. Since the MLA experiment and the Earth-MOLA experiment performed soon thereafter, the mirrors have been recoated and total transmission at 1064 nm is about 70%.

Ground and spacecraft timing

Absolute time and range measurements using a transponder requires tying local event timers to terrestrial time standards. Timing at GGAO was provided by GPS-steered rubidium clocks. A Honeywell precision event time digital counter (TDC) logged the leading-edge times of outgoing and incoming laser pulse triggers with respect to UTC at 10-ps resolution [Kalisz, 2004]. The waveform of each pulse was also digitized by means of a 1-GHz oscilloscope. The centroid time resulting from fitting a Gaussian envelope to the waveforms provided the most precise timing, owing to the extended nature and variable height of the detected pulses (Figure 1). These centroid times were also corrected to UTC seconds of day as recorded by the GPS-steered clock. GPS time errors result in absolute ground clock uncertainty of ~40 ns. Slowly-varying GPS errors do not affect relative times between transmit and receive pulses, which were fit with a root-mean-square residual of 0.39 ns.

Timing was corrected for a 44.2 ns path delay between the transmit laser start detector and the TDC, an optical path delay of 43.8 ns between the transmit detector and the telescope mount reference point, and a 110.2 ns delay from the GPS receiver antenna to the TDC. The latter delay is also applied to the time of the received pulses. The optical path from the telescope mount to the detector assembly and the electronic delay between the detector and the TDC was ~20 ns. Significant forward scattering through clouds likely caused pulse broadening and some delay. Atmospheric refraction delays of tens of ns should also be considered when determining the absolute times of flight, in view of the relatively low 30-35° elevation of the spacecraft above the horizon, but these were not applied. An independent calibration of all timing delays using an earth satellite retroreflector could not obtained during the allotted time owing to cloudy conditions.

The MESSENGER spacecraft [Solomon et al., 2001] employs an ovenized quartz-crystal-based oscillator whose frequency is stable to a few parts in 10^{12} over the course of an hour [Cooper, 2004]. The Mercury Laser Altimeter (MLA) acquires its time base from the spacecraft via a one-pulse-per-second (PPS) tick along with the corresponding mission elapsed time (MET) message over the data bus. The hardware PPS signal provided to MLA was benchmarked at 21 μs uncertainty during ground testing [Cavanaugh et al., 2007]. The PPS offset, and the offset between the MLA event time reference T0 and the PPS tick, are very stable over short intervals of time. The latter is monitored by the instrument at 125-ns resolution. Thus the spacecraft clock can be related to the MLA timing only to tens of microseconds in an absolute sense, but are precisely coupled over intervals of an hour.

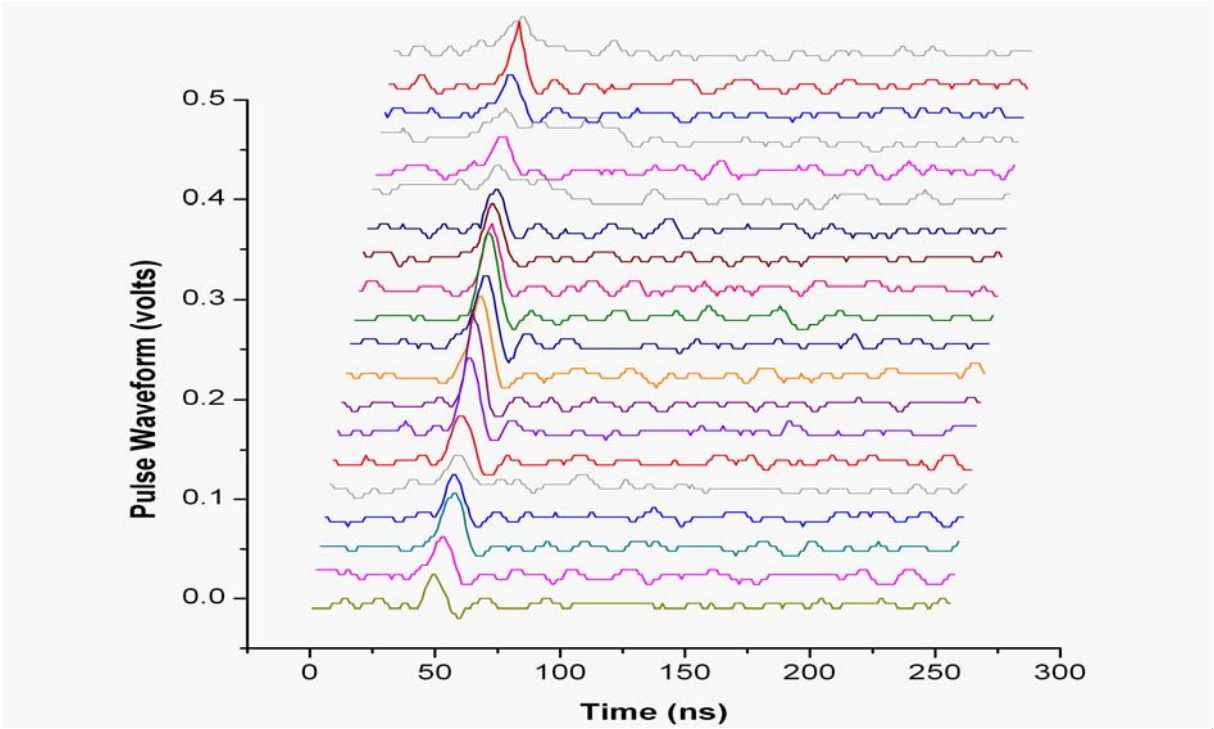

Figure 1. *MLA Pulse waveforms recorded at GGAO on May 27, 2005, along with a few cloud echoes (gray curves) from the ground laser.*

The MLA obtains a 5 MHz clock signal from the spacecraft which drives a coarse event timer. The transmit and receive event timers consist of a set of time-to-digital converters (TDC) based on the tapped delay line technique [Paschalidis et al., 1998]. The tapped lines consist of a series of logic gates that count from an event to the next 5-MHz clock edge. An on-chip delay-lock-loop calibrates the overall delay time against an external reference clock signal, and the delay of each gate is measured on the ground. The combined circuits can time the leading and trailing edges of the transmitted laser pulses and the received echo-pulses to ~400 ps resolution. Coarse and fine clock counts are downlinked via telemetry. A zero-range offset bias of 23.8 ns for high threshold returns and 30.9 ns for low threshold returns is subtracted to account for electronic delays in the receiver relative to the start pulse.

The spacecraft radio telemetry system is used to calibrate MET against time standards at the Deep Space Network (DSN). Spacecraft time must be correlated to a dynamical

time to millisecond accuracy for geodetic purposes, in order to position MESSENGER in space and derive altitude from ranges. The MESSENGER project maintains a clock file giving corresponding MET and Terrestrial Dynamic Times (TDT). An event on the spacecraft at a given MET tick is considered simultaneous with an event at the corresponding terrestrial time, as viewed from the Solar System Barycenter. Owing to special relativity, corresponding times may not appear simultaneous to a terrestrial observer. The Navigation and Ancillary Information Facility (NAIF) toolkit models the travel of light between Earth and MESSENGER in a barycentric inertial frame and was used herein.

MESSENGER Range and Time Transfer Results

During the MLA-Earth experiment, the MESSENGER clock correlation file was updated twice over the course of a week, with coefficients given in Table 1. The clock rate typically varied by <1 part in 10^9 over the period of four days, however, telemetry time coding errors at the DSN on the day before the experiment resulted larger-than-usual variation. Independent verification of the spacecraft timing system integrity was an important goal of the ranging experiment. The downlink time residual was found to be 347 microseconds, while the uplink residual was 351 microseconds. The average residual offset of the spacecraft clock was therefore 349 microseconds. However, post-processing of the spacecraft timing (Stanley B. Cooper, email communication, November 8, 2006) suggests that this clock offset was ~49 microseconds. For reference, the mission requirement is to maintain time correlation to 1 ms.

Table 1*. Spacecraft clock correspondences used during experiment.*

MET	TDT	Rate of MET
25632557	26-MAY-2005T22:11:17.912822	1.00000001564
25963200	30-MAY-2005T18:02:00.917993	1.00000001704
MLA-Earth result, uncorrected for relativistic time delay		
25710307	27-MAY-2005T19:46:03.729662	1.00000001559

Range residuals were calculated via least squares, resulting in a solution from two-way light time of 23,964,675,433.9 m at the 25710307 MET tick, with range decreasing at a rate of 4,154.663 m/s. A spacecraft ephemeris solution using radio tracking data (msgr_20040920_20050823_od032.bsp) predicted a range of 23,964,674,906.35 m. However, the relativistic (Shapiro) delay in the speed of light and bending of light path due to the solar gravitational potential amounted to an equivalent of 486.60 m in each direction, so that the effective range was 23,964,675,392.95 m, or 41 m less than measured by the MLA experiment. There are several sources of error that could account for this discrepancy: the spacecraft ephemeris, errors in the measurement model used for comparison, errors in ground timing and path correction, or combinations of these errors. Such close agreement, to a part per billion in range, is truly remarkable. The formal error in the laser range solution was 0.2 m, or one part in 10^{11}.

MOLA Time Transfer Results

Distances to Mars are well-constrained by years of tracking of spacecraft and landers, and the clock drift on Mars Global Surveyor (MGS) has been very small, so that the

clock correlation file is updated only a few times a year to maintain the specified 10-ms accuracy. The primary purpose of this test was to determine the clock offset between the MOLA data stream and spacecraft time. MGS was commanded to scan twice across a 0.2x0.2° (3.5x3.5 mrad) region of the sky centered on the apparent position of Earth, during each of three nights in September 2005. The 1-3 mrad uncertainty in pointing control of the 9-yr-old spacecraft, as well as the 0.8 mrad detector field of view, made scanning necessary. Passive radiance confirmed that the detector was aimed correctly. MOLA detector threshold was set to produce 1-2 noise counts per second from Earth background light. In each 8-Hz interval, the number of triggers is recorded. A maximum of 6 or 7 shots from the 49-Hz ground laser could have been detected in each interval. In fact, at most 7 triggers above threshold occurred in any single interval, consistent with the expected probability of detection. Roughly 500 such pulses were counted during one successful evening, and from the pattern of counts, it was clear that the pulses were being recorded somewhat later than expected, consistent with a 114-ms skew between the spacecraft time signal and Earth time. Such a bias had earlier been estimated using the altimetry in an eccentric orbit [Rowlands et al., 1999].

Prospects for future experiments

Opportunities to repeat the MLA-Earth experiments occur at several intervals beginning in May 2007, at distances of 100 Gm or more (0.66 to 1 AU). The MESSENGER spacecraft must maintain its sunshade Y-axis within ~12 degrees of the Sun while pointing the instrument Z-axis toward earth, a geometry which also maximizes the elongation of the MLA with respect to the Sun as seen from Earth. The first MLA experiment required several days to complete, even with moderately good visibility. It was severely constrained by the pointing knowledge of the spacecraft, such that no more than 24 shots were received on the ground from MLA during a single observing session. As a result of the experiment, the repeatability of the MLA boresight was determined from passive scans to be within 50 microradians from day to day, and within each scan, the control of each scan line was within its 16-microradian spacing. During several windows through the clouds, the MLA receiver was able to detect ~90 shots from the ground, but never with a probability of detection greater than 1-2%. In 15 events, both a high and a low threshold trigger occurred, with leading and trailing edge times. Such timing allows for estimation of the pulse width and energy, assuming a Gaussian waveform, as detailed in Cavanaugh et al. [2007]. The energy received at the telescope entrance from these events averaged 0.083 fJ, or 0.064 fJ at the detector after transmission losses.

From June 18 to 24, 2007, attempts were made to repeat the MLA experiment at a distance of 104 million km shortly after MESSENGER's second Venus flyby, when the instrument could be safely pointed at Earth. With the improvement in telescope optics, using a single-photon-counting detector, there was sufficient link even with the relatively low ~18 mJ energy of MLA's 1064-nm pulses to range to GGAO at this distance. A 250-mJ laser firing at 48 Hz was employed to improve the probability that a shot would be received within each 14-ms window occurring at 8 Hz, after proper phasing. Communication of a message to the MLA was attempted by modulating the position of each pulse by a variable number of microseconds. However, a myriad of problems with the optical and mechanical ground systems as well as unfavorable weather prevented communication in either direction.

An opportunity for MLA at a similar distance will occur in March 2008, where the elongation of MESSENGER from the Sun will be at a maximum of 44°, with two opportunities in 2009 at elongations of 39° and 36°. It will also be possible to perform the experiment twice per year in Mercury orbit, although solar rejection at the Earth station will require a very narrow field of view. The continued MLA experiments will further demonstrate the ability of lasers to perform precise range measurements, time transfer, and communications throughout the solar system. At these distances the Shapiro delay reaches 10-20 μs. The ability of MLA to see more dramatic effects during solar conjunction is precluded by spacecraft sun avoidance constraints, but the solar avoidance requirements of the MLA optical design itself are minimal. Such experiments could be considered in future interplanetary deployments.

References

[1] Abshire, J.B., X. Sun, G. Neumann, J. McGarry, T. Zagwodzki, P. Jester, H. Riris, M. Zuber, D. E. Smith, "Laser Pulses from Earth Detected at Mars", Conference on Lasers and Electro-Optics (CLEO-06), Long Beach, California, May 2006.

[2] Cavanaugh, J.F., J.C. Smith, X. Sun, A.E. Bartels, L. Ramos-Izquierdo, D. J. Krebs, A. Marie Novo-Gradac, J.F. McGarry, R.Trunzo, J.L. Britt, J. Karsh, R.B. Katz, A. Lukemire, R. Szymkiewicz, D.L. Berry, J.-P. Swinski, G.A. Neumann, M.T. Zuber, D. E. Smith, The Mercury Laser Altimeter Instrument for the MESSENGER Mission, *Space Science Reviews,* in press.

[3] Cooper, S.B., "Design of the MESSENGER Timekeeping System" and "Preliminary Report on MESSENGER Timekeeping Test Results", JHU/APL memos SEA-2003-029, July 11, 2003 and SEA-2004-045, June 7, 2004.

[4] Coyle, D.B., and P.R. Stysley, "The high output maximum efficiency resonator (HOMER) developed for long life, space-based altimetry", IEEE International Aerospace Conference, Big Sky, Montana, 4-11, March 2006.

[5] Degnan, J. J., Asynchronous laser transponders for precise interplanetary ranging and time transfer, *J. Geodynamics* (Special Issue on Laser Altimetry), pp. 551-594, November, 2002.

[6] Faller, J. E., I. Winer, W. Carrion, T. S. Johnson, P. Spadin, L. Robinson, E. J. Wampler, and D. Wieber, Laser beam directed at the lunar retro-reflector array: observations of the first returns, *Science*, 166, 99-102, 1969.

[7] Kalisz, J., Review of methods for time interval measurements with picosecond resolution, *Metrologia*, Vol. 41, pp. 17-32, 2004.

[8] Paschalidis, N., K. Karadomoglou, N. Stamatopoulos, V. Paschalidis, G. Kottaras, E. Sarris, E. Keath, and R. McEntire, "An integrated time to digital converter for space instrumentation", 7th NASA Symposium on VLSI Design, Albuquerque, NM, Oct. 1998.

[9] Rowlands, D.D., D.E. Pavlis, F.G. Lemoine, G.A. Neumann, and S.B. Luthke, The use of laser altimetry in the orbit and attitude determination of Mars Global Surveyor, *Geophys. Res. Lett., 26*, 1191-1194, 1999.

[10] Smith, D.E., M.T. Zuber, X. Sun, G.A. Neumann, J.F. Cavanaugh, J.F. McGarry, and T.W. Zagwodzki, Two-way laser link over interplanetary distance, *Science*, 311, p.53, 2006.

[11] Solomon, S.C., R. L. McNutt Jr, R. E. Gold, M. H. Acu˜na, D. N. Baker, W. V. Boynton, C. R. Chapman, A. F. Cheng, G. Gloeckler, J. W. Head III, S. M. Krimigis, W. E. McClintock, S. L. Murchie, S. J. Peale, R. J. Phillips, M. S. Robinson, J. A. Slavin, D. E. Smith, R. G. Strom, J. I. Trombka, M. T. Zuber, 'The MESSENGER mission to Mercury: Scientific Objectives and Implementation,' *Planetary and Space Science*, Vol. 49, pp. 1445-1465, 2001.

Simulating Interplanetary Transponder and Laser Communications Experiments Via Dual Station Ranging To SLR Satellites

John J. Degnan[1]

1. Sigma Space Corporation, 4801 Forbes, Blvd., Lanham, MD 20706 USA.

Contact: John.Degnan@sigmaspace.com Fax: +01-301-577-9466

Abstract

Laser transponders open up new opportunities for SLR in solar system and planetary science and general relativity, and laser communications offers orders of magnitude more bandwidth in transferring sensor data from our planetary neighbors and their moons. As new missions are proposed by the spacefaring nations to take advantage of these technologies, there will undoubtedly be a need to simulate interplanetary links and test the Earth-based and spaceborne terminals under realistic operational scenarios prior to launch. Dual station ranging to the SLR satellite constellation, in which Station A provides the radiation source received by Station B and vice versa, can provide a realistic testbed for future interplanetary transponder and lasercom systems, simulating not only the high space loss at interplanetary distances (due to the more rapid R^{-4} falloff in signal levels from passive satellites) but also the passage of the transmitted and received beams through the turbulent atmosphere. Satellites which induce minimal pulse spreading are best suited to this application, and the current SLR satellite constellation can simulate interplanetary links as far out as Saturn. The lunar reflectors can simulate distances of 93 AU or more, well beyond the Kuiper belt.

Introduction

In 2005, NASA/GSFC succeeded in performing a two-way asynchronous laser transponder experiment [Degnan 2002] with the Messenger spacecraft at a distance of 24 million km [Smith et al, 2006]. This achievement was followed just three months later by a one way transfer of pulses to the Mars Global Surveyor at a distance of 80 million km. Although these were experiments of opportunity rather than design, they clearly established the feasibility of precise interplanetary laser ranging and wide bandwidth communications. Laser transponders open up new opportunities for SLR in solar system and planetary science and general relativity, whereas laser communications offers orders of magnitude more bandwidth in communicating sensor data from our planetary neighbors and their moons back to Earth. As new missions are proposed by the spacefaring nations to take advantage of these technologies, there will undoubtedly be a need to simulate interplanetary links and test the Earth-based and spaceborne terminals under realistic operational scenarios prior to mission approval and launch. In addition to overcoming large R^{-2} space-losses over interplanetary distances, the laser beams in these future systems must traverse Earth's turbulent atmosphere, which produces effects such as beam spreading, beam wander, and scintillation (fading) [Degnan, 1993]. These effects can become much more pronounced as we attempt to extend the range of transponder or lasercom operations by reducing the uplink beam divergence in order to concentrate more energy on the remote terminal.

End-to-end ground based experiments which can convincingly simulate all aspects of these complex systems are both difficult to envision and expensive to implement. Fortunately, atmospheric transmission and turbulence effects on the uplink and

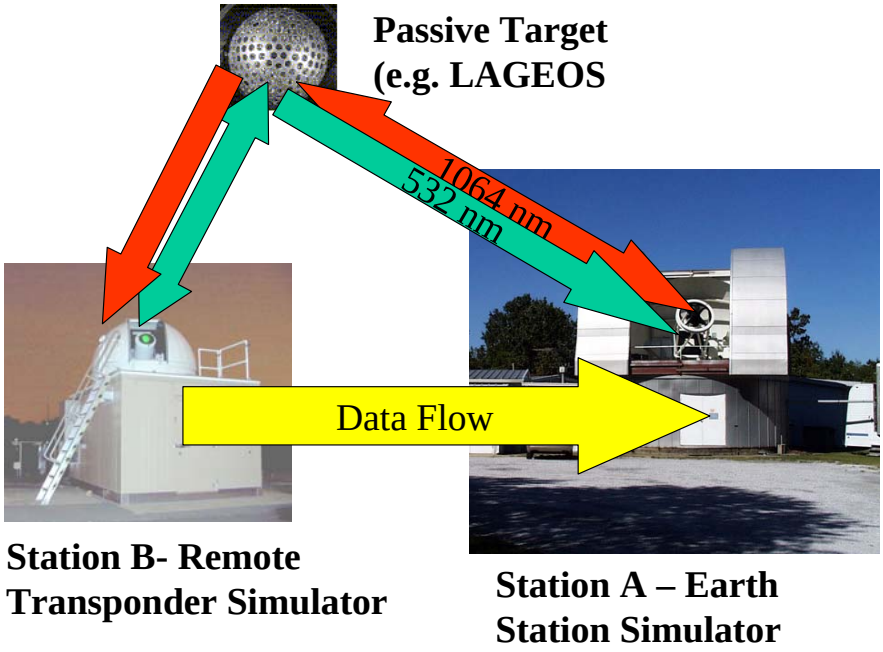

Figure 1: *Dual station laser ranging to LAGEOS with, for example, the GSFC 1.2 meter telescope facility simulating the Earth station and NASA's 40 cm aperture SLR2000 system simulating the remote terminal.*

downlink beams are the same whether the uplink beam is being reflected from a passive high altitude satellite in Earth orbit as in SLR/LLR or transmitted from a distant transponder or lasercom terminal in Deep Space. Dual station ranging to the SLR satellite constellation, in which Station A provides the radiation source received by a nearby Station B and vice versa as in Figure 1, can provide a realistic and inexpensive testbed for future interplanetary transponder and lasercom systems by duplicating not only the high space loss at interplanetary distances (due to the more rapid R^{-4} falloff in signal levels from passive satellites) but also the passage of the transmitted and received beams through the turbulent atmosphere. Each station must be located within the reflected return spot of the other station, and this requirement typically restricts the inter-station separation to within a few hundred meters. The larger terminal, simulating the Earth station, would exchange reflected pulses from the satellite with a smaller station, simulating the remote transponder or lasercom terminal. Figure 1 illustrates GSFC's 1.2 meter telescope facility ranging to LAGEOS in the infrared (1064 nm) while NASA's 40 cm aperture photon-counting SLR2000 system ranges to the same satellite in the green (532 nm). In order to simulate a dual wavelength transponder or lasercom experiment Each station is equipped with a receiver channel at a second wavelength to detect reflected pulses from the sister station. The experiment is self-calibrating since the transponder measures the dogleg defined by Station A – satellite – Station B while the individual ranging systems measure the Station A – satellite and Station B – satellite distances, albeit at slightly different epoch times. Ground surveys typically define the interstation vector, or third leg of the triangle, to better than 2 mm. This provides an accurate way to test the ranging and time transfer algorithms. Similarly, the Bit Error Rate (BER) of an "interplanetary" laser communication system can be obtained by directly comparing the incoming and outgoing bits at the adjacent sites. Such experiments are currently being pursued at NASA [McGarry et al, 2006].

Automated acquisition of the Earth station by the remote terminal can be demonstrated by either turning off or ignoring the closed ranging loop at 532 nm while it searches for the reflected light at 1064 nm. The ability to lock Station A onto the satellite via a closed single ended ranging loop at 1064 nm ensures a steady source of photons from the Earth station for the remote terminal to find and lock onto.

Link Equations

The link equations define the received signal strength at either station. For the infrared link from the Earth station A to the remote terminal B via a passive satellite, the link equation is given by [Degnan, 2001]

$$n_R^{AB} = \frac{4\eta_q^B \eta_t^A \sigma_s \eta_r^B T_A^{2\sec\theta_A}}{h\nu_A \left(\theta_t^A\right)^2 (4\pi)^2} \frac{E_t^A A_r^B}{R_R^4} \tag{1}$$

which depends on the transmitted energy E_t, the receive aperture A_r, detector quantum efficiency η_q, the photon energy $h\nu$, the one-way zenith atmospheric transmission T_a, the satellite zenith angle θ_A, the divergence half-angle of the laser beam θ_t, the target optical cross-section σ_t, measured in square meters, and the optical throughput efficiencies of the transmitter (η_t) and receiver (η_r) optics respectively. The *A* and *B* superscripts and subscripts signify the terminal for which the value applies, and are reversed for the opposite link from terminal *B* to *A*. The quantity R_R.is the slant range to the target satellite. For the nominally circular orbits of typical SLR targets, R_R.can be expressed as a function of the satellite height above sea level *h*, and the satellite zenith angle

$$R_R(h,\theta_A) = -R_E \cos\theta_A + \sqrt{(R_E \cos\theta_A)^2 + h(h + 2R_E)} \tag{2}$$

where R_E = 6378 km is the mean volumetric radius of the Earth and (2) reduces to *h* when $\theta_A = 0$.

For interplanetary transponder or lasercom links, the link equation is given by [Degnan, 2001]

$$n_T^{AB} = \frac{4\eta_q^B \eta_t^A \eta_r^B T_A^{\sec\theta_A} T_B^{\sec\theta_B}}{h\nu_A \left(\theta_t^A\right)^2 (4\pi)} \frac{E_t^A A_r^B}{R_T^2} \tag{3}$$

Setting the mean signal counts equal in (1) and (3), we can derive an expression for the equivalent transponder distance, R_T, in terms of the actual slant range to the satellite, R_R, i.e.

$$R_T(h,\theta_A,\sigma_s) = R_R^2(h,\theta_A)\sqrt{\frac{4\pi}{\sigma_s}\left(\frac{T_B^{\sec\theta_B}}{T_A^{\sec\theta_A}}\right)} \cong R_R^2(h,\theta_A)\sqrt{\frac{4\pi}{\sigma_s}\frac{1}{T_A^{\sec\theta_A}}} \tag{4}$$

where the approximation holds if the remote terminal is in interplanetary cruise phase, in orbit, or sitting on the surface of a planet or moon with little or no atmosphere (T_B ~1).

Since the SLR satellites are normally tracked over the range $0^o \le \theta_A \le 70^o$, Eq. (4) defines a maximum and minimum simulated transponder range for each satellite. These are indicated by the blue curves in Figure 2 for selected satellites where we have assumed a value $T_A = 0.7$ corresponding to the one-way zenith transmission for a

standard clear atmosphere at 532 nm. The red curves are plots of the minimum and maximum interplanetary distances of the Moon and other planets from Earth.

It is worthwhile to note that atmospheric turbulence can influence the effective transmitter beam divergence on the uplink, but this cancels out in our derivation of (4). Furthermore, the fading statistics for the dual station ranging experiment to the passive satellite should be comparable to that of an interplanetary transponder or lasercom experiment, at least to the extent that the satellite adequately mimics a coherent point source of radiation.

Figure 2 demonstrates that a dual station ranging experiment to the lowest of the SLR satellites, Champ, provides a weaker return than a two way lunar transponder. Low elevation angle experiments to Jason are comparable to a Venus or Mars link when they are closest to Earth. Experiments to the LAGEOS and Etalon satellites would simulate ranging to Mercury, Venus, and Mars throughout their synodic cycles while experiments to GPS and LRE (at 25000 km) would simulate links up to and beyond Jupiter and Saturn. Dual station experiments to the Apollo 15 reflector on the lunar surface would simulate transponder links to over 100 AU, well beyond the orbit of Pluto and the Kuiper Belt. These results are summarized in Table 1.

The nine SLR satellites represented in Figure 2 were chosen based on the following criteria:

- The satellite array should not significantly spread nanosecond pulses (important to both transponder and lasercom experiments)
- The satellites should simulate a wide range of equivalent interplanetary distances for experimentation and allow a step-wise demonstration of distance capabilities from the Moon to the inner and outer solar system.
- The satellite suite should permit measurements at a variety of elevation angles to fully explore atmospheric effects which typically worsen at low elevations.

The primary characteristics of these satellites, taken from the ILRS Web Site and used in the computation of equivalent transponder ranges, are also summarized in Table 1.

Another way to interpret Figure 2 is to say that any single SLR station that can track the aforementioned satellites has demonstrated an adequate Energy-Aperture (EA) product for the corresponding transponder link under the same noise background and atmospheric conditions. Since all of the ILRS stations are required to track LAGEOS for membership, they all have adequate EA-product to track out to about 1 AU. About a third of ILRS stations regularly track GPS, which from Figure 2 or Table 1 implies an equivalent transponder range out to 5 AU. The NASA MOBLAS system, with an *EA*-Product of 0.045 Jm^2 and a Power-Aperture (*PA*) Product of 0.23 Wm^2 , falls into this category as does the photon-counting Graz station in Austria with *EA* and *PA* products of only 0.79×10^{-5} Jm^2 and 0.157 Wm^2 respectively. As mentioned previously, three stations have routinely tracked the Apollo reflectors but only at night with low noise background and single photon returns. Nevertheless, the same *EA*-product, which is only about 70% larger than a MOBLAS, should permit transponder links beyond 100 AU under equivalent operating conditions.

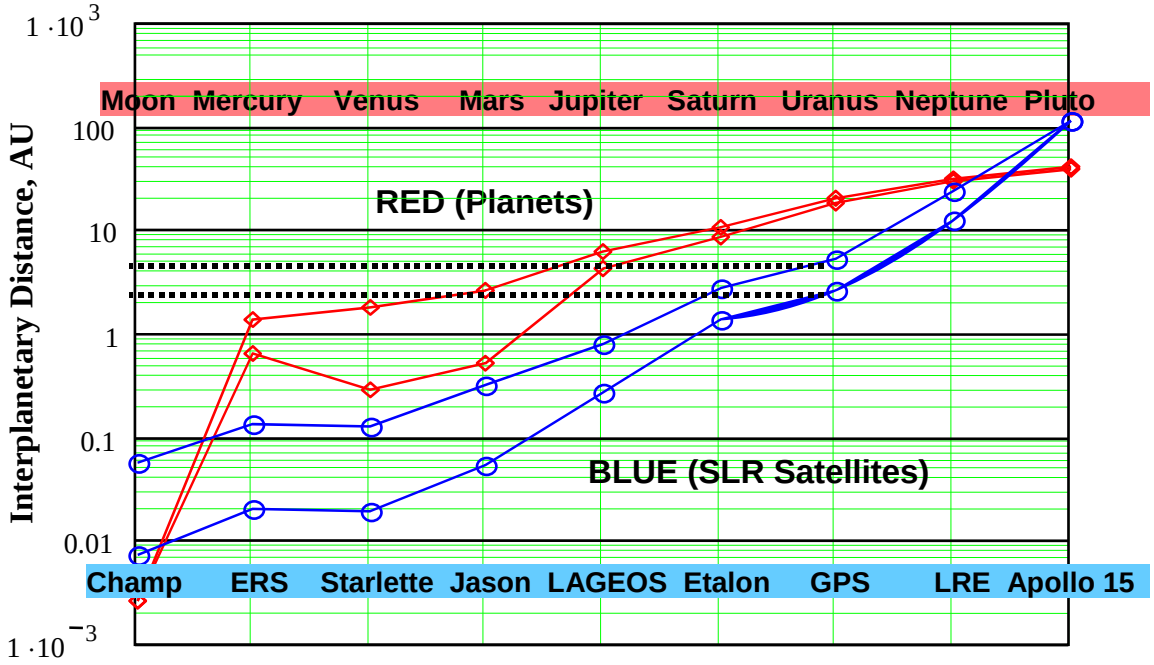

Figure 2: *The minimum and maximum distances from the Earth to the Moon and the 8 planets listed at the top of the graph is illustrated by the two red curves in the figure. The minimum and maximum transponder ranges simulated by the various SLR satellites listed at the bottom of the figure is indicated by the two blue curves.*

Table 1: *Characteristics of selected SLR satellites which can be used to simulate Deep Space transponder or lasercom links (altitudes and cross-sections from ILRS web site).*

Satellite	**Altitude (km)**	**Cross-section (10^6 m^2)**	**Transponder Range (AU)**	**Simulation**
Champ	500	1.0	0.007-0.057	Beyond Lunar (0.0026 AU)
ERS 1 & 2	800	0.85	0.02-0.135	
Starlette/Stella	950	1.8	0.019–0.123	
Jason	1,300	0.8	0.054-0.306	
LAGEOS	6,000	15	0.263-0.771	Mercury, Venus, Mars
ETALON	19,000	55	1.38-2.72	(0.28 to 2.52 AU)
GPS	20,000	19	2.60-5.06	Jupiter near PCA (4.2 AU)
LRE (elliptical)	25, 000 (max)	2	12.52-23.12	Beyond Jupiter, Saturn (4.2 to 10 AU)
Apollo 15	384,000	1,400	111.6	Beyond Outer Planets & Kuiper Belt (40 to 50 AU)

Summary

Based on the recent successful GSFC experiments to the Messenger and MGS spacecraft, the space-qualified technology for decimeter accuracy interplanetary laser transponders is clearly available now. More compact sub-centimeter accuracy photon-counting systems can be made available within 2 to 3 years with very modest technology investments, and interest in fundamental physics experiments using

transponders at NASA is high. Furthermore, detailed exploration of remote planets and moons with modern high data rate sensors previously developed for near-Earth applications will require high bandwidth lasercom systems to transmit the data back to Earth.

The link equations for laser transponders and communications are identical. We have demonstrated that retroreflector arrays on international SLR spacecraft are capable of simulating interplanetary transponder and lasercom links through the turbulent atmosphere. This provides a means for testing potential ground and spacecraft hardware, acquisition procedures, and ranging and time transfer algorithms prior to mission approval. New SLR targets on future HEO/GEO missions could provide an improved testbed with long experiment times and temporally uniform signal strengths. They could also provide better simulations of future missions to the outer planets (e.g. Jupiter and Saturn). In fact, the Jovian moon, Europa, and the Saturnian moons, Titan and Enceladus, have been identified as the top three priorities for exploration by NASA's Outer Planets Advisory Group (OPAG) in their July 2006 report.

The one drawback of using the current SLR target arrays for dual station experiments is that they are composed of large, "spoiled" [Degnan, 1993] retroreflectors. The angularly tight but complex far field patterns produced by these arrays force the stations to lie within a few hundred meters of each other and result in a signal strength which varies with both time and spacecraft-station geometry. Large panels of unspoiled small diameter retroreflectors (~7 mm) placed on future high altitude satellites (GPS/GLONASS altitudes or higher), on the other hand, would relax the proximity requirements for the dual stations to a few km, extend experiment times to several hours or more, and eliminate retroreflector-induced temporal non-uniformities in the return signal strength.

Acknowledgement

This work was initiated following a lively technical discussion on potential ways to demonstrate transponder technologies with Dr. Ulrich Schreiber at the October 2005 ILRS Workshop in Eastbourne, UK.

References

[1] Degnan, J.J., "Millimeter Accuracy Satellite Laser Ranging: A Review", in Contributions of Space Geodesy to Geodynamics: Technology, D. E. Smith and D. L. Turcotte (Eds.), AGU Geodynamics Series, Volume 25, pp. 133-162, 1993

[2] Degnan, J. J., "Asynchronous Laser Transponders for Precise Interplanetary Ranging and Time Transfer", Journal of Geodynamics (Special Issue on Laser Altimetry, pp. 551-594, November, 2002.

[3] Degnan, J. J., "Photon Counting Microlaser Rangers, Transponders, and Altimeters", Surveys in Geophysics, Special Issue on Evolving Geodesy, Vol 22, Nos. 5-6, pp. 431-447, 2001.

[4] McGarry, J., T. Zagwodzki, P. Dabney, P. Dunn, J. Cheek, "Laser Ranging at Planetary Distances from SLR2000", these proceedings, 2006.

[5] Smith, D.E., M. T. Zuber, X. Sun, G. A. Neumann, J. F. Cavanaugh, J. F. McGarry, and T. W. Zagwodzki, *Science*, **311**, p. 53, 2006.

Laser Ranging At Planetary Distances from SLR 2000

J. McGarry[1], T. Zagwodzki[1], P. Dabney[1], P. Dunn[2], J. Cheek[2]

1. NASA / Goddard Space Flight Center
2. Raytheon Information Solutions.

Contact: Jan.McGarry@nasa.gov

Abstract

The SLR2000 prototype system will be participating in two separate planetary transponder laser ranging experiments: (1) as one end of the Goddard in-house asynchronous transponder experiment in 2007, and (2) as the primary ground station for one-way ranging to the Lunar Reconnaissance Orbiter (LRO) in late 2008 and 2009.

The modifications to SLR2000 to participate in these projects are relatively few and are very synergistic with the SLR completion effort. This paper describes the transponder experiments and the changes required at SLR2000.

Introduction

SLR2000 is the prototype for NASA's Next Generation of Satellite Laser Ranging (SLR) Systems. It was originally designed to be a completely automated, eye-safe Satellite Laser Ranging System, with a lower cost of operation, a high reliability, and an accuracy comparable to the existing NASA MOBLAS systems [McGarry]. Because of its arcsecond level pointing capability, its timing accuracy (both absolute and relative) and its ability to independently measure fire and return times, this system is an excellent candidate for transponder work.

The 1.2 metre telescope (aka 48 inch telescope) was developed by Goddard in 1974 as a research and development facility. It has hosted many laser ranging and other experiments over the years including the first successful 2-way asynchronous transponder experiment at 24 million kilometres with the Mercury Laser Altimeter (MLA) on the MESSENGER spacecraft in 2005, and the first successful 1-way laser ranging experiment at ~80 million kilometres with the Mars Obiter Laser Altimeter (MOLA) on the MGS spacecraft orbiting Mars, also in 2005. The 1.2 metre telescope is owned and operated by the Laser Remote Sensing Branch (code 694) at the Goddard Space Flight Center.

Both systems are located at Goddard's Geophysical and Astronomical Observatory (GGAO) which has been the site of most of NASA's ground breaking work in laser ranging, including the some of the first laser ranging returns ever recorded, the development and checkout of the MOBLAS and TLRS systems in the late 1970s and early 1980s, and the MLA and MOLA Earthlink experiments described above. It is also home to MOBLAS-7 which is the NASA SLR Network standard for performance.

Two-way asynchronous transponder demonstration

The goal of this in-house Goddard project is to demonstrate two-way asynchronous acquisition and ranging between two ground systems at Goddard's Geophysical and Astronomical Observatory (GGAO). The 1.2 metre telescope will function as the planetary spacecraft and will transmit at 50Hz in the IR (1064nm) and receive SLR2000's green (532nm) returns. SLR2000 will function as the ground station,

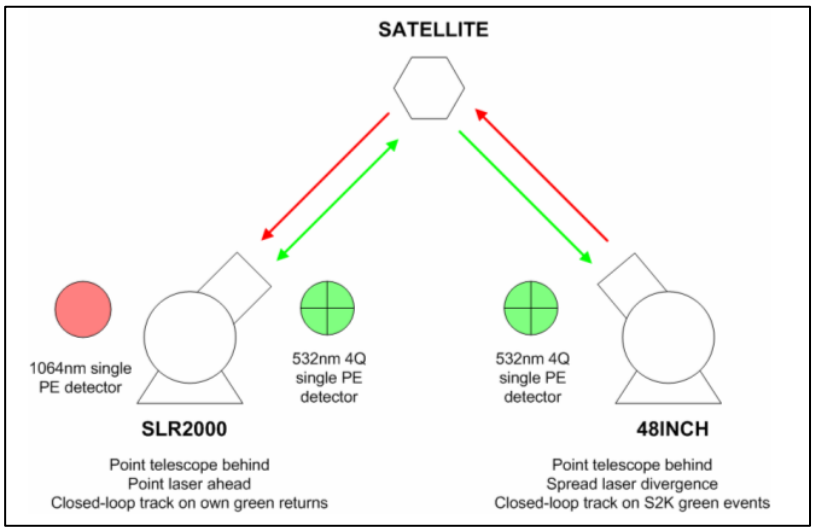

Figure 1: *Two-way asynchronous transponder experiment concept*

firing at 2 khz in the green and receiving the 1.2 metre telescope's IR returns. The laser pulses will be bounced off of retro-reflector equipped satellites to provide the simulation of planetary distances (Figure 1). The stations are sufficiently close that both are within the return footprint from the satellites. SLR2000 will closed-loop track on its own green returns and the 1.2 metre will closed-loop track on the green SLR2000 returns. Fire and return times will be collected by each station. A clock will be used at the 1.2 metre telescope that will simulate the frequency drift of a spacecraft clock. The event information from both stations will be used as input to analysis software that will determine the ranges, clock offset and frequency drift between stations.

Optical breadboard space has been added to SLR2000 to support this experiment along with a dichroic beam splitter (532nm / 1064nm) for the receive channel, beam reduction optics, a narrow band pass filter, and a fiber optic delivery to the 1064nm photodetector (Figure 2). The candidate detector is a Perkin Elmer model SPCM-AQC(4) photodetector with a quantum efficiency of ~2% and better than 500 picosecond jitter. An additional discriminator will be added and one additional event time channel will be used (for the 1064nm returns). There are minimal software changes required to the operational software at SLR2000 to perform this experiment.

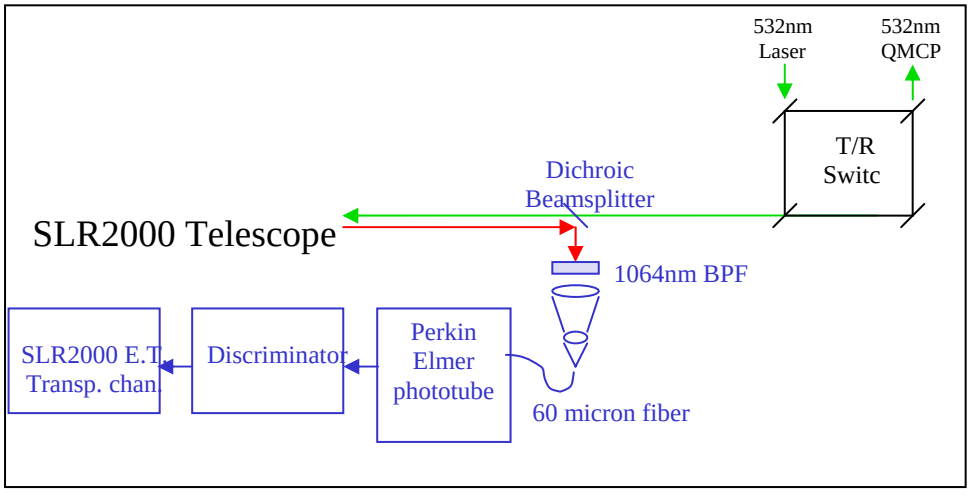

Figure 2: *Additions for 1064nm transponder returns at SLR2000*

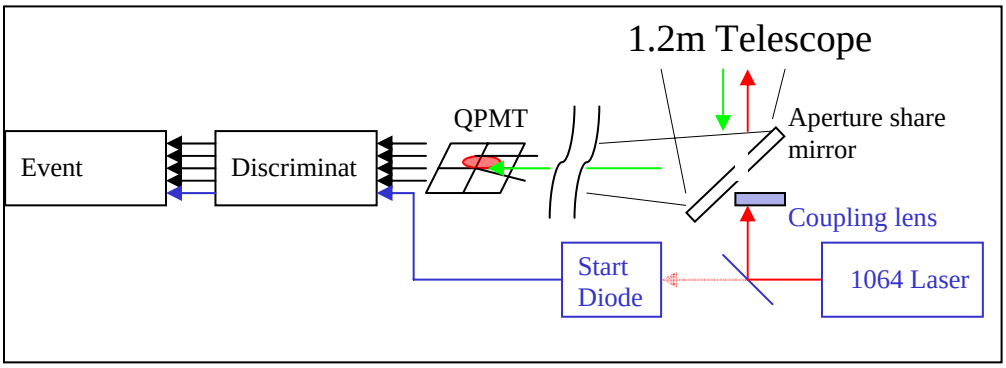

Figure 3: *1.2 meter telescope configuration for transponder experiment*

Modifications to the 1.2 metre telescope configuration include the addition of a 532nm ungated single photon quadrant detector (Hamamatsu metal channel dynode PMT) and four discriminators, along with a band pass filter for the 532nm events from SLR2000 and a 1064nm blocking filter to prevent backscatter from local laser (Figure 3). Much of the configuration used for the MLA-Earthlink and MOLA-Earthlink experiments will be used for this project including the computer, the Time-to-Digital Converter (TDC), the Continuum Inlite II-50 laser (up to 50 Hz at 1064nm with a 6 nanosecond pulse width), and aperture sharing of the transmit-receive. Software modifications include handling of the four quadrant channels for closed-loop tracking.

The transmit and receive times from both SLR2000 and the 1.2m telescope will be processed to remove the noise. The clock bias and drift can be modeled as a linear function of the 1.2 metre telescope's time. The range error can be modeled as a quadratic equation in time. A least squares fit of the fire and receive event data to the resulting equations (shown below in Figure 4) would then provide the ranges as well as the relative clock offset and drift.

Both systems are nearing completion of the required modifications and both have tracked green returns from MOBLAS-7's fires. The 1.2 metre telescope's mirrors are in the process of being recoated in preparation for an upcoming laser communications experiment. When the recoating is complete in the spring of 2007 the two-way asynchronous transponder data collections will begin.

One-way laser ranging to the Lunar Reconnaissance Orbiter

The function of the Earth to LRO laser link is to achieve the mission's precision orbit determination requirement. The requirements on the SLR2000 ground station to accomplish this are:

1. Between 1 and 10 femtoJoules per square centimetre of signal must be delivered to the LRO-LR receiver aperture. For the SLR2000 laser with a 55 microradian laser divergence, this implies 30 milliJoules per pulse.

2. The wavelength must be 532 nm and the 3 Angstrom LRO-LR filter will be tuned to the actual SLR2000 laser in the lab.

3. The laser pulse width must be less than or equal to 8 nanoseconds FWHM.

4. Laser pulses must be delivered into the LOLA earth window at 28Hz.

5. The transmitted pulse time stamp accuracy must be maintained within 100 ns of UTC.

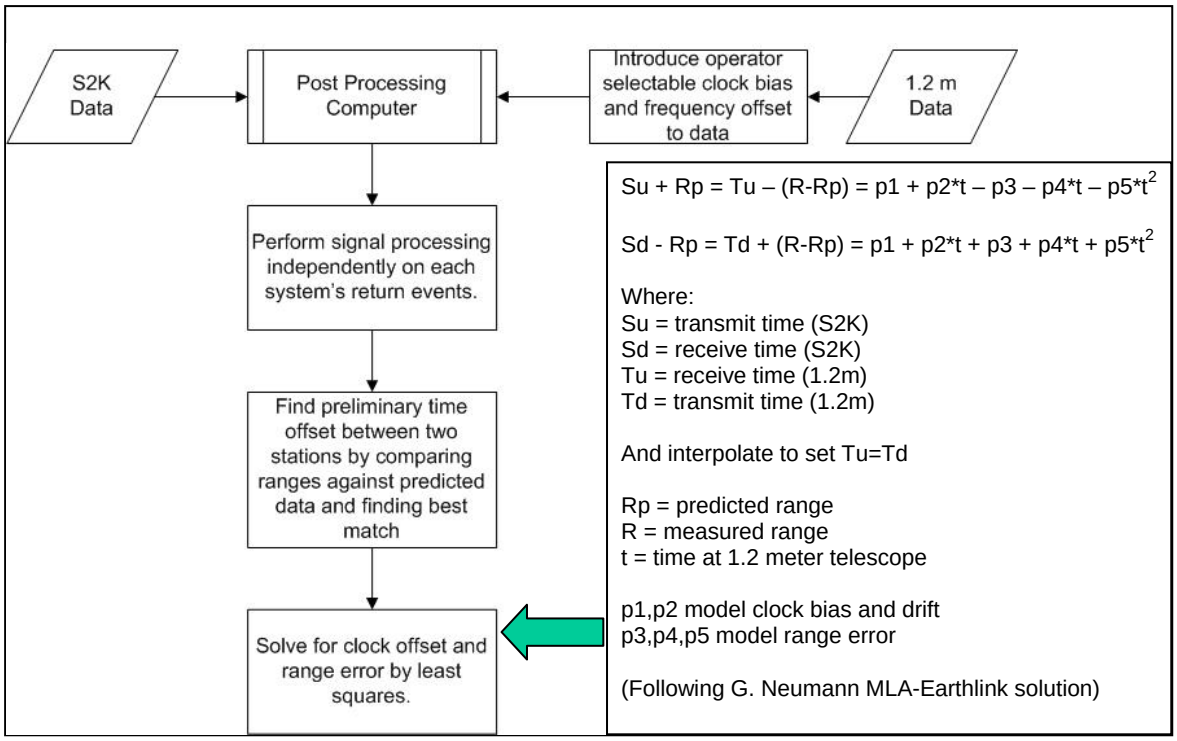

Figure 4: *Post processing of fire and receive event times at two stations*

6. The relative laser time of fire must be measured to better than 200 picoseconds (1 sigma) shot-to-shot over a 10 second period. The laser fire time must be recorded to better than 100 picosecond resolution.

7. The frequency stability of the station's clock must be equal or better than 1.e-12.

8. The system must provide better than 407 hours of ranging data to LRO during year after launch. This number is achievable and takes into account the LRO visibility from the station, the outages due to weather, system failures, as well as aircraft avoidance outages.

To accomplish these requirements SLR2000 is purchasing a 28 Hz diode pumped Nd:YAG master oscillator power amplifier (MOPA) laser that can deliver up to 50 milliJoule per pulse at 532 nm in a 6-8 nanosecond pulse. It is a turn-key system with a projected lifetime of greater than 1 year of continuous use. Additional optical table space has been added for the laser and a removable kinematic mirror mount will be inserted to launch the LRO transmit beam and ensure an easy transition between SLR and LRO lasers. Because this laser is not eye-safe, an aircraft avoidance radar is also being added to the system.

The software for SLR2000 is being modified to handle the new laser parameters, to control the laser fire to hit the earth window on the spacecraft, to take new operator commands for control of the new laser, and to handle predictions for non-earth-orbiting satellites.

LRO-LR will be launched in late 2008. SLR2000 will be staffed to support the mission 10 hours a day, 7 days a week to cover those times when the moon is above 20 degrees elevation. LRO is visible to earth about one hour out of every two.

During the hour that the spacecraft is behind the moon SLR2000 will range to earth orbiting satellites with the eye-safe 2 khz SLR laser.

Summary

Transponder experiments will extend capabilities of SLR2000 and demonstrate the system's ability to do planetary ranging which is the future of laser ranging. Earth orbiting satellite laser ranging and planetary transponder ranging can co-exist in SLR2000 and transitioning between the two will be seamless. The in-house Transponder experiment will complete in late 2007. The LRO mission will run from Fall 2008 through January 2010.

Acknowledgements

The authors would like to thank John Degnan for the original concept of bouncing laser pulses off of earth orbiting satellites to simulate planetary transponder ranging [Degnan].

We would like to thank the LOLA Instrument Principal Investigators David Smith and Maria Zuber for their efforts in getting laser ranging selected for LRO, as well as Xiaoli Sun, Greg Neumann, Ron Zellar, and David Carter for their continued support in the development of the LRO-LR ground system.

We would also like to thank our colleagues who have worked on the transponder experiment and on LRO-LR, including Christopher Clarke, Ray DiSilvestre, Howard Donovan, Julie Horvath, Anthony Mallama, Anthony Mann, Carey Noll, Donald Patterson, Randall Ricklefs, David Rowlands, Mark Torrence, and Susan Valett.

The 2-way asynchronous transponder work is being performed with Goddard in-house IRAD funding. The LRO-LR work is being performed with funding from the Lunar Reconnaissance Orbiter Mission.

References

[1] Degnan, J., "Simulating Interplanetary Transponder and Laser Communications Experiments via Dual Station Ranging to SLR Satellites," in this Proceedings.

[2] McGarry, J., and T. Zagwodzki, "SLR2000: The Path Toward Completion," in this Proceedings.

Laser Ranging to the Lunar Reconnaissance Orbiter (LRO)

David Smith[1], Maria Zuber[2], Mark Torrence[3], Jan McGarry[1], Michael Pearlman[4]

1. NASA / Goddard Space Flight Center, Greenbelt, Maryland, USA,

2. Massachusetts Institute of Technology, Cambridge, Massachusetts, USA

3. SGT Inc, Greenbelt, Maryland, USA

4. Harvard-Smithsonian Center for Astrophysics, Cambridge, Massachusetts, USA

Abstract

LRO will be launched in late 2008 carrying, amongst other payloads, the Lunar Orbiter Laser Altimeter (LOLA) which is a 1064nm laser altimeter for mapping the lunar surface, and the Laser Ranging (LR) receiver which is mounted on the earth-pointed High Gain Antenna (HGA). Laser Ranging with LRO (LRO-LR) is one-way from earth to spacecraft and will be used along with S-band tracking data and the LOLA altimeter data to develop an improved gravity model for both the near and far sides of the moon. SLR2000 will be the primary laser ranging station, but the project would like to extend an invitation to ILRS stations for their participation. The requirements for ranging include satisfying the laser wavelength (to match the onboard filter at 532nm), repetition rate (to hit the range window but minimize impact to the onboard threshold algorithm), transmit energy (to cross the detector threshold), and station timing (to ensure precise transmit time recording). The requirements are very similar to those for earth orbiting satellite laser ranging. We hope that many of you will consider participating in this exciting transponder experiment.

Introduction

LRO is a robotic component of the Moon to Mars vision proposed in January, 2004. LRO will be launched in October 2008 into a polar orbit around the Moon with an average altitude of 50 km. Lunar gravity necessitates orbital maintenance every 30 days (30-70 km altitude range) to maintain the polar orbit for the one-year nominal mapping mission. The LRO spacecraft has a suite of seven instruments: LOLA, a laser altimeter; LROC, a camera; LAMP, a Lyman alpha telescope; LEND, a neutron detector; DIVINER, a thermal radiometer; CRATER, a cosmic ray detector; and the mini-RF, radar technology demonstration. The LOLA altimeter addresses the geodetic measurement objectives of NASA's robotic lunar exploration program, in particular – "Determine the topography of the Moon to geodetic quality from global to landing-site relevant scales." and "Assess metre and smaller-scale features to facilitate safety analysis of potential future lunar landing sites".

The precise determination of the Lunar topography from LOLA data, and positioning of the measurements made by other LRO instrument suite on the lunar surface requires accurate LRO orbits. The LRO orbits will be determined by high quality tracking of LRO and improvement in the knowledge of the Lunar gravity field. To enhance the orbit determination, the LRO mission includes a one-way laser ranging (LR) capability. The LR data will provide a 10 cm precision measurement of the position of LRO. In conjunction with the LOLA data, LRO positional accuracies will be 50 to 100 m along track and 1 metre radially from the Lunar center of mass after improvement of the lunar gravity field. One SLR station (Greenbelt, MD) is presently planned to track LRO; we are hoping for a second US station and help from the international SLR network.

Measurement technique

The LRO-LR measurement is a one way range from earth to spacecraft with the ground station recording the time of the laser fire and the LOLA instrument onboard LRO recording the pulse arrival time. The 2 cm aperture LR receive telescope will be mounted on the spacecraft's High Gain Antenna (HGA). The optical signal will be routed via fiber optic cable to the LOLA instrument (see Figure 1). One of LOLA's five lunar detectors will receive the earth pulses as well as the lunar surface events.

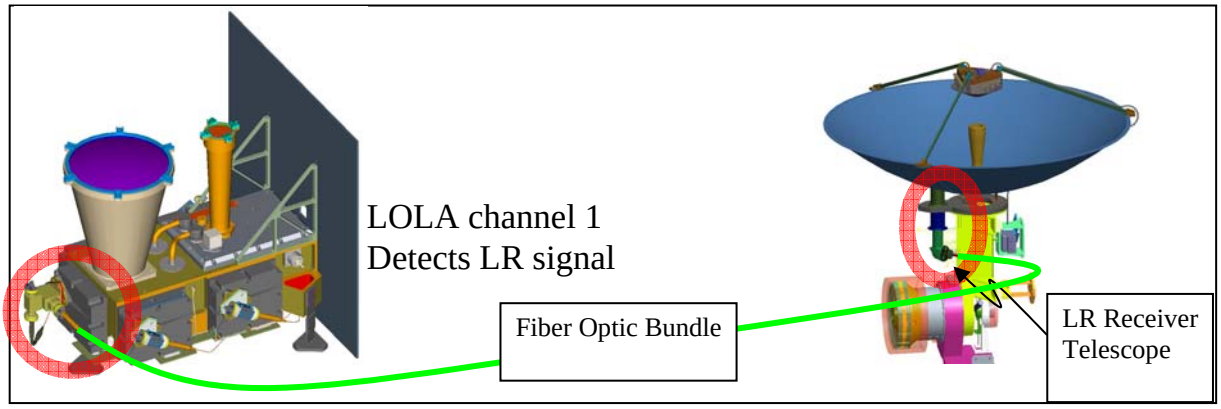

Figure 1: *Optical signal path from HGA to LOLA instrument.*

SLR2000 is the primary ground station for LRO-LR and is required to transmit at 28Hz (the LOLA instrument's fire rate), and to control its laser fire times to ensure that all pulses arrive in the LOLA earth windows as shown in Figure 2 [McGarry]. There is no corresponding requirement for other participating stations to control their laser fire times, however, to ensure a minimum of one pulse per second arrival in the earth window, fire rates of 5 Hz and 10 Hz should be used when the laser fire time is not controlled.

No ground station should fire at LRO faster than 28Hz. Events that occur outside LOLA's range windows (earth or lunar) are interpreted as noise and will affect the threshold level which is controlled by a feedback loop based upon the noise counts outside the windows.

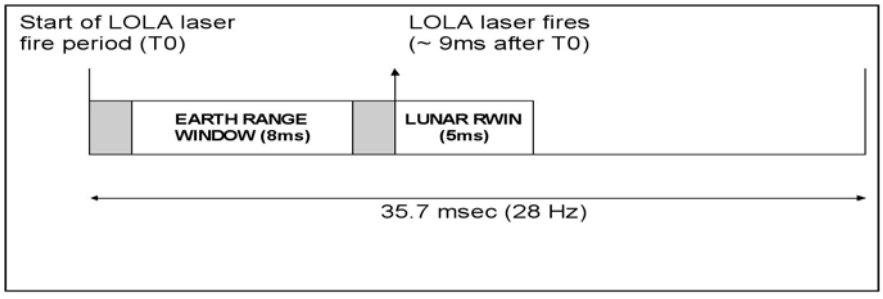

Figure 2: *Timing of LOLA earth window relative to lunar window within the 28Hz laser fire period*

Ground System Requirements

Stations participating in the LRO-LR experiment must satisfy the following requirements:

1. Deliver between 1 and 10 femtoJoules per square centimetre of signal to the receiver aperture. For SLR2000 with its 55 microradian laser divergence this translates into a transmit energy of 30 milliJoules per pulse.
2. The transmitting wavelength must be 532 nm. The exact wavelength will be determined in Spring 2007. The spacecraft filter is 3 Angstroms in width. A filter assembly will be sent to all interested stations later in 2007 to allow each station to determine if its laser meets the requirements.
3. The laser pulsewidth must be less than 8 nanoseconds.
4. The transmitted pulse time stamp accuracy must be maintained within 100 nanoseconds of UTC.
5. The system must measure the relative laser time of fire to better than 200 picoseconds (1 sigma) shot-to-shot over a 10 second period. Laser fire times must be recorded to better than 100 picosecond resolution.
6. The system should deliver at least one laser pulse to the LOLA earth window per second. The laser fire rate cannot exceed 28 Hz.
7. A shot to shot measurement of the output laser energy is desirable.
8. Data should be delivered to CDDIS in new ITDF (simple ASCII format) no slower than daily.

Most ILRS systems should have no problem meeting these requirements.

Other requirements will include coordination with the mission so that coverage can be limited to a single station at a time (at least initially), and reporting so that the mission knows ahead of time which stations will be participating each day.

Operational Considerations

The period of the LRO orbit is approximately 2 hours. The orbit is polar and precesses so that at times the entire 2 hour orbit will be visible from earth. Due to the constraints on the HGA pointing, however, only ~1 hour out of each 2 hour orbit will be available for earth ranging, no matter what the orbital orientation is.

Predictions for LRO will be generated in CPF format. Code for non-earth orbiting satellites will be made available to all ILRS stations by Randy Ricklefs later this year [Ricklefs].

Feedback will be provided from LOLA in its housekeeping telemetry which will be delivered in semi-real-time from the spacecraft, through the LOLA Science Operations Center (SOC), to CDDIS. LOLA will be performing signal processing on the data in the earth window and should be able to recognize earth laser pulses that are fired synchronously to LOLA at 14 or 28Hz. Laser fire rates of 5 and 10 Hz will not be recognized by LOLA, however, the website, http://lrolr.gsfc.nasa.gov ,will contain other information as well (possibly a Go-NoGo flag), so participating stations should check it when ranging to LRO.

The flow of all of the data for LRO-LR is shown in Figure 3.

Stations interested in participating as a ground station for LRO-LR are invited to contact the authors or Michael Pearlman (mpearlman@cfa.harvard.edu).

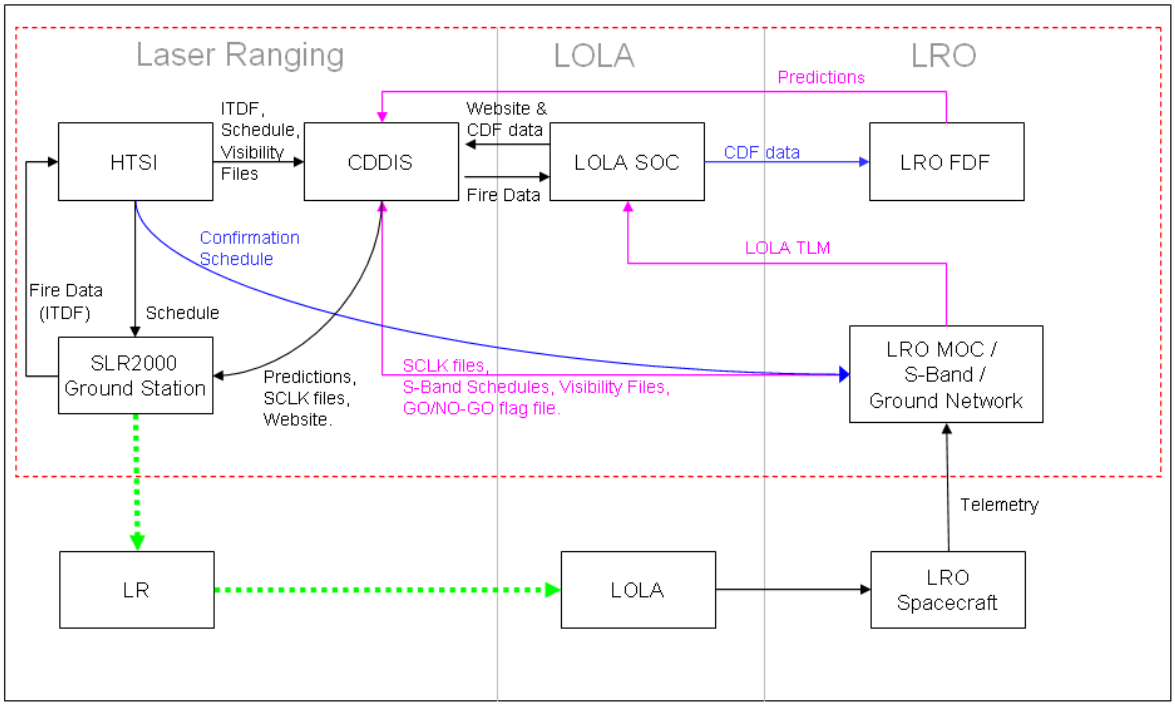

Figure 3: *LRO-LR data flow block diagram.*

References

[1] McGarry, J., and T. Zagwodzki, "SLR2000: The Path Toward Completion," in this Proceedings.

[2] Ricklefs, R., "Consolidated Laser Prediction and Data Formats: Supporting New Technology", in this Proceedings.

UN-COOPERATIVE TARGETS SESSION SUMMARY

Chair: Craig Smith

This short session received fascinating papers from laser ranging groups attempting the most difficult of SLR activities - that is ranging to un-cooperative targets.

From Shanghai Observatory we heard about the numerous upgrades to the system there towards the development of precision tracking for un-cooperative targets (ie targets that do not carry retro-reflectors). We wish Shanghai Observatory well in this endeavor.

From Czechoslovakia and the Graz SLR station in Austria a new technique for provide simultaneous optical and laser tracking of targets was described.

The Experimental Laser Ranging System for Space Debris at Shanghai

Yang Fumin[1], Chen Wanzhen[1], Zhang Zhongping[1], Chen Juping[1], Wang Yuanming[1], K. Hamal[2], I. Prochazka[2)]

1. Shanghai Astronomical Observatory, Chinese Academy of Sciences

2. Czech Technical University in Prague, Czech Republic

Abstract

The paper introduces the performance of the experimental laser ranging system for space debris at the Shanghai Observatory. The output of laser is 2J in 532nm, 10ns, 20Hz, 40W. A new transmitting telescope with the aperture of 210mm is used, and the other parts of the ranging system are the same with the routine SLR system in Shanghai. The ranging system is under testing now.

Introduction

China has launched many spacecrafts into space and had produced many space debris during 30 years. China is one of the members of IADC (Inter-Agency Space Debris Coordination Committee). It is necessary for China to pay great attention to reduce damages from space debris in cooperation with international community. The project of laser ranging to space debris at Shanghai Astronomical Observatory is supported by the Chinese Space Agency. An experimental laser ranging system for space debris at Shanghai is set up in 2006. The goals of the project are as follows: 1) Development of the technology for space debris laser tracking. 2) Experimental observations and orbit determinations for space debris, not routine observations.

2. Performance of the system

The major parts of the space debris ranging system are the same with the SLR system at Shanghai. A China-made 40W Q-switched Nd:YAG laser has been installed and is located at the neighbor room to the mode-locked laser for SLR. There are ten Nd:YAG rods in the laser with the output of 2J in 532nm, 10ns width, 20Hz repetition, 0.6mrad divergence. A new transmitting telescope with 210 mm aperture was installed and replaced the old one with 150mm aperture for better collimating beam. The testing of laser ranging to the satellites with retro-reflectors has been done. The next step will try to ranging to uncooperative space targets soon.

Some photos for the system are shown as follows.

Fig.1. *The Optical Observation Site at Shanghai Observatory, CHINA*

Fig.2. *SLR House in Shanghai*

Fig.3. *SLR Telescope(Aperture 600mm)*

Fig.4. *Electronics Room*

Fig.5. *High Power Laser & Power Supply, Chiller*

Fig.6. *Output of High Power Laser*

Fig.7. *Inside of the 40W Pulsed Nd:YAG Laser*

Fig.8. *Coupling Optics*

Fig.9. *Laser Firing (2J, 20Hz, 40W in 532nm)*

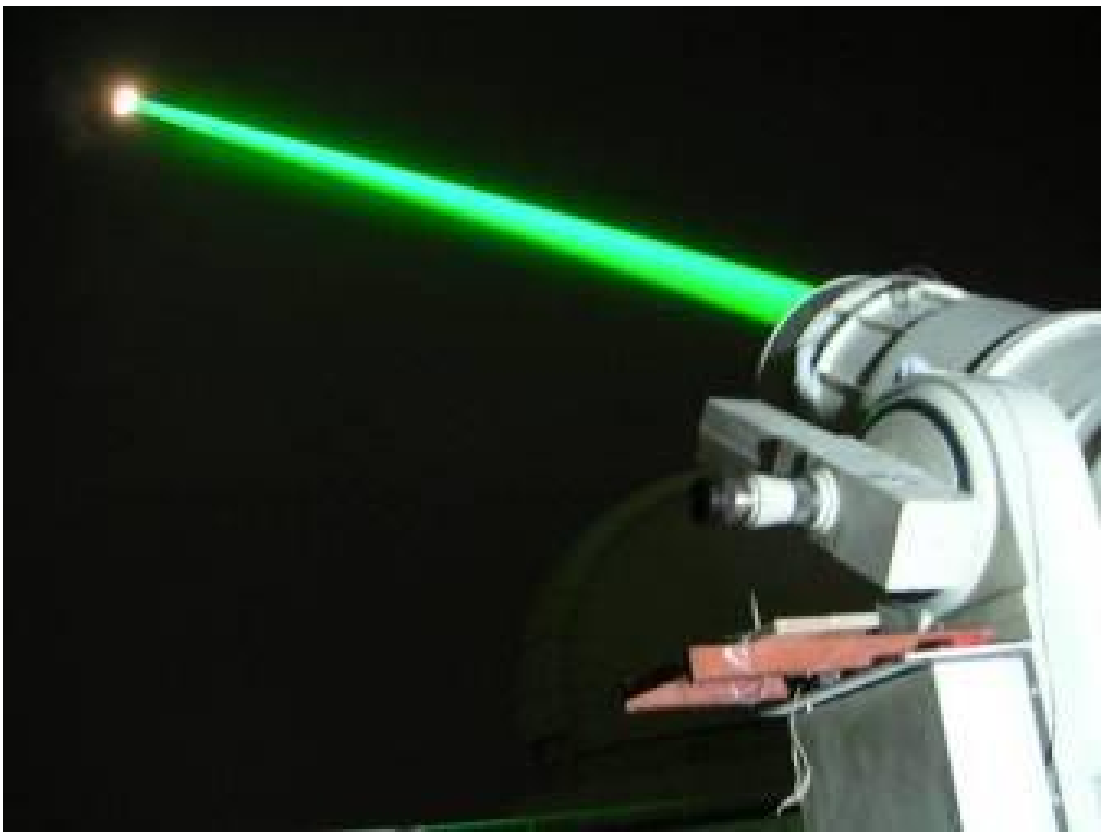

Fig.10. *Laser Firing*

Simultaneous Optical and Laser Space Objects Tracking

M. Němec[1], I. Procházka[1], K. Hamal[1], G. Kirchner[2], F. Koidl[2], W. G. Voller[2]

1. Czech Technical University in Prague, Czech Republic
2. Satellite Laser Station Graz, Austrian Academy of Sciences, Austria

Contact: nemecm1@troja.fjfi.cvut.cz

Abstract

The goal of the presented experiments is the development of new optical tracking techniques for space objects, namely space debris, based on simultaneous CCD and laser measurements: the CCD tracking of a laser illuminated object, the simultaneous CCD tracking and laser ranging and the laser time-tagging of the CCD tracking. The first two experiments can be performed on cooperative - corner retro-reflectors equipped satellites while the third one is applicable to any space object and to space debris in particular. The high accuracy and density of laser ranging data and additional Time-tags in the CCD image, atmospherically back scattered photons, can contribute to the solution stability of computed orbits from data based even on a single tracking location within a single pass.

Simultaneous Optical and Laser Space Objects Tracking

Goals

The goal of the presented experiments is the development of new optical tracking techniques of space objects, namely the space debris, based on simultaneous Optical detection (CCD tracking) and laser measurements:

1) the CCD tracking of laser illuminated object

2) the simultaneous CCD tracking and object laser ranging

3) the nanosecond laser time-tagging of the CCD tracking

The first two techniques can be performed on co-operative retroreflector equipped objects (high power lasers could be further used even for non co-operative [1]).

While the third one is applicable to any space object, the space debris in particular.

Add new applications for Satellite Laser Ranging stations

Martin Němec, FNSPE, CTU in Prague, nemecm1@troja.fjfi.cvut.cz

Simultaneous Optical and Laser Space Objects Tracking

Applications (1/2)
First insight

Classic optical detection

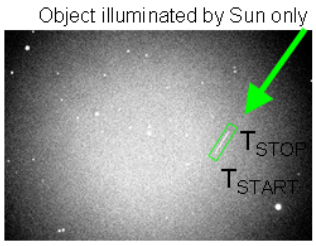

- Technique for determination the orbit of object, based on object's angular positions measurements
- Object illuminated only by Sun
- Telescope synchronized to catalogued stars + object in FOV during exposure -> angular coordinates -> pixels
- 2 Time-tags in the CCD image (Exposure start time and Exposure length) -> times -> pixels
- Problems of the accurate time-tags assigning to subpixels positions in the image (edges detections from signal curve with low SNR)

Laser usage in Optical detection:

- Additional object illumination
  - cooperative objects - Low power laser (usually stronger back reflections (retroreflectros nature) than by Sun only illumination)
  - noncooperative objects - High power laser (object shape reflectivity)
- Additional Time-tags in the CCD images – Low or High power laser
  Time-tags with **nanosecond time precision and subpixel positions** by laser photons backscattered by atmosphere

Martin Němec, FNSPE, CTU in Prague, nemecm1@troja.fjfi.cvut.cz

Simultaneous Optical and Laser Space Objects Tracking

Applications (2/2)
Details

High Precision 3D solution

Object laser ranging + Optical detection with laser time-tagging

- **cooperative objects**
  - Calibration of Optical detection systems
- **noncooperative objects**
  - High power laser strong to get enough returns -> Ranging results -> Orbit estimation
  - Low power laser (only few returns) -> combination of ranging data + high precision angular data (laser time-tagging) -> Orbit estimation

High Precision 2D solution

Optical detection with laser time-tagging

- **cooperative** or **noncooperative objects**
  - several times more of high precision angular data (laser time-tagging) -> Orbit estimation

Martin Němec, FNSPE, CTU in Prague, nemecm1@troja.fjfi.cvut.cz

Simultaneous Optical and Laser Space Objects Tracking

Project scheme

High Precision 3D solution

Optical detection with laser time-tagging

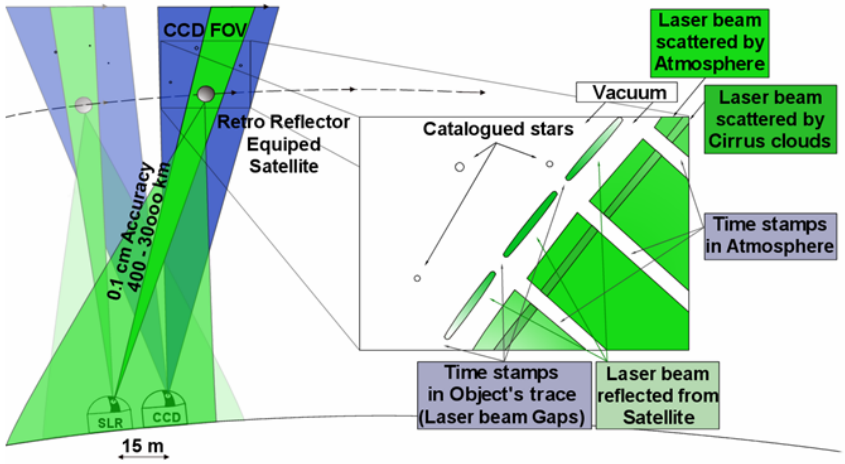

Observatory - Satellite laser ranging station in Graz, Austria

Martin Němec, FNSPE, CTU in Prague, nemecm1@troja.fjfi.cvut.cz

Martin Němec, FNSPE, CTU in Prague, nemecm1@troja.fjfi.cvut.cz

Simultaneous Optical and Laser Space Objects Tracking

Laser Time-Tags without returns

Classic optical detection

- Object illuminated by Sun only
- Only 2 Time-tags (Exposure start time and Exposure length) (more Time-tags using Advanced methods with e.g. rotating shutter)
- Times for Time-tags – milisecond up to microsecond scale (GPS)
- Problems of the accurate time-tags assigning to subpixels positions in the image (edges detections from signal curve with low SNR)
- Accuracy - up to 1 arcsecond
- Nr. of angular measurements during 1 path: usually ~ 10 values/path,

$$\max \sim \frac{\text{path time}}{\text{telescope positioning} + \text{exposure} + \text{image readout times}}$$

Object illuminated by Sun only

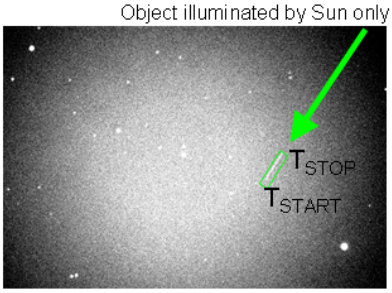

High Precision 2D solution

Optical detection with Laser Time-Tagging

- Object illuminated by Sun and partially by Low-power laser (or by High-power laser only)
- Basic 2 Time-tags (Exposure start time and Exposure length) + **more additional Time-tags** by laser beam modulation or by selection of pulses to be send to the object
- **Higher precision** of the Times for Time-tags – nanosecond scale
- **Higher accuracy** of time-tags assigning to subpixels positions in the image – All image **area** of Atmospherically back-scattered photons could be used - not only edges detections from signal curve
- Accuracy – **better than 1 arcsecond** (first results ~0.2 arcsec/s)
- Nr. of angular measurements during 1 path: **higher productivity**
  Nr. of optical measurements x **Nr. of laser time-tags in image**

Laser beam reflected from satellite

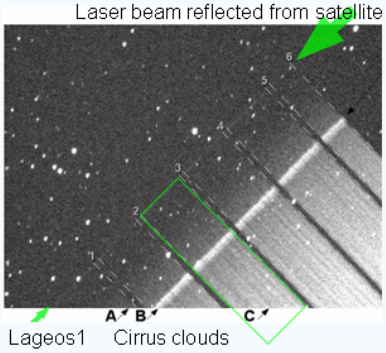

Lageos1 Cirrus clouds

1-5: Laser gaps = 10 Time-tags by laser beam photons backscattered from atmosphere

Simultaneous Optical and Laser Space Objects Tracking

Experiment Setup (1/3)
SLR system

Satellite Laser Ranging System (SLR) station in Graz

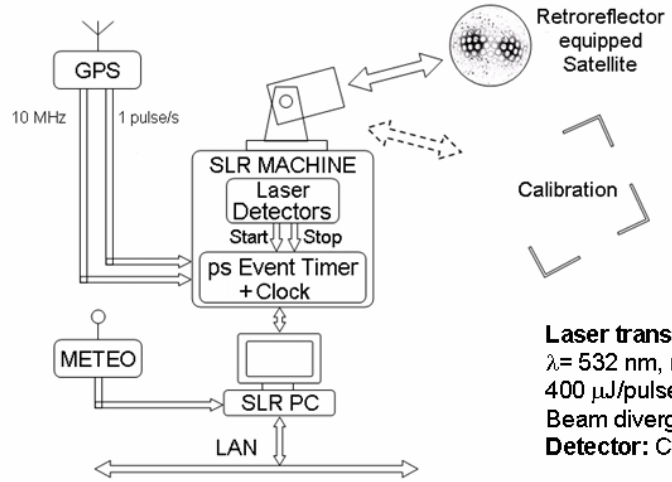

Ranging accuracy ~few mm for Retroreflector equipped satellites in distances of 400-30'000 km

Laser transmitter: HighQLaser, Diode pumped Nd:Van, λ= 532 nm, repetition rate 2 kHz, Pulse length 8 psec, 400 μJ/pulse, Average power up to 1W
Beam divergence θ ~100 μrad
Detector: C-SPAD; Range up to 30 000 km

The SLR station has been modified to provide laser power output modulation (selection of output pulses – gating of Pockel's cells) to serve as a time tagger for the laser illuminated exposures.

The laser is "switched off" for the preset time interval (e.g. 50, 100 or 500 milliseconds, etc.) each one second. The precision of the time-tags is on the nanosecond scale. The time scale accuracy connected to GPS is better than 100 ns.

Martin Němec, FNSPE, CTU in Prague, nemecm1@troja.fjfi.cvut.cz

Simultaneous Optical and Laser Space Objects Tracking

Experiment Setup (2/3)
Telescope and CCD cameras for Optical detection

CCD Telescope:
Meade LX200 16", f/10
Tracking precission 5 arcmin (worse now)

Focal reducers: f/6.3 or f/3.3

Field of View:
CCD1: ~ 23x15 arcmin, 1.8x1.8 arcsec/pixel (bin 3x3)
CCD2: ~ 16.6x12.5 arcmin, 1.2x1.2 arcsec/pixel (bin 2x2)
EMCCD: ~ 9.3x7.0 arcmin, 0.85x0.85 arcsec/pixel

(EMCCD = CCD with internal Electron multiplying register)

CCD cameras:
1: SBIG ST-10ME
Pixel Array:2184x1472
Pixel Size: 6.8x6.8 µmxµm
CCD Size: 14.9x10 mmxmm
Filter:
488-574 nm, green pass

2: SBIG ST-2000XM
Pixel Array:1600x1200
Pixel Size: 7.4x7.4 µmxµm
CCD Size: 11.8x8.9 mmxmm
Filter:
no filter

EMCCD camera:
Andor Luca^{EM}
Pixel Array: 658x496
Pixel Size: 10x10 µmxµm
CCD Size: 6.58x4.96 mmxmm
Filter:
no filter

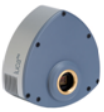

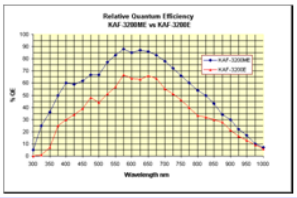

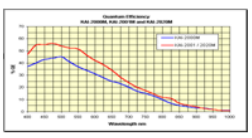

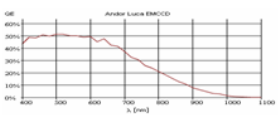

Martin Němec, FNSPE, CTU in Prague, nemecm1@troja.fjfi.cvut.cz

Simultaneous Optical and Laser Space Objects Tracking

Experiment Setup (3/3)
Minimal system configurations

High Precision 3D solution

High Precision 2D solution

* photon detector is not necessary

1. Object path prediction

2. SLR Station:

Telescope - able smooth real-time object tracking (~ 1 arcsecond)

- diameter depending on object shape and reflectivity

Laser – pulse (min. repetition rate > 1 Hz (higher is better)

- depending on Optical detection system FOV, object speed and nr. of laser time-tags)

Pulses gating system + events timing system with high accuracy + photon detector*

Sensitive camera – CCD, EMCCD, ISIT, etc. (optical feedback)

3. Optical detection system:

Telescope

- object tracking precision (~ 5 arcminutes or better, depending on Optical det. system FOV)

- diameter depending on object shape and reflectivity

Sensitive Low-Noise Camera – CCD, EMCCD

- Pixel size, Quantum efficiency depending on object speed, shape and reflectivity (+ telescope properties)

Martin Němec, FNSPE, CTU in Prague, nemecm1@troja.fjfi.cvut.cz

Simultaneous Optical and Laser Space Objects Tracking

Experiment results 1

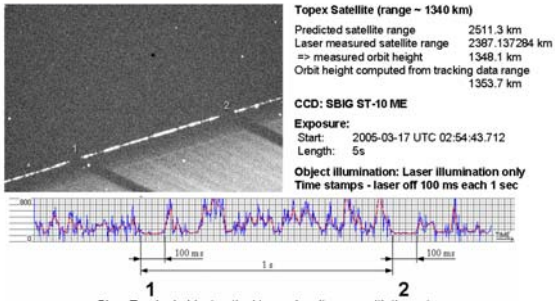

Blue: Tracked object optical trace densitogram with time stamps
Red: Moving AVG (Average) Window graph of optical trace densitogram
(Window: width 5 pixels, height 5 pixels)

Martin Němec, FNSPE, CTU in Prague, nemecm1@troja.fjfi.cvut.cz

Simultaneous Optical and Laser Space Objects Tracking

Experiment results 3

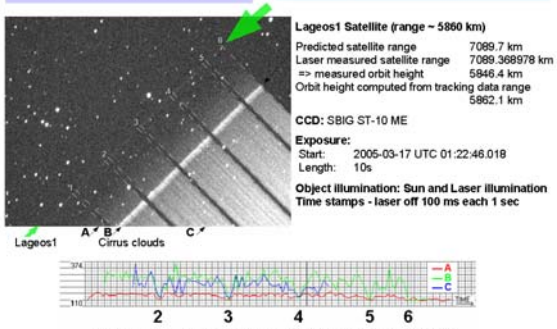

Moving AVG Window graphs of densitograms with time stamps
(Window: width 5 pixels, height 5 pixels)

Martin Němec, FNSPE, CTU in Prague, nemecm1@troja.fjfi.cvut.cz

Simultaneous Optical and Laser Space Objects Tracking

Experiment results 2

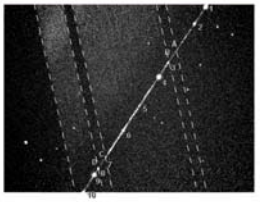

Point	Time [s]	Position [x,y]
A	21.00000002	550.37, 145.97
B	21.10000005	527.67, 180.28
C	22.00000003	323.42, 489.05
D	22.10000001	300.73, 523.36

Base Time: 2005-07-04 UTC 01:47:19.433

Point	Time [s]	Position [x,y]
1	20.5983	641.71, 7.89
2	20.7552	606.01, 61.85
3	21.1217	522.88, 187.52
4	21.2545	492.92, 232.96
5	21.5231	431.77, 325.26

Point	Time [s]	Position [x,y]
6	21.7560	378.69, 405.49
7	22.0012	323.27, 489.28
8	22.1024	300.26, 524.07
9	22.1623	286.64, 544.66
10	22.3192	250.94, 598.62

AJISAI (EGP) is spinning satellite covered with mirrors and retroreflectors.
Adding Time-stamps in atmosphere could increase precision of its spin speed and spin axes orientation measurements

Martin Němec, FNSPE, CTU in Prague, nemecm1@troja.fjfi.cvut.cz

Simultaneous Optical and Laser Space Objects Tracking

Experiment results 4

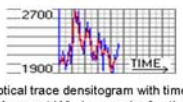

Blue: Optical trace densitogram with time stamps
Red: Moving AVG (Average) Window graph of optical trace densitogram
(Window: width 2 pixels, height 5 pixels)

Martin Němec, FNSPE, CTU in Prague, nemecm1@troja.fjfi.cvut.cz

Simultaneous Optical and Laser Space Objects Tracking

Problems

Atmosphere density – low density => less back-scattered photons

Object tracking Accuracy and Smoothness of the tracking laser movement

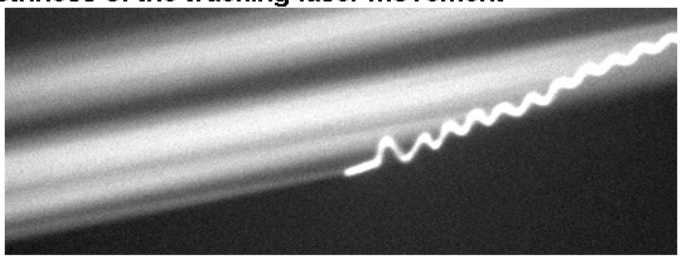

Distance between Laser and CCD telescopes

– too far => low back scattered photons

– too close => low tags resolution - merging

Position of Object, SLR station and CCD telescopes – "Blind Angles"

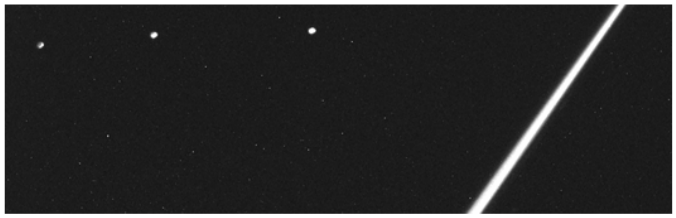

Martin Němec, FNSPE, CTU in Prague, nemecm1@troja.fjfi.cvut.cz

Simultaneous Optical and Laser Space Objects Tracking

Conclusion

Results

The high accuracy and density of laser ranging data **and / or** additional precise laser Time-tags in the CCD image, the atmospherically back scattered photons, can contribute to the high solution stability of computed orbits from data based on a single tracking location within a single pass.

These facts can result in increase the observation productivity and orbit computation stability in comparison to the techniques used recently.

Cooperative targets tracking has been tested by our group in a series of experiments involving combined optical and laser tracking of space cooperative objects at the Observatory of Graz, Austria, March 15-17, 2005 and in September 2006. The laser time-tagging method was also tested on following satellites with retroreflectors: **Champ** (~ 400 km), **ERS2** (~ 800km), **GPS-35** (~ 20ooo km).

Non-cooperative target tracking has been tested by B. Greene [1].

[1] B. Greene et. al., *Advanced Techniques at the EOS Space Research Centre*, 14th International Laser Ranging Workshop, San Fernando, Spain, June 7-11, 2004, published in Boletin ROA No. 4/2004, Real Instituto Observatorion de la Armada, en San Fernando, ISSN 1131-5040, 2004

Future

- Improvement of precision of the image processing methods (now under development)
- Method testing on non-cooperative objects
- Other image time-tagging methods development

Martin Němec, FNSPE, CTU in Prague, nemecm1@troja.fjfi.cvut.cz

SOFTWARE AND AUTOMATION SESSION SUMMARY

Chairs: Werner Gurtner and Jan McGarry

Automation continues to increase throughout the ILRS Network as can be seen in the presentations by Pearson on Mt Stromlo, Pierron on FTLRS, and Xin on TROS. Automation calls for more and more complicated software. Matt Pearson showed that software of the future needs to be modular, loosely coupled, flexible and reusable.

Automation improvements occur in both the hardware and software. Hardware enhancements were presented by Degnan on the SLR2000 beam expander, Wang on new control systems for San Juan, and the use of FPGAs in SLR systems digital design at Beijing by Li and at TROS by Xin.

Chris Moore demonstrated in his presentation that an automated system can perform as well as a manually operated system by giving statistics for Mt Stromlo when it was fully automated and when it was manually controlled.

Werner Gurtner showed that other work can share the telescope system in an automated way with SLR at no performance loss, given the right software to control the system.

New tools and formats are helping SLR stations in their transition to new technologies and in capturing these changes as they happen. This was seen in the presentations by Salminsh on web applications for engineering, and on the Consolidated Prediction and Consolidated Data Formats by Ricklefs.

The presentation by Heiner and Schreiber showed how to improve automated real-time signal processing by reprocessing (looking behind and projecting ahead) which can provide a 10–40% improvement over normal histogram analysis.

Progress in automation, reliability, performance and maintainability continues to be made at stations across the ILRS. Each group has their own approach to improvements. Sharing of these different technical approaches is the most important part of the Workshops.

A Comparison of Performance Statistics for Manual and Automated Operations at Mt Stromlo

C.J. Moore[1]

1. EOS Space Systems Pty. Limited, 111 Canberra Ave., Griffith, A.C.T. Australia.

Contact: cmoore@eos-aus.com

Abstract

The new Mt Stromlo SLR Station was rebuilt in the 12 months following the destruction of the original station by the January 2003 bushfires, and was reopened in April 2004. It became fully operational in December 2004 and since then the station has been operated manually pending completion of the development of a more advanced infra-structure that will support automated operations.

The original station had conducted automated operations for over three years before the bushfires and the performance measures that were in place during this period have continued to be collected for recent operations. This provides a unique opportunity to compare the productivity performance between automated and manual operations undertaken at the same site and with the same management team.

Provided that periods of abnormal events are taken into account, net productivity from these two modes of operation are quite comparable with differences less than about 5% over periods of many months. The fact that automated operations persist for longer periods and in conditions that discourage manual operation appear to compensate for the efficiencies that human interaction can provide.

Introduction

The original Mount Stromlo SLR Station (7849, STRL) was commissioned in Oct 1998, and subsequently performed automated operations from late 1999 until being totally destroyed in the January 2003 Canberra bushfires. A more complete description of the operation of this station has been given by Luck, Moore and Greene (2000). During this period, operations included the automated download of predictions, tracking of satellite and calibration targets, data processing and upload of published data. Automated operations allowed the station to continue operations, collecting and publishing SLR data, while it was unmanned. In fact, such operations were effectively unmanned for 80% of the time.

Productivity metrics were captured for this whole period. As described in Luck et al, these metrics were used for establishing performance criteria required under the contract between EOS and AUSLIG (subsequently incorporated into Geoscience Australia). Processing of productivity data and generation of reports was only partially automated, with a significant component requiring routine, but brief human inspection and assessment of the system and environment.

Subsequent to the 2003 bushfires, the remains of the old station were removed and the new Mount Stromlo SLR Station (7825, STL3) was constructed on the same site. All systems were functional by the official opening in April 2004, less than 14 months later. After undergoing stringent testing of all of the new sub-systems, including a new software system and completing formal acceptance testing, the new station commenced full operations in December 2004. Given the rapid redevelopment of the station, the system (in 2005-2006) was not capable of automation hence the station has been operated manually in a more traditional manner using operators rostered to

cover day and night, seven days a week. The new station was only unmanned when lack of targets or poor weather precluded productive tracking. It should be noted however, that contractual requirements (as well as good practice) required continuing capture of productivity metrics and generation of performance reports. The definition and processing of these data had not changed between the automated and manual operations.

The availability of reasonable long time series in these two data sets, has therefore allowed the relative performance between automated and manual SLR operations to be assessed. It should be remembered that the two stations were both designed by EOS and operated by EOS staff and hence have much in common. It was considered that the physical and technical differences between the two stations did not influence productivity levels to such an extent as data quality and other factors.

Metrics

The metrics used in this assessment include the following;

1. The number of all ILRS satellite passes with a maximum elevation above the 20 degree site horizon.
2. The number of all possible passes – i.e. the number of passes that are trackable, accounting for poor weather, low elevation passes and pass overlaps or priority.
3. The number of attempted passes – i.e. the number of possible passes for which the SLR station fired the laser in an attempt to track the satellite.
4. The number of passes that were successfully tracked – i.e. at least one normal point was generated.

The following figure shows the time series of these metrics for the two periods.

Figure 1: Productivity Metrics

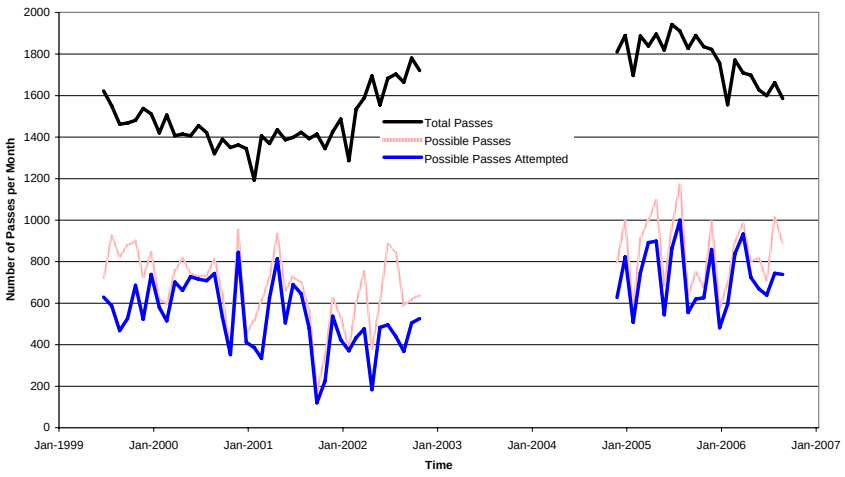

Results

Potential Productivity

Figure 2 provides the number of passes successfully tracked normalized by the number of possible passes. This ratio provides a measure of the system's potential productivity. If the ratio reached 100% then every pass that could realistically be tracked would be tracked. This figure shows that on average the potential productivity of the automated system reached 66% while than manned system was significantly more successful with an average potential productivity of 74%. Note that some exceptional points were excluded from the calculation. The points were associated

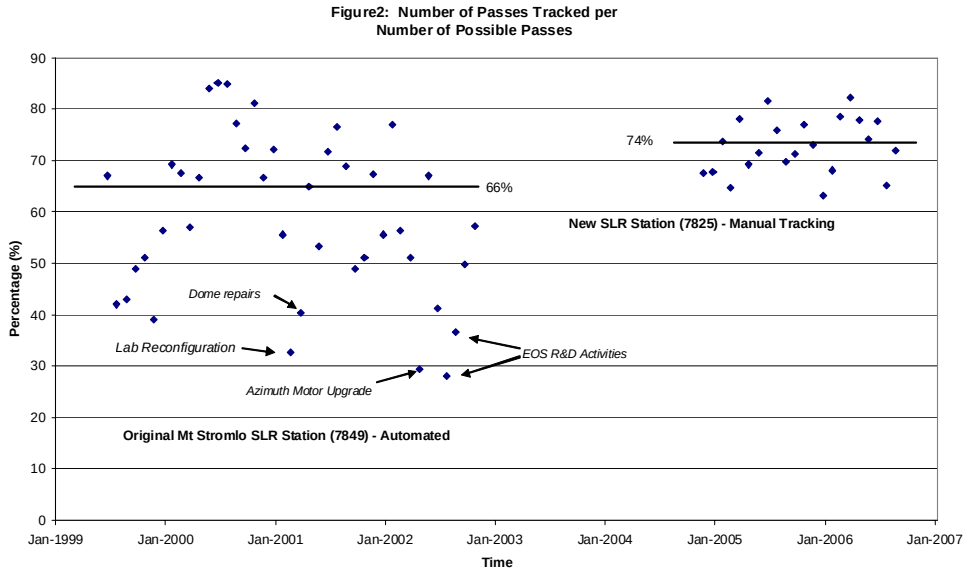

with station activities that significantly affected the ability of the station to perform normal operations. This result suggests that everything else being equal, a human operator should outperform a mechanical system, where for example a human can respond to unusual events such as system failures more quickly.

Tracking Capability

The next figure provides the number of passes successfully tracked normalized by the number of attempted passes. This ratio provides a measure of the system's capability for successfully tracking a target. If the ratio reached 100% then every pass tracked would result in generation of normal points. Figure 3 shows that on average the potential productivity of the automated system was 81% while the manned system was marginally more successful with an average of 87%. Note that a few exceptional points were again excluded from the calculation. For example, at one point the telescope enclosure was slipping due to a mechanical fault such that the system continued to attempt passes, but a misalignment of the telescope and dome meant that no returns were possible.

These results suggest that as long as a pass is attempted, the automated system has on average as nearly as good a chance in successfully acquiring the target as a human operator. Perhaps any skills that an operator may have in acquiring a target is balanced by the persistence of an automated system

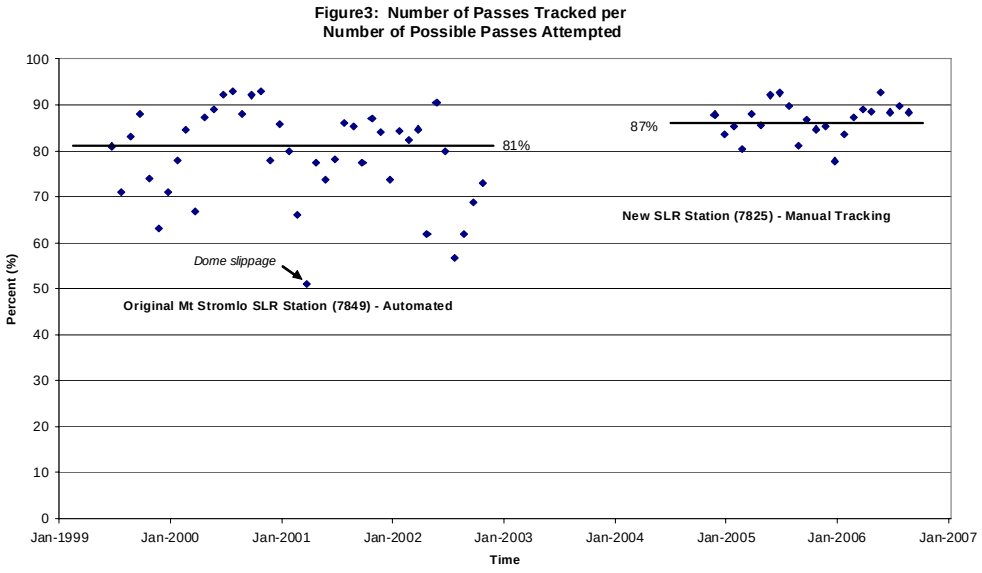

Actual productivity

The final figure provides the number of passes successfully tracked normalized by the total number of passes. This ratio provides a measure of the system's net or actual productivity, or passes tracked irrespective of conditions. In this case if the ratio reached 100% then every pass would have been tracked successfully. Figure 4 shows that on average the actual productivity of the automated system was 32% while that for the manned system was 35%, not a statistically significant difference. Note that some exceptional points were also excluded from the calculation as discussed earlier.

The major contributor to the absolute value of this ratio is of course the weather. It should be noted that during manual operations, the station was often unattended during overcast periods. In contrast, the automated system generally continued operations regardless of weather conditions. It is believed that this difference favoured the automated system, since there would have been opportunities to successful track during breaks in the sky cover or respond quickly to clearing conditions.

Conclusions

Availability of two years or more of productivity data from SLR tracking at one location, using similar techniques and equipment, and the same staff, has allowed an objective assessment of the performance from automation and manual operations.

The results indicate that there was overall very little difference in net productivity between the automated and manual operations. While human operators appear to have an advantage when on-site and undertaking tracking in clement weather, the automated system had an advantage in less ideal condition and could take opportunities that were lost to operators.

Figure 4: Number of Passes Tracked per Number of Total Passes

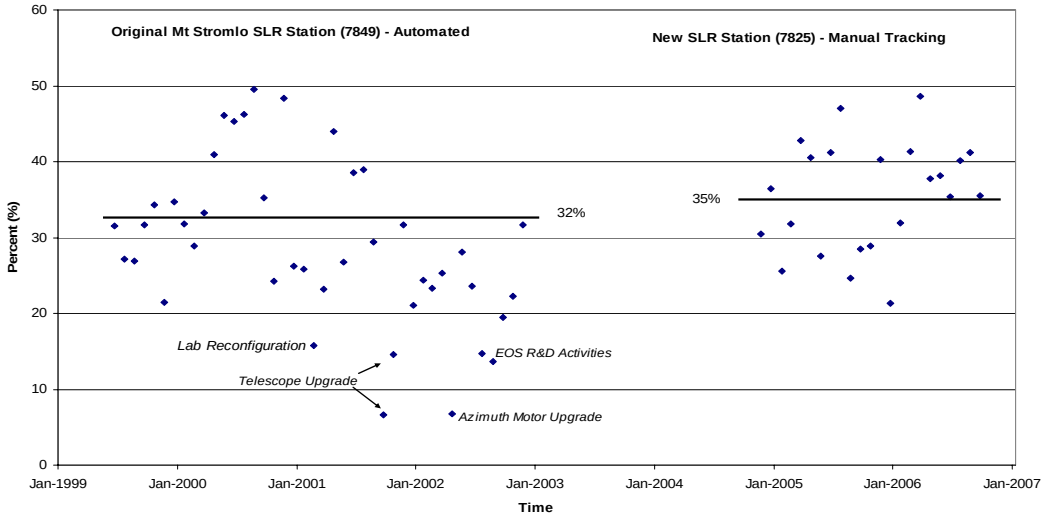

It is therefore clear that sophisticated automation systems can equal, if not better, manual operations. As far as the system at Mount Stromlo is concerned, it is felt that continuing improvements in the software and hardware systems will result in automated operations exceeding manual productivity figures.

References:

[1] Luck, J., C.J. Moore and B. Greene. Autonomous Laser Ranging Results from Mount Stromlo. Twelth International Workshop in Laser Ranging, 2000, Matera.

EOS Software Systems for Satellite Laser Ranging and General Astronomical Observatory Applications

M. Pearson[1]

1. EOS Space Systems Pty. Ltd.

Contact mpearson@eos-aus.com

Abstract

EOS has developed software systems over many years to support Satellite Laser Ranging (SLR) and the delivery of general astronomical observatories to its customers. These software systems are based upon a re-useable software architecture that simplifies systems development. The design objectives of this software architecture are discussed in the context of its evolution and current deployment at the Mt. Stromlo Satellite Laser Ranging facility, located in the Australian Capital Territory.

Introduction

This paper presents a brief overview of the software EOS has developed to support Satellite Laser Ranging at Mount Stromlo, software that has been designed to support not only SLR, but a wide range of astronomical applications.

This software, known as the 'Observatory Control System', supports EOS research and development programmes. It also supports the observatory requirements of several customers, being a flexible and scalable product, which lends itself to re-use across laser ranging and astronomical observatory applications.

Requirements

The basic requirements of the Observatory Control System are:

- it should drive equipment that might be expected at an observatory;
- it should provide some sort of abstraction – an 'Observatory' abstraction – that hides the complexity of the underlying equipment and presents it in terms that end-users and operators are likely to understand;
- it should provide facilities to automate day-to-day operations and routine observatory tasks.

Challenges

With these goals in mind, EOS has developed Observatory Control Systems over many years. But there was a problem; as the complexity of observatories grew, so did the complexity of the supporting software. This led to several challenges which are encountered in all types of software:

- it was becoming monolithic with fewer, larger, more-complex components;
- these components were highly-coupled, so changes to any part of the system could unexpectedly impact seemingly un-related parts;
- these systems were becoming inflexible and difficult to change in order to meet new requirements;
- different observatory solutions were becoming increasingly problem-specific and less re-usable; they were not amenable to solving new problems.

Solution

Under these pressures EOS engaged in a complete re-design of its software, culminating in what is now the 'Observatory Control System'.

The result is that the control system is inherently unaware of its problem domain. It is called an 'Observatory Control System' but it is in fact a generic control system. Its immediate application is to SLR and astronomy, but it could drive any automated industrial facility. It is domain independence that makes the control system highly extensible, flexible and most-importantly for EOS, re-useable.

Basic Architecture

At the highest level the Observatory Control System embodies the system concept:

'a collection of components which work together in order to solve a problem'.

These components include:

- various types of hardware and software;
- usually some sort of network;
- control system and observatory-level software.

The control system software provides facilities including:

- server frameworks;
- client frameworks;
- network interfaces.

The observatory-level software provides facilities including:

- servers;
- clients;
- automation functions.

Refer to Figure 1 for an illustration of these components.

Hardware & Software

Hardware and software include such items as: telescopes, enclosures, lasers, associated software and a variety of other equipment. A common problem with such equipment is that it is often heterogeneous, with different:

- platforms, eg. PC, Mac;
- operating systems, eg. Windows NT, XP, Linux;
- interfaces, eg. serial, CANopen, USB, Bluetooth;
- protocols, eg. sockets, CORBA, COM.

A fundamental feature of the Observatory Control System is that it makes this equipment look, feel and act in a consistent manner. This is achieved by hiding the equipment behind a universal software abstraction – what is called a Device.

Network

Devices are usually accessed through an adapter card and a driver library. But there is a limit to how many devices a given computer can support; at some point a single computer will run out of capacity, or a new device will require a different operating system or computer platform. So most observatories require many computers and the Observatory Control System is network-enabled.

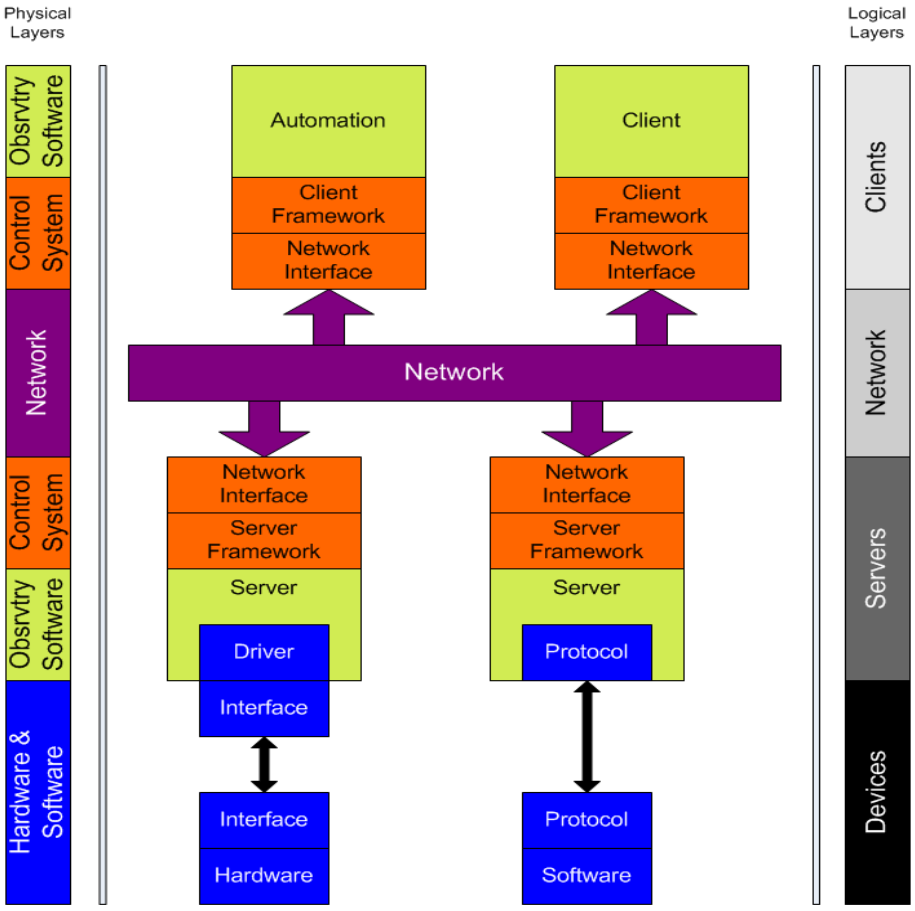

Figure 1. *Basic Software Architecture*

Control System

The Observatory Control System is a Client / Server software architecture. This is a network computing model based on the following concepts; that:

- clients connect to servers;
- clients issue commands to servers;
- servers respond to client commands.

Within the Observatory Control System, device server applications wrap devices and make them available over the network.

Client applications connect to these device servers over the network, or even over the Internet, and drive devices via commands to the relevant device server.

At the heart of the Observatory Control System are several software frameworks; these are code libraries which embody the most-re-useable, but complex and technical aspects of the control system.

These frameworks encourage re-use, and are used by EOS to extend its systems. These frameworks are also available to customers, who can extend their observatories over the longer term, independent of EOS.

Server Framework

Server applications, also known as device servers, are built using a *Server Framework*.

Servers directly manage observatory devices. A device server may manage one or many devices, depending on our requirements.

Servers may be active and/or passive; that is, they may manage devices autonomously and robotically, or in response to user commands.

Servers may participate in a hierarchy, where a parent server may depend on several child servers. Child servers provide services to their parent, which may perform some aggregate function; the parent may itself have a parent, to which it provides services, and so on.

This cooperative, 'building block' approach facilitates a separation of concerns; resulting in simple components from which complex systems can be built.

Client Framework

Client applications are built using a *Client Framework*.

Client applications are the focus of general observatory operators and users. This is where users interface with the observatory. So client applications will usually perform several functions:

- sending commands to / receiving replies from servers;
- displaying server state and responding to server state changes.

The display of server state is by a mechanism called Subscribe / Publish. The subscribing client asks for server state to be delivered at specified intervals, upon which the data is repeatedly published, arriving at the client without the need to keep asking. This asynchronous approach is much more efficient than simply polling for data. It should be noted that efficient network communications are important given the distributed, network-focused nature of the Observatory Control System.

Network Interfaces

In addition to the abstraction which hides the complexities of devices, the network provides its own abstractions – these hide the additional complexity of communicating with devices over the network. The result is that whatever the nature of a device or its location on the network, it can be accessed in a simple manner which is consistent for all devices.

All parts of the Observatory Control System employ the same, universal abstractions to facilitate end-to-end communication between client applications and the device servers which host the observatory devices.

Observatory Software

Observatory software includes client and server applications and automation applications that meet general observatory requirements and specific customer requirements. Domain and problem-specific control system functions are implemented at this level.

Like all parts of the Observatory Control System, this software is built upon a common set of software Frameworks.

It is at this level that the Observatory Control System can be customised, even by customers, with support from EOS if necessary.

Servers

Observatory-level servers will typically drive the hardware and software devices specific to any given observatory.

Clients

Client applications will provide an interface that hides the complexity of the underlying equipment, and present it in terms that end-users and operators are likely to understand.

Automation Functions

Observatory software provides system automation functions at many levels, including:

- device management – automatic management of device behaviour and state by device servers;
- scripted tasks – scripting of automation functions;
- task scheduling – scheduling of robotic tasks to be executed continuously, at scheduled intervals or in response to system events;
- closed loop control – automatic execution of system functions in response to changes in system state.

Case Study – Mount Stromlo

The Mount Stromlo facility contains two ranging systems, for satellite ranging and space debris ranging. These systems have common, but mostly different requirements, and have shared and dedicated components. But both systems were built sharing a single instance of the Observatory Control System.

This integration presented no significant problems or difficulties. Furthermore, no problems are foreseen concerning extensive capability upgrades over the next year. So the Observatory Control System provides technical certainty in terms of EOS' ability to extend and enhance its observatory systems.

Conclusion

The Observatory Control System supports EOS' demanding technical and business requirements. It has evolved over many years and continues to do so. The next evolution may well be a network of stations, where each station is a cooperating instance of the Observatory Control System. This will enable highly coordinated, world-wide observation and ranging programmes.

Currently EOS provides the Observatory Control System with its telescopes and enclosures. There is nothing inherently necessary about EOS' equipment, however; so long as basic requirements are met, the Observatory Control System can operate with any vendor's equipment. So in future EOS may offer the Observatory Control System as a stand-alone product, independent of its telescopes and enclosures.

Finally, the underlying control system is domain-independent. There are no astronomical or observatory-specific concepts embedded in the fundamental control system. So it is plausible that it could be used to drive a range of automated facilities.

Electro-Control System of San Juan SLR Station

Wang Peiyuan[1], Guo Tangyong[1], Li Xin[1], Han Yanben[2], Liu Weidong[2], Wang Tangqiang[3], Qu Feng[3], Tan Yechun[1], Zou Tong[1]

1. Institute of Seismology, China Earthquake Administration
2. National Astronomical Observatories, Chinese Academy of Sciences
3. Chinese Academy of Surveying and Mapping (CASM)
Contact: Yangroot@yahoo.com.cn

Abstract

A new SLR station has been set up in San Juan, Argentina this year, and works well now. Since Feb. 5th, 2006 to the 4th quarter, 2006, a total of 5861 pass (include 1134 Lageos pass) was obtained[1]. Some parts of this station, including servo system, control system, control software, and some observations will be described in this paper.

Telescope Servo System

San Juan SLR station's telescope is a bi-close-loop control system, i.e. position loop and velocity loop. Angle inductosyn and tacho-generator are used for the feedback sensors. When SLR system is tracking, the DAC input is tuned by PC software to drive telescope according to the ephemeris and the telescope position. Then the PID arithmetic theory is used to figure out the PWM voltage, consulting the telescope and theoretical velocity, to drive telescope's moment motor. So using this bi-close-loop control system, the SLR system's tracking can be improved.

The mount is driven by special motion drive IC: LMD18200. Its operating voltage can be up to 55V, and operating current can be up to 3A continuous output.

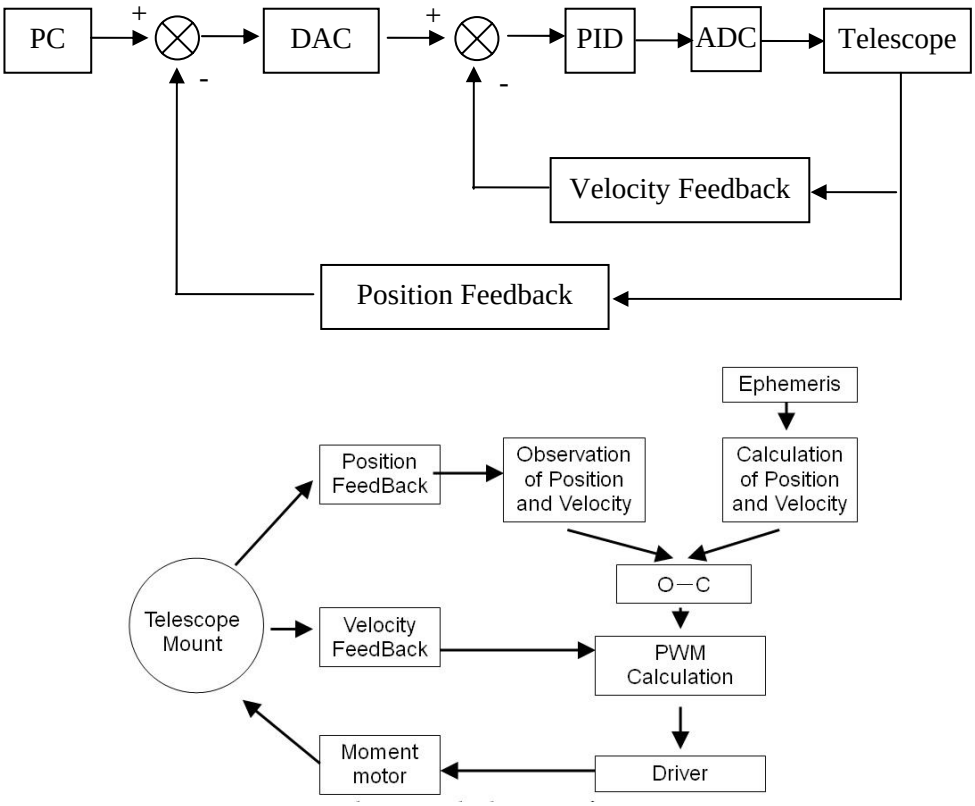

Figure 1: *the principle diagram of servo system*

Control Software

A general computer is needed to run the control software, and Figure 2 is the first picture of San Juan's tracking Lageos. Most control functions are included, such as satellite prediction, data pre-treatment, telescope servo, laser firing, range gate tuning, target measurement, data acquisition, etc.

Figure 2 is the first pass of Lageos in San Juan SLR station on Feb.5th, 2006. In this pass, 1514 samples were achieved between two green lines. The duration is about 15 minutes, and the deviation is very small (white dots).

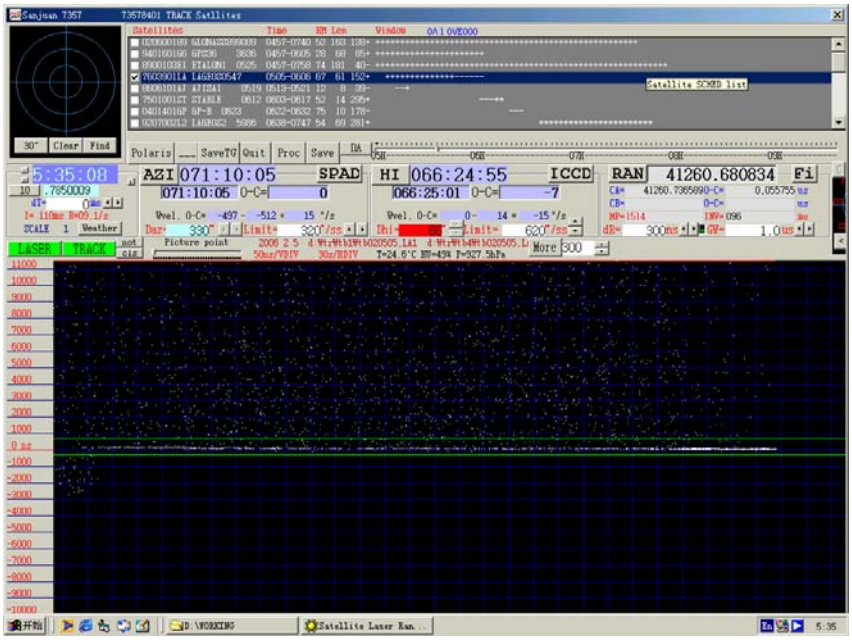

Figure 2: *Interface of control software and the first Lageos pass*

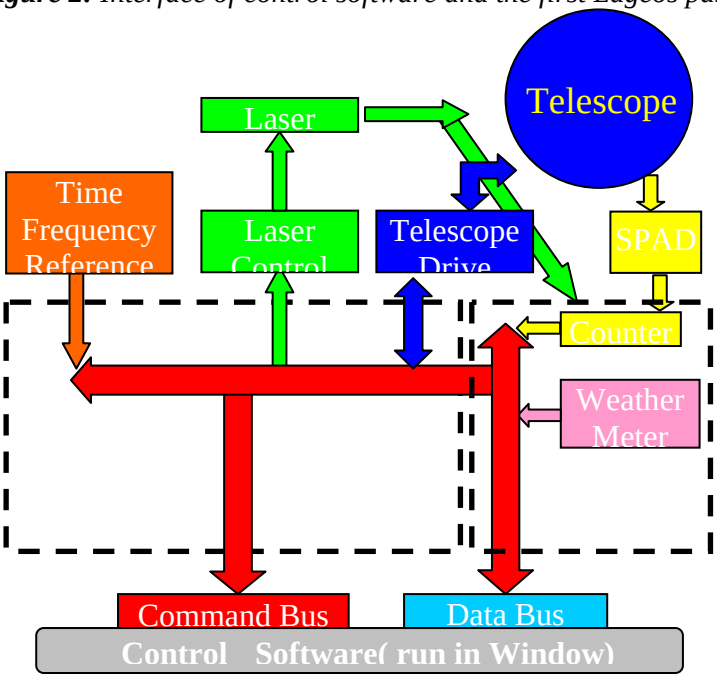

Figure 3: *The diagram of control system*

Results

The South America is lack of SLR station. The running of productive San Juan station will improve performance of the ILRS network.

Site Information		Data Volume									Data Quality		
Column 1	2	3	4	5	6	7	8	9	10	11	12	13	14
Location	Station Number	LEO pass Tot	LAGEOS pass Tot	High pass Tot	Total passes	LEO NP Total	LAGEOS NP Total	High NP Total	Total NP	Minutes of Data	Cal. RMS	Star RMS	LAG RMS
Baseline		1000	400	100	1500								
San_Juan	7406	3846	1134	881	5861	52713	13619	4180	70512	32323	6.5	10.4	12.1

Table 1: *San Juan performance report card[1]*

Reference

[1] SLR Global Performance Report Card July 1, 2005 through June 30, 2006.

[2] Wang Tangqiang, Current Status Of San Juan SLR Station In Argentina, 14th ILRS Workshop Proceedings.

[3] Guo Tangyong, The Performance and Observation of Mobile System TROS-I In China, 14th ILRS Workshop Proceedings.

Integrated Upgrades of Control System for TROS

Li Xin, Guo Tangyong, Zou Tong, Wang Peiyuan, Tan Yechun,
Xia Jiening, Zhou Yunyao, Du Ruilin

1. Institute of Seismology, China Earthquake Administration.

Contact: lxcomcn@yahoo.com.cn /Fax: +86-27-87863471

Abstract

The mobile SLR system TROS has operated for several years. Operations are routine, but the system is not without problems. To solve these problems, we are planning an upgrade to some of the TROS subsystems. These upgrades will enhance the signal return rate, improve the tracking precision and system reliability, provide convenient operational conditions for mobile observation, and relieve the labor intensive nature of the operations and maintenance.

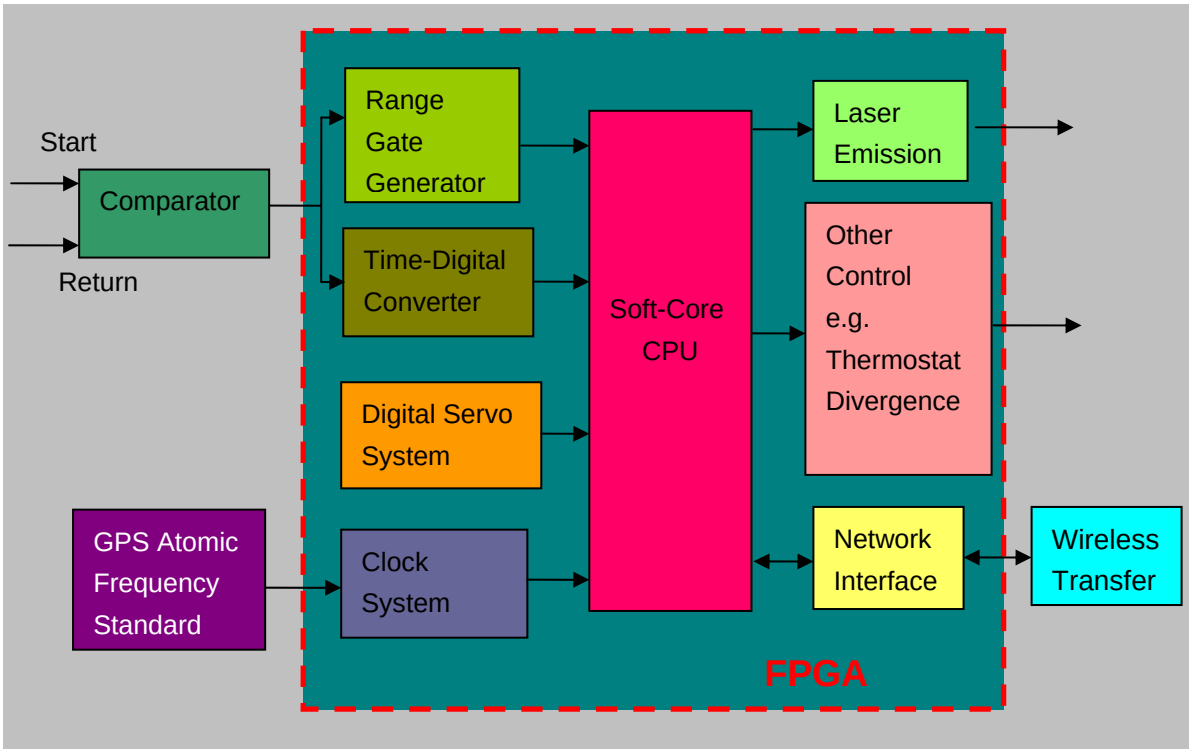

Figure 1. *The principle diagram of the control part*

The new version of TROS will possess the following properties:

1. The electronic components will be integrated into one subsystem, including event counter, GPS locked clock, range gate generator, servo system, and software. This will enhance system reliability.The principle diagram of this part is shown in Figure 1.

2. The control system will provide control for KHz ranging.This will help in target acquisition and tracking and enhance the normal point ranging precision.
3. The integrated event counter will use the time to digital converter to measure the interval in the FPGA.
4. The new electronics will generate the signal of angular position and speed by a photoelectric position encoder for implementing a full digital servo system. This will enhance tracking precision.
5. Operators will be able to run the software to control the system by web browser over wireless link.

CCD and SLR Dual-Use of the Zimmerwald Tracking System

W. Gurtner, M. Ploner

1. Astronomical Institute, University of Bern.

Contact: gurtner@aiub.unibe.ch

Abstract

The Zimmerwald Laser and Astrometric Telescope (ZIMLAT) has been designed for both satellite laser ranging and optical tracking with CCD cameras, the latter mainly for orbit determination of space debris by means of astrometric positions. The paper describes the main characteristics of the control programs, both for CCD and SLR and their interaction during interleaved operation and it summarizes some experiences after several years of dual-use.

Introduction

The Zimmerwald observatory celebrated its 50 years anniversary in 2006. Its original purpose was an astronomical observatory for the University of Bern, Switzerland, mainly designed for sky surveillance (search for supernovae, minor planets and comets). However, it developed more and more into an observatory for space geodesy, starting with optical (photographic) tracking of satellites in the sixties, laser tracking since 1976, permanent GPS (and later GLONASS) tracking since 1991 and finally optical tracking again, mainly of space debris, using CCD cameras and digital image processing. In 1997 we replaced the former SLR tracking system (50 cm telescope, Nd:YAG laser) with a new 1-meter telescope and a two-wavelength Ti:Sapphire laser (846 nm and 423 nm wavelengths). The new ZIMLAT telescope has been designed for dual use, i.e. it serves as transmitting/receiving telescope for satellite laser ranging as well as a telescope for astrometric observations of space objects, mainly space debris.

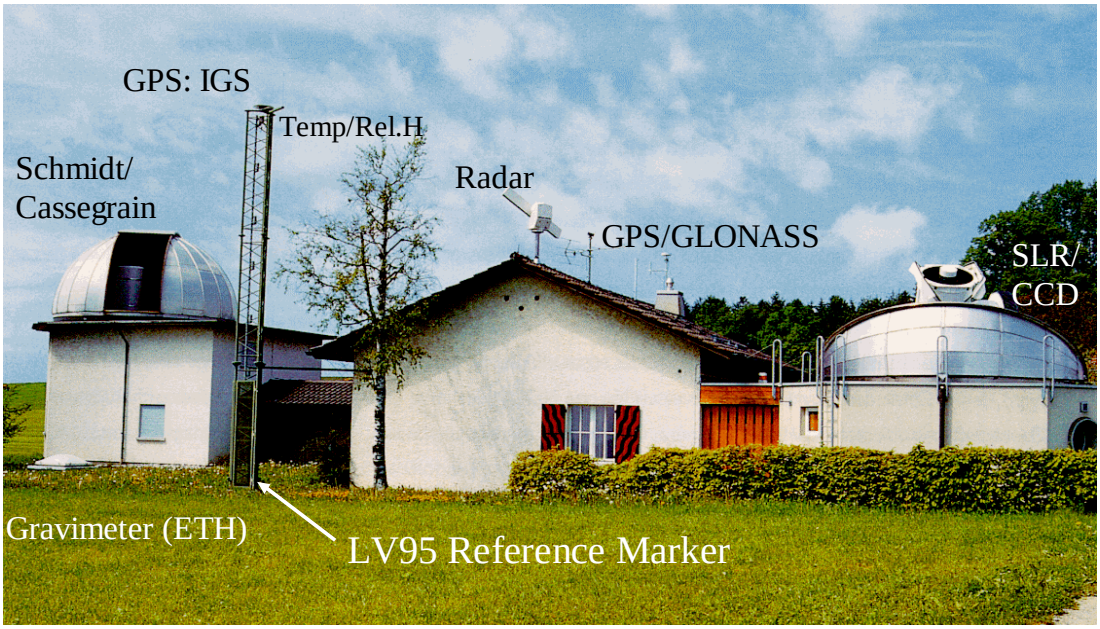

Figure 1: *The Zimmerwald Observatory*

The Zimmerwald Laser and Astrometric Telescope ZIMLAT

The main characteristics of the telescope are as follows:

The diameter of the main mirror is one meter. The telescope is of the Ritchey-Chretien type with main mirror, secondary mirror and a flat 45-degree tertiary mirror reflecting the image sideways into the elevation axis.

A vertical platform on one side of the telescope serves as mounting surface for four optical tables, with reduction optics, filter wheels and CCD cameras (Figure 2). The platform can be rotated around its horizontal axis (independent from the motion of the tube around the elevation axis) to derotate the image on the camera according to various strategies. The camera to be used for observation can be selected by means of a rotating mirror (with four distinct positions) in the center of the platform.

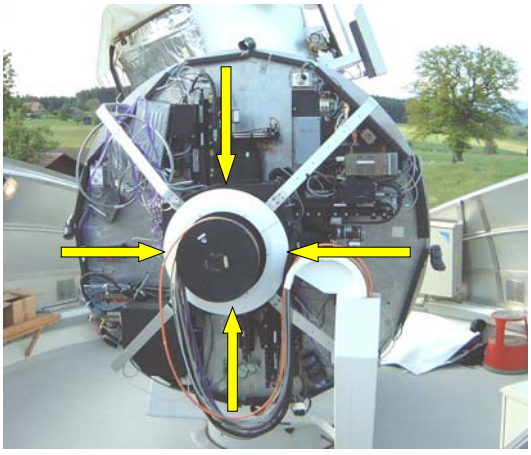

Figure 2: *Instrument platform*

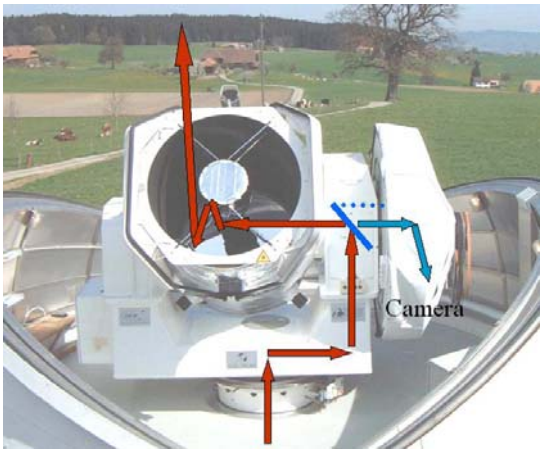

Figure 3: *ZIMLAT telescope*

For Satellite Laser Ranging the laser beam is guided, slightly off-axis, through the Coudé path to the telescope (Figure 3). Its diameter of 1 cm at the exit of the transmit table is increased to 15 cm by the telescope optics. The receiving beam fills the full aperture of the telescope as well as the Coudé path back to the receiving table.

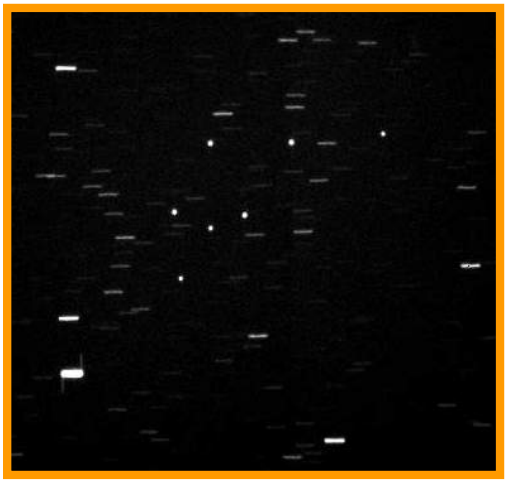

Figure 4: *7 Geostationary Astra satellites (field of view 12x12‘)*

Figure 4 shows a sample image of one of the CCD cameras with 7 geostationary satellites within a field of view of about 12 arc minutes squared. The telescope was

kept fixed during the exposure time, showing the daily rotation of the Earth as short traces of the background stars.

The separation between the CCD and SLR observation modes is done by a fairly large dichroic 45-degree beam splitter mirror in the elevation axis of the telescope. It can be pneumatically removed (tilted) for high-precision CCD imaging. During night-time SLR tracking a video camera on one of the four camera ports can be used for visual verification of the tracking with the dichroic beam splitter inserted.

The Control Systems

The Satellite Laser Ranging part is controlled by the program *ZIMLAS* running on an Alpha workstation (operating system: VMS). It communicates with two specialized PCs for data collection and control of various electronic components and for the control of the telescope. The workstation handles the satellite predictions, generates the observation schedule (example in Figure 6), stores and post-processes the range observations, interacts with the operator in manual mode or controls the whole system in fully automated mode (see also Gurtner et al, 2002).

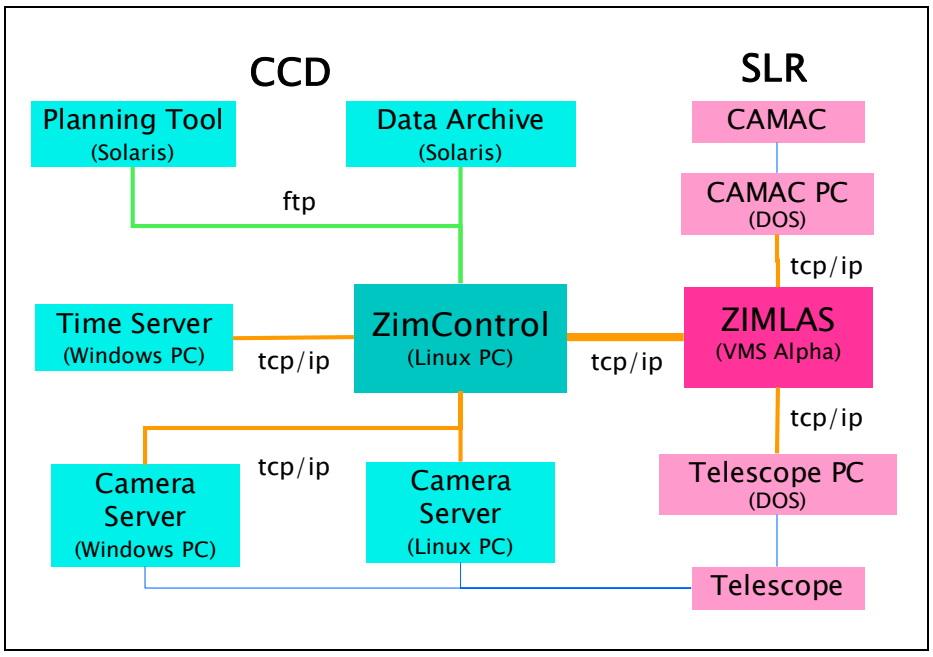

Figure 5: *Control Systems*

The control system for CCD observations (program *ZimControl*) is hosted by a Linux PC. It handles the observation schedule for CCD observations, interacts with the CCD cameras through specialized camera servers, and stores and pre-processes the digital images.

CCD Targets and Observation Plan

The following targets and objects are routinely tracked

- GEO (geostationary objects)
  - Active satellites
  - Space debris
- GTO (geostationary transfer orbit): Upper stages, debris
- Minor planets: Confirmation exposures for Near-Earth Objects

- GPS satellites to check system status (e.g., timing system)
- Photometry: Change of visual magnitude of objects due to their rotation
- Bias and dark current exposures (camera properties)
- Projection parameters, image distortions (telescope and camera properties)
- Focussing exposures (temperature- and elevation-dependent)

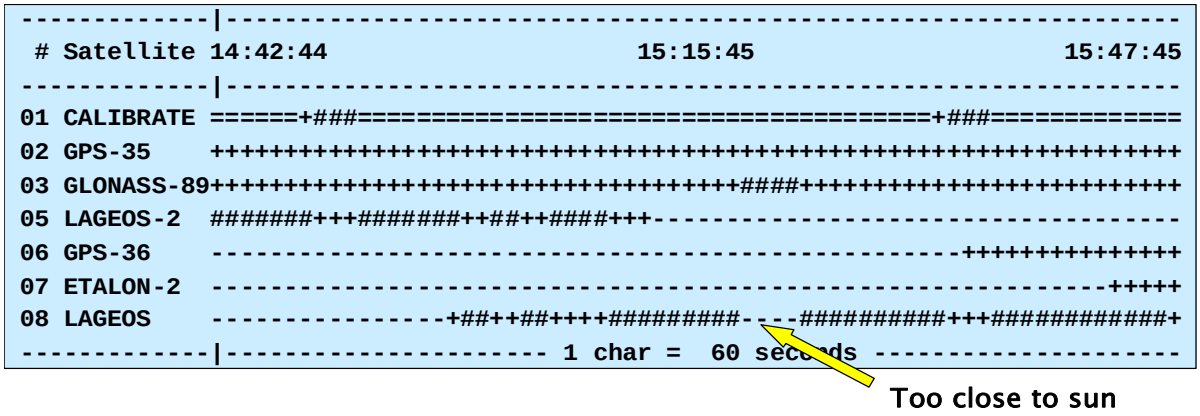

Figure 6: *Automatically generated observation schedule (SLR)*

Figure 7 shows an observation plan with targets and their possible observations periods during one night.

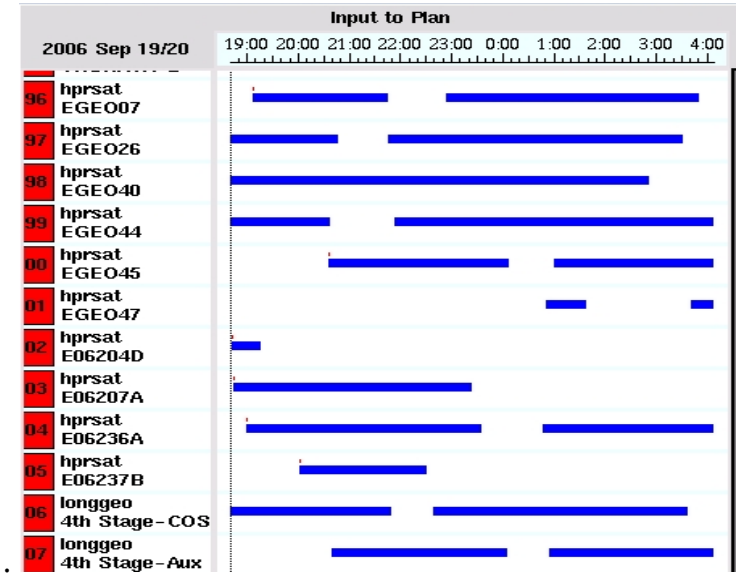

Figure 7: *CCD observation plan*

Insertion of CCD observations into SLR operations

Whenever the sun is more than 9 degrees below the horizon the CCD control system automatically checks if the SLR tracking system is currently operating.

If it is and if there are suitable objects in the observation plan the CCD system starts requesting observation time from the SLR system, starting with a time slot of 10 minutes, gradually reducing its length down to a minimum of 3 minutes if the request is not granted. This process is repeated over and over until a request is granted.

On the other side the SLR system checks each request, compares the requested duration with the current SLR tracking scheme and grants or rejects the request

according to the following conditions:

- Time since last CCD observation “large enough”
- Remaining pass segment of current SLR target “large enough”
- Already a minimum number of successful SLR observations collected
- Currently not in calibration mode
- CCD mode not blocked by operator

“Large enough” depends on the priority of the current SLR target and on the priority assigned to CCD operations.

If the request is granted the SLR system interrupts the current SLR tracking, puts the telescope into CCD mode (removal of the dichroic beam splitter from the elevation axis, pointing of the selection mirror on the platform to the requested CCD camera) and sends the requested object position or trajectory to the telescope control PC for tracking.

The CCD control system commands the camera to take an exposure and stores the digital image for further processing. Depending on the length of the granted observation interval several images of the same object or of different objects may be collected.

At the end of the current CCD observation interval the SLR system puts the telescope back into SLR mode and continues to range to the SLR targets according to the automatically updated tracking scenario.

The CCD control system then starts all over again with new requests for CCD tracking as long as the SLR system is in operation and until dawn.

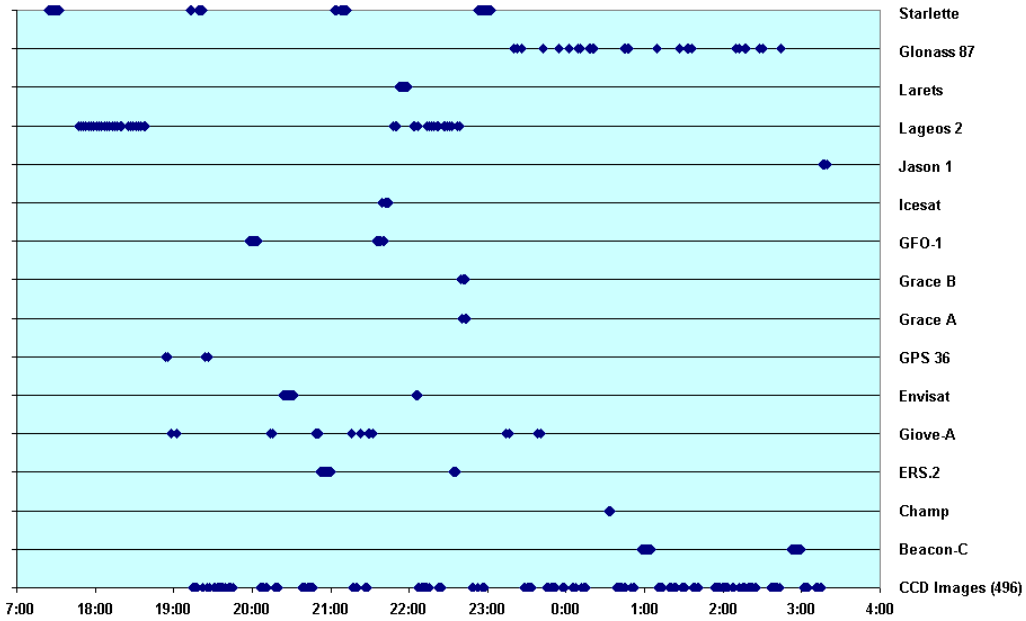

***Figure 8**: SLR/CCD interleaving*

Switching between the two modes SLR and CCD needs all in all less than 30 seconds, repositioning of the telescope included. Figure 8 shows the actual tracking scenario (SLR satellites, CCD observations on the bottom line) of the night of September 1st, 2006. Thanks to the rapid interleaving of CCD into SLR, especially into the long passes of medium-high (Lageos 1,2) and high satellites (navigation satellites and Etalon 1,2) no substantial reduction of the SLR data output could be observed.

Figure 9 shows the monthly number of images collected during the last one and a half years.

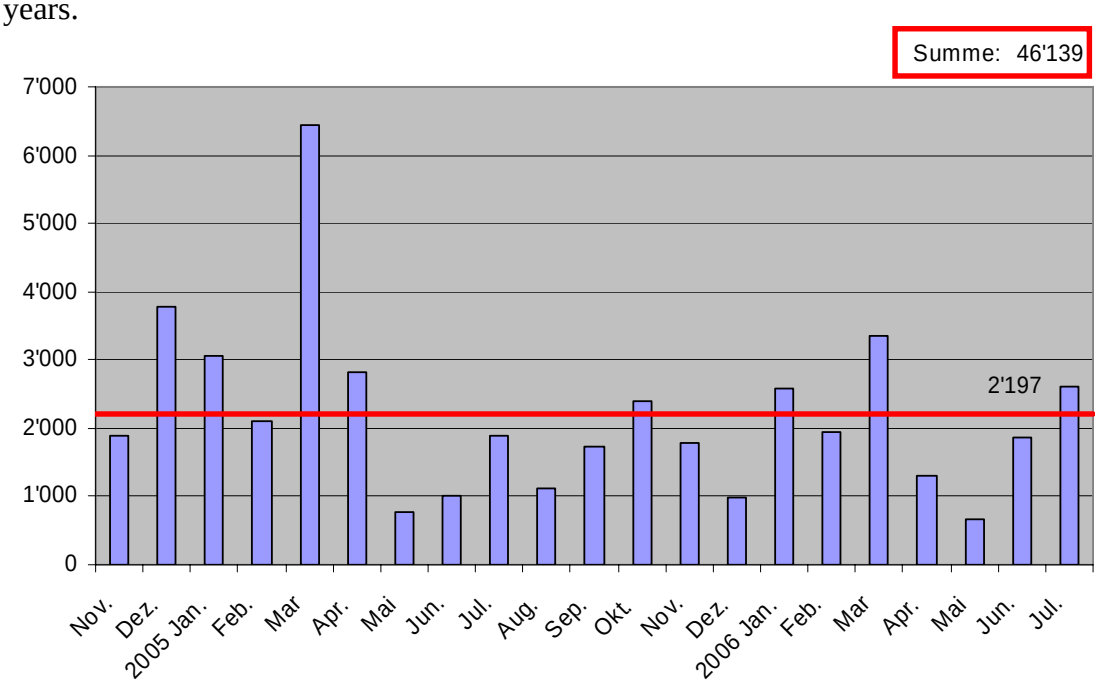

Figure 9: *Monthly number of CCD images Nov 2004 - Jul 2006*

Automation

The two control programs SLR and CCD are independent programs (running on two different computer systems). Either one or both can run completely automatically and unattended or under operator control.

In the extreme case (good and predictable weather conditions provided) several observation sessions of a few hours length each can be set up and submitted in advance by simple commands like

```
AUTO_SLR 20:00 22:00 WG MEDIUM
```

defining start and end time of the session, responsible observer's initials, and the priority assigned to CCD observations. All the rest is taken care of by the two control systems.

Post-processing

SLR data post-processing, i.e.,

- computation and application of an average calibration constant
- data screening
- normal point generation
- exchange format generation and submission of the data to the ILRS data center

can either be done interactively (daylight: mandatory) or fully automatically.

Image processing is automated and runs in the background on a Linux system at the university (the image files are automatically transferred to the university right after acquisition):

- Object recognition
- Reference star selection
- Determine image positions of stars and objects

- Astrometric position of objects
- Image archiving

The automatic processing of the previous night is checked interactively and problematic cases are reprocessed manually.

Conclusions

The dual use of the Zimmerwald Laser and Astrometric Telescope ZIMLAT has proven to be very cost-efficient. Although the telescope's design and operation is more complicated than the one of a single-mode instrument it provides us two different observation techniques for little more than the costs of a simple telescope. Thanks to the high degree of automation the two modes can be used nearly simultaneously without significant reduction of the SLR data output.

References

[1] Gurtner W., E. Pop, J. Utzinger (2002), *Improvements in the Automation of the Zimmerwald SLR Station*, 13th International Workshop on Laser Ranging, October 7-11, 2002, Washington, D.C.

Automated Transmitter Beam Size and Divergence Control in the SLR2000 System

J. Degnan, G. Jodor, and H. Bourges

1. Sigma Space Corporation, 4801 Forbes Blvd., Lanham, MD 20706 USA.

Contact: John.Degnan@sigmaspace.com /Fax: +01-301-577-9466

Abstract

Signal count rates and orbital time bias estimates vary widely over the range of satellite altitudes. In order to obtain an acceptable photon count rate for the higher satellites (e.g. LAGEOS, ETALON, GPS) while still meeting eye safety requirements at the telescope exit aperture, we must tightly control both the SLR2000 transmit beam diameter at the exit aperture and the final beam divergence half angle. For lower satellites, the uncertainty in the satellite angular position and the signal count rates are both relatively high. Thus, the SLR2000 design targets a nominal range of beam divergence half angles between 4 arcsec (larger than the combined effects of mount pointing jitter and atmospherically induced spreading and beam wander) for high satellites and 13 arcsec (adequate to accommodate time bias uncertainties) for LEO satellites. A modified commercial beam expander in the transmitter is used to maintain a constant transmitter beam size at the telescope exit aperture for eye safety while simultaneously varying the beam divergence to accommodate the various satellite altitudes and angular uncertainties.

Introduction

SLR2000 adjusts transmitter beam divergence based on satellite altitude and orbital knowledge, i.e. narrower for high satellites (± 4 arcsec min) and wider for low satellites (± 13 arcsec max). For eye safety reasons, the divergence must be adjusted while keeping the beam diameter at the telescope exit aperture fixed. It has been shown [Klein and Degnan, 1972] that a ratio of telescope diameter to Gaussian beam diameter (between $1/e^2$ intensity points) equal to 1.12 maximizes the amount of energy on the satellite. Thus, for the 40 cm SLR2000 telescope, the optimum beam diameter is 35.7 cm, and final divergence is set by adjusting the phase front curvature of the transmit beam at the telescope exit window. The Special Optics Beam Expander (SOBE) for controlling spot size and divergence is located on the transceiver bench in the transmitter path. This paper outlines our technical approach and additional details can be found elsewhere [Degnan, 2005].

Paraxial ray matrix theory can be applied to Gaussian laser beams if the beam is represented by the complex parameter

$$\frac{1}{q(z)} = \frac{1}{R(z)} - j\frac{\lambda}{\pi\omega^2(z)} \qquad (1)$$

where λ = 532 nm is the laser wavelength in the propagation medium and R(z) and ω(z) are respectively the wavefront curvature and spot radius (measured from the beam center to the $1/e^2$ intensity point) of the Gaussian beam at the location z along the propagation axis. If $q(z_0)$ is the Gaussian beam parameter at the output of the SOBE, then the Gaussian beam parameter at the exit window of the telescope is given by the ABCD Law [Verdeyen, 1989]

$$\frac{1}{q(z)} = \frac{C + D\left(\frac{1}{q(z_0)}\right)}{A + B\left(\frac{1}{q(z_0)}\right)} \tag{2}$$

In (2), A, B, C, and D are the ray matrix coefficients which propagate the rays from the SOBE to the telescope exit aperture. Separating (2) into its real and imaginary parts yields the following expressions for the wavefront curvature and beam spot size at the telescope exit aperture, i.e.

$$R(z) = \frac{\left(A + \frac{B}{R(z_0)}\right)^2 + \left(\frac{B\lambda}{\pi\omega^2(z_0)}\right)^2}{\left(C + \frac{D}{R(z_0)}\right)\left(A + \frac{B}{R(z_0)}\right) + BD\left(\frac{\lambda}{\pi\omega^2(z_0)}\right)^2} \tag{3a}$$

and

$$\omega(z) = \omega(z_0)\sqrt{\left(A + \frac{B}{R(z_0)}\right)^2 + \left(\frac{B\lambda}{\pi\omega^2(z_0)}\right)^2} \tag{3b}$$

We can now compute the ABCD matrix for the transmitter at the satellite target by multiplying the system matrix by the propagation matrix and letting the target range, *r*, approach infinity, i.e.

$$FF = \lim_{r\to\infty}\begin{vmatrix} I & rI \\ 0 & I \end{vmatrix}\begin{vmatrix} A\Gamma' & B\Gamma' \\ C\Gamma' & D\Gamma' \end{vmatrix} = \lim_{r\to\infty}\begin{vmatrix} (A+rC)\Gamma' & (B+rD)\Gamma' \\ C\Gamma' & D\Gamma' \end{vmatrix} \cong \begin{vmatrix} rC\Gamma' & rD\Gamma' \\ C\Gamma' & D\Gamma' \end{vmatrix} \tag{4}$$

Substituting A = rC and B = rD into (3) yields the following expressions for the phase front curvature and spot size at the satellite

$$R(r) = r \tag{5a}$$

and

$$\omega(r) = r\omega(z_0)\sqrt{\left(C + \frac{D}{R(z_0)}\right)^2 + \left(\frac{D\lambda}{\pi\omega^2(z_0)}\right)^2} = r\frac{\omega(z_0)}{m_t}\sqrt{\frac{1}{R^2(z_0)} + \left(\frac{\lambda}{\pi\omega^2(z_0)}\right)^2} \tag{5b}$$

where, for SLR2000, C = 0 and D = $1/m_t$ = 0 where m_t = 30.48 is the total magnification in the transmit path [Degnan, 2005]. As expected, the wavefront curvature in the far field equals the distance from the telescope aperture and the spot size grows linearly with that distance. Equation (5b) can therefore be used to compute the beam divergence half angle (center to $1/e^2$ intensity point) of the transmitter in the far field, i. e.

$$\theta_t \equiv \frac{\omega(r)}{r} = \frac{\omega(z_0)}{m_t}\sqrt{\frac{1}{R^2(z_0)} + \left(\frac{\lambda}{\pi\omega^2(z_0)}\right)^2} = \frac{\lambda}{\pi m_t \omega(z_0)}\sqrt{1 + \left(\frac{\pi\omega^2(z_0)}{\lambda R(z_0)}\right)^2} \tag{6}$$

Note that the far field divergence depends on both the spot size, $\omega(z_0)$, and the phase front curvature, $R(z_0)$, at the output of the SOBE.

Technical Approach

The approach we followed for controlling SLR2000 beam size and divergence was as follows:

1. Measure transmitter gaussian beam radius (.969 mm) at entrance plane to beam expander, raw beam half divergence, and compute gaussian complex q-parameter for the input beam
2. Choose a COTS beam expander with an adequate exit aperture (>40cm/30.48 = 13.1 mm) and magnification range (~13.1 mm/ 2mm = 6.5) and at least two control elements for independently adjusting beam size and phasefront curvature at the output.
3. Develop dynamic ray model for unit including variable lens spacings.
4. Test dynamic ray model against sophisticated ray tracing program such as ZEMAX.
5. Calibrate beam expander servo controllers at various magnifications.
6. For each divergence value, use the gaussian beam propagation law to compute the complex q-parameter of the expander output beam and the lens spacings which produce that parameter.
7. Compute lookup table specific to laser transmitter

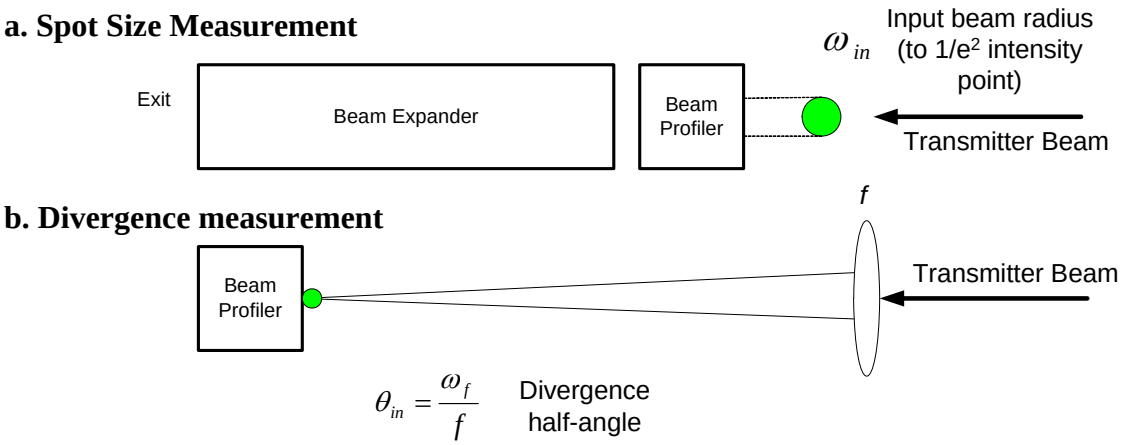

***Figure 1**: Measuring the Gaussian parameters of the raw transmit beam: (a) input radius; and (b) far field beam divergence.*

The beam radius and divergence of the transmitter beam at the input to the SOBE were measured using a standard beam profiler as in Figure 1. The complex Gaussian beam parameter was then computed from the formula

$$\frac{1}{q_{in}} \equiv \frac{1}{R_{in}} - j\frac{\lambda}{\pi\omega_{in}^2} = \frac{\lambda}{\pi\omega_{in}^2}\left(\sqrt{\left(\frac{\pi\omega_{in}\omega_f}{\lambda f}\right)^2 - 1} - j\right) \tag{7}$$

The commercial version of the Special Optics Beam Expander Model 56C-30-2-8X is normally operated under a Labview environment and is designed to provide a wide range of beam magnifications (2X to 8X) at the desired wavelength. Sigma has reconfigured the unit to operate with two National Aperture Motor Controllers under a more flexible software control. The optical unit consists of five lenses: a moving singlet at the input end, a moving doublet in the middle, and a larger aperture stationary doublet at the output end as in Figure 2. The moving singlet and doublet are

driven by two independent stepper motors. Their positions are determined by counting the number of steps from a home position as defined by two limit switches.

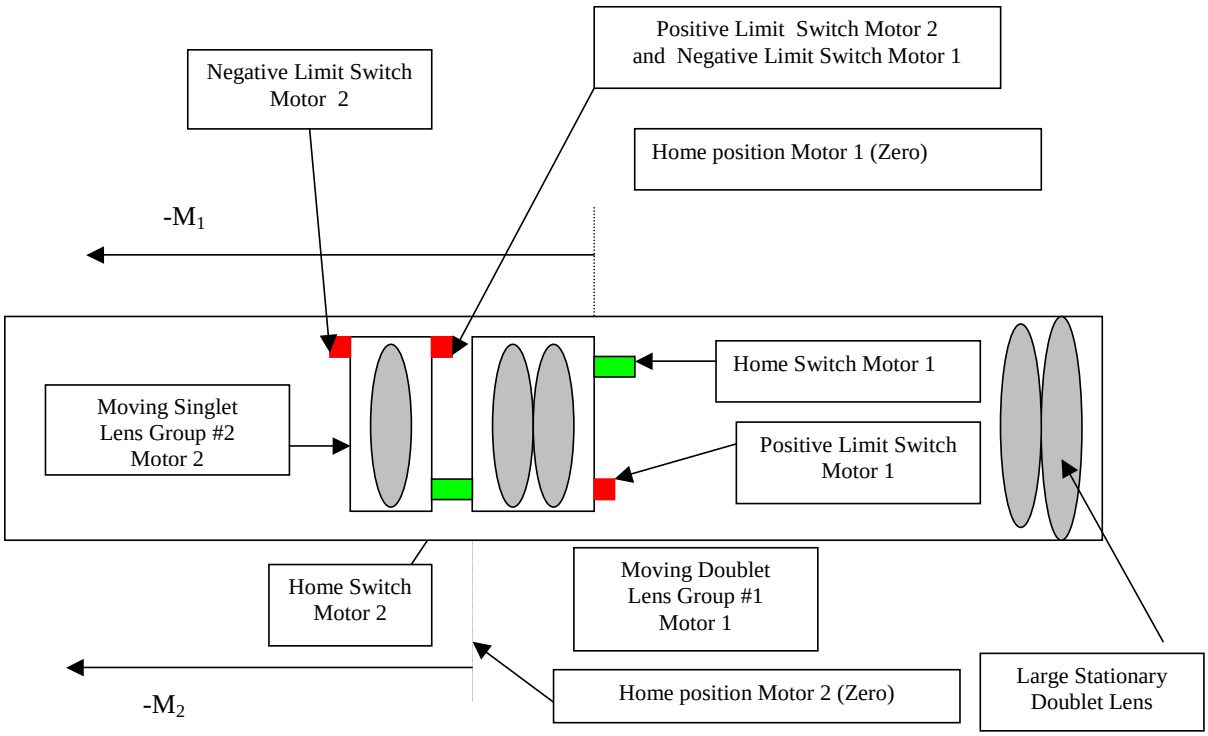

Figure 2: *Optomechanical configuration of Special Optics Beam Expander Model 56C-30-2-8X. The expander has entrance and exit apertures of 10 mm and 30 mm respectively.*

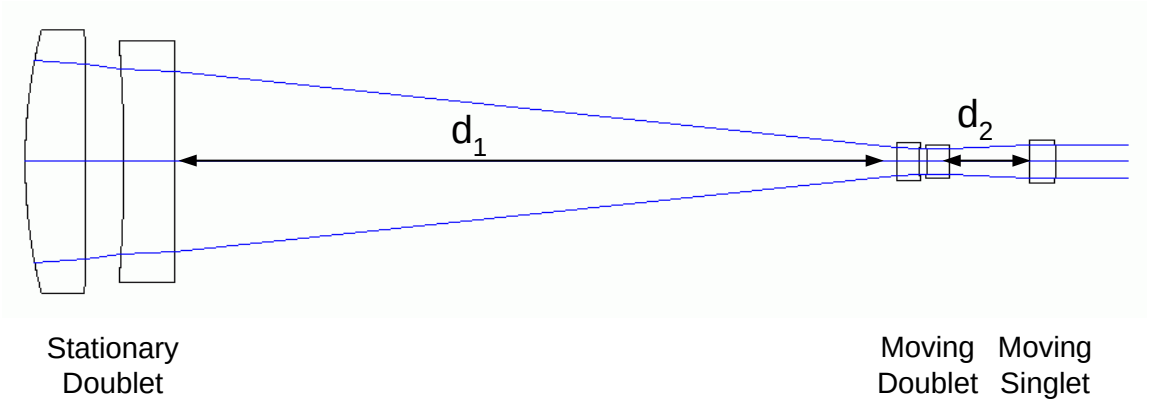

Figure 3: *Optical layout of Special Optics Model 56C-30-2-8X Beam Expander.*

Using an optical prescription provided by Special Optics, we computed a "dynamic ray matrix" for the SOBE depending on the variables d_1 and d_2 defined in Figure 3. The result was

$$M_{SO}(d_1,d_2)=\begin{vmatrix} A_{SO}(d_1,d_2) & B_{SO}(d_1,d_2) \\ C_{SO}(d_1,d_2) & D_{SO}(d_1,d_2) \end{vmatrix} \tag{8}$$

where

$$A_{SO}(d_1, d_2) = A_0 + A_1 d_1 + A_2 d_2 + A_{12} d_1 d_2 \quad (9a)$$

$$B_{SO}(d_1, d_2) = B_0 + B_1 d_1 + B_2 d_2 + B_{12} d_1 d_2 \quad (9b)$$

$$C_{SO}(d_1, d_2) = C_0 + C_1 d_1 + C_2 d_2 + C_{12} d_1 d_2 \quad (9c)$$

$$D_{SO}(d_1, d_2) = D_0 + D_1 d_1 + D_2 d_2 + D_{12} d_1 d_2 \quad (9d)$$

and the computed coefficients appearing in (9) are summarized in Table 1.

Table 1: *Summary of coefficients appearing in the SOBE ray matrix*

Suffix	A	B	C	D
0	1.995665379968	0.028752151456	46.402866180544	1.170293617808
1	63.683551232	1.442710470656	-460.710690944	-10.437108561152
2	-45.765735168	2.505955512	-1230.503704704	67.377646836
12	-1634.569158656	89.502715904	11825.086257152	-647.496210368

Setting C_{SO} =0 and A_{SO} equal to integer magnifications between 2 and 8, the ray matrix predictions of the interlens spacings, d_1 and d_2, computed from (9a) and (9c) were then compared to those of a popular ray tracing program, ZEMAX, and the predictions were found to agree within a few tens of microns for all magnifications. The two motor positions, relative to their respective home limit switches, are related to the interlens spacings via the equations

$$M_1 = a - d_1 \quad \text{and} \quad M_2 = b - d_1 - d_2 \quad (10)$$

Following our inhouse calibration procedure, the constants a = 88.7412 mm and b = 92.9858 mm in (10) were found to differ from the values (a = 88 mm and b = 90 mm) provided by the manufacturer. The next step in the process is to tabulate the values of d_1 and d_2 that produce the desired spot size and divergence at the exit aperture of the telescope. This is accomplished by using the Gaussian propagation law (2) to generate the following approximate expressions for the beam radius and phasefront curvature at the exit aperture of the SOBE

$$\omega_0(\theta_t) \cong \frac{\omega}{m_t} - d_t\theta_t = 0.00585 - 30.84\theta_t(rad)$$

$$\frac{1}{R_0(\theta_t)} \cong \frac{m_t^2\theta_t}{\omega - m_t d_t \theta_t} = \frac{929.0\theta_t\,(rad)}{0.1785 - 940.0\theta_t(rad)} m^{-1}$$

where ω = 0.179 m and θ_t, are the desired beam radius and beam divergence at the telescope exit aperture. For each divergence, we then use the beam expander ray matrix (8) to compute the expander lens positions, $d1$ and $d2$, which yield the above values of ω_0 and R_0. The final step is to compute the corresponding motor positions via (10), convert the latter into encoder counts using a scale factor of 0.304 microns per step, and generate a table lookup of beam divergence versus encoder counts for each motor. Figure 4 gives a graphical representation of the interlens separations in the lookup table as a function of final transmitter beam divergence for SLR2000.

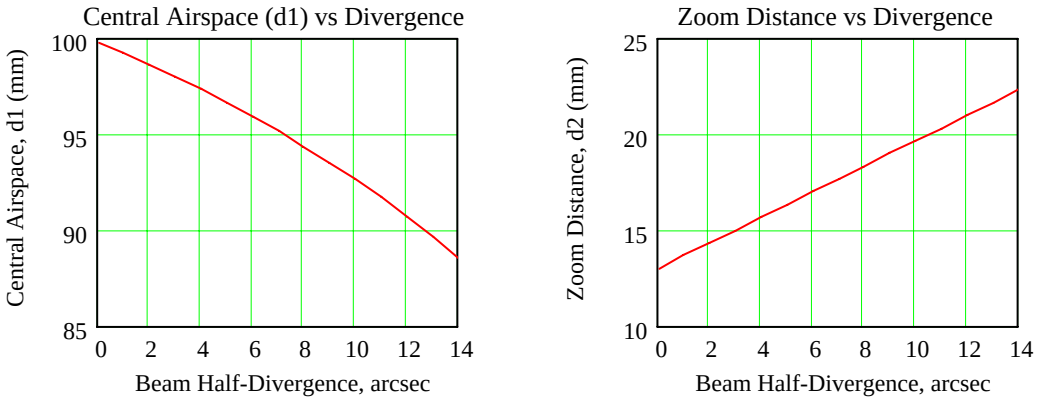

Figure 4: *The computed interlens distances, d_1 and d_2, in the SOBE which produce a given divergence half-angle in the far field while maintaining a constant spot radius of 17.9 cm at the exit aperture of the telescope. A circularized Phase II laser with a mean Gaussian radius of 0.969 mm and a raw half-divergence of 1.265 mrad is assumed as input to the SOBE.*

Summary

Using a computer lookup table, the SLR2000 computer can set two lens spacings in the 5-element transmit beam expander to provide a fixed beam diameter (35.8 cm) at the telescope exit aperture for eye safety while adjusting the phasefront curvature to give the desired final divergence. The lookup table must be updated whenever the transmitter is changed but it is an automated process. The optical half-divergence range of the final SLR2000 transmit beam is theoretically 0.25 arcseconds to 13 arcseconds (1.3 to 65 microradians) but atmospheric turbulence will define the actual lower limit. For verification, GSFC monitors the divergence of the SOBE output via a long focal length lens and CCD camera as outlined in Figure 1 and divides the result by the total magnification in the transmitter path. Presently, an inadvertent defocus in the SLR2000 main telescope is being compensated for by an offsetting defocus in a 3-power telescope on the transceiver bench. As a result, the nominal magnification of 30.48 for perfectly focused telescopes has been reduced to 28.21 for the compensated telescopes [Degnan, 2005].

References

[1] Degnan, J. J., “Ray Matrix Analysis for the Realtime Control of Automated SLR2000 Optical Subsystems”, Chapter 8, Sigma Space Corporation Report, October 2005.

[2] Klein, B. J. and J. J. Degnan “Optical Antenna Gain. I. Transmitting Antennas”, Applied Optics, 13, pp. 2134-2141, 1974.

[3] Verdeyen, Joseph T., Laser Electronics, Chapter 5, Prentice Hall, Englewood Cliffs, New Jersey 1989.

Obtaining the High-resolution Epoch with the FPGA Technology

Q. Li, F. Qu and Z. Wei

1. Chinese Academy of Surveying and Mapping (CASM)

Contact: liqian@casm.ac.cn /Fax:0086-10-68218654

Abstract

In Satellite Laser Ranging it is important to record the transmission epoch of each laser pulse. Currently in the Beijing SLR station many counter-chips are used to accomplish this task. With the popularity of the FPGA technology, engineers find that using FPGA (Field Programmable Gate Array) to design the digital system is a feasible way to reduce the dimension of the circuit board and increase the reliability of the system. We are designing a new epoch measurement system using one Xilinx's Spartan FPGA chip to accomplish what previously had required many counter-chips. The 1pps signals and the time code from the HP58503 are used to get rough epoch information to a one second resolution. The 10 MHz frequency from the HP58503 is used as the system clock. A 24-bit counter module in the FPGA chip, used with the system clock, gives timing information with a resolution of 100 nanoseconds and with a period of one second. To obtain the time code from the HP58503, two UART (Universal Asynchronous Receiver) modules are used, one to communicate with the HP58503, and another to transfer the epoch data to a PC.

Introduction

Fig.1 shows the present module at the Beijing Station that is used to obtain the epoch of the laser pulse. It is the cascade connection of 6 counter-chips. Every chip is only 4 bits, so higher resolution requires more counter-chips. To achieve a higher integrated level, we selected the FPGA chip which would perform the same task in a single module.

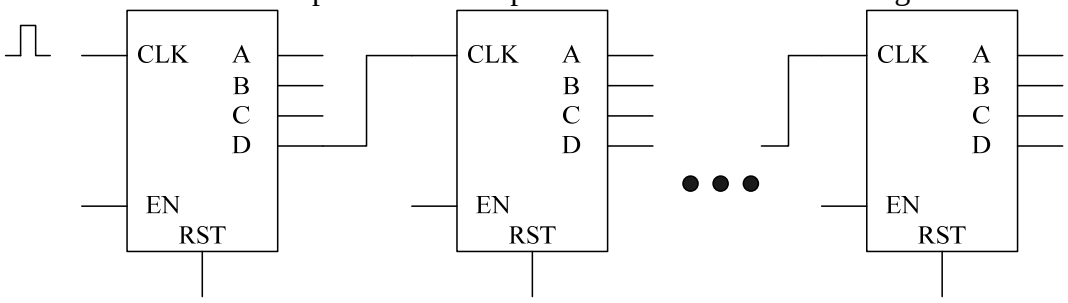

Figure 1: *Present module to obtain the epoch in Beijing Station*

Fig.2 shows the block scheme of the system. The HP58503 supplies the reference frequency, the one-pulse-per-second signal and the time code for the FPGA module to establish a UTC time clock. When a laser pulse arrives, the FPGA module sends the epoch data to the PC through the Serial Interface. MAX3232 is used as the level translator between the RS232 and LVTTL.

Establishment of the UTC time clock

Fig.3 shows the block scheme of the establishment of the UTC time clock. As the input clock frequency is 10MHz, so the time resolution is 100ns. To record one complete second, we must use a counter with at least 24 bits, because,

$$\log_2 \frac{1}{100 \times 10^{-9}} = 23.3$$

It's convenient to design a 24-bit counter in FPGA. Another 16-bit counter is designed to record the number of 1pps events after the reset operation. The 16-bit counter can record the time up to 18 hours, so 18 hours later, another reset operation is needed. Some registers are used to record the time code from the HP58503 to save the datum time.

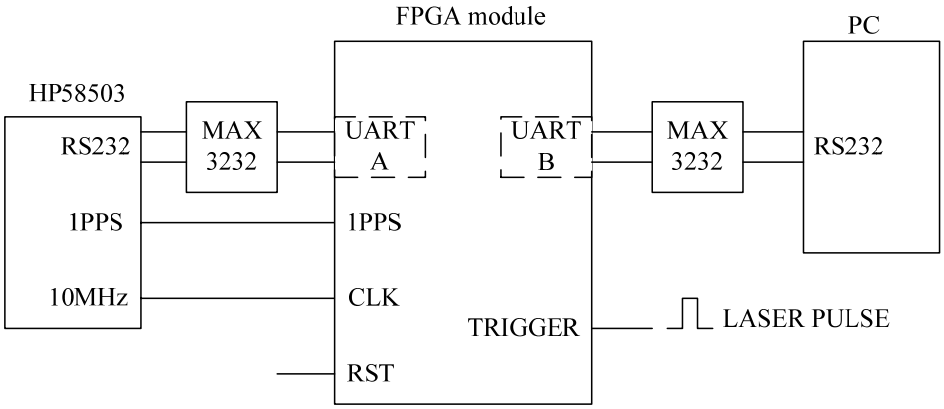

Figure 2: *Block scheme of the system*

Obtaining the epoch of the laser pulse

When a laser pulse arrives, some relative-time-registers are allocated to store the current values of REG1 and REG2. Then the data in the datum-time-registers and relative-time-registers are sent to the PC through UART B. The PC performs the final calculations required to obtain the transmission epoch of the laser pulse.

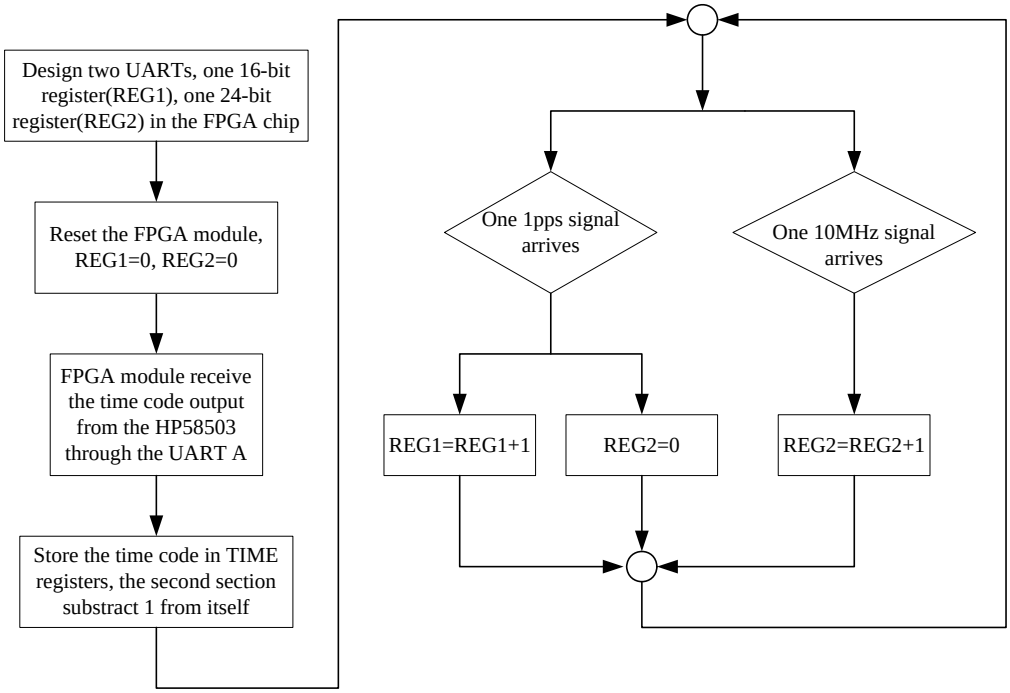

Figure 3*: The Establishment of the UTC time clock*

Comparison experiment and conclusion

A test setup has been designed to make sure that the new module can obtain the time code, 10MHz signal, 1pps signal from HP58503 as well as the laser pulse without disturbing the original system. Comparing the two epoch data shows that the new module has the equivalent function to the original one.

Difficulties in the development process and Future Plans

In the development process, the implementation of the UART is relatively harder than that of the counters. So compared with the microprocessors, the merits and drawbacks of developing a digital system with an FPGA are obvious.

Today, RISC microprocessors with an ARM core are widely used to design digital systems, so the structure “ARM+FPGA” may be a good choice for developing a digital system that can achieve higher resolution, precision, stability, flexibility and integration level as well as shorten the development time.

Platform

- Device:

  - Xilinx’s Spartan FPGA, HP58503, PC

- Software:

  - Xilinx ISE 7.1

  - VC++ 6.0

- Top-level Module type

  - HDL(Verilog HDL)

- Simulator

  - ISE Simulator

- Synthesis

  - XST(VHDL/verilog)

NEW FTLRS software tools for tuning observations schedule and remote control

Monique Pierron and FTLRS staff

1. Observatoire de la Côte d'Azur, Avenue N.Copernic - 06130 Grasse – France.

Contact: Monique.pierron@obs-azur.fr

Abstract

In the goal to facilitate and make more pertinent campaign observations, we have developed:

- *A fully automated mechanism for the CPF predictions: CPF file reception and propagation, prediction generation and orbit display are automatically performed.*
- *An acquired data sky coverage display for any site (per satellite and per date).*
- *A new levelling system for FTLRS, easy to use for observers, efficient and completing the remote controlled capability.*

Introduction

The French Transportable Laser Ranging Station often operates far from our French location in Grasse and it is very important to increase its remote capability, and to facilitate the observer's life.

Fully automated mechanism for the predictions

CPF mail reception

Mail is automatically extracted on the principal computer in Grasse. CPF files are sorted and dispatched in dedicated directories (for example /d/dat/prev/grca if GraceA) and files. File names are based on CPF file headers, for example gracea_060930_7732.gfz is done with target (gracea), date (060930), sequence number (7732) and provider (gfz).

CPF file propagation for FTLRS

For this, we use the rsync command (a free software computer program for Unix) to synchronize CPF files and directories from the Grasse computer to the FTLRS computer. This rsync command is executed every hour via the Crontab unix facility.

Files creation for satellite orbit display

All necessary files to display satellite orbits for the next few hours are created daily on Grasse and FTLRS computers (via cron facility):

- satellite timetable files for one month or more,

- prediction files for satellite passes to come: in this file, the step between positions depends on pass duration, in order to have a continuous curve for orbit display,
- file with next passes list for easy display; each line has the following form: Satellite name, MJD (begin), culmination, azimuth (begin and end), duration, date (hour and minute), prediction file name.

Satellite list and orbit display

At login the following window is displayed and continuously updated.

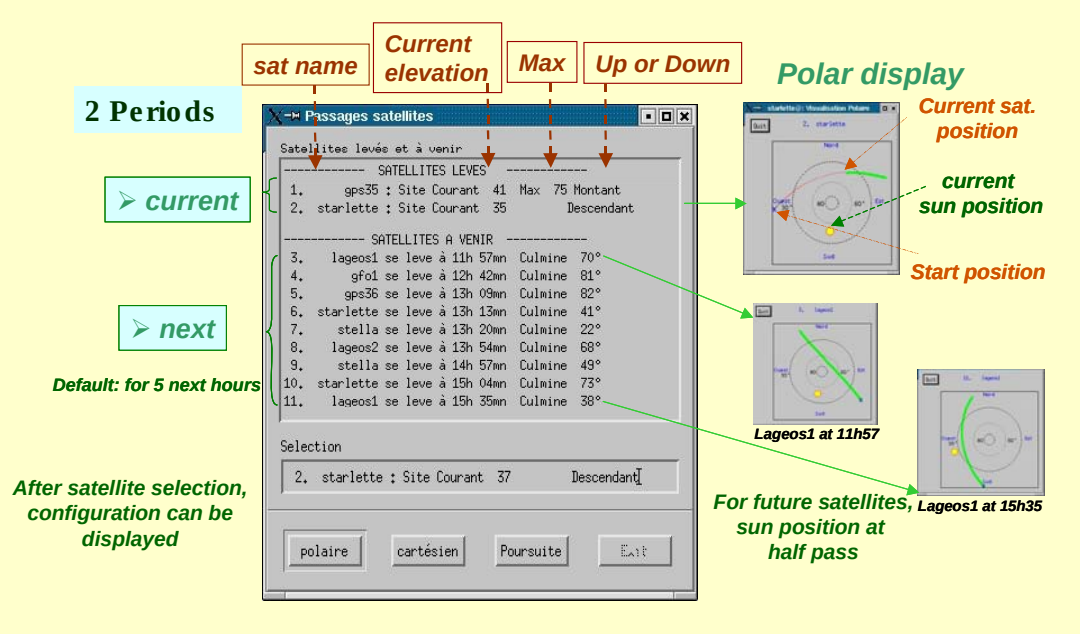

A few minutes before each satellite pass, a window with information appears and a bell rings.

With this mechanism in place, it was then natural and easy to develop the prediction's server on our main computer in Grasse. An executable prediction client (for Windows and Linux) is available. This will be very useful for further operations with MEO station (7845).

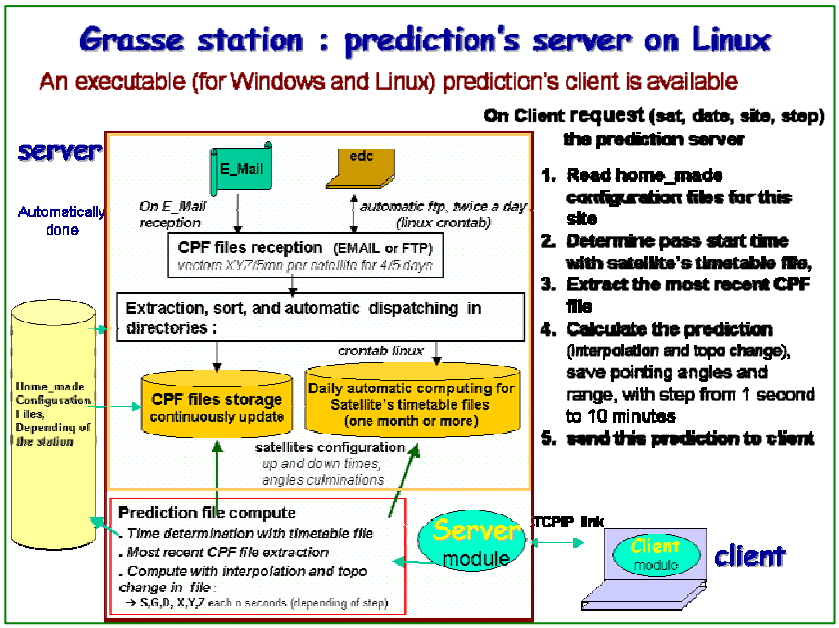

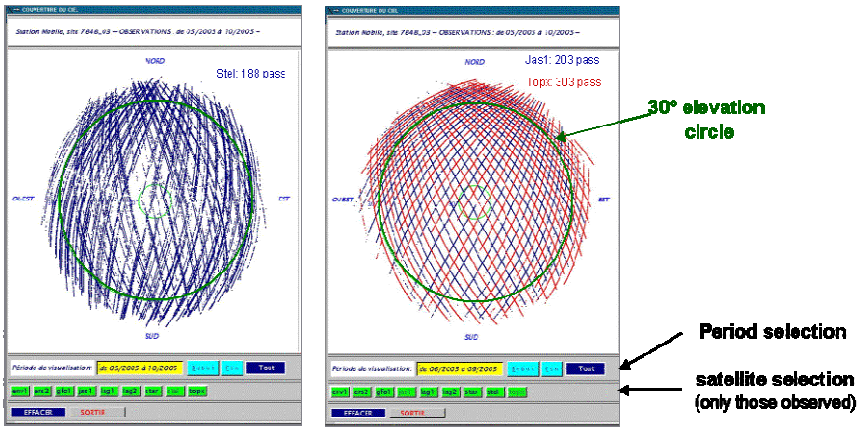

***Figure 1**: Sky coverage for Stella and Jason/Topex - FTLRS - May to October 2005*

Acquired data sky coverage display

This application allows display of data for each Grasse station (FTLRS, MEO and GRSL). Each point on the display is a validated return. The operator has just to choose:

- the satellite(s) in the proposed list, and
- the observation period.

The observation's Grasse station is done with an environment's variable.

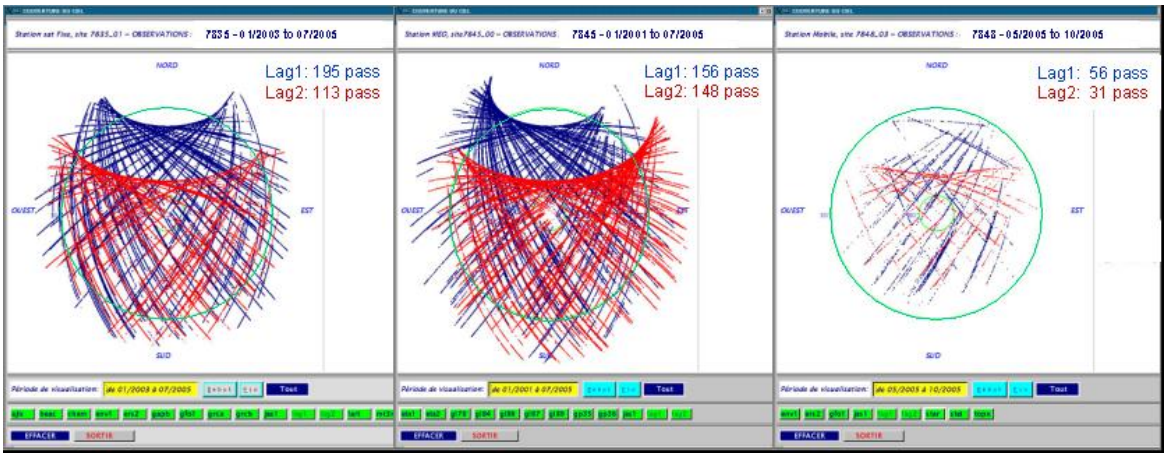

***Figure 2**: Lageos 1/Lageos 2 on Grasse stations: GRSL(7835), LLR(7845) and FTLRS (7848 Ajaccio)*

For FTLRS (7848 station during last Corsica campaign), we observe from the display that:

- the coverage has good repartition on all directions,
- Stella (first part Figure 1) is lost just during culmination,
- for Lageos (third part Figure 2) there were no returns under 30 or 40 degrees.

For GLRS (7835 station) we had a good coverage for all satellites (low satellites to Lageos).

For 7845 station (MEO station used for HEOS) from Lageos:

- the coverage has good repartition on all directions,
- it is easy to have returns when the satellite is low,
- for Lageos, it is very difficult to have returns when higher than 80°; this doesn't exist for higher satellites (Glonass or GPS).

A remote levelling system for FTLRS

We have developed a new system, to process the mount levelling system. The system (laser + telescope) is now on a mechanical device, and this device is levelled with two electrical jacks. These jacks are positioned in perpendicular directions.

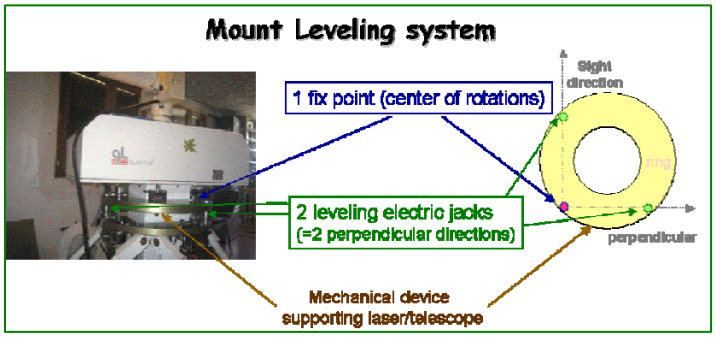

Figure 3: *The new mount Levelling sytem for FTLRS*

These jacks are software controlled via a control panel. Levelling values in two directions are continuously read and displayed, and it is possible to adjust the level:

- manually with the two push buttons on panel, or
- automatically with a servo loop control.

This new remote tool for FTLRS is efficient, easy to use and very important for remote controlled capability.

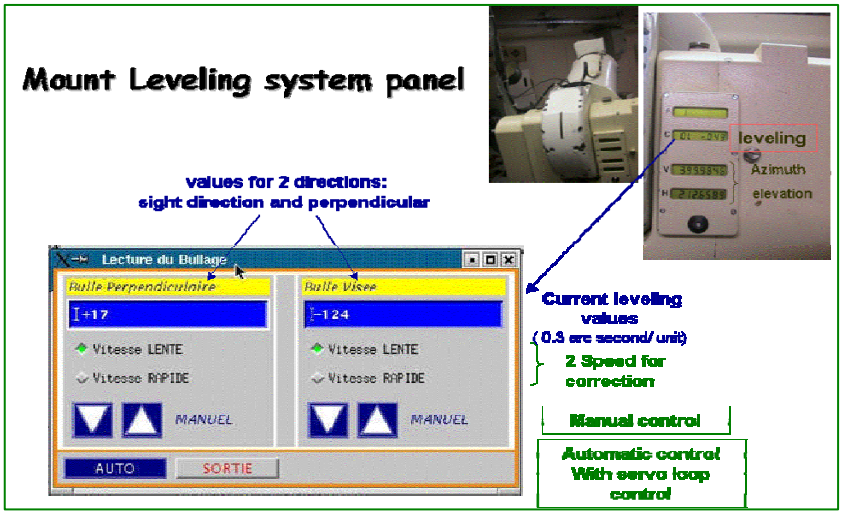

Conclusion

Fully automated mechanisms for the predictions and the new levelling system for FTLRS are major improvements, facilitating the observer's life and completing the remote controlled capability. FTLRS will very soon be operational in our new laboratory in Grasse, and all our staff is very excited to test these new tools and we look forward to our first returns there.

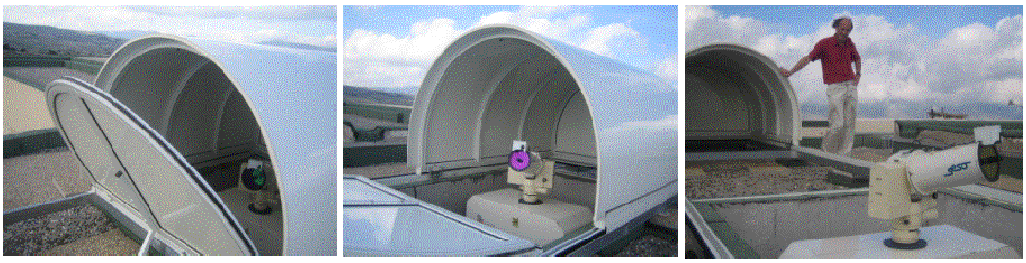

Recursive Filter Algorithm for Noise Reduction in SLR

Michael Hiener[1], Ulrich Schreiber[1], Nikolaus Brandl[2]

1. Forschungseinrichtung Satellitengeodäsie, Technical University of Munich, Fundamentalstation Wettzell, 93444 Bad Kötzting, Germany

2. Bundesamt für Kartographie und Geodäsie, Fundamentalstation Wettzell, 93444 Bad Kötzting, Germany

Contact: schreiber@fs.wettzell.de

Abstract

This report presents the concept and implementation of a recursive filter for the identification of satellite returns in laser ranging in the presence of strong noise. This project was aiming for an increased data yield of automatically filtered satellite laser ranging measurements in order to maximize the number of correctly identified returns. Furthermore the amount of false readings have to be reduced and an automatic timebias-adjustment during ranging was required.

Introduction

Automatic data screening of timer readouts in SLR is widely used by many laser ranging facilities of the ILRS. All of them depend on some type of histogram evaluation of short time slices of measurements throughout the ranging process. The approach uses the fact that return signals from a satellite bunch up at a specific location in the range gate window, while noise readouts caused by background light or intrinsic detector noise are far more spread out throughout the range gate. For satellite passes with reasonable or good signal to noise ratio this method is fully adequate. However, in particular for daylight passes of the GPS and GIOVE satellites, this method is often extracting much fewer returns than actually were recorded by the ranging facility. On top of that a non negligible number of false readings is usually upsetting the normal point generation process, because erratic data points prevent the fitting procedure from converging. Figure 1 shows an example of such a weak satellite pass. One can clearly see time intervals where a reasonable or good signal to noise ratio exists for the measurement. However there are also times where only sparse data is recorded. In order to extract the valid returns out of all the recorded data points in near real-time the control software examines small portions of the pass of a few seconds length. The data is then converted to a histogram and if a suitable bin contains a sufficient number of echoes, these are extracted and stored away as satellite returns. This evaluation process is fast and strictly linear in time. In the presence of very sparse data the threshold criterion is never satisfied and valid data is lost. If on the other side the threshold value is lowered too far, then randomly lumped together background noise events will accidentally be taken as good data and the post-processing can be disrupted.

By using more than one criterion at a time and introducing reprocessing of past data as well as a locally linearized look ahead strategy, one can vastly improve the robustness of the filter procedure. At the same time the data yield improves substantially in particular for passes with a low signal to noise ratio.

Function of the new filter algorithm

The new filter applies two distinctly different methods. A histogram-analysis is used to detect possible satellite returns in a reasonably short time interval. The results then are used to predict the likelihood of valid returns into the future, where it also

successfully recovers valid data-points at a low data rate. Both methods cooperate to not only detect, but also rate identified returns during the ranging activity.

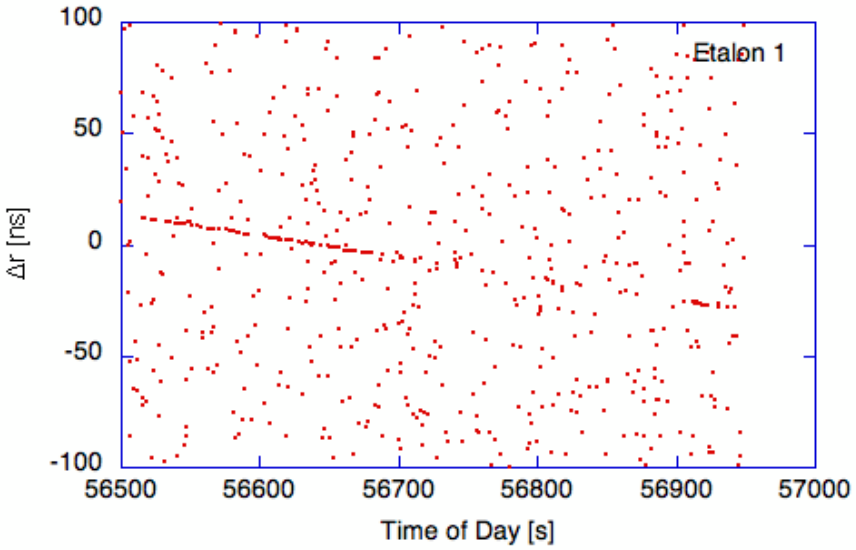

Figure 1: *Example for a measurement window of an ETALON pass with sparse data in daylight.*

From a number of verified satellite returns within a number of time slices, the actually applied time bias value for the momentarily observed satellite pass can be improved. With time bias corrected range residuals the histogram of the analysis process sharpens substantially. As a consequence the width of the rangegate can then be reduced automatically, which in turn enhances the data yield of the ranging operation. The program module works in several layers. The inner loop of the filter procedure is based on time slices of 5 seconds of observations (fig. 2). The length of the time slice is adjusted to the 10 Hz repetition rate and the background noise level typical for the Wettzell Laser Ranging System (WLRS). Other systems will have different settings. If already available a time bias correction is applied to all the data points in that time segment. Then the data is passed on to a histogram analysis routine, which has a bin width of 5 ns. This arbitrarily chosen value too has shown to work well for the WLRS operation parameters.

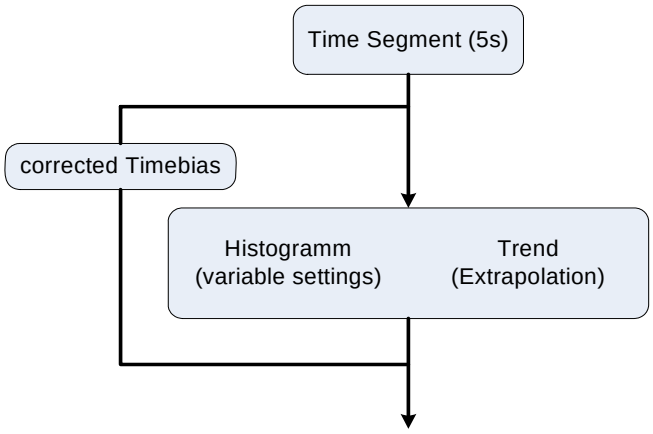

Figure 2: *Flowchart of the inner loop of the data-screening program.*

The threshold value for the histogram evaluation is currently set to 4 events per bin. In order to avoid ambiguities from unfavorable bin boundary settings (see fig. 3) in the histogram analysis, this evaluation is made twice with all the bins shifted to one side by half the bin-width.

When the threshold value of 4 events per bin is exceeded, all data points within that histogram bin are taken as possible returns. If the threshold value is exceeded by a factor of 2 the data within this bin is considered as reliably identified returns. Reliable returns are used twofold for the remainder of the satellite pass. They are used for an updated time bias computation, which feeds back to the next time slice and they are used in order to predict future locations within the range gate for the next few time slices. Figure 5 illustrates the prediction approach. Known trustworthy returns from the most recent past are linked with a straight line. The line is extended into the future and a corridor of ±2.5ns is set around this predicted line. Any single event that happens to fall within this corridor is considered a potential return and subjects it to further verification.

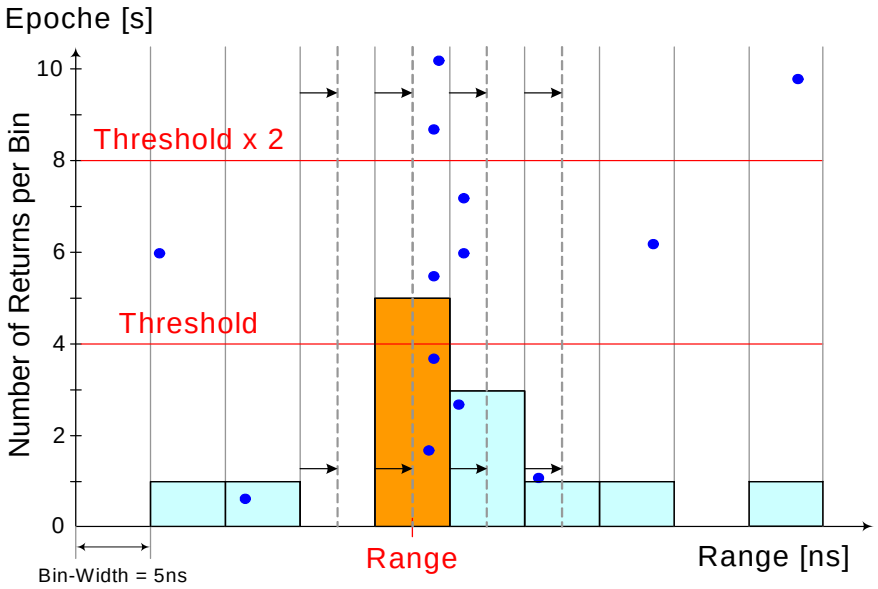

Figure 3: *A histogram of a 5 second long segment of a satellite pass of the WLRS. Unfavorable bin boundary settings are avoided by a re-evaluation with shifted bins.*

Therefore also extremely low return rates well short of the threshold value of 4 can be detected. The predicted linear corridor where future returns are expected expires after about 30 seconds when no further satellite echoes are recorded, because this simplified piecewise linearization of a satellite pass does not represent a valid approximation indefinitely.

Another important aspect of this new approach is a retrospective analysis, which identifies satellite returns that have been overlooked in the near real-time evaluation. A very sparse return rate may cause such lost returns as well as a number of false alarms. The retrospective analysis step revisits the last whole minute of observation. From the time slice analysis a number of returns are found. Some of them will be unambiguously identified as valid returns, while a certain number of returns are only classified as possible candidates. Again a linear regression through all unambiguously identified data points along with a corridor of ±2.5ns selects the part of the range gate where returns are most likely. Three cases may be found:

- All candidates (orange points in fig. 5) within these limits are now recognized as valid returns.
- All candidates outside this corridor are deleted from the list of possible returns.
- All not identified (white) data points inside the corridor are added to the list as possible candidates.

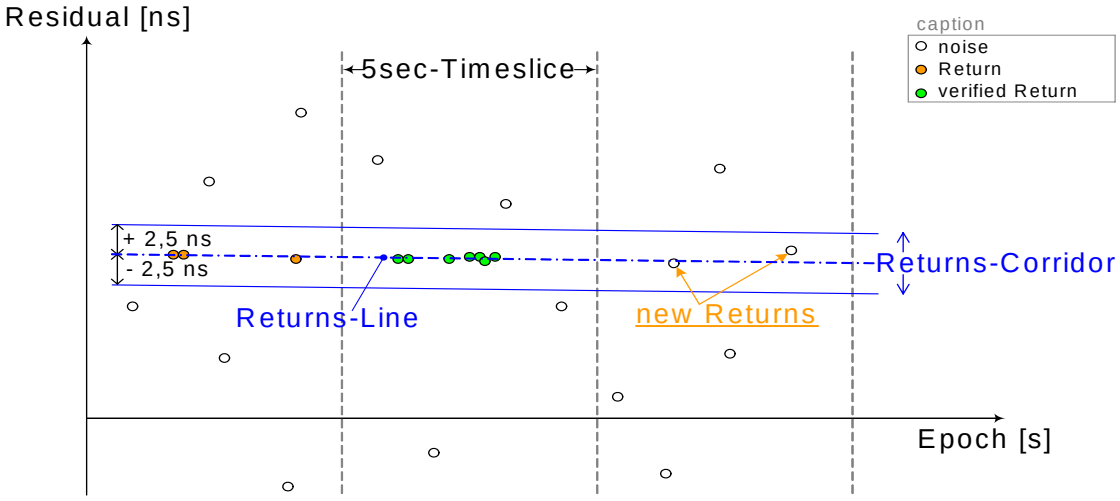

***Figure 4*:** *Reliably identified returns within a time slice of data are extrapolated into the future in order to find otherwise lost data points when the return rate is sparse.*

The linear approach for this screening procedure is justified because only very small segments of a complete pass are analyzed at a time. It has the advantage that this processing is fast and that it does not diverge quickly as polynomials tend to do in the presence of an inhomogeneous data distribution.

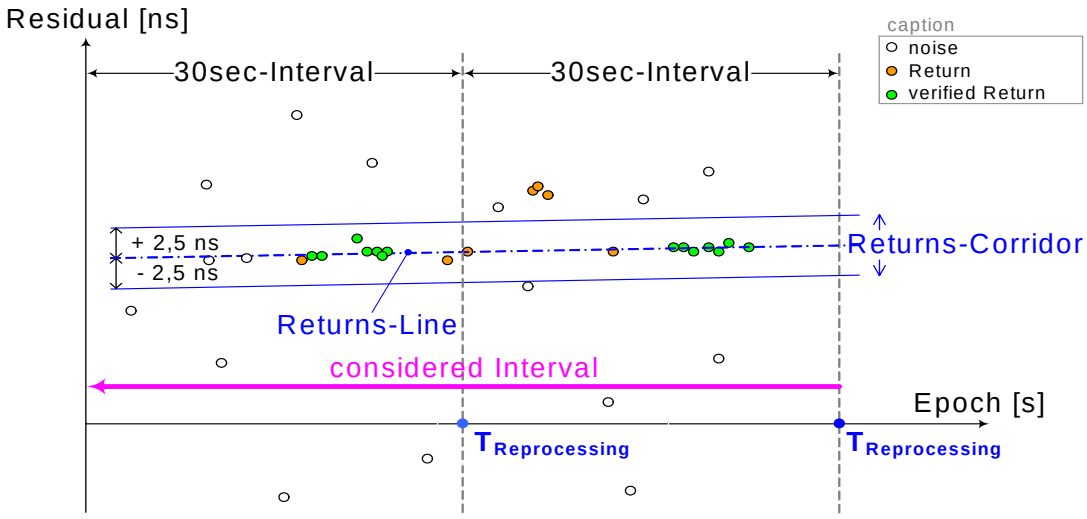

***Figure 5*:** *Reprocessing of the last 60 seconds of data. Reliably identified returns are used to define a return corridor. Potential returns outside this corridor are deleted from the list, while potential returns inside the corridor are turned into verified returns.*

Application Results

When this new data screening approach was integrated into the routine operation software of the WLRS, care was taken that rapid data processing was maintained throughout the ranging operation. We never encountered a situation where the ranging data came in faster than the various processing steps took to evaluate the data. We would expect that this would also apply for higher repetition rate systems, however with an appropriately adapted parameter setting.

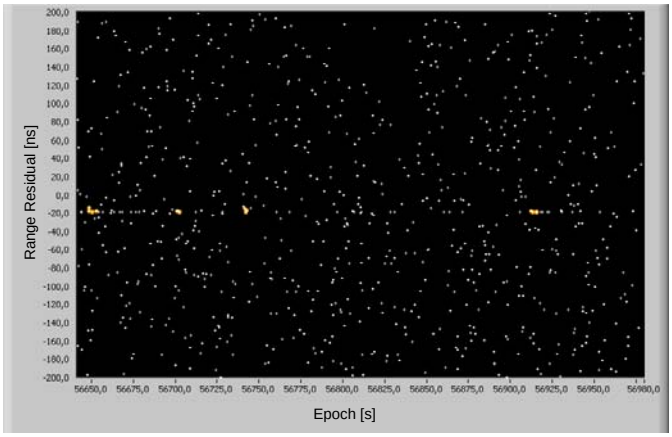

Figure 6*: A Section of an Etalon daylight pass with sparse data with returns identified with the previous screening program. Clearly many valid data points were lost in the past.*

Because of the repeated scanning of recent tracking data some adjustments to the data storage strategy had to be newly introduced. Essentially a larger data buffer is required as a temporal additional storage. As one might expect there is little to no advantage of this recursive screening filter over the simple histogram analysis when there are many satellite returns and almost no noise events. However for a weak signal to noise ratio approaching 1, rather dramatic improvements have been obtained. Figure 6 shows such an Etalon pass. Unfortunate boundary locations of the time slices often cause histograms to remain below the threshold limit. As a consequence a lot of data is lost. In this example only 12 returns were recovered out of the portion of data shown in the diagram.

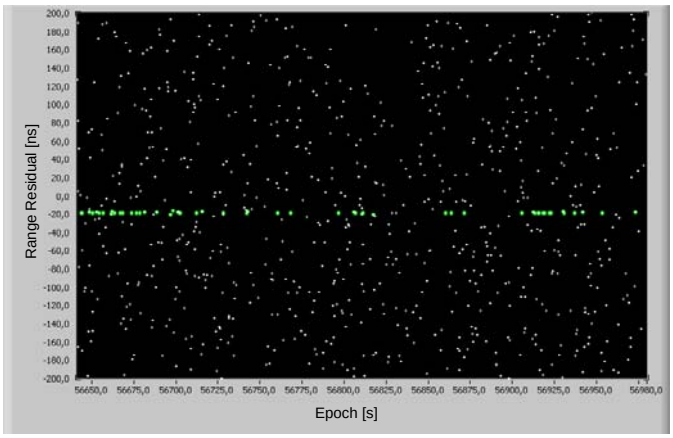

Figure 7: *The same section of the Etalon pass processed with the new screening programme.*

In contrast to fig. 6 the same dataset was re-analyzed with the new screening procedure extracting 50 returns instead of 12. The results are shown in fig. 7. Again this may still not catch all available returns. On the other hand it does not generate false readings either which is also an important aspect for this filter process. The WLRS ranging software was updated to this new filter scheme in December 2006. As far as we can see it improved the efficiency of the WLRS and reduced the number of passes that need manual user intervention for the normal point generation process noticeably.

References

[1] R. Jamal und Herbert Pichlik; LabVIEW Programmiersprache der 4. Generation; Prentice Hall, ISBN 3-8272-589-0, (1999)

[2] M. Chugani, A. Samant, M. Cerna; LabVIEW Signal Processing}; Prentice Hall PTR, ISBN 0-13-972449-4, (www.phptr.com), (1998)

The Impact and Resolution of "Collision Bands" on Tracking Targets at Various Ranges

C.J. Moore[1]

1. EOS Space Systems Pty. Limited, 111 Canberra Ave., Griffith, A.C.T. Australia.

Contact: cmoore@eos-aus.com

Abstract

Symmetric SLR and LLR systems that adopt a spinning disk as an optical switch between transmit and receive laser pulses need to address the problem of losing signal due to transmit and receive pulses being coincident at the disk when targets are at certain "collision band" ranges. These collision bands occur with increasing frequency at larger target ranges and can interrupt tracking of distant targets (> 6,000 km) for significant periods. A general solution to minimize the impact of collision bands based on disk frequency adjustment is presented. Depending on the design of the disk and system requirements, it is possible to eliminate the effect entirely or reduce the impact to a few narrow range bands by applying a relatively simple disk frequency control algorithm.

Introduction

Satellite Laser Ranging (SLR) stations that employ a symmetric (i.e. single telescope) system for their transmit and receive paths must adopt a multiplexing mechanism to allow measurement of the timing of the transmitted and received laser pulses. One popular mechanism involves the use of spinning mirrored disk containing one (or more) small holes that allow passage of the transmit pulse, while the mirrored surface is orientated such that return photons are reflected towards a receive detector. This mechanism has been adopted in recent years by EOS Space Systems for a number of their laser tracking system, including the Mt Stromlo SLR system.

One disadvantage of this mechanism is termed the "collision band" problem where a tracking signal is lost due to coincidence of a transmit hole and returning photons. The collision band thus refers to the band of target ranges that are effectively unmeasurable due to this coincidence. To increase the transmit power it can be advantageous to increase the number of transmit holes, which for a given disk rotation frequency, allows a greater laser fire rate. Unfortunately the greater the number of transmit holes, the greater the number of collision bands that may be experienced with potential loss of signal.

One technique used to minimize of collision bands relies on adjustment of the disk frequency and thus laser fire rate. For example, Titterton (1998) describes this technique to minimize backscatter. This paper describes an analysis of this collision band problem and proposes a technique for the automatic minimization of collision bands and number of disk frequency adjustments for a given range of disk configurations.

Theory

Collision Band Model

Spinning transmit/receive (T/R) disks often have one or two transmit holes, but in general there could be any number subject only to physical restrictions. Figure 1 shows a schematic of such a disk having two transmit holes. In general we can let; **N** = number of holes equally spaced around the disk, **r** = radius of the transmit hole, **R** = radius of 'projected' circle containing the transmit hole centre at fire time, and **f** = disk speed (Hz), giving the laser fire rate as **Nf**. Also let $\boldsymbol{\alpha}$ = angle subtended by each transmit hole such that $\boldsymbol{\alpha} = 2 \sin^{-1} (\mathbf{r}/\mathbf{R})$.

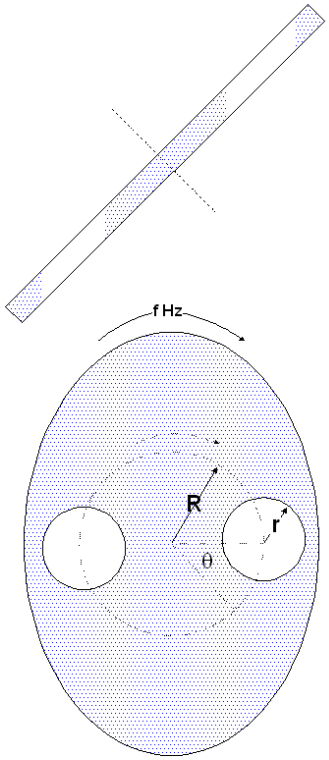

Figure 1: *Schematic of theSpinning T/R Disk*

s = available signal as a ratio, i.e. **s** = 1 when there is no loss and outgoing and incoming signals do not overlap, or **s** = 0 when complete overlap occurs.
d = distance of the target (along the optical path), and **c** = speed of light, such that the two-way time taken for a reflected pulse to leave and return to the disk is $\boldsymbol{\tau = 2d/c}$.
Let $\boldsymbol{\theta}$ = angular displacement on the 'projected' circle. Given the rotation speed of a point on this circle is $\boldsymbol{2\pi f}$, then the disk rotational movement, $\boldsymbol{\Delta\theta}$, in the time it takes for a laser pulse to leave and to return, $\boldsymbol{\Delta\theta = 2\pi f\tau}$, is limited to

$$\frac{2\pi\, i}{N} - s\alpha < \Delta\theta < \frac{2\pi\, i}{N} + s\alpha$$

Here **i** is an integer, equivalent to the number of shots in flight.

Assume that $\boldsymbol{\alpha}$ = 2**r**/**R** to a good approximation and define a geometrical factor, **F** = **sr**/**R**. This equation can be then be rewritten to give the condition for the existence of a collision band, i.e.,

$$\frac{i}{N} - \frac{F}{\pi} < f\tau < \frac{i}{N} + \frac{F}{\pi}$$

which can be expressed simply as,

$$\left| f\tau - \frac{i}{N} \right| < \frac{F}{\pi} \tag{1}$$

The number of pulses in flight, **i**, can be determined from $i = \lceil Nf\tau \rceil$, but it is wise to confirm the inequality using "floor" and "ceiling"values; i.e. $i = \lfloor Nf\tau \rfloor$ and $i = \lceil Nf\tau \rceil$.

Frequency Shifting

Equation (1) indicates that for a given range, **d**, and a given geometrical configuration there is only one parameter that can be adjusted such that the inequality no longer holds and that is the disk frequency, **f**. Hence it may be possible to adopt a scheme where the effect of collision bands can be reduced, or even eliminated, by frequency shifting the spinning disk.

From equation (1) it can be shown that to avoid a collision band at a given range, **d** (or equivalently, $\boldsymbol{\tau}$) then set **f** such that

$$\left| Nf\tau - \lceil Nf\tau \rceil \right| \geq \frac{NF}{\pi} \tag{2}$$

There may be additional system restrictions on the spinning disk frequency, the range of frequency adjustments that can be made and on the rate that adjustments can be made. The restrictions may be such that condition set by equation (2) cannot be met and the collision band cannot be avoided.

The next section describes an analysis of a typical two hole disk used in a laser tracking system and the scheme used to meet, as much as possible, the collision band avoidance condition given by equation (2).

Analysis of a Two Hole T/R Disk

Consider a two-hole disk having a geometrical factor F of 20%. For example, a disk where the transmit holes have a radius (projected at right angles to the laser beam) of 15 mm, at a radius from disk centre of 75 mm, or a disk with transmit holes of radius 12 mm at a distance of 60 mm from the disk centre will have F = 20% assuming no overlap of the return beam footprint on the transmit holes (s = 1.0). For this analysis assume that the maximum laser fire rate is 100Hz and the maximum frequency variation is ±5%. This is just one example of possible design constraints that might apply to systems using this technique. In this case, the value of **f** is limited to a range between 45 and 50 Hz

Table1: *Defined Range Bands*

Range Band	Sample Ranges (km)
Low Earth Orbit (LEO)	500 – 2000 km
Medium Earth Orbit (MEO)	2000 – 12000 km
High Earth Orbit (HEO)	19000 – 29000 km
Lunar	350000 – 400000 km

Table 1 summarises the four range intervals used in this analysis. These represent the typical distribution of earth orbit satellite and lunar targets. Equation (1) was applied to range values in each of these intervals to identify the collision bands occurring over the various ranges. The following sections describe the results from these calculations. In all cases the disk frequency resolution used was 0.05 Hz.

Impact of Tracking LEO Satellites

No collision bands are evident for low earth orbit ranges less than about 1,300 km as shown in figure 2. Unfortunately a collision band occurs for ranges from approximately 1450 km to 1700 km which cannot be avoided using the available disk frequency shift.

An assessment has to be made whether this collision band will cause significant impact on actual target tracking.

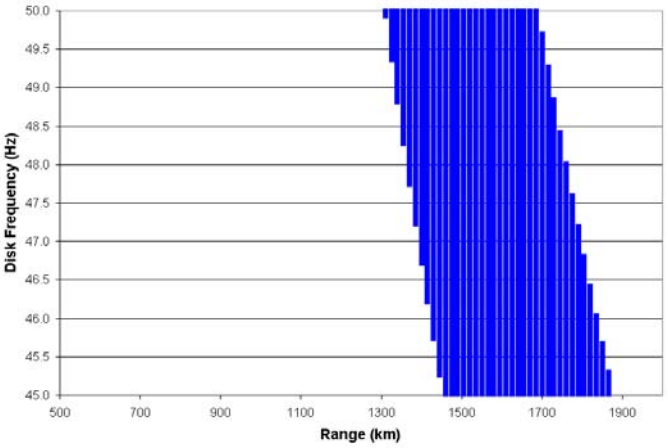

Figure 2*: Collision Bands at LEO Satellite Ranges*

Impact on Tracking MEO Satellites

For ranges between 2,000 and 12,000 km, the collision bands are grouped as shown in figure 3. There are also significant range intervals where there are no collision bands at all. However there is still one range interval where there is an unavoidable collision band, at about 3,000 to 3,200 km. Above this interval there are no ranges that have an unavoidable collision band, as illustrated in figures 3, 4 and 5.

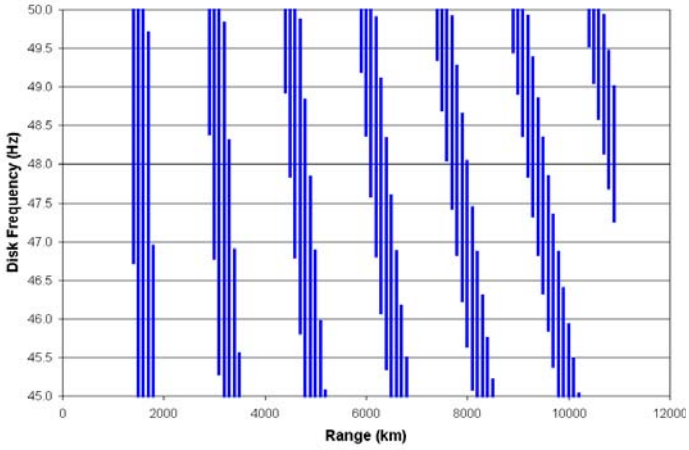

Figure 3*: Collision Bands at MEO Satellite Ranges*

Impact on Tracking HEO Satellites

As ranges increase, the number of collision bands within the disk frequency range increase and become shorter, as illustrated in figures 4 and 5, so the options for avoiding collision bands also increases. However, for any given disk frequency, the probability of a target pass having a number of collision bands also increases.

It is notable that even for one-hole disk systems, the probability that a high satellite pass contains one or more collision bands is quite high, and hence an avoidance scheme is still required.

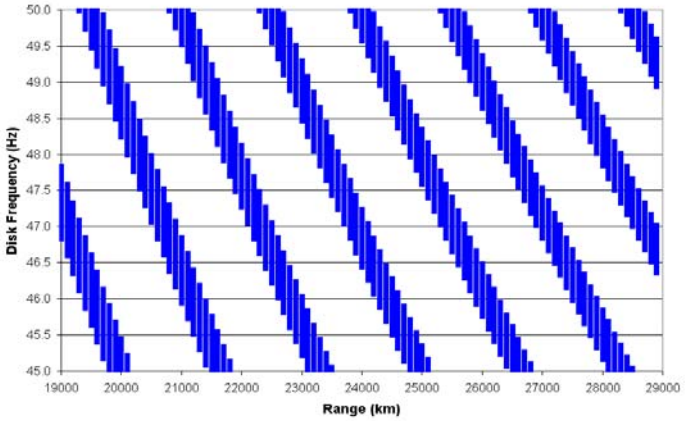

***Figure 4**: Collision Bands at HEO Satellite Ranges*

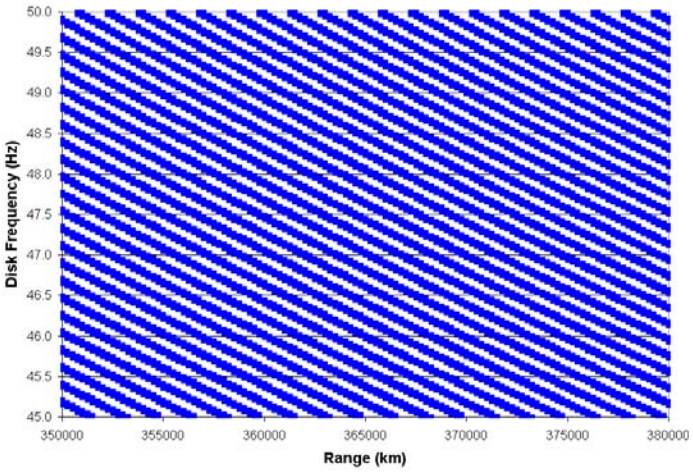

***Figure 5**: Collision Bands at Lunar Ranges*

Impact on Tracking Lunar Targets

At lunar target distances, collision bands are very frequent but very short both in terms of disk frequency and range changes as illustrated in figure 5. With slowly changing ranges, it is possible that a lunar target pass may either be largely free of collision bands or be largely in a collision band. Avoidance at these ranges will require small shifts in disk frequency. Table 2 shows a summary of typical impact of collision bands on tracking a number of ILRS SLR satellites and LLR targets.

***Table 2**: Impact of Collision Bands on ILRS Satellites*

Satellite Groups	Typical Ranges (km)	Impact, no avoidance	Impact with avoidance
GraceA & B, Champ	500 – 1500	None	None
Envisat, ERS2, GFO1, Stella, Starlette	800 – 2000	Lost data around 1500-1700 km (near end of passes)	Lost data around 1500-1700 km (near end of passes).
Ajisai, Jason	1400 – 2900	Lost data near zenith of high passes.	Lost data near zenith of high passes.
Lageos1,2	5900 – 9,000	Lost data in 1 or 2 bands.	None
GPS, Etalon, Giove A, Galileo	19,000 – 27,000	Lost data in 2 or 3 bands.	None
LLR targets	350000 – 420,000	Significant periods of lost data	None

Collision Band Avoidance

Frequency Shifting Algorithm

Using equation (1) it is straightforward to assess, given current range and disk frequency, whether a tracking system is experiencing a collision band. However it is less straightforward to determine what is the best disk frequency to use to avoid such a band. An algorithm was devised such that not only are collision bands avoided (if at all possible) but the number of

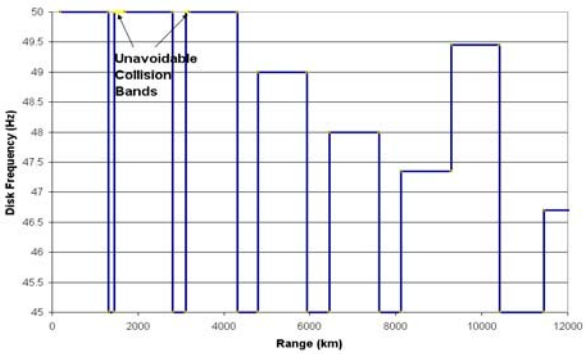

***Figure 6**: Disk Frequency over increasing LEO and MEO Satellite Ranges*

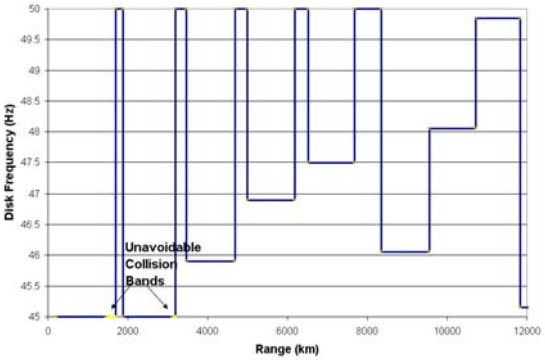

***Figure 7**: Disk Frequency over decreasing LEO and MEO Satellite Ranges*

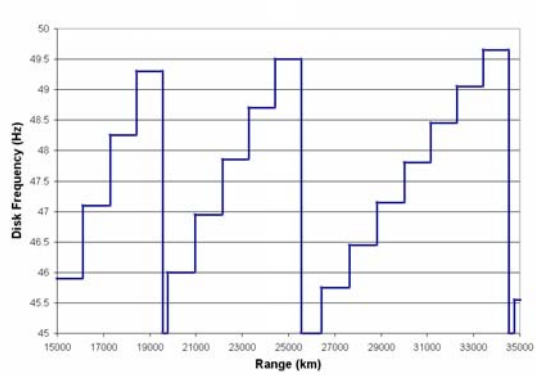

***Figure 8**: Disk Frequency over increasing HEO Satellite Ranges*

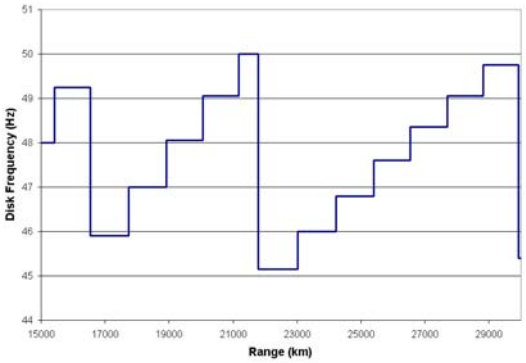

***Figure 9**: Disk Frequency over decreasing HEO Satellite Ranges*

frequency adjustments is minimized. This may be important if the time taken for the laser system to respond to frequency changes is significant.

The algorithm requires determining, for a given range, the disk frequency end points of a given collision band, at the moment that this collision band is first encountered. No action (i.e. frequency adjustment) is necessary when a collision band is not present. If a collision band is encountered when the range is increasing, increase the disk frequency by a small amount and check if the collision band is still present. This is repeated until maximum disk frequency is reached, at which point, the disk frequency is set to the minimum, and then adjusted upwards until no collision band is found or the cycle is completed and avoidance is not possible. A similar procedure is followed when the range is decreasing but in this case the disk frequency is reduced by a small amount.

The following diagrams illustrates the disk frequency changes (for the sample configuration) resulting from the application of this algorithm. Results from increasing and decreasing

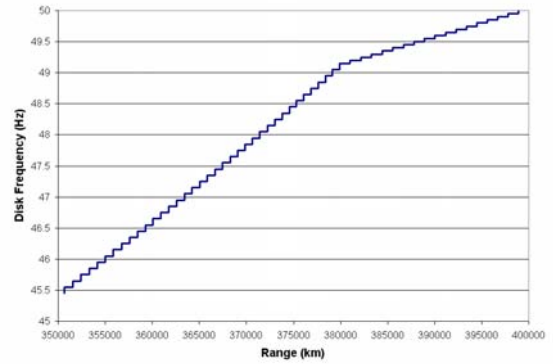

***Figure 10**: Disk Frequency over increasing Lunar Target Ranges*

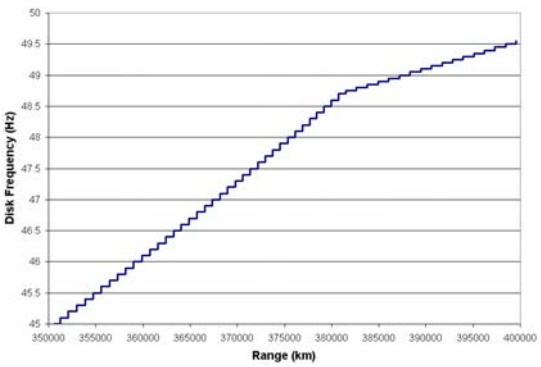

***Figure 11**: Disk Frequency over decreasing Lunar Target Ranges*

ranges are shown.

Low-Medium Earth Orbit Satellite Ranges

The frequency shift patterns for increasing and decreasing distances over the low and medium earth orbit satellite ranges are shown in the figures 6 and 7. Note there are two small ranges where collision bands are unavoidable by frequency shifting for the two hole configuration used.

High Earth Orbit Satellite Ranges

The frequency shift patterns for increasing and decreasing distances over the high earth orbit satellite ranges is shown in the figures 8 and 9. There are no unavoidable collision bands.

Lunar Target Ranges

The frequency shift patterns for increasing and decreasing distances over lunar target ranges is shown in figures 10 and 11. There are no unavoidable collision bands.

Disk Design

Given a geometrical design of the disk, the disk rotation frequency can be used to minimize collision bands as described in the previous section. However can the need for frequency shifting be ameliorated by appropriate disk geometry? The number of transmit holes and the

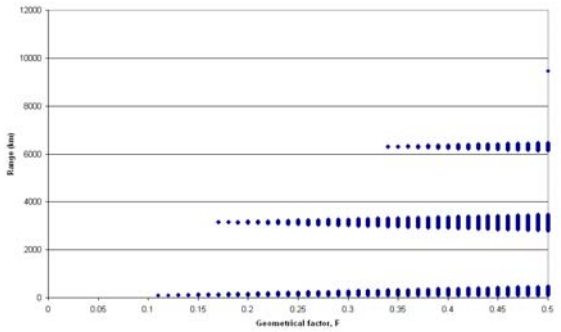

Figure 12: *Unavoidable bands for a 1 hole disk.*

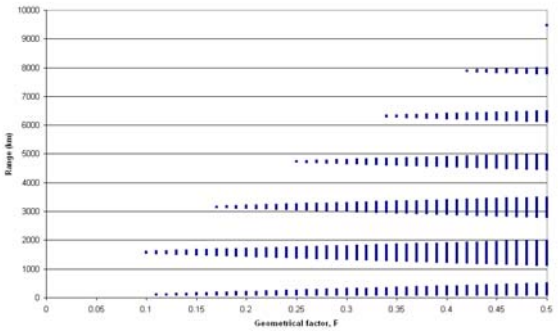

Figure 13: *Unavoidable bands for a 2 hole disk.*

geometrical factor, F, will influence the occurrence of collision bands and this is illustrated in Figure 12 for a 1 hole disk and Figure 13 for a 2 hole disk operating between 45 and 50Hz as in the previous examples. Similar diagrams can be generated for disks having three or more holes. These diagrams show the ***unavoidable*** collision bands at various ranges and various F-factors.

Clearly, more holes will result in a greater number and width of unavoidable bands over ranges up to 8,000 km. However, if the T/R disk and associated transmit hole can be designed such that $F < 0.1$ then the performance of disks with multiple holes (at least up to 3) is greatly improved. If the transmit hole radius had to be greater than, say, 10 mm, to accommodate the laser beam, then to obtain $F = 0.1$, the centre of the transmit hole would have to be greater than 100 mm from the centre of the T/R disk. Whether this is achievable would depend on other design criteria.

References:

[1] Titterton, P., "System/Usage Impact of Operating the SLR2000 at 2 Khz,". Proceedings of the 11th International Workshop on Laser Ranging, 1998, Deggendorf.

Web Application for the Engineering Data Files Processing

K.Salminsh

1. Institute of Astronomy, University of Latvia.

Contact: kalvis@lanet.lv /Fax: +371 7034582

Abstract

One of the problems of introducing new data formats and procedures is a high cost in terms of manpower and time to develop, modify and deploy necessary software across the SLR network. Web applications are a relatively new type of applications located on the server and accessible via the web browsers hence simplifying the software distribution and making any changes and improvements immediately accessible to all users. In this report the web application for the Engineering Data Files (EDF) processing and analysis is considered in more details. Review of the existing functionality and future development is presented.

Introduction

As was shown in [1] the preferable way to handle Engineering Data Files (EDF) processing and analysis is a web application to reduce overall implementation costs accross the ILRS network and to make software and its eventual future changes immediately accessible to the all users. For more detailed information on the EDF's, see [2]. Another advantage of the web applications is their accessibility to everyone with an internet connection and web browser (security restrictions may apply).

EDF Processing Application

Overview of the current implementation of the EDF processing workflow is presented in [2]. Incoming EDF from stations are uploaded via FTP and after preprocessing are moved to the directories for anonymous ftp access and also are inserted in the relational database. Data then can be accessed and processed over the Internet using the dedicated web application. Web application basic functionality, based on the goals stated in [1], can be summarized as following:

- Overview of the used equipment
- Calibration time series and analysis
- Calibration charts
- External interfaces: data export to Excel, web feeds (e.g. RSS)

The use of the application is straightforward. The equipment overview function (Figure 2) allows users to retrieve data about the equipment used in a given period of time for all stations, and to use it as a selection criteria for the calibration time series and to calculate statistics for one or more stations. The selected data can then be compared, plotted or exported to an Excel spreadsheet and downloaded to the user computer. Tabular data view for the Excel export is presented in the Figure 3. Live calibration data can be also published from the database as an RSS feed directly usable in other applications or web sites.

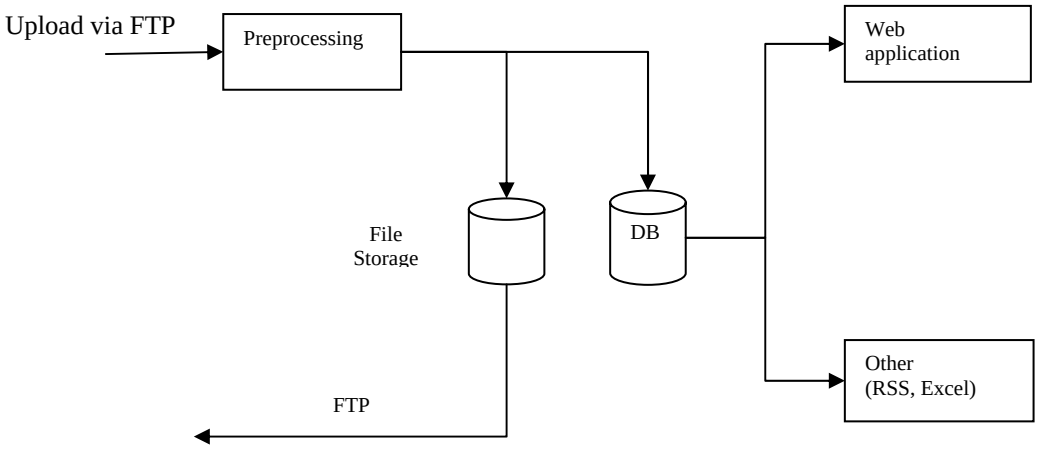

***Figure 1**: EDF processing flow*

Implementation details and future extensions

The EDF processing web application is now deployed on the server at the Institute of Astronomy, Institute of Latvia, and access information will be published on the EDF website [2]. The application is running on a Windows 2003 server and using a Firebird 1.5 relational database for the data storage. The most challenging part of the application is calibration data selection based on the used hardware and data model in the database. This is because it involves optional and station specific data within EDF XML documents and it leads directly to tree data structures which don't map well into the relational database structure. The current solution is to make directly accessible within the database only required parameters from the EDF specification, and to limit the number of parameters available for the data selection. The list of key parameters currently made available for data search and selection are:

- Station
- Calibration epoch
- Detector type
- Timer type
- Laser

Another limitation of the current design and data model is that the station custom data recorded within EDF can be used only as a reference and should be retrieved from the original EDF and stored in the database table as an entity, separately. Hence one of possible future extensions may include migration to the XML database to remove these limitations. Other eventual improvements are related to the user interface and application functionality including improvements in the data model.

Conclusions

One of the main problems in designing the EDF processing application is the absence of a common naming standard for the SLR station basic hardware elements and their parameters which can have an adverse impact on obtaining ranging results. Very likely similar problems will be encountered by others trying to record, process and analyze SLR data.

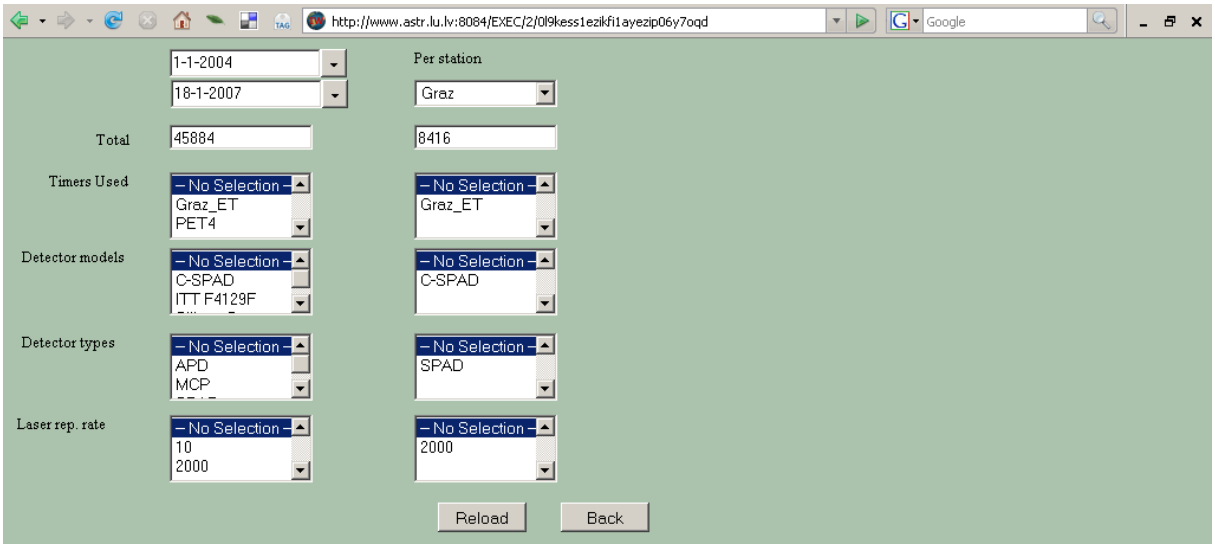

Figure 2: *Hardware overview and selection*

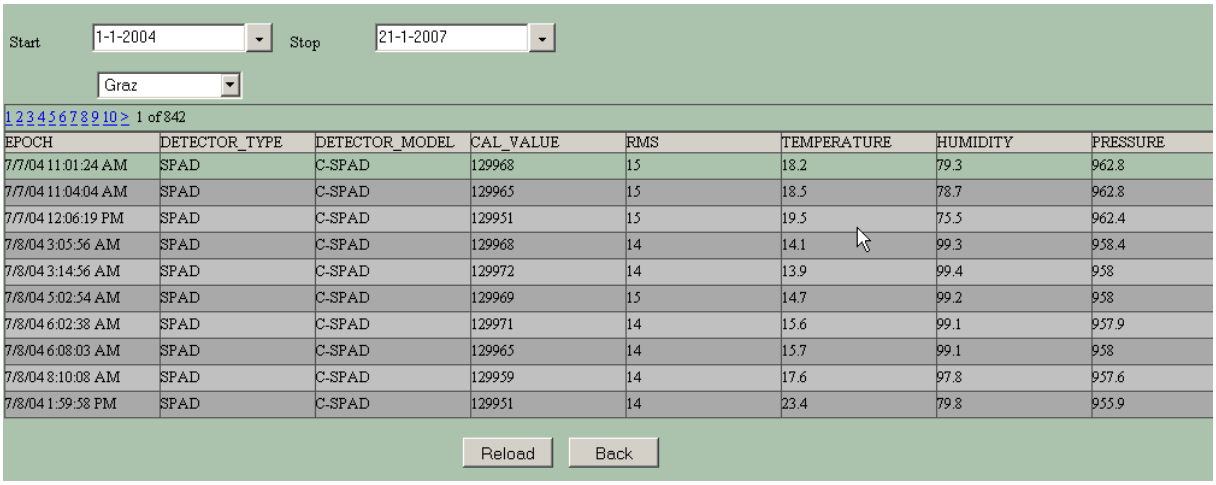

Figure 3*: Calibration time series – table view*

References

[1] Salminsh K. “Engineering Data File Processing and Distribution”, p.377, 14th International Laser Ranging Proceedings, San Fernando 2004.

[2] Website: http://www.astr.lu.lv/EDF

Consolidated Laser Prediction and Data Formats: Supporting New Technology

R. Ricklefs[1]

1. Center for Space Research,The University of Texas at Austin.

Contact: ricklefs@csr.utexas.edu for the ILRS Prediction Format Study Group and the Data Formats and Procedures Working Group

Abstract

The new tabular ILRS Consolidated Prediction Format (CPF) was developed to provide a single format to encompass traditional artificial satellite and lunar ranging targets as well as proposed transponder targets on or around the moon and other planets. As implementation of this format nears completion, the need to effectively handle kilohertz firing rates and transponder data in a new data format has emerged. The proposed Consolidated Laser Ranging Data Format (CRD) carries with it the lessons learned from the CPF: modularity, flexibility, and expandability.

Introduction

At the International Laser Ranging Service (ILRS) Workshop in Matera, Italy in 2000, it was decided that a new prediction format was needed to encompass the existing satellite and lunar ranging targets as well as the often-discussed transponders. In addition, there was a need to improve the predictions for low earth satellites. Thus the consolidated prediction format (CPF) was developed as a single format for all laser ranging targets, present and future. As the process of implementing the CPF is winding down, technological changes, in particular kilohertz repetition rate lasers and the Lunar Reconnaissance Orbiter (LRO) transponder are demanding that the current laser data formats be similarly reformulated. The process of creating the Consolidated Laser Ranging Data Format (CRD) is moving forward to meet LRO mission deadlines.

Consolidated Prediction Format

As described in early documents (Ricklefs, 2004, 2006), the CPF provides a method of ranging to different types of targets using one format. It therefore allows cross-technique ranging attempts, provided that a ranging station has needed hardware capabilities – such as event timers for lunar ranging.

The CPF does not rely on the on-site gravity model, tuning, separate Earth Orientation series, or drag and time bias functions that were required for the older tuned inter-range-vector (TIV) system. Instead, the new format contains untuned state vectors at appropriate intervals, typically in the ITRF system. This so-called format change is actually a change to the entire prediction scheme at the laser station from one of integration to one of interpolation.

Consolidated Prediction Format: Implementation Status

Currently (as of late October, 2006), the CPF is used exclusively in at least 22 out of the 37 ILRS Satellite Laser Ranging (SLR) stations, with one station in late stages of testing and 5 others close behind. Many of the remaining stations are not currently operational. It is expected that all operational stations will be converted by early 2007. In addition, the format is used at the one currently operating Lunar Laser Ranging (LLR) station (McDonald Laser Ranging Station), with other stations experimenting

with the format. The author is also working with the LRO project to generate CPF files. This effort may result in some additional transponder-specific changes to the format.

The results from using the CPF seem to be quite promising. According to one station (Gibbs, 2006), SLR predictions are seen to be much more accurate, with 90% of passes being within +-20nsec and 99% being within +-100nsec of the predicted range.

Consolidated Laser Ranging Data Format: Motivation

The first concern with the existing data formats (ILRS, 1999, 2004) is that transponder data will not fit. Specifically, transponders will often need to deal with one-way ranges. For instance, LRO data will consist of a fire time on the ground and receive time at the satellite. This being the case, there is a need for more accuracy in the fire and receive times, as the difference between the two must accommodate the accuracy expected from a range, usually at the picosecond level. This highlights the third issue, that of clock information. The current time standards, such as GPS are accurate only to about 100ns. Thus, there must be a way of describing the time standard used to record the data – on both the ground station and spacecraft. This is accomplished with a time system flag, a time offset, and a drift rate for both. Calibration is yet another area needing expansion. In the same way that there are laser station system delays, there are similar system delays on the spacecraft that must be accounted for.

In addition to the demand to reshape the data formats for transponders, stations with kilohertz laser firing rates are becoming more common and must be accommodated. Among the advantages, kilohertz laser ranging offers the possibility to study a satellite's signature in more detail than ever before, providing details of the spacecraft rotation rate and corner cube performance (Arnold, et. al., 2004). The existing fullrate data format is cumbersome for use with high-repetition-rate systems, because there is so much redundant information found in each data record. Estimates for the draft version of the format show that fullrate file size should drop by 55-65% at 500 returns/sec and 25-30% at <10 returns/sec.

Consolidated Laser Ranging Data Format: Overview

The intent of the new format is to encompass full rate, sampled engineering, and normal point data in one flexible, ASCII data format. The structure will be similar to that for the Consolidate Prediction Format in that there are several types of header and data records, assembled in a building-block approach, with records capable of specifying data for a particular data type or spacecraft configuration. This makes the format extensible and flexible. An additional section, for system configuration information, is being considered. A configuration section would make the data more self-documenting with more detailed data being available to the analyst. As with the CPF, header records are fixed format, but data (and configuration) records are free format, allowing field sizes to be optimized for each satellite.

Sampled engineering, fullrate, and normal point data could be placed in one file or broken into 3 files. Multiple color data could be included in one file, as could data from one or more satellites or stations. Simple utility programs could facilitate the merging or parsing of files. The hope is to make the format XML-friendly so that the data files could be easily parsed and written into XML files, and an XML representation of the data could easily be written in the CRD format.

In the case of transponders, much of the data required to write the complete CRD file is not available at the ranging stations in real time. The data that is recorded can be transmitted to the mission data center where all the data is collated, quality controlled, and finally submitted to the ILRS data center. Normally, one would expect that the stations would create and submit partially populated CRD files which the mission data center would complete.

Timetable

The LRO mission has become a driver for creation and implementation of the new data format, since its schedule is so tight, with launch in late 2008. At some point a version of the format will need to be frozen for this mission, even if the format is not ready for network-wide implementation. (Fortunately, on-station data for LRO will be written into a compact intermediate format, so 2 versions of the CRD will not be implemented at participating stations.) The version presented here, version 0.09 will probably be used for LRO.

In the near future, the preliminary format will be made available on the ILRS web site. The general community will be invited to submit comments.When the format is finalized, its implementation will take place over a period of a year or so, with stations in most need of the new features implementing it first. These include kilohertz stations, transponders-ranging stations, and lunar stations. The lunar ranging on-station raw format has always contained data not transmitted through the ILRS formats.

There has been some concern on the part of analysts that they would find it disruptive to deal with more than one data format at a time. For this reason, the data centers will translate normal point data received in the new format into the current ILRS format until all stations are using the new format. At some time, historical data, especially normal points, will need to be translated into the new format. This may have to be phased in over a number of years, once the format has been implemented and as resources become available. This topic needs to be discussed in more depth.

Summary

The successful implementation of the new prediction format is drawing to a conclusion at the same time that new technology such as kilohertz ranging and the LRO transponder are demanding that the laser data formats be rewritten. The new data format (CRD) will encompass fullrate, sampled engineering, and normal point data for SLR, LLR, and TLR. As with the CPF, the CRD format will use a building-block approach to permit modularity, expandability and extensibility.

References

[1] Arnold, D., G. Kirchner, and F. Koidl: “Identifying Single Retro Tracks with a 2kHz SLR System – Simulations and Actual Results”, Proceeding of the Fourteenth International Workshop on Laser Ranging, San Fernando, 2004.

[2] Gibbs, P.: Private communications, 2006.

[3] ILRS: “ILRS Fullrate Format Version 3”, http://ilrs.gsfc.nasa.gov/products_formats_procedures/fullrate/fr_format_v3.html, 1999.

[4] ILRS: “ILRS Normal Point Format, Revision 2”, http://ilrs.gsfc.nasa.gov/products_formats_procedures/normal_point/np_format.html, 2004.

[5] Ricklefs, R.: “Consolidated Laser Ranging Prediction Format: Field Tests”, Proceeding of the Fourteenth International Workshop on Laser Ranging, San Fernando, Spain, 2004.

[6] Ricklefs, R.: “Consolidated Laser Ranging Prediction Format”, http://ilrs.gsfc.nasa.gov/products_formats_procedures/predictions/cpf.html. 2006.

Appendix A: New CRD Format Examples

The following data examples are based on the preliminary 0.09 version of the format and are included for demonstration purposes only. Changes being made to the format document will render these examples obsolete.

1. Headers

1.1 Basic header 1

H1 CRD 1 MLRS   2006 9 27 17 0 ENVISAT   test file

Note station and satellite names.

1.2 Basic Header 2

H2   200901 6179   27386 2003 11 11 5 31 24 2003 11 11 5 32 2 52954 7080 24 19 1 0 6 7 2 0

Note the begin and end times and modified julian date of first data record as well as numerical station and satellite IDs.

1.3 Laser color record

H4 1 532.0

One such record is included for each laser color recorded in the file.

1.4 Pass Information

H5 1   -650   0   82   82

This record contains statistical information on the data and calibrations. The final format is likely to include the often-requested skew and kurtosis of the data in addition to the RMS.

1.4 End of Header

H9

Additional headers for transponders and full rate information are not shown here. Headers are fixed format

2. Data records

2.1 Range Record

10 1 2   19880.8466929 1 2   0.010936014472   0

The first long field is the transmit time, and the second long field is either range or receive time at the spacecraft. In the case of a down-link transponder, the first log field would be the transmit time at the satellite, and the second would be the receive time at the ground station. Interpretation of these fields is controlled by flags fields.

2.2 Meteorological record

20   19880.8466929 802.50 288.10   69

This record is written at the beginning of the file and thereafter only when one of the fields change “significantly”. This could be defined as twice the least significant bit of the sensor or an amount based on the field, such as 0.02mB for atmospheric pressure.

2.3 Point angles

30   19880.8466929 1 281.1890 22.4030

Point angles would be written for sampled engineering and fullrate data. After the beginning of the data, additional record are written only when a field changes “significantly.”

2.4 Corrections

40   19880.8466929 1 2   0   0   -650   0

This record includes refraction, center of mass, and system delays. Additional records are written only when a field changes “significantly.”

2.5 Range (with normal point fields)

10 2 2   19884.7472085 1 2   0.010985288919   0   15   37   73   0.0

Note that data records are written in free format.

LUNAR LASER RANGING SESSION SUMMARY

Chair: Tom Murphy

The Lunar Laser Ranging (LLR) session consisted of a single presentation by T. Murphy about the new APOLLO LLR station. Despite this, he McDonald Laser Ranging Station (MLRS) is still actively engaged in LLR. The LLR station at the Grasse is undergoing a major renovation, which was reported by J. Torre in the *Telescopes, Stations, and Upgrades* session. LLR efforts continue at Matera and Mt. Stromlo, Matera having had some success in the past. There is interest in developing a new lunar-capable station in South Africa, though not presented at this conference. A campaign to perform one-way laser ranging to the Lunar Reconnaissance Orbiter (LRO) was discussed by M. Torrence and J. McGarry in the *Transponders* session.

The talk by Murphy, *APOLLO Springs to Life: One-millimeter LLR*, described the progress of the new LLR station at Apache Point in New Mexico. The station began lunar ranging operation in October 2005, attaining science-quality data beginning April 2006. APOLLO routinely achieves a large-enough photon count to achieve one-millimeter statistics. Peak rates approach one photon per pulse at 20 Hz, with ten-minute normal points sometimes consisting of several thousand photons. The 4×4 avalanche photodiode array and 16-channel timing system permits multi-photon returns, the strongest of which to date is 9 photons in a single pulse. Murphy also described the gravitational physics goals of APOLLO, revealing that LLR has already placed 0.1% limits on gravitomagnetism—the phenomenon behind Lense-Thirring precession.

APOLLO SPRINGS TO LIFE: ONE-MILLIMETER LUNAR LASER RANGING

T. W. Murphy, Jr. [1], E. G. Adelberger[2], J. B. Battat[3], C. D. Hoyle[4], E. L. Michelsen[1], C. W. Stubbs[3], and H. E. Swanson[2]

1. UC San Diego, MC-0424, 9500 Gilman Drive, La Jolla, CA 92093-0424, USA;
2. University of Washington, MC-351560, Seattle, WA 98195-1560, USA;
3. Harvard University, Dept. of Physics, 17 Oxford Street, Cambridge, MA 02138, USA;
4. Humboldt State University, Dept. of Physics, Arcata, CA 95521, USA;

Abstract

The Apache Point Observatory Lunar Laser-ranging Operation (APOLLO) obtained its first lunar ranges in October of 2005, achieving over 2000 photons in a 30-minute period. Subsequent operations have seen as many as 2500 photons in less than ten minutes, with a peak photon rate of 0.6 photons per pulse, or 12 per second. The major elements of the system are described, with performance examples and a look at the data precision.

Introduction

Lunar Laser Ranging (LLR) has long provided many of the best tests of gravity, currently claiming the best limits on:

- the weak equivalence principle, to $\Delta a/a < 1.4\times10^{-13}$;
- the strong equivalence principle to $\eta < 4.5\times10^{-4}$;
- time-rate-of-change of the gravitational constant, G, to $< 10^{-12}$ (fractionally) per year;
- gravitomagnetism to < 0.1%;
- geodetic precession to < 0.7%;
- inverse square law to 10^{-10} times the strength of gravity at $\approx 10^{8}$ m scales.

Many of these latest results are presented by Williams et al., (2004) [1]. The gravitomagnetic effect produces six-meter deformations in the lunar orbit at two different frequencies [2], each determined by LLR to sub-centimeter accuracy. Though the phenomenologies of gyroscopic precession (frame dragging) outside a rotating body, orbital (Lense-Thirring) precession of the LAGEOS satellites, and orbital distortions of the lunar orbit may appear to represent distinctly different physics, they all stem from the same term in the equation of motion. This is analogous to the seemingly different rotation of a draining tub and trajectory deflection due to the Coriolis force, though both stem from the same root physical cause.

The APOLLO Apparatus

The APOLLO apparatus is situated at the Apache Point Observatory in southern New Mexico, at 2780 m elevation. The laser is permanently affixed to the 3.5 m telescope, so that a rotation of the telescope tertiary mirror allows efficient sharing with other astronomical programs. The median atmospheric seeing at the site is 1.1 arcseconds (at zenith). The telescope is flexibly scheduled, so that APOLLO is able to get 1.5-hour time slots every few days during the accessible part of the lunar month.

Laser

APOLLO's laser is a Leopard SS-20 model from Continuum Lasers. It is a flashlamp-

pumped Nd:YAG system delivering 120 ps infrared pulses via acoustic mode-locking and cavity dumping, operating at 20 Hz. The infrared is frequency-doubled to 532 nm, delivering about 100 mJ per pulse at a pulse-width < 100 ps.

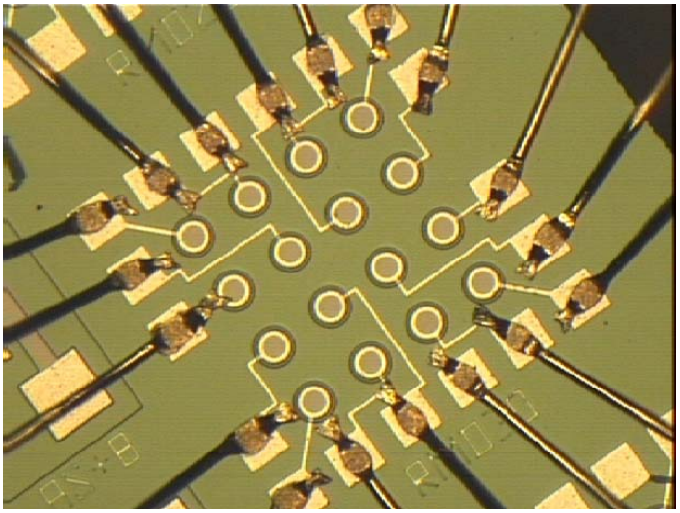

***Figure 1**: 4×4 APD array with 30 μm elements on a 100 μm square grid.*

APD Array Detector

APOLLO uses a 4×4 format avalanche photodiode (APD) array at the re-imaged focal plane (Figure 1). In this way, multiple return photons can be accommodated in a given pulse, each generating a timing signal that is separately time-stamped. A lenslet array placed in front of the detector recovers the fill-factor loss of the bare array. Besides providing multiple "buckets" for the multi-photon return, the resulting 1.4 arcsecond field of view (0.35 arcsec per pixel) yields spatial information about where the telescope is pointing, so that we may maintain tracking lock based on the spatial distribution of the lunar return.

Optical Layout

Figure 2 shows the APOLLO optical layout. Starting at the laser output, the green pulse emerges as a ~7 mm diameter ($1/e^2$) beam with an approximately Gaussian profile, centered 61 mm off of the optical bench. A beam expander (TL1 and TL2) expand the beam to 16 mm diameter prior to the rotating transmit/receive (T/R) optic. Following the T/R optic, the beam encounters a plano-concave lens (L3) that introduces a roughly *f*/10 divergence to the beam so that it may fill the telescope aperture. After L3, the beam experiences two 90° turns on M5 and M4—both of which are multi-layer dielectric coatings for high-efficiency reflection at 532 nm. After this are the telescope's aluminum-coated tertiary, secondary, and primary mirrors (M3, M2, M1). The beam emerges from the primary mirror collimated to well below 0.5 arcsec.

Incoming light from the telescope is brought toward a focus, following the inverse path of the transmit beam, becoming collimated at L3. From here, the path through the T/R optic experiences two 90° turns on M6 and M7, in the process being elevated to ~115 mm off of the optical bench so that it may cross the transmit path. M7 is tip-tilt actuated so that the receiver may be aligned relative to the transmit beam direction. The collimated beam enters the receiver tube via an uncoated glass window, tilted to send the reflected light toward a CCD camera that aids acquisition and alignment. The clear aperture up to this window is maintained to be at least 35 mm so

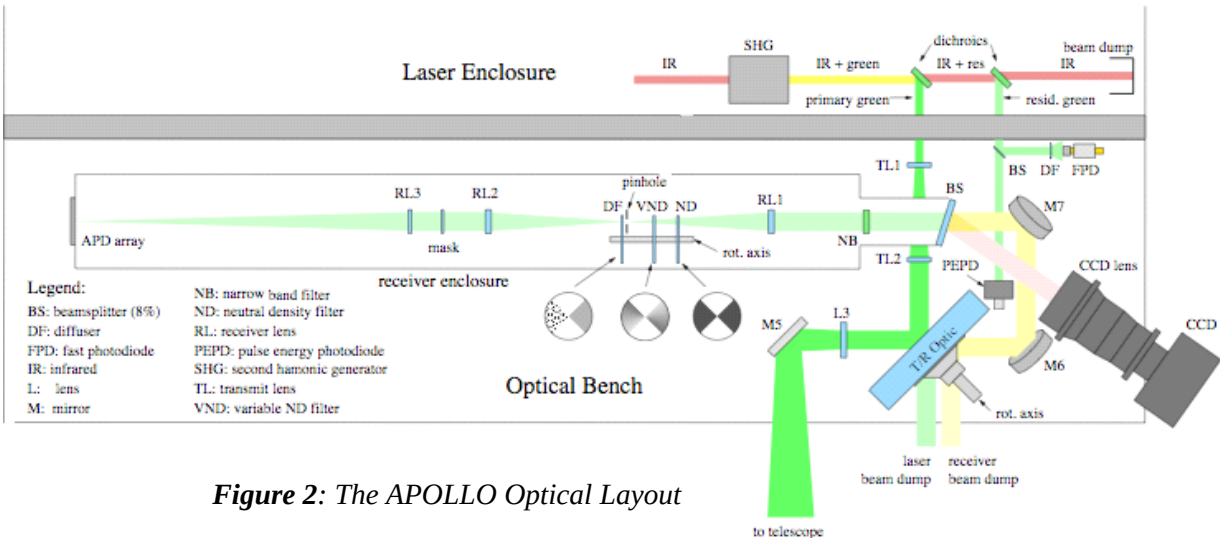

***Figure 2**: The APOLLO Optical Layout*

that a 40 arcsec field of view is preserved for the CCD camera. Past this window, the optics are 25 mm in diameter, which is suitable for the small field of the APD detector array.

A narrow passband filter sits at the front of the receiver tube, with a 1.5 nm FWHM passband centered at 532 nm, and 35% transmission at the center wavelength. Beyond this, a doublet lens (RL1) concentrates the collimated beam to a focus, where a pinhole is placed to act as a spatial filter. The 400 µm hole corresponds to 3 arcsec on the sky. An identical lens (RL2) is placed opposite the pinhole, re-forming the collimated beam. An optional mask in the collimated beam prohibits light originating outside the telescope aperture to proceed. A final lens (RL3) focuses the light onto the detector at the end of the receiver tube. The receiver tube is closely baffled at 50 mm intervals along its entire length so that scattered light from the laser fire is unlikely to survive a trip to the photon-sensitive detector.

Differential Measurement Scheme

APOLLO, like many laser ranging systems, implements a differential timing scheme, referencing its photon arrival times against returns from a local corner cube. This **fiducial** signal (note: often called “calibration” in the SLR community) follows *exactly* the same optical path as the lunar return photons, and is processed by the same timing electronics in the same configuration. The only difference is that optical coatings on the T/R mirror and on the disks near the spatial filter pinhole rotate into

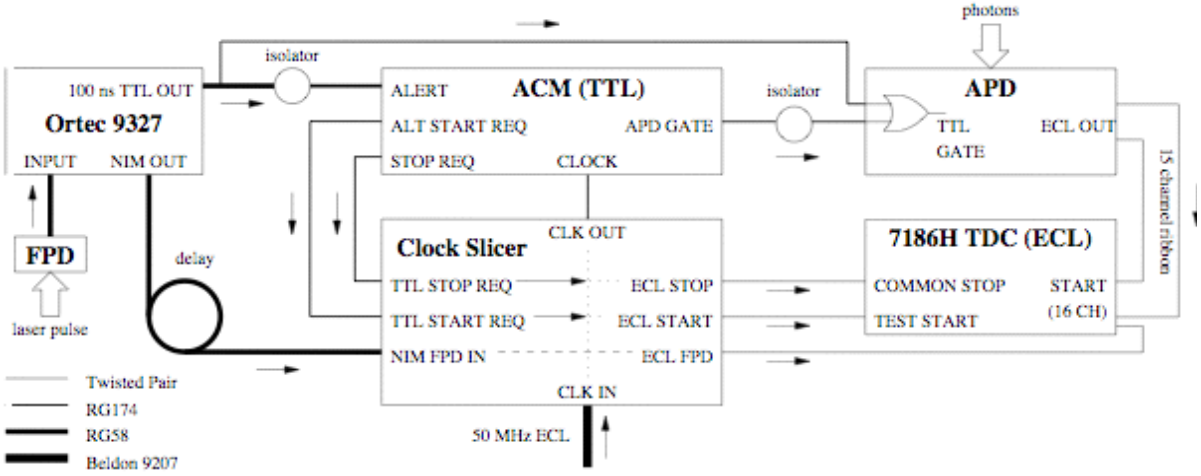

***Figure 3**: The APOLLO Timing System*

the beam to provide an attenuation of ~10^{10}, adjustable over about one order-of-magnitude. The result is a signal level of approximately one photon per pulse (distributed among the APD elements). The disks in the receiver rotate at half the rate of the T/R optic (which itself triggers laser fire events), one side diffusing the fiducial photons to have a roughly uniform distribution within each pupil-imaging APD element. The other side has matching attenuation, but allows the fiducial to be concentrated on each APD element in accordance with the corner cube's spatial location within the telescope entrance aperture. In this way, we can explore the timing bias associated with illumination position within the APD element. See [3] for details on this scheme.

Timing Scheme

The multiplexed timing system for APOLLO is capable of ~20 ps timing on 16 independent channels (common STOP) at rates as high as 4 kHz. The timing system is comprised of:

- a 16-channel time-to-digital converter (TDC): Phillips Scientific model 7186H;
- a Truetime XL-DC GPS-disciplined clock with low phase noise 10 MHz output;
- a 5× clock multiplier producing a 50 MHz ECL clock, preserving low phase noise;
- a custom "clock slicer" module that extracts selected clock pulses out of the train;
- a custom CAMAC module that coordinates gate events and requests clock pulses;
- an Ortec 9327 amplifier/discriminator establishing laser fire time to high precision.

The timing system is depicted in Figure 3. A secondary feature of our setup is the ability to calibrate the TDC by sending pulse pairs based on the 50 MHz clock to the TDC. In this way, we get START/STOP pulse pairs that are integral numbers of 20.00 ns apart. Even so, by arranging the lunar and fiducial photons to use the same 20 ns part of the TDC range (we have control of gate placement up to the clock period), we make the need for this calibration secondary. Running the calibration at 1 kHz at five pulse-pair separations yields 1000 measurements per setting in a five second period.

Example Data Runs

We present here example data from recent APOLLO runs to illustrate the system performance and capabilities.

Figure 4 shows the result of a 10,000 shot (500 second) run on Apollo 15—an array of 300 3.8-cm-diameter corner cubes. The first half of the run was spent optimizing pointing and beam offset. More than three quarters of the return photons fell within the last half of the run, producing an average rate of 0.33 photons per shot.

Figure 5 shows a 10,000-shot run on Apollo 11 (100 3.8 cm corner cubes) that followed the Apollo 15 run shown in Figure 4. Having optimized the signal in the previous run, the signal rate is steady in the Apollo 11 run. The 0.11 photon-per-pulse average return rate is consistent with the 0.33 result from Apollo 15, given the difference in array sizes.

The APOLLO error budget is dominated by the temporal spread arising from the libration-tilted finite-sized corner-cube arrays. Typically contributing about 20–50 mm root-mean-square (RMS) spread (less for the smaller arrays), we need approximately 400–2500 photons to achieve 1 mm random uncertainty. The above examples show that APOLLO is capable of achieving this in few-minute timescales.

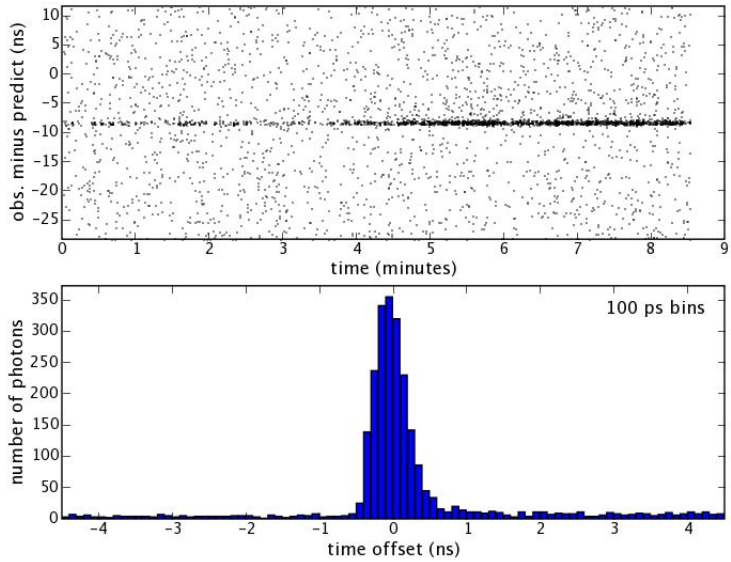

***Figure 4**: Apollo 15 run: 10,000 shots, 2000 lunar returns, 1670 of those in last half (following system optimization). Photon rate average in last half: 0.33 per pulse.*

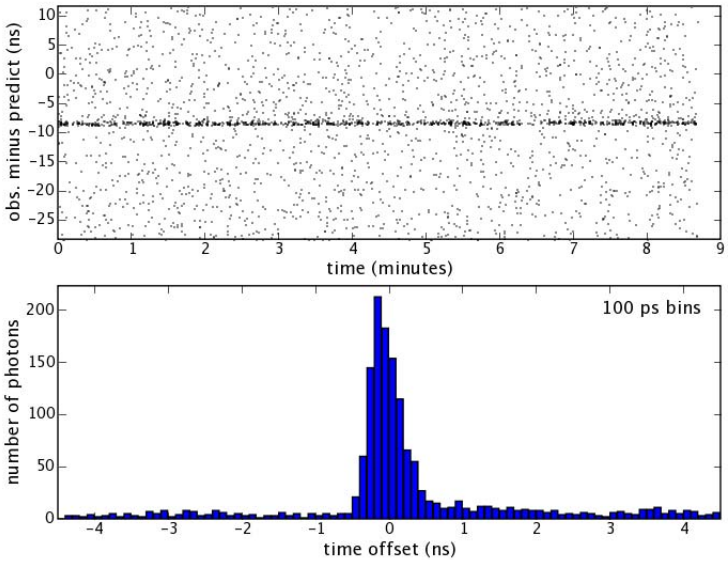

***Figure 5**: Apollo 11 (3 times smaller than Apollo 15) run: 10,000 shots, 1100 lunar returns*

Fiducial Data

An example of APOLLO fiducial data is shown in Figure 6. This particular set coincides with the lunar data presented in Figure 4. Shown here are the time histograms between the arrival of the cable-delayed fast-photodiode signal and the fiducial corner cube APD signal for the various APD channels. The absolute value (about 6 ns on average) is not fundamental, being affected by the cable delay between these signals. The offsets between channels *is* relevant, however, as this information is needed to properly register the lunar return photons among the various APD channels. The consistent shapes indicate that all channels behave similarly in the time domain (channel 8 is an exception). Channels 3 and 5 are inactive. The channel 15 input on the TDC is used to mark the fast photodiode (laser start) reference time. This is expected to fall at a random time relative to our 50 MHz clock, thus producing a uniform histogram 20 ns wide. The time axis is reversed in these histograms

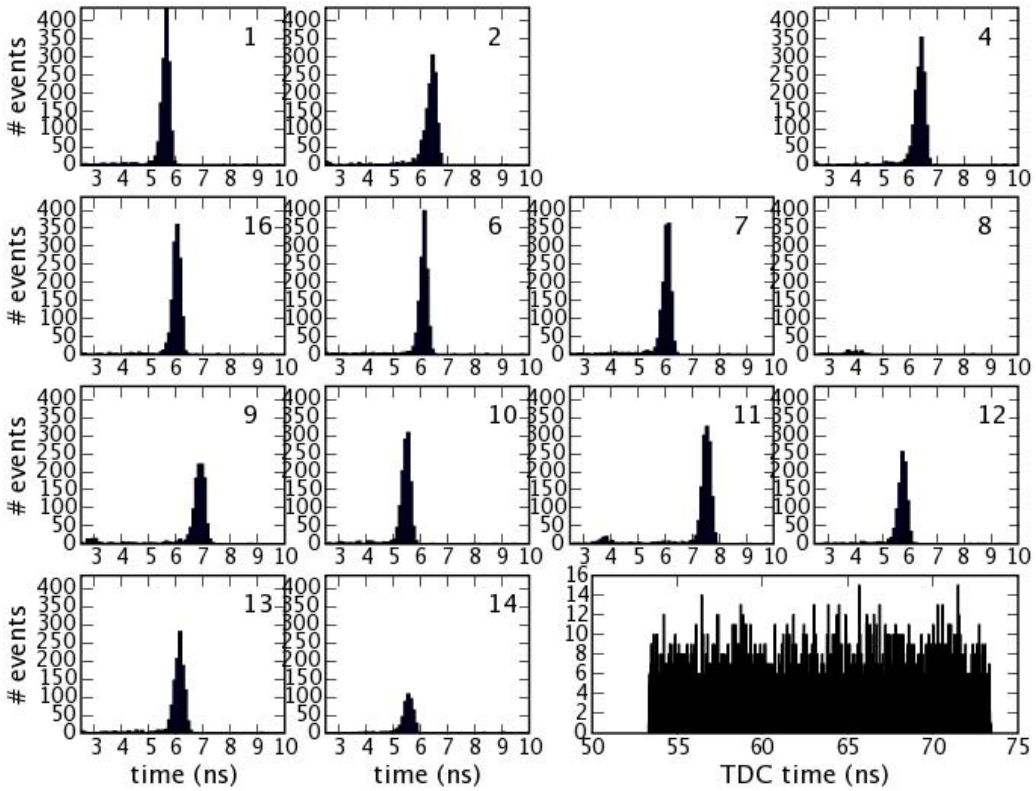

Figure 6*: The fiducial events recorded for the run shown in Figure 4 for each APD channel, at 100 ps per bin. The time axis is reversed from the histogram in Figure 4. Channel 15 is used for the fast photodiode/Ortec signal (pictured in the wide panel), and channels 3, 5, and 8 are effectively inoperative.*

compared to the one shown in Figure 4. The asymmetry is due to the APD response: some photoelectrons take longer to produce an avalanche than the typical, prompt, photoelectron.

APOLLO Performance Summary

APOLLO has achieved routine operational status, and began to gather scientifically useful data beginning in April 2006, with a regular cadence established in October 2006. More than a year of data is needed to see the impact of APOLLO's ranging capability on gravitational physics, so this should come about late in 2007. At this time, some of APOLLO's first year accomplishments are:

- As many as 2500 photons in a 500 second period
- Peak rates of ~0.6 photons per pulse, over 30 second intervals
- Range with ease at full moon (initial October 2005 acquisition at full phase)
- As many as 9 lunar return photons detected in a single pulse
- In strong runs, ~50% of photons arrive in multi-photon groups—even when the average rate is 0.25 photons per pulse

References

[1] Williams, J. G., Turyshev, S. G., and Boggs, D. H., "Progress in Lunar Laser Ranging Tests of Relativistic Gravity," *Physical Review Letters*, **93**, 261101, (2004)

[2] Murphy, T. W., Nordtvedt, K., and Turyshev, S. G., "Gravitomagnetic Influence on Gryoscopes and on the Lunar Orbit," *Physical Review Letters*, **98**, 071102, (2007)

[3] Murphy, T. W. et al., "APOLLO: Meeting the Millimeter Goal," *Proceedings of the 14th International Laser Ranging Workshop*, pp. 165–173, San Fernando, (2004)

TARGETS AND RETURN SIGNAL STRENGTH SESSION SUMMARY

Chair: Tom Murphy

This session consisted of five talks, three of which dealt with target design, testing, and analysis, and two of which dealt with absolute calibration of return signal strengths from laser ranging targets.

D. Arnold presented a summary of analytical results spanning a wide variety of topics, including: range corrections to LAGEOS and LARES; wavelength correction to LAGEOS for 850 and 425 nm light; Apollo lunar array diffraction patterns; hollow cube thermal analysis; retroreflector arrays for high-altitude satellites; diffraction patterns from and thermal analysis of Russian corner cubes; and range corrections associated with multi-photon returns to a single-photon avalanche detector (SPAD).

G. Delle Monache presented an overview of the Space Climatic Facility (SCF) in Frascati—a space/earth/sun simulation facility used to examine the thermal properties of retroreflector arrays in a space environment. The presentation included example thermal images of LAGEOS/LARES corner cubes under simulated space conditions, a description of the SCF's far-field diffraction pattern test capability, preliminary test results of the GPS3 array as part of the ETRUSCO experiment, and plans to test a LAGEOS mock-up in the near future. An invitation was extended to perform thermal tests of other retroreflector systems at the LNF facility.

V. Shargorodsky and V. Vasiliev described a new two-layer nested glass sphere retroreflector target, 17 cm in diameter, 7.5 kg in mass, with a 100,000 m^2 cross-section at 532 nm. The spherical target has been built, and is currently undergoing measurement tests of the return pattern in various conditions. The expected launch date is late 2007. Also presented was a concept possibility for a multi-layer retroreflective sphere that would work at two colors.

T. Murphy presented signal strength results from the APOLLO LLR station, comparing the highest return rates to date with a detailed link budget. Realistic diffraction patterns and de-rating factors were applied to the Apollo arrays. The result was a return signal strength substantially weaker than expected, by a factor of 15. Dust or surface abrasion are likely to blame.

J. Luck and C. Moore presented the results of a study to see if Optus-B or similar targets could be used to calibrate the return strength from other targets. By comparing return strengths from Optus-B and GPS on a variety of nights with similar pointing angles within a given comparison, they found that the measured cross-section ratio agreed with the theoretical ratio to better than 15%—suggesting such inter-comparisons as a viable technique for characterizing the performance of targets in the space environment.

Retroreflector Studies

David A. Arnold

1. 94 Pierce Road, Watertown, MA 02472, USA.

Contact: david-arnold@earthlink.net +1 617-924-3811.

Abstract

This paper discusses studies being done on retroreflectors. Complete reports are available for some, and others are ongoing projects. The studies include a preliminary transfer function for the LARES retroreflector array; computation of the wavelength correction for LAGEOS 850–425 nm; the cross-section of the Apollo lunar retroreflector arrays; parametric thermal analysis of a hollow beryllium retroreflector; retroreflector arrays for high-altitude satellites; measured diffraction patterns of retroreflectors; thermal simulations of coated and uncoated solid cube corners; and modelling of the response of a SPAD detector to various retroreflector arrays.

Introduction

This is an abbreviated version of the paper. The full paper in PDF format is available at http://www.ilrscanberraworkshop2006.com.au/workshop/day6/overview.asp or on the SPWG website in WORD format at http://nercslr.nmt.ac.uk/sig/signature.html.

LARES preliminary transfer function

The variations in range are reduced by the square root of the number of cube corners. Since LAGEOS has 4 times as many cubes as LARES the averaging is better by about a factor of 2. Because the radius of LARES is about half the size of LAGEOS the range correction is smaller. The two effects cancel each other approximately so the variation in the range correction is about the same for both satellites.

Wavelength correction for LAGEOS 850nm-425nm

Table 1 shows the wavelength correction (mm) vs velocity aberration (microradians). The average wavelength correction between 32 and 38 microradians is 2.806 ±.2 mm. The input polarization is circular.

***Table 1**: Range correction as a function of velocity aberration*

30	32	34	36	38	40
2.615000	2.773500	2.891750	2.865250	2.696250	2.465750

Cross section of the APOLLO Lunar retroreflector arrays

The APOLLO Lunar retroreflector arrays use a 1.5 inch diameter uncoated fused silica retroreflector with no intentional dihedral angle offset. The front face is recessed by half the diameter in a cavity with a 1.5 degree flare on the first APOLLO array and a 6 degree flare on the two later arrays. The cutoff angle with no flare would be 27.7 degrees. With the 1.5 degree flare it is 28.3 degrees. With the 6 degrees flare it is 30.3 degrees. Since the APOLLO retroreflectors are uncoated, there is loss of total internal reflection at certain incidence angles. The cross section has been computed vs incidence angle.

Parametric thermal analysis of hollow cubes

Equations have been derived for making order of magnitude estimates of the thermal gradients in a hollow Beryllium retroreflector due to absorption of solar radiation. The performance of the retroreflector can be degraded by thermal warping of the plates or changes in the dihedral angles between the reflecting plates as a result of differential expansion and contraction. The equations consider the case of conduction through the plate and along the plate.

Putting numbers into the equations shows that conduction through the plate is not a problem because the conduction path is wide and the path length short. Conduction along the plate can be a problem because the path length is long and the conduction path is narrow. Thermal distortion of the plates is acceptable as long as the cube corner is not larger than about 2 inches and the plate has a low solar absorptivity such as 7 percent.

Retroreflector arrays for high altitude satellites

Tables 2 and 3 show the area and mass of the cube corners needed to obtain a cross section of 100 million sq meters at the altitude of the GNSS satellites and a cross section of one billion sq meters at geosynchronous altitude.

***Table 2**: GNSS*

Design	# of cubes	Diam. in	Area sq cm	Mass g
uncoated	50	1.3	428	1000
coated	400	0.5	508	460
hollow	400	0.5	508	201
hollow	36	1.4	356	400
GPS	160	1.06	1008	1760

***Table 3**: Geosynchronous*

Design	# of cubes	Diam. In.	Area sq cm	Mass g
Uncoated	165	1.7	2415	7457
Coated	1153	.7	2863	3638
Hollow	1153	.7	2863	1590
Hollow	122	1.8	2003	2863
Single dihedral	22	2.0	446	708

Measurements of Russian cube corners

The data used in this analysis were kindly provided by Vladimir Vasiliev. A measurement of a reference mirror the same size as the cube corner is used for absolute calibration of the cross section of the cube corner. The first cube corner is a very high quality diffraction limited cube and the second is a typical cube corner. The cross section of the typical cube is larger than that of a diffraction limited cube corner past about 20 microradians.

Thermal simulations of Russian cube corner

These simulations were done using a very simple thermal simulation program that has been used only to give order of magnitude effects. The cube corners have no intentional beam spread. The isothermal diffraction does not show sufficient cross section at 26 microradians to account for the nominal cross section of the GPS array. The simulations with solar illumination show that thermal gradients could spread the

beam sufficiently to increase the cross section of the GPS array to 20 million sq meters that is the nominal cross section. The simulations show that the thermal gradients disappear quickly when the solar illumination stops. This could make it difficult to study the effect of thermal gradients in the laboratory. In the absence of a detailed engineering data on the cube corners the only way to know how the Russian cube corners behave is by laboratory testing.

Laboratory tests of cube corners

The space climactic facility at LNF in Frascati, Italy presently has a section of the LAGEOS retroreflector array, a section of LARES cube corners, and the third GPS array that contains Russian cube corners. The plan is to take diffraction patterns similar to those described in section 7 of this report and do thermal vacuum tests to measure the response of the cube corners to solar radiation. These test results can be compared to the simulations given in section 8 of this report. There will probably be significant differences between the simulations and the laboratory tests because of the limitations in the modelling.

Modelling of the response of a SPAD detector to a distributed signal

My analysis programs compute the range correction of a retroreflector array for centroid and constant fraction discriminator detection systems. All single photoelectron systems measure the centroid. For multi-photoelectron signals the range correction for a SPAD detector requires modelling the current vs time as a function of the time of arrival of each photoelectron. The exponential model of a SPAD assumes the number of charge carriers increases exponentially after a photon is detected until the available charge carriers are depleted. Tom Murphy has suggested modelling the number of charger carriers as a quadratic function of time on the assumption that the region of charge carriers is a thin disc whose radius increases linearly with time. The actual behaviour is complex. The rise time of a SPAD detector is a function of the number of photoelectrons. The CSPAD detector compensates for the number of photoelectrons for a point reflector. In the exponential model the rise time is independent of the number of photoelectrons. The exponential model does not explain the observed dependence of the rise time on the number of photoelectrons.

Simulations with the exponential model indicate that the measured range decreases if additional photoelectrons arrive before the current from the first photoelectron has increased to a large value.

***Table 4**: Two-photon bias*

x	0.0	2..6	5.2	10.4	15.6	20.8	26.0	52.0
Δr	3.60	2.66	1.77	0.72	0.28	0.10	0.04	0.00

In Table 4, 'x' is the one-way distance between the reflection points of two photoelectrons. Δr is the decrease in the measured one-way range due to the second photoelectron. For millimeter accuracy ranging the effect is significant for the first centimeter.

The modelling of a SPAD is complex. Unless one has a good model the only way to study the effect of a photoelectron that arrives a short time after the first is to do an experiment. For example, the target calibration vs signal strength could be done with a flat target and with a target where half the area is at position zero and the other half is a few millimeters farther away.

The INFN-LNF Space Climatic Facility for LARES and ETRUSCO

D. Arnold[1], G. Bellettini[2], A. Cantone[3], I. Ciufolini[4], D. G. Currie[5], S. Dell'Agnello[3], G. O. Delle Monache[3], M. Franceschi[3], M. Garattini[3], N. Intaglietta[3], A. Lucantoni[6], T. Napolitano[3], A. Paolozzi[6], E. C. Pavlis[7], R. Tauraso[2] and R. Vittori[8]

1. NASA-GSFC.
2. Univ. of Rome Tor Vergata, Italy.
3. INFN – LNF, Laboratori Nazionali di Frascati, Italy.
4. Univ. of Lecce, Italy.
5. Univ. of Maryland, College Park, USA.
6. Univ. of Rome La Sapienza, Italy.
7. Univ. of Maryland, Baltimore, USA.
8. Italian Air Force.

Abstract

The construction of the LNF Space Climatic Facility (SCF) started in Frascati, Italy, in 2006. The initial purpose was to study the thermal thrusts (TTs) of LAGEOS I/II satellites and to perform the full space-climatic and laser-optical characterization of the new LARES laser-ranged test mass. In late 2004 the construction of LARES was proposed to INFN, which then gave the scientific approval of the LARES experiment in November 2006.

The modular and evolutionary design of the SCF turned out to be well suited to characterize the thermal and optical performance of retro-reflector CCR arrays deployed on GNSS constellations. For this purpose, the groups of INFN-LNF, Rome-Tor Vergata plus R. Vittori in 2006 proposed to INFN a new experiment, ETRUSCO ("Extra Terrestrial Ranging to Unified Satellite COnstellations"). ETRUSCO was approved by INFN in October 2006. This paper describes the SCF and the first preliminary measurements and thermal simulations.

The SCF Apparatus

A schematic view of the SCF is shown in Fig. 1. The steel cryostat is approximately 2 m length by 1 m diameter. Inside this vacuum shell the shield, black painted with the high emissivity paint Aeroglaze® 306, is cooled down to 77 K by forced LNF2 flow. When the SCF is cold, the vacuum is typically 10^{-6} - 10^{-5} mbar.

The thermal input loads are provided by a Solar Simulator (SS) and an infrared (IR) Earth Simulator (ES). The SS is located outside, behind a quartz window (36 cm diameter, 4 cm thickness), which is transparent to the solar radiation up to 3000 nm. The ES located inside, is an Al black-painted disk (diam. 300 mm) held at 254 K by thermo coolers (TECs). A support fixture on the ceiling holds the prototype in front of the simulators. The distance of prototype from the ES is such to provide the CCRs with the same viewing angle in orbit (~60^{o} for LAGEOS). A Germanium window on the right side of the SCF allows for the acquisition of thermograms of the prototypes with an IR digital camera.

The SS (www.ts-space.co.uk) gives a 40 cm diameter beam with close spectral match to the AM0 standard of 1 Sun in space (1366.1 W/m^2), with a uniformity better than ± 5% over an area of 35 cm diameter. The spectrum is formed from the output of two sources, namely an HMI arc lamp (UV-V), together with a tungsten filament lamp (Red-IR). The quartz halogen lamp (with the tungsten filament) has a power of 12 KW, while the metal halide lamp has 6 KW power. These two sources are filtered

such that when the two beams are combined with a beam splitter/filter mirror, the resulting spectrum is a good match to AM0 in the range 400–1800 nm. The spectrum has also been measured also from λ = 1500 nm up to 3000 nm and found to be in reasonable agreement with the AM0 over this extended range. The absolute scale of the SS intensity is established by exposing the beam to a reference device, the *solarimeter*, which is a standard www.epply.com thermopile.

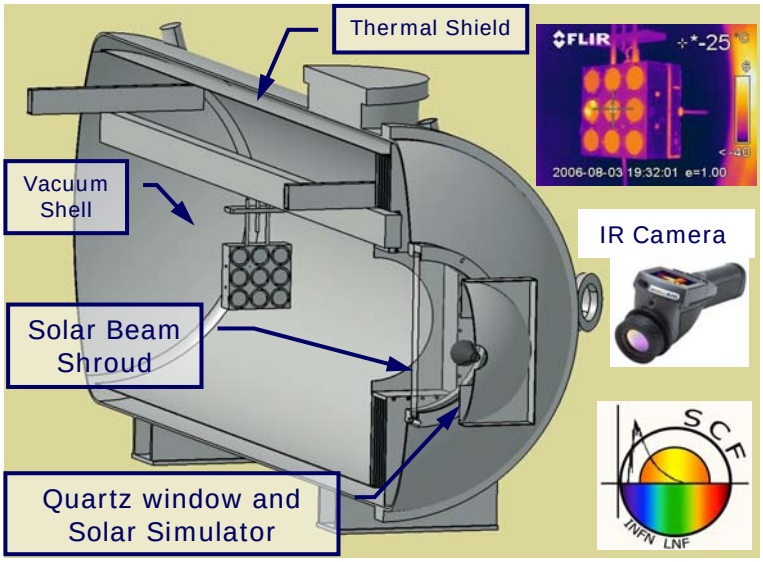

***Figure 1**: The LNF Space Climatic Facility with a retro-reflector array inside.*

The temperature DAQ system consists of an IR camera for non-invasive, high spatial granularity measurements and class-A PT100 RTDs with 4-wire readout. The IR camera is a ThermaCAM® EX320 by http://www.flir.com. The camera focal plane array detector is an un-cooled Vanadium Oxide micro-bolometer with spectral range 7.5 ÷ 13 μm. This camera has a true, built-in 320 x 240 pixel array, field of view/min focus distance 25° x 19° / 0.3 m and thermal sensitivity 80 mK. Since the EX320 factory accuracy is 2 K, the PT100s will be used for cross calibration. The PT100s are certified to have an accuracy of 0.1 – 0.3 K between 273 K and 373 K, which has been checked with a reference thermometer of absolute scale accuracy < 0.1 K, in a range appropriate for LAGEOS. The PT100s are also used below 250 K, outside the working range of the IR camera.

***Figure 2**: The 3×3 LAGEOS matrix built at LNF and the CCR assembly components.*

Thermal Characterization of LAGEOS Retro-reflectors

The thermal relaxation time of LAGEOS and LARES CCRs, τ_{CCR}, has never been measured in realistic climatic conditions. Computations vary by 300%. The goal for LARES and LAGEOS is to measure τ_{CCR} at ≤10% accuracy. This will make the error on the measurement of the Lense-Thirring effect due to thermal perturbations

negligible (permil level; [1] and references therein). A prototype called "3×3 matrix" has been built by LNF to measure directly τ_{CCR} and the time relaxation constant of the retainer Al rings (see fig. 2).

The program of measurements to be done on LAGEOS prototypes is described in [1] and will not be repeated here. The Aluminium base of this prototype has been held at constant temperature by the TECs (for example T(Al) = 298 K), in order to simulate the average temperature of LAGEOS, while the CCR assembly components experience the SS and ES thermal loads in varying climatic configuration. Note that the baseline LARES design uses the same type of LAGEOS CCRs.

The SCF includes thermal software for simulation and parametric design of spacecrafts and/or components. LNF is using the following package from http://www.crtech.com/: Thermal Desktop, the CAD-based geometric thermal modeler, RadCad, the radiation analysis module and orbital simulator, Sinda-Fluint, the solver. With this software, we estimated the overall TTs on LAGEOS during the eclipse due to the Earth shadow (see ref. [1]). With the SCF a preliminary thermal measurement with the ES as the only thermal input has been performed. The measured steady-state temperature of the CCR shows a fair match with the simulated thermal model of the 3×3 matrix (see fig. 3). It should be pointed out, however, that this preliminary test has been carried out with a non-optimized configuration of the screws and retainer rings (in terms of the materials used and of the torque applied to the screws) and that the temperature scale of IR camera was not fully calibrated. Once the thermal model will have been tuned to the final data it can be used for the complete thermal analysis of the LAGEOS satellites (and for the parametric design of LARES).

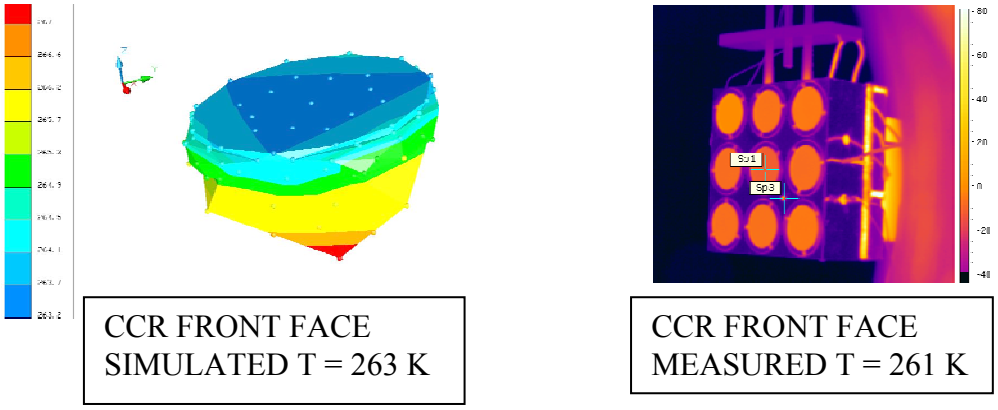

***Figure 3**: Comparison of the steady state CCR temperature measured with the SCF (ES only) and modelled with the thermal software, in a specific test configuration.*

Figure 4 shows the result of another preliminary in-air test at STP conditions, which was performed with the SS as main thermal load (at 75% of the nominal intensity). This was done mainly to exercise the whole system during a maintenance period of the SCF.

The SCF is now being upgraded with one optical-quality fused silica window to measure the far field diffraction patterns (FFDPs) of CCRs inside the SCF in realistic space conditions. Integrated thermal and optical tests will be performed on the CCRs of the LAGEOS "sector" prototype of NASA-GSFC (fig. 5). The finish of its Al surface is believed to be highly emissive (20% - and it will be measured) like for LAGEOS I. The sector contains 37 CCRs of good optical quality (in terms of the

accuracy of the dihedral angle offsets) with an outer diameter of 34 cm, well within the diameter of the SS beam.

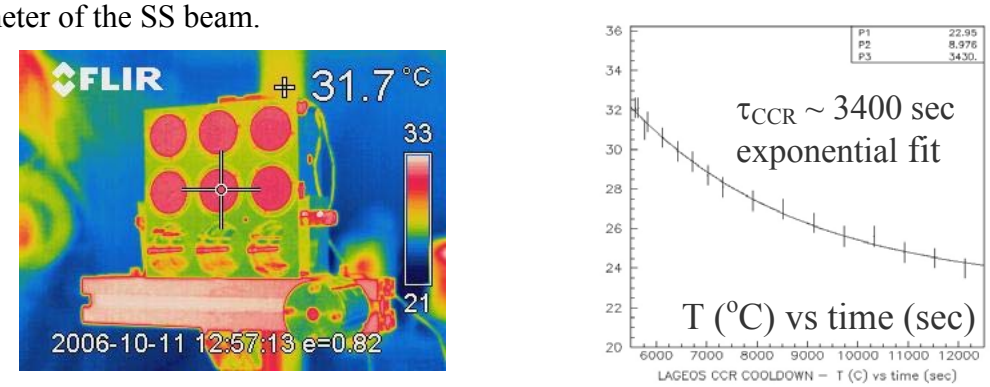

***Figure 4**: Cool-down curve of a LAGEOS CCR in-air and STP conditions.*

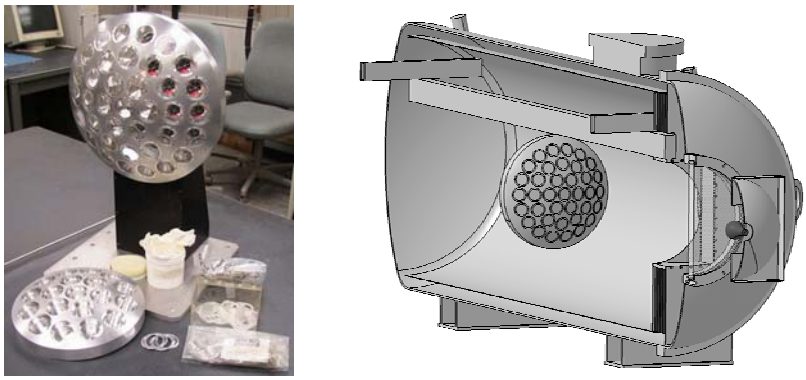

***Figure 5**: Engineering model of LAGEOS (circa 1992) property of NASA-GSFC. This LAGEOS sector is now at LNF for thermal and optical testing at the SCF.*

ETRUSCO (ExtraTerrestrial Ranging to Unified Satellite COnstellations)

The "unification" refers to the addition of laser ranging to the standard microwave ranging of GNSS satellites. Our aim is to perform a complete thermal and laser optical characterization of different CCR arrays used for existing and future GNSS constellations.

A preliminary in-air and STP test of a flight model of the third CCR array to be deployed on a satellite of the GPS block II has been done at LNF. This so-called "GPS3" array is identical to the ones installed on the GPS 35 and 36 satellites in orbit and is property of the University of Maryland (C. O. Alley et al). The three arrays have been manufactured in Russia. Mechanical drawings for its correct modelling have been provided courtesy of V. Vassiliev of the IPIE, Moscow. The GPS3 is currently at LNF, under a special agreement between NASA-GSFC, UMD and INFN-LNF. to be tested at the SCF. A preliminary test was done with the SS as main thermal load (at 75% of the nominal intensity). Two thermograms are shown in Fig. 6.

Figure 7 shows the thermal behaviour of the GPS3 as measured with the IR camera. A space-climatic test will follow in 2007, under the supervision of D. G. Currie of UMD.

Far Field Diffraction Pattern Measurement

The optical circuit for FFPD measurements at STP conditions is shown in fig. 8. The laser beam profiler is a Spiricon CCD camera. Tests are now performed at STP; final one will be performed with the CCR array in SCF.

Figure 9 shows how the SCF is now being upgraded with one optical-quality fused silica window to measure the far field diffraction patterns (FFDPs) of CCRs inside the SCF.

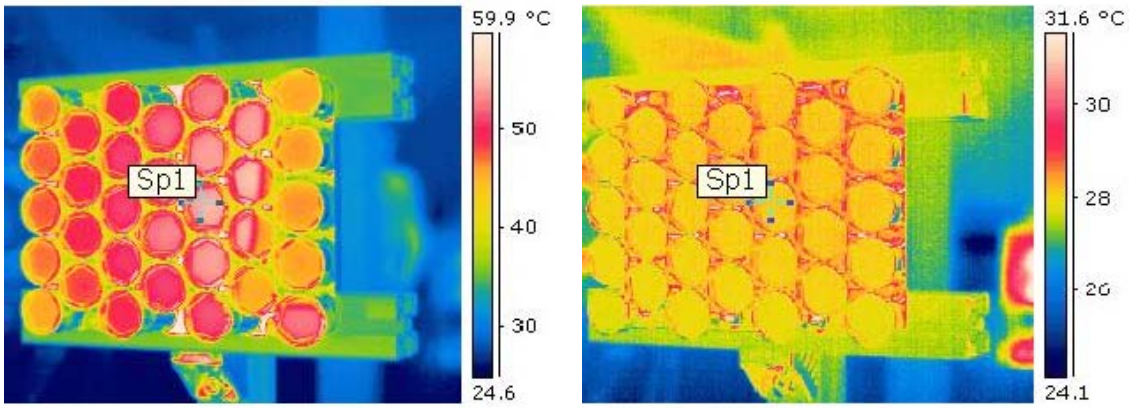

***Figure 6**: Warmest and coolest conditions of the GPS3 retro-reflectors in the LNF STP test.*

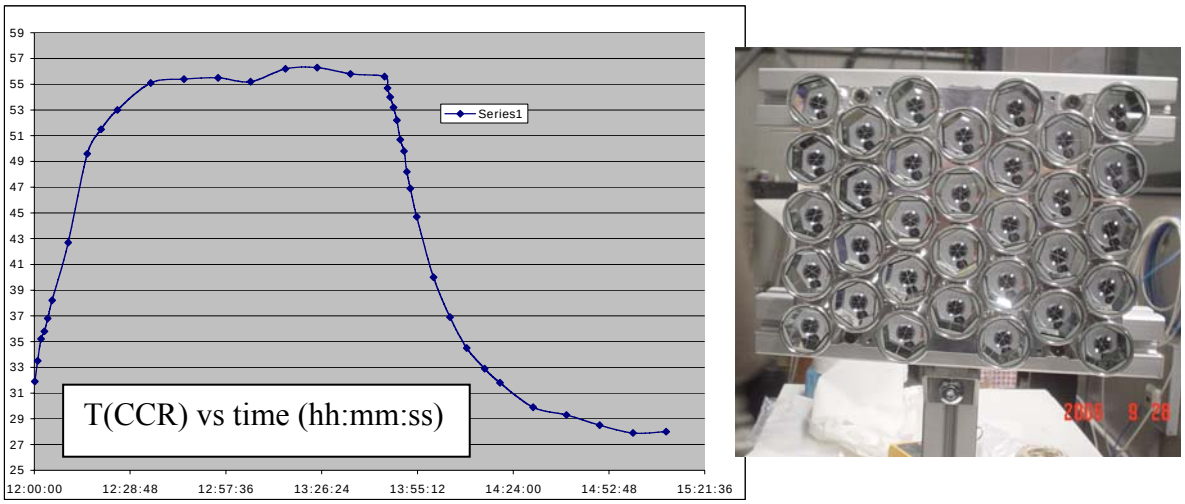

***Figure 7**: Warm-up and cool-down curves of the GPS3, in-ar and at STP at LNF.*

Each CCR will be first exposed to the Sun and the Earth simulators and its thermogram taken by the IR camera from the 45° window. Then, the CCR will be moved in front of the optical window to be exposed to the laser beam and its FFPD recorded (see fig. 10).

Conclusions

At the end of 2006 the SCF has become a permanent, small-size, experimental apparatus of INFN-LNF. The collaboration with ILRS has been very fruitful. Two approved INFN experiments are based for a significant part on the SCF operation: the by-now consolidated LARES mission and the new ETRUSCO experiment. The current upgrade of the SCF, consisting of the integration of the thermal and the laser-optical tests has been funded by INFN, and by LNF, explicitly for ETRUSCO. This funding includes an additional, dedicated optical table to be installed next to the SCF. It does not include the mechanical system(s) for the automated positioning of all the CCRs in the SCF climatic conditions. An endorsement of this work and its scientific motivations by ILRS would be very useful for fund-raising (outside ILRS) and the fulfilment of the ultimate ETRUSCO goals.

References

[1] *Probing Gravity in NEO with High-Accuracy Laser-Ranged Test Masses*, A. Bosco et al, Report INFN-LNF-06-24(P): http://www.lnf.infn.it/sis/preprint/pdf/LNF-06-24(P).pdf. Presented by S. Dell'Agnello at the "Quantum to Cosmos" NASA Int. Workshop, Warrenton (VA), USA, May 2006; to be published in a special issue of Int. Jour. Mod. Phys. D.

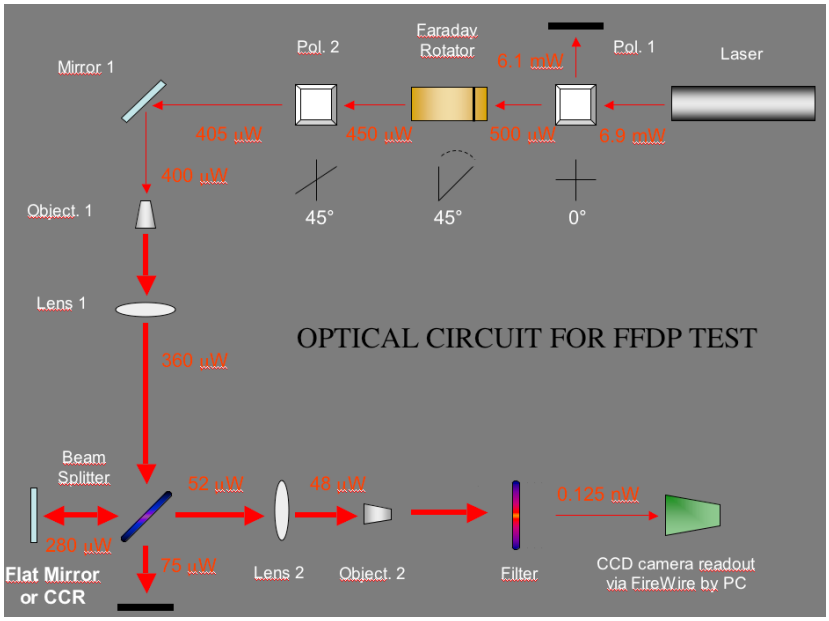

***Figure 8**: Layout of the optical circuit for the FFDP measurement.*

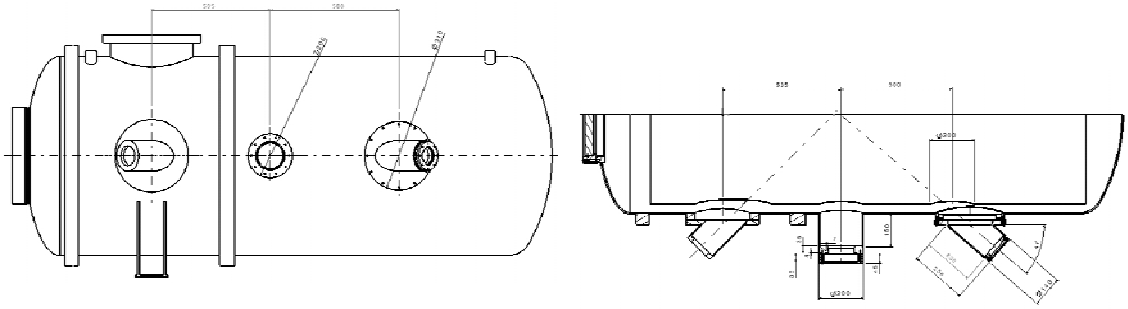

***Figure 9**: Left/central/right windows: IR thermometry, FFDPs and a spare.*

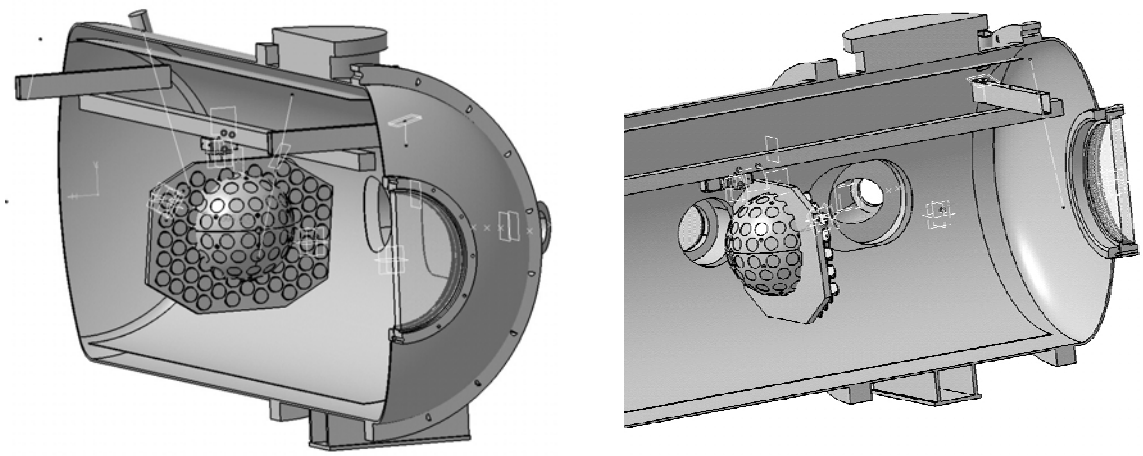

***Figure 10**: The baseline LARES and a GNSS retro-reflector array in the upgraded SCF.*

Absolute Calibration of LLR Signal: Reflector Health Status

T. W. Murphy, Jr. [1], E. G. Adelberger[2], J. B. Battat[3], C. D. Hoyle[4], E. L. Michelsen[1], C. W. Stubbs[3], and H. E. Swanson[2]

1. UC San Diego, MC-0424, 9500 Gilman Drive, La Jolla, CA 92093-0424, USA;
2. University of Washington, MC-351560, Seattle, WA 98195-1560, USA;
3. Harvard University, Dept. of Physics, 17 Oxford Street, Cambridge, MA 02138, USA;
4. Humboldt State University, Dept. of Physics, Arcata, CA 95521, USA;

Abstract

The recently-operational APOLLO lunar ranging station has received lunar return signals as strong as 0.6 photons per pulse over short periods. This signal rate is high enough to allow system optimization and diagnoses that permit careful quantification of system performance. Moreover, observing a spatially flat part of the moon with a well-defined field of view yields a check on the total one-way system efficiency. We are therefore able to compare the lunar signal rate against theoretical expectations as a means of examining the health of the retroreflector arrays after 35 years or more in space. A key part of this analysis is a thorough understanding of the diffraction pattern returned by the corner cube array.

Introduction

Three of the Apollo lunar landing missions placed corner-cube arrays on the lunar surface for the purpose of laser range measurements. The arrays consist of identical 38 mm-diameter uncoated fused-silica corner cubes working via total internal reflection. The Apollo 15 array is three times larger than the first two (Apollo 11 and Apollo 14), making it the preferred target due to its higher return rate. Roughly 85% of laser range measurements to the moon utilize the Apollo 15 array. The present analysis concerns itself only with this array, though results from the others support our conclusions.

The photon count per pulse can be characterized by the link equation,

$$N_{\rm detect} = N_{\rm launch}\eta_{\rm c}^2\eta_{\rm r}\eta_{\rm NB}Qn_{\rm refl}\eta_{\rm refl}\left(\frac{d}{r\phi}\right)^2\left(\frac{D_{\rm eff}}{r\Phi}\right)^2, \qquad (1)$$

where $N_{\rm launch}$ is the number of photons emitted by the laser per pulse, $\eta_{\rm c}$ is the one-way optical efficiency common to both transmit and receive modes, $\eta_{\rm r}$ is the optical efficiency of the receiver, $\eta_{\rm NB}$ is the narrow-band filter peak transmission, and Q is the detector quantum efficiency. The reflector array is composed of $n_{\rm refl}$ corner cubes (300 for Apollo 15), each of diameter, d and efficiency $\eta_{\rm refl}$. The uplink beam has a divergence ϕ, while the downlink divergence is Φ. $D_{\rm ef}$ is the effective diameter of the telescope (such that the collecting area is $\pi D_{\rm eff}^2/4$, and r is the one-way distance between the telescope and the reflector array. The simplified link equation assumes "tophat" diffraction distributions rather than Gaussian or more complicated patterns as a rough estimate of flux in the center of the distribution. We will later abandon this simplification in a refined approach.

The sections below evaluate the terms in the link equation for the recently constructed APOLLO (Apache Point Observatory Lunar Laser-ranging Operation) apparatus [1], comparing the model to observed peak rates. First, the individual terms and their

errors are estimated, followed by a check of the one-way efficiency using the solar-illuminated lunar surface. Then the lunar return is estimated and compared to actual measurements. Ultimately, the calculation is modified to account for a realistic diffraction pattern from the lunar corner cubes. An attempt is made to propagate realistic errors throughout this analysis.

One-Way Throughput

The one-way throughput of the apparatus may be checked by looking at a star or other flux standard using the same detector path employed in detecting lunar laser returns. This checks the quantity $\eta_c \eta_r Q$ in the link equation.

The η_c and η_r terms are composed of a number of optical efficiencies, evaluating to 0.51±0.03 and 0.29–0.58, respectively. Atmospheric transmission, measured to be 0.87 for one airmass at 550 nm at Apache Point, is included in η_c. The large range on η_r stems from the fact that the APOLLO detector only spans 1.4 arcseconds on a side. Therefore, a point source above the atmosphere may overfill the array depending on atmospheric seeing. Despite the large range, given knowledge of the seeing we can estimate this parameter to ~10% precision, leading to a ~12% estimate on η_r. The detector quantum efficiency, *Q*, is roughly 0.30. This number matches theoretical expectations based on device structure, and the flux calibration to a flux standard is in agreement with this figure. The effective diameter of the Apache Point 3.5 meter telescope is 3.26 m.

For the purpose of estimating the one-way throughput when looking at a flux standard, we need to know that the effective bandpass of the narrow-band filter is $\Delta\lambda_{NB}$ = 0.95 nm, and that the integration time is Δt_{APD} = 95 ns per APD gate event. We use the flux calibration standard that a zero-magnitude source at 532 nm wavelength has a flux density of $F_0 = 3.9\times10^{-11}$ W m^{-2} nm^{-1}. The number of photons we see per gate event is then

$$N = \frac{\pi}{4h\nu} F_0 10^{-0.4m} D^2 \Delta\lambda_{NB} \Delta t_{APD} \eta_c \eta_r Q \,, \qquad (2)$$

where *m* is the stellar magnitude, and $h\nu$ is the photon energy. During full moon, we estimate the darker-than-average terrain around the Apollo 15 reflector to have a surface brightness of 3.60 magnitudes per square arcsecond. This translates to 2.87 magnitudes into the 1.4×1.4 arcsecond field of view. Accounting for the fact that only 13 of the 16 APD elements are operational, the expected lunar background rate is: $N_{lunar} = 0.40 \pm 0.08$ photons per gate. Comparing this to the measured full-moon background rate of 0.40 photons per gate, we claim to understand the one-way efficiency of our system. Similar analysis on a focused star yields similar results.

Lunar Return Rate

Simplified Calculation

Populating the terms in Equation (1), we take $\eta_{NB} = 0.35 \pm 0.025$, $N_{launch} = f_{launch} E_{pulse} / h\nu$, with $f_{launch} = 0.6 \pm 0.03$ as the geometrical loss of the Gaussian beam propagating out of the 3.5 meter telescope, and $E_{pulse} = 0.100$ J. Setting $n_{refl} = 300$, d = 0.038 m, $\eta_{refl} = 0.93$, $r = 3.85\times10^8$ m, $\phi = 0.8 \pm 0.12$ arcseconds, and $\Phi = 10 \pm 1.5$ arcseconds, we get an expected lunar return into the APD array (with its particular pattern of dead pixels) of: $N_{detect} = 12.0 \pm 6.1$ photons per pulse. If we use the information we get from the one-way system check, we

reduce the uncertainty by a small amount to ±5.6 photons per pulse.

Observed Lunar Return Rate

The APOLLO lunar return rate is highly dependent on atmospheric seeing and pointing. Not only does the illumination of the reflector scale as the inverse square of the seeing scale, the finite and small APD field of view truncates flux in poor seeing. Seeing of 2.0 arcseconds produces a return rate ten times smaller than at 1.0 arcseconds, if perfectly centered in both cases. For the present analysis, we use the two highest return rates observed in the first six months of APOLLO operation: 9 December 2005, and 17 January 2006. Both nights had exceptional seeing. On each night, we saw return rates of ≈ 0.5 photons per pulse over < 30 second intervals. In each case, telescope pointing and beam offset were optimized for the best signal.

The estimate of expected lunar rate above is 24 times the observed rate. Even though the analysis is a simplified version, the discrepancy is large, and difficult to eliminate through reasonable choices of parameters.

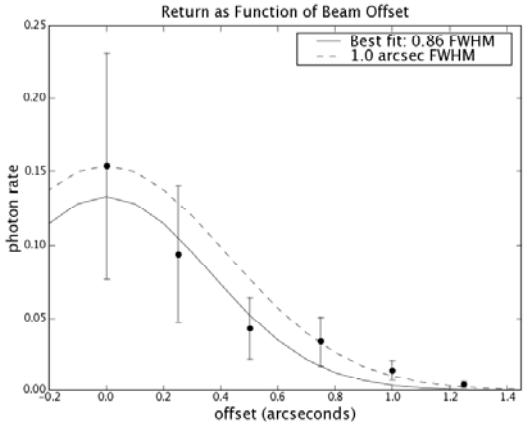

Figure 1*: Beam offset optimization on 9 Dec. 2005. At offset steps of 0.25 arcsec, it is clear that the beam size is less than 1.0 arcsec. Error bars are estimated at 50%.*

The effective beam size on the moon (affected by seeing and optical configuration) is the most obvious place to suspect poor understanding. As for the seeing, the median seeing at the Apache Point Observatory is 1.1 arcsec at zenith. Since the nights used for comparison had especially good seeing, we may assume the seeing to be less than 1.1 arcsec, and likely around 0.8 arcsec. But more convincingly, by rastering the beam pointing on the moon (while keeping the receiver fixed at the same location) we can demonstrate the sensitivity to beam offset, and see directly that the beam illumination footprint on the moon has a full-width at half-maximum (FWHM) less than one arcsecond (Figure 1). Though the best fit in Figure 1 is 0.86 arcsec FWHM, we have chosen 0.8 arcsec in the present analysis because the periods we have chosen for comparison represent the very best 30 second periods within ~10 minute runs. We therefore expect the conditions to have momentarily been better than the average for the run.

It should be noted that the multi-photon capability of APOLLO's detector array renders us insensitive to skewed statistics arising from the structure of the beam's speckle pattern on the moon. In the present analysis, some pulses are seen with as many as 6, 7, or 8 photons. We do not underestimate our return rate by missing these top-heavy events.

Refined Calculation

In the preceding analysis, we made the gross simplifying assumption that the beam patterns were uniform across a circular region—a so-called "tophat" profile. A more realistic calculation should:

- treat the outgoing beam as having a Gaussian profile;
- consider the theoretical diffraction pattern from a perfect corner cube;
- allow for manufacturing tolerance of the corner cubes;
- account for the reduced corner cube throughput as a function of incidence angle;
- de-rate the return strength due to thermal distortions of the corner cube;
- compensate for velocity aberration of the returning beam.

In this section, we treat each of these issues in turn, ultimately producing a more realistic estimate of the return rate, with less uncertainty.

A circularly symmetric Gaussian flux distribution has a peak irradiance that is ln2 ≈ 0.69 times the irradiance of a tophat whose diameter is the same as the Gaussian FWHM and carries the same total flux. Thus we multiply the return rate by this factor.

A corner cube prism employing total internal reflection (TIR) produces a diffraction pattern that is significantly different from that of an equivalent circular aperture. As seen in Figure 2, there is a central core of concentrated flux surrounded by a roughly hexagonal pattern containing significant flux. The core follows the Airy function that would be produced by a perfect circular aperture of the same diameter as the corner cube, but at a peak flux only 27% that of the Airy function, ignoring the two-way reflective surface loss. At normal incidence, the TIR pattern contains 36% of the total energy within the first Airy ring of radius $1.22\lambda/D$, where λ is wavelength and D is the diameter of the aperture [2]. This is compared to 84% for the Airy function.

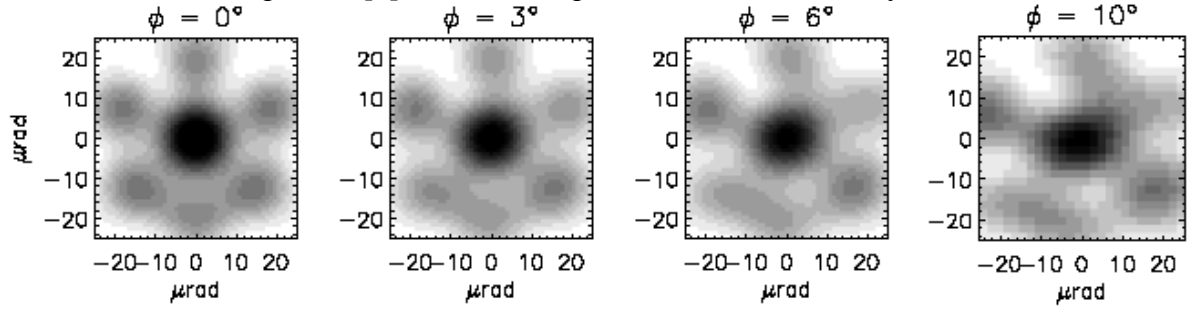

***Figure 2**: Sample diffraction patterns from an Apollo corner cube as a function of incidence angle. Data courtesy David Arnold.*

Compared to a tophat flux distribution with angular diameter λ/D, the normal-incidence TIR diffraction pattern has a central irradiance that is 0.182 times the tophat irradiance if both contain the same total flux. Including the 0.93 two-way front-surface reflection loss from fused silica (η_{refl}), the Apollo corner cubes produce a diffraction pattern with a central irradiance 0.169 times that of the comparison tophat. For the Apollo cubes and $\lambda = 532$ nm, the tophat diameter is 2.89 arcsec.

The manufacturing tolerance for the mutual perpendicular faces of the Apollo corner cubes was specified as ±0.3 arcsec [3]. It was reported that the central intensity of each corner cube selected for flight was at least 90% of the theoretical value. As such, we adopt a factor of 0.93 to provide a representative scaling of manufacturing imperfection.

Corner cubes have an effective cross section that is a function of the incidence angle. For circularly-cut fused silica corner cubes, this function is linear near normal incidence, with 4.3% loss per degree offset. In addition, the Apollo corner cubes are recessed in aluminum mounting structures by half their diameter, or about 1.9 cm. The recesses have conical flares, with half-angles of 1.5° for Apollo 11, and 6° for both Apollo 14 and 15. Together, these factors reduce the throughput by as much as a factor of two for the most extreme libration-induced tilts of 10° (Figure 3).

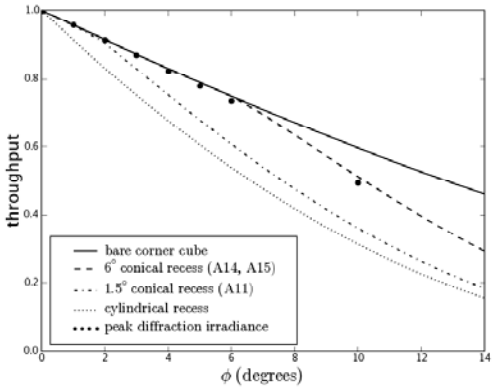

***Figure 3**: Corner cube throughput as a function of incidence angle and recess geometry. The single points come from diffraction patterns (as in Figure 2). Data courtesy Jim Williams.*

The thermal performance of the Apollo reflector arrays in the lunar environment was modeled and tested in great detail prior to flight. The primary performance degradation stems from thermal gradients within the corner cubes, which both deform the optical surfaces and present a refractive index gradient within the material—leading to distortion of the reflected wavefront [4]. For the Apollo 15 array, the central irradiance may be as low as 0.7 times the isothermal value. The original analysis presented plots of degradation as a function of sun angle for the three arrays, from which it is possible to evaluate the thermal degradation factor for any particular lunar phase [5].

Because the lunar reflector is in relative transverse motion with respect to the earth station—due both to the lunar orbit at ≈ 1000 m/s and earth rotation at ≈ 400 m/s—one must account for the angular shift in the diffraction pattern, amounting to $2\Delta v/c$. This amounts to 0.8–1.2 arcsec (4–6 μrad) depending on the vector sum of the relevant velocities. Given the functional form of the central region of the TIR corner cube diffraction pattern, this translates to a signal degradation of 0.64–0.86, or 0.75 on average.

Putting these factors together, we find that the response from the ideal TIR corner cube suffers a factor of 0.20–0.86 degradation. If one then treats the corner cube diffraction pattern as a λ/D tophat function, a pre-factor of 0.034–0.146 must be applied to the link equation. This is equivalent to a tophat function 8–15 arcsec in diameter with no degradation pre-factor.

Analysis of Two Cases

As mentioned before, we use two epochs—both at a return rate of 0.5 photons per pulse—to compare against the return estimate. Table 1 summarizes the various de-rating factors, and estimates resulting from the analysis. The squared atmospheric de-rating as a function of zenith angle has been included (belongs in η_c, technically).

The static factors shown in Table 1 represent the outgoing Gaussian beam profile, the TIR diffraction profile with surface reflection, and the manufacturing tolerance.

***Table 1**: De-rated return rate estimates for the two comparison epochs.*

Parameter	**Epoch 1 value**	**Epoch 1 de-rating**	**Epoch 2 value**	**Epoch 2 de-rating**
Velocity Aber.	1.09 arcsec	0.71	0.86 arcsec	0.81
Angular Offset	3.94°	0.84	4.04°	0.81
Sun Angle	–73°	0.85	35°	0.70
Range	371425 km	1.15	404301 km	0.82
Zenith Angle	50°	0.84	23°	0.97
Static Factors	0.69×0.169×0.93	0.108	0.69×0.169×0.93	0.108
Total de-rating		0.053		0.040
Return Estimate	8.2±3.4 phot./pulse		6.2±2.6 phot./pulse	
Estimate Ratio	16.4		12.4	

Using the de-rating estimates in Table 1 together with Equation (1), and taking the convention that $\Phi = \lambda / D = 2.89$ arcsec, we arrive at the conclusion that we see a return rate approximately 15 times weaker than expected. Given that the estimated net error is about 41%, and considering that this is a multiplicative problem, a one-sigma deviation would correspond to multiplying the estimate by (1 – 0.41) = 0.59. A two-sigma deviation corresponds to multiplying by $0.59^2 \approx 0.35$. To bring the discrepancy down to unity, we must be approximately five standard deviations away—a significant result.

To illustrate the robustness of this result, imagine that our estimate of the beam width—our least certain parameter—is less certain than our ±15% estimate. We could achieve the discrepant ratios by letting the beam profile be as large as 2.8–3.2 arcsec, which is not at all consistent with Figure 1, or APOLLO experience in general.

We conclude that the lunar reflectors have suffered performance degradation (ratios between reflectors are as expected) in their > 35 years on the lunar surface. We cannot tell whether the degradation is due to dust or surface abrasion. Recent work proposing a dynamic fountain of dust on the moon may be relevant [6].

References

[1] Murphy, T. W. et al., "APOLLO Springs to Life: Millimeter Lunar Laser Ranging," *Proceedings of the 15th International Laser Ranging Workshop*, Canberra, (2006)

[2] Chang, R. F., Currie, D. G., Alley, C. O., and Pittman, M. E., "Far-Field Diffraction Pattern for Corner Reflectors with Complex Reflection Coefficients," J. Opt. Soc. America, **61**, 431, (1971)

[3] Kokurin, Y. L., "Laser Ranging to the Moon," *Proceedings of the P. N. Lebedev Physics Institute*, **91**, p. 161

[4] Faller, J. E.., "The Apollo Retroreflector Arrays and a New Multi-lensed Receiver Telescope," *Space Research XII*, Akademie-Verlag, p.235, (1972)

[5] Faller, J. E. et al., "Laser Ranging Retroreflector," Chapter 14 of the NASA post-mission report on the Apollo 15 mission

[6] Stubbs, T. J., Vondrak, R. R., and Farrell, W. M., "A dynamic fountain model for lunar dust," *Advances in Space Research*, **37**, 59, (2005)

Experimental Return Strengths from Optus-B and GPS

John McK. Luck[1] and Chris Moore[1]

1. EOS Space Systems Pty.Ltd., Canberra, Australia

Abstract

The return signal strengths from the retroreflector arrays on the Optus-B satellites in geostationary orbits have been compared with those from GPS targets using the High Energy Laser on the 1.8 metre space debris tracking system adjacent to the Mount Stromlo SLR. In the experiments conducted in mid-2006, we performed alternate ranging to an Optus-B then to a GPS while the two targets were in close proximity to minimize atmospheric differences. Each measurement was the setting of the receive-path Neutral Density filter required to extinguish returns, having first maximized the return rate by fine pointing adjustment.

The ratios of the results, after judicious editing of outliers, were in broad agreement with Dave Arnold's calculations of the respective array cross sections. They suggest that this could be a viable technique for calibrating actual performance of arrays in their space environment.

Satellite Retroreflector Arrays

The constellation OPTUS-B1 and OPTUS-B3 constitutes the space segment of the Australian satellite communications system. They are in geostationary orbits. B1 was launched in 1992 and is at longitude 160°E. B3 (1993) is at 156°E. B2 crashed after launch. Each contains a 20cm x 18cm tray of 14 solid cubes of Herseus fused silica, Amasil grade. Their front faces are tri-roundular with inscribed diameter 38 mm coated with indium tin oxide (ITO) over an anti-reflection dielectric layer. Their rear faces are also coated with ITO and have dihedral angles of 0".8 (James et al, 1990; Luck, 1994). The cross-section of each array is $\sigma_O = 46 \times 10^6$ m^2 (Arnold, 2006).

GPS-35 and GPS-36 each host trays of 32 solid hexagonal cubes 27 mm across with aluminium-coated rear faces. The cross-section of each array is $\sigma_G = 20 \times 10^6$ m^2 (Arnold, 2006). The theoretical ratio of cross-sections is therefore $\kappa = \sigma_G/\sigma_O = 0.43$.

Experimental Method

The method was to range to a pair of satellites, one Optus and 1 GPS, in "bursts" in rapid succession while the selected GPS satellite was "close" to the Optus satellite. During each burst, the Neutral Density (ND) filter was adjusted so that returns were just extinguished. The measurement was the ND value at extinguishment. The UTC, ND setting and GPS elevation angle were recorded at that instant. This method relies on the assumption that the photon detection threshold of the detector is both significant and constant.

"Close" means within a few degrees (<10°) in elevation, to minimize variations in atmospheric attenuation, and also in azimuth to minimize cloud attenuation variation. A "burst" was just long enough to optimize the pointing for maximum return rate, then to adjust the ND until extinguishment, ideally less than 5 minutes. Then a burst was done on the other target.

Observations were made on the 1.8 metre space debris-tracking telescope STRK (7826) adjacent to Stromlo SLR at wavelength 1064 nm, power 2-12 W at 50 Hz.

Data Reduction

Define "brightness" B as the return signal strength (e.g. photons/sec at the detector) when pointing is optimized, and let B_e be the brightness at extinguishment so that it corresponds to the detection threshold. B_e is assumed constant. Let P be the measured average power, effectively equivalent to energy per shot since pulse-width, fire rate etc. are constant. Also let N be the transmission through the ND filter, T be one-way atmospheric transmission, R be the range from station to satellite, and S be the actual array cross-section. Then:

$$B = \alpha P N T^2 . S/R^4$$

where α is a proportionality constant. The observed ratio of cross-sections is then:

$$k = S_G/S_O = (R_G/R_O)^4 . P_O N_O T_O^2 / P_G N_G T_G^2$$

where subscripts G and O refer to GPS and OPTUS respectively. We used $N = 10^{-ND}$ where ND is the Neutral Density wheel setting, and:

$$T = \exp[-0.21072\exp(-h/1.2)/\sin E]$$

where *h* is height above sea level (0.8 Km for Stromlo) and *E* is target elevation angle (Degnan, 1993). The two-way transmission is illustrated in Fig.1.

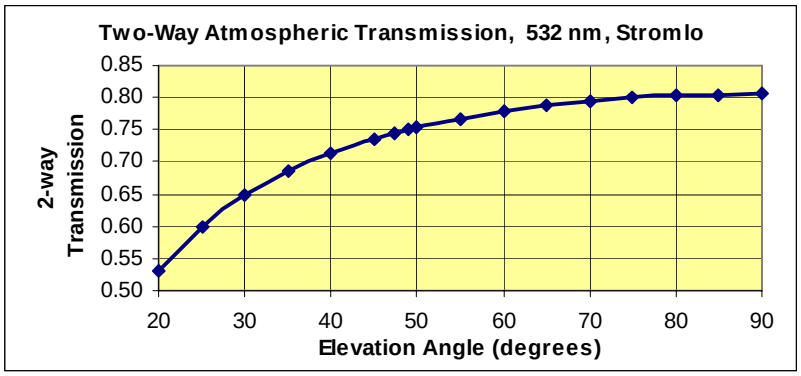

***Figure 1**: Standard atmospheric transmission as a function of elevation angle, Stromlo*

A "standardized brightness" V can be defined for a satellite observed on a given ranging system, as if there was no atmosphere and no ND filter and the transmitted power was 1, normalized to the detection threshold. Thus:

$$V = B_e/PNT^2 \quad \text{and hence} \quad S=R^4V/\alpha.$$

The ratio $\beta = V_G/V_O$ gives the relative standard brightness. Its expected value with R_O = 37180 km (B3, nominal) and RG = 20931 km (GPS36, typical at 49° elevation) is β = 4.28.

Results

Measurements made on 4 clear nights in May 2006 are shown in the Table 1. The column R_G/R_O is the ratio of range (Stromlo to GPS) relative to range (Stromlo to OPTUS). Column S is the cross-sections in square metric (but otherwise arbitrary) units, and column V the standardized brightnesses. There are huge variations, so the greatest and least values of S_G and of S_O were discarded, as were those of V_O and V_G, yielding mean values of:

$S_G = 14.2$ $V_G = 145.8$

$S_O = 34.6.$ $V_O = 34.6$

The ratios of averaged observed cross-sections, and of standardized brightnesses, are:

$S_G/S_O = 0.41$ $V_G/V_O = 4.2.$

The observed cross-section ratio is remarkably close to the predicted $\kappa = 0.43$ given above. The observed brightness ratio similarly is also remarkably close to the predicted $\beta = 4.28$.

Conclusion

It may be that this excellent result is a fluke, but we certainly did not continue observing until we got the right answer! It suggests that this technique might indeed be viable for determining relative cross-sections of retroreflector arrays in actual orbit, provided that a sufficient number of measurements are taken.

***Table 1**: Summary of observations and resulting cross-sections. Optus cross-sections are in green. Rejected outliers are flagged in the right-hand column.*

Date	UTC		Sat	R/R(Opt)	El	P	ND	T	V	S	Rej
May-06	hh	mm			(deg)	(Watts)		(1-way)			
10	9	50	GPS36	0.544	75.9	9	2.75	0.894	78.10	6.84	
	11	2	B1	1	47.4	9	2.15	0.863	21.06	21.06	
	11	9	GPS36	0.598	39.5	9	0.50	0.844	0.49	0.06	*
	11	26	B3	1	48.9	9	4.00	0.866	1480.67	1480.67	*
13	11	0	B3	1	48.9	2	2.00	0.866	66.63	66.63	
	11	10	GPS 36	0.610	40.9	2	3.00	0.848	695.81	96.34	*
	11	20	B3	1	48.9	2	2.00	0.866	66.63	66.63	
15	9	20	B3	1	48.9	12	3.00	0.866	111.05	111.05	
	9	33	GPS36	0.545	85.0	2	1.90	0.897	49.35	4.35	
	9	42	B3	1	48.9	2	0.90	0.866	5.29	5.29	
	9	59	GPS36	0.556	63.6	2	2.30	0.886	127.02	12.14	
	10	3	GPS36	0.560	61.7	2	2.90	0.884	507.80	49.94	
	10	9	B3	1	48.9	2	0.60	0.866	2.65	2.65	
	10	19	GPS36	0.568	55.6	2	2.40	0.877	163.25	16.99	
	10	26	B3	1	48.9	2	0.80	0.866	4.20	4.20	
	10	32	GPS36	0.580	46.2	2	2.10	0.861	84.95	9.61	
	10	42	B3	1	48.9	2	0.80	0.866	4.20	4.20	
	10	44	B3	1	48.9	2	1.00	0.866	6.66	6.66	
	11	0	GPS36	0.603	33.6	2	1.00	0.822	7.39	0.98	
16	9	28	GPS36	0.546	74.8	12	3.50	0.894	329.76	29.31	
	9	44	B3	1	48.9	12	0.60	0.866	0.44	0.44	*
	10	0	GPS36	0.559	62.0	2	1.70	0.885	32.02	3.13	
	10	27	B3	1	48.9	12	2.80	0.866	70.07	70.07	
	10	35	GPS36	0.583	44.4	2	1.20	0.857	10.80	1.25	
	10	42	B3	1	48.9	12	2.30	0.866	22.16	22.16	

Further Suggestions

- Repeat the experiment at 532nm wavelength.
- Extend to GLONASS, GIOVE, ETS-VIII, LARES and others.
- The GPS array is theoretically about 1500 times brighter than Apollo 15, corresponding to ND 3.2, so if GPS is still observable at a station with this setting then LLR should also be acquirable.

- Systems having readouts for return signal strength would be well suited to doing an equivalent of this experiment, more easily. In fact, by using our method as well as their own, our method could be tested.
- Similarly, comparisons of return rates in controlled experiments might assist in validation of the technique.

References

[1] Arnold, D.: Private communications, 2006.

[2] Degnan, J.J.: "*Millimetre Accuracy Satellite Laser Ranging: A Review*", in "Contributions of Space Geodesy to Geodynamics: Technology", David E. Smith & Daniel L. Turcotte (Eds), Geodynamics Series Vol.25, American Geophysical Union, Washington D.C., esp. pp.139-140 (1993)

[3] James, W.E., W.H. Steel & Evans, N.O.J.L: "*Design and Testing of a Cube-Corner Array for Laser Ranging*", SPIE Vol.1400 Optical Fabrication and Testing, p.129 (1990)

[4] Luck, J.McK. & J.R. Woodger: "*Laser Ranging Support for TV Time Transfer Using Geostationary Satellites*", Proc. 8th European Frequency and Time Forum, Technical University Munich, March 9-11, 1994.

Spherical Glass Target Microsatellite

V.D. Shargorodsky, V.P. Vasiliev, M.S. Belov, I.S. Gashkin, N.N. Parkhomenko

1. Institute for Precision Instrument Engineering, Moscow, Russia.

Contact: www.niipp-moskva.ru

Abstract

A new SLR target microsatellite based on the optical Luneberg lens concept is now undergoing ground testing. It will be launched from the carrier spacecraft METEOR-M next year, and will be the first autonomous retroreflector satellite of this type, providing an extremely low target error.

Some parameters are presented of the microsatellite and its orbit, as well as far-field diffraction patterns measured on test bench.

Introduction

Most of the current SLR target satellites are spherical structures carrying a number of corner cube retroreflectors; with the rapid progress in SLR precision during the last decades, some disadvantages of such targets, being insignificant during the first years of SLR development, became increasingly more significant with the passing years.

The disadvantages are:

- It is difficult to obtain target errors less than 1 mm if return signals come from several cube corners having different positions relative to the CoM (Center of Mass) of the satellite.
- Even if the "one direction - one reflector" principle is used (e.g. in the WESTPAC or LARETS satellite design), the active retroreflector position varies relatively to the CoM, and the cube corner internal delay time also varies when the active retroreflector moves away from the line connecting the SLR system with the satellite CoM.
- The return signal strength varies significantly with the satellite rotation.
- The satellite shape is not an ideal sphere, especially for a design using the "one direction - one reflector" principle (WESTPAC, LARETS).
- Interaction with the Earth magnetic field (due to eddy currents induced in the massive metal body): slow-down of spinning, some disturbance of orbital motion.

There is a way to overcome the above difficulties. Instead of a multitude of corner cube prisms mounted on a spherical metal body, the target may be a single spherical retroreflector made of glass.

The initial idea was to use a device similar to the Luneberg lens proposed in 1944 and used in some radio-frequency systems (Figure 1). A planar electromagnetic wave coming from any direction is there focused on opposite surface of the spherical lens and if this surface is a reflective one, the device acts as a retroreflector.

Unfortunately, there are currently no suitable optical materials for correct implementation of such a device operating in the optical waveband.

A possible solution is using of a ball lens made of a glass with an index of refraction exactly equal to 2 (Figure 2). However, it requires a special extra-dense glass of a

high optical quality; this is currently a very hard task. Moreover, calculations show that only a small part of the ball aperture may be effectively used because of the spherical aberration.

The first practical solution was a two-layer glass ball, where the inner part is made of a flint glass having a relatively large index of refraction (1.75), while the outer layer is made of a crown glass with a low index of refraction (1.47). Such a device has been implemented and successfully tested showing acceptable retroreflector parameters [1] (Figure 3).

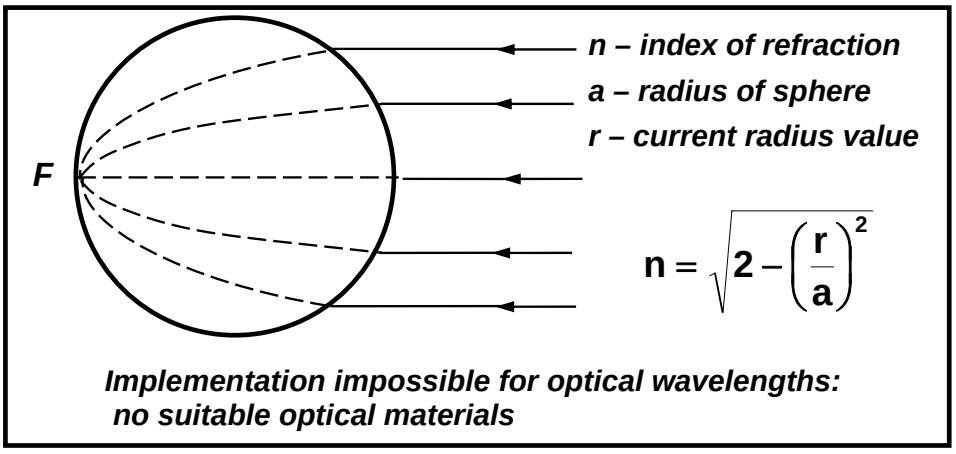

Figure 1. *Luneberg lens principle*

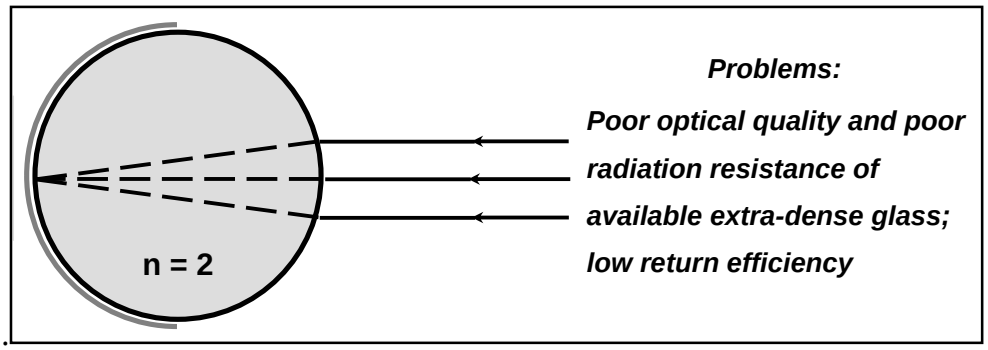

Figure 2. *Ball lens made of glass with index of refraction n = 2*

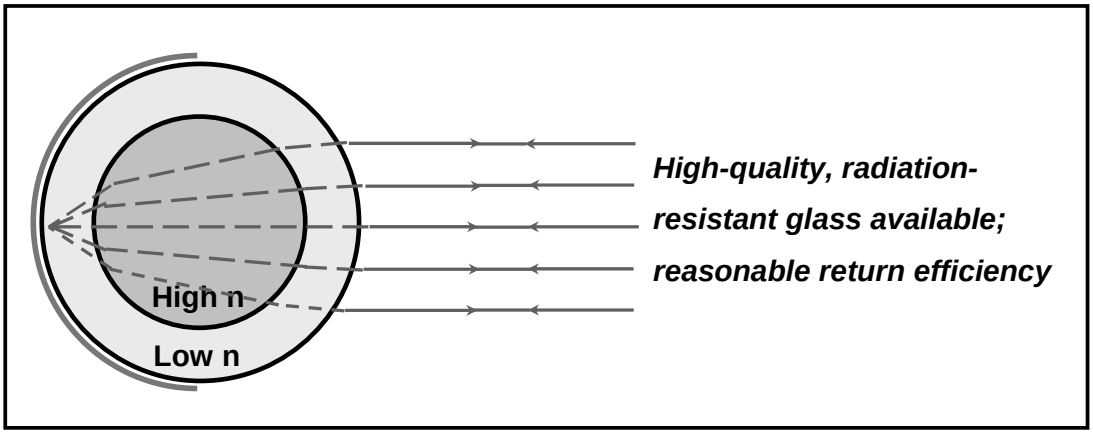

Figure 3*. Spherical retroreflector: a two-layer ball lens*

An experimental 60-mm-diameter spherical retroreflector of this type [2], after being tested in laboratory conditions, has been 10 December 2001 launched into space on board of the METEOR-3M(1) satellite having a 1018.5-km-high circular orbit (Figure 4). During four years of operation, the spherical retroreflector provided precision orbit determination for the SAGE-III experiment.

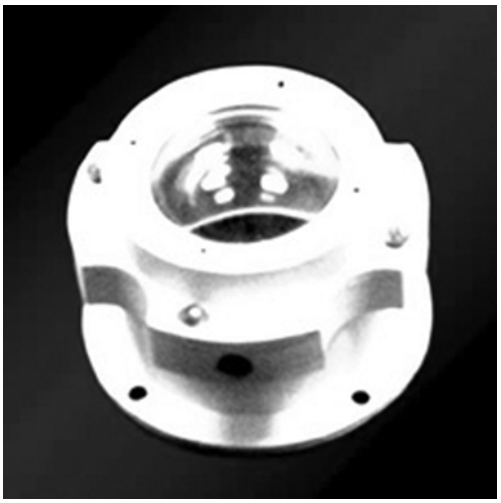

Figure 4*. An experimental 60-mm-diameter spherical retroreflector, launched into space on board of the METEOR-3M(1) 10 December 2001*

The lidar cross-section of this target was low (about 10^4 sq.m at the initial phase of flight), making SLR observations difficult and even impossible for a large part of the ILRS network stations.

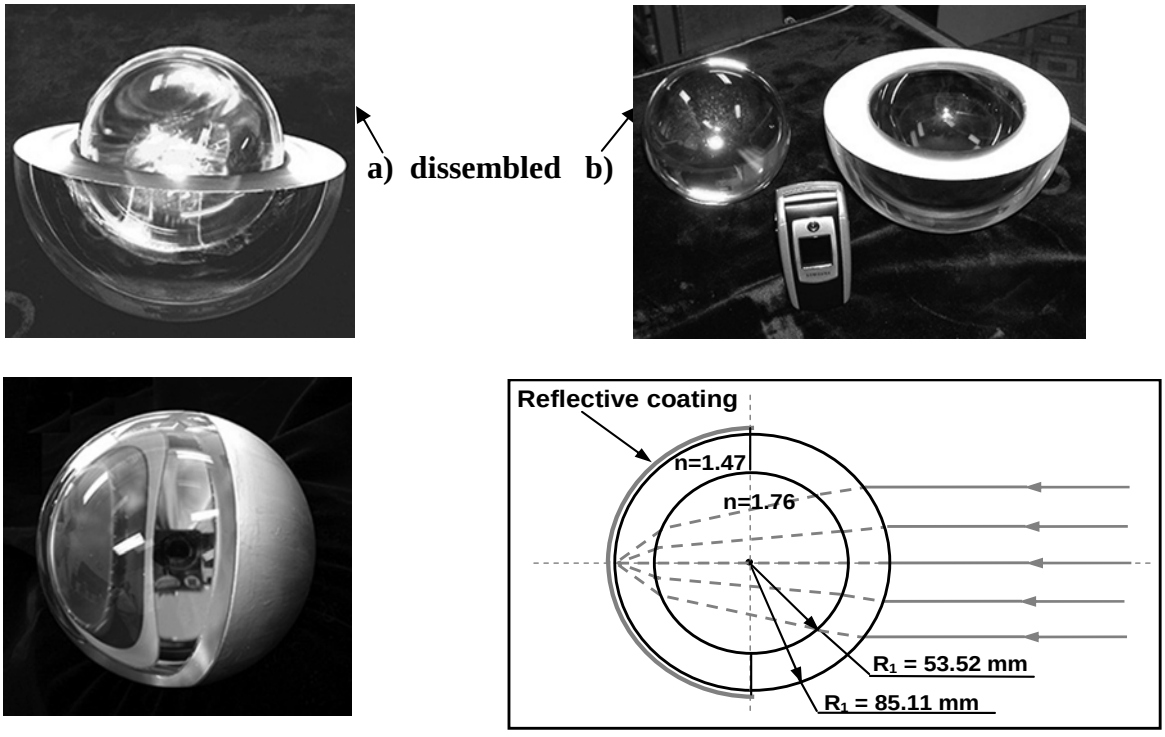

Figure 5. *17-cm-diameter spherical retroreflector*

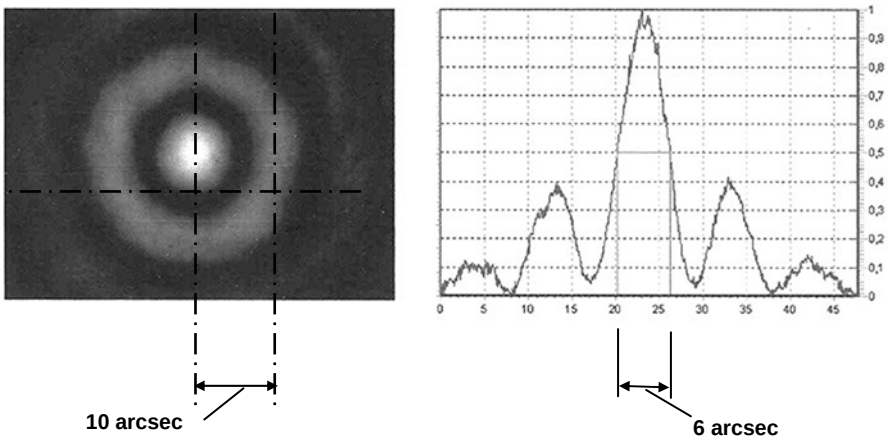

Figure 6. *Far-field diffraction pattern*

We have therefore developed and fabricated a medium-size (17 cm in diameter) spherical retroreflector of this type, which can be used as an autonomous SLR target.

Figure 6 shows the far-field diffraction pattern of this device measured on a test bench. It can be seen from the picture, that most of the return signal energy is in the first-order side lobe (the product of its amplitude and solid angle is more than that of the center lobe).

It is intended to launch this device as an autonomous SLR target, as a piggyback load on the Meteor-M spacecraft. The basic parameters of this micro-satellite are shown in Table 1.

Table 1. *Zero-signature spherical retroreflector micro-satellite*

Microsatellite parameters	
Diameter	17 cm
Mass	7.45 kg
Cross-section	~100,000 sq.m at λ=532 nm
Current status	
Return pattern measurement under varying ambient conditions	
Separation system development	
Mission	
Carrier satellite	METEOR-M
Carrier satellite parameter	Height: 835 km (circular) Inclination: 99.7°
Planned launch date	Late 2007

The separation system (now under development) should provide a spin rate of at least 6 rpm, while the spin axis lies in the plane dividing the ball lens surface into the coated and uncoated parts.

SLR targets of this type may be improved in the following ways:

1. To increase the lidar cross-section, more than two layers of glass may be used. Calculations show that a three-layer ball lens may provide a significantly higher cross-section value than a two-layer one.
2. To provide operation on two widely separated wavelengths (e.g., 532 nm and 1064 nm), a design may be used shown in Figure 7. In the future, such an SLR-target may be attractive for minimization of the atmosphere refraction error using simultaneous two-wavelength ranging.
3. If (or rather when) super-dense optical glass with reflection index values ≥2 with good optical quality becomes available, it may be used for manufacturing of a ball-lens retroreflector microsatellite with a high mass to aperture cross-section ratio.

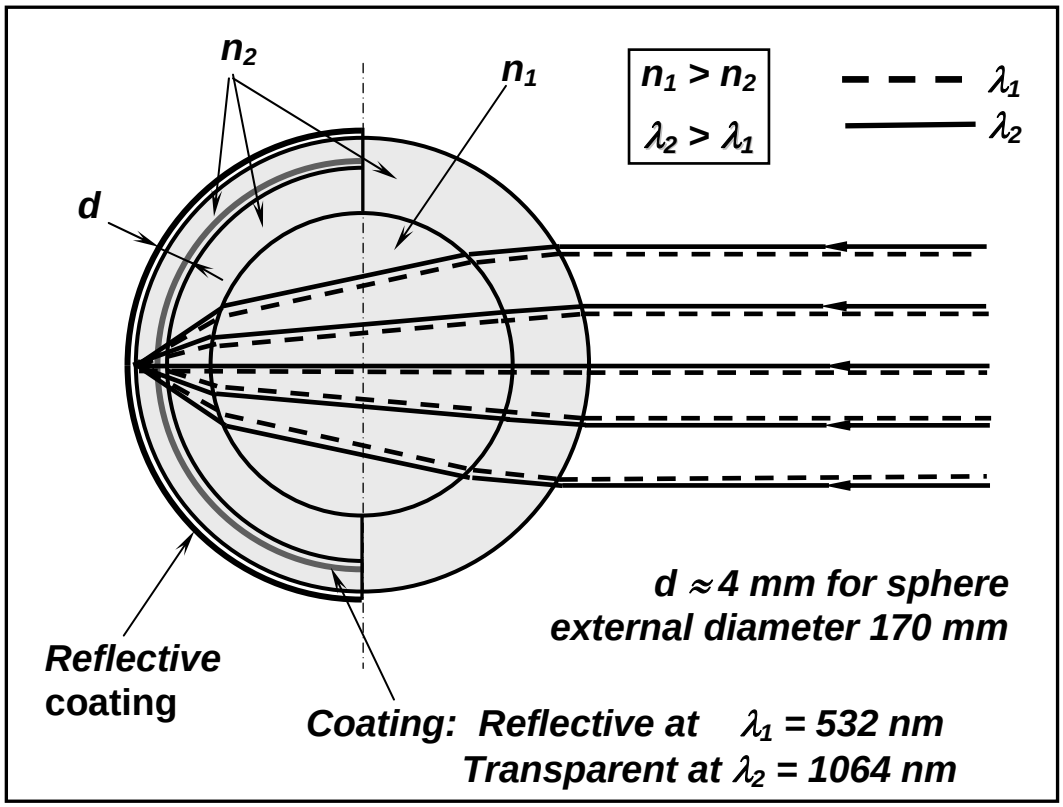

Figure 7. *Spherical retroreflector for operation at two widely separated wavelengths*

References

[1] Vasiliev V. P., Gashkin I. S., Belov M. S., Shargorodsky V. D., A New Approach to a Submillimeter SLR Target Design. Proceedings of 11th International Workshop on Laser Ranging, Deggendorf, Germany, Sep. 1998

[2] Shargorodsky V. D., Vasiliev V. P., Soyuzova N. M., Burmistrov V.B., Gashkin I. S., Belov M. S., Khorosheva T. I., Nikolaev E. A. Experimental Spherical Retroreflector on Board of the Meteor-3M Satellite. Proceedings of 12th International Workshop on Laser Ranging, Matera, Italy, 2000

OVERFLOW SESSION SUMMARY

Chair: Mike Pearlman

Andrew Dmytrotsa gave a paper on the recent upgrading of the Simiez SLR Station. Software and optics upgrades have improved data yield. The laser power supply was replaced with a loaner from the Katzively station after the on-site system failed. Upgrades continue with new servo drivers for the stepper motors.

Julie Horvath reported that the TLRS-4 system has been refurbished, upgraded, and transferred to a new site at Haleakala in Maui. The collocation with Moblas-7 at GSFC achieved closure to 1 - 2 mm and demonstrated full capability on both low satellites and LAGEOS. Operations are anticipated by the end of the year.

Nobuo Kudo gave a paper on "Using SLR, the GPS accuracy verification experiment of ALOS". Twelve selected stations from the ILRS network supported the GPS-SLR validation campaign from August 14 to 31, 2006. The satellite had a payload vulnerable to laser light and this campaign used the new restricted tracking procedures implemented by the ILRS network last year. The campaign showed that the offset between the GPS and the SLR orbits was within a few centimeters RMS, well within the mission requirement.

Hyung Chul Lim presented the "Korean Plan for SLR system development". He described the structure and activities of the Korea Astronomy and Space Science Institute (KASSI). KASSI is building two satellites STSAT-2 and KOMPSAT-5 to be launched in 2007 and 2009 respectively. Both will carry retroreflector arrays for POD. Korea now has about 80 GPS stations and three VLBI stations and plans to build a mobile SLR station and a Fundamental Station that would include a permanent SLR. The development period for these systems will be about 2 years for the mobile system and 5 years for the Fundamental Station. In the meantime, the Chinese will provide a mobile system for use at a site in Korea for some period starting in 2007 to support the STSAT-2 satellites and ILRS requirements.

You Zhao reported on the "Fulfillment of the SLR daylight tracking of Changchun Station". The main thrust of the program is to improve orbit predictions, provide better filtering of sky noise, increase the alignment of the transmitting and receiving beams, and reduce stray light. The plan includes improved spatial, timing, and spectral filtering. The hardware and software improvements are nearly ready for testing. Work had been delayed because the Changchun Station was selected as the main Chinese tracking support for GIOVE-A, and tracking on this satellite took highest priority, but system testing is anticipated by early 2007.

Vladimir Glotov presented "GLONASS status updates; MCC activity in GLONASS Program". The paper reviewed the background and mission of the GLONASS Program which is building toward a 24 satellite complex in the 2009 timeframe. The International GLONASS – Pilot Project (IGLOS-PP) is a pilot service of the IGS to track and analyze data from the satellite constellation. The ILRS provides very important support for GLONASS by tracking three of the constellation satellites as designated by IGLOS. The need will continue and hopefully the tracking will increase. GLONASS provides a "colocation in space", a key tool to strengthening the reference frame. IGLOS-PP demonstrates the ability of IGS to accommodate other microwave satellite systems.

Current Status of ''Simeiz-1873'' Station

A.I. Dmytrotsa[1] , O.A. Minin[1], D.I. Neyachenko[1]

1. SRI Crimean Astrophysical observatory, Crimea, Ukraine.

Contact: dmytrotsa@gmail.com

Abstract

The SLR station "Simeiz-1873" was founded in 1989. After modernization in 2000 we have increased the amount of ranging data by approximately three times. With this modernization we have probably reached a limit of the equipment, due mainly to the shortcomings of the laser transmitter. Independent analysis groups have shown stability problems in of our data.

A permanent GPS receiver was installed at the site in 2000. "Simeiz-1873" became a permanent IGS station (GPS-CRAO) in 2004. Recently in our station began processing GPS data using the GLOBK/GAMIT software. We have obtained and analyzed data for the period 2002-2005.

Introduction

Regular satellite laser ranging started in our observatory in 1976 as an INTERKOSMOS Station with a laser system installed by K. Hamal on a KRIPTON telescope. In 1988 the Crimean Astrophysical Observatory installed a new station (near the old station). Colocations with the IFAG MLTRS system were conducted in 1991.

A modernization program was undertaken in 2000 under a CRDF grant (thanks for M. Pearlman and D. Nugent). New angular encoders and a new time interval counter were installed. After modernization we increased the amount of ranging data by approximately three times (Fig.2).

A permanent GPS receiver has been operating near “Simeiz-1873” since 2000. In 2004 it became an IGS site “GPS-CRAO” (Fig.3, right). The “Simeiz-1873” is a one of four Ukrainian SLR stations. (GLSV-1824, Lviv-1831, KTZL-1893)

Current status

Modernization of station proceeds. It is necessary to carry out the following items:

- Implementation of the new CPF prediction format into the software;
- installation of a new modern control system of engines;
- updating of optical system of a telescope for a new calibration target and replacement of a prism with a mirror;
- ground calibration tests with the new target at 77m east;
- continue processing GPS data with GAMIT/GLOBK.

Ranging and GPS proceeding

In 2006 we suffered appreciable downtime due to two failures of the laser power unit. The Katzively station (1893) has installed a new laser systems and loaned their old power unit to us. The loaned unit also failed and required considerable, time-consuming repair.

As you can see in Fig.2, data has increased with the modernization activities, but we have probably reached the limit with our equipment; the laser transmitter is 18 years

old! The second problem is in tracking. In 2006 we purchased new servo-drivers for the stepper motors and we hope that this will help improve our tracking capability.

Figure 1. *SLR-1873. General view.*

Table 1. *Main elements.*

Element	Description
Mount	Alt-Az. 1m mirror.
Angular encoders	FARRAND CONTROLS, 0.4”
Time interval counter	SR620
PMT	H6533
Time & Freq standard	TC-74, sec. from GPS.
Laser	350 ps, 5Hz. (18 years old)
Software	GUI on a JAVA, server on a C++, low level modules on a C. LINUX.
Ephemeredes	CPF, (on a F77).

Analysis by two independent groups shows that the stability of the station SLR data still needs considerable work. Results from the Ukrainian Center of Determination of the Earth Orientation Parameters (Bolotina, 2006) are shown in fig.3 (left). Similar results were found by S. Schillak by processing our LAGEOS ranging data for period 1999-2003. (See Schillak, 2004).

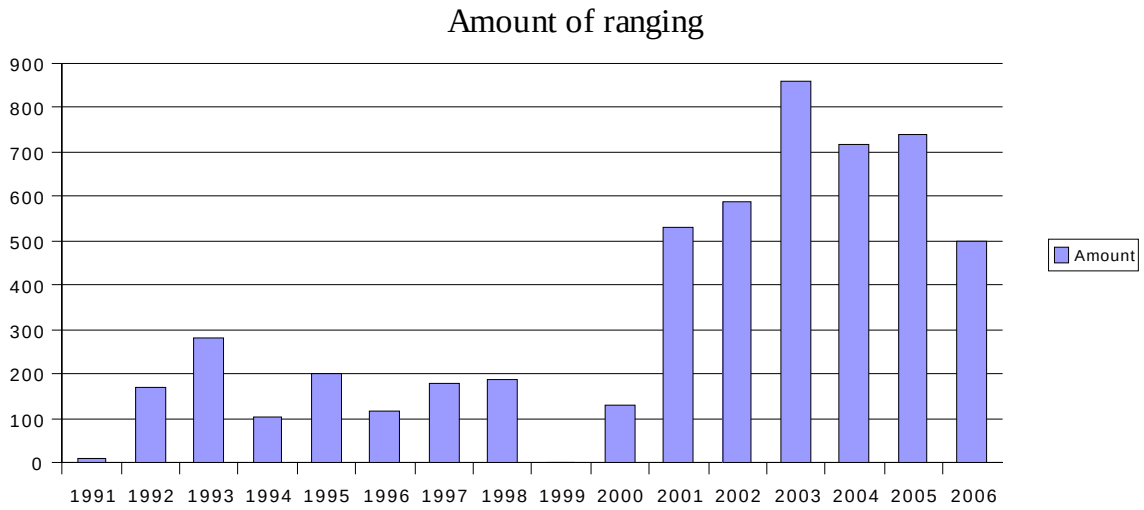

Figure2. *Amount of ranging from 1991 to 2006.*

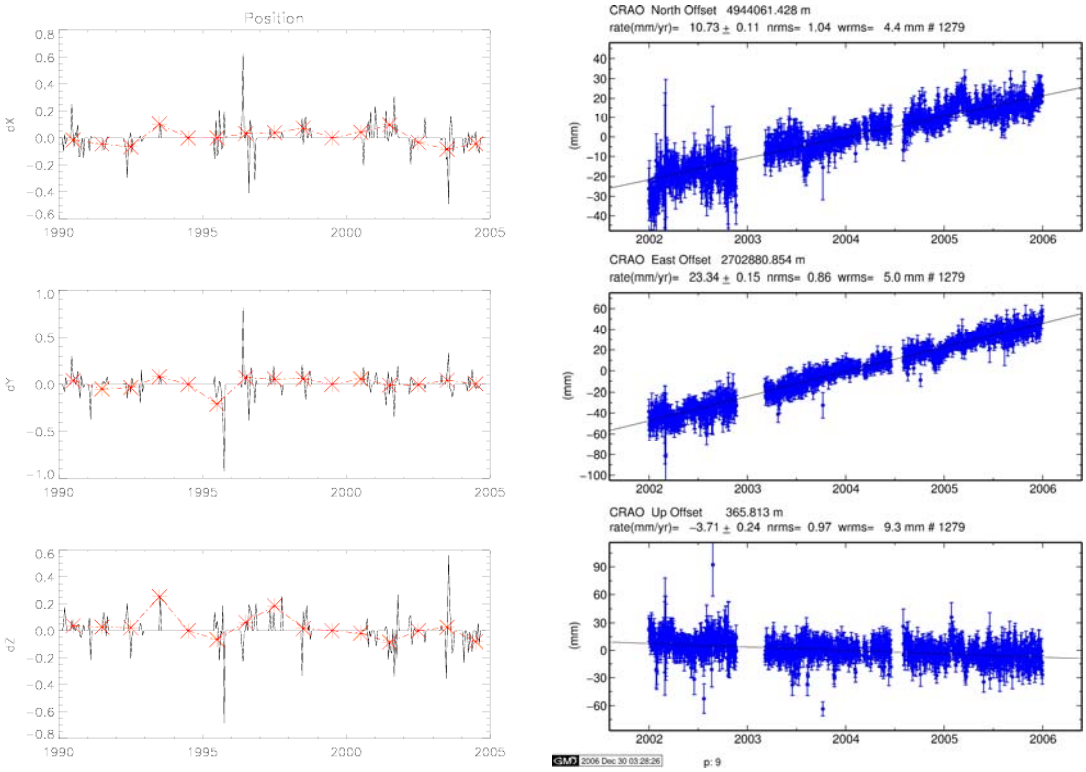

Figure 3. *Geocentric coordinates (delta from mean value) obtained by SLR (left) for 1991-2005 (red is a mean by year), meters; topocentric coordinates (delta from mean value) obtained by GPS (right) for 2002-2006, mm*

We have also processed GPS data with the GAMIT/GLOBK software on our station (fig.3, right). As you see, results from our SLR location are not comparable with results received by GPS. Also on the GPS results a trend is evident. It not detectable in the lower precision SLR data.

Summary

The analysis of results has shown that we still have stability problems with the Simiez ranging systems; likely causes of the problems are the old laser transmitter, inadequacies in the calibration system, and greater breaks in ranging to LAGEOS because of equipment failure and poor weather.

The basic directions of work will be: creation of a new telescope mount model; better operations procedures, and hopefully, replacement of the laser on new.

Acknowledgments

We acknowledge and thank to Stanislaw Schillak and to Olga Bolotina for processing our SLR results. We acknowledge and thank the Local Organize Committee of the 15th Workshop for financial assistance.

References

[1] Bolotina, O., Medvedskij M, Investigation of the stability of the Ukrainian SLR network, preprint, 2006

[2] Schillak, S. Determination of the station coordinates for quality control of the satellite laser ranging data. p387-394, Proc. 14th International Laser Ranging Workshop.

Overview and Performance of the Ukrainian SLR Station "Lviv-1831"

Martynyuk-Lototsky K., Blahodyr Ja., Bilinskiy A., Lohvynenko O.

1. Astronomical Observatory of Ivan Franko National University of Lviv, Ukraine, 79005, Lviv, Kiril and Mephodij St.8.

Contact: langure@mail.ru

Abstract

Satellite laser ranging station "Lviv-1831" was found in 1998. In August 2002, it was registered as an associate SLR station in the ILRS. It is also a member of the Ukrainian network of UCEOP (Ukrainian Center for Earth Orientation Parameters).

The station is based on the following equipment: 1 m telescope TPL-1M on alt-azimuth mounting, an SL-212 laser with 150 ps pulses at 532 nm and a repetition rate 5 Hz, a Latvian A911 timer with internal precision of 40 ps. The current fire-receiving system can only operate at ranges above 900 km [1].

During 2005 the station ranged to 138 passes of LAGEOS with an RMS of 50 mm. The short term stability over 2005 was about 35 mm, and the long term stability was 25 mm.

At present, the station team is testing a new receiver with a Hamamatsu module H6780-20 PMT, a neutral density filters wheel for return signal strength control, and a new electromechanical shutter. Implementation of these improvements in the system should increase the performance and the accuracy of ranging results by a factor of about three. The next step in station modernization is the improvement of fire-receiving system for ranging to very low satellites at altitudes about 500 – 900 km.

References*:*

[1] A.Bilinsky, Ya.Blagodyr, A.Lohvynenko, S.Ternavska Station reports: Lviv, Ukraine // International laser Ranging Service 2003-2004 Annual Report, June 2005, pp.B-26 – B-27.

Results of the TLRS-4 / moblas-7 Intercomparison test

Julie Horvath[1], Maceo Blount[1], Christopher Clarke[1], Howard Donovan[1], Craig Foreman[1], Michael Heinick[1], Anthony Mann[1], Donald Patterson[1], Dennis McCollums[1], Thomas Oldham[1], Scott Wetzel[1], David Carter[2]

1. Honeywell Technology Solutions Inc. 7515 Mission Dr. Lanham, MD USA 20706
2. NASA Goddard Space Flight Center, Code 453, Greenbelt, MD, USA 20771

Contact: julie.horvath@honeywell.com

Abstract

In March 2005, Honeywell Technology Solutions Inc. (HTSI) was tasked to restore the Transportable Laser Ranging System 4 (TLRS-4) to operational capability. This was in preparation for replacement of the Hollas SLR system, located on Mt. Haleakala that had ceased operations in 2004.

Introduction

The TLRS-4 had ended routine operations following a successful tracking campaign in Richmond, Florida on May 22, 1995 and was held at the Goddard Geophysical and Astronomical Observatory (GGAO) at the NASA Goddard Space Flight Center in a semi- operational status until 1999. Less than six months after beginning the restoration of the TLRS-4, the system was providing quality ground and satellite tracking. This culminated in the validation of the TLRS-4 by a direct intercomparison of TLRS-4 with the Network Standard, Moblas-7. The TLRS-4 / Moblas-7 Intercomparison occurred from August 1st – September 6th, 2005. Results of this test were presented at a NASA Operational Readiness Review on September 15th, 2005 to a panel of ILRS members and other NASA management.

This paper provides a description of the work performed to restore the TLRS-4 to operational status, a description of the intercomparison test, the analysis of simultaneous satellite tracking data along with ground target tests and the results of the test.

History

The TLRS-4 system has a history that dates back to the early 1980's when two identical TLRS systems (Transportable Laser Ranging Systems) -3 and -4, were originally designed and built by NASA. These systems were designed as compact and transportable,

and were deployed to many diverse locations for short (2-6 months) SLR tracking campaigns. HTSI, as NASA's mission contractor, was tasked to maintain, operate, and deploy each system for these tracking campaigns. TLRS-4 was assigned to North American locations.

In 1995, after a major decrease in the NASA SLR budget, TLRS-4 returned to GSFC. Since 1995, HTSI maintained the system in caretaker status at the GGAO under NASA SLR Mission contract. HTSI maintained TLRS-4 while supporting all other NASA SLR systems, as well as operating two systems at the GGAO and Monument Peak, CA (Moblas-7 and Moblas-4). TLRS-4 was frequently used as a test-bed to support SLR engineering projects, and was used for spare parts to support operational stations. In March of 2005, NASA tasked SLR to return the TLRS-4 to operational status. The system required a major engineering effort to return the system to regular operations.

Repairs/Upgrades

The TLRS-4 system's pre-upgrade status was that of an inoperable system missing both hardware and software upgrades that had been installed into all other systems in the NASA Network. Major repairs and upgrades were required for every major subsystem of the TLRS-4. The Laser subsystem required new oscillator and amplifier heads, a solid state pulse slicer, a laser interlock system, a laser collimation lens, dye pump power supply, calibration transmit filter, laser bracket, and a laser warning light. The telescope/optics subsystem required a new 10Å Daylight Filter, a complete upper deck upgrade, and a diassembly and cleaning of the telescope. The transmit/receive subsystem required a T/R Switch motor and synch board, installation of the Photek MCP upgrade, and installation of a low-loss receive cable. The computer subsystem required a fully upgraded processing computer, a new administration computer, modifications to software for the controller computer, and upgraded Internet communications. The console subsystem required a new trackball board and microprocessor, a new tracking scope, and a new HP5370B Time Interval counter. The timing subsystem required a modification to the Time Code Generator for 4pps, the modification for 4/5 pps Auto switch, and updated CNS Clock Software. The facility subsystem was upgraded with dome control sensors, dome weather protection, a new remote operated dome shutter, and a complete refurbishment of the Instrumentation van and Support trailer. The safety subsystem was completely overhauled and coordinated through GSFC Code 250 for laser safety compliance.

System Operations Verification Tests (SOVT)

In July 2005, after all system upgrades and repairs were completed, HTSI began SOVT testing of the TLRS-4 system. SOVT Tests are performed subsequent to each relocation and prior to any laser system beginning operational support. SOVT's are comprehensive testing that ensures that the system is ready for operations by addressing every major and minor subsystem. These include tests for verifying station communications; station timing; mount level and dome control; interface of the tracking computer, mount, and data interface system; processing computer; performance of the data measurement

system; operations of the Continuum Laser system; safety interlock system; telescope pointing; star calibration performance; ground tracking; and controller computer operations. All SOVT Testing was successfully completed on July 15th, 2005.

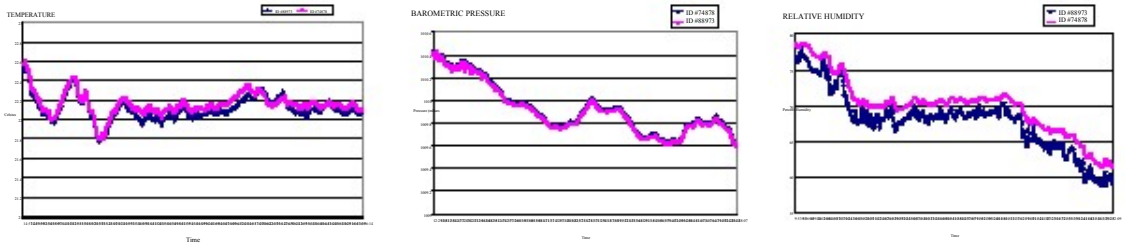

System Validation

The NASA SLR program validates newly built, or newly upgraded SLR systems with an Intercomparison or Collocation Technique developed at NASA and HTSI in the 1980's. Designed to directly compare an upgraded SLR system to an established SLR tracking system (Moblas-7 at GGAO currently operates as the NASA Global Standard SLR system), this technique characterizes and verifies the operational performance and laser ranging capabilities of the upgraded system prior to establishing routine operations. During this project, system performance of the TLRS-4 system was compared, relative to that of Moblas-7 with an Intercomparison between the two systems. Both datasets were also compared against known orbits. The Intercomparison was achieved by using NASA SLR- developed Intercomparison software packaged called Polyquick and orbit comparisons were achieved by using the NASA-developed GEODYN software package. Polyquick was developed to identify laser system ranging anomalies by utilizing intercomparison geometry to isolate station dependent, systematic ranging errors from other external sources of systematic errors such as refraction and orbital errors. Directly comparing these two stations will provide a reliable technique to accurately calibrate the TLRS-4's SLR performance at the centimeter and sub-centimeter accuracy level.

A pre-intercomparison phase was established to ensure that all prerequisites for the Intercomparison were completed. Prerequisites included a first order system survey to establish the DX, DY, DZ components between the two systems, simultaneous ground tests to establish stability and dependency issues, simultananeous satellite tracking to establish performance, comparison of the two systems MET systems, comparison of the two systems station timing, and finally a configuration freeze.

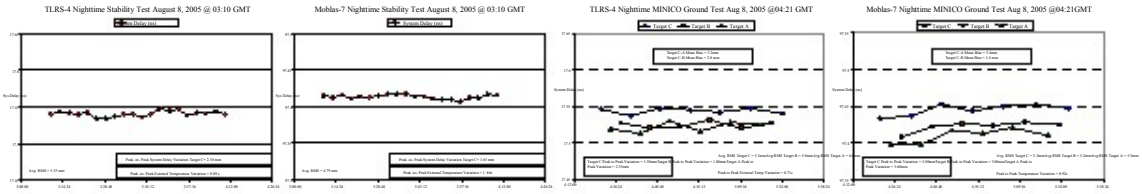

STATION	LATITUDE	LONGITUDE	HEIGHT(m)
7105	39° 01′ 14.17743″ N	76° 49′ 39.69784″ W	19.194
7130	39° 01′ 15.27139″ N	76° 49′ 38.82201″ W	18.632

On August 1st, 2005, the configuration of both the Moblas-7 and TLRS-4 systems were frozen for the formal Intercomparison phase of the TLRS-4 Return to Operations Project. An Intercomparison test consists of simultaneous satellite and ground tracking where an evaluation is done for data quantity and data quality, as well as simultaneous data analysis to establish any biases or dependencies between the two systems. The Moblas-7, the NASA Network standard, was established as the base system because of its known performance, and was to be tested against the unknown TLRS-4 system.

Intercomparison Requirements:

– Data Quantity and Quality:

– Minimum of 15 simultaneous Lageos-1 or Lageos-2 passes must be tracked during the Intercomparison period.

– Minimum of 20 low orbital satellite passes will be tracked during the Intercomparison period.

– Both systems must achieve the specified data quality standards for any pass to be qualified for the test pass total. The quality criteria are as follows:

System Calibration RMS (mm) Calibration Shift (mm)	Lageos RMS (mm)	LEO's RMS (mm)
TLRS-4< 7.0< 10.0	< 15.0	12.0 - 30.0
Moblas-7< 7.0< 10.0	< 15.0	12.0 - 30.0

Data Analysis Requirements:

– All systematic biases between the TLRS-4 and Moblas-7, operating under normal conditions will be less than ±15 millimeters

– Only passes with 30 full-rate observations for Moblas-7 are qualified for Intercomparison data analysis

– Minimum of 10 simultaneous points per Polyquick bin per station.

– Analyses by Polyquick will be performed for each simultaneous pass taken during the Intercomparison test period.

- Range Difference Computation
- Bias Tests
  - – Range-dependent Range Bias Test
  - – Range-rate dependent Bias Test
  - – Elevation Dependent Range Bias Test
  - – Azimuth Dependent Range Bias Test
  - – Energy Dependent Range Bias Test
  - – Test for Long Term Mean Range Bias Stability
  - – Test for Diurnal Effects
  - – System Delay Range Bias Test
  - – Sky Coverage Test
  - – Orbital comparison Test

- Data Analysis:

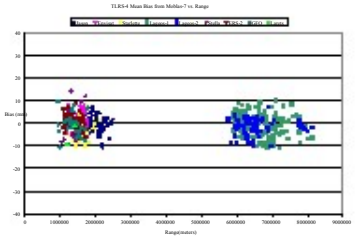
TLRS-4 Mean Bias from Mobllas-7 vs. Range
Range(meters)

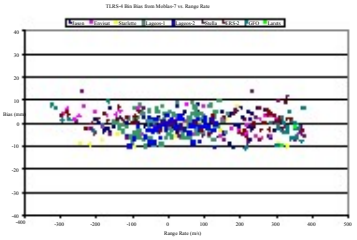
TLRS-4 Bin Bias from Mobllas-7 vs. Range Rate
Range Rate (m/s)

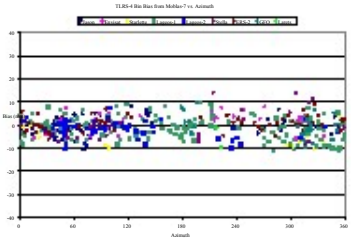
TLRS-4 Bin Bias from Mobllas-7 vs. Azimuth
Azimuth

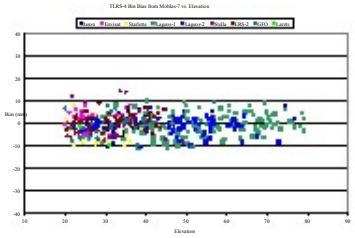
TLRS-4 Bin Bias from Mobllas-7 vs. Elevation
Elevation

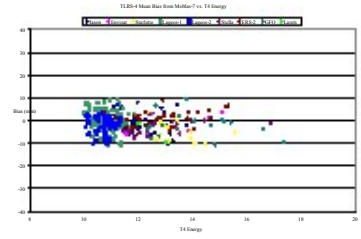
TLRS-4 Mean Bias from Mobllas-7 vs. T4 Energy
T4 Energy

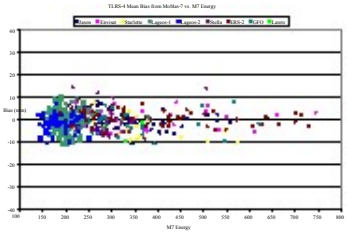
TLRS-4 Mean Bias from Mobllas-7 vs. M7 Energy
M7 Energy

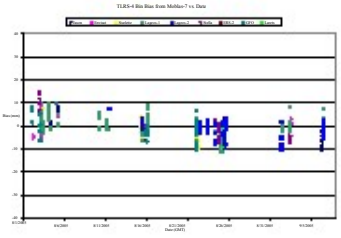
TLRS-4 Bin Bias from Mobllas-7 vs. Date
Date (GMT)

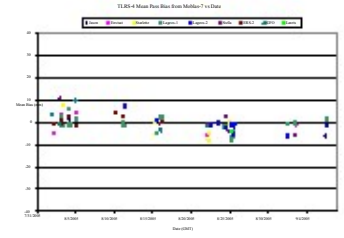
TLRS-4 Mean Pass Bias from Mobllas-7 vs Date
Date (GMT)

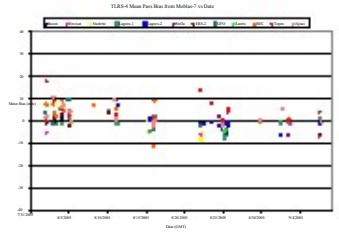
TLRS-4 Mean Pass Bias from Mobllas-7 vs Date
Date (GMT)

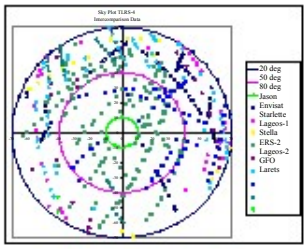
Sky Plot TLRS-4
Intercomparison Data
20 deg
50 deg
80 deg
Jason
Envisat
Starlette
Lageos-1
Stella
ERS-2
Lageos-2
GFO
Larets

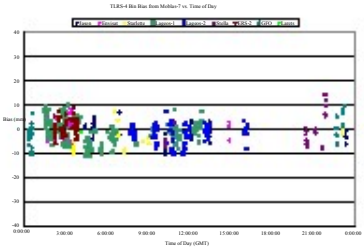
TLRS-4 Bin Bias from Mobllas-7 vs. Time of Day
Time of Day (GMT)

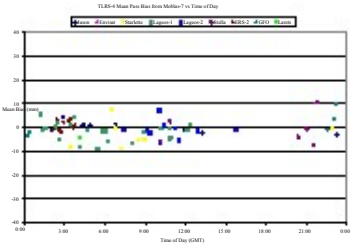
TLRS-4 Mean Pass Bias from Mobllas-7 vs Time of Day
Time of Day (GMT)

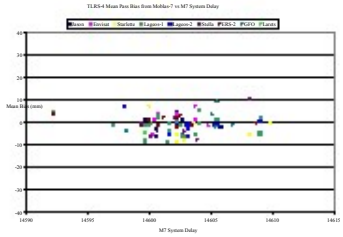
TLRS-4 Mean Pass Bias from Mobllas-7 vs M7 System Delay
M7 System Delay

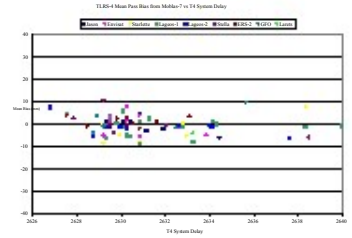
TLRS-4 Mean Pass Bias from Mobllas-7 vs T4 System Delay
T4 System Delay

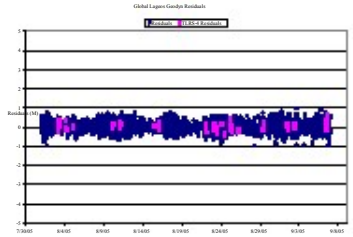
Global Lageos Geodyn Residuals
Residuals
TLRS-4 Residuals

Intercomparison				
TOPIC	TLRS-4	Moblas-7	TLRS-4 Results	Moblas-7 Results
Minimum Simultaneous Passes				
Lageos-1 & Lageos-2	15	15	29	29
LEO's	20	20	123	123
Fullrate Data RMS				
Calibration	≤ 7 mm	≤ 7 mm	5.44 mm	5.49 mm
Calibration Shift	≤ 10 mm	≤ 10 mm	0.31 mm	0.71 mm
Lageos-1 & Lageos-2	≤ 15 mm	≤ 15 mm	11.25 mm	9.17 mm
LEO's	≤ 12 - 30 mm	≤ 12 - 30 mm	16.11 mm	11.21 mm
Ground Test Delay Variations				
Stability Test	≤ 8 mm	≤ 8 mm	2.55 mm	1.73 mm
Extended MINICO	≤ 8 mm	≤ 8 mm	2.95 mm	2.13 mm
Intercomparison Bias				
TLRS-4 Mean Pass Bias from Moblas-7	± 15 mm		1.07 mm	
Lageos-1 & Lageos-2	± 15 mm		0.91 mm	
LEO's	± 15 mm		1.67 mm	

Results

The TLRS-4 / Moblas-7 Intercomparison produced some of the best intercomparison results ever achieved by a NASA system. The TLRS-4 system bias from Moblas-7 was 1.07 mm, far exceeding the ±15 mm requirement. The system exceeded every other intercomparison requirement and was declared an operational system after the NASA Operational Readiness Review on September 15, 2005. TLRS-4 was deployed to Maui, Hawaii on April 19th, 2006. It was then moved to the summit of Haleakala on September 7, 2006, and will return laser ranging to a critical global geographical position in the very near future.

The Accuracy Verification for GPS Receiver of ALOS by SLR

Nobuo Kudo, Shinichi Nakamura, Ryo Nakamura

1. Japan Aerospace Exploration Agency, 2-1-1 Sengen, Tsukuba-city, Ibaraki, 305-8505.

Contact : kudoh.nobuo@jaxa.jp / Fax: +81-29-868-2990

Abstract

The Advanced Land Observing Satellite (ALOS) provides precise geographical data for making global precise map. ALOS has a dual-frequency GPS receiver to determine geographic positions corresponding to points on satellite images. In order to confirm the orbit determination accuracy by GPS, we carried out a restricted laser ranging campaign with the support of the International Laser Ranging Service (ILRS). We found the GPS orbit agreed with the SLR orbit to within the resolution range of the SLR analysis.

Introduction

Recently, the positioning accuracy achieved by dual-frequency GPS receivers is within few dozens of cm. However we needed to verify the ALOS onboard GPS receiver because it was newly developed.

Overview of ALOS

Advanced Land Observing Satellite (ALOS), also called “DAICHI”, was launched from Tanegashima Space Center in Japan on 24 January 2006. ALOS performs earth observations at a high resolution, which is expected to contribute to a wide range of fields such as map compilation, regional observation, notice of disaster situations and resource mapping. Detailed review of the ALOS mission and its advanced technology were reviewed in Iwata et al [1] and Hamazaki [2]. The orbit information of ALOS is described in Table 1.

Table 1: *The value of the orbit*

Orbit Type	Solar synchronous, sub-recurrent, frozen
Height	691.65km (above the equator)
Period	98.7 min
Eccentricity	1/1000
Inclination	98.16deg
Recurrent days	46 days

ALOS is one of the largest Earth observing satellites ever developed. ALOS has a GPS receiver and a laser reflector as tools for orbit determination.

Orbit Determination accuracy of ALOS

In order to make a precise map, it is necessary to observe the earth with high resolution and specify geographical positions corresponding to observed images. Thus, high positioning accuracy and directional precision are required for ALOS [3]. Orbit determination accuracy is required to be within 1m after processing on the ground. There are two tools for precise orbit determination for ALOS, that is, GPS receiver and laser reflector (LR) for Satellite Laser Ranging (SLR). The ALOS GPS receiver was newly developed for this mission. Detailed description of the GPS receiver is given in Toda *et al* [4]. The result of orbit determination using the GPS data is reported in

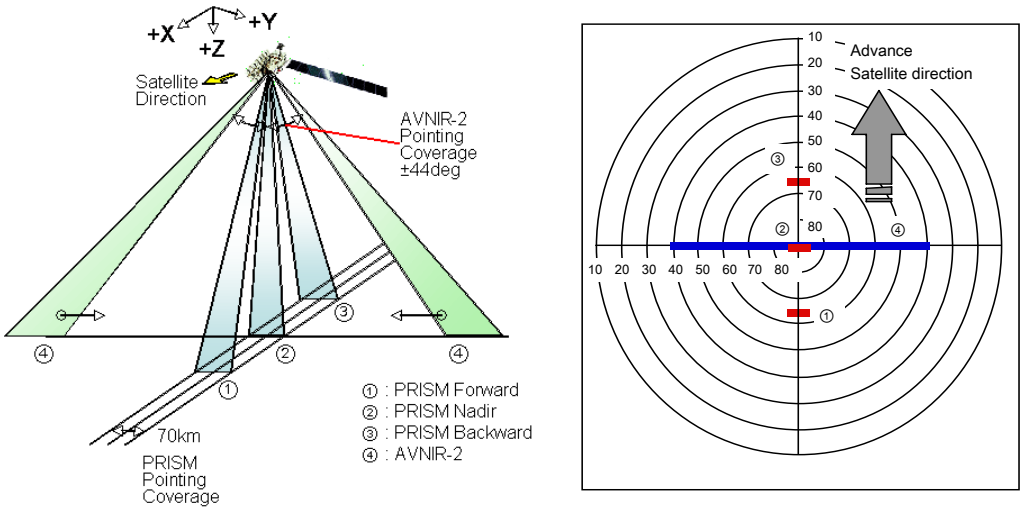

Figure 1. *Image of the ranging restriction.*

Nakamura *et al* [5]. The ALOS LR consists of nine Corner Cube Reflectors (CCR). A more detailed analytical result is described in the ALOS Tracking Standard [6].

Interference between ALOS's earth observation sensors and SLR laser beam

ALOS has two earth observation sensors (PRISM, AVNIR-2) which are vulnerable to the SLR laser radiation wavelength at 532nm. The CCD of each sensor can be destroyed when the incident energy exceeds $5x10^{14}$[W/m^2]. We checked the possibility of damage to these sensors using the specifications of some typical SLR stations. As a result, the laser of SLR could damage the CCDs of sensors if the laser beam impinges on the sensors. The results are similar for almost all stations of the world. Therefore we needed to carry out restricted laser tracking to avoid damaging sensors.

Restricted Laser Tracking

The method of restricted laser tracking is standardized by the ILRS[7]. JAXA carried out restricted laser tracking to ALOS using this method. Figure 1 shows the restricted area. The pass of ALOS is sometimes divided into two, three, or four regions.

Table 2: *List of participating station for ALOS Tracking*

SLR Stations	**ID**	**Nation**
Mt. Stromlo	STL3	Australia
RIGA	RIGL	Latvia
Koganei(KOGC)	KOGC	Japan
Simosato	SISL	Japan
Monument Peak(Moblas-4)	MONL	USA
Hartebeesthoek (Moblas-6)	HARL	South Africa
Yarragadee(Moblas-5)	YARL	Australia
Tanegashima	GMSL	Japan
Zimmerwald	ZIML	Swiss land
Herstmonceux	HERL	United Kingdom
Greenbelt (MOBLAS-7)	GODL	USA

SLR data acquisition and ILRS campaign

We asked ILRS to provide support for ALOS SLR. Thanks to ILRS support, eleven SLR stations (Table 2) participated in the ALOS SLR campaign. We carried out the

ALOS SLR campaign from UT 00:00:00 on 14 August 2006 to UT 16:00:00 on 31 August 2006. We obtained 100 passes and 2979 data points.

The accuracy of orbit determination using GPS data

First, we review the accuracy of orbit determination using GPS data. The details of method of orbit determination using GPS are described in Nakamura *et al*[5].

The accuracy of orbit determination using GPS data

Figure 2 and Table 3 shows the accuracy of orbit determination using GPS data during ALOS SLR campaign. The accuracy of orbit determination is evaluated by overlap comparison and expressed in terms of the RMS value during the orbit determination period. Figure 2 and Table 3 show that the accuracy of orbit determination using GPS data is within a few cm.

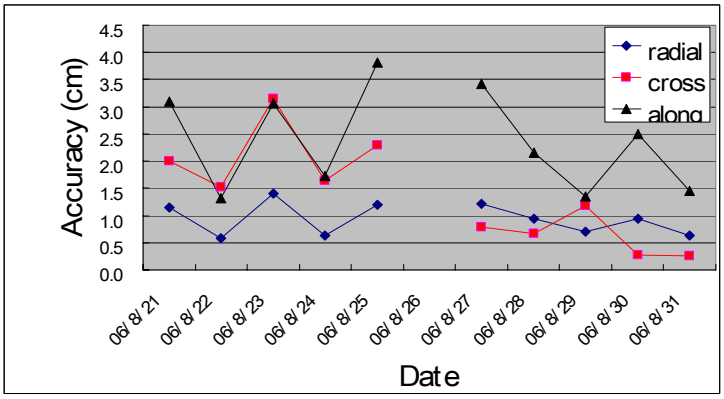

Figure 2. *Accuracy of orbit determination using GPS data (RMS) The horizontal axis is date and the vertical axis is the accuracy of orbit determination.*

Table 3. *Summary of GPS OD Accuracy (cm)*

	Radial(ave)	Radial(sig)	Cross(ave)	Cross(sig)	Along(ave)	Along(sig)
GPS Overlap	-0.04	0.94	0.03	1.38	0.56	2.39

Analysis

Our SLR analyses used both global arc and short arc methods.

Global arc analysis

We compared GPS data with SLR data and evaluated the residual of SLR data. Figure 3 shows a typical result and Table 4 shows the statistic result.

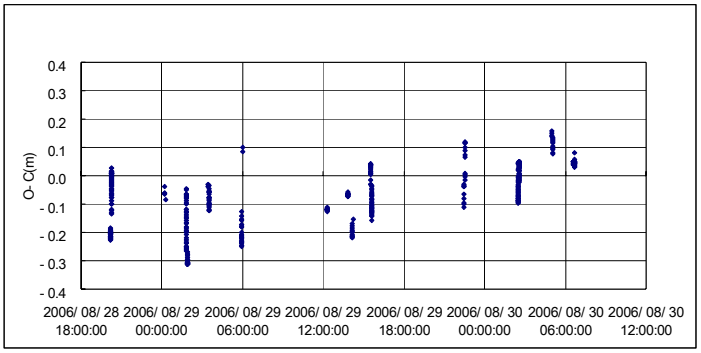

Figure 3. *Difference between GPS orbit and Laser ranging data (as example)*

Our analysis shows that the SLR data is within -4.8 ± 12.0 cm of the GPS orbits. What is noteworthy is that the standard deviation value is larger than the average value. This means that the difference between GPS-determined orbit and SLR data is well within the margin of error; there is no significant difference.

Table 4. *Results of residual (cm)*

	Average	St Dev
SLR O-C Analysis	-4.78	12.03

Short arc analysis

The above analysis cannot separate the radial, cross, and along components of GPS-determined orbit. Next we performed the orbit determination using only SLR data and compared it with the orbit determination using GPS data in each direction. Because SLR is an independent method from GPS, this analysis provides an objective evaluation of the ALOS onboard GPS receiver specifications.

Several passes are needed to perform orbit determination using SLR data. If we used daily data sets, the accuracy of orbit determination would be degraded because of the irregularity in data density. Therefore we performed the orbit determination using SLR data acquired during periods when more than three stations carried out SLR within a few orbital cycles. This means that our analysis is not the short arc analysis in a strict sense.

We calculated only the six orbital elements for the orbit determination using SLR data. We used a polyhedral model to represent the satellite and also considered the attitude model of ALOS. We didn't estimate the range bias for each station data. (We used the calibration data of each station.) And the analysis was performed for the periods where SLR data existed.

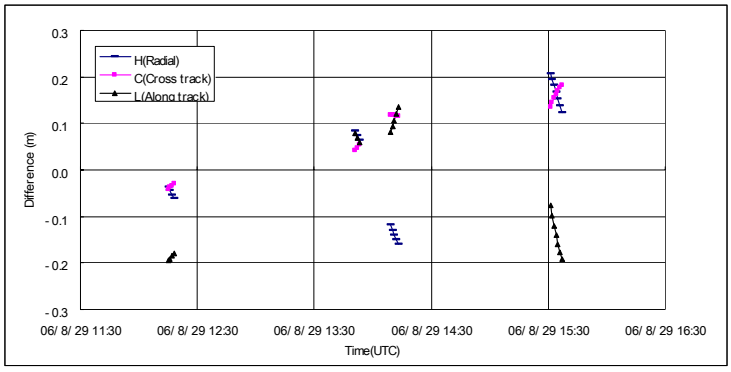

Figure 4. *The difference between the orbit determinations using SLR and* GPS

We compared the two orbit determinations of SLR and GPS approaches, and verified each direction (Cross, Along, Radial) result. The summary of result is shown in Table 5.

Table 5. *Summary of Difference between SLR and GPS (cm)*

	R(ave)	R(sig)	C(ave)	C(sig)	A(ave)	A(sig)
SLR-GPS	-2.98	20.54	-4.69	38.32	-5.44	28.76

These results show that the position estimated by GPS overlap method, and the position estimated by comparison of GPS orbit determination and SLR orbit determination fell within the margin of error (1sigma).

Conclusion

The analysis using the overlap method is a relative evaluation of GPS-based orbit determination and the analysis using SLR data is an absolute evaluation of GPS-based orbit determination. In other words, the overlap method is the evaluation of random error and the analysis using SLR data is the evaluation of bias error.

From this analysis, the error estimated by GPS overlap method was small compared to the error estimated by the analysis using SLR data. This means that the error estimated by GPS overlap method is negligible. The result of global arc analysis shows that there is no significant difference between the SLR and GPS data. Next we checked the difference in each direction between SLR determined-orbit and GPS determined-orbit by short arc-like analysis. As a result, the position estimated by GPS overlap method, and the position estimated by comparison of GPS orbit determination and SLR orbit determination agreed to within the margin of error (1sigma). Because the ALOS onboard GPS receiver was newly developed, we needed to verify the specifications. The result of this analysis showed that ALOS GPS receiver provides correct positioning information, to at least within the accuracy confirmed by our SLR-based analysis. In this analysis, 1 sigma was about 30 cm. This means that the accuracy of the ALOS onboard GPS receiver satisfies the requirement from ALOS mission, which is within 1m (peak to peak).

Acknowledgements

ALOS tracking campaign was performed successfully with the cooperation of ILRS and participating SLR stations, to all of whom we would like to express our deep appreciation. And we also would like to express our deep appreciation to Mr. Iwata, Mr. Toda and Mr. Matsumoto of ALOS project team, who explained the structure of ALOS in detail.

References

[1] Iwata. T et al, “The Advanced Land Observing Satellite (ALOS) – Preliminary Design”, 49th IAF, IAF-98-B.2.01, Melbourne, Australia, 1998.

[2] Hamazaki. T, “Key technology development for the Advanced Land Observing Satellite”, XIXth ISPRS Congress, Amsterdam, The Netherlands, July 2000

[3] Iwata. T, “Precision attitude and position determination for the Advanced Land Observing Satellite (ALOS)”, SPIE 4th International Asia-Pacific Environmental Remote Sensing Symposium: Remote Sensing of the Atmosphere, Ocean, Environment & Space, Honolulu, U.S.A., November 9,2004

[4] Toda. K et al, “GPS Receiver and Precision Position Determination for the advanced Land Observing Satellite (ALOS): Flight Result”(in Japanese), in print

[5] Nakamura. S et al, “Precise Orbit Determination for ALOS” (in press)

[6] Uchimura. T, “ALOS Tracking Standard”, http://god.tksc.jaxa.jp/al/source/source.html

[7] Werner Gurtner, Restricted Laser Tracking of satellites, May 2, 2005, http://ilrs.gsfc.nasa.gov/satellite_missions/restriction.html

Fulfilment of SLR Daylight Tracking In Changchun Station

ZHAO You, HAN Xinwei, FAN Cunbo, DAI Tongyu

1. National Astronomical Observatories/Changchun Observatory, CAS

Abstract

The paper introduces the performance and progress for Satellite Laser Ranging (SLR) system daylight tracking in Changchun station. This paper first introduces the problems and difficulties facing this system for daylight tracking—mount model, the separation of emitting and receiving parts of the telescope, control range gate, installing narrower filter. Third it presents some work which was done in the system for daylight tracking: system stability improvement, laser stability improvement, mount model adoption, control system, etc. From these analysis and work which have been done, the system performance has been greatly improved. A routine operation system in daylight tracking has been set up.

***Keywords*:** SLR, daylight tracking

Introduction

Some main technical problems for daylight tracking

The daylight tracking is necessary and the tendency of SLR in the future. Many stations in the world can take the daylight observations. According to the experience at the most successful station, recent years, Changchun station has been working on the daylight tracking technique. Some things to consider:

- Precise orbit prediction

Predictions of position and range of satellites and pointing of tracking mount with high accuracy. No problem for current CPF predictions.

- Reduce the effect of daylight sky background noise on photoelectric detector

Day background noise level is higher in SLR daylight tracking. Pointing of the telescope; Mount model problem for the telescope; Generating control range gate narrower; the application narrow Spectrum filter; the receiver filed of view want to be small, above all will efficiency reduces amount of background light.

- Parallelism of transmitting and receiving paths

For our station using telescopes with separated transmit and receive, it is sometimes difficult to maintain correct laser beam pointing due to Coude path mirror drifts. It required good collimation.

- Intensive light protective methods

To avoid the damage of the detector by focused Intensive light.

Progress for Daylight Tracking in Changchun SLR System

Even there are so many difficulties, we still have done some work to try to fulfill daylight tracking, such as system stability improvement, laser stability improvement, mount model adoption, control system, etc. In order to improve the system stability, a new control system has been adopted, including an industrial control computer, data collecting board and counter card for timing and range gate. Control and data preprocessing software are also updated so that all work can be done automatically. For

laser stability, the room is air-conditioned. The cooling system is also improved for its liable working, including some system protections. In order to improve the pointing accuracy, mount model correction is also adopted in the satellite prediction. A spherical harmonics pointing model was built by using astronomical observation at our telescope system. It is proved that the pointing model is an effective correction to the system error. This makes the pointing bias become very small in most directions. The design of tracking optical scheme on Changchun SLR system is shown in Figure 1.

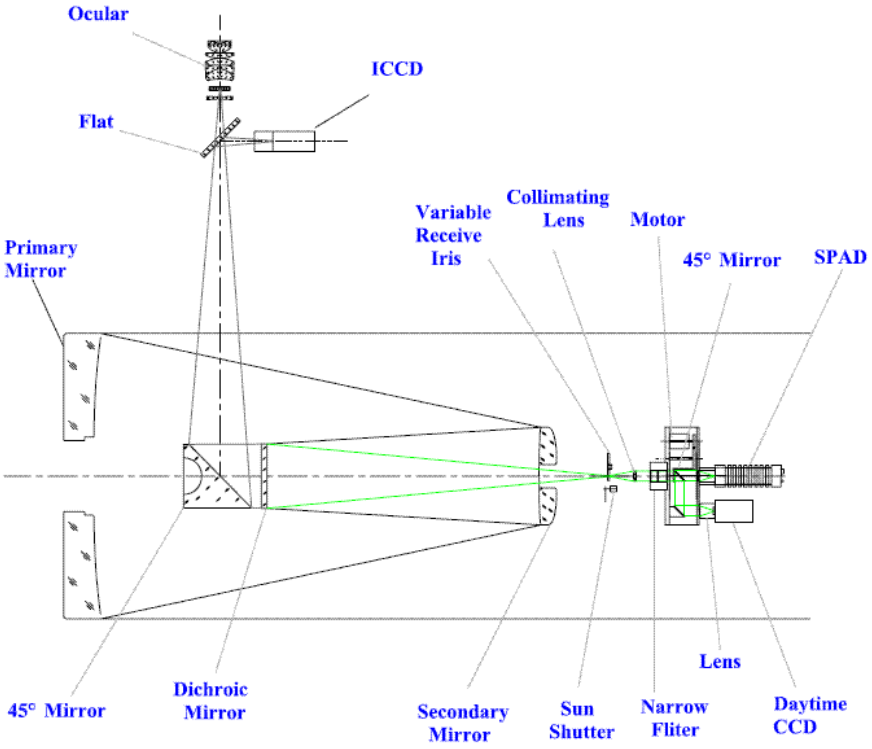

Figure 1. *Optical scheme of Changchun SLR system*

Ways to reduce effect of daylight background noise

Space filter

The electric-powered adjustable iris is used for field of view.
Receiving Field of view: 45"-12'. Figure 2 shows receiving iris diaphragm.

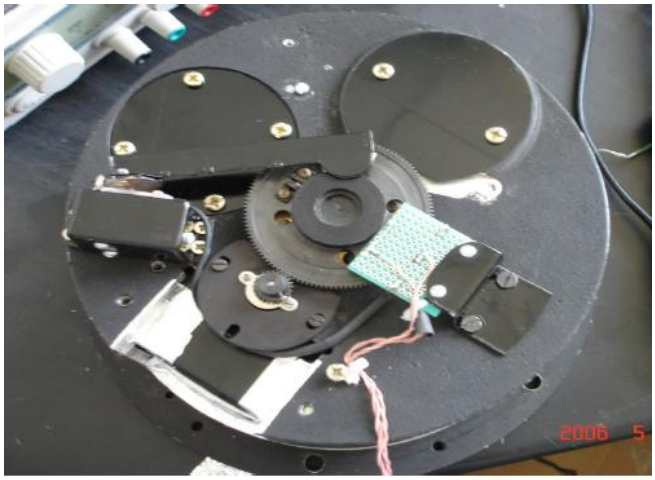

Figure 2. *Variable Receiving Iris diaphragm*

Timing filter

We designed and developed the precise range gate generator.
It can produce 1ns range gate to make the time closer to the arrival echo. We provide two devices to generate range gate:

AD9501: Programmable digital delay generator.10ps precision time delay, delay: 2.5ns—10us (capacitance and resistor);

DS1020: 8 bit programmable delay device, serial parallel mode. Max. Delay time: 48.25ns (fast mode), 520ns (slow mode). Figure 3 is the control precise range gate Generate Circuit Chart.

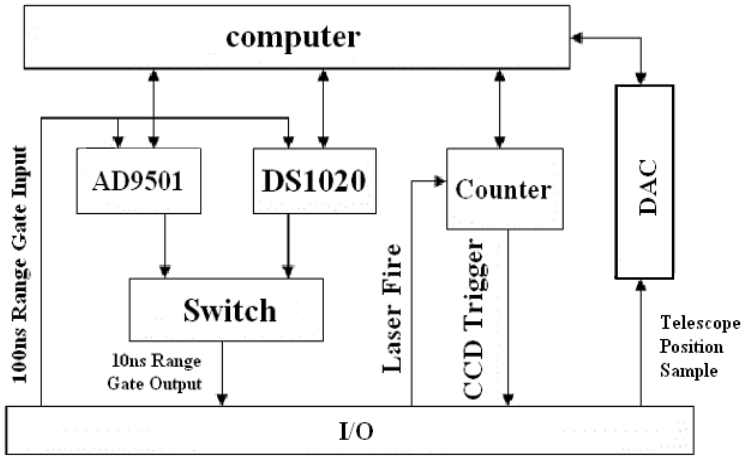

Figure 3. *Control precise range gate Generate Circuit Chart*

Spectrum filter

The application of 0.3nm narrow band pass interference filter form Andover Corp**.** and the constant temperature box to cut more background noise and to make the filter working in a constant temperature environment. The temperature controller provides protection against the influences of ambient temperature fluctuation. The specs of Andover Narrow Band Interference Filter are: Center Wavelength: 531.9 nm; Bandwidth: 0.3±0.1 nm; Peak transmission: 41.30 %; Ambient temperature: 23ºC; Size:Φ25.00 ± 0.25 mm. Figure 4 is the photograph.

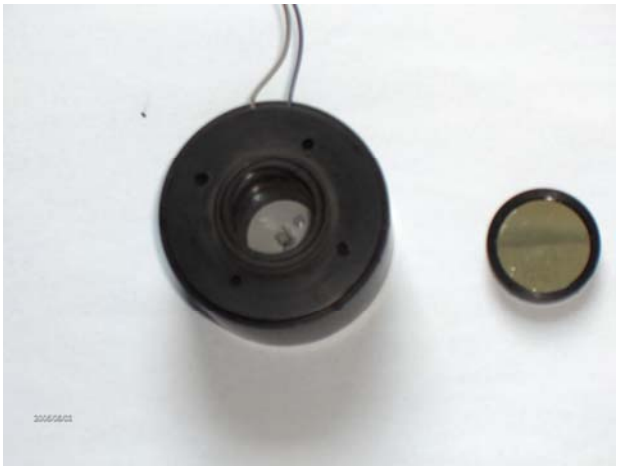

Figure 4. *Spectrum filter and constant temperature box*

Pointing of the telescope

- Mount leveling Collimation measurement

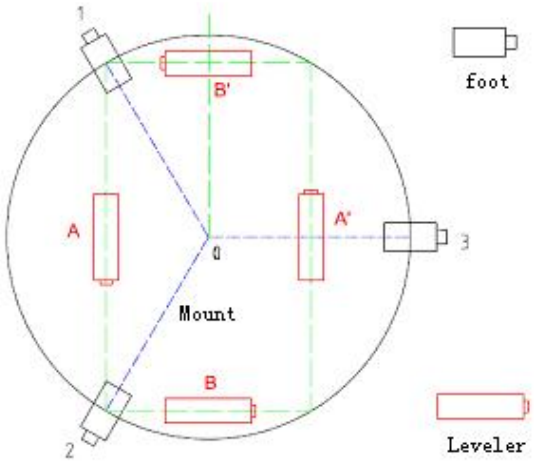

Figure 5. *Mount leveling Collimation measurement*

The first step is mount leveling. The data of mount leveler is recorded each 30 degree.

After leveling

$$i = \sqrt{a_1^{\,2} + b_1^{\,2}}$$

$$A = \arctan\left(\frac{a_1}{b_1}\right)$$

where

$$a_1 = \frac{1}{6}\sum_{j=0}^{11} f(\alpha_j)\cos(30^\circ \cdot j); b_1 = \frac{1}{6}\sum_{j=0}^{11} f(\alpha_j)\sin(30^\circ \cdot j)$$

After calculation: the azimuth angle perpendicular to the slant direction is A=1.2"

- Collimation measurement

$$C = (A_R - A_L \pm 180^o)/2$$

RMS = 3'02"

- Zero error measurement of encoder

Polestar observation the error of encoder zero position:

$$\Delta A_0 = 180.682431^o$$

$$\Delta E_0 = 0.01684^o$$

- Star Calibration

Observe positions of known stars (calculation from FK5) using night camera. Mark reference position on screen of night camera. Our system can to gather data from 48--60 stars in 1 hour. Compare observed (encoder readings) with calibration position (O-C). The Least Squares to fit the mount model parameters (13 parameters each axis). Application of current mount model provides a good fit for elevations from 15 degrees to 80 degrees. System pointing is at the few arc second level.

RMS of fit: Azimuth: 5.5"

Altitude: 4.8"

Parallelism of transmitting and receiving paths

1) Adjustment of sensitive area of detector.
2) Coude path fine adjustment.
3) Monitor laser beam during daylight.

We have installed a CCD camera in the receiver path; a switched mirror can direct this green light into the CCD or into the SPAD. This CCD is triggered by the laser start pulse that is delay 153us; an exposure time of down to 1/20000 s. Using software image / contrast enhancement techniques to display the backscatter of laser beam in real time.
4) Directional adjustment of output laser beam.

To adjust the laser beam direction with remote control of the last Coude mirror to fit the parallelism of transmitting and receiving path. Figure 6 is the image of daylight laser beam.

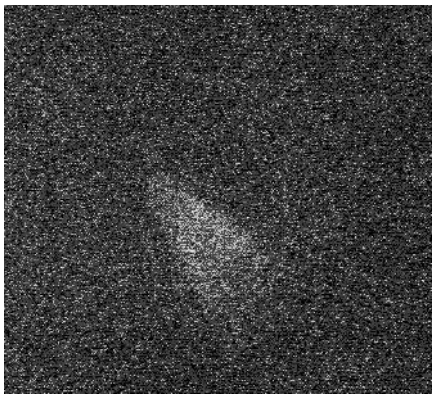

Figure 6. *Image of Daylight Laser Beam*

Intensive light protective methods

In order to avoid the damage of the C-SPAD detector by focusing sunlight, we must prevent the mount from pointing to the Sun. The double methods were used:

Hardware protection

Four strong light detectors were adopted on the top of mount, when the telescope moves to the place with strong light (such as to the sun or moon), the detectors will trigger a circuit to shut off the emergency shutter of the field of view. Figure 7 shows the electronic circuit diagram.

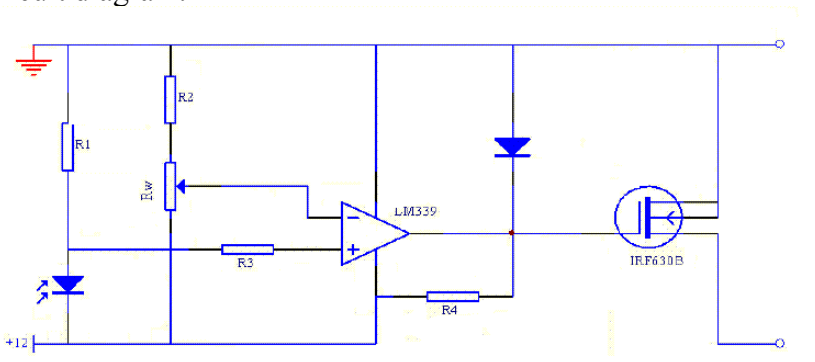

Figure 7. *Electronic diagram of light protective circuit*

Software protection

The software will control the telescope to avoid the sun when the satellite path travels across the sun area (less than 15º distance to sun) and stop the laser. It can choose a tracking path automatically when multi-satellite alternative tracking.

Conclusion

Almost everything, including hardware and software, is ready since the end of last year. Because of the cold weather we decided to do the test at the beginning of this year. In March of 2006, Galileo project was launched. Changchun station was selected to track Galileo satellite by Chinese government and ESA. So we have to change our plan and daylight tracking test has to be delayed. The Galileo project of first phase was finished, but the acceptance is not done. We have to wait for until it is over. But we are sure the condition is suitable for daylight tracking. And we will try the daylight tracking in the near future.

Acknowledgement

The authors would like to thank the financial support of the knowledge innovation project of the Chinese Academy of Sciences. And helpful discussion with Prof. Yang Fumin, Ms. Chen Wanzhen of Shanghai Astronomical Observatory, CAS of China, Dr. George Kirchner of Graz station of Austria.
The authors gratefully acknowledge the support of K.C.Wong Education Foundation, Hong Kong.

References

[1] ZHAO You, ZHANG Jun-rong, CUI Dou-xing: “The improvement of Changchun satellite laser ranging system”, Proceedings of SPIE Vol. 3501, pp.453 -460, 1998 Beijing, China.

[2] Zhao You: “Upgrade of Changchun SLR System”, Proceedings of 11th International Workshop on Laser Ranging, pp. 188 - 196, Sep. 1998 Deggendorf, Germany.

[3] Zhao You, Kunimori H., Hamal K., Prochazka I: “PCS in Changchun Station”, Proceedings of 11th International Workshop on Laser Ranging, pp.174 - 180, Sep. 1998 Deggendorf, Germany.

[4] LIU Chengzhi, ZHAO You, FAN Cunbo, CUI Douxing, HAN Xingwei, YANG Fumin: “Performance and observation summary of Changchun Satellite Laser Ranging Station”, Chinese Science Bulletin, Vol. 47, No. 13, pp.1070 - 1072, July 2002.

[5] You ZHAO, Cunbo FAN, Chengzhi LIU, Xinwei HAN, Jianyong SHI, Xinhua ZHANG, Haitao ZHANG: “System Stability Improvement of Changchun SLR”, Proceedings of 13th International Workshop on Laser Ranging. Oct. 2002, USA.

[6] ILRS publications SLR Station Performance Report Card 2003, on the Internet.

[7] Werner Gurtner, Ulrich Schreiber: “Daylight Tracking”, ILRS Technical Workshop, Kötzting, Germany, October 28 - 31, 2003.

[8] Yang Fumin, Xiao Zhikun, Chen Wanzhen, et al., “Design and Observations of the Satellite Laser Ranging System for Daylight Tracking at Shanghai Observatory”, Science in China, Series A, Vol.42, No.2, pp.198 - 206, 1999.

[9] Zhao You, Cunbo Fan, Xinwei Han, Chengzhi Liu, Xinhua Zhang, Jianyong Shi: “Progress for daylight tracking in Changchun SLR system”, Proceedings of 14th International Workshop on Laser Ranging, June of 2004, Spain, pp179 – 182.

GLONASS status update. MCC activity in GLONASS program.

V.D. Glotov, S.G. Revnivykh, V.V. Mitrikas

1. Russian Mission Control Center

Introduction

The Global Navigation Satellite System (GLONASS) is a government satellite navigation system which is designed for providing a continuous all-weather support of an unlimited number of aeronautical, maritime, terrestrial and space-born users with high-precision position-fixing and timing information at any point of the Earth and in the near-Earth outer-space. The Russian Federation Presidential Directive No. 38-RP of February 18, 1999 designated the GLONASS system as a dual-purpose space facility applied for solving the scientific, industrial, economical, social, defense, security and other relevant problems. It was also specified that the Federal Space Agency (Roscosmos) is a co-customer of the GLONASS system on equal footing with the Russian Ministry of Defence.

GLONASS Status

The first GLONASS satellite was launched into orbit on October 12, 1982. The GLONASS system formally attained the initial operation capability with a reduced-scale orbital configuration on September 24, 1993. The fact was approved with Presidential Directive No. 658 RP. Russian Federation Government Directions No. 237 of March 07, 1995 assigned a mission to implement a full-scale deployment of the GLONASS orbital constellation (24 satellites), to provide for mass-production of user equipment and to introduce the GLONASS system as an integral element of the international satellite navigation system for civil users.

The Russian Federation Government approved a long-term program of the GLONASS system modernization on August 20, 2001. It is designated as the Global Navigation System (GNS) federal objective program. The GNS Program covers improvement of space, ground-based and user equipment segments of the GLONASS system. Government commitments are associated with appropriation of funds to the Program for ten years by the State Budget Act.

There are new main tasks with the Presidential Directives issued at January 18, 2006 and at April 19, 2006:

- To ensure GLONASS minimum operational capability (constellation of 18 NSV) by the end of 2007
- To ensure GLONASS full operational capability (constellation of 24 NSV) by the end of 2009
- To ensure GLONASS performance comparable with that of GPS and GALILEO by 2010
- To ensure the navigation equipment mass production: encourage the industry in the manufacture renovation
- Mass market development

The Federal GLONASS Program update was approved by the Government Resolution at July 14 2006, No423.

Main reasons for SLR data application to GLONASS

There are a lot of the civil and scientific applications where navigation data from GPS are not enough for the complete analysis. The GLONASS navigation data are useful and helpful in these situations. Thus it's very important to use the same geodetic base with GPS by the GLONASS data generation. From this point of view it is necessary to calibrate geodetic base, the navigation signals accuracy for GLONASS system as good as possible. On the other hand the Russian Ground-Based Control Facility (GBCF) provides for management of the GLONASS orbital constellation and consists of the GLONASS Control Center and a network of tracking/control stations deployed in different areas of the Russian Federation only. SLR data from world wide stations net is the source of calibration data for ephemeris determination, international geodetic base providing and accuracy factor improving for GNSS etc.

So SLR data from ILRS network provide:

- Improving of the geodetic base for GLONASS on the way to ITRF
- Studying and improving of the SC motion model etc.
- Calibration and validation of the microwave means
- Testing and validation of the software and analysis results
- Monitoring of the real on-board ephemeris and clock

IAC activity in GLONASS Program

Informational Analytical Center (IAC - the department of the Russian Mission Control Center) since August, 15, 2006 has been formally assigned by the Federal Space Agency as the GLONASS official information portal for users with the next issues:

- Daily brief bulletins for GLONASS and GPS status based on the global data available (IGS network)
- GLONASS Control Center (Space Force) information
- NAGU generation
- Monthly bulletins with deep analysis of GLONASS performance
- GLONASS news
- GLONASS ICD, etc.

So, IAC is now acting as positive feed-back in the GLONASS control segment.

The IAC has been making contributions to the International GPS Service (IGS) by providing precise orbits based on SLR observations for those GLONASS satellites that are observed by the ILRS network. These independent orbits help to validate and evaluate precise orbits computed by Analysis Centers from the IGS tracking network observations. Since 1995, the MCC has permanently supported orbit determination of GLONASS satellites based on SLR data. Orbits for GLONASS satellites (in SP3 format) are regularly sent to the CDDIS for the determination of the final orbits based mainly on the GLONASS "phase" data.

GLONASS SLR data analysis

The global products from the International GLONASS service as part of the IGS should facilitate the use of combined GLONASS and GPS observations and analysis results for the civil scientific and engineering applications in the frame of the prototype Global Navigation Satellite System (GNSS). The ILRS supports this effort by a continuous tracking of three GLONASS satellites as part of their standard tracking protocol and by delivering precise GLONASS orbits through one of its Analyses Centers (MCC). Average number of the SLR data pro month for three GLONASS satellites is 500 – 700 passes from 15-18 stations (see the Table 1 as example of the month SLR tracking.)

Table 1.
Time interval: 30.07.2006 – 26.08.2006

SC	Passes	Stations
GLONASS-07	**133**	**14**
GLONASS-22	**154**	**15**
GLONASS-03	**220**	**16**
Total	**507**	**18**

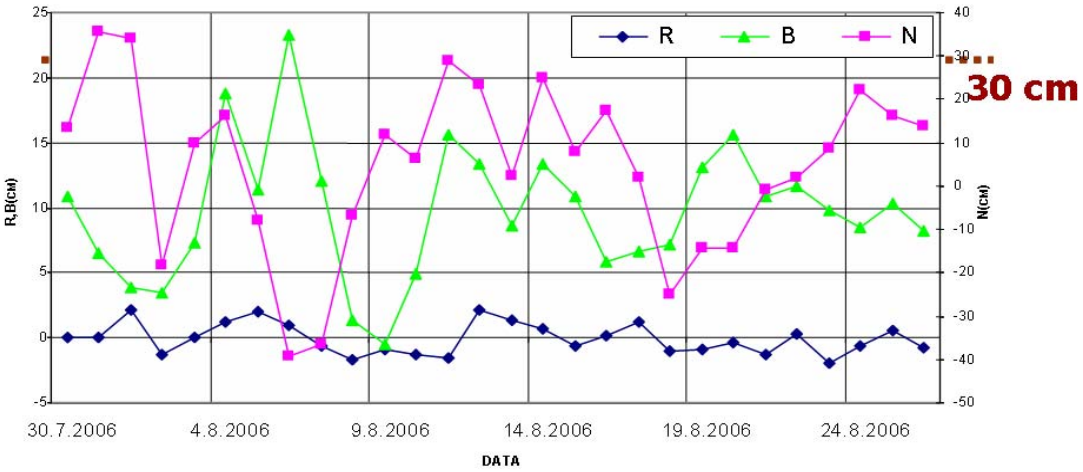

Figure 1. *The average difference between SLR and navigation orbits for GLONASS-89 (August 2006)*

Figure 1 shows the average difference between SLR and "microwave" orbits as potential GLONASS Performance (R-radial, B-across orbit, N- along orbit).

Figure 2 shows the improving of the on-board ephemeris & clock data for GLONASS constellation in the last years (since July 2005).

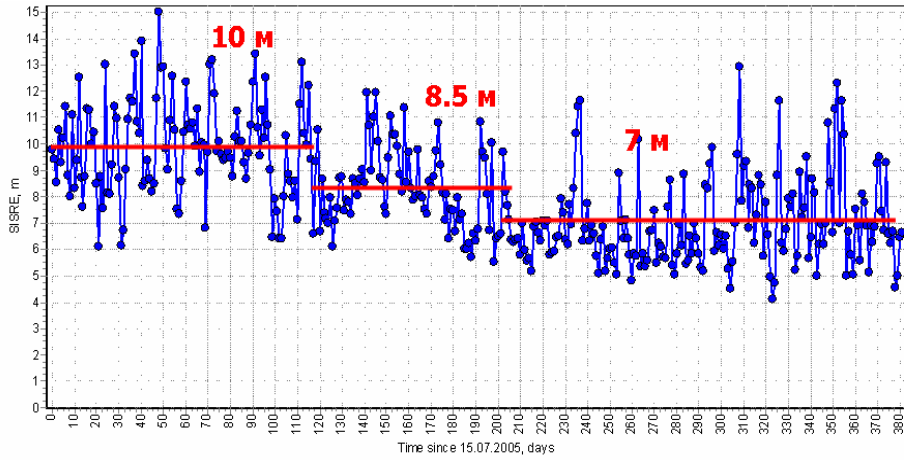

***Figure 2**. Average Signal In Space Range Error (SISRE), м (Since July, 2005)*

Conclusions

- ILRS support is very important for GLONASS modernization by the way to the Global Navigation Satellite System
- Need to continue/increase tracking of GLONASS satellites by ILRS for the realization of the real collocation in space (Microwave / Laser)
- The International GLONASS - Pilot Project demonstrates the extensibility of IGS to accommodate other microwave systems (GLONASS, GALILEO).

REGISTRANTS

Last Name	First Name	Organisation	Email
Altamimi	Zuheir	Institut Geographique National, France	altamimi@ensg.ign.fr
Appleby	Graham	NERC Space Geodesy Facility, UK	gapp@nerc.ac.uk
Arnold	David	Watertown, MA, USA	david-arnold@earthlink.net
Baltuck	Miriam	CSIRO, Canberra Deep Space Complex, Australia	mbaltuck@cdscc.nasa.gov
Beutler	Gerhard	Astronomical Institute of the University of Bern, Switzerland	Gerhard.beutler@aiub.unibe.ch
Bianco	Giusseppe	ASI/CGS, Matera, Italy	Guiseppe.bianco@asi.it
Burmistrov	Vladimir	Institute for Precision Engineering, Russia	Natalia.n@g23.relcom.ru
Burris	Harris	NRL / RSI, USA	
Carman	Randall	MOBLAS 5 Yarragadee, EOS, Australia	moblas@midwest.com.au
Carter	David	NASA Goddard Space Flight Centre, USA	david.l.carter@nasa.gov
Chuanyin	Zhang	Beijing SLR Station of Chinese Academy of Surveying and Mapping, China	bjslr@casm.ac.cn
Clarke	Christopher	NASA SLR / Honeywell TSI, USA	christopher.clarke@honeywell-tsi.com
Coulot	David	IGN/LAREG, France	David.Coulot@ensg.ign.fr
Davis	Mark	Naval Research Lab, Honeywell TSI, USA	mark.davis@nrl.navy.mil
Degnan	John	Sigma Space Corporation, USA	John.Degnan@sigmaspace.com
Deleflie	Florent	OCA/ GEMINI – GRGS, Grasse, France	Florent.deleflie@obs-azur.fr
Delle Monache	Giovanni	INFN LNF, Italy	Giovanni.dellemonche@lnf.infn.it
Dmytrotsa	Andriy	SRI Crimean Astrophysical Observatory, Ukraine	dymtrotsa@gmail.com
Donovan	Howard	NASA Satellite Laser Ranging Program, USA	howard.donovan@honeywell-tsi.com
Dunn	Peter	SGT Inc, USA	Peter.Dunn@raytheon.com
Feng	Qu	Beijing SLR Station of Chinese Academy of Surveying and Mapping, China	bjslr@casm.ac.cn
Forman	Michael	EOS, Canberra, Australia	mforman@eos-aus.com
Fumin	Yang	Shanghai Astronomical Observatory, China	yangfm@shao.ac.cn
Gambis	Daniel	Observatoire de Paris, France	daniel.gambis@obspm.fr
Gao	Yue	EOS, Canberra, Australia	ygao@eos-aus.com
Garate	Jorge	San Fernando Naval Observatory, Spain	jgarate@roa.es
Gibbs	Philip	NERC Space Geodesy Facility, UK	pgib@nerc.ac.uk
Glotov	Vladimir	Russian Mission Control Centre, Moscow, Russia	Vladimir.glotov@mcc.rsu.ru
Govind	Ramesh	Geoscience Australia, Canberra, Australia	Ramesh.Govind@ga.gov.au
Greene	Ben	EOS, Canberra, Australia	bengreene@bengreene.net
Gurtner	Werner	Astronomical Institute, University of Bern, Switzerland	werner.gurtner@aiub.unibe.ch
Hamal	Karel	Czech Technical University, Prague, Czech Republic	prochazk@troja.fjfi.cvut.cz
Horvath	Julie	NASA SLR / Honeywell TSI, USA	julie.horvath@honeywell-tsi.com
Izumi	Tadashi	NICT, Kogenai, Japan	slr-kog@slr.nict.go.jp
Jianli	Wang	Changchun Institute of Optics Mechanics and Physics, CAS, China	wangjianli@ciomp.ac.cn
Jingxu	Zhang	CIOMP, Chinese Academy of Sciences, Changchun, China	wangjianli@ciomp.ac.cn
Johnston	Gary	Geoscience Australia, Canberra, Australia	gary.johnston@ga.gov.au
Juping	Chen	Shanghai Astronomical Observatory, China	zzp@shao.ac.cn

Kim	Kyunhee	KAIST / STRC, Korea	
Kirchner	Georg	Austrian Academy of Sciences, Graz, Austria	kirchner@flubpc04.tu-graz.ac.at
Klosko	Steven	SGT Inc., USA	sklosko@sgt-inc.com
Koidl	Franz	Austrian Academy of Sciences, Graz, Austria	koidl@flubpc04.tu-graz.ac.at
Kolbl	Josef	Deggendorf University of Applied Sciences, Germany	josef.koelbl@fh-deggendorf.de
Kucharski	Daniel	Space Research Centre, Polish Academy of Sciences, Poznan, Poland	Kucharski@cbk.poznan.pl
Kudo	Nobuo	Japan Aerospace Exploration Agency, Tsukuba-City, Japan	kudoh@nobuo@jaxa.jp
Kulagin	Oleg	Institute of Applied Physics, RAS, Nizhny Novgorod, Russia	ok@appl.sci-nnov.ru
Kunimori	Hiroo	NICT, Koganei, Japan	kuni@nict.go.jp
Lee	Sang Hyun	KAIST / STRC, Korea	
Lemoine	Frank	NASA Goddard Space Flight Centre, USA	flemoine@puuoo.gsfc.nasa.gov
Lewova	Dana	Czech Technical University, Prague, Czech Republic	Lew.Dana@gmail.com
Li	Xin	Institute of Seismology, China Earthquake Administration, China	lxcomcn@yahoo.com.cn.
Lim	Hyung-Chul	Korea Astronomy & Space Science Institute, Daejeon, Korea	
Lu	Ma	UAO	
Luceri	Vincenza	e-GEOS, CGS, Matera, Italy	cinzia.luceri@telespazio.com
Luck	John	Stromlo SLR, EOS, Canberra, Australia	John-luck@bigpond.com
Luton	Geoff	Geoscience Australia, Canberra, Australia	Geoff.luton@ga.gov.au
McClure	David	Honeywell Technology Solutions Inc., USA	david.mcclure@honeywell-tsi.com
McGarry	Jan	NASA/GSFC, Greenbelt, USA	Jan.McGarry@nasa.gov
Michaelis	Harald	DLR, Institute of Planetary Research, Berlin, Germany	harald.michaelis@dlr.de
Moore	Chris	Stromlo SLR, EOS, Canberra, Australia	cmoore@eos-aus.com
Moshkov	Vladislav	IPIE, Moscow, Russia	Natalia.n@g23.relcom.ru
Mueller	Horst	DGFI, Muenchen, Germany	mueller@dgfi.badw.de
Mullaney	Jennifer	Registration Coordinator, EOS, Australia	
Murphy	Tom	University of California at San Diego, La Jolla, USA	tmurphy@physics.ucsd.edu
Nemec	Martin	Czech Technical University, Prague, Czech Republic	nemecM1@troja.fjfi.cvut.cz
Noomen	Ron	Delft University of Technology, The Netherlands	r.noomen@tudelft.nl
Noyes	Vince	MOBLAS 5 Yarragadee, EOS, Australia	moblas@midwest.com.au
Ogaja	Clement	Geoscience Australia, Canberra, Australia	clement.ogaja@ga.gov.au
O'Gara	Daniel	University of Hawaii Institute for Astronomy, Maui, USA	ogara@ifa.hawaii.edu
Osipova	Liene	Institute of Astronomy, University of Latvia, Riga, Latvia	lieneosipova@inbox.lv
Otsubo	Toshimichi	NICT, Japan	t.otsubo@srv.cc.hit-u.ac.jp
Parkhomenko	Natalia	Institute for Precision Instrument Engineering, Moscow, Russia	Natalia.n@g23.relcom.ru
Pavlis	Erricos	JCET/UMBC Nasa Goddard SFC, USA	epavlis@umbc.edu
Pearlman	Michael	Harvard-Smithsonian Centre for Astrophysics, Cambridge MA, USA	mpearlman@cfa.harvard.edu
Pearson	Matthew	EOS, Canberra, Australia	mpearson@eos-aus.com
Peltier	Richard	University of Toronto, Canada	peltier@atmosp.physics.utoronto.ca

Pierron	Monique	Observatoire de la Cote d'Azur, Grasse, France	monique.pierron@obs-azur.fr
Pierron	Francis	Observatoire de la Cote d'Azur, Grasse, France	francis.pierron@obs-azur.fr
Qian	Li	Beijing SLR Station of Chinese Academy of Surveying and Mapping, China	bjslr@casm.ac.cn
Ricklefs	Randall	University of Texas, Center for Space Research, Austin, USA	ricklefs@csr.utexas.edu
Salminsh	Kalvis	Institute of Astronomy, University of Latvia, Riga, Latvia	kalvis@lanet.lv
Sang	Jizhang	EOS, Canberra, Australia	jsang@eos-aus.com
Schreiber	Ulrich	Fundamental Station Wettzell, Germany	schreiber@fs.wettzell.de
Seemueller	Wolfgang	DGFI, Munich, Germany	seemueller@dgfi.badw.de
Shargorodsky	Victor	Institute for Precision Instrument Engineering, Moscow, Russia	Natalia.n@g23.relcom.ru
Shelus	Peter	Center for Space Research, University of Texas, Austin, USA	pjs@astro.as.utexas.edu
Sierk	Bernd	TIGO Observatory (BKG), Concepcion, Chile	sierk@tigo.cl
Smith	Craig	EOS, Canberra, Australia	csmith@eos-aus.com
Sperber	Peter	University of Applied Sciences, Deggendorf, Germany	peter.sperber@fh-deggendorf.de
Tangyong	Guo	Institute of Seismology, China Earthquake Administration, Wuhan, China	guoty@21cn.com
Tanqiang	Wang	Beijing SLR Station of Chinese Academy of Surveying and Mapping, China	bjslr@casm.ac.cn
Thompson	Ron	EOS, Canberra, Australia	ronthompson@eos-aus.com
Titov	Oleg	Geoscience Australia, Canberra, Australia	Oleg.titov@ga.gov.au
Torre	Jean-Marie	Observatoire de la Cote d'Azur, Grasse, France	torre@obs-azur.fr
Torrence	Mark	SGT Inc/NASA-GSFC, Greenbelt, USA	mark.h.torrence1@gsfc.nasa.gov
Tregoning	Paul	School of Earth Sciences, Australian National University, Canberra, Australia	Paul.tregoning@anu.edu.au
Urschl	Claudia	Astonomical Institute, Uni of Bern, Switzerland	claudia.flohrer@aiub.unibe.ch
Varghese	Thomas	Cybioms Corporation, Rockville MD, USA	tvarghes@cybioms.com
Wang	Peiyuan	Institute of Seismology, China Earthquake Administration, Wuhan, China	yangroot@yahoo.com.au
Wanzhen	Chen	Shanghai Astronomical Observatory, China	cwz@shao.ac.cn
Wasiczko	Linda	US Naval Research Laboratory, USA	linda.wasiczko@nrl.navy.mil
Wetzel	Scott	NASA SLR / Honeywell TSI, USA	scott.wetzel@honeywell-tsi.com
White	Nathan	EOS, Canberra, Australia	nwhite@eos-aus.com
Wiant	Jerry	McDonald Observatory, University of Texas, USA	jrw@astro.as.utexas.edu
Wilson	Peter	Stromlo SLR, EOS, Canberra, Australia	pwilson@eos-aus.com
Xiangming	Zheng	Yunnan Observatory, National Astronomical Observatories China (NAOC), Kunming, China	KMzxm@hotmail.com
Yechun	Tan	Institute of Seismology, China Earthquake Administration, Wuhan, China	tanyechun@21cn.com
Zhao	You	Changchun Observatory of NAOC, China	youzhao@cho.ac.cn
Zhongping	Zhang	Shanghai Astronomical Observatory, China	zzp@shao.ac.cn
Zhulian	Li	Yunnan Observatory, NAOC, Kunming, China	KMzxm@hotmail.com

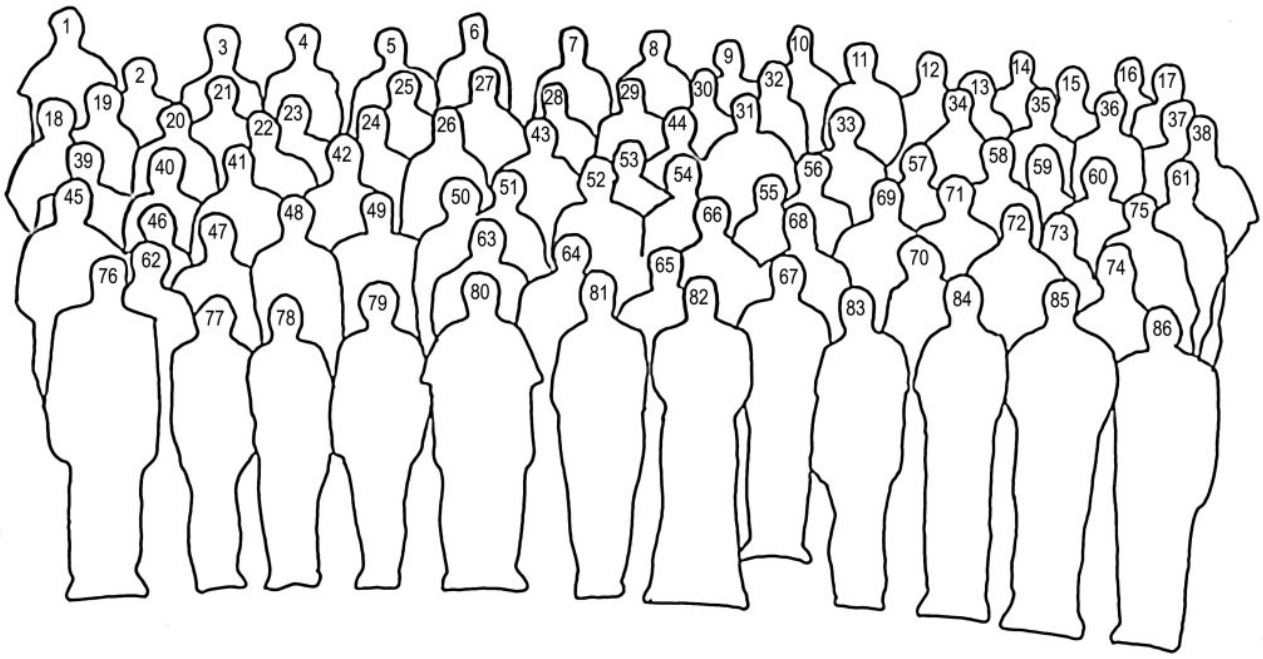

1 Paul Tregoning
2 Hyung-Chul Lim
3 David McClure
4 Howard Donovan
5 Christopher Clarke
6 Ron Noomen
7 Randy Ricklefs
8 Tom Murphy
9 Jerry Wiant
10 Nathan White
11 Mike Pearlman
12 Georg Kirchner
13 Steve Klosko
14 Daniel Kucharski
15 Vlasislav Moshkov
16 John Luck
17 Zuheir Altamimi
18 Wang Peiyuan
19 Kyung-Hee Kim
20 Zhang Zhongping
21 Sang-Hyun Lee
22 Dan O'Gara
23 Franz Koidl
24 Jean-Marie Torre
25 Vince Noyes
26 Ulrich Schreiber
27 Mark Davis
28 Jorge Garate
29 Pippo Bianco
30 Giovanni Delle Monache
31 David Coulot
32 Cinzia Luceri
33 Li Xin
34 Toshi Otsubo
35 Mark Elphick
36 Nobuo Kudo
37 Zhao You
38 Bernd Sierk
39 Craig Smith
40 Chris Moore
41 Scott Wetzel
42 Kalvis Salminsh
43 Pete Shelus
44 Florent Deleflie
45 Vladimir Burmistrov
46 Galina Glotova
47 Nina Platova
48 Ma Lu
49 Guo Tangyong
50 Philip Gibbs
51 Jan McGarry
52 Peter Dunn
53 Graham Appleby
54 Horst Mueller
55 Frank Lemoine
56 Hiroo Kunimori
57 Dave Arnold
58 Yang Fumin
59 Li Zhulian
60 Zheng Xiangming
61 Martin Nemec
62 Natalia Parkhomenko
63 Peter Sperber
64 Wolfgang Seemueller
65 Erricos Pavlis
66 Werner Gurtner
67 Ramesh Govind
68 Harald Michaelis
69 Dave Carter
70 Monique Pierron
71 Francis Pierron
72 Clement Ogaja
73 Dana Lewova
74 Andriy Dmytrotsa
75 Karel Hamal
76 Vladimir Glotov
77 Julie Horvath
78 Tan Yechun
79 Chen Wanzhen
80 Mark Torrence
81 Jennifer Mullaney
82 Ron Thompson
83 Claudia Urschl
84 Randall Carman
85 Peter Wilson
86 Viktor Shargorodsky